

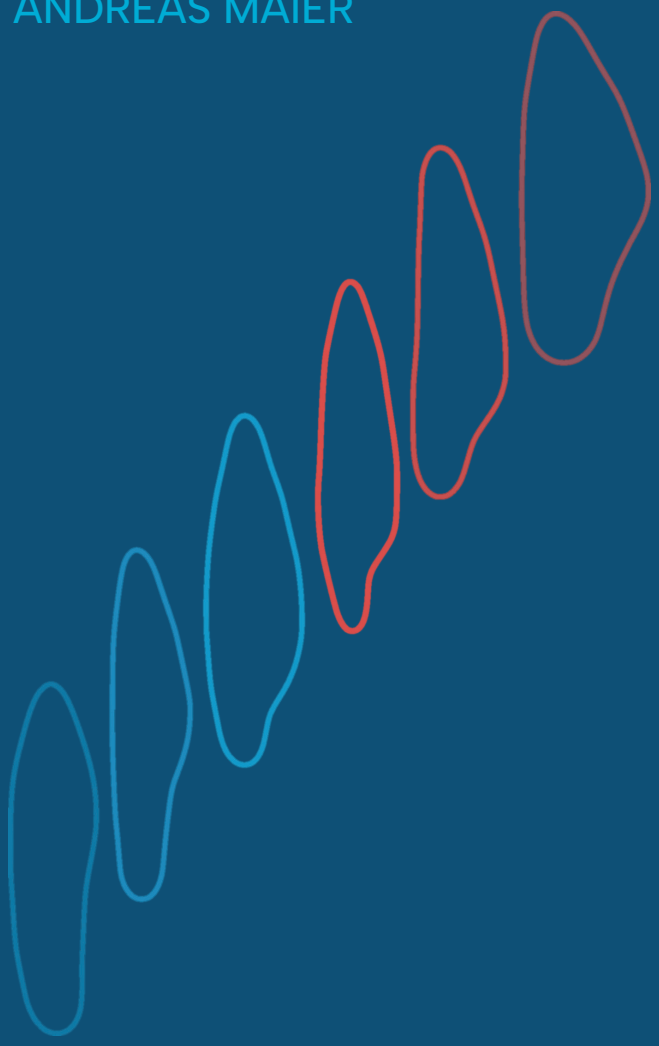
UNIVERSITÄT
ZU KÖLN

*The Cologne Prehistoric Series* *Volume 4*

# QUANTIFYING MORPHOLOGICAL VARIABILITY AND CHANGE IN LITHIC PROJECTILE POINTS OF THE UPPER PALAEOLITHIC IN EUROPE

ROBIN JOHN

EDITED BY ANDREAS MAIER



INSTITUTE FOR PREHISTORIC ARCHAEOLOGY

*The Cologne Prehistory Series* *Volume 4*

# QUANTIFYING MORPHOLOGICAL VARIABILITY AND CHANGE IN LITHIC PROJECTILE POINTS OF THE UPPER PALAEOLITHIC IN EUROPE

ROBIN JOHN

358 pages, 146 figures, 8 maps, 69 tables, 168 plates, 18 appendix tables

Oktober/November 2026

Funded by the Helga-Raddatz-Scholarship of the Stiftung NRW,
hosted at the Neanderthal Museum

Cover and Layout: Anja Rüschmann
Typesetting: Anja Rüschmann
Editing: Robin John

INSTITUT FÜR UR- UND FRÜHGESCHICHTE

# QUANTIFYING MORPHOLOGICAL VARIABILITY AND CHANGE IN LITHIC PROJECTILE POINTS OF THE UPPER PALAEOLITHIC IN EUROPE

Inaugural-Dissertation
zur Erlangung des Doktorgrades der Philosophischen Fakultät
der Universität zu Köln

im Fach Ur- und Frühgeschichte
vorgelegt von

**Robin John**
geb. am 26.11.1993
in Leipzig
Köln, den 10.10.2025

**Erstbetreuer:** Prof. Dr. Andreas Maier, Universität zu Köln, Deutschland/Germany
**Zweitbetreuer:** Prof. Dr. Felix Riede, Aarhus Universität, Dänemark/Danmark
**Gutachterin:** Prof. Dr. Silviane Scharl

# ACKNOWLEDGMENTS

This research was made possible through the generous Helga-Raddatz-Scholarship of the Stiftung NRW and was hosted by the Neanderthal Museum, Mettmann. I am extremely grateful to all the institutions involved for providing me with the opportunity to conduct my research over the past three years. I would also like to extend my sincere thanks to everyone affiliated with these institutions whose support and contributions helped make this project possible. In particular, I would like to express my deep gratitude to Anna Riethus, MA, research coordinator at the Neanderthal Museum, for her invaluable assistance and dedicated support in all organisational matters.

I am also deeply grateful to Dr. Isabell Schmidt, Dr. Gerda Koert, Prof. Dr. Mircea Anghelinu, Dr. Loredana Niţă, Dr. Walpurga Antl-Weiser and Veronika Kaudela, MA, for kindly providing images essential to this study. Special thanks go to Dr. Bernhard Paul Weninger for his kind support with the CalPal software.

My sincere thanks also go to Tjaark Siemsen, MA, for many stimulating discussions and his thoughtful, constructive criticism throughout the development of this work. I would also like to thank Dr. Georg Roth for educational and insightful conversations on statistical methods – some of which extended well into the night. Further appreciation is extended to my second supervisor, Prof. Dr. Felix Riede, for his valuable input, particularly regarding the theoretical framework. Isabelle Helle, I would like to thank for her meticulous and dedicated work in reviewing the texts for both grammatical and orthographic accuracy.

Above all, I would like to express my deepest gratitude to my primary supervisor, Prof. Dr. Andreas Maier. It was he who first sparked my interest in evolutionary archaeology and who laid the conceptual foundation for this research by introducing the initial ideas on the implementation of standardised morphometrical analysis. His unwavering support, insightful guidance, and constant encouragement – particularly during challenging periods of slow progress – were invaluable in sustaining my motivation and driving this project forward. His genuine interest in both the process and the outcomes of this research has been a continuous source of inspiration.

I thank all three reviewers for their thorough examination of my work and for their constructive comments.

Lastly, I am deeply grateful to my family for their steadfast support, for encouraging me to pursue this project, and for making it possible to fully dedicate myself to the work.

# TABLE OF CONTENTS


ACKNOWLEDGEMENTS 4

List of Abreviations 8

1. INTRODUCTION 9
!.1 APPLYING EVOLUTIONARY ARCHAEOLOGY 9
1.2 METHODOLOGICAL AND THEORETICAL CONSTRAINTS 11
1.3 CASE STUDY 12
1.4 BENEFITS, IMPLICATIONS AND OUTLOOK 13

2. MATERIAL 15
2.1 DATA COLLECTION AND EVALUATION 15
2.2 DATASET STRUCTURE 16
2.3 CHRONOLOGICAL AND GEOGRAPHICAL FRAMEWORK 17

3. METHODS 32
3.1 DATA RECORD 32
3.2 MORPHOMETRIC FEATURES 32
3.2.1 Intercorrelations between Morphometric Features 35
3.2.2 Categorisation of Morphometric Features 36
3.2.3 Style and Function 37
3.2.4 Constraints and Biases of Morphological Change 37
3.2.5 Problem of Preservation 38
3.3 ANALYTICAL METHODS 38
3.3.1 Identifying Timing and Duration of Evolutionary Trends 40
3.3.2 Mrasuring Variation 40
3.3.3 Calculating Tempo, inferring Mode 41
*3.3.3.1 Change Rates* 43
*3.3.3.2 Correlation* 44
3.3.4 Relations 44
3.4 VISUALISING METHODS 47

4. RESULTS 48
4.1 RESULTS ON THE 'CHRONOLOGICALLY INFORMED' PERSPECTIVE 48
4.1.1 Redundancy Analysis 48
*4.1.1.1 Entire Investigated Period* 48
*4.1.1.2 Periodisation* 49
*4.1.1.2.1 5000 year Periodisation* 49
*4.1.1.2.2 4000 year Periodisation* 50
*4.1.1.2.3 3000 year Periodisation* 53
*4.1.1.2.4 2000 year Periodisation* 57
*4.1.1.2.5 1000 year Periodisation* 61
*4.1.1.3 Optimal Periodisation* 65

4.1.2 Coefficient of Variation 65
4.1.3 Change Rates and Correlations 73
*4.1.3.1 Morphometric Features* 73
*4.1.3.2 Sections* 82
*4.1.3.3 Directness of Change Rates* 83
4.1.4 Combining Variation and Change 87
4.1.5 Summary of the Results on the 'Chronologically Informed' Perspective 87
4.2 RESULTS ON THE ARCHAEO-STRATIGRAPHICALLY INFORMED' PERSPECTIVE 91
4.2.1 Within Taxonomic Units 91
*4.2.1.1 Redundancy Analysis* 91
*4.2.1.1.1 Late Gravettian* 91
*4.2.1.1.2 Upper Solutrean* 94
*4.2.1.1.3 Non-Solutrean LGM Industries* 99
*4.2.1.1.4 Upper/Late-Final Magdalenian* 101
*4.2.1.1.5 Hamburgian* 104
*4.2.1.2 Coefficient of Variation* 106
*4.2.1.1.1 Late Gravettian* 106
*4.2.1.1.2 Upper Solutrean* 107
*4.2.1.1.3 Non-Solutrean LGM Industries* 110
*4.2.1.1.4 Upper/Late-Final Magdalenian* 113
*4.2.1.1.5 Hamburgian* 115
*4.2.1.3 Change Rates* 117
*4.2.1.3.1 Change Rates for Sections* 120
*4.2.1.3.2 Change Rates for Morphometric Features* 120
*4.2.1.3.3 Directedness of Change Rates* 123
*4.2.1.4 Combining Variation and Change* 125
4.2.2 Between Taxonomic Units 125
*4.2.2.1 Late Gravettian – Upper Solutrean* 136
*4.2.2.1.1 27th–26th millenium BP* 136
*4.2.2.1.2 26th–25th millenium BP* 137
*4.2.2.2 Upper Solutrean – Non-Solutrean LGM Industries* 138
*4.2.2.2.1 25th–24th millenium BP* 138
*4.2.2.2.2 24th–23th millenium BP* 140
*4.2.2.2.3 23th–22th millenium BP* 146
*4.2.2.2.4 22th–21th millenium BP* 148
*4.2.2.3 Middle Magdalenian – Upper/Late Magdalenian* 153
*4.2.2.4 Late Upper Palaeolithic Industries* 154
*4.2.2.4.1 17th–16th millenium BP* 154
*4.2.2.4.2 16th–15th millenium BP* 155
*4.2.2.4.3 15th–14th millenium BP* 158
4.2.3 Summary of the Results on the 'Archaeo-Stratigraphically Informed' Perspective 161
4.3 CLUSTER ANALYSES 162
4.3.1 Unconstrained Clustering 163
*4.3.1.1 Cluster Distribution and Diversity* 164
*4.3.1.2 Variation within Clusters* 165
*4.3.1.3 Morphometrics across chronologically sorted Clusters* 167
*4.3.1.4 Chronological Distance and Morphometric Difference* 168
4.3.2 Chronologically-Constrained Clustering 168
*4.3.2.1 1% Time-weighting* 168
*4.3.2.2 2% Time-weighting* 172
4.3.3 Adding Geographical Proximity 173
4.4 BRIDGING THE GAP? SCALENE BLADELETS AND SHOULDERED POINTS 176

5. DISCUSSION 185
5.1 EVOLUTIONARY DYNAMICS 187
5.1.1 What is Changing? 189
5.1.2 Morphometrics and Dynamics in Palaeodemography and Enviromental Conditions 193
5.2 SHOULDERED POINT LINEAGES 197
5.2.1 From the Late Gravettian to the Upper Solutrean: Heritable Continuity or Re-Innovation of Shouldered Points? 198
5.2.2 Relationships during the Last Glacial Maximum 202
*5.2.2.1 The Epigravettian and the West* 202
*5.2.2.2 The Salpetrian: A Regional Expression of the Solutrean?* 203
*5.2.2.3 The Badegoulian Phenomenon* 203
*5.2.2.4 The Emergance of the Magdalenian* 204
5.2.3 Magdalenian Shouldered Point Tradition? 204
5.2.4 The Late Upper Palaeolithic Shouldered Points 205

6. OUTLOOK: PREDICTIVE POTENTIAL OF MORPHOMETRICS 207
6.1 PREDICTION METHOD 207
6.2 TAXONOMIC PREDICTION 209
6.2.1 Late Gravettian – Upper Solutrean 209
6.2.2 Upper Solutrean – Salpetrian 212
6.3 TYPOLOGICAL PREDICTION 212
6.4 CHRONOLOGICAL PREDICTION 217
6.4.1 Berdyzh 217
6.4.2 Baume d'Oullins, layer D 218

7. SUMMARY 221
*Duration And Timing* 221
*Variation* 221
*Change* 222
*Alignment with Palaeodemographic Studies* 222
*Taxonomic Relations and the Limits of Typology* 222
*Predictive Potential of Morphometrics* 222

REFERRENCES 224–250

PLATES 251–302

APPENDIX TABLES 303–358

## List of Abbreviations

AMS = Accelerator Mass Spectrometry
BP = before present
cal = calibrated
CON = conventional dating
CV = Coefficient of Variation
e.g. = exempli gratia
ka = kiloyear
lat. = latitude
long. = longitude
PCA = Principal Component Analyses
RDA = Redundancy Analyses
SP = shouldered point
WA = Weighted Average

# QUANTIFYING MORPHOLOGICAL VARIABILITY AND CHANGE IN LITHIC PROJECTILE POINTS OF THE UPPER PALAEOLITHIC IN EUROPE

ROBIN JOHN

## 1. INTRODUCTION

Culture is the shared beliefs, values, norms and knowledge, that individuals of a community acquire through social learning and manifest in behaviours and material products (Boyd & Richerson 1985). It serves as an adapting mechanism for responding to changing environments, influencing, modifying, or even diverging from the trajectory of natural selection (Whitehead et al. 2019). A key human adaptation – perhaps most evident over the past 150 years – is the progressive and cumulative change of culture over time, as reflected in all facets of human life (Hill et al. 2009).

In archaeology, cultural change serves not only as the foundation for subdividing the discipline into specialised fields – such as Palaeolithic, Bronze Age, or Medieval archaeology – but also underpins the methodological approaches and interpretive frameworks employed to study the past. The notion that artefacts change in form and style over time is deeply embedded in archaeological thought and is reflected in early seminal works like Oscar Montelius' *'Die Methode'* (1903).

The dynamism and complexity of human culture set it apart from the cultural expressions observable in other animals, which are assumed to be insufficiently stable to affect genetic evolution (Boyd & Richerson 1985; Feldman & Laland 1996). For example, while chimpanzees (e.g., Sanz & Morgan 2009), crows (e.g., Hunt 1996) and wrasses (e.g., Jones et al. 2011) use tools, and orcas exhibit group-specific vocal dialects (Ford & Fisher 1983), these traits show little evidence of cumulative progression over time (Heinrich 2016). Early hominins may have shared this minimal form of cultural expression. Snyder et al. (2022) suggest that the transmission of know-how through social learning may not be necessary for the production of simple stone tools and the basic ability to make such tools may be part of our biological inheritance. Social learning, however, is also not a uniquely human trait (on this: Whiten et al. 2011; and e.g., Gunasekaram et al. 2024), but in humans it eventually became the driver of a far more powerful evolutionary process.

At a certain point in human history – variously argued to coincide with the Middle to Upper Palaeolithic transition (e.g., Mellars 1994), the Middle to Late Stone Age transition (e.g., Klein 1994), or, as more recently proposed, with the onset of the Middle Stone Age (McBrearty & Brooks 2000; Scerri & Will 2023), or perhaps even as far back as the emergence of geographical variability within Acheulean handaxes (Vaughan 2001; Sharon 2007) – human culture began to exhibit mechanisms characteristic of evolutionary systems. These include the transmission, heritability and loss of cultural traits (Cavalli-Sforza 1986), the introduction of variation through processes such as copying errors, transmission noise, or innovation (Perry et al. 2021), and the differential persistence of traits over time, whether driven by stochastic processes or selective pressures (Neiman 1995).

### 1.1 APPLYING EVOLUTIONARY ARCHAEOLOGY

Accepting human cultural change as an evolutionary process enables the application of methodological and theoretical perspectives that form the foundation of Evolutionary Archaeology. In this study, Evolutionary Archaeology is understood as the application of Darwinian evolutionism, rooting in the publication of Charles Darwin's *'On the Origin of Species'* (1859), to the analysis of human material cul-

ture. The concept of 'cultural evolution' was introduced in Richard Dawkins' *'The selfish Gene'* (1976), where he introduced the term 'meme' – a unit of culture that carries much of the *evolutionary* burden, as opposed to 'gene' as the traditional unit of heredity. The application of Darwinian evolutionary theory in archaeology can be traced back to the work of archaeologist Robert Dunnelll (1978a, 1978b, 1980), who introduced the concept of cultural transmission and variation as evolutionary processes, emphasising how artefacts and behaviours undergo selection, analogous to biological traits. These contributions set the groundwork for what later became known as Evolutionary Archaeology, integrating Darwinian principles into the study of material culture. The focus on the evolution of specific cultural phenomena distinguishes this approach to Evolutionary Archaeology from theories that emphasise the evolution of culture as a whole, such as the early works of Tylor (1871) and Morgan (1877), which significantly influenced processual archaeology, or later perspectives, often referred to as 'Whitean cultural evolution' (Dunnelll 1980), by White (1945, 1959) and e.g., Childe (1951). The proposal to apply Darwinian evolutionary theory in archaeology was met with significant debate within the scientific community (see, for example, Maschner 1998; Preucel 1999; Fracchia & Lewontin 1999). Critics argue that cultural change does not operate under the same constraints as biological evolution, thereby questioning the direct applicability of concepts, such as natural selection, variation, and inheritance to archaeological objects.

Evolutionary Archaeology, in the Darwinian sense, conceptualises archaeological objects as extensions of the human phenotype – that is, observable traits shaped by the interaction between an individual's genotype (its inherited genetic makeup) and its environment (Dawkins 1982; Griffiths et al. 2020) and temporally enduring manifestations of individual behaviour (O'Brien & Lyman 2003a). In doing so, it acknowledges that while the individuals who created and used these objects were subject to evolutionary processes, the objects themselves are adaptive reflections and active components of it (O'Brien & Lyman 2000, 7). By treating archaeological objects as extensions of biology through culture (Whiten 2017) – much like biologists consider, for example, spider webs to be temporary functional extensions of a spider's body (Dawkins 1982, 198) – this approach is argued to enable the application of Darwinian evolutionary biological concepts such as variation, selection, drift, innovation/mutation and heritability (Mesoudi et al. 2004).

However, cultural evolution, although analogies exist, is not biological evolution (Laland & O'Brien 2023), and cultural selection is not natural selection (Cavalli-Sforza & Feldman 1981). Biological evolution, in the Darwinian sense, is an unconscious and comparatively slow process. Variation – phenotypic differences observed among individuals within a population (Hansen 2006) – arises through random mutations. Variants are filtered by natural selection acting on reproductive success, either promoting the survival of advantageous traits or eliminating less advantageous ones, leading to adaptation. In this way, the direction of evolutionary change is shaped by environmental pressures. However, evolutionary change can also be effected by random processes called (genetic) drift. Cultural evolution, by contrast, can be both conscious and unconscious, and often unfolds at a much faster speed than biological evolution (Feldman & Laland 1996; Boyd et al. 2013), with changes possible within a single human generation or even a few years. Variation emerges through processes, such as innovation and copying or transmission errors, or individual choices (Cavalli-Sforza & Feldman 1981; Eerkens & Lipo 2005; Kempe et al. 2012; Fogarty et al. 2015). Selective pressures in cultural evolution are primarily social – driven by perceived usefulness, social influence, or cultural prestige (Boyd & Richerson 1985) – but can also include natural factors. Cultural traits can, however, also show signs of neutral drift (Bentley et al. 2004). The direction of cultural change is thus largely determined by social goals, preferences, and conventions but can also, to varying degrees, be influenced by environmental pressures.

As the adaptation of the title of O'Brien & Lyman's (2007) seminal book for this sub-chapter should suggest, the aim of this study is not to contribute to the theoretical discourse on cultural evolutionary archaeology, but rather to empirically apply key concepts to an extensive dataset and interpret the results through the lens of cultural evolution. It primarily addresses the question of how variation and, with it, the

speed and direction of change in cultural traits, particularly in archaeological objects can be measured.

## 1.2 METHODOLOGICAL AND THEORETICAL CONSTRAINTS

Despite the growing body of archaeological research framed within an evolutionary perspective (e.g., Kandler & Shennan 2015; Crema et al. 2016), and a particular interest in trait-based quantitative methods and their application to evolutionary research questions among archaeologists (e.g., O'Brien et al. 2014; O'Brien et al. 2016), the discipline still lacks well established standardised quantitative methods for measuring morphological variation and change in archaeological objects – methods that are well established in evolutionary biology and palaeobiology since at least George Gaylord Simpsons *'Tempo and Mode in Evolution'* (Simpson 1944). This methodological gap limits our ability to systematically trace cultural dynamics over time and to incorporate such results in broader contexts.

This methodological shortcoming is closely linked to the way archaeologists traditionally record information on artefact morphology. Specifically, information on (Palaeolithic) artefact morphology is traditionally recorded in terms of typologies (e.g., de Sonneville-Bordes & Perrot 1954; 1955: 1956; Bordes 1967; Klejn 1982; Debénath & Dibble 1994). In typological approaches, artefacts are recorded and categorised based on the presence of characteristic traits, which can but do not have to be present. Smaller differences between individual artefacts can be overlooked in favour of overarching similarities. While this makes typologies effective at capturing diversity across archaeological material – types – it often fails to adequately account for variation within individual types in a way that is suitable for quantitative analysis. It is noteworthy that the concept of 'types' was subjected to far earlier and more comprehensive critique in biology, where they are restricted to serving as name-bearing specimens (Simpson 1940).

In contrast to traditional typologies, several trait-based recording systems have been proposed to shift the analytical focus towards the technological characteristics of individual artefacts (e.g., Auffermann et al. 1990; Tostevin 2003; Nigst 2012; Simon & Moreau 2012). These systems emphasise discrete morphological or technological traits rather than overarching categorisations. Despite these efforts, a comprehensive and widely accepted trait-based systematics for tools has yet to be established in the field, although notable attempts have been made (Laplace 1972). Over the past two decades, the limitations inherent to typologies have been increasingly recognised, prompting the development of alternative methodologies aimed at capturing (intra-type) variation more effectively. Among these, Geometric Morphometrics (GMM) has emerged as a prominent tool in archaeology, particularly since the availability of user-friendly code-scripts (Bonhomme et al. 2014), offering a quantitative framework for the study of artefact shape. A substantial body of GMM-based studies focusses predominantly on shape – occasionally integrating technological information – while either entirely excluding or only briefly addressing size-related dimensions (e.g., Archer et al. 2016; Hoggard et al. 2019; Delpiano & Uthmeier 2020; Leplengeon et al. 2020; Weiss 2020; Matzig et al. 2021; Falcucci et al. 2022; Timbrell et al. 2022; Bischoff 2023; Rossini et al. 2023; Tsirintoulaki et al. 2023). Notably, exceptions that incorporate size parameters do exist (e.g., Weiss et al. 2018).

With 'PyREnArA', a new approach was introduced in 2023 (John et al. 2023), which places a stronger emphasis on morphometrics in the strict sense – integrating both shape and size to provide a more holistic understanding of artefact variability and its change. Such data can be utilised in methods specifically designed for the analysis of variation and change through time and space. PyREnArA has only been applied once before (Maier et al. 2023), with further applications currently in preparation (Siemssen et al. in prep.; Vogelsang et al. in prep.).

With the resurgence of interest in cultural evolution (Boyd & Richerson 2024), recent years have seen the emergence of new computational and quantitative approaches (e.g., Fogarty et al. 2024; Riede et al. 2024). The present study aims to contribute to the development of a robust methodological framework for quantifying morphological variation and tracking diachronic change. To achieve this, it draws on statistical approaches adapted from

disciplines such as evolutionary biology and ecology, where the analysis of shape change and trait evolution is well established (e.g., Haldane 1949; Hennig 1950; Simpson 1951; MacFadden 1988). These analytical methods have been implemented within PyREnArA, further developing it towards a more powerful and versatile tool, and are directly applied to the morphometric data it generates. This interdisciplinary framework enables the integration of evolutionary theory with high-resolution morphometric analysis. In doing so, the study seeks to bridge the gap between archaeological inquiry and evolutionary modelling, offering novel insights into the dynamics of cultural and technological change.

## 1.3 CASE STUDY

The application of such a methodological framework necessitates a case study that meets specific criteria: a sufficient chronological span, clear morphological consistency, and a well-established chronological sequence.

In a classical typological understanding, the shouldered point (SP) is a recurrent element of Upper Palaeolithic hunter-gatherer toolkits across Europe dating from approximately 30,000 to 14,000 years before present (BP). The typological classification of SP was first established by Henri Breuil (1913), who based it on an artefact from the Cueva de Ambrosio site, as part of his systematisation of the Upper Palaeolithic. They are defined by a concave retouch along one lateral edge, forming a notch (German: *Kerbe*, hence *Kerbspitze*; French: *cran*, hence *pointes à cran*) that gives rise to the characteristic shoulder. The point itself can be shaped by a steeply retouched truncation. These retouches may merge into a continuous retouch or remain separated by an unretouched section (Floss 2012). Additionally, SPs can be shaped entirely through surface retouch (e.g., Smith 1966).

Beyond these technological features, the typological definition of SPs does not encompass aspects of overall shape composition – for instance, the shoulder's position, which influences the relative proportions of a potential hafting part versus the actual penetrating part – nor does it consider size dimensions. Despite attempts to integrate morphological and technological data (Onoratini 1978) and to apply geometric morphometric methods for shape analysis (Schmidt & Mom 2015; Schmidt 2015), differentiation within the typology of SPs has thus far primarily relied on technological or stylistic criteria (de Sonneville-Bordes & Perrot 1956; Monmejan et al. 1964; Leroi-Gourhan 1964; Bordes 1965; Brézillon 1971). This has resulted in a multitude of sub-types that link technological, stylistic, and morphological characteristics of SPs to taxonomic units – such as the "classic Eastern European shouldered points" (Demars & Laurent 1992), the *'pointes à cran du Salpêtrien ancien'* (Boccaccio 2005), the *'pointes à cran du Tardigravettien'* (Livache & Brochier 1976), or the *'pointes à cran magdaléniennes'* (Lenoir 1975) – which complicates, if not completely hinders, diachronic analysis.

Although different hafting arrangements are functionally plausible (Beckhoff 1967; Lund 1993; Weber 2009; Muñoz Ibáñez et al. 2017, 48–49), SPs can be classified as latero-frontally hafted implements, combining the properties and functions of both laterally and frontally hafted tools within a single artefact (Maier et al. 2023). In a classical configuration, the penetrating part is positioned frontally, while the lateral edge opposite the shoulder may protrude from the shaft (Plisson & Geneste 1989, 91, Fig. 21; Kufel-Diakowska et al. 2016). This interpretation may be supported by the presence of retouched notches opposite the shoulder in some specimens (e.g., Onoratini 1994, Fig. 1.10), which may have served to facilitate binding or wrapping.

The first appearance of SPs around 30,000 years ago in Central Europe forms part of a change in the lithic toolkit, marking the onset of the Late Gravettian or Willendorf-Kostenkian (e.g., Svoboda 1996 and 2007). While this change is thought to have comprised a shift from axisymmetric projectile points – including tanged points, bifacial points, flechettes, Milovice points, or Pavlovian bipoints – to non-axisymmetric morphologies (Maier et al. 2021) – foremostly Gravette points, SPs may represent yet another transition: from laterally hafted forms – primarily Gravette points – to latero-frontally hafted projectile points (Maier et al. 2023). Although this has been recently questioned (Polanská et al. 2021; Niţă et al. 2021), for decades, shouldered points were considered as *fossils directeurs* of this Cen-

tral and Eastern European phenomenon (e.g., Otte 1981; Svoboda 2007), even giving rise to the term 'Shouldered Point Horizon' (e.g., Kozlowski 2008). In Western Europe, SPs occur for the first time around 25,000 years calBP during the Solutrean, where they play an essential role in defining its Upper phase (Jordá Cerdá 1955; Straus 1983; Zilhão 1997). Whether this appearance reflects the spread of SPs from their Eastern European distribution during the Late Gravettian, as suggested by Tiffagom (2006), or represents an independent development remains uncertain. On first impression, the technological difference, however, is evident – many of the specimens are shaped by facial retouching. SPs also occur in non-Solutrean assemblages during the Late Glacial Maximum sensu Mix et al. (2001), associated with taxonomic units like the Salpetrian (Boccacio 2005), the Late Badegoulian (Ducasse 2010), the Epigravettian or Epigravettiano in Italy (Mussi 2002) and the Lower Magdalenian (Langlais 2007). Throughout the Magdalenian, they remain a typical component of the lithic inventory, albeit with varying frequencies. Between roughly 20,000 and 16,000 years calBP, however, they occur only very rarely in Epigravettian and Middle Magdalenian contexts. Maier (2020) explains this near absence of classic SP-forms with the onset of functional probably similar 'scalene bladelets' at around 19,000 years calBP. These forms however disappear around 16,000 years calBP and SPs reappear numerously throughout central-northern Europa within the Upper/Late and Final Magdalenian, as well as in the Hamburgian (Weber 2009). With their presence continuing into in the slightly more recent Havelte phase (Tromnau 1975b, Pedersen et al. 2019), SPs then disappear from the archaeological record.

Even though the uninterrupted tradition of SPs as a universal design concept and a persisting hafting arrangement is questionable, the recurrent and consistent morphological feature – a single lateral notch – allows for inter-comparability. The exceptionally long duration of production and use of what typologically is framed as SPs, combined with the relatively precise chronological attribution of individual specimens, presents a rare and valuable opportunity to investigate long-term morphological developments within a well-defined temporal framework.

Additionally, as components of hunting equipment, projectile points are generally closely linked to subsistence strategies and are therefore assumed here to be particularly responsive to adaptive processes. It is widely accepted that SPs functioned as projectile points, a view that is supported not only by the exceptional finds of shouldered point fragments embedded in a horse scapula at the Solutrean site of Combe-Saunière (Castel 1999), as well as in two mammoth ribs at the Gravettian site of Kraków Spadzista (Wojtal et al. 2019), but also by repeated confirmations from use-wear analyses and fracture studies conducted on specimens from various contexts (Geneste & Plisson 1986 and 1989; Broglio et al. 1993; Boccaccio 2005; Schmidt 2015; Kufel-Diakowska et al. 2016; Tomasso & Rots 2021; Rossini et al. 2025). However, it remains plausible to argue that SPs may also have served alternative purposes, such as cutting or scraping, and were not necessarily components of hunting equipment in the strictest sense. Nevertheless, for the purposes of this study, a projectile function is assumed for all analysed SPs.

## 1.4 BENEFITS, IMPLICATIONS AND OUTLOOK

At first glance, after this introduction, focusing on a single constructed artefact type may seem counterintuitive when discussing cultural evolution. However, this deliberately narrow framework serves a specific purpose: it minimises analytical 'noise' that arises when artefact diversity is too great, enabling a clearer examination of variation in measurable traits and how they change over time and space. It is important to emphasise that this study does not aim to create new sub-types or taxonomic divisions within the artefact class under consideration. Instead, the intention is to use a clearly defined unit as a consistent reference point. As O'Brien & Lyman (2000, 352 f.) aptly note: *"you can define a species any way you want – biologically, paleobiologically, stratophenetically,* [typologically,] *or whatever. Just do not get so wrapped up in such units that you lose sight of the real goal, which is measuring variation, tracking it through time and across space, and then explaining it."* In this sense, the artefact type functions less as

a rigid taxonomic boundary and more as a methodological tool – an anchor for tracing patterns of morphological change, cultural transmission, and adaptation. The ultimate objective is to better understand the dynamics of variation itself: how it emerges, persists, spreads, and transforms.

The introduction of a novel methodological framework – at least from an archaeological perspective – for quantifying morphological variation and tracing its diachronic development, produces unprecedented data within the field of Palaeolithic archaeology. For the first time, morphological variation and transformation in stone tools are systematically measured and quantified in such a manner. The results are evaluated through multiple lenses: one emphasising chronological trends, and another integrating taxonomic classifications and geographic distribution.

While this study follows a macro-archaeological approach, prioritising large-scale, diachronic patterns across broad geographic and temporal frameworks, it intentionally deprioritises the analysis of individual assemblages or single artefacts. This trade-off allows for a better capture of overarching evolutionary trends in the morphology that transcend local or site-specific variation. Such an approach is typically referred to as macroevolutionary (Prentiss et al. 2009; Prentiss et al. 2022). By abstracting from micro-contextual details, the study aims to reveal structural regularities and long-term dynamics in material culture – SPs in particular – thereby contributing to a broader understanding of cultural evolution and technological change throughout the Upper Palaeolithic of Europe. However, a macro-approach is not a prerequisite to the application of the proposed methodological framework.

Cultural change – or cultural evolution – is not an undriven phenomenon. Rather, it is shaped by a complex interplay of factors, including biologically rooted developments, such as altered neural configurations (e.g., Pinson et al. 2022), environmental fluctuations (e.g., Collard et al. 2013a and 2013b; Maier et al. 2021), and feedback processes between artefacts and their producers or users (e.g., Hodder 2012; Malafouris 2013). Another widely discussed factor – long recognised among biologists (Charlesworth 2009) – that also plays a crucial role in cultural evolution is demographic dynamics (e.g., Henrich 2004; Shennan 2001). Over the past decade, paleodemography has produced increasingly quantified data on population size and density during the Upper Palaeolithic (e.g., Maier et al. 2022), enabling direct comparison with observed patterns of morphological change. This study primarily interprets its findings through the lens of the latter, with particular emphasis on the influence of human population dynamics on the observed patterns.

Not barely acknowledging but fully engaging with recent concerns regarding the significance of taxonomic units – such as techno-complexes and archaeological cultures – (e.g., Reynolds & Riede 2019), this study additionally provides insights into potential morphological relationships between the SPs of individual taxonomic assignments proposed by the literature. This offers a basis for exploring how certain traits may be shared, inherited, or diverge over time. These observed relationships, in turn, inform a broader discussions on the significance of taxonomic units and taxonomic continuity or discontinuity, overlap, or transformation, shedding light on processes such as cultural transmission, innovation, convergence, or evolutionary branching within and between techno-complexes.

The approach presented here offers an initial demonstration of the framework's potential, serving as a foundational case study for future research. Additionally, this study assembles the thus far largest collection of SP depictions, accompanied by detailed chronological, taxonomic, bibliographic, and morphological data. This unique dataset is well suited for integration into further analyses and, owing to its transparency, is readily usable by other researchers in the field. While individual case studies can yield valuable insights into past dynamics, the broader objective is to encourage the development of comparable datasets that, collectively, contribute to a more comprehensive understanding of long-term morphological change.

The systematic analysis of variation and change in artefacts through time offers an additional opportunity: the recursive classification of undated or ambiguous artefacts. As both an outlook and a demonstration of the potential of the approach developed here, this study explores this application.

# 2. MATERIAL

## 2.1 DATA COLLECTION AND EVALUATION

Through an extensive review of archaeological literature and personal communications (see references in *Table 2*), complete and near-complete tools classified as SPs by the respective authors were identified. As the completeness of artefacts is essential for accurate two-dimensional morphometric analysis, only intact SPs were considered. If broken, they had to be published in a refitted condition. Small missing portions of the tip were accepted if their original shape was either indicated by the author or could be reliably inferred from the convergence of the outline. In such cases the missing part was reconstructed (e.g. Appendix Plate 26). However, artefacts with missing basal sections were more difficult to reconstruct. Consequently, SPs with such incompleteness were not recorded. This ensures precise and unbiased measurements of key properties such as length, area, angles, and symmetry, providing a reliable foundation for comparative analysis. The exclusion of heavily fragmented SPs, however, means that a substantial portion of the published artefacts were not incorporated. Fragmentation – depending on the fracture type – is often indicative of use, suggesting that these pieces were selected for their properties after manufacture. In contrast, complete pieces may never have been used. Therefore, analysing only complete specimens could introduce an unnoticed *bias* into the dataset. Nevertheless, this potential *bias* is considered acceptable, as broken and complete pieces generally exhibit highly similar morphologies.

Artefact plates containing drawings or photographs of such SPs were scanned from the original literature using a handheld scanning device (IRIScan™ Book WiFi). Following scanning, the resulting images underwent a series of processing steps. Initially, a black filled one-by-one centimetre square, used by PyREnArA – a code-script for recording and analysing the morphometrics of artefacts (see Methods – Data Recording, Chapter 3.1) – as a reference to calculate the pixel-to-millimetre ratio, was extracted from the original scale and positioned in the upper left corner. Subsequently, all elements not relevant to the study – such as lateral and ventral views of the artefacts, scales, artefact numbers, and arrows indicating striking directions – were removed from the image. The refined image was then imported into a vector graphic software (Inkscape) for further processing. Using a brightness cut-off detection mode, the image was vectorised into a bitmap. This step allowed for resizing artefact depictions to a standardised scale, eliminating background noise from the original scan, and ensuring consistent image quality. In some cases, where the depiction quality was insufficient or photographs were used, internal details (e.g., negatives) could not be retained. In such cases, the artefact area was instead filled in black. Additionally, some depictions obtained through personal communication were provided only as silhouettes. These too were filled in black. Finally, to standardise measurements of symmetry, all SPs were oriented with the notch facing to the right. These standardised and cleaned images ensured a trouble-free usage of the images in PyREnArA and facilitate direct comparison and analysis. In total, 168 such assemblage-specific images were compiled, depicting 687 complete or completed SPs (see Appendix Plates).

For each assemblage, three types of background data were recorded: geographical location, taxonomic association, and radiocarbon data. While taxonomic associations were accepted directly from the original literature from which the images were sourced, the radiocarbon dates required further evaluation. Available radiocarbon dates were documented alongside their respective laboratory numbers. Where possible, the type of dated material (e.g., bone, antler, or charcoal) and the identified species (e.g., horse, reindeer, or pine tree) were recorded also, accompanied by the specific bibliographic references. When radiocarbon dates or specific details for individual dates could not be obtained by the review of the literature, the Radiocarbon Palaeolithic Europe database (Vermeersch 2023) was consulted. In total, 628 radiocarbon measurements from 109 assemblages were compiled (see Appendix Table 15 and 16). 315 of the measurements derive from Accelerator Mass Spectrometry (AMS), which is known for being more precise than conventional dating (CON).

The quality of each measurement was assessed singly based on some of the evaluation criteria compiled by Maier (2020), while,

where available, incorporating assessments from previous researchers (Grimm & Weber 2008; Barshay-Szmidt et al. 2016; Haesearts et al. 2016; Delage 2018). Key criteria for rejecting dates include:

1. standard deviation in years exceeding 1.5% of the measured radiocarbon age,
2. failure in the z-test for statistical consistency – date(s) differ(s) statistically from other dates outside acceptable limits (1.96*σ),
3. conflict with AMS date(s) – when CON dates conflict with AMS dates, AMS dates are preferred,
4. conflict with date(s) from humanly modified artefact(s) from the same layer – in such cases, the latter are preferred.

This procedure is necessary to provide a maximum level of precision, ensuring the significance of later results on chronological developements. It is acknowledged that measurements on certain materials (e.g., burned bone) may be of insufficient quality (Pettitt et al. 2003, 1687) as well as the fact, that single dates are problematic due to the impossibility of cross-evaluation (ibid, 1690). Nonetheless, given the limited number of radiocarbon measurements for most assemblages, such dates were included if they met the predefined criteria, even though they might not yield the preferred precision (e.g., Ua-3588 for Cueto de la Mina, Appendix Table 15). Additionally, no examination of the context of the individual radiocarbon measurements was undertaken.

The radiocarbon measurments remaining after the application of the above-stated criteria were then calibrated, and for assemblages with multiple measurements, weighted averages (WA) were calculated in CalPal (Weninger 2022) using the IntCal 2020 curve (Reimer et al. 2020). 'ka calBP' – denoting the calibrated age of the assemblage – and millennium BP – indicating the calibrated millennium before present within the respective assemblage dates *(Figure 1)* – were subsequently added as metadata. However, the exclusion of a date through this evaluation, does not necessarily imply that these dates should be entirely disregarded. Dates with a high standard deviation may be reconsidered in certain analyses where precise chronological placement is not strictly required.

## 2.2 DATASET STRUCTURE

The radiocarbon dates for 88 of the assemblages, encompassing 381 SPs, provided sufficient calibrated WAs. These assemblages, used to establish the chronological framework (*Figure 3* and Appendix Table 15), are referred to as the 'Class I' dataset. Among these, 63 assemblages yield multiple specimens, forming the 'Category A' dataset with 356 SPs. Another 25 well-dated assemblages, each containing only a single complete specimen, make up the 'Category B' dataset. Additionally, the remaining 77 undated or insufficiently dated (dates in Appendix Table 16) but chrono-stratigraphically or taxonomically assigned assemblages containing 303 SPs were classified as the 'Class II' dataset, which consists of two groups: 50 assemblages with multiple specimens (276 SPs), forming the 'Category C' dataset, and 27 assemblages with only single specimens forming the 'Category D' dataset. Lastly, the 'Category E' dataset includes five specimens from four assemblages, which were excluded from the analysis for various reasons. The single SP from Grotta Romanelli (E-1) was excluded due to its anomalously young calibrated WA of only 12.0 ka (Appendix Table 16). The specimen from Vrbička Cave (E-2; Appendix Plate 167), although classified as an SP by Borić & Christiani (2016) and associated with a plausible radiocarbon date, was excluded due to its rather atypical morphology. The SP from Grotta Paglicci (E-3; Appendix Plate 73), reportedly originating from one of the older lay-

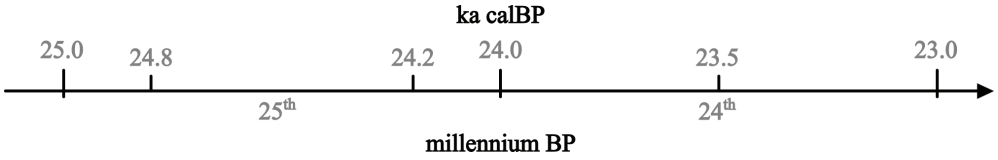



Figure 1: Conceptual use of 'ka calBP' in relation to 'millennium BP'.

ers (23–22) (Palma di Cesnola 2006), was excluded because of its unusually old calibrated age of at least 30.8 ka (Appendix Table 16) and its divergent morphological features. Additionally, two specimens labelled as 'Pointe à cran périgordienne, atypique' (de Sonneville-Bordes & Perrot 1956, 551, *Fig. 2*) were recorded. Owing to their isolated geographical and taxonomic occurrence within the Gravettian of Central France, as well as uncertainties regarding this attribution, they were excluded from the analysis but are discussed in the text.

The established structure of the dataset allows for analysis from two distinct perspectives: first, a macroevolutionary approach within a chronologically controlled framework (Chapter 4), which investigates diachronic evolutionary dynamics such as variation, selective pressure, and random drift; and second, an exploratory approach (Chapter 6), which evaluates the recursive applicability of the framework developed beforehand for the chronological attribution of undated or insufficiently dated SPs. Furthermore, the division into Category A and B assemblages provides an opportunity to validate the robustness of the results by testing whether individual specimens exert a disproportionate influence on the overall patterns. *(Table 1)*

## 2.3 CHRONOLOGICAL AND GEOGRAPHICAL FRAMEWORK

The chronological framework of this study is defined by the presence of SPs in Europe and is directly derived from the calibrated ages of the dated assemblages (class I dataset, categories A and B). It spans approximately 17,000 years, ranging from 30.0 to 13.5 ka calBP, providing an extensive and densely represented timeframe, highly suitable for investigating long-term evolutionary processes in material culture. As the results are presented and treated as individual case studies, the structure of the underlying dataset is outlined prior to each analysis.

The number of assemblages containing SPs, as well as the total count of SPs themselves, fluctuates significantly across the observed timeframe *(Figure 2)*. At the beginning of the sequence, the 30$^{th}$ and the 29$^{th}$ millennium BP display notably low counts, followed by a marked increase during the 28$^{th}$ and the 27$^{th}$ millennium BP. A sharp decline is evident in the 26$^{th}$ millennium BP, with a subsequent recovery leading to a first peak in the 24$^{th}$ millennium BP. From the 23$^{rd}$ to the 20$^{th}$ millennium BP, numbers remain relatively elevated. In contrast, the 19$^{th}$ and the 18$^{th}$ millennium BP are characterised by a near absence of assemblages and specimens. Counts begin to rise again in the 17$^{th}$ millennium BP, culminating

Table 1: Organisation of the Dataset. Numbers without brackets = assemblages; Numbers in brackets = SPs.

| I | | II | | | |
|---|---|---|---|---|---|
| **A** | **B** | **C** | **D** | **E** | **total** |
| 63 (356) | 25 (25) | 50 (276) | 27 (27) | 4 (5) | |
| 88 (381) | | 77 (303) | | | 169 (689) |
| – well dated<br>– archaeo-stratigraphically assigned | | – insufficiently dated<br>– archaeo-stratigraphically assigned | | questionable artefact or dates | |

in the second-highest values during the 16th millennium BP and reaching a maximum in the 15th millennium BP. This is followed by a notable decrease in the 14th millennium BP.

The chronological framework illustrated in Figure 4 reveals distinct phases of dataset density. Periods characterised by a steeper slope in the curve – particularly between 27,000–25,000, 25,000–23,000, and after 15,000 calBP – indicate a higher density of dated assemblages. In contrast, flatter segments of the curve correspond to intervals with fewer available dates, notably between approximately 25,500–24,500 and 20,000–16,000 calBP. Throughout the entire period of investigation, SPs appear in inventories associated with eighteen distinct archaeological taxonomic units. Among these, ten major units provide sufficiently large sample sizes for analysis: the Late Gravettian, the Upper Solutrean, the non-Solutrean LGM industries – including the Salpetrian, Late Badegoulian, Epigravettian, and Lower Magdalenian – the Middle Magdalenian, the Upper/Late–Final Magdalenian, the Hamburgian and the Creswellian *(Figure 3)*.

Geographically, the assemblages span a broad area, extending from the Eastern European Plain through Eastern and Central Europe to Central and Southern France and the Iberian Peninsula. Notably, the geographical distribution of SPs follows a chronologically driven pattern. As previously noted, the earliest SPs originate from Central and Eastern European assemblages associated with the

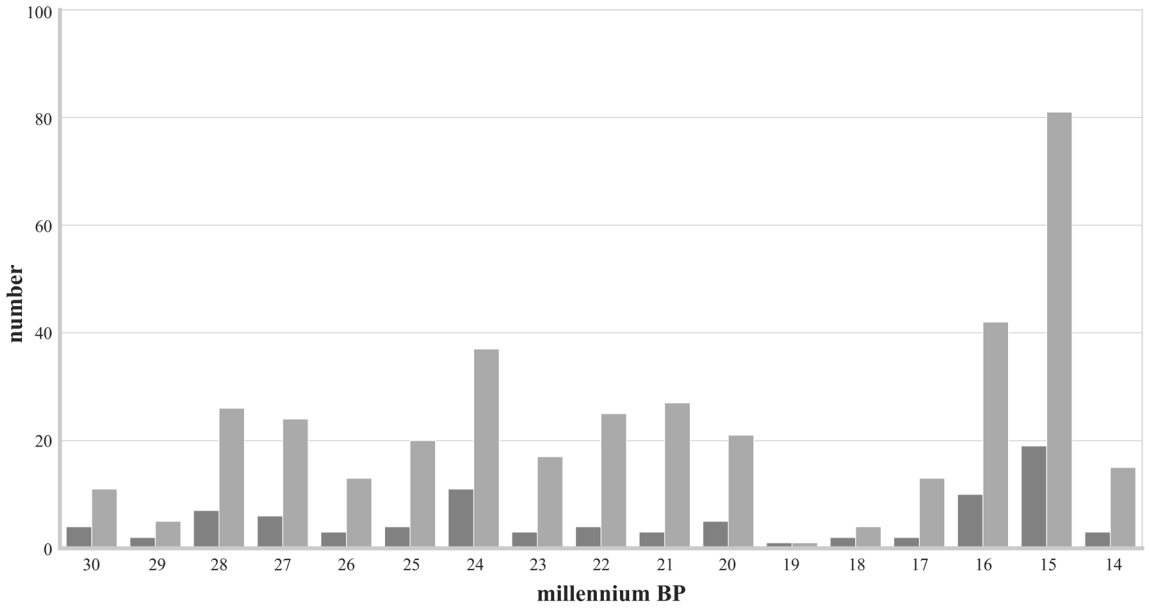



Figure 2: Chronological distribution of assemblages and SPs (dark grey, left bar = assemblages; light grey, right bar = SPs).

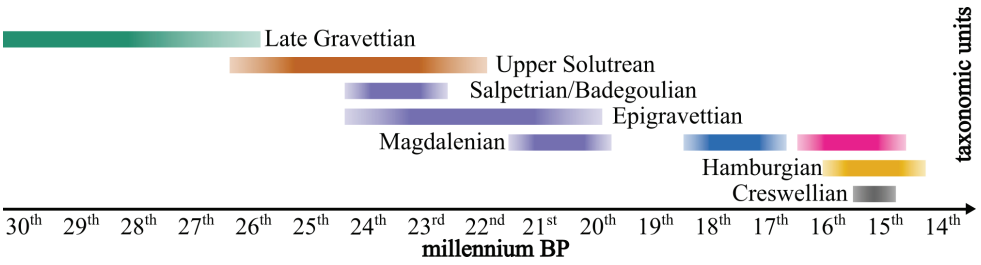



Figure 3: Chronological distribution of taxonomic units (coloured by major group: violet = non-Solutrean LGM industries; blue = Middle Magdalenian; pink = Upper/Late–Final Magdalenian).

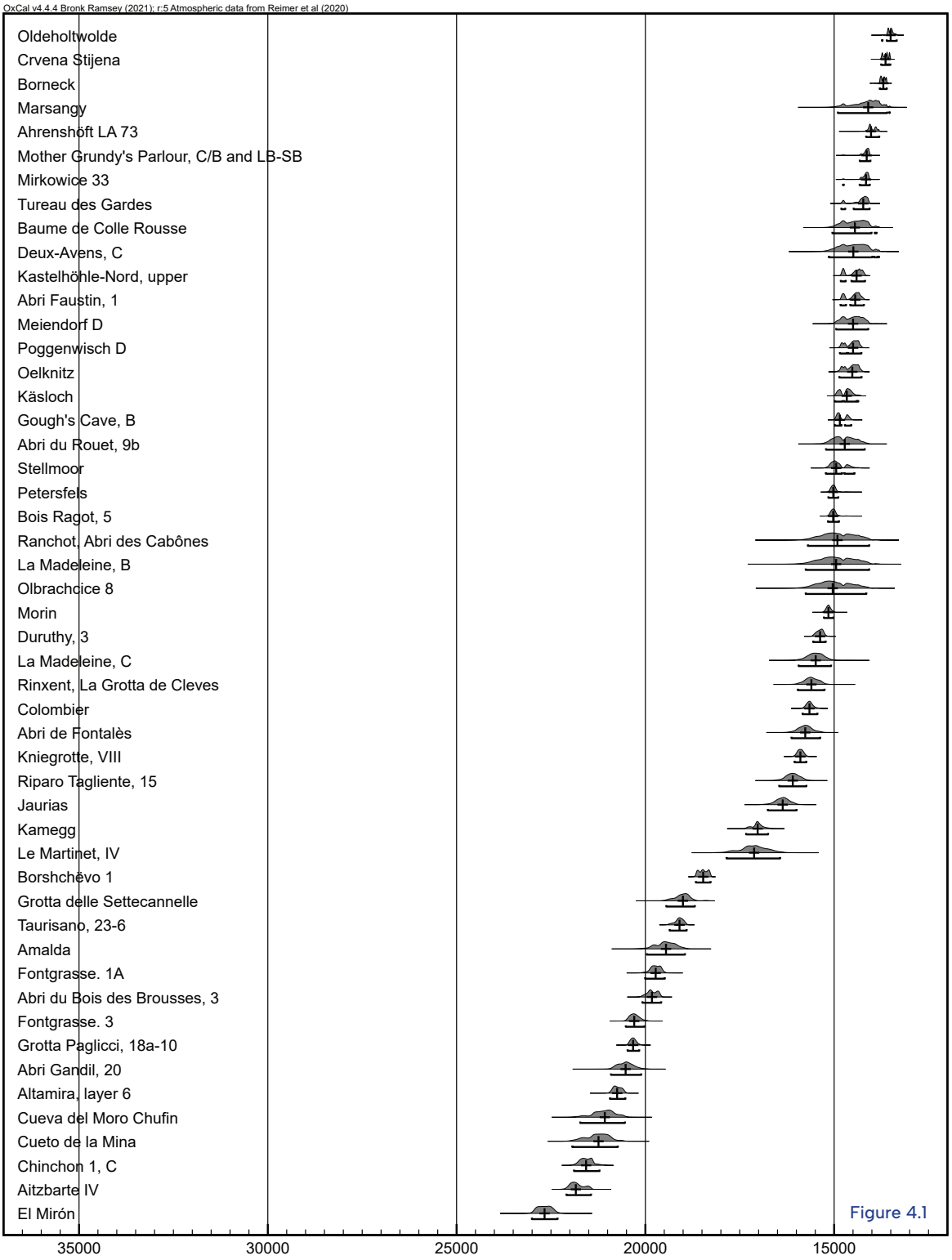



Figure 4: Chronological framework (weighted averages (WA) or single dates (calBP) calibrated in CalPal (Weninger 2022) using IntCal20 (Reimer et al. 2020); see Appendix Table 14; figure produced in OxCal v4.4 (Bronk Ramsey 2021)).

Late Gravettian. Around the 26th millennium BP, SPs begin to appear in Upper Solutrean contexts on the Iberian Peninsula, followed shortly thereafter by occurrences in France, while simultaneously disappearing almost entirely from Eastern and Central European inventories. From that point until approximately the 16th millennium BP, the distribution of SPs is largely confined to the Iberian Peninsula, Central and Southern France, and Italy. An Austrian site, Kamegg (B-11), which yields a single SP attributed to the Middle Magdalenian, may represent an early re-occurrence of SPs north of the Alps. Beginning in the 16th millennium BP, SPs appear frequently in assemblages from southern France, the Paris Basin, northern Italy and become common in German, Polish, and Swiss assemblages within Upper Magdalenian and Hamburgian contexts, eventually extending to the British Isles in Creswellian contexts. Interestingly, by this later phase, SPs are no longer present in Iberian or Southern French assemblages. A major exception to this pattern is the isolated Austrian assemblage from Kammern-Grubgraben, layers 2 and 3 (A-39), dated to approximately 23,000 calBP. *(Figure 4.1 and 4.2, Table 2, Map 1 and 2)*

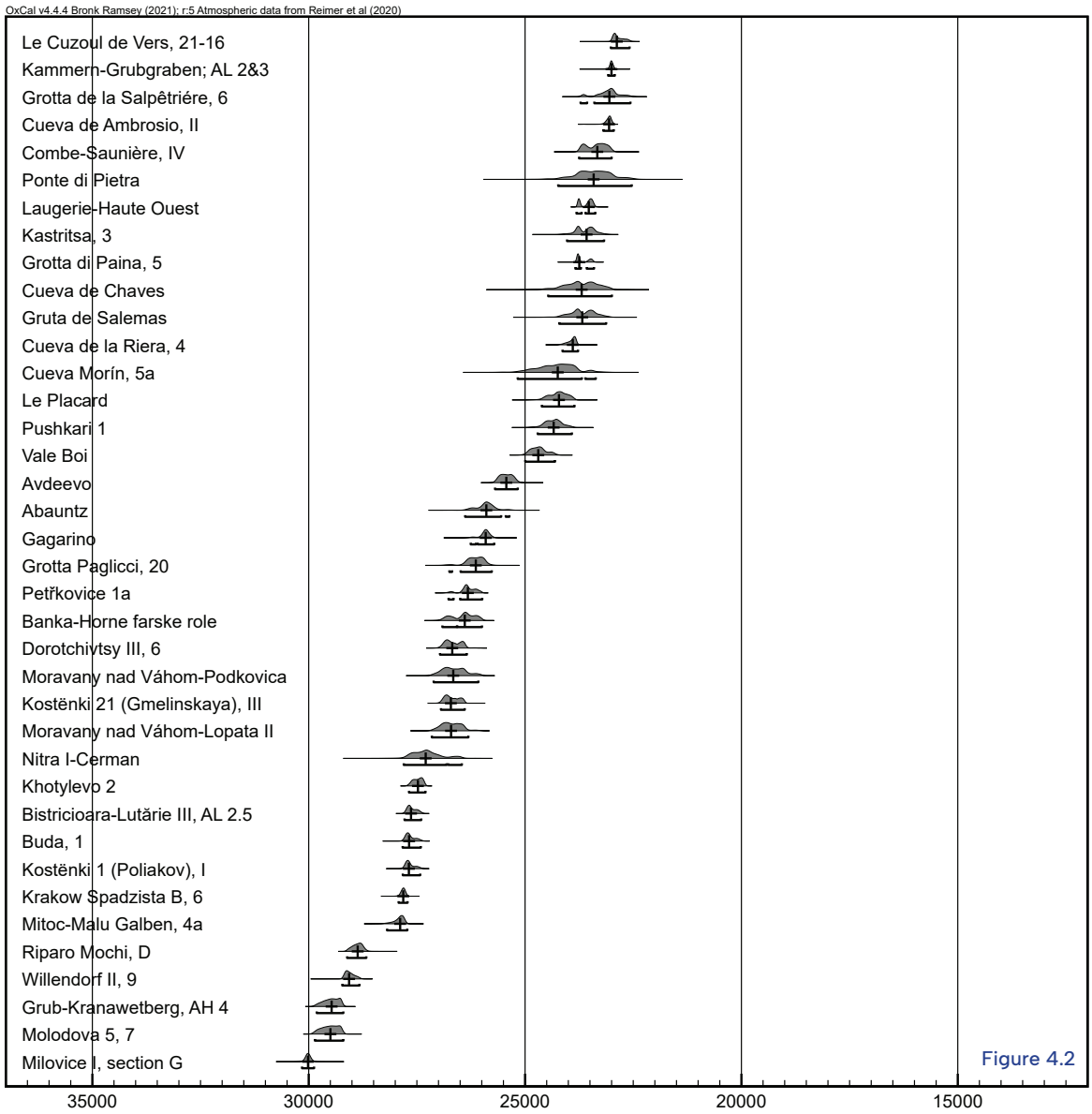


Figure 4.2

Table 2: Database of SPs (ka calBP = calibrated ages based on IntCal20 (see Appendix Table 14); / = no radiocarbon date available; ? = contradicting radiocarbon dates (no WA possible); italic = radiocarbon dates available but problematic; grey = questionable artefact and/or age; n = number of complete or nearly complete SPs available). Image courtesy of: (1) I. Schmidt & G. Koert; (2) M. Anghelinu; (3) W. Antl-Weiser (unpubl.); (4) V. Kaudela (Krahuletzmuseum Eggenburg, Austria).

| ID | site | layer/level/conc. | ka calBP | taxonomic unit | long. | lat. | reference | n |
|---|---|---|---|---|---|---|---|---|
| A-1 | Oldeholtwolde | | 13.5 | Havelte Group | 6.0081 | 52.9151 | Johansen & Stapert 2004 | 7 |
| A-2 | Borneck | | 13.7 | Hamburgian | 10.2500 | 53.6833 | Rust 1958 | 7 |
| A-3 | Marsagny | | 14.1 | Late Magdalenian | 3.2488 | 48.0999 | Schmider 1992 | 2 |
| A-4 | Mirkowice 33 | | 14.2 | Hamburgian | 17.4119 | 52.7688 | Chłodnicki & Kabaciński 1997 | 2 |
| A-5 | Mother Grundy´s Parlour | C/B and LB-SB | 14.2 | Creswellian | -1.1964 | 53.2627 | Campbell 1977 | 4 |
| A-6 | Meiendorf 2 | | 14.5 | Hamburgian | 10.1760 | 53.6260 | Rust 1937 | 17 |
| A-7 | Abri Faustin | 1 | 14.5 | Final Magdalenian | 0.1667 | 44.7333 | Lenoir & Terraza 1971 | 6 |
| A-8 | Oelknitz | | 14.6 | Upper Magdalenian | 11.6666 | 50.8350 | Gelhausen 2015 | 2 |
| A-9 | Poggenwisch D | | 14.6 | Hamburgian | 10.2030 | 53.6400 | Rust 1958 | 23 |
| A-10 | Abri du Rouet | 9b | 14.7 | Tardigravettian | 5.1524 | 43.3310 | Brochier & Livache 2003a | 3 |
| A-11 | Käsloch | | 14.7 | Late Magdalenian | 7.9330 | 47.3645 | Zuberbühler Koch 2002 | 5 |
| A-12 | Gough's Cave | B | 14.8 | Creswellian | -2.7665 | 51.2818 | Campbell 1977 | 6 |
| A-13 | Ranchot, Abri des Cabônes | | 14.9 | Late Magdalenian | 5.7000 | 47.1500 | David 1996 | 2 |
| A-14 | Stellmoor | | 14.9 | Hamburgian | 9.3623 | 53.1520 | Rust 1943 | 2 |
| A-15 | Bois Ragot | 5 | 15.0 | Upper Magdalenian | 0.6833 | 46.3667 | Chollet & Dujardin 2005 | 2 |
| A-16 | Olbrachcice 8 | | 15.0 | Hamburgian | 16.3752 | 51.7759 | Burdukiewicz 1981; 1986 | 8 |

Table 2, continued 1,

| ID | site | layer/level/conc. | ka calBP | taxonomic unit | long. | lat. | reference | n |
|---|---|---|---|---|---|---|---|---|
| A-17 | Petersfels | | 15.0 | Upper Magdalenian | 8.8000 | 47.8616 | de Sonneville-Bordes 1969 | 13 |
| A-18 | Morin | | 15.2 | Upper Magdalenian | -0.3330 | 44.7314 | Lenoir 2003 | 6 |
| A-19 | Duruthy | 3 | 15.4 | Upper Magdalenian | -1.0630 | 43.5210 | Arambourou et al. 1978 | 3 |
| A-20 | Abri de Fontalès | | 15.5 | Upper Magdalenian | 0.8167 | 43.7167 | Darasse & Guffroy 1960 | 2 |
| A-21 | La Madeleine | C - Magd. VI | 15.5 | Upper Magdalenian | 1.0356 | 44.9675 | Taylor 2012 | 5 |
| A-22 | Riparo Tagliente | 15 | 16.1 | Epigravettian | 11.0056 | 45.5406 | Guerreschi & Leonardi 1984 | 2 |
| A-23 | Jaurias | | 16.4 | Lower Magdalenian | -0.2887 | 44.8261 | Lenoir 2003 | 11 |
| A-24 | Le Martinet | IV | 17.1 | Lower Magdalenian | 1.0167 | 44.6000 | Le Tensorer 1981 | 3 |
| A-25 | Grotta delle Settecannelle | | 19.0 | Epigravettian | 11.7533 | 42.5455 | Ucelli Gnesutta & Cristiani 2002 | 10 |
| A-26 | Taurisano | 23-6 | 19.1 | Epigravettian | 18.2018 | 39.9629 | Bietti 1979 | 5 |
| A-27 | Fontgrasse | 1a | 19.7 | Lower Magdalenian | 4.5324 | 43.9686 | Bazile 1999 | 4 |
| A-28 | Fontgrasse | 3 | 20.2 | Lower Magdalenian | 4.5324 | 43.9686 | Bazile 1999 | 2 |
| A-29 | Grotta Paglicci | 18a-10 | 20.3 | Epigravettian | 15.6153 | 41.6540 | Mezzena & Palma di Cesnola 1967 | 22 |
| A-30 | Abri Gandil | 20 | 20.5 | Lower Magdalenian | 1.6667 | 44.0500 | Ladier 2000 | 3 |
| A-31 | Cueva del Moro Chufin | | 21.0 | Upper Solutrean | -4.4607 | 43.2921 | 1 | 2 |
| A-32 | Cueto de la Mina | | 21.3 | Upper Solutrean | -4.8600 | 43.4256 | 1 | 14 |
| A-33 | Chinchon 1 | C | 21.6 | Tardigravettian | 5.0857 | 43.9308 | Paccard 1964; Paccard & Dumas 1977 | 5 |

Table 2, continued 2,

| ID | site | layer/level/conc. | ka calBP | taxonomic unit | long. | lat. | reference | n |
|---|---|---|---|---|---|---|---|---|
| A-34 | Aitzbarte IV | | 21.7 | Upper Solutrean | -1.9044 | 43.2654 | 1 | 4 |
| A-35 | Altamira | 7 | 22.8 | Upper Solutrean | -4.1192 | 43.3775 | 1 | 13 |
| A-36 | Le Cuzoul de Vers | 21-16 | 22.8 | Late Badegoulian | 1.5534 | 44.4859 | Ducasse et al. 2021 | 3 |
| A-37 | Cueva de Ambrosio | II | 23.0 | Upper Solutrean | -2.0956 | 37.8319 | Ripoll Lopez & Cacho Ouesada 1990 | 10 |
| A-38 | Grotta de la Salpêtriére | 6 | 23.0 | Salpetrian | 4.5383 | 43.9478 | Onoratini 1982; Boccaccio 2005 | 5 |
| A-39 | Kammern-Grubgraben | AL2 and 3 | 23.0 | LGM | 15.6667 | 48.4667 | 4 | 4 |
| A-40 | Combe-Saunière | IV | 23.4 | Upper Solutrean | 0.8836 | 45.2307 | Geneste & Plisson 1986 | 3 |
| A-41 | Ponte di Pietra | | 23.4 | Epigravettian | 12.9590 | 43.4999 | Broglio & Lollini 1982 | 2 |
| A-42 | Kastrisa | 7/ Stratum 3 | 23.6 | Epigravettian | 20.9166 | 39.6333 | Adam 2007 | 2 |
| A-43 | Laugerie-Haute Ouest | Niv. p. à cran | 23.6 | Upper Solutrean | 1.0015 | 44.9523 | Smith 1966 | 2 |
| A-44 | Cueva de Chaves | | 23.7 | Upper Solutrean | -0.1420 | 42.2130 | Utrilla & Mazo 1994 | 3 |
| A-45 | Gruta de Salemas | | 23.7 | Upper Solutrean | -9.2122 | 38.8685 | Zilhão 1997 | 4 |
| A-46 | Le Placard | | 24.2 | Upper Solutrean | 0.4197 | 45.6897 | Smith 1966, Geneste & Plisson 1989 | 13 |
| A-47 | Vale Boi | | 24.7 | Upper Solutrean | -8.8150 | 37.0944 | 1 | 5 |
| A-48 | Avdeevo | | 25.4 | Late Gravettian | 35.5000 | 51.7667 | Gvozdover 1995 | 5 |
| A-49 | Abauntz | | 25.9 | Upper Solutrean | -1.6411 | 43.0156 | Utrilla & Mazo 1994 | 3 |
| A-50 | Gagarino | | 25.9 | Late Gravettian | 38.9000 | 52.8325 | Tarasov 1979 | 5 |

Table 2, continued 3,

| ID | site | layer/level/conc. | ka calBP | taxonomic unit | long. | lat. | reference | n |
|---|---|---|---|---|---|---|---|---|
| A-51 | Petřkovice | 1a | 26.3 | Late Gravettian | 17.9510 | 49.5463 | Novák 2008 | 3 |
| A-52 | Dorotchivtsy III | 6 | 26.6 | Late Gravettian | 25.8697 | 48.5939 | Kulakovska et al. 2014 | 2 |
| A-53 | Moravany nad Váhom-Podkovica | | 26.6 | Late Gravettian | 17.8863 | 48.6087 | Bárta 1965 | 3 |
| A-54 | Kostënki 21 (Gmelinskaya) | III | 26.7 | Late Gravettian | 39.0453 | 51.4043 | Reynolds 2014 | 14 |
| A-55 | Nitra I-Čermáň | | 27.2 | Late Gravettian | 18.0660 | 48.3060 | Kaminska 2015 | 4 |
| A-56 | Khotylëvo 2 | | 27.5 | Late Gravettian | 34.1079 | 53.3445 | Zaverniaev 1991; Reynolds 2014 | 4 |
| A-57 | Bistricioara-Lutărie III | AH 2.5 | 27.6 | Late Gravettian | 25.9480 | 47.0557 | Niţă et al. 2021; 2 | 7 |
| A-58 | Kostënki 1 (Poliakov) | I | 27.6 | Late Gravettian | 39.0415 | 51.3953 | Efimienko 1958; Rogachev et al. 1982 | 4 |
| A-59 | Krakow Spadzista B | 6 | 27.8 | Late Gravettian | 19.8972 | 50.0561 | Chmielewsky et al. 1975 | 5 |
| A-60 | Mitoc-Malu Galben | 4a | 28.0 | Late Gravettian | 27.0360 | 48.1110 | Otte et al. 2007 | 4 |
| A-61 | Willendorf II | 9 | 29.0 | Late Gravettian | 15.4050 | 48.3227 | Felgenhauer 1957 | 4 |
| A-62 | Grub-Kranawetberg | AH 4 | 29.5 | Late Gravettian | 16.1102 | 48.0810 | 3 | 3 |
| A-63 | Molodova V | 7 | 29.5 | Late Gravettian | 27.1483 | 48.5736 | Chernysh 1961 | 3 |
| B-1 | Crvena Stijena | | 13.6 | Epigravettian | 18.4817 | 42.7788 | Borić & Cristiani 2016 | 1 |
| B-2 | Ahrenshöft | LA 73 | 14.0 | Hamburgian | 9.0713 | 54.5581 | Clausen 1998 | 1 |
| B-3 | Marolles/Tureau des Gardes | | 14.3 | Upper Magdalenian | 3.0519 | 48.3667 | Burdukiewicz & Schmider 2000 | 1 |
| B-4 | Baume de Colle Rousse | | 14.5 | Upper Magdalenian | 6.7000 | 43.5333 | Onoratini et al. 1994 | 1 |

Table 2, continued 4,

| ID | site | layer/level/conc. | ka calBP | taxonomic unit | long. | lat. | reference | n |
|---|---|---|---|---|---|---|---|---|
| B-5 | Deux-Avens | C | 14.5 | Upper Magdalenian | 4.0800 | 44.5100 | Combier 2003 | 1 |
| B-6 | Kastelhöhle-Nord | upper layer | 14.5 | Upper Magdalenian | 7.5833 | 47.4167 | Nielsen 2009 | 1 |
| B-7 | La Madeleine | B - Magd. V | 14.9 | Upper Magdalenian | 1.0356 | 44.9675 | Taylor 2012 | 1 |
| B-8 | Grotte de Cleves, Rinxent | | 15.6 | Upper Magdalenien | 1.7390 | 50.8000 | Fagnart 1984 | 1 |
| B-9 | Colombier | | 15.7 | Upper Magdalenian | 4.4999 | 44.3120 | Combier 2003 | 1 |
| B-10 | Kniegrotte | VIII | 15.9 | Upper Magdalenian | 11.6557 | 50.6816 | Feustel 1974 | 1 |
| B-11 | Kamegg | | 17.0 | Middle Magdalenian | 15.6547 | 48.6120 | Neugebauer-Maresch 1999 | 1 |
| B-12 | Borshevo 1 | | 18.5 | Epigravettian | 39.0905 | 51.3622 | Nuzhnyi 2015 | 1 |
| B-13 | Amalda | | 19.5 | Upper Solutrean | -2.2008 | 43.2274 | 1 | 1 |
| B-14 | Abri du Bois des Brousses | 3 | 19.8 | Epigravettian | 3.5675 | 43.7138 | Bazile 2011 | 1 |
| B-15 | El Mirón | | 22.7 | Upper Solutrean | -3.4691 | 43.1440 | Straus & Gonzáles Morales 2009 | 1 |
| B-16 | Grotta di Paina | 5 | 23.6 | Epigravettian | 11.5485 | 45.4290 | Broglio et al. 1993 | 1 |
| B-17 | Cueva de la Riera | 4 | 23.9 | Upper Solutrean | -4.8565 | 43.4248 | Straus & Clark 1986 | 1 |
| B-18 | Cueva Morín | 5a | 24.3 | Upper Solutrean | -3.8588 | 43.3586 | 1 | 1 |
| B-19 | Pushkari I | | 24.3 | Late Gravettian | 33.1833 | 52.1400 | Nuzhnyi 2015 | 1 |
| B-20 | Grotta Paglicci | 20 | 26.1 | Late Gravettian | 15.6153 | 41.6540 | Palma di Cesnola 1976 | 1 |
| B-21 | Banka-Horné farské role | | 26.5 | Late Gravettian | 17.8500 | 48.5833 | Alexandrowicz et al. 2000 | 1 |

Table 2, continued 5,

| ID | site | layer/level/conc. | ka calBP | taxonomic unit | long. | lat. | reference | n |
|---|---|---|---|---|---|---|---|---|
| B-22 | Moravany nad Váhom-Lopata II | | 27.0 | Late Gravettian | 17.8863 | 48.6087 | Hromada 2000 | 1 |
| B-23 | Buda | 1 | 27.6 | Late Gravettian | 26.4131 | 46.4007 | Bitiri-Ciortescu et al. 1989 | 1 |
| B-24 | Riparo Mochi | D | 28.9 | Late Gravettian | 7.5348 | 43.7841 | Blanc 1953 | 1 |
| B-25 | Milovice I | section G | 30.0 | Late Gravettian | 16.6976 | 48.8501 | Oliva 1999, 2009 | 1 |
| C-1 | Grotte de la Bouviere | | / | Arénien | 6.6539 | 43.5145 | Onoratini 1978 | 9 |
| C-2 | Grotte des Enfants à Grimaldi | | 14.4 | Arénien | 7.5329 | 43.7847 | Onoratini 1978 | 5 |
| C-3 | Hengistbury Head | | ? | Creswellian | -1.7333 | 50.7000 | Barton 1992 | 2 |
| C-4 | Deimern 42 | | / | Hamburgian | 9.8965 | 53.0304 | Tromnau 1975 | 9 |
| C-5 | Hasewisch | | / | Hamburgian | 10.2002 | 53.6380 | Rust 1958 | 2 |
| C-6 | Heber 118 | | / | Hamburgian | 9.8667 | 53.0833 | Tromnau 1975 | 14 |
| C-7 | Heber 127 | | / | Hamburgian | 9.8667 | 53.0833 | Tromnau 1975 | 17 |
| C-8 | Liny 1 | | / | Hamburgian | 15.8678 | 52.9701 | Kobusiewicz 1975 | 3 |
| C-9 | Rogow Opolski 9 | | / | Hamburgian | 17.9333 | 50.5167 | Rothert 1936 | 2 |
| C-10 | Siedlnica | 17a | / | Hamburgian | 16.3333 | 51.7667 | Burdukiewicz 1987 | 2 |
| C-11 | Teltwisch | | / | Hamburgian | 10.2037 | 53.6414 | Tromnau 1975b | 12 |
| C-12 | Ureterp 1 | | / | Hamburgian | 6.1667 | 53.1167 | Bohmers 1947 | 9 |
| C-13 | Fußgönheim I | | / | Late Magdalenian | 8.2886 | 49.4553 | Stodiek 1987 | 4 |

Table 2, continued 6,

| ID | site | layer/level/conc. | ka calBP | taxonomic unit | long. | lat. | reference | n |
|---|---|---|---|---|---|---|---|---|
| C-14 | Fußgönheim II | | / | Late Magdalenian | 8.2886 | 49.4553 | Stodiek 1987 | 3 |
| C-15 | Abri Schweizersbild | | ~14.5 | Upper Magdalenian | 8.6395 | 47.7241 | Höneisen & Peyer 1994 | 2 |
| C-16 | Cepoy/La Pierre aux Fées | | / | Upper Magdalenian | 2.7484 | 48.0442 | Allain 1974 | 4 |
| C-17 | Köpfli | | / | Upper Magdalenian | 7.9331 | 47.3645 | Zürcher 1969 | 4 |
| C-18 | Blazi Cave | Tr. 5, layer 4 | / | Epigravettian | 20.0101 | 41.7421 | Hauck et al. 2017 | 2 |
| C-19 | Cenciano Diruto | IV-I | / | Epigravettian | 12.2768 | 42.3838 | Pennacchioni & Tozzi 1984 | 2 |
| C-20 | Fondo Focone | Trench B | / | Epigravettian | 18.1638 | 39.8641 | Cancellieri 2018 | 5 |
| C-21 | Madonna dell'Ospedale | | / | Epigravettian | 13.2280 | 43.3850 | Silvestrini et al. 2008 | 2 |
| C-22 | Riparo di Biedano | VI-II | / | Epigravettian | 11.9451 | 42.4937 | Pennacchioni & Tozzi 1986 | 2 |
| C-23 | Cadenet | | / | Salpetrian | 5.3738 | 43.7347 | Boccaccio 2005 | 2 |
| C-24 | La Rouviére | | / | Salpetrian | 4.0645 | 44.4443 | Gallet 1973 | 5 |
| C-25 | Baío | | / | Upper Solutrean | -9.4167 | 39.0833 | Zilhão 1997 | 3 |
| C-26 | Baume d´Oullins | D | 24.7 | Upper Solutrean | 4.4576 | 44.3418 | Bazile 1990; Boccacio 2005 | 5 |
| C-27 | Cueva de les Mallaetes | III | ~19 | Upper Solutrean | -0.2996 | 39.0210 | Fortea Pérez & Jordá Cerda 1976 | 3 |
| C-28 | Cueva de los Morceguillos | | / | Upper Solutrean | -2.0165 | 40.1824 | Ripoll Lopez & Cacho Ouesada 1990 | 2 |
| C-29 | Cueva del Boquete Zafarraya | | 22.9 | Upper Solutrean | -4.1267 | 36.9512 | 1 | 2 |
| C-30 | Cueva del Parpalló | 4.25–4.00 | 21.7 | Upper Solutrean | -0.2750 | 39.0018 | Muñoz Ibáñez 2000 | 13 |

Table 2, continued 7,

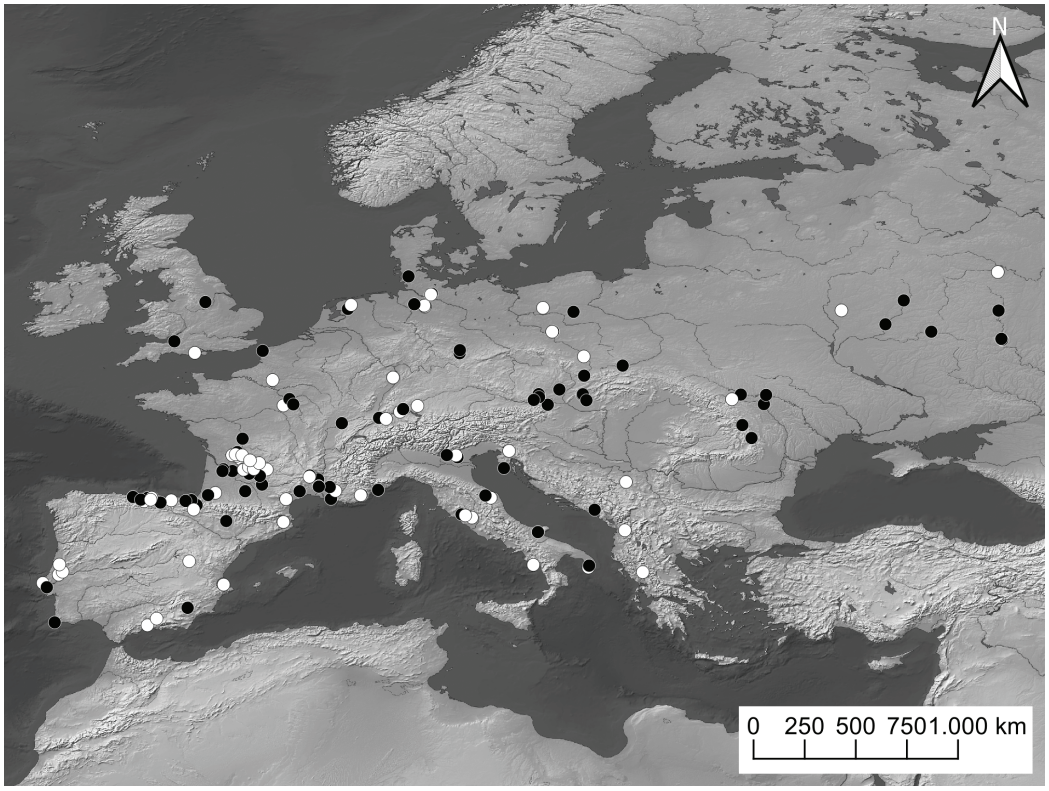
| ID | site | layer/level/conc. | ka calBP | taxonomic unit | long. | lat. | reference | n |
|---|---|---|---|---|---|---|---|---|
| C-31 | Cueva del Parpalló | 4.00–3.75 | / | Upper Solutrean | -0.2750 | 39.0018 | Muñoz Ibáñez 2000 | 17 |
| C-32 | Cueva del Parpalló | 4.50–4.25 | / | Upper Solutrean | -0.2750 | 39.0018 | Muñoz Ibáñez 2000 | 21 |
| C-33 | Cueva del Reclau Viver | | ? | Upper Solutrean | 2.7484 | 42.1610 | 1 | 3 |
| C-34 | Davant Pau | | / | Upper Solutrean | 2.7475 | 42.1612 | 1 | 2 |
| C-35 | El Pendo | | / | Upper Solutrean | -3.9135 | 43.3877 | Corchon 1971 | 2 |
| C-36 | Fourneau du Diable | Sol. sup. I | / | Upper Solutrean | 0.5943 | 45.3346 | Smith 1966 | 5 |
| C-37 | Fourneau du Diable | Sol. sup. II | / | Upper Solutrean | 0.5943 | 45.3346 | Smith 1966 | 10 |
| C-38 | Fourneau du Diable | Sol. sup. III | / | Upper Solutrean | 0.5943 | 45.3346 | Smith 1966 | 9 |
| C-39 | Gavechou | | / | Upper Solutrean | 0.3500 | 45.4900 | Smith 1966 | 2 |
| C-40 | Gruta do Almonda | | / | Upper Solutrean | -8.6153 | 39.5050 | Zilhão et al. 1991 | 2 |
| C-41 | Gruta do Caldeirão | ABC-D/Eb | ? | Upper Solutrean | -8.4167 | 39.6500 | Zilhão 1997 | 2 |
| C-42 | Les Jean-Blancs | | / | Upper Solutrean | 0.7333 | 44.7974 | Smith 1966 | 6 |
| C-43 | Oreille-d´Enfer | | / | Upper Solutrean | 0.9971 | 44.9480 | Smith 1966 | 2 |
| C-44 | Pech de la Boissière | | / | Upper Solutrean | 1.2500 | 44.8333 | Geneste & Plisson 1989 | 6 |
| C-45 | Petite Grotte de Bize | | / | Upper Solutrean | 2.8833 | 43.3167 | Sacchi 1986 | 11 |
| C-46 | Tourtoirac | | / | Upper Solutrean | 1.0586 | 45.2714 | Smith 1966 | 2 |
| C-47 | Berdyzh | | ~27 | Late Gravettian | 30.9568 | 52.8420 | Kaletchitz 1984 | 5 |

Table 2, continued 8,

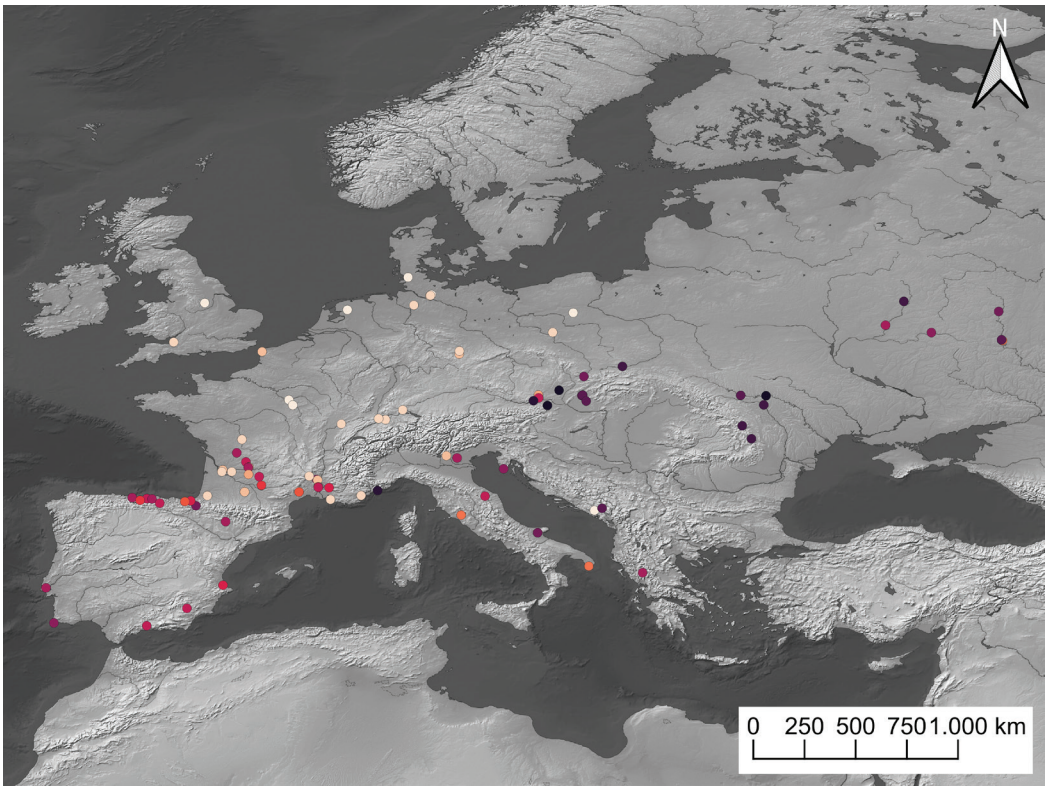
| ID | site | layer/level/conc. | ka calBP | taxonomic unit | long. | lat. | reference | n |
|---|---|---|---|---|---|---|---|---|
| C-48 | Moravany nad Váhom-Noviny | | / | Late Gravettian | 17.8867 | 48.6000 | Bárta 1965 | 12 |
| C-49 | Zamostya I | | / | Late Gravettian | 25.4241 | 48.3587 | Ambrojevici & Popovici 1938 | 2 |
| C-50 | Zaraisk | | ? | Late Gravettian | 38.8628 | 54.7762 | Troussov 1998; Amirkhanov 2000 | 4 |
| D-1 | Schussenquelle | F | / | Late Magdalenian | 9.5272 | 48.0219 | Schuler 1994 | 1 |
| D-2 | Grotta del Fanciulli | D-C | / | Epigravettian | 7.5329 | 43.7847 | Palma di Cesnola 1979 | 1 |
| D-3 | Grotta della Cala | P-M | ? | Epigravettian | 15.3812 | 40.0010 | Martini 1978 | 1 |
| D-4 | Grotta Trene | | ~23 | Epigravettian | 11.4744 | 45.5214 | Broglio et al. 2009 | 1 |
| D-5 | Jama v Lozi | 5 | / | Epigravettian | 14.1536 | 45.7498 | Brodar 1986 | 1 |
| D-6 | Kastrisa | Stratum 5 | ? | Epigravettian | 20.9166 | 39.6333 | Adam 2007 | 1 |
| D-7 | Šalitrena Pecina | 4 | / | Epigravettian | 20.0664 | 44.1819 | Mihailovic & Mihailovic 2007 | 1 |
| D-8 | Sandalja II | c/d | 24.9 | Epigravettian | 13.8967 | 44.8825 | Malez 1987 | 1 |
| D-9 | Atxuri | | / | Upper Solutrean | -2.9217 | 43.2541 | Straus 1983 | 1 |
| D-10 | Brassempouy | | / | Upper Solutrean | -0.6954 | 43.6309 | Smith 1966 | 1 |
| D-11 | Cueva de la Meaza | | / | Upper Solutrean | -4.2973 | 43.2030 | 1 | 1 |
| D-12 | Cueva del Pantano de Cubillas | | / | Upper Solutrean | -3.6625 | 37.2883 | Ripoll Lopez & Cacho Ouesada 1990 | 1 |
| D-13 | Grand Abri de Mazerat | | / | Upper Solutrean | 0.7035 | 44.8215 | Smith 1966 | 1 |
| D-14 | Grotte des Eyzies | | / | Upper Solutrean | 1.0136 | 44.9364 | Smith 1966 | 1 |

Table 2, continued 9.

| ID | site | layer/level/conc. | ka calBP | taxonomic unit | long. | lat. | reference | n |
|---|---|---|---|---|---|---|---|---|
| D-15 | Gruta do Ourão | | / | Upper Solutrean | -8.5800 | 40.0167 | Zilhão 1997 | 1 |
| D-16 | La Balutie | | / | Upper Solutrean | 1.1652 | 45.0639 | Smith 1966 | 1 |
| D-17 | La Mouthe | | / | Upper Solutrean | 1.0173 | 44.9243 | Smith 1966 | 1 |
| D-18 | La Pasiega | | / | Upper Solutrean | -3.9658 | 43.2889 | Corchon 1971 | 1 |
| D-19 | Lacam | | / | Upper Solutrean | 1.9136 | 44.8152 | Smith 1966 | 1 |
| D-20 | Lachaud | | / | Upper Solutrean | 1.3000 | 45.1167 | Smith 1966 | 1 |
| D-21 | Legintxiqui | | / | Upper Solutrean | -1.7900 | 42.7932 | Nuin 1988/1989 | 1 |
| D-22 | Les Vachons | | / | Upper Solutrean | 0.1578 | 45.5322 | Smith 1966 | 1 |
| D-23 | Noailles | | / | Upper Solutrean | 2.2000 | 49.3269 | Smith 1966 | 1 |
| D-24 | Pré-Aubert | | / | Upper Solutrean | 1.5203 | 45.1340 | Smith 1966 | 1 |
| D-25 | Roc de Sers | | / | Upper Solutrean | 0.3294 | 45.5750 | Smith 1966 | 1 |
| D-26 | Saint-Front-de-Corgnac | | / | Upper Solutrean | 0.6600 | 45.5300 | Smith 1966 | 1 |
| D-27 | Hubina | | ? | Late Gravettian | 17.8869 | 48.6177 | Hromada & Žemla 2000 | 1 |
| E-1 | Grotta Romanelli | E-B | 12.0 | Romanellian | 18.4334 | 40.0161 | Palma di Cesnola 1985 | 1 |
| E-2 | Vrbička Cave | | 27.4 | Late Gravettian | 18.8707 | 42.8908 | Boric & Christiani 2016 | 1 |
| E-3 | Grotta Paglicci | 23-22 | 30.8 | Late Gravettian | 15.6153 | 41.6540 | Palma di Cesnola 2006 | 1 |




Map 1: Geographical distribution of assemblages (n = 168; black = Class I (n = 88); white = Class II (n = 80)).




Map 2: Geographical distribution of dated (Class I) assemblages (n = 88; coloured by millennium BP, dark = older, light = younger).

# 3. METHODS

## 3.1 DATA RECORDING

The morphometric data of the SPs is recorded using the half-automated system PyREnArA (Python-R-Environment for Artefact Analysis) (John et al. 2023). PyREnArA detects the artefact outlines on the input image and subsequently orients them with their longest extend placed vertically in order to ensure the standardisation of measurement. It extracts traditional as well as new traits – morphometric features – of object size and shape (Maier et al. 2023).

This study records and employs only data observable from the dorsal or ventral view of the artefacts. It is assumed – though yet to be empirically tested – that for most Upper Palaeolithic projectile points produced on flakes, blades, or bladelets, thickness plays only a minor discriminant role. Focusing exclusively on two-dimensional characteristics also allows for the integration of the extensive published data, which often lack lateral views of the artefacts. Nevertheless, it is acknowledged that lateral shape – particularly curvature (e.g., Aleo et al. 2021) or twistedness (e.g., Lucas 1997) – may have been crucial for functionality and therefore represents an important discriminant feature in some cases. Recent methodological advances in three-dimensional analyses of stone tool morphology (e.g., Falcucci & Peresani 2022) are therefore of considerable value.

## 3.2 MORPHOMETRIC FEATURES

Following Boëda (2018), lithic tools can be subdivided into three functional parts: an energy-receiving part, an energy-transmitting part, and an energy-transforming part. In the case of lithic projectile points, the energy-receiving part corresponds to the hafting area, where the point is inserted into the (fore)shaft and thus receives energy from the propulsion of the entire projectile. The transformative part is the actual penetrating part, which converts the energy imparted by propulsion into penetrative force. As stone tools can only be shaped through reduction – what Weißmüller (1995, 13) termed the "subtractive law" – the transmitting part of the projectile point, which connects the shaped parts for hafting and penetration, is defined by the tool's widest, largely unretouched section. In SPs, this is typically marked by the part between the shoulder and the narrowing towards the tip *(Figure 6, A)*. Accordingly, the transformative part corresponds to the distal, or upper, part above the shoulder, whereas the hafting part refers to the proximal, or lower, part below it. However, the subdivision by the position of the widest dimension does not work for all specimens. In a subset of SPs – primarily those from Upper Solutrean, Upper Magdalenian, and Hamburgian contexts – the outline of the transformative part may exceed the width at the position just above the shoulder.

When subdivided along the longest dimension, the edges of a SP can be distinguished into what is here referred to as a primary cutting edge (opposite the shoulder) and a secondary cutting edge (above the shoulder) *(Figure 6, B)* – even though these edges may bear retouches and thus not necessarily possess cutting properties. This classification draws on the assumption of the latero-frontally hafting of SPs *(Figure 5)*.



Figure 5:
Schematic illustration of latero-frontally hafting of SPs.

Closely related to the lengths of the cutting edges is the vertical symmetry *(Figure 6, D)*. SPs, which have their longest extend near the centre of the vertical axis are referred to as axis-symmetric, while those with the maximum length shifted markedly to the left side are classified as asymmetric. As all SPs are oriented with the shoulder facing right, marked shifts to the right are not expected. Finally, each SP also comprises two extremities: the tip (distal end) and the base (proximal or basal end) *(Figure 6, C)*.

PyREnArA extracts a wide range of morphometric features (John et al. 2023), including the key metrical variables width, length, area, contour length, the length-width-index (l-w-index), the lengths of the upper and lower parts and their ratio (upper–lower ratio), the widths of the left and right parts and their ratio

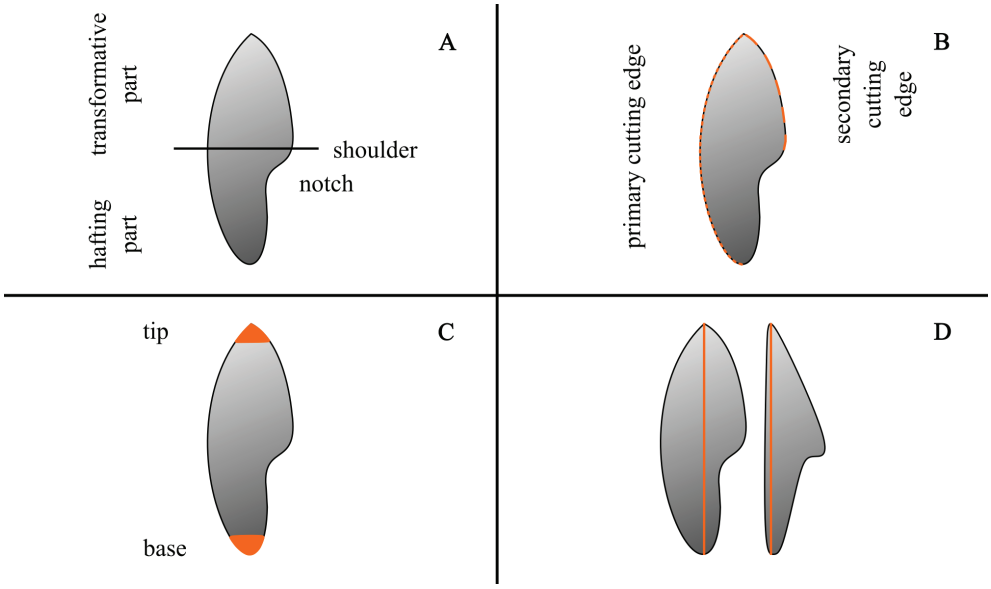



Figure 6: Morphological components of SPs (A = transformative and hafting part; B = primary and secondary cutting edge; C = tip and base; D = y-axis/vertical symmetry: left = symmetric, right = asymmetric).

(left–right ratio), tip angle, and the horizontal (x) and vertical (y) offsets of the centre of mass. In the following, the features and their respective calculation are documented:

**width:** Euclidean distance in millimetre between the two points with the most extreme x-coordinates (widest extend) *(Figure 7, B)*.

**length:** Euclidean distance in millimetre between the two points with the most extreme y-coordinates (longest extend) *(Figure 7, A)*.

**area:** Two-dimensional surface area in square millimetre *(Figure 7, C)*.

**contour length:** Length of the two-dimensional outline/contour in millimetre *(Figure 7, D)*.

**l–w–index:** *length divided by width*; Higher values indicate slenderer forms whereas lower values indicate stouter forms.

**length lower part:** Euclidean distance in millimetre between y-coordinate of the widest extent and the point with the lowest y-coordinate *(Figure 7, E)*. Refers to the length of the hafting part.

**length upper part:** Euclidean distance in millimetre between y-coordinate of the widest extent and the point with the highest y-coordinate *(Figure 7, E)*. Refers to the length of the transformative part.

**upper–lower–ratio:** *length upper part divided by length of the lower part*; Values equal or close to one indicate that the widest extent of the artefact is situated (approximately) at its centre. Specimens with such values are therefore described as exhibiting x-axis or horizontal symmetry *(e.g., Figure 7, H, left)*. Values higher than one indicate a shift of the position of the widest extent towards the base, resulting in a relatively longer transformative part *(e.g., Figure 7, H, right)*. Values less than one indicate a shift of the position of the widest extent towards the tip, causing a reduced length of the transformative part respectively a more pronounced hafting part. For a few specimens, where the upper–lower–ratio could not be determined automatically, it had to be measured manually instead.

**width left part:** Euclidean distance in millimetre between the x-coordinate of the longest extent and the point with the lowest x-coordinate *(Figure 7, F)*. Correlates with the length of the cutting edge on the left side – the primary cutting edge.

**width right part:** Euclidean distance in millimetre between the x-coordinate of the longest extent and the point with the highest x-coordinate *(Figure 7, F)*. Correlates with the length of the cutting edge on the right side – the secondary cutting edge.

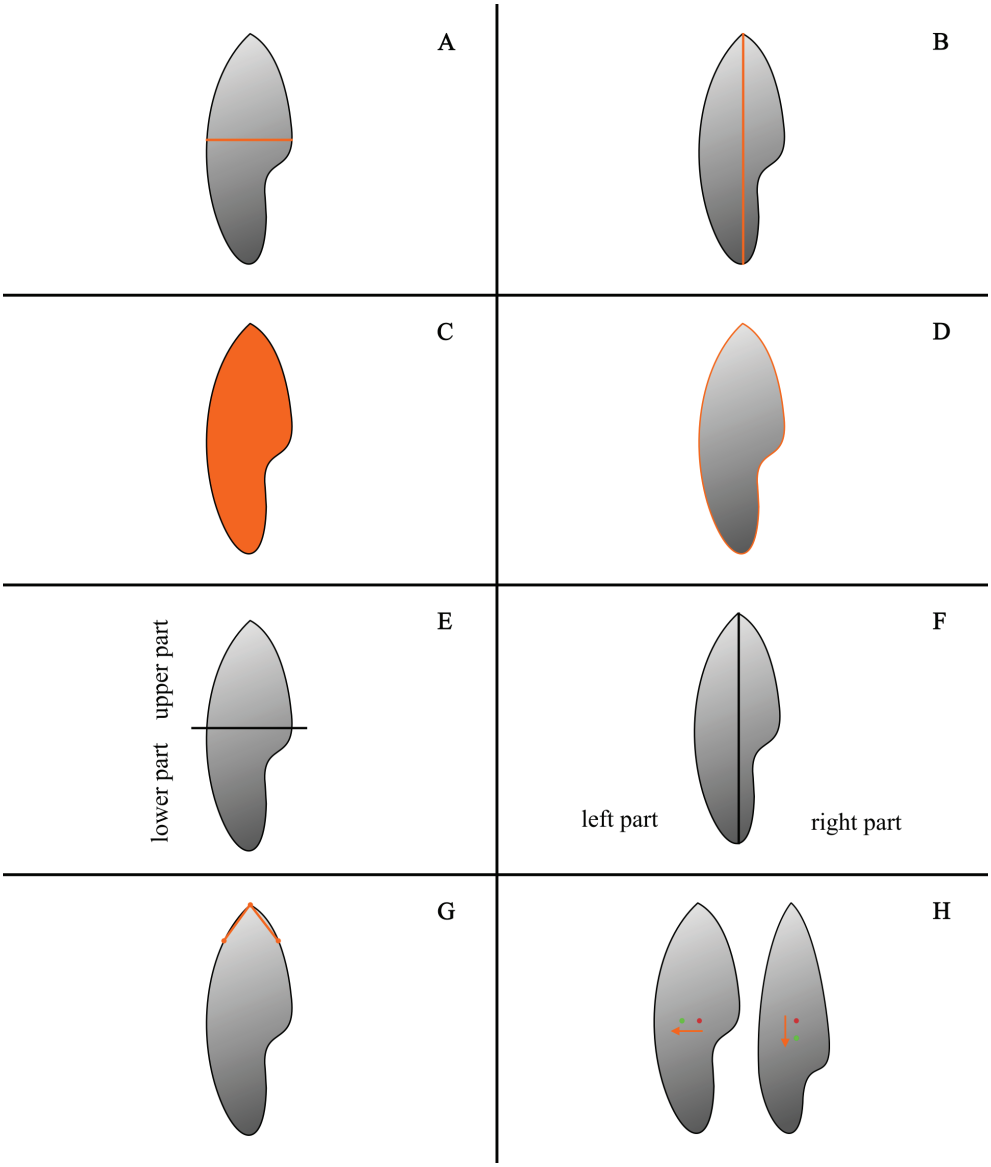



Figure 7: Main metrical features (A = width; B = length; C = area; D = contour length; E = length of upper and lower part; F = width of left and right part; G = tip angle; H = MP–CM x- and y-offset).

**left-right-ratio:** *width of left part divided by width of the right part*; Values equal to or close to one indicate that the longest extent of the artefact is situated (approximately) at its centre. Specimens with such values are therefore described as exhibiting y-axis or vertical symmetry *(Figure 6, D, left)*. Values higher than one indicate a shift of the position of the longest extent to the right side resulting in a longer primary cutting edge. Values less than one indicate a shift of the position of the longest extent towards left, causing a reduced length of the primary cutting edge respectively a more pronounced secondary cutting edge *(Figure 6, D, right)*.

**tip angle:** Angle in degree between two points on the contour line with the same y-value and the tip. The points on the contour line are determined as the uppermost pair of three pairs of points along the contour line of the transformative part equally distributed between the tip and the widest extent. The returned value is a standardised approximation of the tip angle *(Figure 7, G)*.

**MP-CM-x-offset:** Vector between the x-coordinates of the geometric centre (MP: *x = width / 2, y = length / 2*) and the centre of mass (CM) (Grosman 2016); Values equal to or close to zero indicate artefacts that are horizontally symmetric along the x-axis. Positive values indicate a shift of mass towards right. Negative values indicate a shift of mass towards left *(Figure 7, H)*.

**MP-CM-y-offset:** Vector between the y-coordinates of the geometric centre (MP: *x = width / 2, y = length / 2*) and the centre of mass (CM) (Grosman 2016); Values equal to or close to zero indicate artefacts that are vertically symmetric along the y-axis. Higher values indicate a shift of mass towards the tip, which, in the specific case of SPs is most likely caused by a shift of the position of the widest extend towards the tip. Lower values indicate a shift of mass towards the base, which in turn is most likely caused by a shift of then position of the widest extend towards the base *(Figure 7, H)*.

### 3.2.1 Intercorrelations between Morphometric Features

The morphometrical features were initially examined for intercorrelations to avoid redundant signals in the primary analysis. A first inspection of the Kendall's tau correlation results between the key morphometric variables *(Figure 8)* reveals a high degree of intercorrelation among the features width, length, area, and contour length. While the correlation between width and length is moderate (r = 0.46), both show strong correlations with area (width = 0.69; length = 0.75). The slightly higher correlation between length and area, as opposed to width and area, is expected for artefacts produced on blades or bladelets, which typically permit more variability in length than in width. Contour length is highly correlated with all three of these features (width = 0.46; length = 0.93; area = 0.80), suggesting that it provides redundant information. The length-width-index (l-w-index) shows only moderate correlations with other features. It is negatively correlated with width (τ = -0.27), the width of the right part (τ = -0.27), and tip angle (τ = -0.39), suggesting that wider artefacts generally have more obtuse tip angles. Although the absolute values of the length of the upper and the lower part as well as the width of the left and the right part are highly correlated with width, length, area, and contour length, their derived ratios – the upper-lower-ratio and the left-right-ratio – only show pronounced correlations with their respective constituent dimensions *(Figure 8)*. Tip angle exhibits notable negative correlations with both the l-w-index (τ = -0.39) and the upper–lower-ratio (τ = -0.37) – indicating that slenderer artefacts and artefacts with longer transformative parts tend to have pointier tips. Tip angle also positively correlates with the vertical offset of the centre of mass (MP-CM-y-offset, τ = 0.36), implying that artefacts with lower centres of mass tend to have more acute tip angles. The horizontal offset of the centre of mass (MP-CM-x-offset) is strongly influenced by asymmetry, as shown by its negative correlation with the width of the right part (τ = -0.56) and positive correlation with the left-right-ratio (τ = 0.52). In contrast, the vertical offset (MP-CM-y-offset) correlates only with tip angle, as described above.

With regard to these results, nine morphometric features were selected for further analysis: length, width, area, l-w-index, upper-lower-ratio, left-right-ratio, tip angle, and the x- and y-offsets of the centre of mass. Contour length was excluded due to redundancy. The individual dimensions of the upper and the lower part and the left and the right part were omitted in favour of their respective ratios.

It must be emphasised that the intercorrelations between individual morphometric features vary depending on the artefact under study, and the feature set chosen here is by no means universally optimal. It is therefore recommended to assess intercorrelations prior to the main analysis. For example, artefacts with an almost rectangular outline will likely display stronger intercorrelations among size-related features and with the l-w-index, whereas drop- or pear-shaped artefacts are more likely to exhibit strong correlations involving the upper-lower-ratio. Future methodological advances should aim at developing algorithms that enable a more standardised and reproducible selection of morphometric features, replacing the current reliance on manual selection.

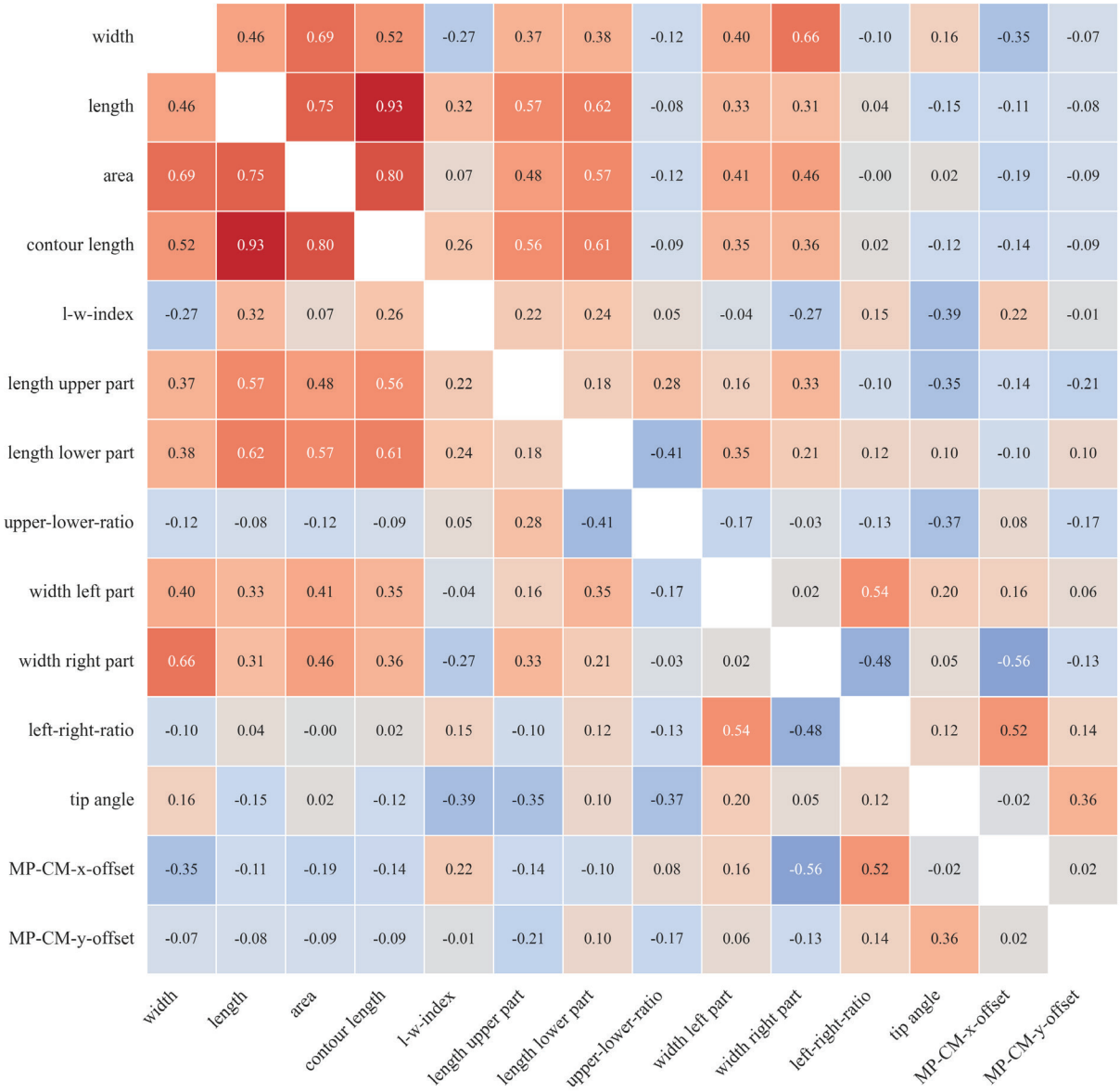



Figure 8: Confusion matrix of Kendall's tau (T) correlations for a selection of metrical features.

### 3.2.2 Categorisation of Morphometric Features

Based on the morphometric information each feature provides, they can be categorised into two groups: size-related and shape-related features *(Table 3)*. While size generally refers to the actual dimensions, shape is defined as the total information that remains invariant under translation, rotation, and isotropic rescaling – that is, the aspects that do not change with position, orientation, or overall scale (Kendall 1989; Small 1996). Size-related features therefore include length, width and area. Shape-related features encompass the upper-lower-ratio, the left-right-ratio, the tip angle, and the centre of mass features (MP-CM-x and y-offset). While the l-w-index is invariant under translation, rotation, and isotropic rescaling, it also does not convey information about absolute dimensions in a strict sense. It was therefore categorised as a shape-related feature.

Table 3: Categorisation of morphometric features.

| width | length | area | l-w-index | upper-lower-ratio | left-right-ratio | tip angle | MP-CM-x-offset | MP-CM-y-offset |
|---|---|---|---|---|---|---|---|---|
| size-related | | | shape-related | | | | | |
| blank production, selection and initial pre-modification | | | shaping | | | | | |

The features length, width, l-w index, and area are primarily influenced by the dimensions of the blank from which the artefact is produced, as well as any modifications made to the blank prior to shaping the final product itself. As such, these attributes likely reflect variations and thus allow for inferences on changes in blank production, selection, or pre-modification strategies. In contrast, the left-right ratio, upper-lower ratio, tip angle, and centre of mass features are predominantly influenced by the artefact's final modification processes. These features, therefore, provide insights into differences or changes in design concepts and may further indicate variations in hafting techniques or even broader shifts in hunting weapon composition.

### 3.2.3 Style and Function

Palaeolithic tools exhibit different aspects that are considered to be of different diagnostic value for the interpretation of evolutionary changes: style and function (Sackett 1977; Dunnelll 1978b). The functions of tools are constrained by physical requirements (see Chapter 3.2.4), leaving relatively little room for significant alteration in their material design. Style, in contrast, is far less constrained and shows greater variability. While functional attributes are often considered subject to natural selection, affecting the "Darwinian fitness of the populations in which they occur" (Dunnell 1978b, 199), stylistic features are thought to be selectively neutral and shaped largely by stochastic factors (Neiman 1995).

This style-function dichotomy is frequently framed in terms of whether a trait is payoff correlated – that is, whether it directly affects an individual's fitness or utility (Brantingham 2007). Under this view, functional traits are payoff correlated, whereas stylistic traits are not. Because stylistic elements are less constrained by performance demands, they are more susceptible to innovation, copying errors, drift, or personal preference (e.g., Neiman 1995). Some scholars, however, propose that style and function typically operate side by side (Bettinger et al. 1996).

Most of what the morphometric features capture in this study is likely closely tied to functionality – affecting hafting efficiency, durability, repairability, penetration capacity, and overall hunting performance. Therefore, changes in these features may reflect selective processes and adaptive behaviours. Some characteristics may also reflect stylistic preferences rather than purely functional requirements, though distinguishing between the two is challenging in the context of lithic projectile points. Also, some features might shift in and out of selective pressure, thus behaving sometimes directed, somtimes stochastically. Therefore, instead of assining certain traits generally and a priori to the functional or stylistic domain, these aspects should be treated as an emprical question.

### 3.2.4 Constraints and Biases of Morpho-logical Change

Developmental constraints and developmental *biases* describe how developmental processes shape evolutionary change by limiting or directing phenotypic variation. Developmental constraints restrict the range of phenotypes that can arise, preventing certain forms from evolving regardless of their potential adaptive value (Hansen 2015). In contrast, developmental *biases* do not prohibit variation but make some phenotypes more likely to emerge than

others because of the underlying structure of developmental systems (Uller et al. 2018). Thus, whereas developmental constraints define the limits of possible evolutionary change, developmental *biases* influence the direction evolution is more likely to take.

Both concepts can be applied to the evolution of stone tool morphology (Eren et al. 2018; O'Brien & Lala 2023). Since stone tools are shaped exclusively through reduction, the primary constraints on morphological evolution are the breaking mechanics of the lithic raw material and the dimensions of the blank. Likewise, developmental *biases* are inherent to stone tools, as evolutionary changes and variations are confined by a limited morphological range, channelling possible pathways in certain directions (McGhee 2018). These constraints are particularly relevant when focusing on a specific stone tool type, as done in this study. All morphometric features presented above are subject to developmental constraints, each confined to a specific range of possible variation. Size-related features, are naturally restricted by the dimensions of the blanks, which likewise place limitations on the l-w-index. The tip angle is constrained by the functional requirements of projectile points, as only angles within a certain range ensure both effectiveness and durability. Beckhoff (1966), for example, argues that tip angles exceeding 55° should no longer be considered functionally viable. Similarly, Friis-Hansen (1990) demonstrates that the most effective tip angles fall within the range of 20° to 40°. The hafting part must reach a minimum length to allow for secure hafting, while the transformative part must exceed a certain length to ensure the point serves as a functional latero-frontally projectile implement, which in turn sets a lower limit for the upper-lower-ratio. Similarly, the left-right-ratio is constrained by the morphology of the shoulder and the primary cutting edge of the point. As in this study, all SPs are oriented with the shoulder facing right, the left part can, in theory, approach zero in cases of extreme straightness of the primary cutting edge. However, such a reduction is not feasible for the right part of the SP, meaning the left-right-ratio is inherently bounded. Finally, the centre-of-mass offsets (MP-CM-x- and y-offset) are physically constrained by the possible geometric configurations of the point. Extremely high values would indicate non-sensical or functionally implausible forms, and thus are not expected to occur within the archaeological record. Additionally, some features, by the nature of their calculation, are also mathematically bounded. The left-right-ratio and the upper-lower-ratio, for example, cannot fall below zero.

### 3.2.5 Problem of Preservation

It is acknowledged here that some of the morphometric features yield high potential for not being preserved in a state reflecting the original design concept of the SP. Resharpening, maintenance, and curation of artefacts, well-recognised especially among American archaeologists (e.g., Buchanan 2006; Shott & Ballenger 2007; Buchanan & Collard 2010) but also for European Palaeolithic contexts (e.g., Richter 1997; Jöris 2012; Beyries & Cattin 2015; Schmidt 2015; Uthmeier 2016; Shimelmitz et al. 2017; Weiss 2020; Tsanova et al. 2024), can significantly affect key morphometric traits, such as overall length, tip angle, and upper-lower-ratio, as restoration efforts were likely focused on broken tip areas. Certain periods and regions may have seen more frequent resharpening, maintenance and curation than others, thereby exerting a stronger influence on overall variation. Additionally, Schmidt (2015) demonstrated that some bifacially retouched SPs of the Upper Solutrean were recycled from broken bifacial points, suggesting that their dimensions reflect opportunistic reuse rather than the deliberate production of a specific SP form. However, at the macroscale level addressed in this study, the impact of resharpening, maintenance, curation and recycling on morphometric variation is initially set aside, but may be revisited in further studies.

## 3.3 ANALYTICAL METHODS

The main focus of this study is the analysis and the quantification of possible trends in the evolution of material culture. In pursuing this goal, it faces several difficulties. A major difficulty lies in the way change takes place. Simpson (1944) challenged classical Darwinian gradualism by demonstrating that evolution occurs at varying speeds and in different ways across

different lineages. He argued that evolutionary patterns are not uniform and depend on ecological and genetic factors. Consequently, the choice of where measurements are taken becomes crucial to the interpretation of results. This issue is illustrated in *Figure 9*, where the evolutionary rate between time points $t_2$ and $t_5$ differs markedly from that between $t_1$ and $t_5$, for example. Alongside this challenge comes the issue of scale: conclusions about evolutionary tempo or rate are highly dependent on the temporal scale applied with short-term studies often revealing rapid phenotypic shifts, while long-term patterns often appear more constrained (see e.g. Perrier & Charmantier 2018). Whether one considers the entire timeframe shown in *Figure 9* at once, or subdivides it into smaller intervals – such as isolating the steep increase between $t_2$ and $t_3$, or the pronounced decrease between $t_3$ and $t_4$ – can substantially alter the observed patterns. However, the apparent reduction in evolutionary rates observed across extended timescales may often reflect statistical *biases* inherent in ratio-based metrics rather than genuine changes in the underlying rate of evolution (De Lisle & Svensson 2023).

Another difficulty when quantitatively addressing change in archaeological objects is variation. As handcrafted and thus more or less unique items, archaeological artefacts inherently display a degree of variation that is typically more pronounced than what is observable in biological species (see e.g., Feldman & Laland 1996 for difference between genetic and cultural evolution). This variation is a natural outcome of human production, shaped by factors such as individual choices, skills, raw material constraints, and also varying standards in learning communities.

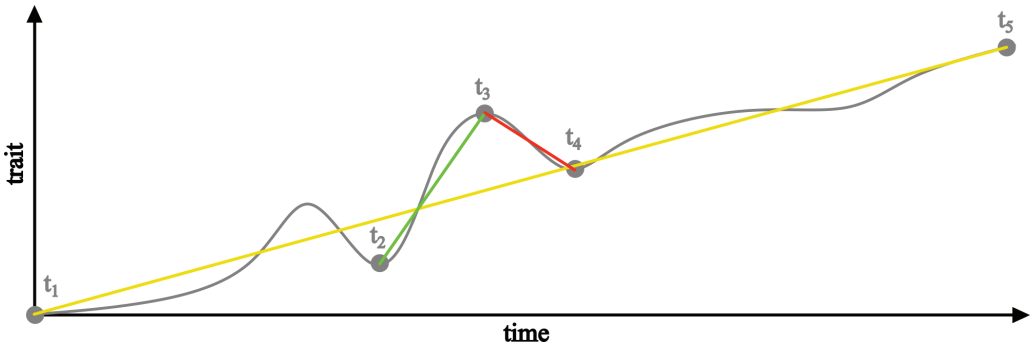



Figure 9: Evolutionary change of a single trait and the implications of non-linear evolution for change rate calculation (yellow = increasing trend $t_1$–$t_5$; green = increasing trend $t_2$–$t_3$; red = decreasing trend $t_3$–$t_4$).

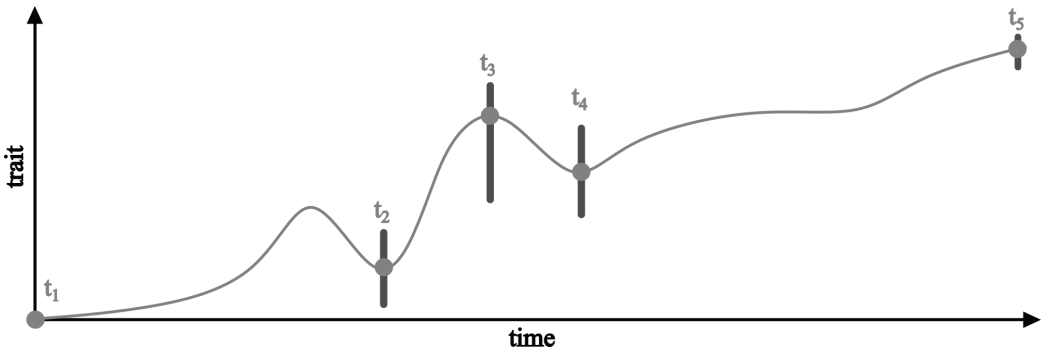



Figure 10: Evolutionary change of a single trait and the implications of variation for change rate calculation (dark grey vertical lines = variation at measuring points $t_2$–$t_5$).

While there are methods applied in archaeological praxis specifically designed to capture variation, and other methods aimed at calculating morphological change, an effective integration of both aspects remains largely absent in current archaeological practice. Consequently, in this study, when discussing morphological change or difference, variation can only be acknowledged, rather than fully incorporated into a formal model of change. This limitation is especially important when interpreting evolutionary trends in artefact morphologies, where distinguishing between meaningful evolutionary patterns and random variation is a methodological challenge.

While this might oversimplify the actual pattern, the methods for calculating change employed in this study generally rely on averages to avoid measurement inconsistencies arising from variation. For example, the substantial difference between measuring change from the lowest point of the data distribution at $t_2$ to the highest point at $t_3$, or *vice versa (Figure 10)*.

To establish a statistically supported and quantifiable understanding of chronological change, this study applies a systematic set of methods. This foundation enables the discussion of evolutionary trends and the factors influencing them. Another goal of this study is to explore the morphometric relationships between SPs. To achieve this, methods are employed to identify patterns and structural similarities within the dataset, thereby aiding in the assessment of potential evolutionary and cultural linkages between different SPs.S

### 3.3.1 Identifying Timing and Duration of Evolutionary Trends

To explore the timing of evolutionary trends and assess the extent to which variation is influenced by chronological factors rather than random variation, Redundancy Analysis (RDA) is conducted as a first analytical step. This method is a direct extension of multiple regression, designed to model the effect of an explanatory matrix X ($n \times p$) on a response matrix Y ($n \times m$) (Legendre & Legendre 2012; Roth 2022). RDA can be understood as a two-step process. The first step involves performing multiple regressions, where each variable in Y is regressed on the explanatory variables in X, resulting in a fitted matrix, Y-fit. The second step involves applying Principal Component Analysis (PCA) to Y-fit, which reduces dimensionality and provides eigenvalues and eigenvectors (Hotelling 1933). This process yields a matrix Z, containing the canonical axes that represent linear combinations of the explanatory variables in the space of X. In this study, the calibrated ages ('ka calBP') of the category A and B datasets are used as X in order to investigate chronological developments represented by the morphometric features as Y.

The linearity of the combinations of X is crucial to the RDA. It focuses solely on the effect of X on Y between the initial stage *(Figure 9, $t_1$)* and the final stage *(Figure 9, $t_5$)* of X. Non-linear developments, such as fluctuating effects *(Figure 9, $t_2$–$t_4$)*, rectified but stronger trends *(Figure 9, $t_2$–$t_3$)* or counter-trends *(Figure 9, $t_3$–$t_4$)* occurring in between, are not accounted for. Therefore, the selection of the dataset's extent directly influences the results of the RDA.

Two output values of the RDA are important to this study: $R^2$, representing the explanatory power of the canonical variable (Legendre & Legendre 2012, 630 f. and Fig. 11.4), and p (p-value), which is the probability of the result estimated by a permutation test (Legendre & Legendre 2012, 25–28). When p is higher than 0.05, the result is rejected for not being significant. If p is lower than 0.005, the result is referred to as highly significant. Values for $R^2$ higher than 5% (0.05), are considered in this study to indicate notably strong explanatory powers.

RDA is applied in this study using the 'vegan' package (Oksanen et al. 2020) in R (R Core Team 2021), integrated within PyREnArA, following along application advices by Borcard et al. (2011). This implementation enables fast and user-friendly processing of the acquired morphometric data.

### 3.3.2 Measuring Variation

When analysing artefacts, two distinct forms of multiplicity are important to consider: diversity and variability. Diversity refers to the range of different categories within a classification system – such as various tool types like scrapers, borers, or points (see Chapter 1.2). In contrast, variability pertains to the differenc-

es observed within a single category, such as variations in point shapes or specific modifications like retouched bases. While these concepts both deal with multiplicity, they operate at different analytical levels. Keeping diversity and variability separate in analysis is crucial for understanding cultural evolution, as each can respond differently – or even oppositely – to external influences like temporal changes or spatial patterns (on this see Maier et al. 2023). For example, a shrinking population might be linked to fewer types of tools (lower diversity) but greater variation within the remaining types (higher variability) (Maier et al. 2021). Since this study focuses exclusively on a single tool type – SPs – the primary aim is to explore the morphological variation found within this specific category.

Variation further is a fundamental prerequisite for any form of evolution driven by selection (Darwin 1859, 101–102). To properly assess evolutionary change, variation must be quantified, allowing the calculation of appropriately scaled rates of change later on. Any absolute or proportional change is only meaningful when considered in relation to the existing distribution of variation available for selection or drift (Gingerich 2011). High variation may facilitate and indicate evolutionary change, but it can also result from stochastic processes. Conversely, low variation may reflect phases of stabilisation and standardisation.

While different methods for capturing variation in archaeological material are frequently applied – e.g., measures of richness, of *evenness* or heterogeneity (see Lyman & O'Brien 2000) – these methods are originally not designed for the analysis of metrical data. To assess the overall morphometric variation within a specific unit, the Coefficient of Variation (*CV*) is calculated. The CV is a widely used statistical measure in evolutionary biology for comparing trait variation in, for example, species, so called phenotypic plasticity (e.g., Fajarado & Piper 2011), and the 'evolvability' of traits (e.g., Houle 1992). Although applications in palaeolithic archaeology are relatively uncommon, they are not entirely absent (e.g., Roux 2003), and applications in Neolithic contexts is more frequently seen (e.g., Zimmermann 1998, 139; Scharl 2017, 117).

It is calculated as the ratio of the standard deviation ($\sigma$) to the average ($\bar{x}$), and it is expressed as a percentage value.

$$CV=(\sigma_{trait}/\bar{x}_{trait})$$

The CV is especially useful for comparing the variation of the different morphometric features with different scales. However, as both features for the offset of the centre of mass (MP-CM-x- and y-offset) can exhibit negative values, the calculation of the CV does not follow the same principles as the other features, which is why both features are excluded from the calculation of the CV here.

### 3.3.3 Calculating Tempo, inferring Mode

Simpson (1944) separated two variables of evolution – tempo and mode. Tempo he referred to as the rate of change over time, while mode can be understood as the process over time and its pattern. Both are, of course, inextricably linked (Hunt 2012). Canonically, there are three modes of evolution: directional evolution, random walk and stasis (Hunt 2010). Directional evolution corresponds to gradual change in the Darwinian sense, where traits evolve consistently in a particular direction over time *(Figure 11, A)*, reflecting adaptational processes. This evolutionary mode can occur at any tempo – whether rapid or slow. Stasis, on the other hand, represents a pattern of no evolutionary change, with traits fluctuating around a stable average value *(Figure 11, B)*. Random walk describes independent changes in traits, where both increases and decreases occur with equal probability, but without any inherent directional trend *(Figure 11, C)*.

Additionally, Simpson (1944) showed that major transitions (e.g., the rise of mammals) often occur in bursts rather than steady, gradual changes, what he described as 'quantum evolution'. This concept was later revisited by researchers under the term of 'Punctuated Equilibrium' (e.g., Eldredge 1971; Eldredge & Gould 1972). In a Punctuated Equilibrium, the rate of change – the tempo – fluctuates between longer periods of morphological and taxonomical stasis and bursts of change *(Figure 11, D)*, which is the result of speciation, represented by morphological diversification

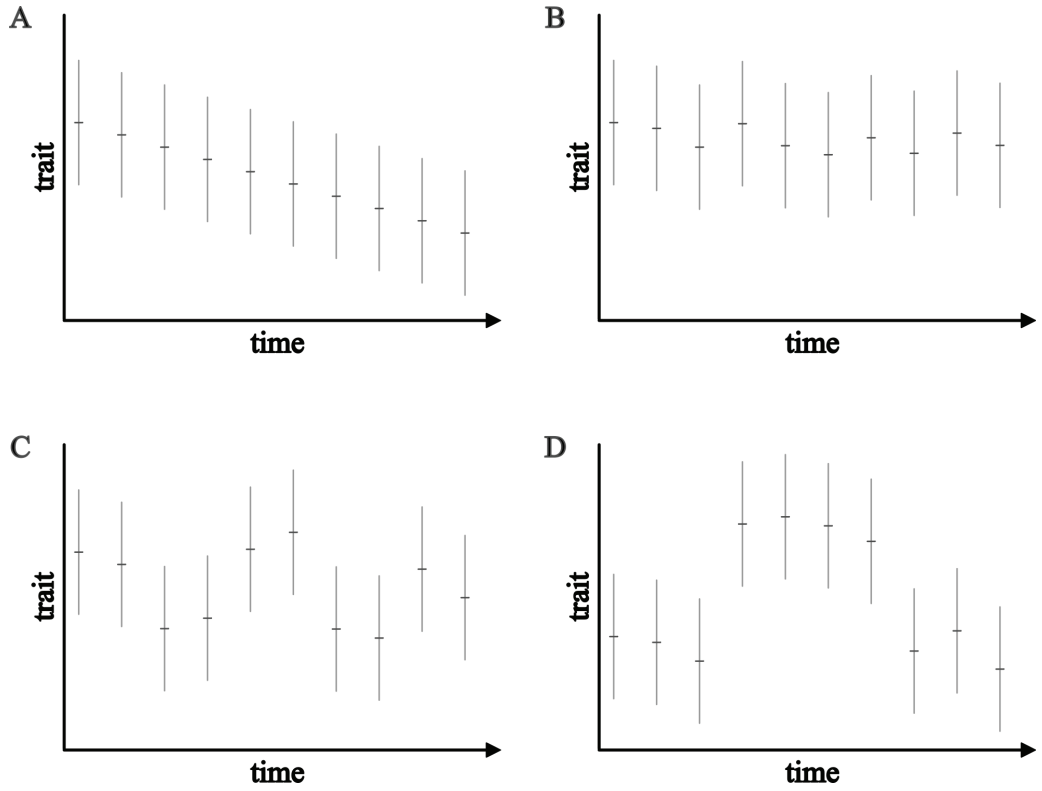



Figure 11: Modes of change. Each vertical line represents the range of variation at a given measuring point in a specific morphological trait (A = gradual change, where the mean shifts uniformly in one direction over time; B = stasis, where the mean does not move in one direction; C = random walk, where the mean shifts in different directions over time; D = Punctuated Equilibrium, where the mean shifts suddenly after a period of stasis, which is then eventually followed by another period of stasis. After Martin & Barnosky 1993; Hunt 2010 and O'Brien & Lyman 2023).

(Gould 1982). While Gould (1982) suggested such bursts should comprise less than one percent of the lineage's duration, archaeological datasets usually lack the necessary chronological sensitivity.

One phenomenon that can account for sudden bursts in human material culture and thus be treated as equivalents to biological speciation is the occurrence of inventions and innovations. Inventions refers to the creation of a novel idea, while innovation is a novelty that has successfully diffused through a population (Duran-Nebrada et al. 2022). Among humans, both invention and innovation are fundamental processes for generating and propagating new variants (O'Brien & Holland 1990 and 1995; Fogarty et al. 2015; Kolodny et al. 2015; Kolodny et al. 2016).

Martin & Barnosky (1993) emphasise that different morphological traits may undergo distinct modes of change, resulting in what they termed a 'mosaic change' (ibid., 7). They argued that while one trait may change gradually, randomly, or in bursts, another may follow a different mode of change, collectively forming a mosaic pattern. However, the mere coexistence of stasis in one trait and change in another does not constitute such a mosaic pattern, as stasis is common across many traits. Distinguishing different evolutionary tempos, however, requires the specification of a unit of change over time, as well as a definition of the magnitude of such unit that is to be understood as modal, slow, or fast.

### 3.3.3.1 Change Rates

In evolutionary biology, the tempo of evolutionary change in traits, such as body size, limb length, or beak shape, is widely assessed by Haldane's 'Darwin' (Haldane 1949) or Gingerich's 'Haldane' (Gingerich 1993) (for reviews on both, see Gingerich 2009; Hendry & Kinnison 1999). The application of 'Darwin' as a unit of evolutionary change to the evolution of material culture would allow for direct comparisons with biological evolution. However, due to the nature of these units, the relatively short-term observations for material culture will naturally produce higher values than those typically seen in long-term biological evolution (Gingerich 1983), biasing the comparison. For instance, a 'Darwin' can mathematically be expressed as:

$$d = [log(x_2) - log(x_1)]/\Delta t$$

with $x_1$ and $x_2$ being the trait values at two different times and Δt the time interval in millions of years (Haldane 1949, 52). Considering a change in length between artefacts of the same type – one dated to 24,000 calBP ($x_1$) with a length of 50 mm and another at 23,000 calBP ($x_2$) measuring 60 mm – the resulting evolutionary rate would be 9.691 * 10-5 Darwins or 96.91% per million years. In comparison to Haldane's own example concerning the evolution of horse teeth, which exhibits a rate of just 3.6 * 10-8 Darwins or 3.6% per million years (Haldane 1949, 53), the calculated example rate for material culture appears exceptionally high. This contrast highlights the fundamental difference between biological and cultural evolution, where the latter can undergo rapid transformations due to factors such as innovation, social transmission, and environmental adaptation, rather than the slower genetic changes observed in biological systems (Feldman & Laland 1996). Moreover, estimating evolutionary rates using the 'Haldane' metric requires the definition of 'generations' (Gingerich 1993, 457), which poses a significant challenge when applied to material culture, as it involves non-living artefacts rather than biological populations.

Therefore, in this study, a directly interpretable calculation of change rates is applied, which returns percentage change. The change rate for each morphometric feature is here determined by calculating the average value per chronological unit for the respective feature, subtracting the older value ($\bar{x}_1$) from the younger value ($\bar{x}_2$), and dividing the difference by the older value:

$$change\ rate = (\bar{x}_2 - \bar{x}_1)/x_1$$

This formula calculates the average change in each morphometric feature from one chronological unit to the next. The overall average change rate for each morphometric feature is then calculated as the average of all chronological units. Based on the average, the standard deviation ($\sigma$) for each feature is also calculated. To identify extraordinary values, a significance threshold was established, encompassing the conventional 95% of the data distribution (assuming a normal distribution) (Fisher 1925), as follows:

$$significance\ threshold = \bar{x} + 1.96 * \sigma$$

Change rates are purposefully based solely on average values and do not account for variation within each chronological unit. This approach is designed to focus on large-scale developments in (the morphometric) features, offering valuable insights into the speed or extend of change over time. It allows moving beyond localised or assemblage-specific variation and focuses on broader temporal processes, such as evolutionary shifts, cultural adaptations, or technological innovations. It further provides a simplified summary of potentially complex morphometric datasets, reducing them to a single, interpretable metric. This makes it easier to communicate findings and enables integration into broader studies or comparative analyses with other datasets or research domains. However, this oversight can obscure important patterns or outliers that may indicate meaningful local processes or subtrends within the broader temporal framework. Features with high internal variation might yield misleading or incomplete interpretations when only averages are considered. Additionally, outliers exert a disproportionate influence on the calculated averages, potentially skewing the results. As such, they must be carefully identified, evaluated, and, where necessary, excluded to ensure the reliability and integrity of the analysis.

Also, the granularity of the chronological units strongly influences the results (on this, see Hendry & Kinnison 1999, Fig. 2). Coarse divisions may dilute significant changes within shorter timeframes, while overly fine divisions can amplify noise, reducing the clarity of overarching patterns (see Chapter 3.3). This sensitivity highlights the need for carefully chosen chronological units to balance resolution and interpretability. Returning to the example given in *Figure 9*, if, for example, the rate of change were calculated between $t_2$ and $t_4$, the result would be much weaker than that between $t_2$ and $t_3$ *(Figure 9)*. The method further assumes a linear relationship between successive chronological units, which may not reflect the true nature of changes in morphometric features. Nonlinear changes may be misrepresented or entirely overlooked by the change rate approach *(e.g., Figure 9, $t_1$–$t_3$)*. The application of change rates should therefore be approached with caution and carefully supervised – e.g., by RDA – to ensure accurate and meaningful results. To complement and enhance the findings, additional methods, such as correlation analyses, can be employed to provide further context and validation.

### *3.3.3.2 Correlation*

In order to investigate the relationship between the actual values of the morphometric features and the progression of time, represented by the calibrated ages ('ka calBP') of the assemblages, Kendall's tau (Kendall 1938) correlation is applied. Kendall's tau (T) is preferred over other correlation coefficients due to its unique characteristics and advantages. Kendall's tau is a rank-based correlation coefficient, meaning it does not assume a linear relationship or require the data to be normally distributed. It is robust to outliers and skewed distributions, unlike Pearson's correlation (Pearson 1895), which is sensitive to these issues. Whereas Pearson's correlation only measures linear monotonic relationships, Kendall's tau assesses the strength and direction of nonlinear nonmonotonic relationships, where the variables tend to move together in a consistent direction, not necessarily linearly (e.g. Alshahrani 2026). Additionally, Kendall's tau often performs better with smaller sample sizes than Pearson's correlation, providing more accurate and reliable estimates in small datasets. Since the calibrated ages decrease as time progresses, a positive correlation indicates that the values are decreasing over time, and *vice versa*.

### 3.3.4 Relations

When assessing interactions between Palaeolithic groups and suggesting degrees of relatedness, shared tool types are often seen as strong indicators (Binford 1972, 116). For instance, the occurrence of SPs in both Badegoulian and Salpetrian inventories has been interpreted by some as evidence of contact between these groups (Boccaccio 2021). However, using tool types as indicators of interaction is at best problematic (see Maier 2015, 41 ff.; Sauer & Riede 2019). This issue parallels the broader shortcomings of typological approaches discussed earlier (Chapter 1.2), particularly their inability to capture the full extent of variability. Since this study focuses on a single constructed type – the SP – it emphasises variability and change within this category and thus highlights its non-uniform nature. Consequently, methods beyond simple presence–absence observations are required to assess potential relationships.

In palaeobiology, phylogenetics – the study of evolutionary history based on observable characteristics of organisms – has a long tradition of use and plays a vital role in inferring relationships among organisms (see e.g., Zimmermann 1937; Hennig 1950). Archaeologists as well have long been interested in establishing artefact 'lineages', primarily based on similarities in morphological traits, and estimating the (relative) chronological position of individual 'members' within them – an endeavour that has fuelled seminal works such as Montelius' '*Die Methode*' (1903). The application of phylogenetic approaches to the study of artefact lineages has gained increasing popularity, particularly among American archaeologists (e.g., O'Brien et al. 2001; O'Brien & Lyman 2003b; Darwent & O'Brien 2006; Buchanan & Collard 2008; O'Brien et al. 2012) and promising and sophisticated model-based methods employing Bayesian phylodynamic to infer phylogenies have also been introduced (Matzig et

al. 2024). To the author's knowledge, no established method currently exists for assessing phylogenetic relationships using explicitly morphometric data.

Darwin (1859) already identified the problem of distinguishing between analogous traits – traits that have a similar function but evolved independently in species that do not share a recent common ancestor – and homologous traits – traits that are similar in species because they are inherited from a common ancestor. A key factor contributing to morphological similarity without direct relatedness – frequently discussed in the context of stone tools (Eren et al. 2018; Charbonneau 2018; McGhee 2018; Diachenko et al. 2023; Abdolahzadeh et al. 2025) – is what biological evolutionary theory terms 'convergent evolution' (e.g., McGhee 2011). It is generally understood that certain morphological or technological characteristics in stone tools may emerge independently in contexts with low variation – analogously – throughout prehistory. This problem, in turn, leads to the challenge of identifying relationships between archaeological artefacts comparable to biological taxonomy. As Darwin (1859, 74 f.), who had no knowledge of genes and thereby faced the same problem, observed, it is impossible to distinguish varieties – related but different forms – from species – different forms that might or might not be related – unless intermediate linking forms are found or a certain indefinite degree of difference is not surpassed. Hence, from a morphological perspective, similarity can be observed as a fact, whereas homology must be inferred as a hypothesis (Patterson 1982; 1988). Returning to Dunnell's (1978b) dichotomy and definition of style versus function, O'Brien & Leonard (2001, 4) note that "traits, or features, that confer Darwinian fitness on an organism – Dunnell's functional traits – may arise among different breeding populations as independently generated features – analogs – or as products of a common developmental history – homologs".

This study does not aim to resolve the broader and largely unresolved theoretical issues surrounding these questions. Instead, it operates on the assumption of a strong interrelationship among the archaeological artefacts – provided that a) morphological differences are not significant – what has been paraphrased "the more similar, the more closely related" (Hennig 1950) – and that spatial and chronological distances remain within reasonable bounds. By focusing on these three parameters, the study aligns with established archaeological frameworks. Willey (1953, 361) identified "form, space, and time" as the three basic factors of archaeological analysis, while Spaulding (1960, 439) defined archaeology as the study of the interrelationship between "form, temporal locus, and spatial locus." A similar perspective is found in biology, where, for example, Gingerich (1980) described these dimensions as the three 'principal components of evolutionary space.' A related conceptual framework is employed by researchers applying frequency seriation – a method that tracks the relative frequencies of traits across specimens and analyses the diversity of variants over time (Lyman et al. 1997) – to the investigation of artefact lineages (e.g., Lipo et al. 1997; Neiman 1995). To ensure that the patterns observed reflect heritable continuity – rather than simply a chronological sequence of variation – this approach requires that the artefacts under study originate from the same time span, geographic locality, and cultural tradition (e.g., Cowgill 1972; Dunnelll 1970).

It must be emphasised again that, while borrowing methods from biology, the focus here is not on relationships between artefacts themself. Rather, it lies on the relationship between ideas and concepts – the 'recipes' (Lyman & O'Brien 2003) – for artefacts that may be regarded as replicators in Dawkins' terms (1976). These are expressed by the producers through artefact morphology, which is eventually transmitted, and finally reflected in lineages. In this sense, artefacts, as part of the phenotypic expression of the producer or user, can be regarded as manifestations of a cultural trait (Crema et al. 2024), that can be shared or not.

In this study, Hierarchical Cluster Analysis (HCA) is applied to investigate the morphometric relationships among SP samples over time, providing insights into temporal patterns of morphological variation. HCA is an unsupervised multivariate technique used to identify natural groupings among a set of objects based on their similarity or dissimilarity across one or more measured variables (Johnson 1967). In archaeological research, HCA can help identify cultural or chronological groupings among assemblages based on technological, typological, or stylistic traits (e.g., Shennan 1997; Baxter 2003).

Unlike partitioning methods (e.g., k-means), HCA does not require the number of clusters to be specified a priori. Instead, it produces a nested hierarchy of clusters that can be visualised using a dendrogram, allowing researchers to explore relationships at multiple levels of granularity (Murtagh & Contreras 2012). HCA operates in two main phases: calculating pairwise distances between data points using a dissimilarity metric (e.g., Euclidean, Manhattan, or custom metrics), and then linking those points into a tree-like structure using an agglomerative (bottom-up) or divisive (top-down) algorithm (Lance & Williams 1967). In agglomerative clustering – the most commonly and thus here employed approach – each observation starts as its own cluster and is successively merged with its nearest neighbour until all data points belong to a single cluster (Murtagh & Legendre 2014). The result is a tree that reflects both the relative similarity among samples and the sequence in which they are grouped (Sneath & Sokal 1973). A critical consideration in HCA is the choice of distance metric and linkage method (e.g., single, complete, average, Ward's method), as these can significantly influence the resulting cluster structure (Kaufman & Rousseeuw 2005).

Here, HCA is applied based on a distance matrix calculated from change rates (Chapter 3.3.3.1) between the averages of individual units using an average linkage method. The average linkage method allows a sample to join a group at the mean of the distances between this sample and all member of the group. While the use of change rates again overrides intra-group variation and may oversimplify potential linkages, it enhances the accessibility and comparability of the results throughout this study, enabling more direct interpretation. Future research should focus on implementing methods that account for in-group variation and evaluate distances between groups relative to that variation, such as Mahalanobis distance (Mahalanobis 1936).

Distance matrices can be extended or modified to incorporate additional information, such as temporal or spatial weighting, allowing the HCA to produce more contextually sensitive classifications. While unconstrained HCA is robust for identifying structure in multivariate data, it assumes all variables or dimensions are equally relevant and that samples are exchangeable with respect to time and space. In archaeological and historical research, however, such assumptions are often unrealistic. Artefacts are not only defined by their attributes but also by their chronological and spatial context, both of which may have shaped their development. While such implications have not been widely addressed in archaeology to date, researchers in other disciplines have developed sophisticated methods for applying weights to distance matrices in order to tailor subsequent analyses to their specific needs (e.g., Legendre et al. 1985; Legendre & Legendre 2012; Lamb et al. 2020).

Weighting in HCA modifies the original distance matrix to favour particular relationships. For example, in time-weighted HCA, the chronological proximity of samples can be introduced into the distance matrix by computing an additional time-distance component and combining it with the trait-based dissimilarity (e.g., linearly or via a weighted sum). A relatively simple approach is chosen here, once again prioritising the accessibility and comparability of the results throughout this study. It can be expressed mathematically as:

$$D_{ij}\ combined = D_{ij}\ traits + D_{ij}\ time * \alpha$$

where $D_{ij}\ traits$ is the original dissimilarity between samples i and j based on traits, $D_{ij}\ time$ is the absolute difference in time, and $\alpha$ is a weighting factor that tunes the influence of temporal proximity. This approach can enhance the interpretability of clusters, especially in diachronic studies where cultural transmission, innovation, or continuity over time are key hypotheses. It helps prevent the formation of ahistorical clusters that group samples with similar attributes but that are chronologically implausible. As such, time weighting serves as a heuristic to guide the algorithm toward historically meaningful solutions, without imposing hard constraints. When $\alpha = 0.01$ – the weighting is 1% – a chronological difference of one millennium adds 0.01 to the morphometric distance *(Table 4)*. Given that the maximum chronological difference in the dataset is 16,000 years, the maximum temporal weight that could be added to the morphometric distance is 0.16.

To further constrain the resulting clusters and prioritise spatially proximate samples, geographic distance is incorporated into the

Table 4: Example matrices for time-constrained HCA (A = Metrical distance matrix for between the samples $x_1$–$x_3$, representing a time sequence of three consecutive millennia; B = Weighted time distance matrix with α= 0.01; C = combined matrix used in a constrained HCA).

A

| | $x_1$ | $x_2$ | $x_3$ |
|---|---|---|---|
| $x_1$ | | 0.1 | 0.2 |
| $x_2$ | 0.1 | | 0.15 |
| $x_3$ | 0.2 | 0.15 | |

B

| | $x_1$ | $x_2$ | $x_3$ |
|---|---|---|---|
| $x_1$ | | 0.01 | 0.02 |
| $x_2$ | 0.01 | | 0.1 |
| $x_3$ | 0.02 | 0.1 | |

C

| | $x_1$ | $x_2$ | $x_3$ |
|---|---|---|---|
| $x_1$ | | 0.11 | 0.22 |
| $x_2$ | 0.11 | | 0.16 |
| $x_3$ | 0.22 | 0.16 | |

clustering approach in an additional analytical step. This is done by calculating the haversine distance between the average coordinates of the samples, expressed in kilometres. These distances are then scaled by a factor of 0.00005, such that 1000 km corresponds to a value of 0.05. As a result, the maximum geographical distance between any two sample averages in the dataset – approximately 4000 km – contributes an additional 0.2 to the morphometric distance metric.

By applying chronological and spatial constraints to the clustering analyses, this approach approximates what Spaulding (1953, 305), who employed a quantitative, formal approach to critique traditional notions – subjective classifications – of artefact typology, emphasising a more empirical basis for defining types, termed "real types".

## 3.4 VISUALISING METHODS

To visualise key morphometric results beyond raw numbers and simple data plots, this study employs Geometric morphometrics (GMM). GMM is a set of methods for quantifying and analysing shapes using geometry rather than just simple linear measurements. Instead of measuring distances, angles, or ratios separately, GMM captures the overall geometry of a structure so that it can statistically be analysed (Rohlf & Marcus 1993).

Building on the seminal work of Thompson (1945), GMM has become a widely applied method in modern biology for estimating structural changes in species based on topology (e.g., Machado et al. 2025). Its application in archaeology has also increased in recent years (Archer et al. 2016; Weiss et al. 2018; Hoggard et al. 2019; Delpiano & Uthmeier 2020; Leplengeon et al. 2020; Weiss 2020; Matzig et al. 2021; Falcucci et al. 2022; Timbrell et al. 2022; Bischoff 2023; Rossini et al. 2023; Tsirintoulaki et al. 2023), particularly due to the availability of user-friendly code scripts (Bonhomme et al. 2014).

In this study, GMM is used exclusively for visualisation purposes. To this end, meanshapes are calculated (Claude 2008) from respective outlines of the SPs recorded with PyREnArA. It is important to highlight that the meanshape-approach utilises a Procrustes and Elliptic Fourier analysis, which translates, rotates, and scales shapes to achieve the best possible alignment (Claude 2008, 156–166). While this analysis effectively captures and preserves shape characteristics, it does not account for size variation. As a result, all generated meanshapes are standardised to the same size, which facilitates shape comparison but obscures potential size-related differences. It must also be emphasised that both the number of outlines and the degree of shape variation among them strongly influence the resulting meanshape. A large sample of highly similar outlines will produce a much smoother meanshape than a small sample with considerable shape differences.

# 4. RESULTS

In order to investigates the morphological ariation of SPs over time and its relationship to chronological change, two complementary analytical frameworks are employed: a chronologically informed approach, which focuses exclusively on temporal patterns without considering taxonomic assignment or geographical distribution, and an archaeo-stratigraphically informed approach, which integrates all available contextual information. This dual methodology facilitates the identification of overarching evolutionary trends across the examined timeframe, while simultaneously assessing the extent to which established archaeological taxonomic units shape morphometric variation. In a subsequent step, morphological relationships are explored more broadly, independent of strict chronological constraints.

## 4.1 RESULTS ON THE 'CHRONOLOGICALLY INFORMED' PERSPECTIVE

This chapter is dedicated solely to tracking variation over time and identifying fundamental chronological processes. To this end, it intentionally excludes taxonomic units and geographical locations, focusing exclusively on the chronological positioning of the analysed assemblages. By doing so, the influence of individual assemblages is deliberately minimised to prioritise the identification of broader, overarching patterns. This approach necessarily involves some degree of generalisation, relying primarily on average values while recognising that variation within the data is only partially captured. While this focus on chronological patterns is methodologically justifiable, the exclusion of taxonomic units and geographical positions introduces limitations. Morphometric changes may be significantly influenced by regional or taxonomic factors, which could confound or even drive the observed chronological variation. These aspects will, however, be addressed in greater detail in Chapter 4.2 to provide a more comprehensive analysis. This layered approach ensures that each dimension – chronology, taxonomy, and geographic location – is properly understood before integrating them into a holistic interpretation. By acknowledging its limitations and transparently presenting the scope of this analysis, this chapter lays the groundwork for identifying the fundamental chronological processes shaping morphometric variation.

### 4.1.1 Redundancy Analysis

Redundancy Analysis (RDA) is applied to assemblages of the dataset class I, categories A and B. The primary aim is to assess the extent to which the passage of time explains variation and thereby determines the timing of chronologically directed changes in morphometric features, including width, length, area, l-w-index, upper-lower-ratio, left-right-ratio, tip angle, MP-CM-x- and y-offset. Therefore, the calibrated ages ('ka calBP') of the examined assemblages are utilised as the canonical variable. To assess whether a coarser temporal scale affects the results obtained from precise chronological positions (calibrated ages), additional analyses were conducted using millennium BP as the temporal variable. The results were then compared to those based on calibrated ages to evaluate their robustness.

#### *4.1.1.1 Entire Investigated Period*

In a first step, the entirety of the dated assemblages in the dataset class I, categories A and B is analysed for the explanatory power of the canonical variable – the calibrated ages of all examined assemblages – in explaining the variation in the morphometric features. RDA indicates that 2.89% of the variation in the morphometric features can be highly significantly ($p = 0.001$) explained by the passage of time. When limiting the analysis to category A assemblages, 2.85% of the variation in the morphometric features can be explained with high significance ($p = 0.001$). Although the proportions of explained variation are low, these findings confirm that chronologically directed changes in the morphometry of this projectile point type occurred over the entire timeframe of SPs in Europe. This challenges the notion of SPs as a fixed, unchanging unit, suggested by the uniform use of the typological term 'shouldered point'. However, it is im-

portant to note that these results reflect only linear changes across the observed period. This means more complex dynamics, such as trends, counter-trends, or periods of stasis, which could exhibit higher or lower explanatory power, are obscured. To gain deeper insights into the temporal dynamics at play and to address further questions as of when, how fast, in which mode and in which features SPs change, it is necessary to focus on smaller, well-defined analytical units within the dataset.

### *4.1.1.2 Periodisation*

In the next step, the dataset is subdivided into arbitrary periods of different lengths, ranging from a coarse chronological resolution with periods spanning 5000 years, gradually decreasing in increments of 1000 years, down to periods of 1000 years. Doing so, it is not only tried to investigate for the timing and the length of chronologically directed trends, but to identify the optimal length of the observation periods for subsequent analysis in order to avoid an a priori determination.

#### *4.1.1.2.1 5000 year Periodisation*

By subdividing the dataset on a coarse scale with sections spanning 5000 years, four distinct sections emerge. With the exception of the youngest 5000 year section, the number of assemblages within each section is distributed relatively evenly. The specimen count in each section is generally high, with the final section yielding the largest number of specimens. *(Figure 12)*

The first 5000 year section ranges from the 30th to the 26th millennium BP. It comprises a total amount of 79 SPs from 22 assemblages, of which 16 yield multiple complete or nearly complete specimens (A-63–A-48) and six only a single specimen (B-25–B-20). Applying RDA to the entirety of the class I assemblages of this section, the calibrated ages as canonical variable explain only 2.4% ($R^2$ = 0.0241) of the variation in the morphometrical features. The result is not significant (p = 0.096). Applying RDA to the category A assemblages of this section only, the result is not altered much ($R^2$ = 0.0268, p = 0.08) (Appendix Table 1).

The second 5000 year section ranges from the 26$^{th}$ to the 22$^{nd}$ millennium BP. It comprises a total amount of 112 SPs from 25 assemblages, of which 20 yield multiple complete or nearly complete specimens (A-50–A-31) and five only a single specimen (B-19–B-15). Applying RDA to the entirety of the class I assemblages of this section, the calibrated ages as canonical variable highly significantly (p = 0.006) explain 3.7% ($R^2$ = 0.0365) of the variation in the morphometrical features. Applying RDA to the category A assemblages of this section only, the result is not altered much ($R^2$ = 0.0379, p = 0.003) (Appendix Table 1).

The third 5000 year section ranges from the 22nd to the 18th millennium BP. It comprises a total amount of 78 SPs from 15 assemblages, of which 11 yield multiple complete or nearly complete specimens (A-34–A-24) and four only a single specimen (B-14–B-11). Applying RDA to the entirety of the class I assemblages of this section, the calibrated ages as canonical variable significantly (p = 0.025) explain 3.5% ($R^2$ = 0.0349) of the variation in the morphometrical features. Applying RDA to the category A assemblages of this period only, the result is not altered much ($R^2$ = 0.0347, p = 0.029) (Appendix Table 1).

The fourth 5000 year section ranges from the 18th to the 14th millennium BP. It comprises a total amount of 154 SPs from 35 assemblages, of which 24 yield multiple complete or nearly complete specimens (A-24–A-1) and 11 only a single specimen (B-11–B-1). Applying RDA to the entirety of the class I assemblages of this section, the calibrated ages as canonical variable explain only 1% ($R^2$ = 0.0108) of the variation in the morphometrical features. The result is not significant (p = 0.146). Applying RDA to the category A assemblages of this section only, the result is not altered much ($R^2$ = 0.0117, p = 0.134) (Appendix Table 1).

The RDA values – the amount of variation in the morphometric features explainable by the passage of time – is comparably low in all four periods. Two sections on the 5000 year periodisation returned a significant result in RDA: the section from the 26$^{th}$ to the 22$^{nd}$ millennium BP and the subsequent section from the 22$^{nd}$ to the 18$^{th}$ millennium BP. The number of specimens and assemblages that were taken into account for the older section (26$^{th}$–22$^{nd}$ millennium BP) is quite large and rather evenly distributed chronologically, so that the result can be accepted not only mathematically but also archaeologically as a period, in which SPs

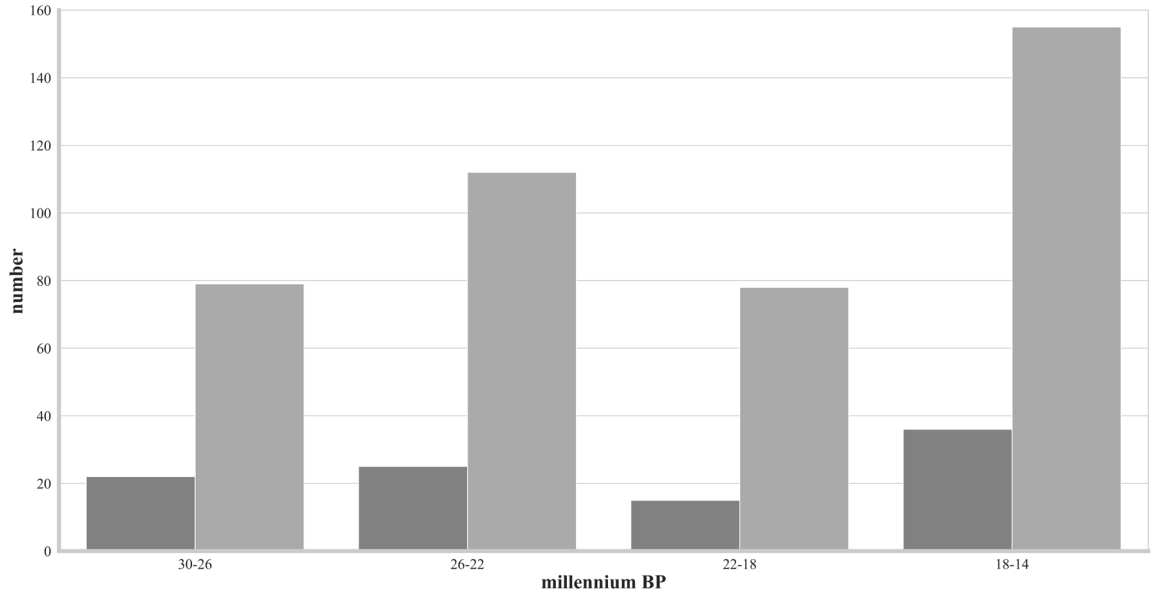



Figure 12: Number of assemblages and artefacts per 5000-year section (dark grey, left bar = assemblages; light grey, right bar = artefacts).

have been subject to chronologically directed change in morphometry. The section from the 22nd to the 18th millennium BP yielded a sufficient sample size too, but most of the assemblages date to the oldest three millennia, which might have an impact on the result. Surprisingly, no changes are calculatable for the youngest period from the 18th to the 14th millennium BP, even though the dataset for this section is by far the largest. The lack of variation that is explainable by the passage of time therefore must be taken seriously and signalises a 5000 year lasting period of apparently no chronologically directed changes in the morphometry of SPs. The reduction of the dataset to category A assemblages only, only had a weak effect on the results of the RDA. *(Table 5, Figure 13)*

If 'millennium BP' – the millennia, in which the respective assemblages are dated – are used as the canonical variable in the RDA instead of the calibrated ages, the results remain largely unchanged (Appendix Table 2). For the first 5000 year section, the analysis still does not yield a significant result ($p = 0.066$), with the explained variation in the morphometric features remaining low ($R^2 = 0.0256$). In the second 5000 year section, the use of 'millennium BP' returns a significant result ($p = 0.001$), with a marginally higher explanatory power ($R^2 = 0.0418$), compared to the calibrated ages. Conversely, in the third 5000 year section, the result is weaker ($R^2 = 0.0265$) when 'millennium BP' is used as the canonical variable, and returns as not significant ($p = 0.075$). The same pattern is observed in the fourth 5000 year section, where using 'millennium BP' as the canonical variable yields an almost negligible explained variation ($R^2 = 0.0091$) and no significance ($p = 0.278$). While the proportions of explained variation shift slightly when 'millennium BP' is used as the canonical variable, the overall pattern identified by the RDA analysis with the calibrated ages as the canonical variable is effectively replicated.

#### *4.1.1.2.2 4000 year Periodisation*

By subdividing the dataset into sections spanning 4000 years, five distinct sections emerge. Given that the total observed timeframe spans 17 millennia, the first section in this periodisation corresponds to the first 5000 year section, ranging from the 30th to the 26th millennium BP, in order to accomodate the supernumerary millenium resulting from this subdivision.. Both the number of assemblages and specimens are distributed relatively evenly across the first three 4000 year sections. Following a notable decline in both assemblage and spec-

Table 5: RDA results for the 5000-year periodisation with calibrated ages ('ka calBP') as canonical variable for all Class I assemblages (dark red = p ≤ 0.05).

| mil. BP | 30th–26th | 26th–22th | 22th–18th | 18th–14th |
|---|---|---|---|---|
| SPs | 79 | 112 | 78 | 154 |
| assemblages | 22 | 25 | 15 | 35 |
| p | 0.096 | 0.006 | 0.025 | 0.146 |
| $R^2$ | 0.0241 | 0.0365 | 0.0349 | 0.0108 |

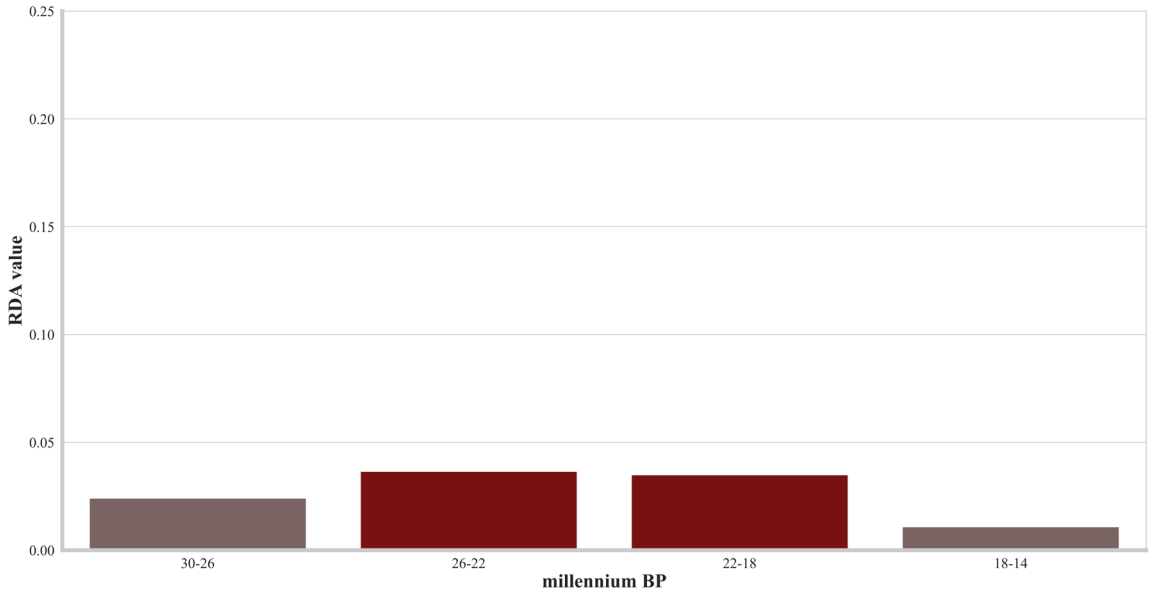



Figure 13: RDA values ($R^2$) for the 5000-year periodisation with calibrated ages ('ka calBP') as canonical variable for all Class I assemblages (dark red = p ≤ 0.05, pale red = p > 0.05).

imen numbers in the section from the 20th to the 17th millennium BP, the numbers increase significantly in the final 4000 year section. (*Figure 14*)

The second 4000 year section ranges from the 26th to the 23rd millennium BP. It comprises a total amount of 87 SPs from 21 assemblages, of which 16 yield multiple complete or nearly complete specimens (A-50–A-35) and five only a single specimen (B-19–B-15). Applying RDA to the entirety of the class I assemblages of this section, the calibrated ages as canonical variable highly significantly explain 4.4% of the variation in the morphometrical features (p = 0.003, $R^2$ = 0.0435). Applying RDA to the category A assemblages of this section only, the result is not altered much ($R^2$ = 0.0445, p = 0.004) (Appendix Table 3).

The third 4000 year section ranges from the 23rd to the 20th millennium BP. It comprises a total amount of 90 SPs from 15 assemblages, of which twelve yield multiple complete or nearly complete specimens (A-36–A-25) and three only a single specimen (B-15–B-13). Applying RDA to the entirety of the class I assemblages of this section, the calibrated ages

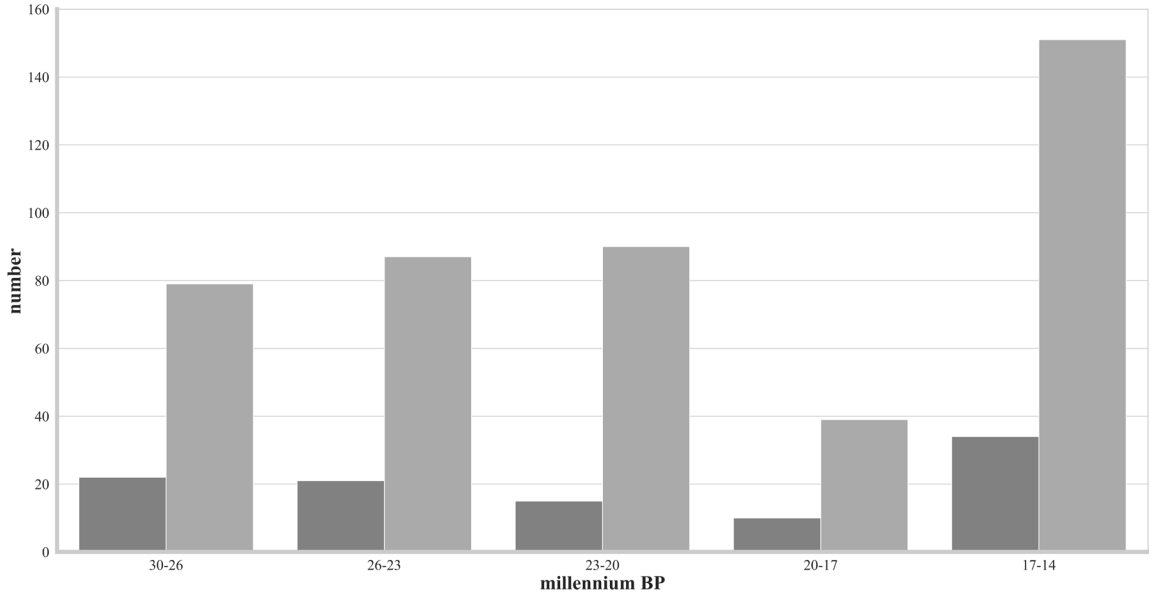



Figure 14: Number of assemblages and artefacts per 4000-year section (dark grey, left bar = assemblages; light grey, right bar = artefacts).

as canonical variable significantly explain 3.8% of the variation in the morphometrical features ($p = 0.006$, $R^2 = 0.0379$). Applying RDA to the category A assemblages of this section only, the result is not altered much ($R^2 = 0.0353$, $p = 0.013$) (Appendix Table 3).

The fourth 4000 year section ranges from the 20th to the 17th millennium BP. It comprises a total amount of 39 SPs from ten assemblages, of which six yield multiple complete or nearly complete specimens (A-27–A-22) and four only a single specimen (B-14–B-11). Applying RDA to the entirety of the class I assemblages of this section, the calibrated ages as canonical variable significantly explain 6.6% of the variation in the morphometrical features ($p = 0.037$, $R^2 = 0.0655$). Applying RDA to the category A assemblages of this section only, the result is a bit stronger ($R^2 = 0.0707$, $p = 0.037$) (Appendix Table 3).

The fifth 4000 year section ranges from the 17th to the 14th millennium BP. It comprises a total amount of 150 SPs from 33 assemblages, of which 23 yield multiple complete or nearly complete specimens (A-23–A-1) and ten only a single specimen (B-10–B-1). Applying RDA to the entirety of the class I assemblages of this section, the calibrated ages as canonical variable explain only 1% ($R^2 = 0.0098$) of the variation in the morphometrical features. The result is not significant ($p = 0.182$). Applying RDA to the category A assemblages of this section only, the result is not altered much ($R^2 = 0.0114$, $p = 0.153$) (Appendix Table 3).

In comparison to the previous periodisation (5000 year periodisation) the result has not changed intensely for the older part of the dataset. It is still shown, that the period from the 26th millennium BP onwards seems to be a time of chronologically directed changes in the morphometry of the SPs, even though the period under consideration is 1000 years shorter here. What is added is the high value for the section from the 20th to the 17th millennium BP. Still, the youngest section from the 17th to the 14th millennium BP does not show any chronologically directed changes over the observed timeframe of 4000 years while being the by far best represented section. The reduction of the dataset to category A assemblages only, again, did not had a strong effect on the results of the RDA. *(Table 6, Figure 15)*

If 'millennium BP' – the millennia, in which the respective assemblages are dated – are used as the canonical variable in the RDA in-

stead of the calibrated ages, the results remain largely unchanged (Appendix Table 4). In the second 4000 year section (26th–23rd millennium BP), 'millennium BP' shows an only slightly higher explanatory power ($R^2$ = 0.0553) compared to the calibrated ages, while remaining significant (p = 0.003). The same applies to the third (23rd–20th millennium BP) ($R^2$ = 0.0385, p = 0.009) and the fourth 4000 year section (20th–17th millennium BP) ($R^2$ = 0.0688, p = 0.025). In the fifth 4000 year section (17th–14th millennium BP), the explanatory power for 'millennium BP' is lower ($R^2$ = 0.0083) and also not significant (p = 0.281). Overall, while there are slight shifts in the proportions of explained variation when using 'millennium BP' instead of the calibrated ages, the general pattern and significances remain unchanged.

#### *4.1.1.2.3 3000 year Periodisation*

By subdividing the dataset into sections spanning 3000 years, a total of eight sections emerge. Starting from the oldest section, the number of assemblages and specimens increases steadily until the section from the 24th to the 22nd millennium BP. Following a slight decline, the counts drop sharply for the sec-

Table 6: RDA results for the 4000-year periodisation with calibrated ages ('ka calBP') as canonical variable for all Class I assemblages (dark red = p ≤ 0.05).

| mil. BP | 30th–26th | 26th–23rd | 23rd–20th | 20th–17th | 17th–14th |
|---|---|---|---|---|---|
| SPs | 79 | 87 | 90 | 39 | 150 |
| assemblages | 22 | 21 | 15 | 10 | 33 |
| p | 0.096 | 0.003 | 0.006 | 0.037 | 0.182 |
| $R^2$ | 0.0241 | 0.0435 | 0.379 | 0.655 | 0.0098 |

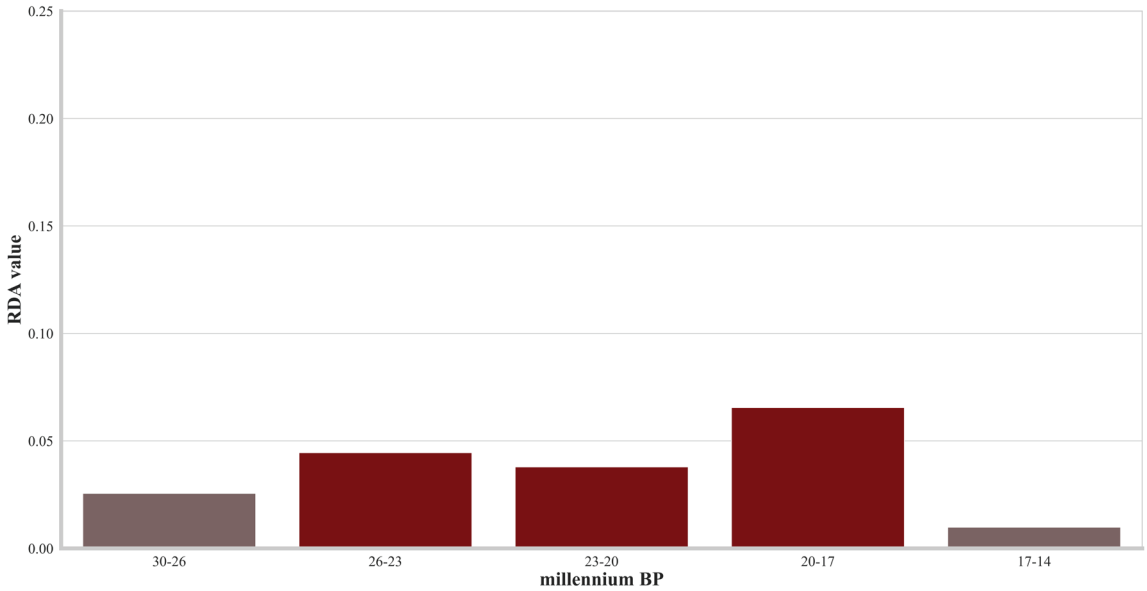



Figure 15: RDA values ($R^2$) for the 4000-year periodisation with calibrated ages ('ka calBP') as canonical variable for all Class I assemblages (dark red = p ≤ 0.05, pale red = p > 0.05).

tion from the 20th to the 18th millennium BP. In the subsequent section from the 18th to the 16th millennium BP, the numbers rise again. The youngest section shows the highest counts by far. *(Figure 16)*

The first 3000 year section ranges from the 30th to the 28th millennium BP. It comprises a total amount of 42 SPs from 13 assemblages, of which nine yield multiple complete or nearly complete specimens (A-63–A-55) and four only a single specimen (B-25–B-22). Applying RDA to the entirety of the class I assemblages of this section, the calibrated ages as canonical variable explain only 2.1% ($R^2$ = 0.0208) of the variation in the morphometrical features. The result is not significant (p = 0.494). Applying RDA to the category A assemblages of this section only, the result is not altered much ($R^2$ = 0.0201, p = 0.605) (Appendix Table 5).

The second 3000 year section ranges from the 28th to the 26th millennium BP. It comprises a total amount of 63 SPs from 16 assemblages, of which twelve yield multiple complete or nearly complete specimens (A-59–A-48) and four only a single specimen (B-23–B-20). Applying RDA to the entirety of the class I assemblages of this section, the calibrated ages as canonical variable explain only 3.2% ($R^2$ = 0.032) of the variation in the morphometrical features. The result is not significant (p = 0.084). Applying RDA to the category A assemblages of this section only, the result is not altered much ($R^2$ = 0.0334, p = 0.085) (Appendix Table 5).

The third 3000 year section ranges from the 26th to the 24th millennium BP. It comprises a total amount of 70 SPs from 18 assemblages, of which 14 yield multiple complete or nearly complete specimens (A-50–A-37) and four only a single specimen (B-19–B-16). Applying RDA to the entirety of the class I assemblages of this section, the calibrated ages as canonical variable significantly explain 4.2% of the variation in the morphometrical features (p = 0.023, $R^2$ = 0.0417). Applying RDA to the category A assemblages of this section only, the result is not altered much ($R^2$ = 0.0431, p = 0.027) (Appendix Table 5).

The fourth 3000 year section ranges from the 24th to the 22nd millennium BP. It comprises a total amount of 79 SPs from 18 assemblages, of which 15 yield multiple complete or nearly complete specimens (A-45–A-31) and three only a single specimen (B-15–B-13). Applying RDA to the entirety of the class I assemblages of this section, the calibrated ages as

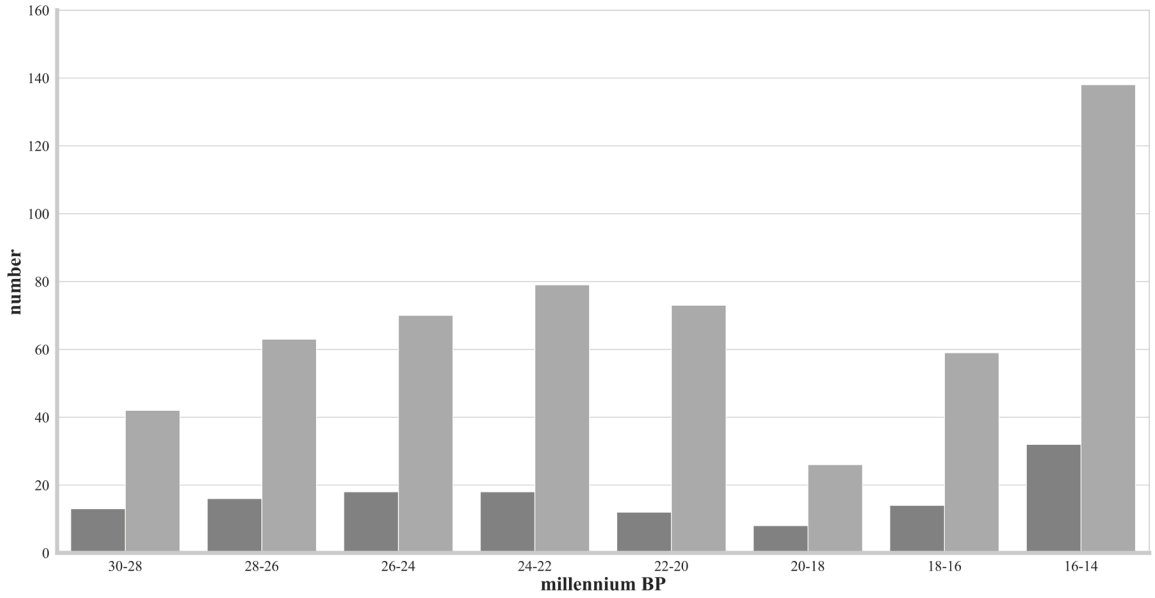



Figure 16: Number of assemblages and artefacts per 3000-year section (dark grey, left bar = assemblages; light grey, right bar = artefacts).

canonical variable significantly explain 3.9% of the variation in the morphometrical features ($p = 0.007$, $R^2 = 0.0385$). Applying RDA to the category A assemblages of this section only, the result is not altered much ($R^2 = 0.0405$, $p = 0.018$) (Appendix Table 5).

The fifth 3000 year section ranges from the 22nd to the 20th millennium BP. It comprises a total amount of 73 SPs from 12 assemblages, of which ten yield multiple complete or nearly complete specimens (A-34–A-25) and two only a single specimen (B-14 & B-13). Applying RDA to the entirety of the class I assemblages of this section, the calibrated ages as canonical variable significantly explain 4.7% of the variation in the morphometrical features ($p = 0.008$, $R^2 = 0.0472$). Applying RDA to the category A assemblages of this section only, the result is not altered much ($R^2 = 0.0507$, $p = 0.01$) (Appendix Table 5).

The sixth 3000 year section ranges from the 20th to the 18th millennium BP. It comprises a total amount of 26 SPs from eight assemblages, of which four yield multiple complete or nearly complete specimens (A-27–A-24) and four only a single specimen (B-14–B-11). Applying RDA to the entirety of the class I assemblages of this section, the calibrated ages as canonical variable explain only 1.7% ($R^2 = 0.0173$) of the variation in the morphometrical features. The result is not significant ($p = 0.837$). Applying RDA to the category A assemblages of this section only, the result is much stronger but not significant also ($R^2 = 0.0573$, $p = 0.309$) (Appendix Table 5).

The seventh 3000 year section ranges from the 18th to the 16th millennium BP. It comprises a total amount of 59 SPs from 14 assemblages, of which ten yield multiple complete or nearly complete specimens (A-24–A-15) and four only a single specimen (B-11–B-8). Applying RDA to the entirety of the class I assemblages of this section, the calibrated ages as canonical variable highly significantly explain 14.4% of the variation in the morphometrical features ($p = 0.001$. $R^2 = 0.1437$). Applying RDA to the category A assemblages of this section only, the result is not altered much ($R^2 = 0.1413$, $p = 0.001$) (Appendix Table 5).

The eighth 3000 year section ranges from the 16th to the 14th millennium BP. It comprises a total amount of 59 SPs from 31 assemblages, of which ten yield multiple complete or nearly complete specimens (A-24–A-15) and four only a single specimen (B-11–B-8). Applying RDA to the entirety of the class I assemblages of this section, the calibrated ages as canonical variable highly significantly explain 3.3% of the variation in the morphometrical features ($p = 0.003$, $R^2 = 0.0326$). Applying RDA to the category A assemblages of this section only, the result is a bit stronger ($R^2 = 0.0431$, $p = 0.002$), but is still comparably weak (Appendix Table 5).

Setting the periodisation to 3000 years, the two oldest sections remain not significant. As for the periodisation before, the period from the 26th to the 20th millennium BP is further identified as a time when pronounced chronologically directed changes are taking place. As suggested by the not significant results in this period for the previous periodisation (4000 year periodisation), the section between the 20th and the 18th millennium BP lacks significance. Notable directed change in the morphometric features seems to happen in the period from the 18th to the 16th millennium BP, potentially driving the strong result calculated for the previous periodisation. As there are not a lot of assemblages dating within the 18th and the 17th millennium BP, the reliability of this result is questionable from an archaeological point of view. The youngest section from the 16th to the 14th millennium BP returns a weak but significant result, indicating some minor chronologically directed trends taking place in this period within 3000 years.

The reduction of the dataset to category A assemblages only, again, did not had a strong effect on the results of the RDA. The only exception from that is the section from the 20th to the 18th millennium BP, where explanatory power of the calibrated ages is much higher when excluding the single specimens. This, however, is most likely due to the low sample size (19th millennium BP is not represented in the category A assemblages).

When 'millennium BP' is used as the canonical variable in the RDA instead of the calibrated ages, the results remain largely consistent with the previous analysis (Appendix Table 6). In the first 3000 year section (30th–28th millennium BP), 'millennium BP' yields a slightly stronger but still not significant result ($R^2 = 0.0463$, $p = 0.098$). In the second 3000 year section (28th–26th millennium BP), the result is weaker ($R^2 = 0.0273$) compared to the results with

the calibrated ages as canonical variable and also not significant (p = 0.126). For the third 3000 year section (26th–24th millennium BP), 'millennium BP' explain 6.2% ($R^2$ = 0.0623, p = 0.003) of the variation, a result that is well stronger than with the calibrated ages as canonical variable. Similarly, in the fourth 3000 year section (24th–22nd millennium BP), 'millennium BP' highly significantly (p = 0.001) explain 6 % ($R^2$ = 0.0538) of the variation, a result well stronger than with the calibrated ages. In the fifth 3000 year section (22nd–20th millennium BP), the RDA result with 'millennium BP' as canonical variable is a bit weaker than with the calibrated ages ($R^2$ = 0.0348, p = 0.036). In the sixth section (20th–18th millennium BP), the results with the calibrated ages as canonical variable are well resembled by 'millennium BP' as canonical variable ($R^2$ = 0.0145, p = 0.87). For the seventh section (18th–16th millennium BP), 'millennium BP' significantly (p = 0.001) explain 11.8% ($R^2$ = 0.118) of the variation, which is a bit weaker than with the calibrated ages as canonical variable. Finally, in the eighth section (16th–14th millennium BP), 'millennium BP' highly significantly (p = 0.001) accounts for 3.6% ($R^2$ = 0.0359) of the variation – slightly more than with the calibrated ages as canonical variable. *(Table 7, Figure 17)*

Table 7: RDA results for the 3000-year periodisation with calibrated ages ('ka calBP') as canonical variable for all Class I assemblages (dark red = p ≤ 0.05).

| mil. BP | 30th–28th | 28th–26th | 26th–24th | 24th–22nd | 22nd–20th | 20th–18th | 18th–16th | 16th–14th |
|---|---|---|---|---|---|---|---|---|
| SPs | 79 | 63 | 70 | 79 | 73 | 26 | 59 | 59 |
| assemblages | 22 | 16 | 18 | 18 | 12 | 8 | 14 | 31 |
| p | 0.494 | 0.084 | 0.023 | 0.007 | 0.008 | 0.837 | 0.001 | 0.003 |
| $R^2$ | 0.0208 | 0.032 | 0.0417 | 0.0385 | 0.0472 | 0.0173 | 0.1437 | 0.0326 |

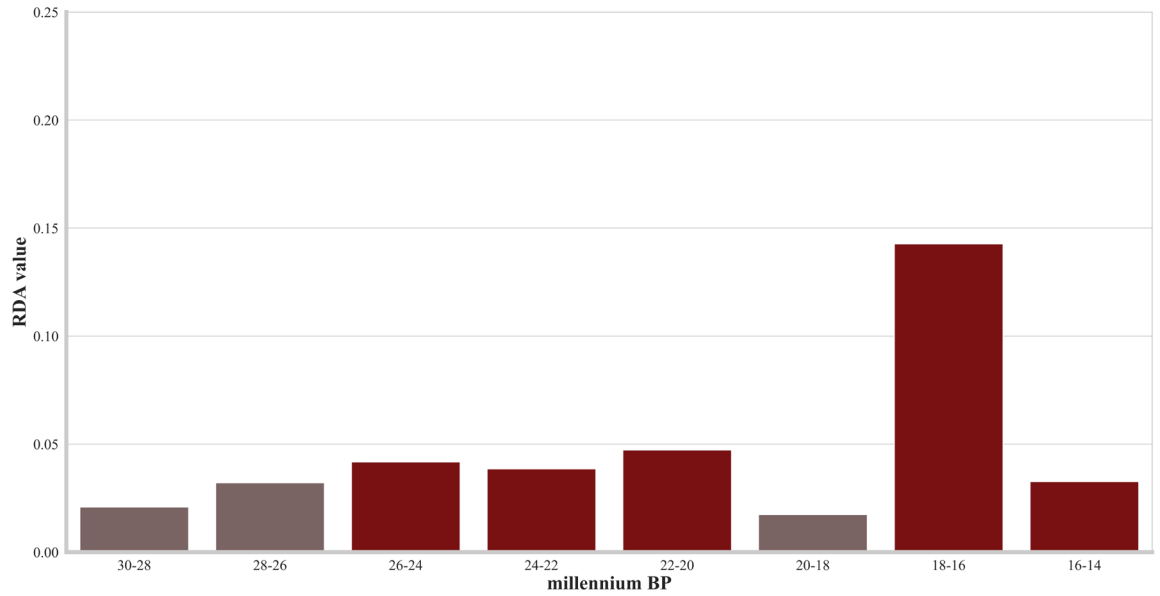



Figure 17: RDA values ($R^2$) for the 3000-year periodisation with calibrated ages ('ka calBP') as canonical variable for all Class I assemblages (dark red = p ≤ 0.05, pale red = p > 0.05).

#### *4.1.1.2.4 2000 year Periodisation*

By subdividing the dataset into sections spanning 2000 years, a total of 16 sections emerge. Following an initial rise in the number of assemblages and specimens up to the section from the 28th to the 27th millennium BP, the numbers begin to decline. Starting from the section from the 25th to the 24th millennium BP, both assemblage and specimen counts remain consistently high for five consecutive sections. However, beginning with the section from the 20th to the 19th millennium BP, the numbers decline sharply. By the section from the 19th to the 18th millennium BP, almost no assemblages or specimens were available to this study. Although still low, the numbers begin to rise again in the section spanning the 18th to the 17th millennium BP. Exceptionally high numbers of both assemblages and specimens are observed in the youngest two sections. *(Figure 18)*

Due to the low number of specimens available for the first 2000 year section ranging from the 30th to the 29th millennium BP – only 16 points from six sites, the calibrated ages as canonical variable does not significantly (p = 0.188) explain the variation in the morphometric features. Especially because for the 29th millennium BP only two assemblages (A-60 and B-24) are available, the high RDA-value of 9.8% ($R^2$ = 0.0979) rather represents the difference in SP morphology of A-60 (Mitoc-Malu Galben, layer 4a) than a chronological trend. Applying RDA to the category A assemblages of this section only, the result is even stronger ($R^2$ = 0.1377, p = 0.115) (Appendix Table 7).

The second 2000 year section ranges from the 29th to the 28th millennium BP. It comprises a total amount of 31 SPs from nine assemblages, of which five yield multiple complete or nearly complete specimens (A-60–A-55) and three only a single specimen (B-24–B-22). Applying RDA to the entirety of the class I assemblages of this section, the calibrated ages as canonical variable explain 3.5% ($R^2$ = 0.0352) of the variation in the morphometrical features. The result however is not significant (p = 0.388). Applying RDA to the category A assemblages of this period only, the calibrated ages, due to the low number of cases not significantly (p = 0.179), explain 5.6% ($R^2$ = 0.0595) of the variation in the morphometric features. As it was stated for the previous section, the 29th millennium BP is represented by only one site yielding multiple specimens, which makes the latter result not resilient (Appendix Table 7).

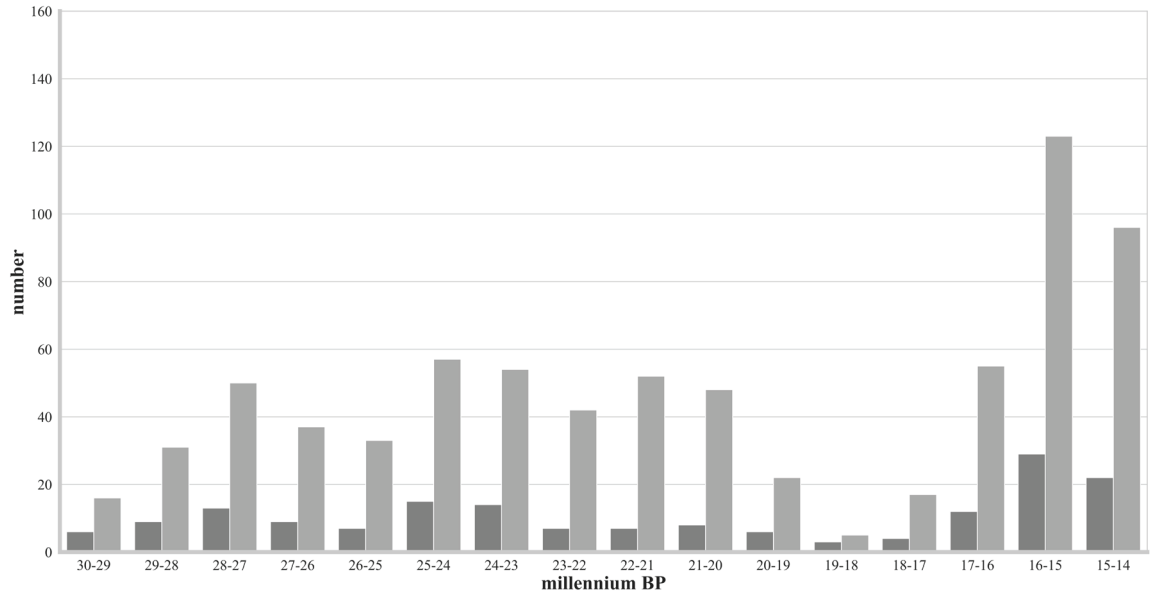



Figure 18: Number of assemblages and artefacts per 2000-year section (dark grey, left bar = assemblages; light grey, right bar = artefacts).

The third 2000 year section ranges from the 28th to the 27th millennium BP. It comprises a total amount of 50 SPs from 13 assemblages, of which nine yield multiple complete or nearly complete specimens (A-59–A-51) and four only a single specimen (B-23–B-20). Applying RDA to the entirety of the class I assemblages of this section, the calibrated ages as canonical variable explain 3.9% ($R^2$ = 0.0386) of the variation in the morphometrical features. The result is not significant (p = 0.087). Applying RDA to the category A assemblages of this section only, the result is slightly stronger and significant ($R^2$ = 0.0461, p = 0.05) (Appendix Table 7).

The fourth 2000 year section ranges from the 27th to the 26th millennium BP. It comprises a total amount of 37 SPs from nine assemblages, of which seven yield multiple complete or nearly complete specimens (A-54–A-48) and two only a single specimen (B-21 & B-20). Applying RDA to the entirety of the class I assemblages of this section, the calibrated ages as canonical variable significantly explain 10.1% of the variation in the morphometrical features (p = 0.002, $R^2$ = 0.1011). Applying RDA to the category A assemblages of this section only, the result is not altered much ($R^2$ = 0.1067, p = 0.003) (Appendix Table 7).

The fifth 2000 year section ranges from the 26th to the 25th millennium BP. It comprises a total amount of 33 SPs from seven assemblages, of which five yield multiple complete or nearly complete specimens (A-50–A-46) and two only a single specimen (B-19 & B-18). Applying RDA to the entirety of the class I assemblages of this section, the calibrated ages as canonical variable significantly explain 11.8% of the variation in the morphometrical features (p = 0.002, $R^2$ = 0.1177). Applying RDA to the category A assemblages of this section only, the result is much stronger ($R^2$ = 0.1467, p = 0.002) (Appendix Table 7).

The sixth 2000 year section ranges from the 25th to the 24th millennium BP. It comprises a total amount of 57 SPs from 15 assemblages, of which 12 yield multiple complete or nearly complete specimens (A-47–A-37) and three only a single specimen (B-19–B-16). Applying RDA to the entirety of the class I assemblages of this section, the calibrated ages as canonical variable significantly explain 7.1% of the variation in the morphometrical features (p = 0.004, $R^2$ = 0.0708). Applying RDA to the category A assemblages of this section only, the result is slightly stronger ($R^2$ = 0.085, p = 0.004) (Appendix Table 7).

The seventh 2000 year section ranges from the 24th to the 23rd millennium BP. It comprises a total amount of 54 SPs from 14 assemblages, of which 11 yield multiple complete or nearly complete specimens (A-45–A-35) and three only a single specimen (B-17–B-15). Applying RDA to the entirety of the class I assemblages of this section, the calibrated ages as canonical variable explain only 2.4% ($R^2$ = 0.0237) of the variation in the morphometrical features. The result is not significant (p = 0.262). Applying RDA to the category A assemblages of this section only, the result is even weaker ($R^2$ = 0.0187, p = 0.437) (Appendix Table 7).

The eighth 2000 year section ranges from the 23rd to the 22nd millennium BP. It comprises a total amount of 42 SPs from seven assemblages, of which six yield multiple complete or nearly complete specimens (A-36–A-31) and one only a single specimen (B-15). Applying RDA to the entirety of the class I assemblages of this section, the calibrated ages as canonical variable explain only 3.5% ($R^2$ = 0.0345) of the variation in the morphometrical features. The result is not significant (p = 0.205). Applying RDA to the category A assemblages of this section only, the result is not altered much ($R^2$ = 0.0322, p = 0.234) (Appendix Table 7).

The ninth 2000 year section ranges from the 22nd to the 21st millennium BP. It comprises a total amount of 52 SPs from seven assemblages, all yielding multiple complete or nearly complete specimens (A-36–A-31). Applying RDA, the calibrated ages as canonical variable significantly (p = 0.008) explain 6.1% ($R^2$ = 0.0613) of the variation in the morphometrical features.

The tenth 2000 year section ranges from the 21st to the 20th millennium BP. It comprises a total amount of 48 SPs from seven assemblages, of which five yield multiple complete or nearly complete specimens (A-30–A-25) and two only a single specimen (B-14 & B-13). Applying RDA to the entirety of the class I assemblages of this section, the calibrated ages as canonical variable significantly explain 7.3% of the variation in the morphometrical features (p = 0.005, $R^2$ = 0.0727). Applying RDA to the category A assemblages of this section only, the result is not altered much ($R^2$ = 0.0758, p = 0.006) (Appendix Table 7).

The eleventh 2000 year section ranges from the 20th to the 19th millennium BP. It comprises a total amount of 22 SPs from six assemblages, of which three yield multiple complete or nearly complete specimens (A-30–A-25) and three only a single specimen (B-14–B-12). Applying RDA to the entirety of the class I assemblages of this section, the calibrated ages as canonical variable explain 8.6% ($R^2$ = 0.086) of the variation in the morphometrical features, but, due to the low number of specimens, the result is not significant (p = 0.085). The number of specimens coming from category A assemblages is too low to conduct a valid calculation.

The twelfth 2000 year section ranges from the 19th to the 18th millennium BP. It comprises a total amount of only five SPs from three assemblages, of which only a single assemblage yields multiple complete or nearly complete specimens (A-24) and two only a single specimen (B-12 & B-11). The low amount of specimens is not enough to conduct a valid calculation.

The thirteenth 2000 year section ranges from the 18th to the 17th millennium BP. It comprises a total amount of only 17 SPs from four assemblages, of which three yield multiple complete or nearly complete specimens (A-24–A-22) and one only a single specimen (B-11). Applying RDA to the entirety of the class I assemblages of this section, the calibrated ages as canonical variable explain 11.3% ($R^2$ = 0.1126) of the variation in the morphometrical features, but, due to the low number of specimens, the result is not significant (p = 0.097). Applying RDA to the category A assemblages of this section only, the result is stronger but also not significant ($R^2$ = 0.1307, p = 0.082) (Appendix Table 7).

The fourteenth 2000 year section ranges from the 17th to the 16th millennium BP. It comprises a total amount of 55 SPs from 12 assemblages, of which nine yield multiple complete or nearly complete specimens (A-23–A-15) and three only a single specimen (B-10–B-8). Applying RDA to the entirety of the class I assemblages of this section, the calibrated ages as canonical variable highly significantly explain 14.7% of the variation in the morphometrical features (p = 0.001, $R^2$ = 0.147). Applying RDA to the category A assemblages of this section only, the result is not altered much ($R^2$ = 0.1489, p = 0.001) (Appendix Table 7).

The fifteenth 2000 year section ranges from the 16th to the 15th millennium BP. It comprises a total amount of 122 SPs from 28 assemblages, of which 19 yield multiple complete or nearly complete specimens (A-21–A-3) and nine only a single specimen (B-10–B-2). Applying RDA to the entirety of the class I assemblages of this section, the calibrated ages as canonical variable highly significantly explain 3.2% of the variation in the morphometrical features (p = 0.009, $R^2$ = 0.0318). Applying RDA to the category A assemblages of this section only, the result is slightly stronger (p = 0.001, $R^2$ = 0.0502) (Appendix Table 7).

The sixteenth 2000 year section ranges from the 15th to the 14th millennium BP. It comprises a total amount of 95 SPs from 21 assemblages, of which 14 yield multiple complete or nearly complete specimens (A-14–A-1) and seven only a single specimen (B-7–B-1). Applying RDA to the entirety of the class I assemblages of this section, the calibrated ages as canonical variable explain only 1.7% ($R^2$ = 0.0171) of the variation in the morphometrical features. The result is also not significant (p = 0.148). Applying RDA to the category A assemblages of this section only, the result is even weaker ($R^2$ = 0.0156, p = 0.222) (Appendix Table 7).

Reducing the periodisation to sections of 2000 years leads to a slightly altered result. Even though the result for the first section is particularly strong, there still seems to be no significant chronologically directed change in the morphometry of SPs taking place at the very beginning of their production and use. Nevertheless, the first weakly chronologically directed changes seem to happen quite early. Against the findings for the previous periodisation (3000 year periodisation), the section from the 27th to the 26th millennium BP returns significant, indicating chronologically directed changes taking place in this early period. The following two sections refine the results of the previous periodisation, indicating quite strongly chronologically directed changes taking place in the period between the 26th and the 24th millennium BP. The period between the 24th and the 22nd millennium BP, that returned significant in the previous periodisation, now subdivided into two sections, does not return significant anymore. Supporting the findings of the previous periodisation, the two sections between the 22nd and the 20th millen-

nium BP both returned comparably weak but significant results. As indicated by the previous periodisation, no chronologically directed changes seem to have taken place in the period between the 20th and the 18th millennium BP. However, besides not returning significant, most likely to the low number of assemblages, especially for the 18th millennium BP, the result for the section from the 18th to the 17th millennium BP is among the highest. The comparably high value for the section from the 17th to the 16th millennium BP suggests that the changes calculated for the previous section from the 18th to the 17th millennium BP are probably rather taking place in the younger millennium. While the section from the 15th to the 14th millennium BP did not yield significant results, the section from the 16th to the 15th millennium BP shows a very weak but significant signal. This suggests that the changes previously identified in the youngest section of the 3000 year periodisation likely occurred at its beginning rather than towards its end. Combining these findings, the overall results suggest a cyclic pattern, characterised by recurring periods, starting with abruptly increasing chronologically directed change, follwed by periods of slow decline. *(Table 8, Figure 19)*

When 'millennium BP' is used as the canonical variable in the RDA instead of the calibrated ages – when the values of the morphometric features of the two subsequent millennia are compared with each other – the results remain largely consistent with the previous analysis, with some notable differences (Appendix Table 8). A significant divergence is observed in the first 2000 year section (30th–29th millennium BP), where RDA with 'millennium BP' as the canonical variable yields an significant ($p = 0.04$) extreme value of 15.5% ($R^2 = 0.1552$) explained variation in the morphometric features. This result, however, is likely heavily influenced by a strong signal from the uniquely shaped SPs of A-60 (Mitoc-Malu Galben, layer 4a: 29th millennium BP). For the second 2000 year section (29th–28th millennium BP), the result with 'millennium BP' shows higher explanatory power ($R^2 = 0.0628$) than with the calibrated ages, but it is still not significant ($p = 0.086$). For the 2000 year section from

Table 8: RDA results for the 2000-year periodisation with calibrated ages ('ka calBP') as canonical variable for all Class I assemblages (dark red = $p \leq 0.05$).

| mil. BP | 30th–29th | 29th–28th | 28th–27th | 27th–26th | 26th–25th | 25th–24th | 24th–23rd | 23rd–22nd |
|---|---|---|---|---|---|---|---|---|
| SPs | 16 | 31 | 50 | 37 | 33 | 57 | 54 | 42 |
| assemblages | 6 | 9 | 13 | 9 | 7 | 15 | 14 | 7 |
| p | 0.188 | 0.388 | 0.087 | 0.002 | 0.002 | 0.004 | 0.262 | 0.205 |
| $R^2$ | 0.0979 | 0.0352 | 0.0386 | 0.1011 | 0.1177 | 0.0708 | 0.0237 | 0.0345 |

| mil. BP | 22nd–21st | 21st–20th | 20th–19th | 19th–18th | 18th–17th | 17th–16th | 16th–15th | 15th–14th |
|---|---|---|---|---|---|---|---|---|
| SPs | 52 | 48 | 22 | 5 | 17 | 55 | 122 | 95 |
| assemblages | 7 | 7 | 6 | 3 | 4 | 12 | 28 | 21 |
| p | 0.008 | 0.005 | 0.085 | / | 0.097 | 0.001 | 0.009 | 0.148 |
| $R^2$ | 0.0613 | 0.0727 | 0.086 | / | 0.1126 | 0.147 | 0.0318 | 0.0171 |

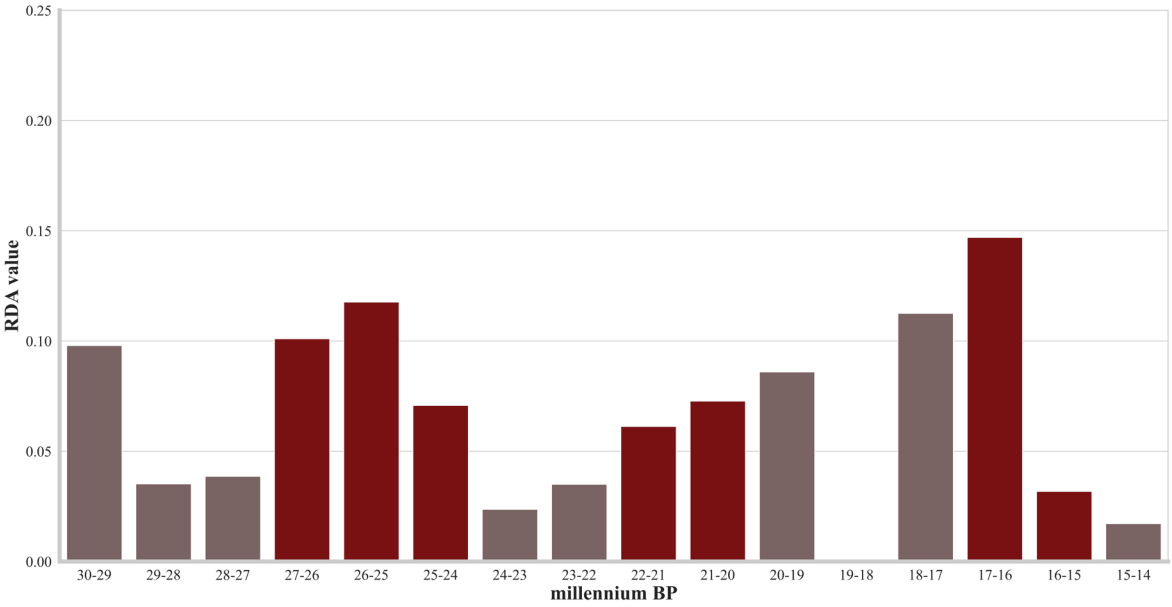



Figure 19: RDA values ($R^2$) for the 2000-year periodisation with calibrated ages ('ka calBP') as canonical variable for all Class I assemblages (dark red = $p \leq 0.05$, pale red = $p > 0.05$).

the 28th to the 27th millennium BP, the results align well, as the explanatory power of 'millennium BP' is only slightly weaker ($R^2$ = 0.0247, p = 0.277). For the section from the 27th to the 26th millennium BP, the explanatory power returns much weaker and not significant ($R^2$ = 0.0515, p = 0.107). The result for the section from the 26th to the 25th millennium BP is a bit weaker ($R^2$ = 0.1057, p = 0.005). Conversely, the result for the section from the 25th to the 24th millennium BP ($R^2$ = 0.0991, p = 0.002) is stronger than with the calibrated ages as canonical variable. The period of apparent lack of chronologically directed change between the 24th and 22nd millennium BP is consistently replicated (24th–23rd millennium BP: R2 = 0.0197, p = 0.418; 23rd–22nd millennium BP: $R^2$ = 0.032, p = 0.233). Also, the results for the two subsequent sections from the 22nd to the 21st millennium BP and from the 21st to the 20th millennium BP are well replicated ($R^2$ = 0.065, p = 0.007; R2 = 0.0705, p = 0.006). No calculations could be conducted for the period between the 20th and the 17th millennium BP due to insufficient sample sizes. The section from the 17th to the 16th millennium BP yields weaker but still significant result ($R^2$ = 0.1207, p = 0.001). The result for section from the 16th to the 15th millennium BP is slightly higher ($R^2$ = 0.0407, p = 0.001). The youngest 2000 year section (15th–14th millennium BP) does not yield significant results, with the explanatory power remaining extremely low ($R^2$ = 0.0063, p = 0.72), just as with the calibrated ages as canonical variable.

#### *4.1.1.2.5 1000 year Periodisation*

Here, the results of the RDA on the *small*est scale – for each of the 17 millennia – are presented. The structure of the dataset was described in the Material Chapter 2.

For the 30th millennium BP 11 SPs from four assemblages, including the oldest SP in the entire dataset from Milovice I, section G (B-25) with an the calibrated ages of 30.0 ka calBP, as well as three assemblages yielding multiple complete or nearly complete specimens (A-63–A-61) are available. RDA implies quite strong explanatory power for the calibrated ages as canonical variable. 11.9% ($R^2$ = 0.156) of the variation in the morphometric features can be explained by the calibrated ages of the four available assemblages. Due to the low amount of specimes, the result is not significant

(p = 0.131) though. Applying RDA to the category A assemblages of this section only, the result is slightly stronger ($R^2$ = 0.1603, p = 0.205) (Appendix Table 9).

The 29th millennium BP comprises only five SPs from two assemblages, of which one yields multiple complete or nearly complete specimens (A-60) and one only a single specimen (B-24). The low amount of specimens are not enough to conduct a valid calculation.

The 28th millennium BP comprises 26 SPs from seven assemblages, of which five yield multiple complete or nearly complete specimens (A-59–A-55) and two only a single specimen (B-23 & B-22). Applying RDA to the entirety of the class I assemblages of this millennium, the calibrated ages as canonical variable significantly (p = 0.043) explain 9.2% ($R^2$ = 0.0917) of the variation in the morphometrical features. Applying RDA to the category A assemblages of this section only, the result is much stronger ($R^2$ = 0.1638, p = 0.005) (Appendix Table 9).

The 27th millennium BP comprises 24 SPs from six assemblages, of which five yield multiple complete or nearly complete specimens (A-54–A-51) and two only a single specimen (B-21 & B-20). Applying RDA to the entirety of the class I assemblages of this millennium, the calibrated ages as canonical variable significantly eplain 11.4% of the variation in the morphometric features (p = 0.015, $R^2$ = 0.1135). Applying RDA to the category A assemblages of this section only, the result is much stronger ($R^2$ = 0.1466, p = 0.005) (Appendix Table 9).

The 26th millennium BP comprises only 13 SPs from only three assemblages, all yielding multiple complete or nearly complete specimens (A-50–A-48). Applying RDA, the calibrated ages as canonical variable significantly eplain 35.7% of the variation in the morphometric features (p = 0.002, $R^2$ = 0.3568).

The 25th millennium BP comprises 20 SPs from only four assemblages, of which two yield multiple complete or nearly complete specimens (A-47 & A-46) and two only a single specimen (B-19 & B-18). Applying RDA to the entirety of the class I assemblages of this millennium, the calibrated ages as canonical variable highly significantly eplain 32.5% of the variation in the morphometric features (p = 0.001, $R^2$ = 0.3254). Applying RDA to the category A assemblages of this section only, the result is even stronger ($R^2$ = 0.367, p = 0.002). These results however rather resemble pronounced differences between the assemblages A-47 and A-46, than chronological directed changes.

The 24th millennium BP comprises 37 SPs from 11 assemblages, of which nine yield multiple complete or nearly completes specimens (A-45–A-37) and two only a single specimen (B-17 & B-16). Applying RDA to the entirety of the class I assemblages of this millennium, the calibrated ages as canonical variable highly significantly eplain 6.5% of the variation in the morphometric features (p = 0.046, $R^2$ = 0.0647). Applying RDA to the category A assemblages of this section only, the result is slightly weaker and not significant ($R^2$ = 0.0597, p = 0.07) (Appendix Table 9).

The 23rd millennium BP comprises only 17 SPs from only three assemblages, of which two yield multiple complete or nearly complete specimens (A-36 & A-35) and one only a single specimen (B-15). Applying RDA to the entirety of the class I assemblages of this millennium, the calibrated ages as canonical variable explain only 2.4% ($R^2$ = 0.0236) of the variation in the morphometrical features. The result is also not significant (p = 0.86). The low amount of specimens in the category A assemblages of this section is not enough to conduct a valid calculation.

The 22nd millennium BP comprises only 25 SPs from only four assemblages, all yielding multiple complete or nearly complete specimens (A-34–A-31). Applying RDA, the calibrated ages as canonical variable highly significantly eplain 22% of the variation in the morphometric features (p = 0.001, $R^2$ = 0.22).

The 21st millennium BP comprises only 27 SPs from only three assemblages, all yielding multiple complete or nearly complete specimens (A-30–A-28). Applying RDA to the entirety of the class I assemblages of this millennium, the calibrated ages as canonical variable explain only 2.1% ($R^2$ = 0.0211) of the variation in the morphometrical features. The result is also not significant (p = 0.764).

The 20th millennium BP comprises only 21 SPs from five assemblages, of which three yield multiple complete or nearly complete specimens (A-27–A-25) and two only a single specimen (B-14 & B-13). Applying RDA to the entirety of the class I assemblages of this millennium, the calibrated ages as canonical variable explain 8.2% ($R^2$ = 0.0819) of the

variation in the morphometrical features. The result, however, is not significant (p = 0.147), most probably due to the low amount of specimens. Applying RDA to the category A assemblages of this section only, the result is much stronger ($R^2$ = 0.1728, p = 0.015) (Appendix Table 9). However, since only three assemblages, of which two dating closely together, were taken into account, the result is to be treated with caution.

As only a single specimen is available for the 19th millennium BP (B-12), no calculations can be conducted.

The low amount of specimens for the 18th millennium BP – only four SPs from two assemblages (A-24 & B-11), are not enough to conduct a valid calculation.

The 17th millennium BP comprises only 13 SPs from only two assemblages (A-23 & A-22). RDA returns not significant ($R^2$ = 0.146, p = 0.139), and rather resembles pronounced difference between the two assemblages than chronological directed changes.

The 16th millennium BP comprises 42 SPs from ten assemblages, of which nine yield multiple complete or nearly complete specimens (A-21–A-15) and three only a single specimen (B-10–B-8). Applying RDA to the entirety of the class I assemblages of this millennium, the calibrated ages as canonical variable highly significantly eplain 15.8% of the variation in the morphometric features (p = 0.001, $R^2$ = 0.1582). Applying RDA to the category A assemblages of this section only, the result is much stronger ($R^2$ = 0.2533, p = 0.001) (Appendix Table 9).

The 15th millennium BP comprises 80 SPs from 18 assemblages, of which twelve yield multiple complete or nearly complete specimens (A-14–A-3) and six only a single specimen (B-7–B-2). Applying RDA to the entirety of the class I assemblages of this millennium, the calibrated ages as canonical variable significantly eplain 3.1% of the variation in the morphometric features (p = 0.035, $R^2$ = 0.0307). Applying RDA to the category A assemblages of this section only, the result is not altered much, but is not significant anymore ($R^2$ = 0.0249, p = 0.104) (Appendix Table 9).

For the 14th millennium BP only 15 SPs from three assemblages (A-2, A-1 & B-1). Applying RDA to the entirety of the class I assemblages of this millennium, the calibrated ages as canonical variable significantly eplain 19.5% of the variation in the morphometric features (p = 0.009, $R^2$ = 0.1946). Applying RDA to the category A assemblages of this section only, the result is slightly stronger ($R^2$ = 0.2054, p = 0.017) (Appendix Table 9). These results, however, rather resemble pronounced differences between the assemblages A-2 and A-1, than chronological directed changes.

Setting the periodisation down to one millennium, relevant patterns seen for the previous periodisation (2000 year periodisation) are supported. Still, the period between the 28th and the 24th millennium BP yields high explanatory values, indicating chronological directed changes taking place, even on the millennium-scale. Also, RDA returned high values for the 16th millennium BP, which coincides with the findings made for the 2000 year section from the 17th to the 16th millennium BP. The significant results for 15th as well as for the 22nd millennium BP also coincide with the findings of the 2000 year periodisation, resembling signals seen before (22nd–21st and 16th–15th millennium BP) are rather taking place in a single millennium. In several millennia, including the 23rd, the 21st and the 20th millennium BP, the calibrated ages exhibit limited explanatory power with non-significant results, suggesting minimal chronological influence. Many other millennia, particularly the 29th, the 19th, and the 18th millennium BP, lacked sufficient data for valid statistical analysis. Even where calculations were feasible, small sample sizes often reduced the robustness and significance of observed trends or indicated high intra-assemblage variation rather than chronologically directed trends (e.g., in the 14th millennium BP).

Reducing the dataset to category A assemblages significantly impacted the RDA results. In millennia with a sufficient number of cases, such as the 28th and the 27th millennium BP, the results were notably strengthened. However, in millennia with insufficient cases, the previously identified issues were exacerbated. Due to the lack of sufficient data for many millennia, the one-millennia-scale proves unsuitable for further investigations, as it fails to provide the statistical robustness required for reliable analysis. *(Table 9, Figure 20)*

The results of the RDA across the different temporal periodisation underscore the complexity of the timing and the duration of diachronic morphometric changes in SPs

across their time of production and use. While chronologically directed trends are evident in certain periods throughout multiple periodisations – most notably between the 26th and the 24th millennium BP, the 22nd and the 20th millennium BP, and between the 17th and the 15th millennium BP – the lack of significant patterns in many other intervals, particularly in the older sections and the youngest section as well as the period from the 24th to the 22nd millennium BP, suggests episodes of stochastic rather than consistently directional change or no change at all. These observations already argue against a linear morphometric evolution in SPs. Moreover, some short-term patterns, particularly those observed in the 1000- and 2000-year intervals within the 26th to 22nd millennium BP timeframe, appear to be segments of longer-term trends captured across all periodisation schemes. In contrast, patterns detected between the 17th and 14th millennium BP do not align with any broader, longer-term trajectories, underscoring the presence of punctuated changes or potentially taxonomically specific morphometric developments.

The comparison to the analysis using 'millennium BP' as the canonical variable underscores the reliability of the results obtained with the calibrated ages ('ka calBP) as the canonical variable. Even when the resolution was coarsened, thereby reducing the emphasis on the fine-chronological positions of individual assemblages, the results were largely replicated, demonstrating the robustness of the original findings. While it might be argued that relying on the calibrated ages could introduce *bias* by overfitting to fine-chronological positions, the consistent outcomes with 'millennium BP' further validate the reliability and generalisability of the results. Also, the results on category A assemblages only were mostly close to the results made for all assemblages, further highlighting the robustness of the conducted analysis. This demonstrates also that the methodology is reliable, flexible and not overly sensitive to minor adjustments in how chronological data is structured.

Table 9: RDA results for the 1000-year periodisation with calibrated ages ('ka calBP') as canonical variable for all Class I assemblages (dark red = $p \leq 0.05$).

| mil. BP | 30th | 29th | 28th | 27th | 26th | 25th | 24th | 23rd |
|---|---|---|---|---|---|---|---|---|
| SPs | 10 | 4 | 24 | 22 | 13 | 18 | 35 | 16 |
| assemblages | 3 | 1 | 5 | 4 | 3 | 2 | 9 | 2 |
| p | 0.205 | / | 0.005 | 0.005 | 0.002 | 0.002 | 0.07 | / |
| $R^2$ | 0.1603 | / | 0.1638 | 0.1466 | 0.3568 | 0.4074 | 0.0597 | / |

| mil. BP | 22nd | 21st | 20th | 19th | 18th | 17th | 16th | 15th | 14th |
|---|---|---|---|---|---|---|---|---|---|
| SPs | 25 | 27 | 19 | / | 3 | 13 | 39 | 74 | 14 |
| assemblages | 4 | 3 | 3 | / | 1 | 2 | 7 | 12 | 2 |
| p | 0.001 | 0.764 | 0.015 | / | / | 0.139 | 0.001 | 0.104 | 0.017 |
| $R^2$ | 0.22 | 0.0211 | 0.1728 | / | / | 0.146 | 0.2533 | 0.0249 | 0.2054 |

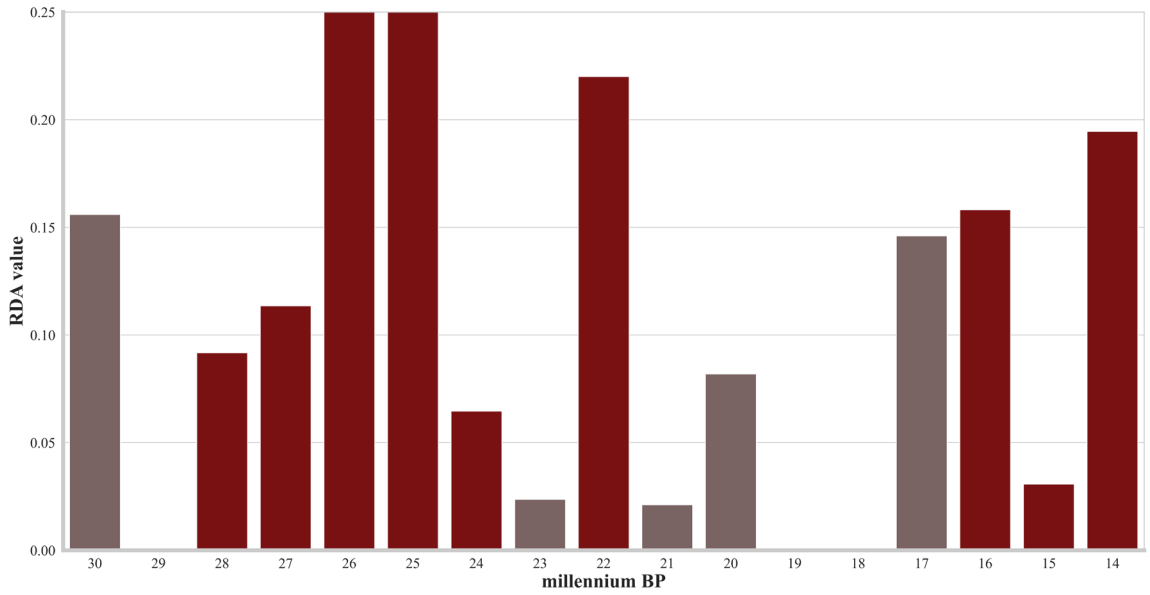



Figure 20: RDA values ($R^2$) for the 1000-year periodisation with calibrated ages ('ka calBP') as canonical variable for all Class I assemblages (dark red = $p \leq 0.05$, pale red = $p > 0.05$).

#### *4.1.1.3 Optimal Periodisation*

These results also highlight the decisive influence of the chosen temporal scale: coarser periodisation tend to obscure shorter-term trends while better capturing long-term developments, whereas finer scales exaggerate short-lived fluctuations, while failing to reflect longer-term dynamics. As an example, the period between the 28th and the 26th millennium BP did not return significant for the 3000 year periodisation, but for the 2000 year and the 1000 year periodisation. At the finest resolution (1000 year periodisation) however, the data for many periods becomes sparse, leading to unreliable or non-significant results due to small sample sizes and overemphasised variation within assemblages.

The 2000 year periodisation seems to strike the best balance between detail and statistical robustness. While avoiding excessive granularity that might complicate interpretations, it is detailed enough to identify relatively short-termed (e.g. 17th–16th millennium BP) as well as long-lasting periods of change (e.g. 28th–24th millennium BP) as well as periods of stasis (22nd–20th millennium BP). It aggregates assemblages effectively, reducing the impact of small sample sizes, ensuring that the results are both archaeologically and mathematically reliable. Also, the offered timeframes are manageable for interpreting the results in a broader context of e.g. taxonomic units or palaeodemography. Thus, the 2000 year resolution is considered to be the most effective arbitrary periodisation for observing diachronic changes in SP morphometry within the examined dataset and will be used in further analysis.

However, the period ranging from the 20th to the 18th millennium BP is poorly represented in both assemblages and specimens within the 2000 year periodisation, making the respective sections unsuitable for further statistical analysis.

### 4.1.2 Coefficient of Variation

After demonstrating that the amount of variation in the morphometric features explained by the passage of time varies significantly across the entire of the observed timeframe, the focus now shifts to analysing the actual amount of variation within each 2000 year section. Therefore the calculation of Coefficients of

Variation (CV) is applied. This analysis serves two purposes: first, it provides a deeper understanding of how variation fluctuates over time; second, it establishes a foundation for subsequent calculations of the rate of change. Sections with high internal variation in morphometric features may indicate potential for changes driven by chronological factors, while sections with low variation could suggest phases of high standardisation in the morphometry of SPs or stasis in chronologically directed change.

The average overall variation in the morphometric features analysable with the CV-method of the entire dataset is 37% ($\bar{x}$ = 0.37) *(Table 10)*. The highest average CV is calculated for the upper-lower-ratio (0.53). The left-right-ratio also yields quite high values resulting in an average of 0.52. L-w-index (0.26) and tip angle (0.27) do not seem to exhibit as much overall variation, neither does width (0.27) and length (0.27). Area, however, seems to vary more on average throughout the entire dataset (0.46).

In the following, each 2000 year period will be analysed separately, while for the 2000 year sections including the 19th and the 18th millennia BP were left out due to the insufficient sample size.

The average of the overall variation for the first section ranging from the 30th to the 29th millennium BP ($\bar{x}$ = 0.41) is higher than the average for the entire dataset and the highest among the RDA not-significant periods. Whereas the CV for the features related to the size of the SPs are particularly low (width = 0.25, length = 0.24, area = 0.34), remaining below the averages of the CV of the respective morphometric features, the values for the features related to the shape are among the highest in the entire dataset. The values for the left-right-ratio (0.75) and the tip angle (0.34) are the highest in the entire dataset. Among the highest in the entire dataset is the CV for the upper-lower-ratio (0.67). The value yielded for the l-w-index (0.29) is well over the average CV of this feature. *(Figure 21)*

The average of the overall variation for the second section ranging from the 29th to the 28th millennium BP is not very different from the previous section and also higher than the average for the entire dataset ($\bar{x}$ = 0.39). Width (0.34) and area (0.54) show the highest CV for the sections not returning significant in the RDA. Also, the value for length (0.3) is among the highest and clearly exceeding the averages of the CV of the respective features. Additionally, this section yields the highest CV for the l-w-index (0.34). The CV for the upper-lower-ratio (0.5) is slightly below the average CV for this feature. The CV value for the tip angle (0.31) is also among the highest values in this feature, exceeding the average value. On the contrary, left-right-ratio (0.4) does not exhibit particular high variation and is far below the average value for this feature. *(Figure 22)*

The average of the overall variation for the third section ranging from the 28th to the 27th millennium BP is more or less equal to the average for the entire dataset ($\bar{x}$ = 0.36). All features related to the size are particularly high, exceeding the averages of the CV of the respective features (width = 0.32, length = 0.3, area = 0.55). Whereas the CV for the l-w-index is the highest within RDA significant sections (0.3), the other morphometric features related to the shape remain below the averages of the CV of the respective features (upper-lower-ratio = 0.41, left-right-ratio = 0.42, tip angle = 0.26). *(Figure 23)*

The average of the overall variation for the fourth section ranging from the 27th to the 26th millennium BP is well higher than the average for the entire dataset ($\bar{x}$ = 0.43). Whereas the CV value yielded for width (0.39) is the highest in the entire dataset and the values for area (0.58) are well over respectively equal to the average CV of the respective feature, the CV yielded for length (0.26) is just below its average CV. Also, the CV yielded for the upper-lower-ratio (0.90) is the highest in the dataset, while the other shape related features are below the averages of the CV of the respective feature (l-w-index = 0.25, left-right-ratio = 0.39, tip angle = 0.25). The extreme value in the upper-lower-ratio within this section however derives from a single assemblage (A-49, Abauntz_03; see Appendix Table 17), marking the oldest assemblage from Iberian Upper Solutrean contexts, yielding three SPs with extreme high upper-lower-ratios. *(Figure 24)*

The average of the overall variation for the fifth section ranging from the 26th to the 25th millennium BP are the highest in the entire dataset ($\bar{x}$ = 0.44). All size-related features

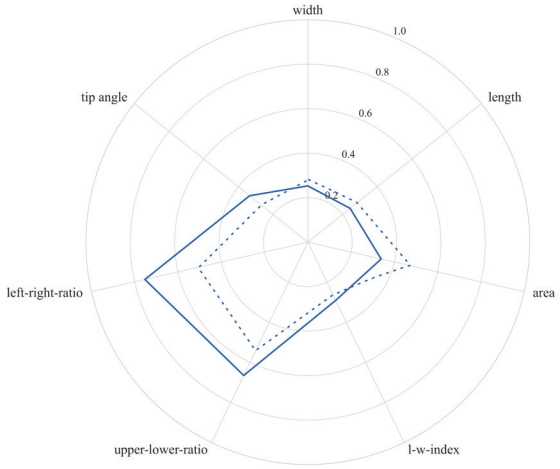



Figure 21: Coefficient of Variation (CV) of morphometric features for the section from the 30th to the 29th millennium BP (dotted line = average CV for the entire dataset).

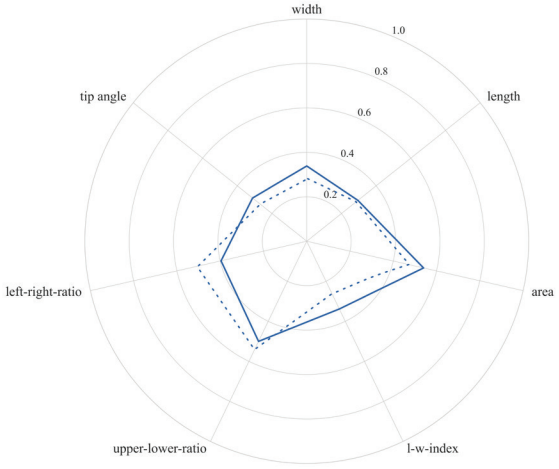



Figure 22: Coefficient of Variation (CV) of morphometric features for the section from the 29th to the 28th millennium BP (dotted line = average CV for the entire dataset).

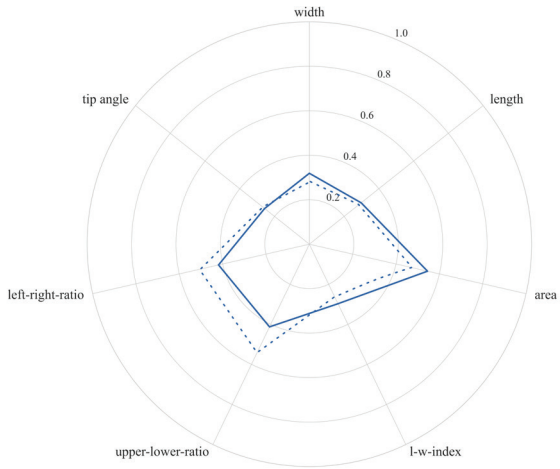



Figure 23: Coefficient of Variation (CV) of morphometric features for the section from the 28th to the 27th millennium BP (dotted line = average CV for the entire dataset).

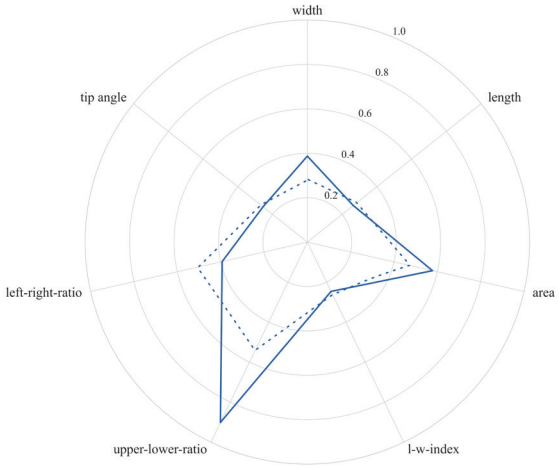



Figure 24: Coefficient of Variation (CV) of morphometric features for the section from the 27th to the 26th millennium BP (dotted line = average CV for the entire dataset).

yield CV among the highest within the respective feature (width = 0.37, length = 0.38, area = 0.56). The CV yielded for the upper-lower-ratio (0.71) is well over the respective average CV. The CV for the tip angle (0.32) is the highest value in this feature for the RDA significant sections. The values for the l-w-index (0.24) and the left-right-ratio (0.48) are just below the average CV for this feature. *(Figure 25)*

The average of the overall variation for the sixth section ranging from the 25th to the 24th millennium BP is well higher than the average for the entire dataset ($\bar{x}$ = 0.4). The CV yielded for length (0.42) and area (0.65) are all the highest for the respective feature in the RDA significant sections. The CV for width (0.32) is well over the respective average CV and among the highest values for width in the entire dataset. All shape-related features are below the respective average CV (l-w-index = 0.25, upper-lower-ratio = 0.47, left-right-ratio = 0.41), except from the tip angle (0.31). *(Figure 26)*

The average of the overall variation for the seventh section ranging from the 24th to the 23rd millennium BP is just above the average for the entire dataset ($\bar{x}$ = 0.37). All size-related features yield CV above the respective average CV (width = 0.28, length = 0.31, area = 0.5). Even if the CV for length is the highest within the not-significant RDA sections, they are well lower than the values for the RDA significant sections. With the exception of the tip angle (0.31), all shape-related features yield CV below the respective average CV (l-w-index = 0.25, upper-lower-ratio = 0.52, left-right-ratio = 0.41). *(Figure 27)*

The average of the overall variation for the eighth section ranging from the 23rd to the 22nd millennium BP is well below the average for the entire dataset ($\bar{x}$ = 0.32). The variation in all morphometric features remains below the average values of the respective feature (width = 0.19, length = 0.25, area = 0.40, l-w-index = 0.22, upper-lower-ratio = 0.44, left-right-ratio = 0.48, tip angle = 0.24). The CV for the l-w-index and the upper-lower-ratio are among the lowest values for the respective feature. *(Figure 28)*

The average of the overall variation for the ninth section ranging from the 22nd to the 21st millennium BP is well below the average for the entire dataset and among the lowest values ($\bar{x}$ = 0.30). The variation in all morphometric features remains well below the average values of the respective feature and are among the lowest in the entire dataset (width = 0.16, length = 0.23, area = 0.35, l-w-index = 0.22, upper-lower-ratio = 0.46, left-right-ratio = 0.44, tip angle = 0.22). The CV for width, l-w-index and the tip angle are the lowest values for the respective feature. *(Figure 29)*

The average of the overall variation for the tenth section ranging from the 21st to the 20th millennium BP is well below the average for the entire dataset and among the lowest values ($\bar{x}$ = 0.31). The variation in all morphometric features remains well below the average values of the respective feature and are among the lowest in the entire dataset (width = 0.22, length = 0.25, area = 0.43, l-w-index = 0.23, upper-lower-ratio = 0.42, left-right-ratio = 0.41, tip angle = 0.23), some of which are among the lowest in the entire dataset. *(Figure 30)*

The average of the overall variation for the fourteenth section ranging from the 17th to the 16th millennium BP is just above the average for the entire dataset ($\bar{x}$ = 0.37). The variation in all size-related features remains well below the average values of the respective feature and are among the lowest in the entire dataset (width = 0.25, length = 0.22, area = 0.38). The CV for the shape-related features however, with the exception of the CV for the tip angle (0.22), are all above the respective average CV (l-w-index = 0.29, upper-lower-ratio = 0.54), including the highest CV for the left-right-ratio within the RDA significant sections (0.7). However, this signal unfortunately is an artefact of PyREnArA, which struggles to properly orient some of the SPs from the last three millennia. These SPs are characterised by a straight back opposing the notch and a straight base, leading to them being tilted. Therefore, these signals can be disregarded at this stage. *(Figure 31)*

The average of the overall variation for the fifteenth section ranging from the 16th to the 15th millennium BP is below the average for the entire dataset ($\bar{x}$ = 0.34). The left-right-ratio yields a comparably high CV (0.68). However, as discussed in the previous section, this is likely not of analytical significance. Also, the CV for the l-w-index (0.28) is well above the average CV. The CV for the upper-lower-ratio (0.54) is just above the average CV.

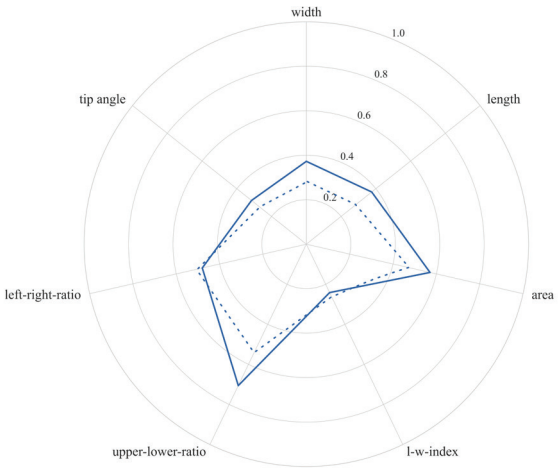



Figure 25: Coefficient of Variation (CV) of morphometric features for the section from the 26th to the 25th millennium BP (dotted line = average CV for the entire dataset).

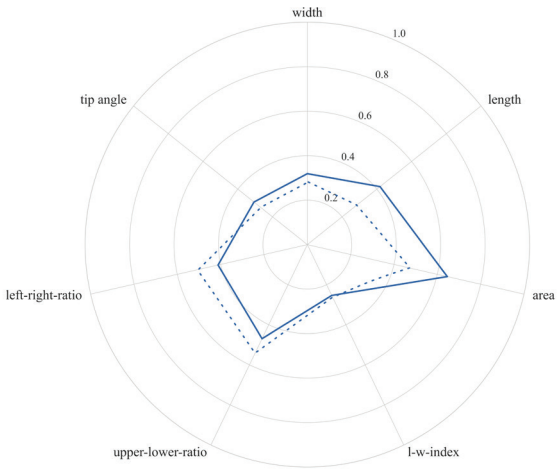



Figure 26: Coefficient of Variation (CV) of morphometric features for the section from the 25th to the 24th millennium BP (dotted line = average CV for the entire dataset).

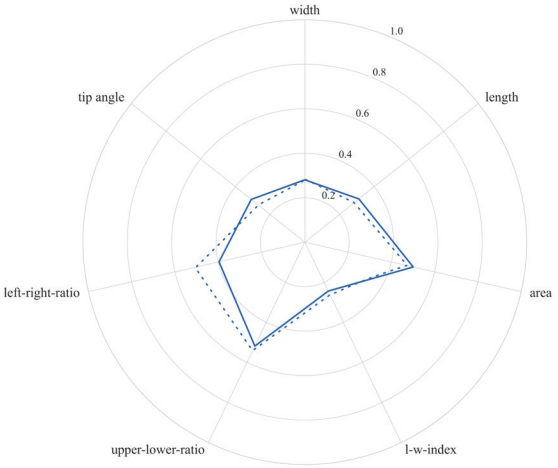



Figure 27: Coefficient of Variation (CV) of morphometric features for the section from the 24th to the 23rd millennium BP (dotted line = average CV for the entire dataset).

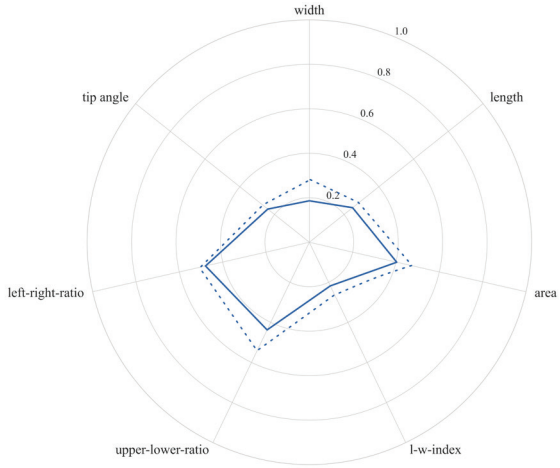



Figure 28: Coefficient of Variation (CV) of morphometric features for the section from the 23rd to the 22nd millennium BP (dotted line = average CV for the entire dataset).

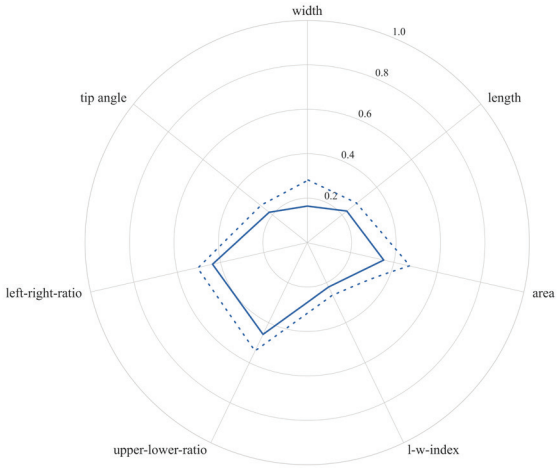



Figure 29: Coefficient of Variation (CV) of morphometric features for the section from the 22nd to the 21st millennium BP (dotted line = average CV for the entire dataset).

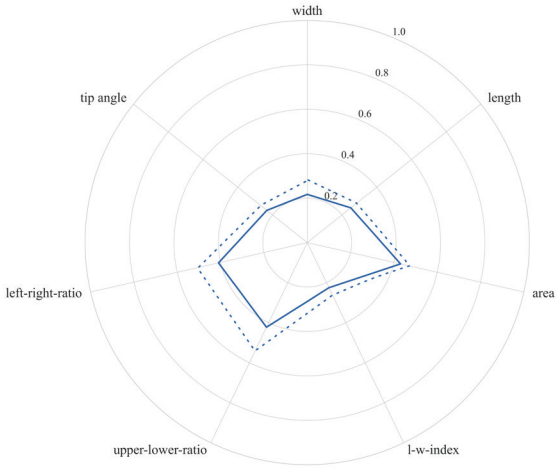



Figure 30: Coefficient of Variation (CV) of morphometric features for the section from the 21st to the 20th millennium BP (dotted line = average CV for the entire dataset).

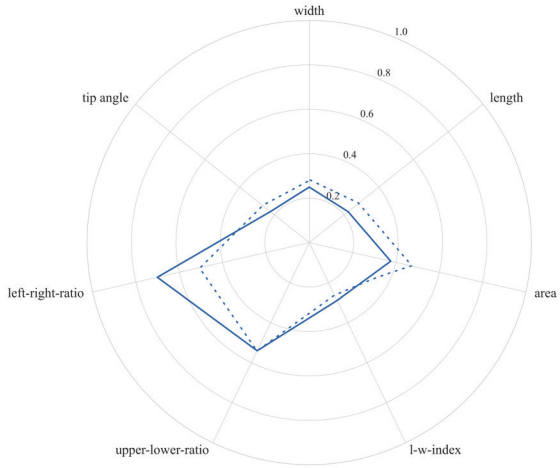



Figure 31: Coefficient of Variation (CV) of morphometric features for the section from the 17th to the 16th millennium BP (dotted line = average CV for the entire dataset).

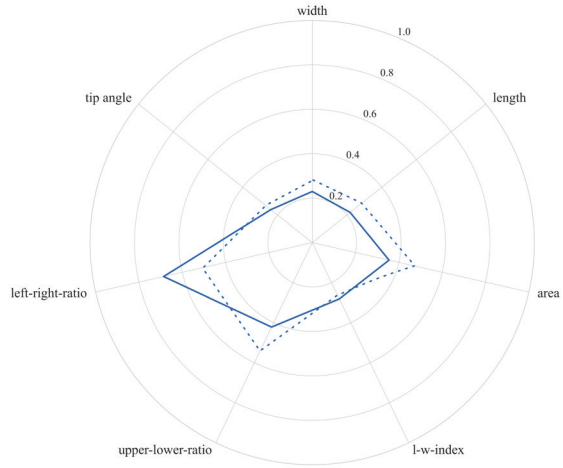



Figure 32: Coefficient of Variation (CV) of morphometric features for the section from the 16th to the 15th millennium BP (dotted line = average CV for the entire dataset).

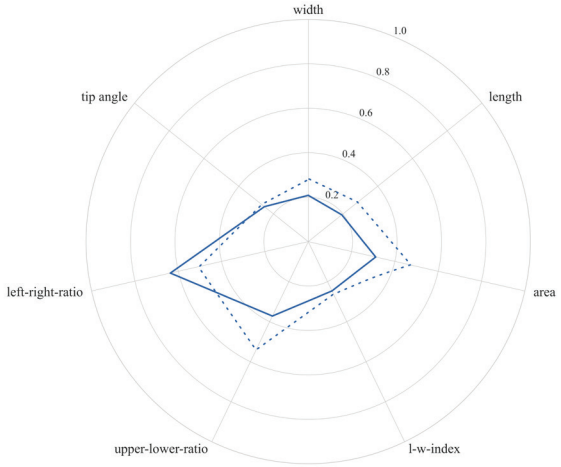



Figure 33: Coefficient of Variation (CV) of morphometric features for the section from the 15th to the 14th millennium BP (dotted line = average CV for the entire dataset).

The CV for the tip angle (0.22) as well as for all size-related features remain below the respective average CV (width = 0.23, length = 0.22, area = 0.35). *(Figure 32)*

The average of the overall variation for the sixteenth section ranging from the 15th to the 14th millennium BP is the lowest in the entire dataset ($\bar{x}$ = 0.31). The CV for the left-right ratio (0.64) is the only feature exhibiting pronounced variation. However, as discussed in the previous section, this is likely not of analytical significance. The CV for all other features remain well below the respective average CV (width = 0.21, area = 0.31, l-w-index = 0.25, tip angle = 0.25). Some of which are even the lowest in the entire dataset (length = 0.19, upper-lower-ratio = 0.37). *(Figure 33 and 34)*

The CV for the morphometric features reveals a notable differences between variation in size-related and shape-related features, with shape-related features ($\bar{x}$ = 0.39) generally exhibiting greater overall variation compared to size-related features ($\bar{x}$ = 0.33). This is true for all sections, with the exception of the sections spanning the 29th to 24th millennia BP. The pronounced variation in shape-related features may indicate a greater sensitivity to

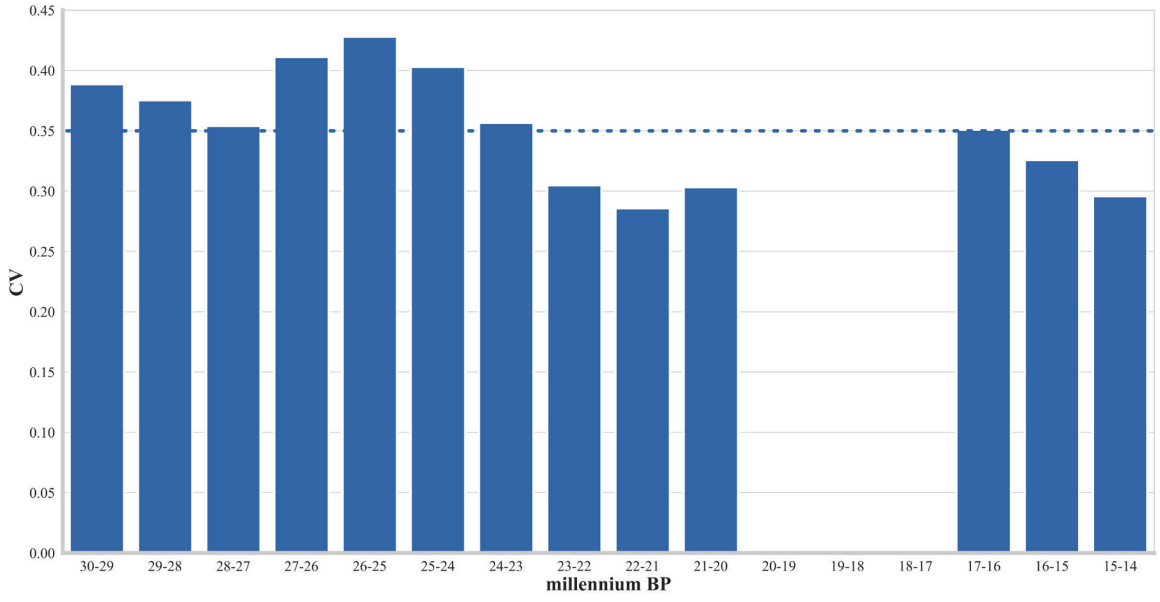



Figure 34: Averages ($\bar{x}$) of Coefficient of Variation (CV) *per section* in millennium BP (dotted line = average CV for all periods).

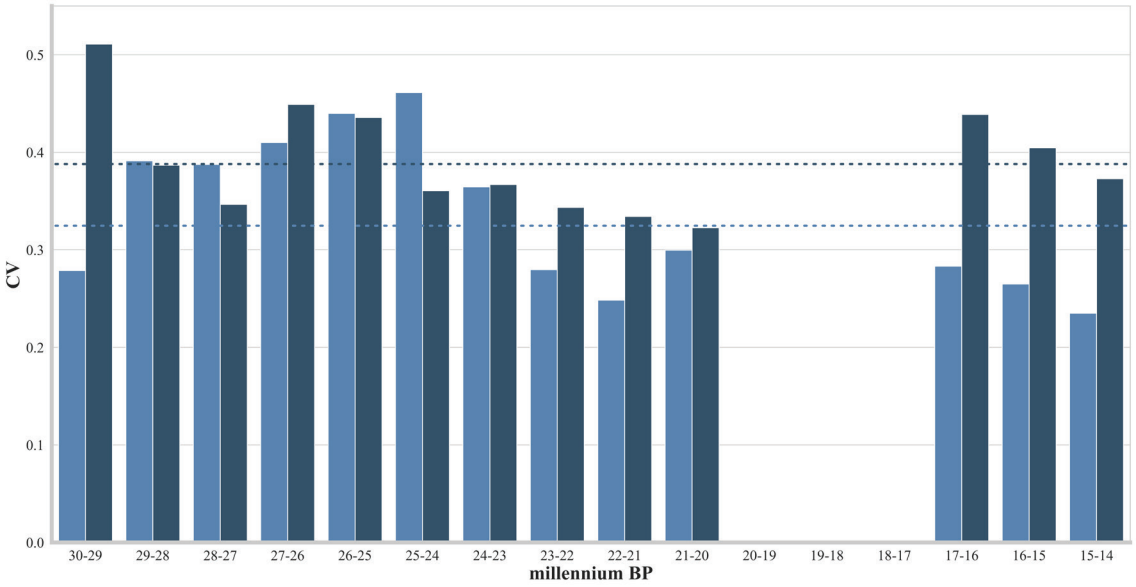



Figure 35: Averages ($\bar{x}$) of Coefficient of Variation (CV) for features related to size and shape *per se*ction in millennium BP (size = light blue, shape = dark blue; dotted line = average CV for all sections).

selective pressures. In contrast, the relatively lower variation in size-related features suggests greater stability, potentially due to stronger constraints on size-related metrics.

Additionally the shape- and the size-related features show distinct trajectories. Size-related features exhibit a relatively steady increase in variation until the 25th to the 24th millennium BP. In contrast, shape-related features display an alternating pattern during the same timeframe. This pattern begins with elevated variation for the 30th to the 29th millennium BP, followed by a decline between the 29th and the 27th millennium BP, then a resurgence of higher variation between the 27th and the 25th millennium BP, and finally a sharp drop in the section from the 25th to the 24th millennium BP. Between the 24th to the 20th millennium BP, variation in size-related features undergoes a consistent decrease, reaching a low point by the 21st to the 20th millennium BP. Conversely, shape-related features show a more gradual and less pronounced decrease during this period. In the youngest three sections, both size- and shape-related features follow a similar declining trend, although the decrease is somewhat more pronounced for shape-related features. This divergence and eventual convergence in the variation-trajectories of size- and shape-related features might reflect differing constraints influencing these morphometric attributes over time. *(Figure 35)*

The analysis of the CV across all investigated millennia reveals distinct patterns of morphometric variation. Temporal trends indicate that earlier SPs in the period between the 30th and the 25th millennium BP exhibit higher average CV values, with size-related features often surpassing their respective averages, and punctuated high CV values for shape-related features. The overall variation during this earlier period exhibits an intriguing cyclic trajectory, characterised by elevated values at the beginning, a decline to lower values in the mid-period, and a subsequent increase toward the end *(Figure 34)*. Conversely, the period between the 24th and the 20th millennium BP shows a decreasing trend over all variation towards exceptional low values, possibly reflecting a standardisation in both size- and shape-related morphometric features. While variation is quite high in the beginning of the youngest three sections (17th–16th, 16th–15th and 15th–14th millennium BP) and decreases constantly towards the end of the observed timeframe, this period illustrates a marked disparity between size and shape-related variation, with shape-related features driving overall varia-

tion due to isolated high variation values and size-related features maintaining consistent low in variation.

These results, together with the insights obtained from RDA, provide a foundational framework for further analyses aimed at quantifying the extent of change. Periods exhibiting high variation in morphometric features and returning significant in the RDA – in which, to a certain amount, variation in the morphometric features is chronologically directed and not just a matter of stochastic variation – present greater potential for detecting pronounced chronological trends compared to periods of lower variation. However, high variation might also imply the influence of factors beyond chronology (e.g. spatial distribution or different taxonomic units), which is tested for in the next chapter. *(Table 10)*

### 4.1.3 Change Rates and Correlations

Having demonstrated that specific timeframes exhibit higher morphological variation in SPs than others, and that this variation is, in some instances, better explained by the passage of time, it is now of interest to calculate the amplitude of change. This involves quantifying the rate at which change occurs in the morphometric features, providing insights into the dynamics and the pace of change through time. To achieve this, change rates for each morphometric feature are calculated between the two consecutive millennia within each 2000 year section. Additionally, the resulting values are compared to the significance threshold (see Chapter 3.3.3. *Change Rates*) of each respective feature. This approach is systematically applied across all sections, enabling a comprehensive assessment of the amount of change, calculated as an average of the absolute values of the change rates for each morphometric feature, and its variation over time.

By applying the calculation of Kendall's tau correlation coefficient between the actual values in the morphometric features and the calibrated ages of the assemblages in the corresponding section, it is further assessed for the relevance of the change rates in the respective morphometric feature. While the change rates highlight overarching developments between two consecutive sections, the correlations account for the chronological arrangement of the underlying assemblages. Therefore, the correlations do not necessarily have to support the change rates. The change rate between the mean values of two conequetive millennia might indicate substantial change taking place, while the actual trajectory of the change is less linear and therefore not as strong.

A preliminary examination of the calculated change rates *(Table 12)* reveals some extreme values for the centre of mass offsets (MP-CM-x and y-offset). These anomalies likely derive from the characteristics of these features, which include both positive and negative as well as very minute values, coupled with inter-assemblage differences. Given that these outliers exert a significant influence on the averages, the values in both features are acknowledged but excluded from further calculations to ensure the integrity and relevance of the analysis. However, this exclusion does not imply a lack of archaeological or mathematical significance in these extremes. In fact, some of these values are supported by significant Kendall's tau correlation calculations, revealing meaningful relationships between the variation in the respective morphometric features and the passage of time (see description in the further text).

#### *4.1.3.1 Morphometric Features*

The average rate of change – calculated from the absolute values of the individual change rates – in morphometric features between two subsequent millennia is 17% *(*$\bar{x}$ = 0.173, *Table 12)*. Nearly all peak values for change rates – the highest amount of change – in the individual morphometric features occur during the RDA-significant sections, with exceptions noted during the two oldest sections ($30^{th}$–$29^{th}$ and $29^{th}$–$28^{th}$ millennium BP). The features exhibiting the highest average change rates include the MP-CM-y-offset ($\bar{x}$ = 0.32), the upper-lower-ratio ($\bar{x}$ = 0.23), area ($\bar{x}$ = 0.22), and the left-right-ratio ($\bar{x}$ = 0.21). In contrast, the average change rates for width ($\bar{x}$ = 0.11), length ($\bar{x}$ = 0.12), and the l-w-index ($\bar{x}$ = 0.11), while being notably similar, are not only low, but also significantly below the overall average for the entire dataset. The average change rate for the MP-CM-x-offset ($\bar{x}$ = 0.16) and the tip angle ($\bar{x}$ = 0.15) are only slightly below the feature-specific average.

Table 10: Coefficient of Variation (CV) for each morphometric feature and section (highlighted in red = RDA significant sections; bold and underlined = highest change rate in feature; grey = value below respective average CV).

| section m. BP | width | length | area | l-w-index | upper-lower-index | left-right-ratio | tip angle | $\bar{x}$ |
|---|---|---|---|---|---|---|---|---|
| 15th–14th | 0.21 | 0.19 | 0.31 | **0.24** | 0.37 | **0.64** | 0.25 | 0.31 |
| 16th–15th | 0.23 | 0.21 | 0.35 | **0.27** | 0.43 | **0.68** | 0.24 | 0.34 |
| 17th–16th | 0.25 | 0.22 | 0.38 | **0.29** | **0.54** | **<u>0.70</u>** | 0.22 | **0.37** |
| 18th–17th | | | | | | | | |
| 19th–18th | | | | | | | | |
| 20th–19th | | | | | | | | |
| 21th–20th | 0.22 | 0.25 | 0.43 | 0.23 | 0.42 | 0.41 | 0.23 | 0.31 |
| 22th–21th | 0.16 | 0.23 | 0.35 | 0.22 | 0.46 | 0.44 | 0.22 | 0.30 |
| 23rd–22nd | 0.19 | 0.25 | 0.40 | 0.22 | 0.44 | 0.48 | 0.24 | 0.32 |
| 24th–23rd | **0.28** | **0.31** | **0.50** | 0.24 | 0.52 | 0.40 | **0.31** | **0.37** |
| 25th–24th | **0.32** | **<u>0.42</u>** | **<u>0.65</u>** | 0.25 | 0.47 | 0.41 | **0.31** | **0.40** |
| 26th–25th | **0.37** | **0.38** | **0.57** | 0.24 | **0.71** | 0.48 | **0.32** | **<u>0.44</u>** |
| 27th–26th | **<u>0.39</u>** | 0.26 | **0.58** | 0.25 | **<u>0.90</u>** | 0.39 | 0.25 | **0.43** |
| 28th–27th | **0.32** | **0.30** | **0.55** | **0.30** | 0.41 | 0.42 | 0.26 | **0.36** |
| 29th–28th | **0.34** | **0.30** | **0.54** | **<u>0.34</u>** | 0.50 | 0.40 | **0.31** | **0.39** |
| 30th–29th | 0.25 | 0.24 | 0.34 | **0.29** | **0.67** | **<u>0.75</u>** | **<u>0.34</u>** | **0.41** |
| $\bar{x}$ | 0.27 | 0.27 | **0.46** | 0.26 | **0.53** | **0.51** | 0.27 | **0.37** |

***width***

The highest change rates in width occur in the section from the 27th to the 26th millennium BP (0.24), with almost similarly high values noted in the section from the 25th to the 24th (-0.22) and the 17th to the 16th millennium BP (0.21), exceeding the average change rate for width. These three sections are the only ones to yield change rates supported by significant Kendall's tau correlations, further emphasising the importance of these values (27th–26th millennium BP: $\tau = -0.39$, $p = 0.003$; 25th–24th millennium BP: $\tau = 0.27$, $p = 0.008$; 17th–16th millennium BP: $\tau = -0.5$, $p < 0.001$). The oldest two sections from the 30th to the 29th and the 29th to the 28th millennium BP (0.14 and 0.13) as well as the period between the 24th and the 22nd millennium BP (0.1 and 0.11) show values around the average change rate for width. The two youngest sections (16th–15th and 15th–14th millennium BP) exhibit particularly low change rates (-0.07 and -0.02), as does the period between the 22nd and the 20th millennium BP (0.01, 0.01), indicating almost no chronologically directed changes in width taking place at these times. None of the values exceeds the significance threshold for width (0.27).

Table 11: Kendall's correlation for morphometric features and calibrated ages ('ka calBP') across successive millennia (bold and green = significant correlation ($p \leq 0.05$); red = RDA-significant sections; n = number of significant correlations).

| section m. BP | width | length | area | l-w-index | upper-lower-index | left-right-ratio | tip angle | MP-CM-x-offset | MP-CM-y-offset | n |
|---|---|---|---|---|---|---|---|---|---|---|
| 15th–14th | 0.14 | **0.15** | **0.24** | 0.01 | −0.05 | −0.06 | 0.1 | −0.07 | −0.05 | **2** |
| 16th–15th | 0.11 | 0.11 | **0.2** | −0.02 | **−0.29** | 0.07 | **0.22** | −0.02 | 0.04 | **3** |
| 17th–16th | −0.5 | 0.11 | **−0.27** | **0.42** | 0.20 | 0.11 | **−0.46** | **0.22** | −0.16 | **5** |
| 18th–17th | | | | | | | | | | |
| 19th–18th | | | | | | | | | | |
| 20th–19th | | | | | | | | | | |
| 21th–20th | 0.12 | **0.34** | **0.26** | **0.31** | −0.01 | −0.02 | **−0.23** | −0.03 | −0.01 | **4** |
| 22th–21th | 0.07 | −0.06 | 0.01 | −0.15 | **0.43** | **0** | 0.06 | 0.15 | −0.15 | **1** |
| 23rd–22nd | −0.11 | 0.08 | 0 | **0.27** | 0.14 | **0.27** | −0.12 | 0.2 | −0.16 | **2** |
| 24th–23rd | 0.01 | 0.07 | 0.03 | 0.04 | **−0.22** | 0.06 | −0.07 | −0.04 | 0.1 | **1** |
| 25th–24th | **0.27** | **0.29** | **0.29** | 0.12 | **−0.22** | −0.17 | −0.05 | −0.17 | −0.02 | **4** |
| 26th–25th | −0.22 | **−0.41** | **−0.34** | **−0.3** | −0.22 | **0.38** | 0.2 | **0.55** | −0.2 | **5** |
| 27th–26th | **−0.39** | −0.17 | **−0.33** | **0.3** | −0.11 | −0.24 | −0.07 | −0.21 | **0.3** | **4** |
| 28th–27th | 0.06 | **0.21** | 0.15 | 0.13 | −0.13 | 0.07 | 0.04 | −0.07 | 0.05 | **1** |
| 29th–28th | 0.2 | 0.24 | 0.21 | 0.05 | 0.13 | 0.09 | −0.10 | −0.11 | −0.11 | **0** |
| 30th–29th | −0.01 | −0.15 | −0.14 | −0.01 | 0.01 | −0.07 | 0.05 | −0.27 | **0.46** | **1** |
| **n** | **3** | **5** | **7** | **5** | **4** | **2** | **3** | **2** | **2** | |

Table 12: Change rates across successive millennia ($\bar{x}$ = averages of absolute change rates; signi. = significance threshold ($\bar{x} + 1.96 \times \sigma$); highlighted in red = RDA significant sections; green = change rate supported by significant Kendall's tau correlation ($p \leq 0.005$); bold and underlined = highest change rate in feature/sections; faint = value below respective average change rate; italic = extreme values excluded from averages; ! = value exceeding significance threshold).

| section m. BP | width | length | area | l-w-index | upper-lower-index | left-right-ratio | tip angle | MP-CM-x-offset | MP-CM-y-offset | $\bar{x}$ |
|---|---|---|---|---|---|---|---|---|---|---|
| 15th–14th | -0.02 | **-0.04** | **-0.11** | -0.04 | -0.04 | -0.08 | -0.09 | 0.09 | 0.18 | 0.06 |
| 16th–15th | -0.07 | -0.02 | **-0.14** | 0.04 | **0.36** | -0.19 | **-0.16** | -0.04 | -0.23 | 0.14 |
| 17th–16th | **0.21** | 0.02 | **0.29** | **-0.13** | -0.54 | **0.48** | **0.35** | **-0.25** | 0.14 | **0.29** |
| 18th–17th | | | | | | | | | | |
| 19th–18th | | | | | | | | | | |
| 20th–19th | | | | | | | | | | |
| 21th–20th | 0.01 | **-0.2** | -0.15 | **-0.2** | 0 | -0.03 | **0.2** | 0.06 | 0.32 | 0.11 |
| 22th–21th | 0.01 | **0.13** | 0.1 | 0.15 | **-0.41** | 0.12 | -0.07 | -0.14 | 0.26 | 0.14 |
| 23rd–22nd | 0.11 | **0.04** | 0.16 | **-0.08** | **0.02** | **-0.25** | 0.06 | -0.25 | 0.02 | 0.1 |
| 24th–23rd | 0.1 | **0.09** | 0.16 | **-0.02** | **0.32** | -0.03 | -0.04 | 0.06 | -0.9! | 0.11 |
| 25th–24th | **-0.22** | **-0.3** | **-0.47** | **-0.08** | **0.31** | 0.33 | 0.02 | 0.39 | -0.47 | 0.25 |
| 26th–25th | -0.12 | **0.19** | **0.03** | **0.21** | **0.06** | **-0.44** | -0.25 | ***-2.09*** | 0.41 | 0.19 |
| 27th–26th | **0.24** | **0.05** | **0.36** | **-0.11** | **0.71** | 0.19 | 0.02 | **0.47!** | ***-3.49!*** | 0.24 |
| 28th–27th | -0.08 | **-0.15** | -0.24 | -0.09 | 0.09 | -0.12 | 0.01 | -0.14 | *1.55!* | 0.11 |
| 29th–28th | 0.13 | **0.03** | 0.3 | -0.12 | -0.32 | 0.14 | **0.44!** | 0 | *1.03!* | 0.21 |
| 30th–29th | 0.14 | **0.26!** | 0.29 | 0.21 | 0.58 | -0.28 | -0.3 | -0.06 | ***-5.53!*** | 0.3 |
| **$\bar{x}$** | **0.11** | **0.12** | **0.22** | **0.11** | **0.28** | **0.21** | **0.15** | **0.16** | **0.32** | **0.17** |
| **signi.** | 0.27 | 0.31 | 0.45 | 0.24 | 0.75 | 0.49 | 0.43 | 0.44 | 0.79 | 0.32 |

***length***

The highest change rates in length occur in the two sections between the 26th and the 24th millennium BP (0.19 and 0.3), and in the section from the 21st to the 20th millennium BP (0.2), all of which exceeding the average change rate for length. These three sections yield change rates supported by significant Kendall's tau correlations (26th–25th millennium BP: $\tau = -0.41$, $p = 0.002$; 25th–24th millennium BP: $\tau = 0.29$, $p = 0.004$; 21st–20th millennium BP: $\tau = 0.34$, $p = 0.002$). The oldest section (30th–29th millennium BP) also shows a high change rate (0.26), which however is not supported by a significant correlation. Conversely, particularly low change rates are found in the three most recent sections (0.02, 0.02, 0.04) and from the 23rd to the 22nd (0.04), the 27th to the 26th (0.05) as well as the 29th to the 28th millennium BP (0.03), indicating almost no chronologically directed changes in length are taking place at these times. However, the low change rate in length for the section from the 15th to the 14th millennium BP is supported by a barely significant ($p = 0.048$) and weak ($\tau = 0.15$) correlation. None of the values exceeds the significance threshold for length (0.31).

***area***

The highest change rates in area occur in the section from the 25th to the 24th millennium BP (-0.47), exceeding the significance threshold for area (0.45). Also, the two oldest sections (30th–29th millennium BP: 0.29; 29th–28th millennium BP: 0.3) as well as the sections from the 27th to the 26th millennium BP (0.36) and from the 17th to the 16th millennium BP (0.29) show comparatively high values, exceeding both the average change rate for area and overall morphometric features. With the exception of the values for the oldest two sections, all of these change rates are supported by significant Kendall's tau correlations, further emphasising the importance of these values (27th–26th millennium BP: $\tau = -0.33$, $p = 0.008$; 25th–24th millennium BP: $\tau = 0.29$, $p = 0.003$; 17th–16th millennium BP: $\tau = -0.27$, $p = 0.008$). Relatively low change rates, neither exceeding the average change rate for area nor for overall morphometric features are calculated for the period between the 24th and the 20th millennium BP (0.16, 0.16, 0.1, -0.15) and for the two youngest sections (16th–15th millennium BP: -0.14, 15th–14th millennium BP: -0.11). Almost no changes in area occur between the 26th and the 25th millennium BP (0.03). None of the latter values is reflected in significant Kendall's tau correlations.

***l-w-index***

The highest change rates in the l-w-index occur in the section from the 26th to the 25th millennium BP (0.21), with similarly high values for the oldest section (30th–29th millennium BP: 0.21) and for the section from the 21th to the 20th millennium BP (-0.2), both of the latter exceeding the average change rate for l-w-index as well as the overall average change rate. However, only the values for the section from the 26th to the 25th millennium BP ($\tau = -0.37$, $p = 0.027$) and from the 21st to the 20th millennium BP ($\tau = 0.31$, $p = 0.005$) are actually supported by significant Kendall's tau correlations, further emphasising the importance of these values. Average change rates are noted for the period between the 29th and the 26th millennium BP (-0.12, -0.09, -0.11), for the sections from the 22nd to the 21st (0.15) and from the 17th to the 16th millennium BP (-0.13). Interestingly, the latter is supported by a significant correlation, highlighting the importance of this value ($\tau = 0.42$, $p < 0.001$). The youngest sections (16th–15th millennium BP: 0.04 and 15th–14th millennium BP: -0.04) and the sections in the period between the 25th and the 22nd millennium BP (-0.08, -0.02, -0.08) show almost no chronologically directed changes in l-w-index. None of the values exceeds the significance threshold for the l-w-index (0.24).

***upper-lower-ratio***

The highest change rate in the upper-lower-ratio occurs for the section from the 27th to the 26th millennium BP (0.71). This high value however, derives from the divergence between strong signals from three specimens from a single assemblage (Abauntz, A-49, Appendix Table 17), resembling the oldest Iberian Upper Solutrean SPs in the dataset, and the relative low values for the rest of the specimens. Apart from this outstanding values, the highest change rates in the upper-lower-ratio have been calculated for the sections from the 30th to the 29th (0.58), which is most likely also the result of a single assemblage (Mitoc-Malu Galben, layer 4a, A-60, Appendix Table 17) yielding outstanding values, and from the 17th and the 16th millennium BP (-0.54). Change rates

just around the average change rate for the upper-lower-ratio are calculated for the sections from the 29th to the 28th (-0.32) and the two sections from the 25th to the 24th millennium BP (0.31) and from the 24th to the 23rd millennium BP (0.32). Change rates significantly higher than the average change rates for the upper-lower-ratio occur for the sections from the 16th and the 15th millennium BP (0.36) and from the 22nd to the 21st millennium BP (-0.41). Comparably low change rates are calculated for the sections from the 28th to the 75th (0.09), the 26th to the 25th millennium BP (0.06), the 23rd to the 22nd millennium BP (0.02) and the youngest section from the 15th to the 14th millennium BP (-0.04). Almost no chronologically directed changes in the upper-lower-ratio seems to happen in the section from the 21st to the 20th millennium BP (0). Most interestingly, the elevated change rates for the sections from the 24th to the 24th, from the 24th to the 23rd, from the 22nd to the 21st and from the 16th to the 15th millennium BP are supported by significant Kendall´s tau correlations (25th–24th: $\tau = -0.22$, $p = 0.03$; 24th–23rd: $\tau = -0.22$, $p = 0.03$; 22nd–21st: $\tau = 0.43$, $p < 0.001$; 16th–15th: $\tau = -0.29$, $p < 0.001$). However, the extreme values observed for the sections from the 30th to the 29th and from the 27th to the 26th millennium BP are not statistically supported by Kendall´s tau correlations. Additionally, when low change rates occur, Kendall´s tau correlations remain low and not significant (e.g. 21st–20th millennium BP: $\tau = -0.01$, $p = 0.895$). None of the values for the upper-lower-ratio (0.75) exceed the significance threshold, though the value for the section from the 27th to the 26th millennium BP comes close.

***left-right-ratio***

The highest change rates in the left-right-ratio occur between the 17th and the 16th (0.48) and between the 26th and the 25th millennium BP (-0.44). Also the change rates for between the 30th and the 29th (-0.28) and between the 25th and the 24th millennium BP (0.33) are well over the average change rate for the left-right-ratio as well as over the average change rate for overall morphometric features. However, only the change rate for the section from the 26th to the 25th millennium is supported by significant Kendall's tau correlations, further emphasising the importance of these values ($\tau = 0.38$, $p = 0.006$). Change rates around the average change rates for both left-right-ratio and overall morphometric features are calculated for between the 27th to the 26th (0.19), the 23th and the 22th (-0.25), actually supported by a significant correlation ($\tau = 0.27$, $p = 0.031$) and the 16th and the 15th millennium BP (-0.19). Almost no chronologically directed changes in the left-right-ratio seem to happen between the 24th and the 23rd (-0.03), the 21st and the 20th (-0.03) and the 15th and the 14th millennium BP (-0.08).

***tip angle***

The average change rate for the tip angle (0.15) is slightly below the overall average change rate. The highest change rates in tip angle occur between the 29th and the 28th (0.44), exceeding the significance threshold for the tip angle (0.43), and the 17th and the 16th millennium BP (0.35), but only the latter is supported by a significant Kendall´s tau correlation ($\tau = -0.46$, $p < 0.001$). Also the change rates for the sections from the 30th to the 29th (-0.3), the 26th to the 25th (-0.25) as well as the 21st to the 20th millennium BP (0.2) are well over the average change rates for both tip angle. A change rate just around the average change rate for tip angle are calculated between the 16th and the 15th millennium BP (-0.16), which however is supported by a significant correlation, highlighting the importance of this value ($\tau = 0.22$, $p = 0.001$). Almost no chronologically directed changes in tip angle seem to happen in the periods from the 28th to the 26th (-0.01, 0.02) and from the 25th to the 21st (0.02, -0.04, 0.06, -0.07). None of the values exceeds the significance threshold for the tip angle (0.72).

***MP-CM-x-offset***

By far the highest change rates in the MP-CM-x-offset occur between the 26th and the 25th millennium BP (-2.09). This high change rate is supported by a significant Kendall´s tau correlation ($\tau = 0.55$, $p < 0.001$), further highlighting its importance. However, as stated above, this extreme value is not considered in further calculations for its disproportionate influence on the result. Apart from this outstanding value, the most change in MP-CM-x-offset is calculated for the previous sections from the 27th to the 26th millennium BP (0.47) and the subsequent section between the 25th and the 24th millennium BP (0.39), the first even exceeding the significance threshold for the

MP-CM-x-offset (0.44; calculated without the extreme value) while both not being supported by significant correlation. The change rates for the sections from the 23rd to the 22nd and from the 17th to the 16th millennium BP (-0.25 both) are also comparatively high. The latter is even supported by a significant correlation (τ = 0.22, p = 0.033). The values for all other sections are far below the average change rate for MP-CM-x-offset, indicating almost no chronologically directed change in MP-CM-x-offset taking place at these times (30th–29th millennium BP: -0.06, 29th–28th millennium BP: 0; 24th–23rd millennium BP: 0.06, 16th–15th millennium BP: -0.04, 15th–14th millennium BP: -0.09).

***MP-CM-y-offset***

By far the highest change rate in the MP-CM-y-offset is calculated for the oldest section between the 30th and the 29th (-5.53). This extreme value is supported by a significant Kendall´s tau correlation (τ = 0.46, p = 0.023), underlining its importance. Further striking high values occur for sections in the period between the 29th and the 26th millennium BP (1.03,1.55, -3.49). The change rate for the youngest section of this period (27th–26th millennium BP) is supported by a significant correlation (τ = 0.3, p = 0.018). As stated at the beginning of this Chapter, these extreme values are not considered in further calculations for their disproportionate influence on the result. Reasonable high amounts of change are calculated for the three subsequent sections in the period from the 26th to the 23rd millennium BP (0.41, -0.47, -0.9). The latter value even exceeds the significance threshold for the MP-CM-y-offset (0.5; calculated without the extreme value) but not supported by a significant correlation. Comparably low change rates are calculated for all sections from the 22nd to the 14th millennium BP (0.26, 0.32, 014, -0.23, 0.18). Almost no chronologically directed change seems to take place between the 23rd and the 22nd millennium BP.

The significant correlations support some of the observed change rates, predominantly the extreme values but also, in certain instances, lower ones, underscoring the meaningfulness of the underlying changes not only on a coarse scale but also in finer detail. Conversely, when change rates are particularly low, the correlations do not indicate any significant signal, highlighting the significance of phases where no apparent change occurs in the morphometric features. The most significant correlations are observed in the size-related features length (n = 5), area (n = 7), and in the l-w index (n = 5). *(Figure 36, Table 11)*

The comparison of average change rates between features associated with size (n = 3) and those associated with shape (n = 4) across the sections reveals significant differences in the magnitude and the pattern of morphometric change over time. On average, the change rate for shape-related features ($\bar{x}$ = 0.19) is higher than that for size-related features ($\bar{x}$ = 0.15), indicating a general trend of shape exhibiting greater dynamism over time than size. This observation holds true for most sections, with a few notable exceptions: the sections from the 28th to the 27th millennium BP, the sections between the 25th and the 22nd millennium BP as well as the section from the 21st to the 20th millennium BP.

In the oldest section (30th–29th millennium BP), both the averages for size-related ($\bar{x}$ = 0.24) and shape-related features ($\bar{x}$ = 0.34) exceed their respective averages for the entire observed timeframe, with shape-related features showing the highest average rate of change. In the following section (29th–28th millennium BP), shape-related features ($\bar{x}$ = 0.26) continue to exceed their average change rate, while the average change rate for size-related features ($\bar{x}$ = 0.12) falls below their average for the entire timeframe. Again, these strong signals for shape-related features are probably largely driven by the distinct SP forms of Mitoc-Malu Galben, layer 4a (A-60). For the section from the 28th to the 27th millennium BP, the trend is inverted, with size-related features ($\bar{x}$ = 0.15) showing a higher average rate of change than shape-related features ($\bar{x}$ = 0.08), which do not exceed their average for the entire timeframe. For the section from the 27th to the 26th millennium BP, both the averages for size- ($\bar{x}$ = 0.19) and shape-related features ($\bar{x}$ = 0.26) yet again exceed their respective averages for the entire timeframe, though shape-related features show a higher average rate of change. In contrast, during the section from the 26th to the 25th millennium BP, the average change rate for size-related features drops significantly ($\bar{x}$ = 0.12), while shape-related features show a notable high average rate of change ($\bar{x}$ = 0.24). The section

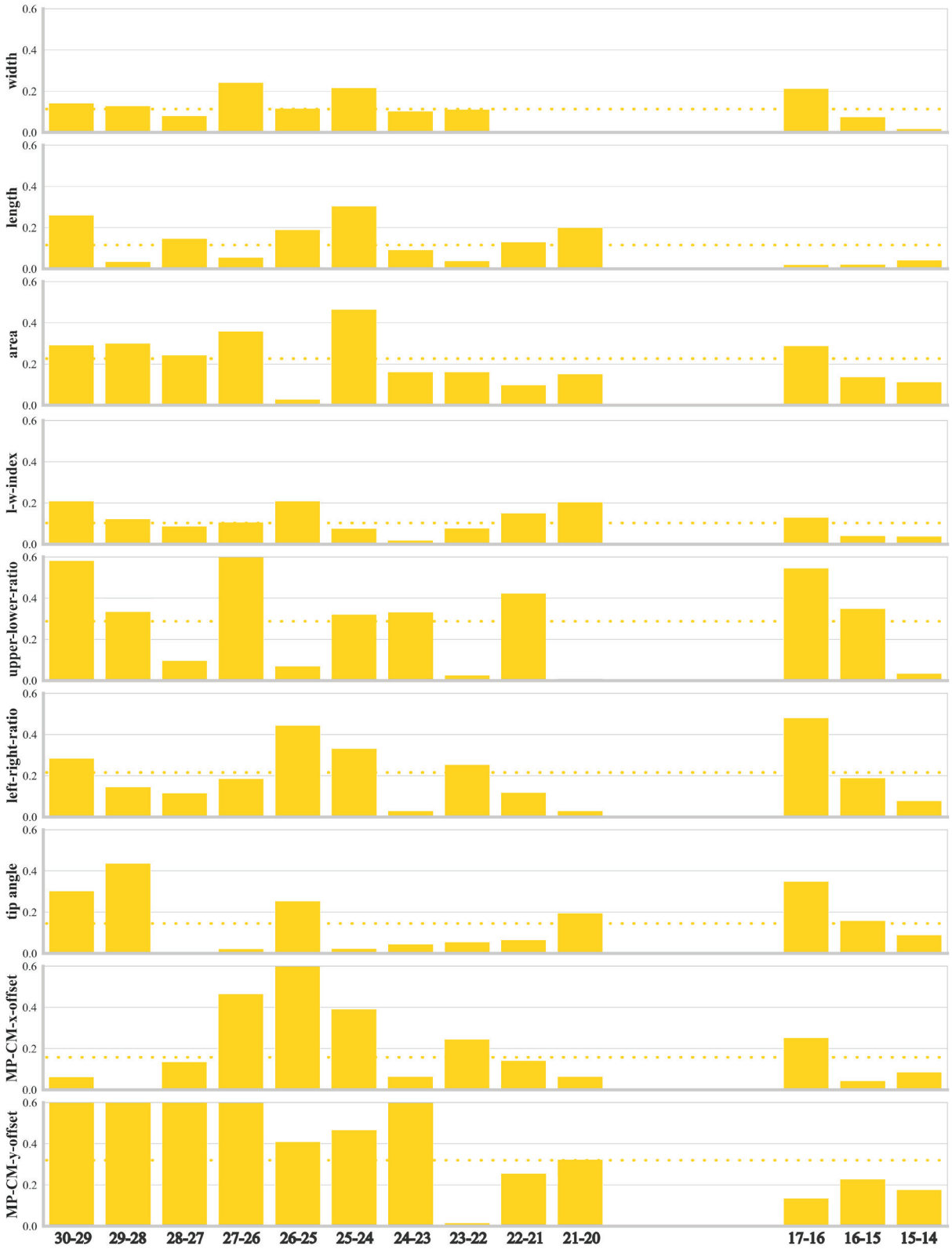



Figure 36: Absolute values of change rates for each morphometric feature *per s*ection in millennium BP (dotted line = average change rate for all sections).

from the 25th to the 24th millennium BP displays another inversion, with size-related features ($\bar{x}$ = 0.32) exhibiting the highest average change rate observed across all sections, more than double their average for the entire timeframe. Shape-related features in this section display a lowered average rate of change ($\bar{x}$ = 0.18), not exceeding the average change rate for shape-related features. From the 24th to the 20th millennium BP, the average rates of change for both size- and shape-related features generally remain below their respective averages for the entire timeframe. During this period, size- and shape-related features generally show almost equally low amounts of change, with the exception of the section from the 22nd to the 21st millennium BP, where shape-related features ($\bar{x}$ = 0.19) show more than twice the amount of change than size-related features ($\bar{x}$ = 0.8). In the final three sections, the amount of change in shape-related features is almost double that in size-related features. In the section from the 17th to the 16th millennium BP, the average change rates for both size-related ($\bar{x}$ = 0.14) and shape-related features ($\bar{x}$ = 0.34) exceed their respective averages for the entire timeframe, with shape-related features showing the second-highest average rate of change. However, in the youngest two sections, the average rates of change for both size and shape fall well below their respective averages.

In the earliest three sections, the average rates of the change rates in shape-related features follows a consistent decreasing trend. From both peak values observed for the section from the 27th to the 26th and from the 26th to the 25th millennium BP on, a linear decreasing trend in the amount of change in the shape-related features is observable, continuing, with the exception of the interspersed elevated value for the section from the 22nd to the 21st millennium BP, until the last section before the period of apparent absence of SPs (21st–20th millennium BP).

After the high value for the oldest section from the 30th to the 29th millennium BP, the amount of change in size-related features increases continuously until its peak value in the section from the 25th to the 24th millennium BP, with only one regression for the section from the 26th to the 25th millennium BP. Afterwards the amount of change in size-related features follows the same continuous decreasing trend as the shape-related features. Conversely to the shape-related features, the trend for features related to size is continuous and lasts until the section from the 21st to the 20th millen-

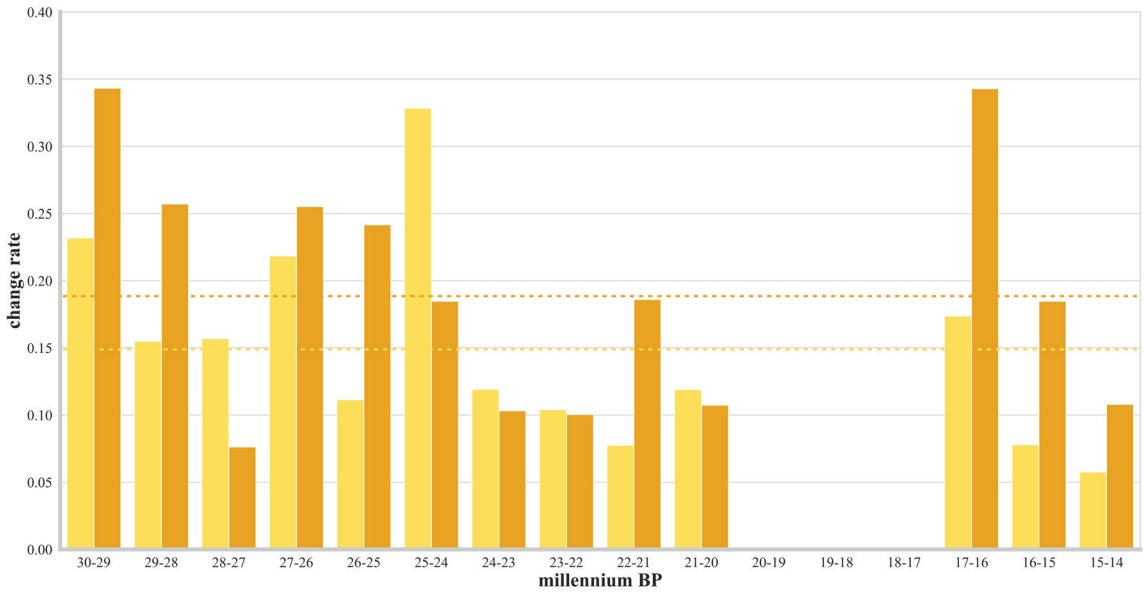



Figure 37: Averages ($\bar{x}$) of absolute change rates for features related to size and shape *per se*ction in millennium BP (size = light yellow, shape = dark yellow; dotted line = average change rate for all sections).

nium BP. In this section, the amount of change in size-related features rises again slightly, but remains low. From the section spanning the 17th to the 16th millennium BP onward, a rapid linear decrease in the amount of change in both size- and shape-related features is evident, although this is much more distinct for the shape-related features. *(Figure 37)*

### *4.1.3.2 Sections*

The average rate of change in the morphometric features between two consecutive millennia or respectively within a 2000 year section is 17% ($\bar{x}$ = 0.1655). Nearly all peak values for change rates – the highest amount of change – in the sections occur during the RDA-significant sections, with exceptions noted during the two oldest section from the 30th to the 29th millennium BP ($\bar{x}$ = 0.29) and from the 29th to the 28th millennium BP ($\bar{x}$ = 0.19). Also, although returning significant in the RDA, the sections from the 22nd to the 21st millennium BP ($\bar{x}$ = 0.13), the 21st to the 20th millennium BP ($\bar{x}$ = 0.12) and the 16th to the 15th millennium BP ($\bar{x}$ = 0.13) yield notable low change rates.

Despite the high average change rate for the oldest section described above, the highest change rate is calculated for the section from the 17th to the 16th millennium BP ($\bar{x}$ = 0.26). The next highest values are calculated for the sections from the 25th to the 24th millennium BP ($\bar{x}$ = 0.25) and from the 27th to the 26th millennium BP ($\bar{x}$ = 0.22). A bit lower although above the average are the change rates for the sections from the 26th to the 25th millennium BP ($\bar{x}$ = 0.18) and, as mentioned above, for the section from the 29th to the 28th millennium BP ($\bar{x}$ = 0.19). As can be inferred from the change rates for the morphometric features, notably low change rates are calculated for the section from the 28th to the 27th millennium BP ($\bar{x}$ = 0.11), in the period between the 24th and the 20th millennium BP ($\bar{x}$ = 0.11, 0.1, 0.13, 0.12) as well as for the youngest two sections from the 16th to the 15th millennium BP ($\bar{x}$ = 0.13) and the 15th to the 14th millennium BP ($\bar{x}$ = 0.06), all of which not exceeding the average change rate for the entire observed timeframe. *(Figure 38)*

When analysing the frequency of correlations between morphometric features and the passage of time, represented by the calibrated ages of the assemblages within each section, the highest frequencies are observed during

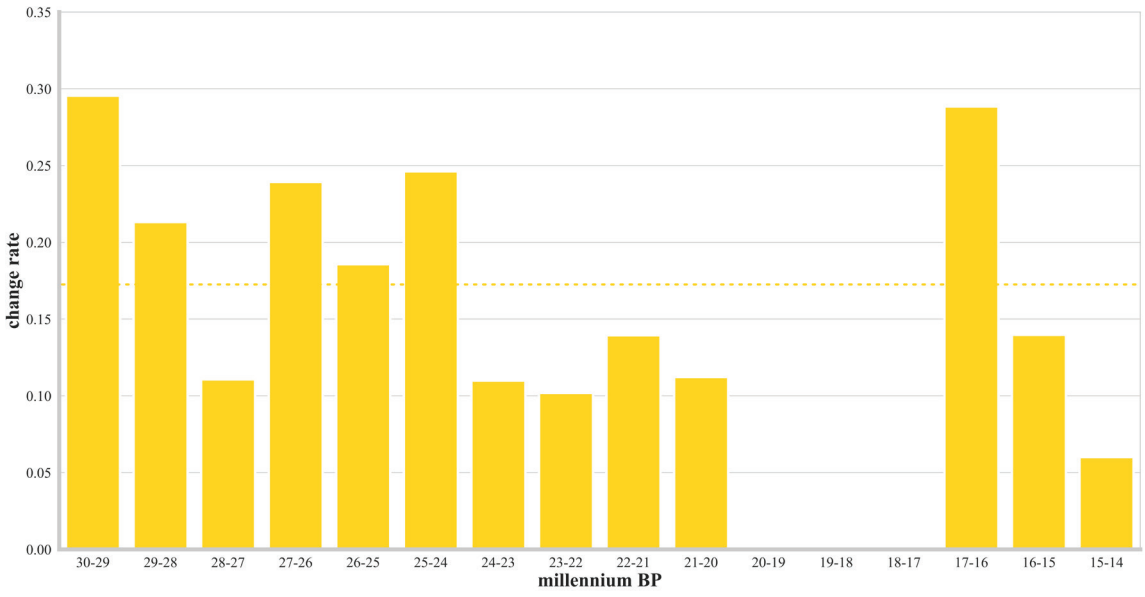



Figure 38: Averages ($\bar{x}$) of change rates *per* section in millennium BP (dotted line = average change rate for all sections).

the RDA-significant sections (*see Table 5*: 27th–26th millennium BP: n = 4, 26th–25th millennium BP: n = 5, 25th–24th millennium BP: n = 4, 21st–20th millennium BP: n = 4, 17th–16th millennium BP: n = 5). In the two oldest sections, no significant correlations are present, except for the positive correlation of the MP-CM-y-offset in the section from the 30th to the 29th millennium BP, suggesting random changes during this initial period. In the section from the 28th to the 27th millennium BP, one significant correlations was calculated, potentially marking a first weak onset of chronologically directed changes. Between the 24th and 21st millennia BP, only a few significant correlations are found: two positive correlations for the l-w-index and the left-right-ratio in the section from the 23rd to the 22nd millennium BP as well as two correlations for the upper-lower-ratio. These low numbers further highlights this period as one of minimal or no chronologically directed change. In contrast, the youngest two sections show relatively high numbers of significant correlations (16th–15th millennium BP: n = 3, 15th–14th millennium BP: n = 2), despite the change rates being very low and the RDA results not being significant for the youngest section.

As inferred from the results of the RDA and the correlations, the very beginning of the existence of SPs is marked by some pronounced but not chronologically directed – random varying – changes taking place until the 27th millennium BP. The section from the 27th to the 26th millennium BP then marks the beginning of a phase of chronologically directed changes that lasts until the 24th millennium BP with a peak in change between the 25th and the 24th millennium BP. After the 24th millennium BP, a phase of roughly 4000 years of only minor, mostly chronologically probably undirected changes far below the expected amount of change follows, which ends in a hiatus of classical SPs of 2000 years until the 17th millennium BP. It can be expected that with the return of classical SPs to the hunter-gatherer toolkit, fast chronologically directed changes are taking place in the morphometry. These are than again followed by probably not chronologically directed changes of only low intensity.

Supporting the findings made in Chapter 4.1.1 (RDA), the results of the change rates made evident, that a simple, linear mode of change in SP morphometry throughout the entire period under investigation can be ruled out. Instead, the data reveal a pattern of punctuated shifts, where phases of accelerated change are interspersed with periods of relative stability or slower transformations. Notably, two phases of more intense morphological change stand out: the period between the 27th and the 24th millennium BP, and the section between the 17th and the 16th millennium BP. During these phases, intensive significant alterations in size and shape occurred, possibly indicating periods of intensified selective pressure and adaptation. In contrast, these bursts of change are followed by phases of more gradual shifts of lower intensity or even stagnation. These phases could reflect periods of reduced selective pressures, during which the existing characteristics were retained or only minorly modified.

### *4.1.3.3 Directedness of Change Rates*

Having identified periods in which morphometric features exhibit particularly high rates of chronological change, as well as differences in the magnitude of change among individual features, the next step is to examine the direction of these changes. To this end, the sign of the change rates (positive or negative) is taken into account.

***width***

Besides a slight regression of the values in the 27th millennium BP, the width of the SPs underlies a stable increasing trend throughout the first five millennia of the observed period (30th–26th millennium BP). Afterwards, width shows a countertrend for over 2000 years leading to again narrower forms until the 24th millennium BP, where the values among the lowest in the entire dataset (as low as in the two oldest millennia). From the 24th millennium BP on a quite pronounced increasing trend lasting 2000 years is calculated, restoring the values from before the decreasing trend. This is than followed by another 2000 years of stable values in width. The strong change rate for the section between the 17th and the 16th millennium BP described above derives from a distinct increase in width. Within the two youngest millennia, there seems to be almost no change in width taking place.

***length***

Besides a two millennia lasting phase of SPs becoming shorter between the 27th and the 26th millennium BP, the SPs seem to increase consistently in length within the oldest five millennia. Between the 25th and the 24th millennium BP, this trend is interrupted by a distinct drop in length, which however, is followed by another increasing trend until the 21st millennium BP. From the 21st to the 20th millennium BP, the values drop again. The values for length then stay quite stable throughout the youngest four millennia (17th to 14th millennium BP).

***area***

The course of change in area is very much comparable to the changes in width and length but much more distinct. The almost consistent increasing trend in size within the oldest five millennia calculated for length and width is reproduced in area. Even the short regression around the 27th millennium BP is shown. After the 25th millennium BP, the values for area of course also drop for one millennium just to recover steadily until the 21st millennium BP. Also, the rapid increase in size from the 17th to the 16th millennium BP, implied by the distinct trend for width, is displayed.

***l-w-index***

After a pronounced increase in the l-w-index between the 30th and the 29th millennium BP, SPs seem to underlie a steady trend towards slenderer forms until the 26th millennium BP. With the section to the 25th millennium BP, again a pronounced, short termed increase in values is marked. Afterwards again, although a bit weaker, a steady decreasing trend until the 22nd millennium BP is observable. From the 22nd to the 21st millennium BP, once more a sudden, pronounced increase in values is marked. With the exception of the slight decrease in values for the section between the 17th and the 16th millennium BP, no changes seem to happen in the l-w-index during the youngest four millennia (17th to 14th millennium BP).

***upper-lower-ratio***

In the beginning of the observed timeframe stands a peak change rate between the 30th and the 29th millennium BP described above, indicating SPs with much shorter hafting parts in relation to their transformative parts in the 29th millennium BP. With the 28th and the 27th millennium BP, the values are a bit lower again. From the 27th millennium BP on, the upper-lower-ratio starts to show an almost linear, consistent increasing trend until the 22nd millennium BP, indicating a gradual decrease in the relative length of the hafting part, or conversely, an increase in the relative length of the transformative part over this period. This long-lasting trend is followed by a 2000 year period of a low degree of regression and stagnation between the 22nd and the 20th millennium BP. The strong change rate for the section between the 17th and the 16th millennium BP described above derives from a distinct decrease in the upper-lower-ratio, lowering the values back to the level from around the 25th and 24th millennium BP. However, this development is restored immediately with the subsequent 15th millennium BP. From the 15th to the 14th millennium BP a slight decrease in values is indicated. Inspecting the last three millennia as a unit, the values for the upper-lower-ratio seem to follow a stochastic trajectory, indicating fluctuations around a central value.

***left-right-ratio***

During the first five millennia, the change in left-right-ratio does not seem to follow any directed course. It rather shows slight variations around a more or less stable value. With the section between the 27th and the 26th millennium BP, a pronounced decrease in the values is marked, which however is compensated again with the subsequent section. For the 24th and the 23rd millennium BP, values are more or less identical, implying a short-term phase of relative stasis. For the section between the 23rd and the 22nd millennium BP a distinct shift in the left-right-ratio is observable, actually indicating more asymmetric SPs in the 22nd millennium BP. The values than remain low until the 20th millennium BP. Inspecting the period from the 24th to the 20th millennium BP as a unit, a slight but not entirely linear (interrupted by the abrupt shift between the 23rd and the 22nd millennium BP), negative trend is observable, indicating a tendency towards more asymmetric SPs. For the 17th millennium BP the values for the left-right-ratio are quite low too. With the 16th millennium BP the values abruptly change significantly to higher values. Even though the values remain quite high, the left-right-ratio subsequently shows a slight negative trend until the 14th millennium BP again.

***tip angle***

Besides the distinct drop of the values in the 29th millennium BP, the tip angle stays quite stable throughout the first five millennia of the observed period (30th–26th millennium BP). This is especially true for the period between the 28th and the 26th millennium BP. With the section from the 26th to the 25th millennium BP, a noticeable reduction in the tip angle takes place. Afterwards again a stable period of five millennia follows, where only minor fluctuations around a central value can be observed. With the section from the 21st to the 20th millennium BP, a slight change towards more obtuse tip angles takes place. From the 17th to the 16th millennium BP a substantial, abrupt change towards more acute tip angles is calculated. This development is then countered by a consistent trend towards more obtuse angles between the 16th and the 14th millennium BP.

***MP-CM-x-offset***

After the values for the oldest three sections until the 27th millennium BP are almost unchanged, a significantly strong positive change is takes place between the 27th and the 26th millennium BP. This is countered by an even stronger negative change – the extreme high value for between the 26th and the 25th millennium BP. After this pattern, a constant increasing trend between the 25th and the 23rd millennium BP is observable. Subsequently, between the 23rd and the 21st millennium BP, a constant decreasing trend follows. Between the 21st and the 20th millennium a short phase of stasis in the values seems to occur. With the 17th millennium BP, for which the values are slightly higher again, a stable decreasing trend in the MP-CM-x-offset values until the 14th millennium BP is shown.

***MP-CM-y-offset***

After the section between the 30th and the 29th millennium BP, where extreme differences in the MP-CM-y-offset have been calculated, an extremely pronounced, two millennia lasting increasing trend is shown. This trend is followed by a significant abrupt negative change from the 27th to the 26th millennium BP. After a slighter positive change between the 26th and the 25th millennium BP, a quite strong constant decreasing trend until the 23rd millennium BP is observable. Subsequently almost no change is happening from the 23rd to the 22nd millennium BP. Between the 22nd and the 20th millennium BP a constant increasing trend in the MP-CM-y-offset is shown, almost restoring the values from before the decreasing trend beforehand. Between the 17th and the 14th millennium BP, the values are alternately increasing and decreasing, seemingly varying around a central value.

The findings made above, identified some general patterns. Morphometric features related to the size consistently follow a similar pattern of an early growth trend (30th–25th millennium BP), a short-termed decrease (25th–24th millennium BP), a recovery trend or in other words second growth trend (24th–21st millennium BP), a short-termed increase (17th–16th millennium BP) and a final stabilisation (16th–14th millennium BP). While the trajectories in shape-related features tend to be more complex, there are some notable interrelations in the morphometric features. The l-w-index, highly influenced by the developments in width and length is the only shape-related features, that exhibits a more or less consistent trend in the early millennia (30th–25th millennium BP), indicating SPs become stouter over time. Additionally, the upper-lower-ratio, following an initial phase of apparent stasis until the 27th millennium BP, exhibits a consistent increasing trend until the 22nd millennium BP. This development suggests a gradual decrease in the relative length of the hafting part, or conversely, an increase in the relative length of the transformative part over this period. The other features either show stochastic trajectories (left-right-ratio) or stasis interrupted by abrupt changes (tip angle, MP-CM-x- and y-offset).

Visible in most shape-related features is a short-termed change between the 26th and the 25th millennium BP, most interestingly preceding the abrupt changes observable in the size-related features. This is then followed by consistent trends in the l-w-index (decreasing), the upper-lower-ratio (increasing) and the left-right-ratio (not linear but decreasing) until the 22nd millennium BP. Interestingly, these trends end one millennium before the second growth pattern in the size-related features. The tip angle in this period shows a stochastic trajectory. Both the MP-CM-x and y-offset show a cyclic pattern of an initial increase and a subsequent decreasing trend. The period between the 22nd and the 20th millennium BP

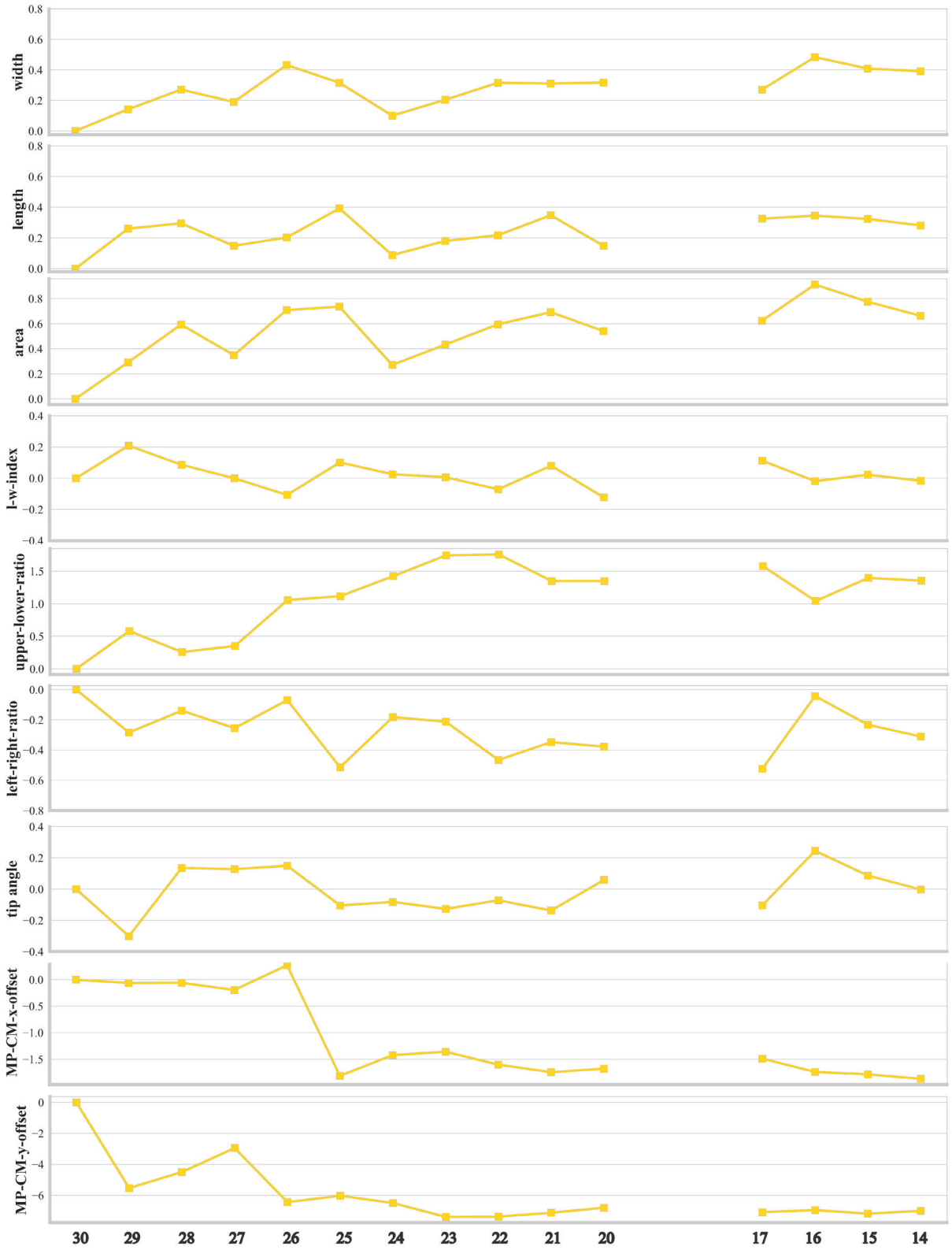



Figure 39: Summed change rates for each morphometric features, illustrating the course and the direction of change.

is then marked by stochastic variation or stasis in the shape-related features. Noticeable here are the abrupt changes in the l-w-index (decreasing) and the tip angle (increasing) for the section from the 21st to the 20th millennium BP. With the exception of the MP-CM-y-offset, all shape-related features show an abrupt change in the section from the 17th to the 16th millennium BP. The final period from the 16th millennium BP on is then marked by stasis in the l-w-index and the MP-CM-x-offset, a stochastic variation in the upper-lower-ratio and consistent decreasing trends in the left-right-ratio, the tip angle and the MP-CM- y-offset.
*(Figure 39, Table 12)*

### 4.1.4 Combining Variation and Change

Plotting variation against change rates for each chronological section reveals a diagonal separation across the plot *(Figure 40)*. Five sections – namely the RDA-significant sections 27th–26th, 26th–25th, and 25th–24th millennium BP, along with the earliest two sections (30th–29th and 29th–28th millennium BP) – cluster in the upper-right quadrant. This indicates a co-occurrence of high variation and high change rates. In the case of the RDA-significant sections, this pattern might suggest the influence of strong selective forces. For the two oldest sections, on the contrary, the results appear to be strongly influenced by the distinctive morphology of SPs from a single assemblage (A-60, Mitoc Malu-Galben) again, once more implying that the observed change rate and variation likely reflect regional peculiarity rather than selective pressure. Another RDA-significant section, the section from the 17th to 16th millennium BP, exhibits average variation paired with a high change rate, again suggesting directed evolutionary processes. Conversely, five additional sections – 22nd–21st, 21st–20th, and 16th–15th millennium BP (all RDA-significant), as well as the sections 28th–27th, 23rd–22nd and 15th–14th millennium BP – are situated in the lower-left quadrant, where both variation and change rates are low. Even though, RDA signalised chronologically directed changes taking place, these results are indicative of potential stabilising forces or only weak directed changes. The 24th–23rd millennium BP section is located very close to the upper-left quadrant, marked by average variation but a low rate of change, which may point to stochastic processes or other influences that increase variation without affecting the change rate. Such could be regionalisation characterised by the development of differing forms or short lived innovations of distinguished SP forms that do not occur before or after these two millennia.

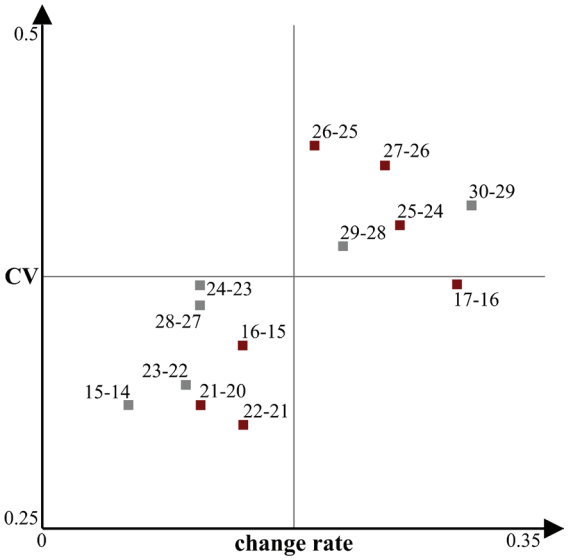



Figure 40: Scatterplot of Coefficient of variation (CV) and change rate for each section (vertical line = average change rate, 0.17; horizontal line = average CV).

### 4.1.5 Summary of the Results on the 'Chronologically Informed' Perspective

While RDA was employed to define the target periodisation, which was found to be 2000 year sections, it also identified seven distinct 2000 year sections where chronologically directed changes occurred. Notably, the three sections spanning the period between the 27th and 24th millennium BP stand out for their significant results. Additionally, two sections within the 22nd to 20th millennium BP period also returned significant changes. Lastly, the results for the two sections between the 17th and 15th millennium BP indicate yet another phase of chronologically directed transformations, suggesting multiple key intervals of morphologi-

cal evolution across the observed timeframe interspersed with phases of apparently no directed changes.

The analysis of variation across the individual 2000 year sections revealed a diverse pattern. The average amount of variation in the morphometric features within a 2000 year section is approximately 34%. At the beginning of the observed timeframe, the variation in the morphometric features of the SPs is relatively high but decreases until the section from the 28th to the 27th millennium BP. In the following three sections, variation increases significantly, peaking in the 26th to 25th millennium BP section. Afterward, a steady decline in variation is observed until the section from the 22nd to 21st millennium BP. In the final three sections, variation remains comparatively low, while declining gradually until the end of the observed timeframe. For most of the sections, shape-related features showed much more variation than features related to size.

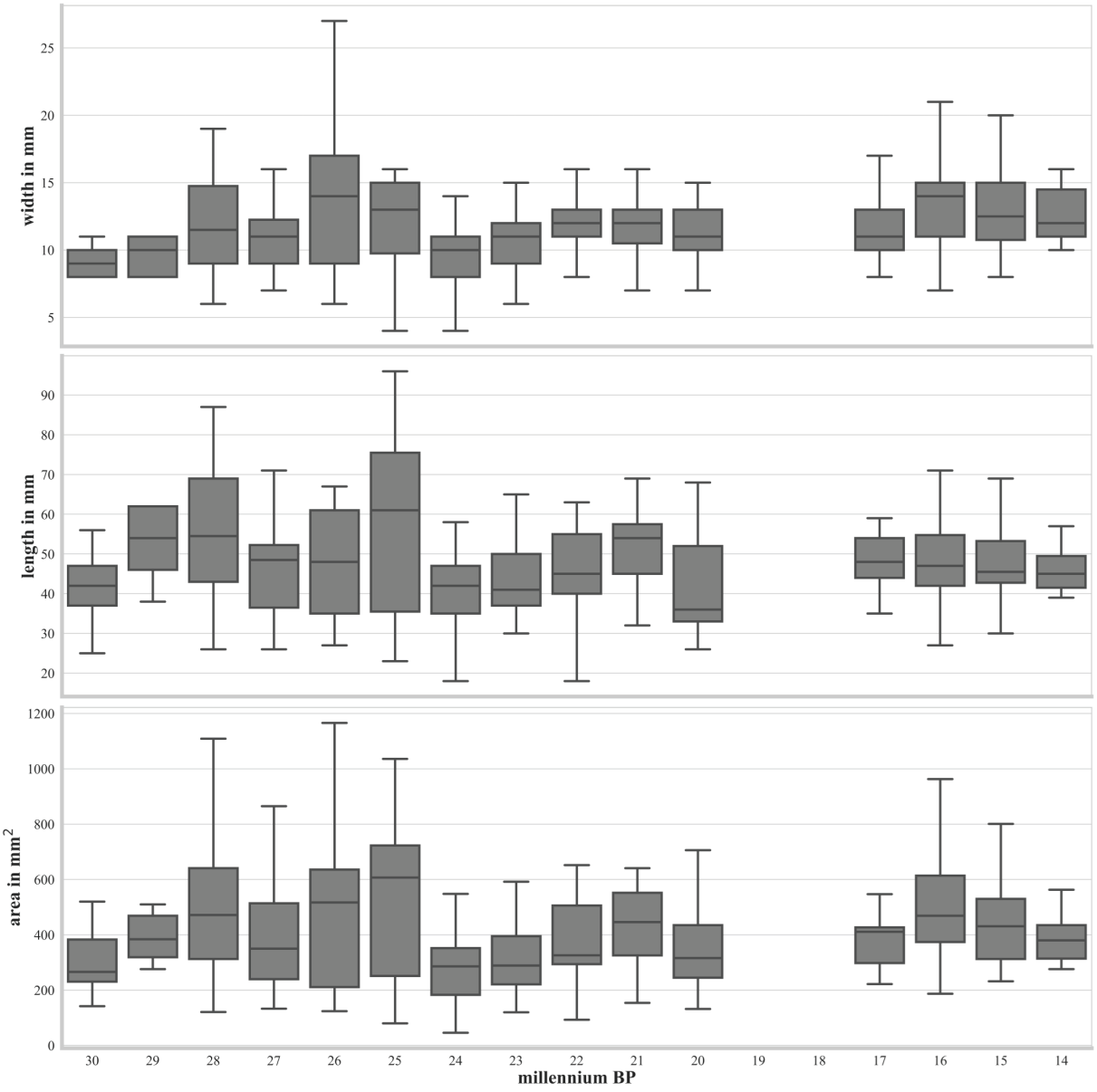



Figure 41: Box-plots of real values of size-related features (outliers and values for the 19th and 18th millennium BP excluded).

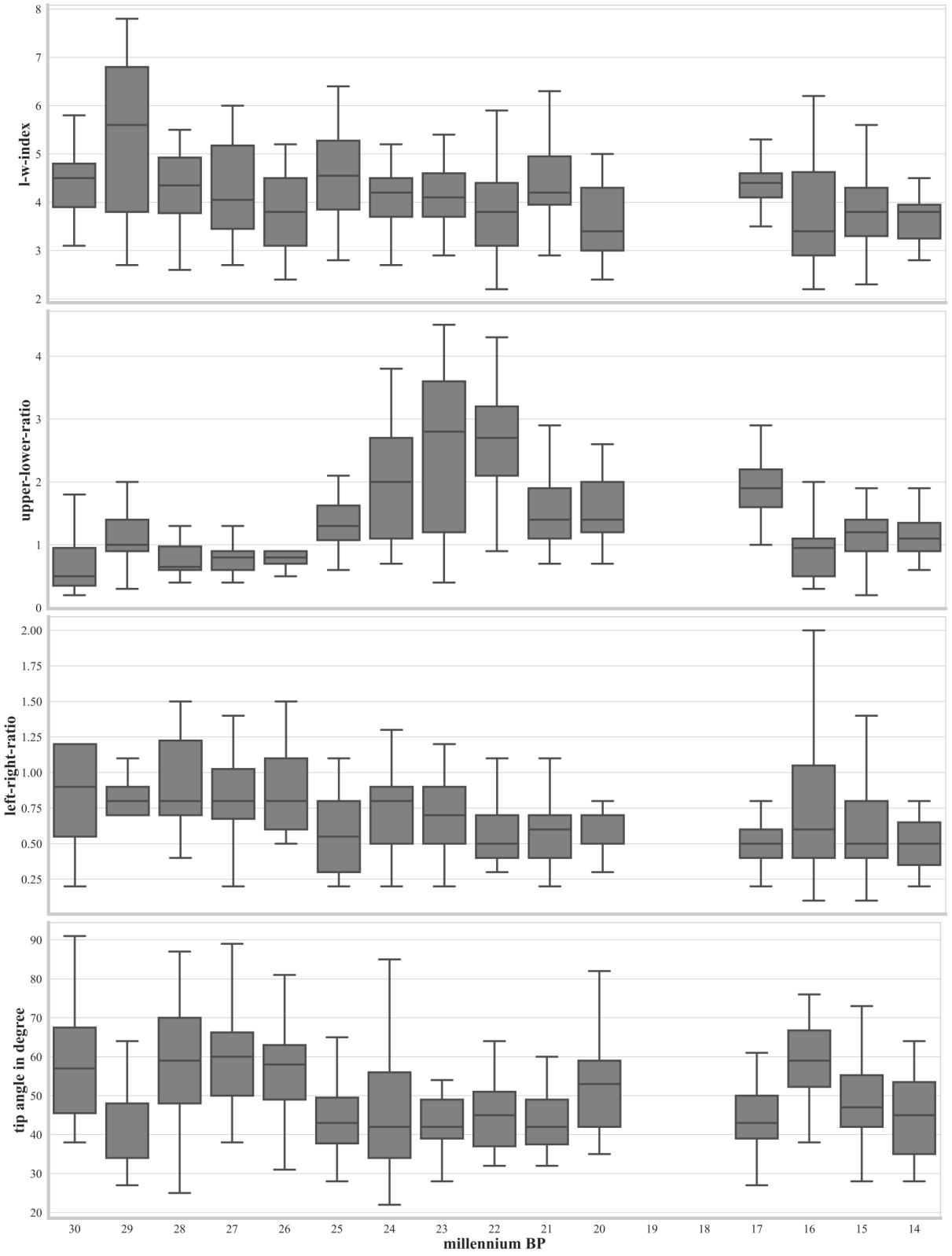



Figure 42: Box-plots of real values of shape-related features (outliers and values for the 19th and 18th millennium BP excluded).

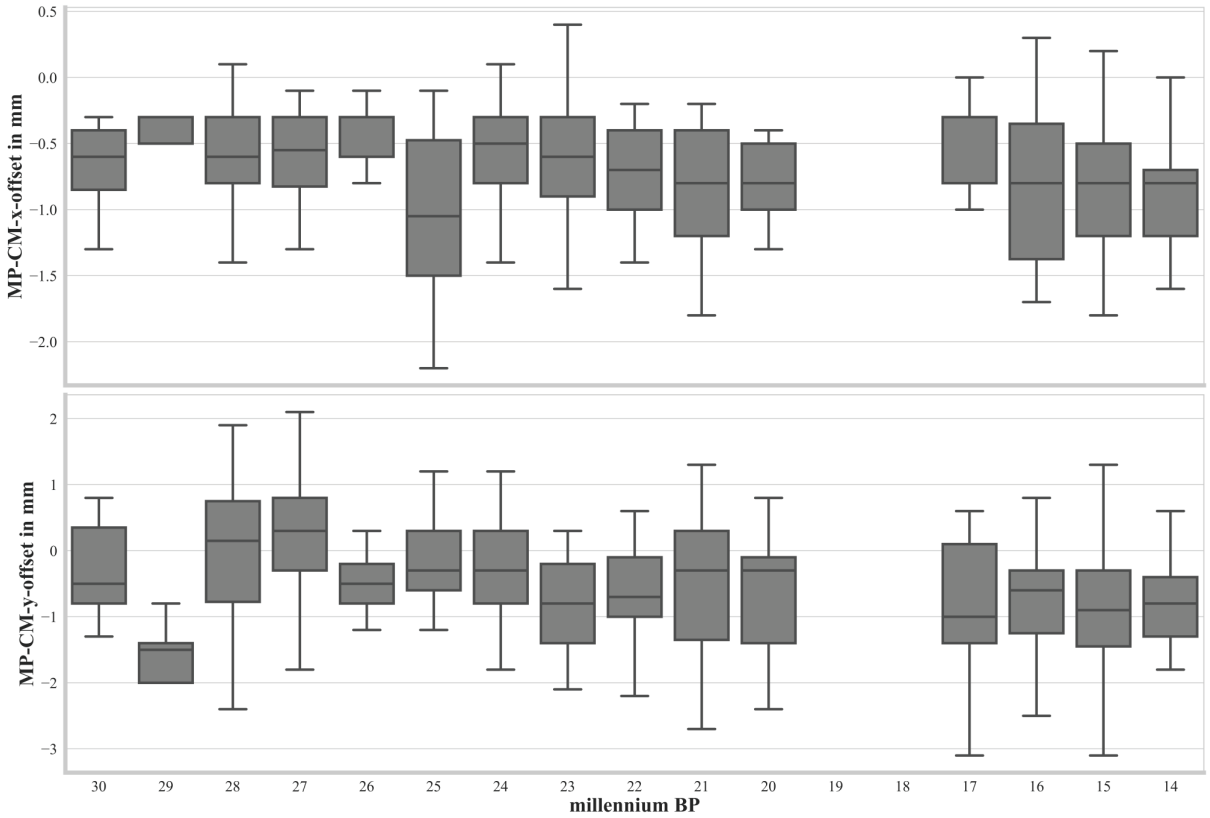



Figure 43: Box-plots of the real values of the centre of mass offset features (outliers and values for the 19th and the 18th millennium BP excluded).

The calculation of change rates across individual 2000 year sections provided multiple insights into the dynamics of morphometric change in SPs. Firstly, the average change rate, or the expected amount of change between two consecutive millennia or within a 2000 year section, is approximately 17%. The pattern observed for variation is reflected in the change rates across the sections. Following an extremely high value in the oldest section, change rates decline rapidly until the section from the 28th to 27th millennium BP. The period between the 27th and 24th millennium BP then exhibits elevated change rates, followed by a 4000 year phase of relatively low change until the 20th millennium BP. A notable increase in change is observed in the section from the 17th to the 16th millennium BP, after which change rates decline sharply until the end of the observed timeframe. Once again, shape-related features contribute significantly more to the average change rates than size-related features. The features exhibiting the highest average change, and therefore are expected to perform best for chronological distinction, are area, the left-right-ratio, the upper-lower-ratio, and the MP-CM-y-offset.

The combined analysis of variation and change rates reveals a clear differentiation among sections: those in which selective forces are a plausible explanatory factor – namely the sections 27th–26th, 26th–25th, and 25th–24th millennium BP, along with the earliest two sections (30th–29th and 29th–28th millennium BP) and the section from the 17th to the 16th millennium BP – though regionalisation or innovation of new, short lived SPs forms may also have contributed –; those likely influenced by stabilising forces – 28th–27th, 22nd–21st, 21st–20th, and 16th–15th millennium BP (all RDA-significant), as well as 23rd–22nd and 15th–14th millennium BP – and a single section suggestive of stochastic influences or, alternatively, pronounced regionalisation or innovation dynamics – the section from the 24th to the 23rd millennium BP.

Combining the insights from the various methodological approaches, the following pattern emerges: at the initial appearance of SPs, high variation and a lack of clearly directed change likely indicate a phase of stochastic variation – although some developmental trends are observable – driven by both intra- and inter-assemblage diversity. Beginning with the section from the 27th to the 26th millennium BP, directed changes begin to occur. Until the 24th millennium BP, a phase marked by both high variation and strong chronologically directed change unfolds, suggesting that selective forces were actively shaping SP morphologies during this time. This is followed by the section from the 24th to the 23rd millennium BP, which exhibits high variation but a low rate of change, along with non-significant RDA results – conditions that likely reflect regionalisation or incipient innovation dynamics. Subsequently, a steady decline in variation and change rate is observed until the 20th millennium BP, suggesting a period influenced by stabilising forces. With the pronounced re-emergence of SPs in European Upper Palaeolithic inventories, a new phase of strong, chronologically directed change begins, likely driven again by selective forces. The final two sections are characterised by both low variation and low change rates, indicating a return to stabilisation. *(Figures 41–43)*

## 4.2. RESULTS ON THE 'ARCHAEO-STRATIGRAPHICALLY INFORMED' PERSPECTIVE

The analysis in this chapter is conducted with sensitivity to both taxonomic units and geographical context. By examining chronological signals within and between major taxonomic groups, the study seeks to reveal temporal dynamics that might be obscured in aggregated datasets or overlooked in analyses based solely on chronological ordering. Furthermore, since several strong signals observed in the chronologically informed perspective coincide with the timing of taxonomic transitions, particular emphasis is placed on assessing the impact of such on these results.

Given the limited number of samples in certain minor taxonomic units, the analysis focusses on the major taxonomic units yielding SPs *(Figure 3)*. Where feasible, multiple minor taxonomic units were aggregated into a larger, composite unit to ensure sufficient sample size for robust statistical analysis. As demonstrated in the analysis of the previous chapter, limiting the calculations to category A assemblages did not significantly impact the results. Consequently, while the dataset composition will be acknowledged, such restrictions will only be applied where sample sizes permit, thereby avoiding further limitations to already constrained datasets.

### 4.2.1 Within Taxonomic Units

The analytical methods presented in Chapter 4.1 are also applied to examine variation within individual taxonomic units. This allows an assessment of whether the chronological trends in SP morphometry identified in the chronologically informed analysis are consistently observed when each taxonomic unit is analysed separately.

#### *4.2.1.1 Redundancy Analysis*

Again, RDA is employed on the 2000 year periodisation to establish a foundational understanding of the temporal dynamics.

##### *4.2.1.1.1 Late Gravettian*

For the Late Gravettian, 77 SPs from 22 ClassI assemblages across central and eastern Europe, dating between 30.0 and 25.4 ka calBP are available. 16 sites yield more than a single SP, containing a total amount of 70 SPs – category A assemblages – and six category B assemblages yielding only a single specimen.

At the very beginning of the Late Gravettian, the number of assemblages and associated specimens is notably limited (30th millennium BP: 4 assemblages, 11 SPs; 29th millennium BP: 2 assemblages, 5 SPs). A significant increase in both assemblages and SPs occurs during the 28th and the 27th millennia BP, with these two periods collectively contributing over half of the entire dataset (28th millennium BP: 7

assemblages, 26 SPs; 27th millennium BP: 6 assemblages, 24 SPs). Following this peak, the numbers decline sharply during the 26th millennium BP (2 assemblages, 10 SPs) and drop off entirely after the 25th millennium BP (1 assemblage, 1 SP), marking the end of the Gravettian. *(Figure 44)*

20 of these assemblages are spatially clustering in three more or less distinct core areas *(Map 3)*. Two more sites are located outside these core areas. Core area one is formed by nine sites – Milovice I, section G (B-25), Grub-Kranawetberg, AH4 (A-62), Willendorf II, layer 9 (A-61), Krakow Spadzista B, layer 6 (A-59), Nitra I-Čermáň (A-55), Moravany nad Váhom-Lopata II (B-22), Moravany nad Váhom-Podkovica (A-53), Banka-Horné farské role (B-21), Petřkovice, layer 1a (A-51) – located in lower Austria, Moravia, Poland and Slovakia, yielding 25 specimens. The calibrated ages of the available radiocarbon dates ranging from 30.0 to 26.5 ka calBP, including the oldest SP of the entire dataset from Milovice I, section G (B-25) and covering most of the time period assigned to the Late Gravettian.

Core area two is formed by five sites – Molodova V, layer 7 (A-63), Mitoc-Malu Galben, layer 4a (A-60), Buda, layer 1 (B-23), Bistricioara-Lutărie III, AH 2.5 (A-57) and Dorotchivtsy III, layer 6 (A-52) – located at the Outer Eastern Carpathians in Romania and the Dniester valley in south-western Ukraine, yielding 17 specimens. The calibrated ages of the available radiocarbon dates ranging from 29.5 to 26.6 ka calBP, which gives it a comparable period of time to core area one.

Core area three is formed by six sites - Kostënki 1 (Poliakov), layer I (A-58), Khotylëvo 2 (A-56), Kostënki 21 (Gmelinskaya), layer III (A-54), Gagarino (A-50), Avdeevo (A-49) and Pushkari I (B-19) – located close to the rivers Desna, Seym and Don in Russia, yielding 33 specimens. The calibrated ages of the available radiocarbon dates ranging from 27.6 and 25.4 ka calBP (24.3 ka calBP for the single specimen from Pushkari I (B-19)), which makes this core area slightly younger than both more western ones.

The two assemblages not clustering within these core areas are the two Italian sites Riparo Mochi, layer D (B-24) in Liguria with one of the oldest calibrated ages in the entire dataset of

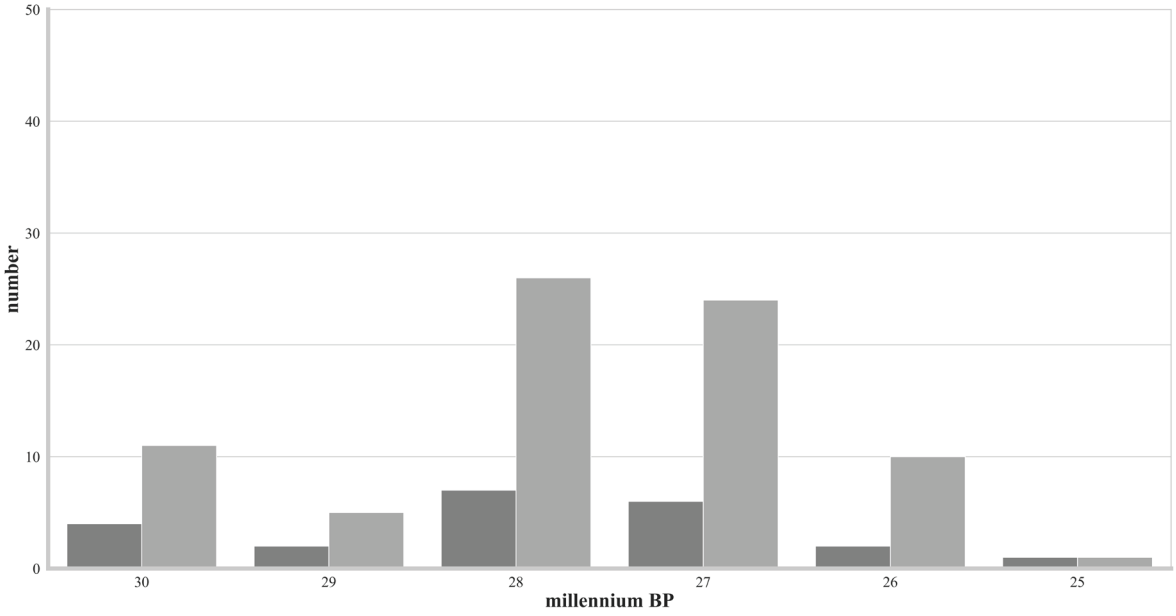
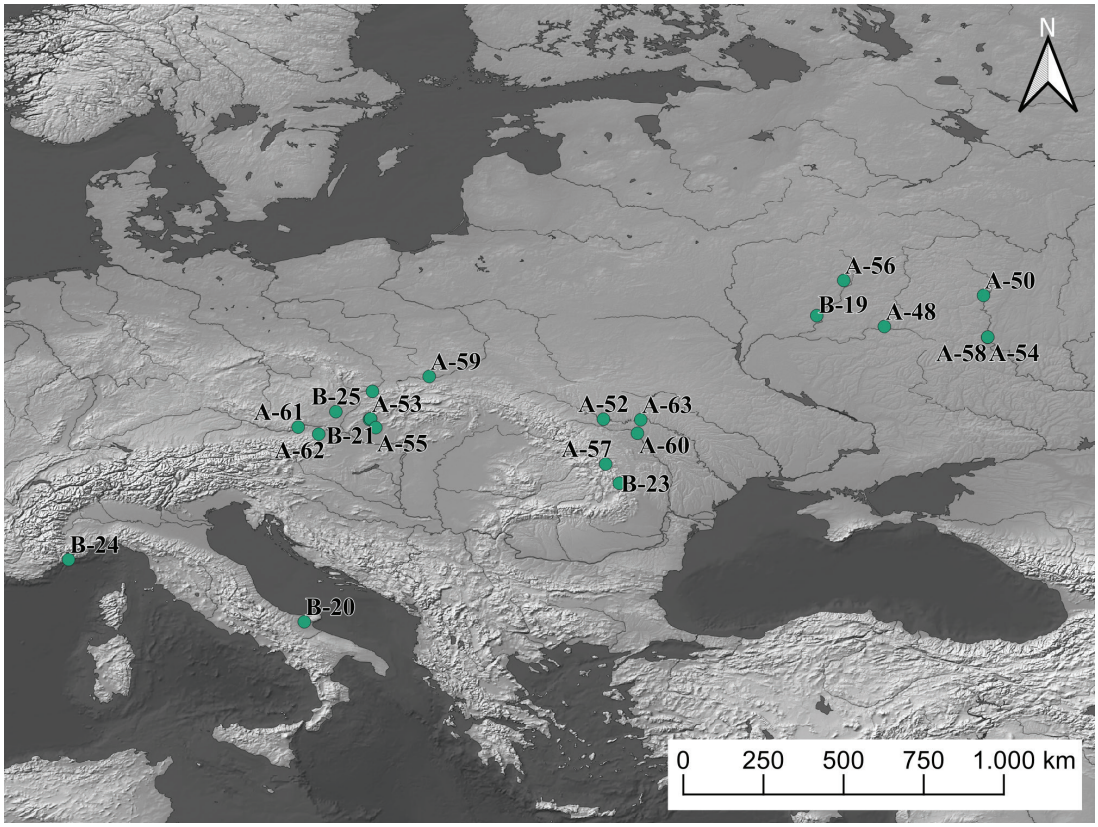



Figure 44: Number of assemblages and artefacts per millennium BP of the Late Gravettian (dark grey, left bar = assemblages; light grey, right bar = artefacts).




Map 3: Class I assemblages of the Late Gravettian (n = 22; labels = IDs).

28.9 ka calBP and Grotta Paglicci, layer 20 (B-20) in Puglia dating quite young to around 26.1 ka calBP. *(Table 13)*

Using the calibrated ages as canonical variable for all dated specimens assigned to the Late Gravettian, the result of the RDA is weak ($R^2$ = 0.014) and not significant (p = 0.367), indicating no chronologically directed changes across the entirety of the Late Gravettian. The same outcome is observed when only category A assemblages are considered ($R^2$ = 0.0174, p = 0.265).

The oldest section, ranging from the 30th to the 29$^{th}$ millennium BP, is represented by three assemblages from core area one (B-25, A-62, A-61), two from core area two (A-63, A-60), and a single SP from Italy (B-24), yielding a total of 16 SPs. The second section, covering the 29$^{th}$ to the 28$^{th}$ millennium BP, includes three assemblages from core area one (A-59, A-55, B-22), three from core area two (A-60, B-23, A-57), two from core area three (A-58, A-56), and again a single SP from Italy (B-24), yielding a total of 31 SPs. The best-represented section of the Late Gravettian, spanning the 28$^{th}$ to the 27$^{th}$ millennium BP, consists of six assemblages from core area one (A-59, A-55, B-22, A-53, B-21, A-51), three from core area two (B-23, A-57, A-52), three from core area three (A-58, A-56, A-54), and a single SP from Italy (B-20), yielding a total of 50 SPs. The final section suitable for analysis, ranging from the 27$^{th}$ to the 26$^{th}$ millennium BP, comprises three assemblages from core area one (A-53, B-21, A-51), one from core area two (A-52), three from core area three (A-54, A-50, A-49), and a single SP from Italy (B-20), yielding a total of 34 SPs.

The first three section-wise RDA values for the Late Gravettian can be directly inferred from Chapter 4.1.1, as there are no other taxonomic units yielding SPs until the 26$^{th}$ millennium BP. These earlier results include a strong but not significant signal in the section from the 30$^{th}$ to the 29$^{th}$ millennium BP ($R^2$ = 0.0979, p = 0.188) and two relatively weak and not significant signals for the sections from the 29$^{th}$ to the 28$^{th}$ millennium BP ($R^2$ = 0.0352, p

Table 13: Chronological and geographical distribution of dated Late Gravettian assemblages.

| mil. BP | core area 1 | core area 2 | core area 3 | other |
|---|---|---|---|---|
| **25th** | | | B-19 | |
| **26th** | | | A-50, A-49 | |
| **27th** | A-53, B-21, A-51 | A-52 | A-54 | B-20 |
| **28th** | A-59, A-55, B-22 | B-23, A-57 | A-58, A-56 | |
| **29th** | | A-60 | | B-24 |
| **30th** | B-25, A-62, A-61 | A-63 | | |

= 0.388) and from the 28th to the 27th millennium BP ($R^2$ = 0.0368, p = 0.087). For the fourth section from the 27th to the 26th millennium BP, new calculations were necessary to exclude the earliest Upper Solutrean assemblage yielding SPs (Abauntz (A-49), see above). Following this adjustment, the calibrated ages for this modified section significantly (p = 0.008) explain 9.8% ($R^2$ = 0.0981) of the variation in the morphometric features. *(Table 14, Figure 45)*

Conducting an RDA for all dated specimens in core area one, the calibrated ages as the canonical variable explain 7.3% ($R^2$ = 0.0729) of the variation in morphometric features. However, the result is not significant (p = 0.116), most likely due to the low sample size. A subdivided analysis for 2000 year sections is only feasible for the 28th to 27th millennium BP. However, for the small remaining number of assemblages (n = 6), the result is not significant (p = 0.187), despite the calibrated ages explaining 8.9% ($R^2$ = 0.0891) of the variation in the morphometric features. In core area two, the calibrated ages explain 7.4% ($R^2$ = 0.0742) of the variation in morphometric features, though the result is not significant (p = 0.333). Due to the limited sample size, a subdivided analysis for 2000 year sections is not feasible. In core area three, the calibrated ages explain 5.9% ($R^2$ = 0.0587) of the variation, or 6.5% ($R^2$ = 0.0653) when excluding the single specimen from Pushkari I (B-19), which dates comparably young. In both cases, the results remain non-significant (p = 0.1 / p = 0.072 without Pushkari I). However, conducting an RDA for the 28th to 27th millennium BP in core area three yields a striking result: 14.1% ($R^2$ = 0.141) of the variation in morphometric features is highly significantly explained by the calibrated ages (p = 0.016). A comparably high value is also calculated for the section from the 27th to the 26th millennium BP in core area three, where the calibrated ages significantly (p = 0.003) explain 16.3% ($R^2$ = 0.1627) of the variation. *(Table 15)*

This initial analysis suggests no significant chronologically directed changes across the entire Late Gravettian dataset. However, breaking the timeframe down to 2000 year sections, it is indicated that chronologically directed changes seem to occur at the end of the Late Gravettian. Additionally, while some results remain statistically weak, the individual core areas exhibit strong chronological trends. Overall, the findings indicate regionally distinct developments, probably obscuring each other.

#### *4.2.1.1.2 Upper Solutrean*

The Upper Solutrean dataset comprises 80 SPs from 16 dated assemblages across central and western Europe, dating between 25.9 and 19.5 ka calBP. Of these, 12 assemblages contribute more than a single specimen, collectively accounting for 76 SPs. The majority of SPs and assemblages yielding SPs are concentrated in the classical Upper Solutrean period, between the 25th and the 22nd millennium BP. This period encompasses 19 SPs from three assemblages in the 25th millennium, 23 SPs from six assemblages in the 24th, 14 SPs from

Table 14: RDA results with calibrated ages ('ka calBP') as canonical variable for the Late Gravettian sections (dark red: p-value <= 0.05).

| mil. BP | 30th–29th | 29th–28th | 28th–27th | 27th–26th |
|---|---|---|---|---|
| SPs | 16 | 31 | 50 | 34 |
| assemblages | 6 | 9 | 13 | 8 |
| p | 0.188 | 0.388 | 0.087 | 0.008 |
| $R^2$ | 0.0979 | 0.0352 | 0.0368 | 0.0981 |

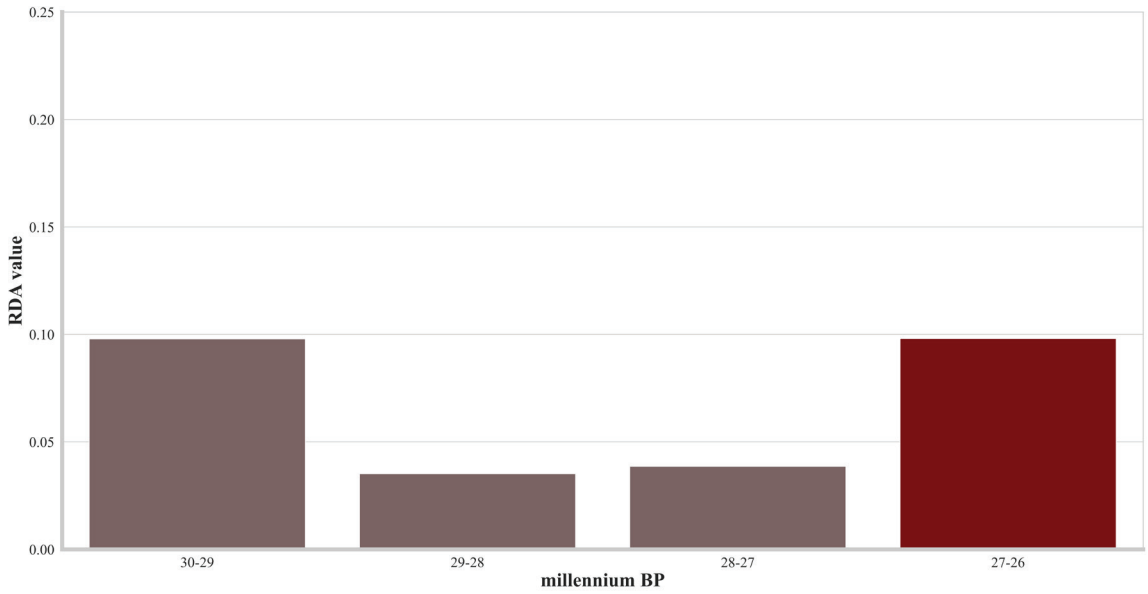



Figure 45: RDA values ($R^2$) for 2000-year sections of the Late Gravettian with calibrated ages ('ka calBP') as canonical variable (dark red = p ≤ 0.05, pale red = p > 0.05).

two assemblages in the 23rd, and 20 SPs from three assemblages in the 22nd millennium BP – together comprising 95% of all dated Upper Solutrean SPs. The oldest Upper Solutrean assemblage, Abauntz (A-49), yielding three SPs, likely dates to the 26th millennium BP, while the youngest SP, assigned to the Upper Solutrean, originates from Amalda (B-13) and is most likely dated to the 20th millennium BP. *(Figure 46)*

Nine sites – Abauntz (A-49), Cueva Morín (B-18), Cueva de la Riera, layer 5a (B-17), Altamira, layer 7 (A-35), El Mirón (B-15), Aitzbarte IV (A-34), Cueto de la Mina (A-32), Cueva del Moro Chufin (A-31), and Amalda (B-13) – are situated along the northern Spanish coast *(Map 4)*, spanning the entire timespan of the Solutrean dataset and collectively yielding 40 SPs. The calibrated ages of the radiocarbon dates for this cluster range from 25.9 to 19.5 ka calBP, encompassing both the oldest and youngest Upper Solutrean assemblages. However, the majority of SPs (n = 32) from

Table 15: RDA results with calibrated ages ('ka calBP') as canonical variable for the Late Gravettian core areas (dark red = p ≤ 0.05).

| mil. BP | core area 1 | core area 2 | core area 3 |
|---|---|---|---|
| **SPs** | 25 | 17 | 33 |
| **assemblages** | 9 | 5 | 6 |
| **p** | 0.116 | 0.333 | 0.1 |
| **$R^2$** | 0.0729 | 0.0742 | 0.0587 |

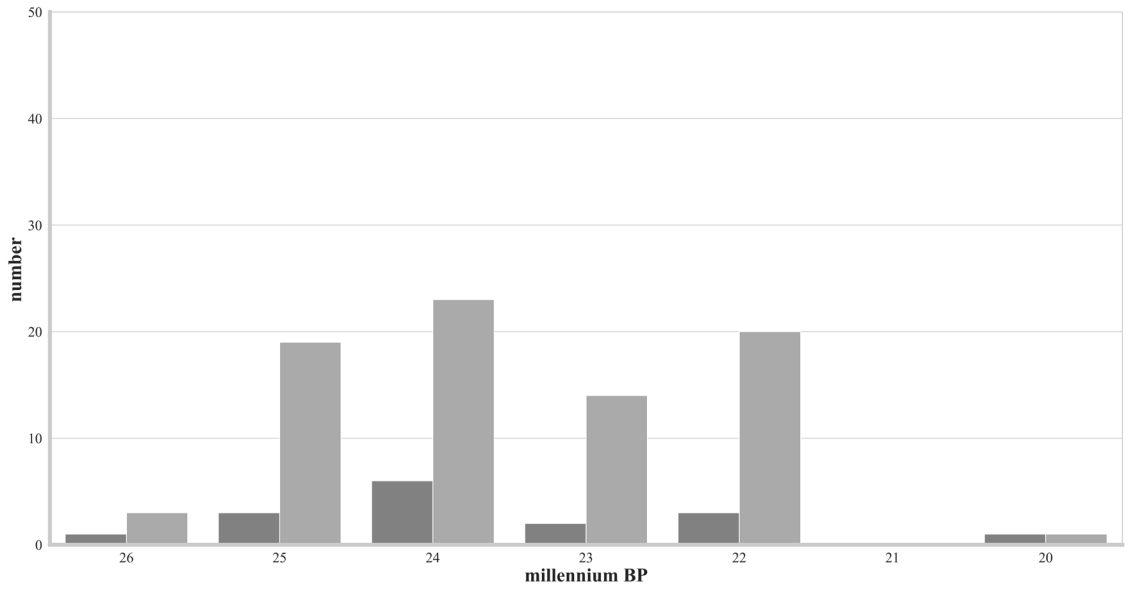
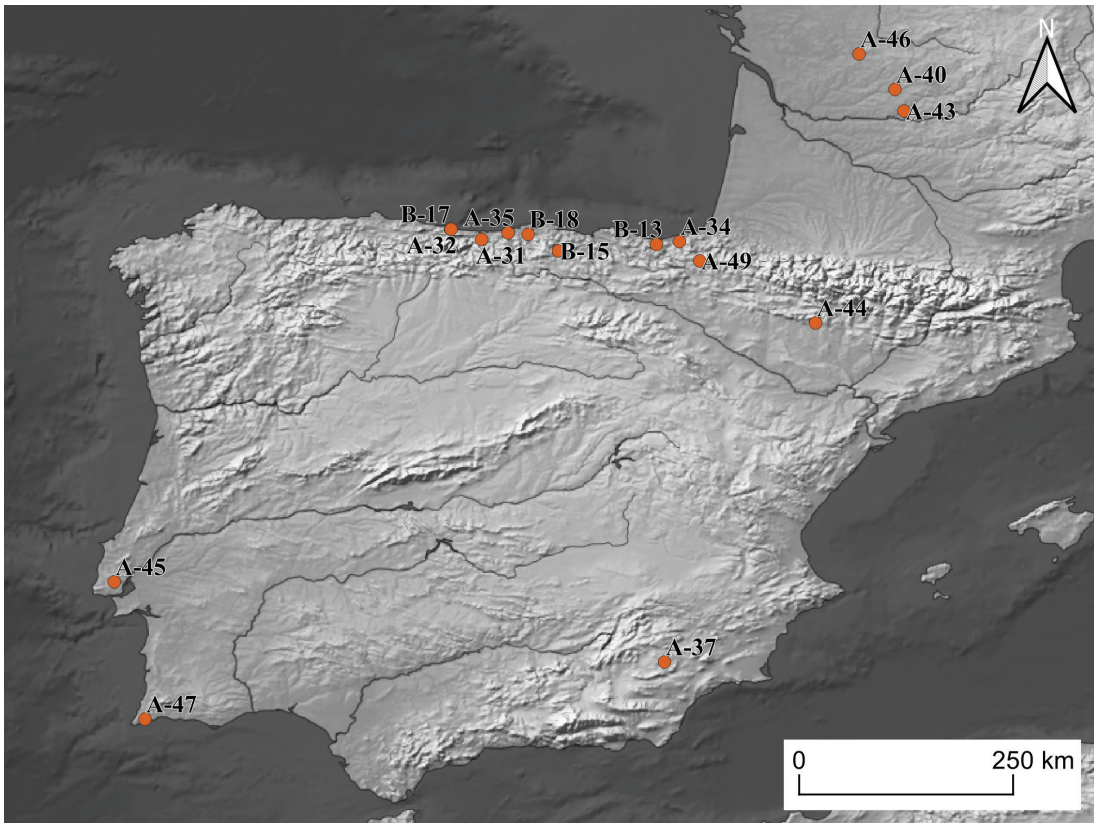



Figure 46: Number of assemblages and artefacts per millennium BP of the Upper Solutrean (dark grey, left bar = assemblages; light grey, right bar = artefacts).

this cluster originate from four assemblages (A-35, B-15, A-34, and A-32) dated between 22.8 and 21.3 ka calBP. Nearby, a single site – Cueva de Chaves (A-44) – is located on the southern foothills of the Pyrenees.

Three additional sites – Le Placard (A-46) Laugerie-Haute Ouest, Niveau pointe à cran (A-43) and Combe-Saunière, layer IV (A-40) – are clustered on the eastern edge of the Massif Central, between the Dordogne and Vienne rivers in France, and yield 18 SPs. The calibrated ages for this cluster range from 24.2 to 23.4 ka calBP, making it nearly 1000 years older than most specimens from the northern Spanish coast cluster. Another single site, Cueva de Ambrosio, layer II (A-37), located in the north eastern Betic Cordillera in south eastern Spain, yields 10 SPs. *(Map 4, Table 16)* Two more sites are positioned along the Portuguese coast: one at the mouth of the Tejo River on the east coast - Gruta de Salemas (A-45) – and the other at Cabo de São Vicente in the south - Vale Boi (A-47). With calibrated ages of 24.7 ka calBP (A-47) and 23.7 ka calBP (A-45), these sites yield a combined total of nine SPs (A-47: 5; A-45: 4).

Using the calibrated ages as canonical variable for all dated specimens assigned to the Upper Solutrean, the result of the RDA returns a highly significant (p = 0.004) result. 4.8%




Map 4: Class I assemblages of the Upper Solutrean (n = 16; labels = IDs).

Table 16: Chronological and geographical distribution of dated Upper Solutrean assemblages.

| mil. BP | n. Spanish coast cluster | French cluster | other |
|---|---|---|---|
| 20th | B-13 | | |
| 21st | | | |
| 22nd | A-34, A-32, A-31 | | |
| 23rd | A-35, B-15 | | |
| 24th | B-17 | A-43, A-40 | A-44, A-45, A-37 |
| 25th | B-18 | A-46 | A-47 |
| 26th | A-49 | | |

($R^2$ = 0.0484) of explained variation, implying chronologically directed trends taking place along the entirety of the Upper Solutrean.
Breaking the entire timespan of the Upper Solutrean SPs down into 2000 year sections, four such sections emerge. The first section from the 26th to the 25th millennium BP encompasses only the three SPs from Abauntz (A-49) for the 26th millennium BP and respectively one assemblage from the northern Spanish coast cluster (B-18) and the French cluster (A-46) as well as one assemblage from Portuguese (A-47) for the 25th millennium BP. The result is therefore not completely reliable. In total, the dataset only comprises 22 SPs (three from the 26th and 19 from the 25th millennium BP), which adds additional potential for suspicion on the result. However, the calibrated ages of the assemblages in this section significantly (p = 0.019) explain 14.6% ($R^2$ = 0.1458) of the variation in the morphometric features.

The second 2000 year section from the 25th to the 24th millennium BP comprises nine assemblages, including all dated French assemblages (A-46, A-43, A-40), both Portuguese assemblages (A-47, A-45), Cueva de Ambrosio, layer II (A-37) as well as two single specimens from two assemblages of the northern Spanish coast cluster (B-18 and B-17). Together this section comprises 42 SPs. The calibrated ages of these assemblages significantly (p = 0.013) explain 8% ($R^2$ = 0.0798) of the variation in the morphometric features.

The third 2000 year section of the Upper Solutrean, ranging from the 24th to the 23rd millennium BP, comprises 37 SPs from eight assemblages. These assemblages include the two younger French assemblages (A-43 and A-40), Cueva de Ambrosio, layer II (A-37), three assemblages from the northern Spanish coast cluster (B-17, A-35 and B-15), Gruta de Salemas (A-45) on the Portuguese coast and Cueva de Chaves (A-44) located on the southern foothills of the Pyrenees. The result of the RDA using the calibrated ages as canonical variable is comparably weak ($R^2$ = 0.0404) and not significant (p = 0.204).

The last 2000 year section feasible for analysis ranges from the 23rd to the 22nd millennium BP. It comprises a total of 34 SPs from five assemblages, all of which cluster along the northern Spanish coast – Altamira, layer 7 (A-35), El Mirón (B-15), Aitzbarte IV (A-34), Cueto de la Mina (A-32), Cueva del Moro Chufin (A-31). The calibrated ages of these assemblages significantly (p = 0.034) explain 8% ($R^2$ = 0.0727) of the variation in the morphometric features. *(Table 17, Figure 47)*

Conducting a RDA with all dated specimens from the nine assemblages at the northern Spanish coast, the calibrated ages as canonical variable highly significantly (p = 0.001) explain 13.1% ($R^2$ = 0.131) of the variation in the morphometric features. However, as shown beforehand for the 2000 year section of the Upper Solutrean ranging from the 23rd to the 22nd millennium BP, the main portion of the changes implied here for the entirety of the Upper Solutrean timespan in the northern Spanish coast cluster are not taking place in the youngest two millennia, where the dataset shows sufficient density. The high explanatory power therefore is rather the result of the difference between older pieces, rarely represented in this dataset, and the ones dating younger.

The calibrated ages of the assemblages clustering in France explain 13.9% ($R^2$ = 0.139) of the variation in the morphometric features. Most likely due to the low sample size, the result, however, is not significant (p = 0.063), highlighting the questionable reliability of this result. This high value has a significant influence on the result for the 2000 year section ranging from the 25th to the 24th millennium BP, overprinting a low ($R^2$ = 0.0293) and not significant (p = 0.653) explanatory power of the calibrated ages when the French assemblages are excluded. *(Table 18)*

The result of the initial analyses suggests that chronologically directed changes occur throughout the Upper Solutrean. However, when dividing the timespan into 2000 year sections, it becomes evident that the most significant changes take place at the very beginning of the Upper Solutrean. Further refining the analysis by examining geographical clusters often results in statistically insignificant findings or relies on small sample sizes, making the archaeological validity of these results questionable. An exception is the cluster at the northern Spanish coast, which potentially shows a high disparity between older and younger Upper Solutrean SPs.

Table 17: RDA results with calibrated ages ('ka calBP') as canonical variable for the Upper Solutrean sections (dark red: p-value <= 0.05).

| mil. BP | 26th–25th | 25th–24th | 24th–23rd | 23rd–22nd |
|---|---|---|---|---|
| SPs | 22 | 42 | 37 | 34 |
| assemblages | 4 | 9 | 8 | 5 |
| p | 0.019 | 0.013 | 0.204 | 0.034 |
| $R^2$ | 0.1458 | 0.0798 | 0.0404 | 0.0727 |

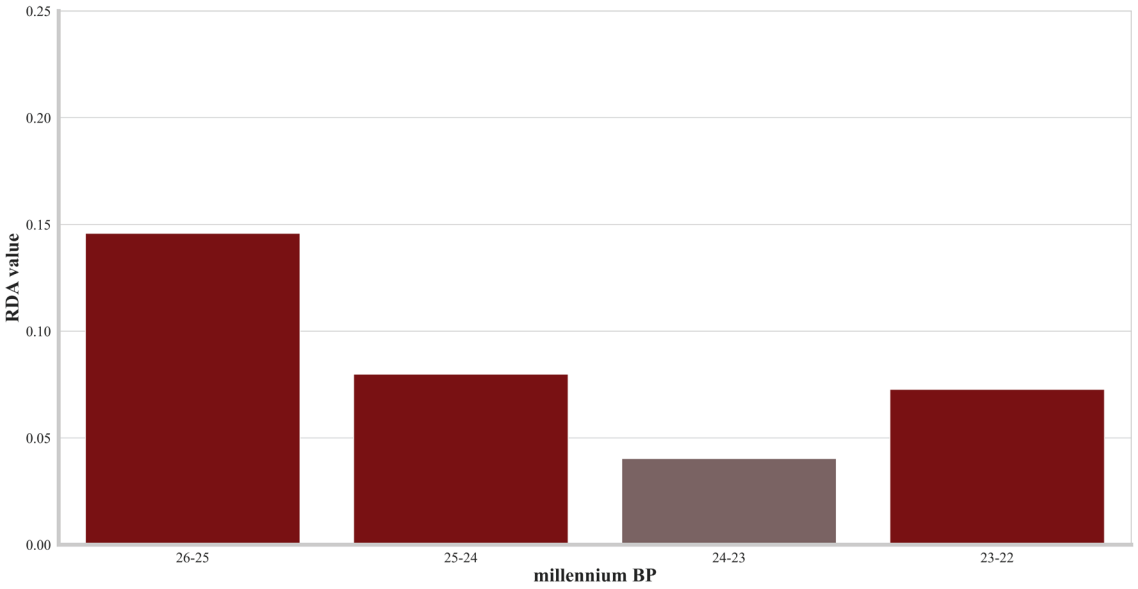



Figure 47: RDA values ($R^2$) for 2000-year sections of the Upper Solutrean with calibrated ages ('ka calBP') as canonical variable (dark red = $p \leq 0.05$, pale red = $p > 0.05$).

#### *4.2.1.1.3 Non-Solutrean LGM Industries*

To form a dataset of analysable size, assemblages assigned to the smaller taxonomic units of the Salpetrian, Late Badegoulian, Lower Magdalenian, and Epigravettian – dating within the Last Glacial Maximum (LGM) sensu lato (Mix et al. 2001) – are aggregated here. While the Epigravettian contributes a relatively robust sample size, with eight assemblages and 48 specimens, the Late Badegoulian and the Salpetrian are each represented by only a single well-dated assemblage (Le Cuzoul de Vers, layers 21–16, A-36; Grotta de la Salpêtriére, layer 6, A-38). The Lower Magdalenian dataset is similarly limited, originating from just two sites, respectively three dated assemblages (Fontgrasse, layer 3, A-28; Fontgrasse, layer 1a, A-27; Abri Gandil, layer 20, A-30), yielding a total of nine SPs. Additionally, the chronological distribution within these smaller taxonomic units presents further challenges. While the majority of Epigravettian SPs originate from the 20th and 21st millennium BP, some assemblages date to the 24th and 22nd millennium BP, introducing a degree of temporal dispersion.

Table 18: RDA results with calibrated ages ('ka calBP') as canonical variable for the Upper Solutrean core areas and for the section from the 25th to the 24th millennium BP exclusive the French assemblages (dark red = p ≤ 0.05).

| mil. BP | northern Spanish coast | France | 25th–24th mil. BP (– Fr. assembl.) |
|---|---|---|---|
| SPs | 40 | 18 | 24 |
| assemblages | 9 | 3 | 6 |
| p | 0.001 | 0.063 | 0.653 |
| $R^2$ | 0.131 | 0.139 | 0.0293 |

The Salpetrian assemblage is dated to the 24th millennium BP, while the Late Badegoulian assemblage is dated to the 23rd millennium BP. In contrast, the Lower Magdalenian SPs derive exclusively from assemblages dating to the 21st and 20th millennia BP. The final aggregated dataset comprises 64 SPs from 13 sites or respectively 14 assemblages across southern central Europe, dating between 23.6 and 19.0 ka calBP. Only two assemblages contribute a single specimen each: Grotta di Paina, layer 5 (B-16), and Abri du Bois des Brousses, layer 3 (B-14). The majority of SPs in this dataset come from the 24th millennium BP (14 SPs from three assemblages) and the youngest two millennia - 21st millennium BP (27 SPs from four assemblages) and 20th millennium BP (15 SPs from three assemblages). The 23rd and 22nd millennia BP are weakly represented, with only one assemblage each, yielding three and five SPs, respectively. Given these limitations, patterns deriving from the smaller taxonomic units have to be interpreted with caution. While the dataset provides valuable insights into broad trends for the LGM-period, its fragmentary nature means that any apparent developments must be assessed critically, avoiding overemphasis on signals that may be driven by sample size constraints and inter-sample variation rather than genuine chronological changes in morphology. The chronological scattering complicates direct comparisons and may obscure potential patterns of technological or morphological change within and across these taxonomic units. *(Figure 48)*

A noteworthy cluster of sites emerges in the Rhône Valley *(Map 5)*, comprising five sites respectively six assemblages – Grotta de la Salpêtriére, layer 6 (A-38), Le Cuzoul de Vers, layers 21-16 (A-36), Chinchon 1, layer C (A-33), Fontgrasse, layer 3 (A-28), Abri du Bois des Brousses, layer 3 (B-14) and Fontgrasse, layer 1a (A-27) – dated between 23.0 and 19.7 ka calBP.

These assemblages are assigned to the Salpetrian, Late Badegoulian, Epigravettian or Tardigravettian, and Lower Magdalenian, collectively yielding 20 SPs. While each of the youngest millennium (20th) include two assemblages, the three older millennia (24th–21st) are represented by a single assemblage each. However, the four older assemblages contribute 15 SPs, whereas the younger ones yield only five. Given the broad chronological span of over 3000 years, the assignment of assemblages to four different taxonomic units, and the relatively small sample sizes, the results for this cluster should be interpreted with caution. One site, Abri Gandil, layer 20 (A-30), is located just across the Massif Central, near the Rhône Valley. In Italy, five sites are present, two of which – Grotta di Paina, layer 5 (B-16), and Ponte di Pietra (A-41) – date to the 24th millennium BP, while three – Grotta Paglicci, layers 18a–10 (A-29), Taurisano, layers 23–6 (A-26), and Grotta delle Settecannelle (A-25) – date to the 20th millennium BP. Due to the significant chronological gap between these radiocarbon ages, this Italian cluster is not suitable for the upcoming analysis. Additionally, two sites – Kammern-Grubgraben, AL2 in Lower

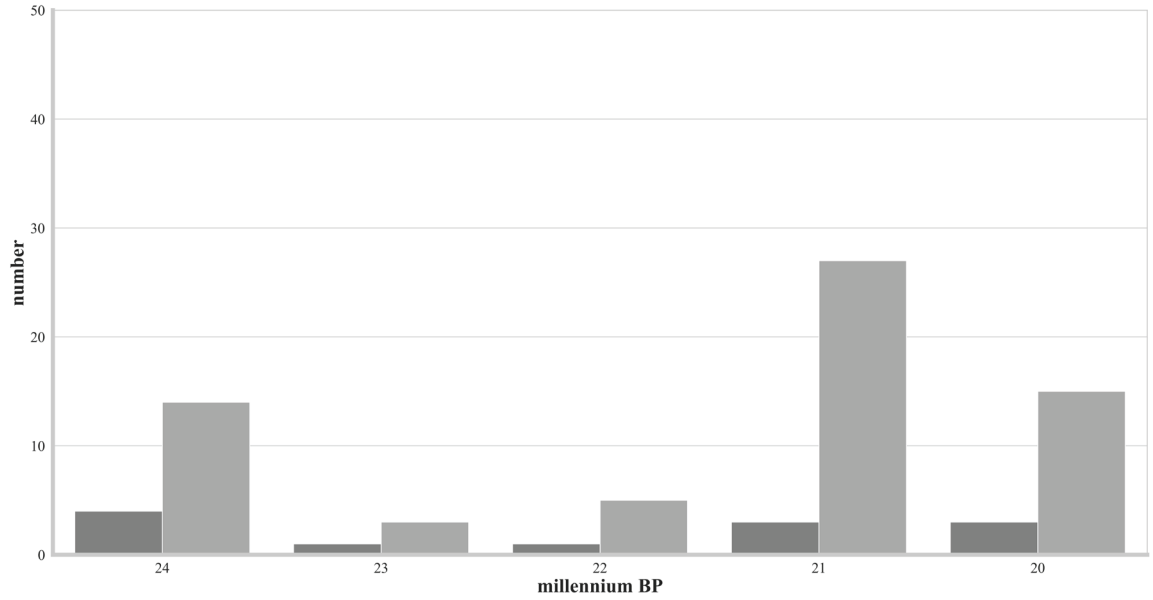



Figure 48: Number of assemblages and artefacts per millennium BP of the non-Solutrean LGM (dark grey, left bar = assemblages; light grey, right bar = artefacts)

Austria (A-39) and Kastrisa, layer 7/Stratum 3 (A-42) in western Greece – do not belong to a distinct regional group, although Kastrisa is quite close to the Italian site Grotta Paglicci. *(Table 19, Map 5)*

Applying RDA to the entirety of the class I assemblages assigned to non-Solutrean LGM Industries unit, the calibrated ages as canonical variable significantly ($p = 0.004$) explain 7.2% ($R^2 = 0.072$) of the variation in the morphometrical features.

Conducting a RDA with all specimens from the assemblages in the Rhône-valley, the calibrated ages as canonical variable highly significantly ($p = 0.009$) explain 18.5% ($R^2 = 0.1847$) of the variation in the morphometric features.

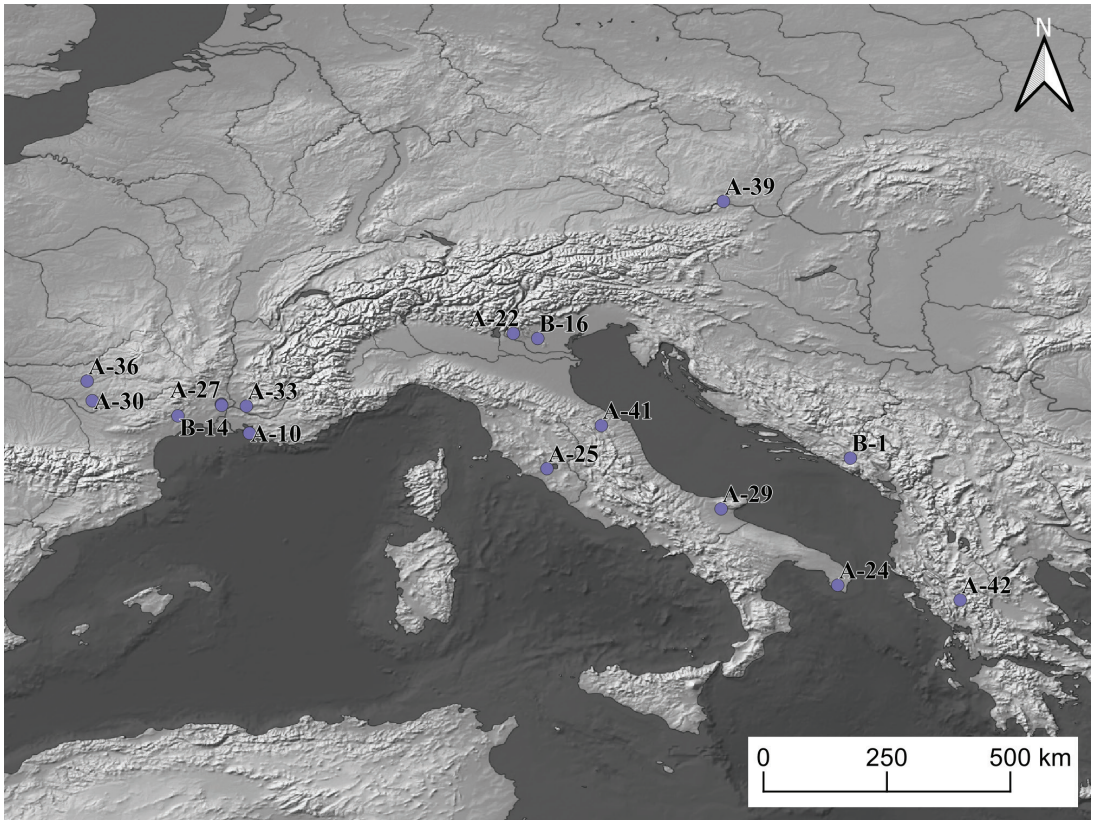
These findings from the dataset excluding the Solutrean, despite the inability to refine the analysis into 2000 year sections due to low sample sizes, provide valuable insights into the period between the 24$^{th}$ and 20$^{th}$ millennium BP, indicating comparably weak but significant signals for chronologically directed changes during this period. Additionally, pronounced shifts are observed within the regional cluster in the Rhône Valley.

#### *4.2.1.1.4 Upper/Late–Final Magdalenian*

The Upper/Late – Final Magdalenian dataset comprises 54 SPs from 18 sites, respectively 19 assemblages across central and western Europe, dating between 15.9 and 14.1 ka calBP. Of these, 11 assemblages contribute more than a single specimen, collectively accounting for 48 SPs. This dataset unifies assemblages assigned to the Upper, the Late and the Final Magdalenian. While there are clearly more SPs darting to the 16$^{th}$ (n = 34) than to the 15$^{th}$ millennium BP (n = 20), the numbers of assemblages are almost evenly distributed (16$^{th}$ = 9, 15$^{th}$ = 10). Apart from Abri Faustin, layer I (A-7), all assemblages are assigned to the Upper or the Late Magdalenian. *(Figure 49)*

A cluster worth mentioning is formed by seven assemblages – Abri de Fontales (A-20), Abri Faustin (A-7), Bois Ragot (A-15), Duruthy (A-19), La Madeleine, C - Magd. VI (A-21) and B - Magd. V (B-7) and Morin (A-18) – located around the Dordogne and Vienne rivers in France *(Map 6)*, dating between 15.5 and 14.5 ka calBP. These assemblages yield a combined total of 25 SPs. *(Table 20, Map 6)*

Applying RDA to the entirety of the class I assemblages assigned to the Upper/Late – Final Magdalenian, the calibrated ages as canonical variable only explain 1.7% ($R^2 = 0.0169$)




Map 5: Class I non-Solutrean assemblages dating between the 24th and the 20th millennium BP (LGM sensu lato) (n = 14; labels = IDs).

Table 19: Chronological and geographical distribution of dated non-Solutrean LGM assemblages.

| mil. BP | Rhône Valley | other |
|---|---|---|
| **20th** | B-14, A-27 | A-26, A-25 |
| **21st** | A-28 | A-29 |
| **22nd** | A-33 | |
| **23rd** | A-36 | |
| **24th** | A-38 | B-16, A-42, A-41, A-39 |

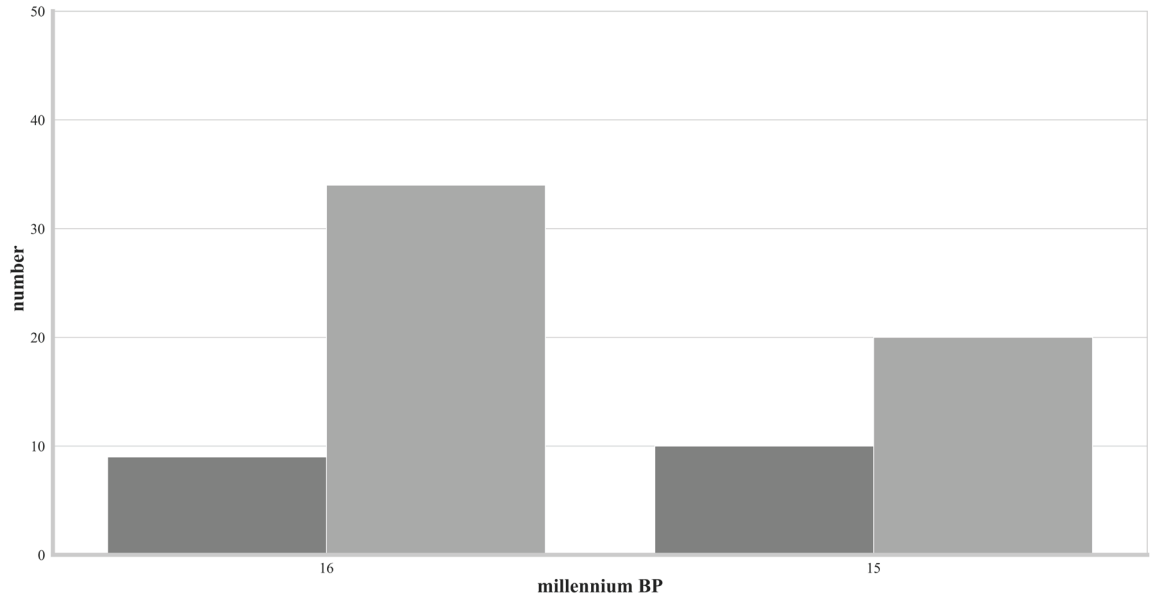
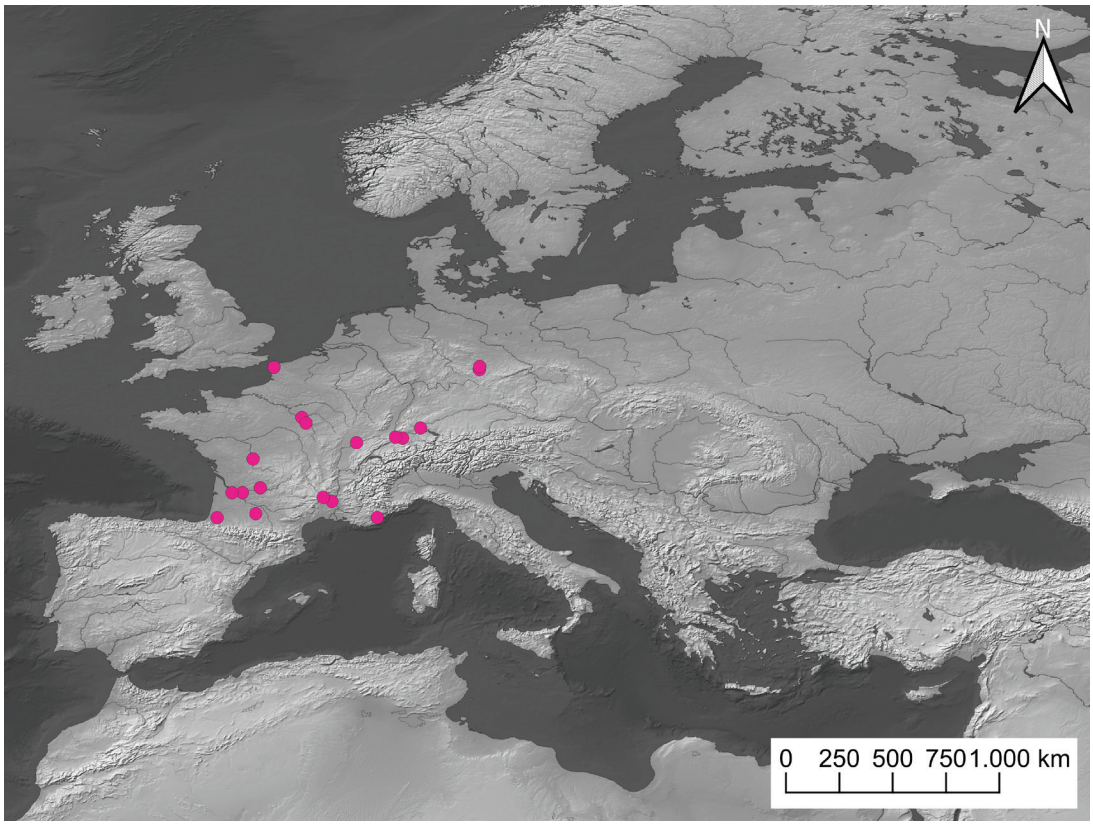



Figure 49: Number of assemblages and artefacts per millennium BP of the Upper/Late and Final Magdalenian (dark grey, left bar = assemblages; light grey, right bar = artefacts).




Map 6: Class I assemblages of the Upper/Late and Final Magdalenian (n = 19; labels = IDs).

Table 20: Chronological and geographical distribution of dated Upper/Late and Final Magdalenian assemblages.

| mil. BP | French cluster | other |
|---|---|---|
| 15th | A-7, B-7 | A-13, A-11, B-4, B-5, A-8, B-6, B-3, A-3 |
| 16th | A-21, A-20, A-19, A-18, A-15 | B-10, B-9, B-8, A-17 |

of the variation in the morphometrical features. The result is not significant (p = 0.451). When applying RDA exclusively to the French cluster, the result is comparably weak and not significant ($R^2$ = 0.0457, p = 0.317).

Even though the sample size for the Upper/Late-Final Magdalenian dataset is relatively large, RDA did not reveal any significant chronologically directed changes. This remains true even when focusing on the regional cluster in France. These findings contrasts the results from the chronologically informed perspective (Chapter 4.1.2), where significant changes were detected for the section from the 16th to the 15th millennium BP.

#### *4.2.1.1.5 Hamburgian*

The Hamburgian dataset comprises 60 SPs from seven assemblages located in northern Germany and central Poland, dating between 15.0 and 13.7 ka calBP. Only a single assemblage – Ahrenshöft, LA 73 (B-2) – yields a single specimen. The majority of the SPs comes from two assemblages in norther Germany – Poggenwisch D (A-9) (n = 23) and Meiendorf 2 (A-6) (n = 17) – dating to 14.6 and 14.5 ka calBP, together comprising two thirds of the Hamburgian dataset. *(Figure 50)*

Seven sites – Stellmoor (A-14), Poggenwisch D (A-9), Meiendorf 2 (A-6), Ahrenshöft, LA 73 (B-2) and Borneck (A-2) – cluster remarkably close together in the North German Plain, while the two remaining sites – Olbrachcice 8 (A-16) and Mirkowice 33 (A-4) – are about 130 km apart from each other in mid Poland *(Map 7, Table 21)*

Applying RDA to the entirety of the class I assemblages assigned to the Hamburgian, the calibrated ages as canonical only explain 3.2% ($R^2$ = 0.0316) of the variation in the morphometrical features. The result is also not significant (p = 0.1). However, when applying RDA exclusively to the North German Plain cluster, the calibrated ages of the assemblages significantly (p = 0.004) explain 6.9% ($R^2$ = 0.0694) of the variation in the morphometric features.

While the sample size of five assemblages is relatively small and should be interpreted with caution, this result suggests the possibility of chronologically directed changes in SP morphometry occurring in northern Germany between the 15th and 14th millennium BP.

The results of the RDA across the different taxonomic units revealed some chronological dynamics unidentified by the previous, the chronologically informed, analysis. Still the period between the 27th and the 24th millennium BP returns as a period of intensified chronologically directed changes in the morphometry of SPs. However, it is now able to state that the high RDA values of the period between the 27th and the 25th millennium BP not only derive from the transition between the two mayor taxonomic units of the Late Gravettian and the Upper Solutrean (which will be analysed in Chapter 4.2.2. Late Gravettian – Upper Solutrean) and the geographical shift in the occurrence of SPs, but rather high chronologically directed changes at the end of the Late Gravettian and independently at the beginning of the Upper Solutrean. For the Upper Solutrean, it can be shown that there must have been different chronologically trends taking place in Northern Iberia and France, that, to an only smaller amount, might have shared certain developements. Also, disconnected from the Upper Solutrean assemblages, the non-Solutrean LGM, assemblages, although a division into smaller chronologically units was not feasible, give a significant signal for the period between the 24th and the 20th millennium BP. When fo-

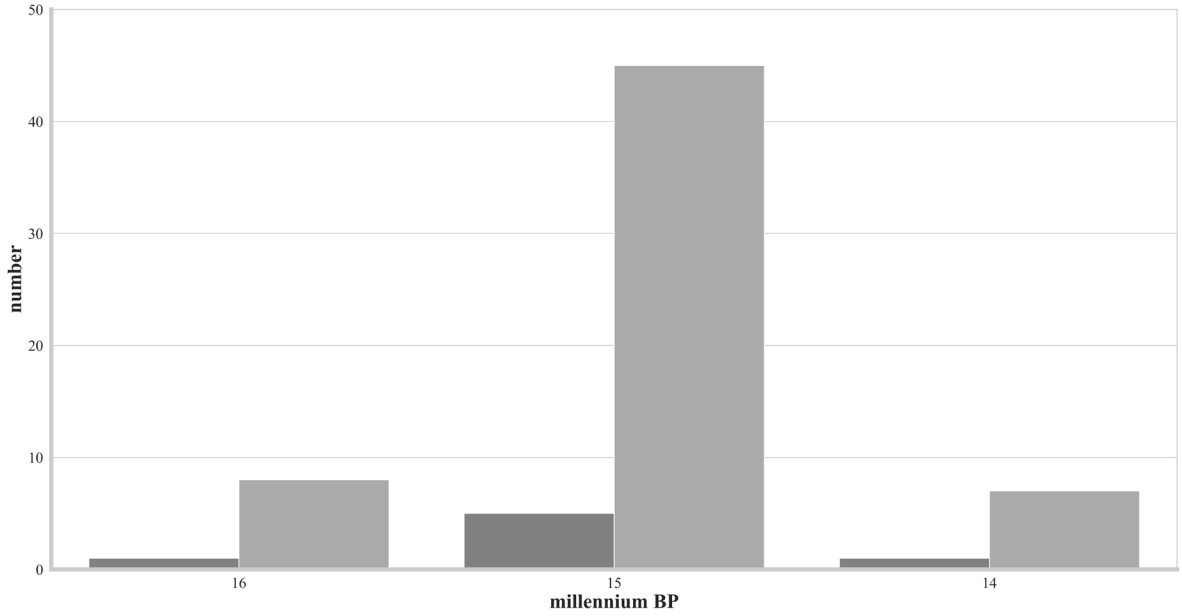
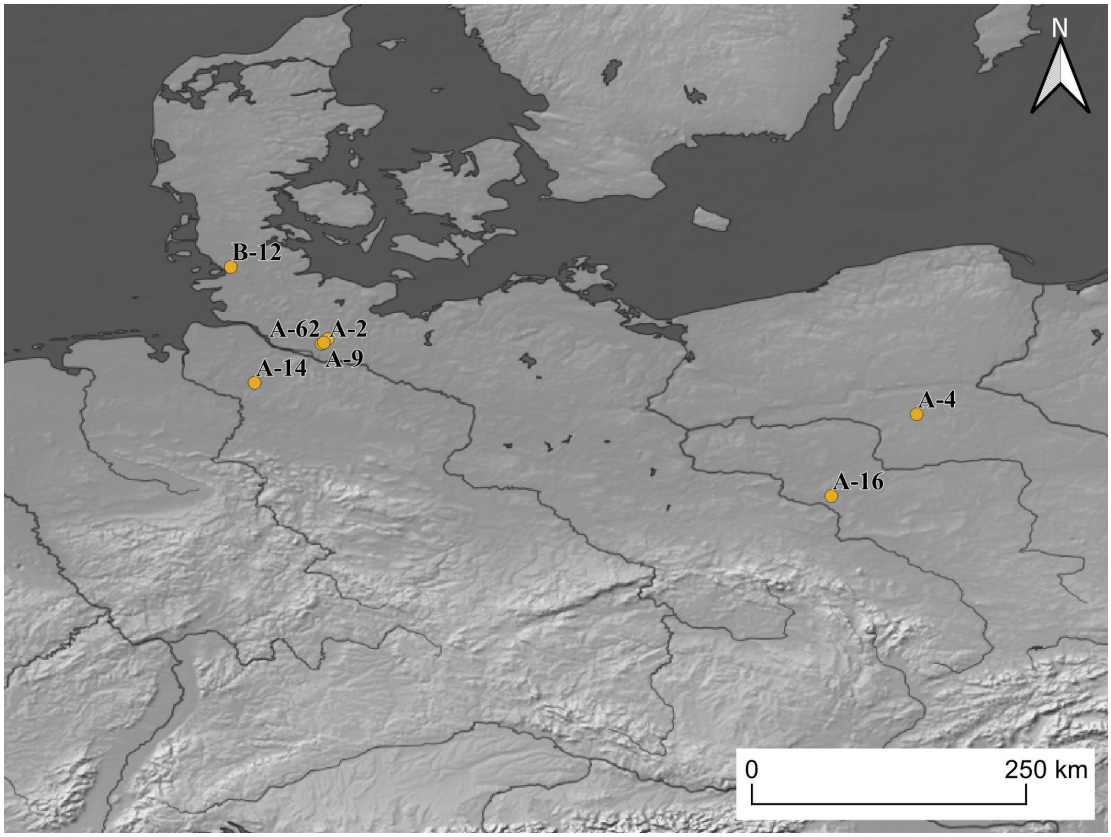



Figure 50: Number of assemblages and artefacts per millennium BP of the Hamburgian (dark grey, left bar = assemblages; light grey, right bar = artefacts).




Map 7: Class I assemblages of the Hamburgian (n = 7; labels = IDs).

Table 21: Chronological and geographical distribution of dated Hamburgian assemblages.

| mil. BP | North German Plain | Polish sites |
|---|---|---|
| 14th | A-2 | |
| 15th | A-14, A-9, A-6, B-2 | A-4 |
| 16th | | A-16 |

cussing on assemblages located in the Rhône valley only, the signal becomes even stronger. Taking only Upper/Late and Final Magdalenian assemblages into account, RDA returns a quite weak and non-significant result for the time between the 16th and the 15th millennium BP. Focusing on the Hamburgian assemblages, RDA also is not significant for the entirety of the Hamburgian, implying no chronologically directed changes taking place in this taxonomic unit either. When restricting the analysis to the small cluster of Hamburgian sites in northern Germany, however, returns a significant signal.

Although some of the latter results are based on low sample sizes and therefore lack statistical and archaeological significance, certain general conclusions can be drawn for taxonomic units beyond the Late Gravettian and Upper Solutrean. During the LGM, chronologically directed changes are evident not only in the Upper Solutrean, but it remains questionable to what extent. However, after the hiatus of traditional SP forms, such changes appear absent in the Upper/Late and Final Magdalenian. Similarly, no overarching chronologically directed changes are observed in the Hamburgian, despite comparably weak signals detected within a regional subgroup. The disparity between the findings made here and the significant results made on the chronologically informed perspective for the section from the 16th to the 15th millennium BP requires further analyses.

### 4.2.1.2 Coefficient of Variation

After it has been demonstrated that the amount of variation in the morphometric features explained by the passage of time varies significantly across and within the taxonomic units under investigation, the focus now shifts to analysing the amount variation within each section. Therefore again the calculation of CV is applied.

#### 4.2.1.2.1 Late Gravettian

Considering the entire Late Gravettian dataset, the average CV is 0.40. The most pronounced variations occur for the upper-lower-ratio (0.46), area (0.58) and the left-right-ratio (0.52). The other morphometric features exhibit less variation even though all values are clearly above the average CV for the respec-

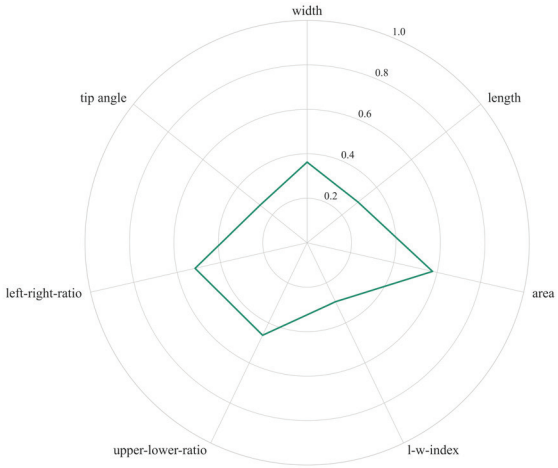



Figure 51: Coefficient of Variation (CV) of morphometric features for the entirety of the Late Gravettian assemblages.

tive feature calculated in Chapter 4.1.2 (width = 0.36, length = 0.29, l-w-index = 0.29, tip angle = 0.27). *(Figure 51)*

Breaking the analysis down into 2000 year sections, the results for the first three sections again can be inferred from the chronologically informed perspective (Chapter 4.1.2). The highest variation is observed in the two oldest sections (30th–29th: $\bar{x}$ = 0.39 and 29th–28th: 0.38), while the values for the two younger sections are slightly lower (both $\bar{x}$ = 0.35) *(Table 22)*. These elevated values can actually not be attributed to the special morphology of the SPs from Mitoc-Malu Galben, layer 4a (A-60, 29th millennium BP), as the results are not altered much – the upper-lower-ratio and the tip angle are virtually the only features that are alterd – excluding the Mitoc SPs (30th–29th: $\bar{x}$ = 0.41; 29th–28th: $\bar{x}$ = 0.38). When averaging the morphometric features across these sections, the overall pattern of variation for the Late Gravettian dataset is well resembled. The upper-lower ratio ($\bar{x}$ = 0.48), the left-right ratio ($\bar{x}$ = 0.49), and area ($\bar{x}$ = 0.51) continue to exhibit the most pronounced variation. In contrast, the other morphometric features show comparatively lower average variation: width = 0.33, length = 0.28, l-w index = 0.29, and tip angle = 0.29.

Whereas within the section from the 30th to the 29th millennium BP the CV for the features related to size are particularly low (width = 0.25, length = 0.24, area = 0.34), remaining below the averages of the CV of the respective morphometric features for the Late Gravettian, the values for the shape-related features are among the highest in the entire dataset, exceeding their averages (left-right-ratio = 0.75, tip angle = 0.34, upper-lower-ratio = 0.67). The value yielded for the l-w-index (0.29) is equal to the average CV of this feature. *(Figure 52)*

In the section from the 29th to the 28th millennium BP, apart from the left-right-ratio (0.4), all CV for the morphometric features exceed their respective averages: width = 0.34, length = 0.3, area = 0.54, l-w-index = 0.34, upper-lower-ratio = 0.5 and tip angle = 0.31. *(Figure 53)*

For the section ranging from the 28th to the 27th millennium BP all features related to the size are particularly high, exceeding the averages of the CV of the respective features for the Late Gravettian by a bit (width = 0.32, length = 0.3, area = 0.55). Again, apart from the left-right-ratio (0.42) and the upper-lower-ratio (0.41) all morphometric features related to the shape exceed the averages of the CV of the respective features: l-w-index = 0.3, left-right-ratio = 0.42, tip angle = 0.26. *(Figure 54)*

While the variations for the section ranging from the 27th to the 26th millennium BP inmost features including length (0.27), l-w-index (0.25), the upper-lower-ratio (0.35) and the tip angle (0.24) are lower than for the entire Late Gravettian, the values for width (0.4) and area (0.61) are a bit higher. The variation in the left-right-ratio however is a lot lower (0.4). *(Figure 55)*

#### *4.2.1.2.2 Upper Solutrean*

Considering the entire Upper Solutrean dataset, the average CV is 0.38. The most pronounced variations occur for area (0.56), the left-right-ratio (0.44) and the upper-lower-ratio (0.49). The other morphometric features exhibit less variation. While most values are above the average CV for the respective feature calculated in Chapter 4.1.2 (width = 0.27, length = 0.37, tip angle = 0.27), the l-w-index exhibits a particularly low average CV (0.22). *(Figure 56)*

Breaking the analysis down into 2000 year sections, the highest variation is observed in the two oldest Upper Solutrean 2000 year sections (26th–25th: $\bar{x}$ = 0.38 and 25th–24th: $\bar{x}$ = 0.41), whereas the values for the two younger sections are significantly lower (24th–23rd: $\bar{x}$ = 0.35 and 23rd–22nd: $\bar{x}$ = 0.29). When averaging the morphometric features across these sections, the overall pattern of variation for the Upper Solutrean dataset is well resembled. Area (0.51), the left-right-ratio (049) and the upper-lower-ratio (0.48) continue to exhibit the most pronounced variation. In contrast, the other morphometric features show comparatively lower variation: width = 0.27, length = 0.35, l-w-index = 0.20, and tip angle = 0.27.

With the exception of the tip angle (0.25) and area (0.48), all morphometric features for the 2000 year section ranging from the 26th to the 25th millennium BP exhibit CV higher than the average CV for the entire Upper Solutrean (width = 0.28, length = 0.37, l-w-index = 0.22, upper-lower-ratio = 0.59, left-right-ratio = 0.49). *(Figure 57)*

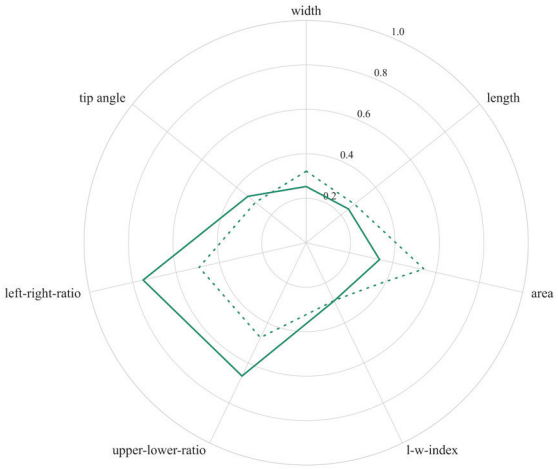



Figure 52: Coefficient of Variation (CV) of morphometric features for Late Gravettian assemblages dating in the section from the 30th to the 29th millennium BP (dotted line = average CV for the Late Gravettian assemblages).

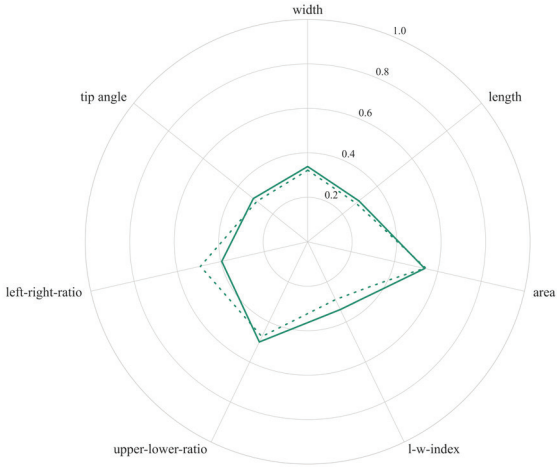



Figure 53: Coefficient of Variation (CV) of morphometric features for Late Gravettian assemblages dating in the section from the 29th to the 28th millennium BP (dotted line = average CV for the Late Gravettian assemblages)

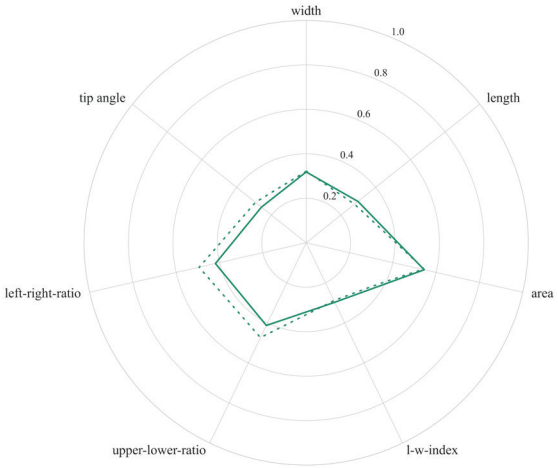



Figure 54: Coefficient of Variation (CV) of morphometric features for Late Gravettian assemblages dating in the section from the 28th to the 27th millennium BP (dotted line = average CV for the Late Gravettian assemblages).

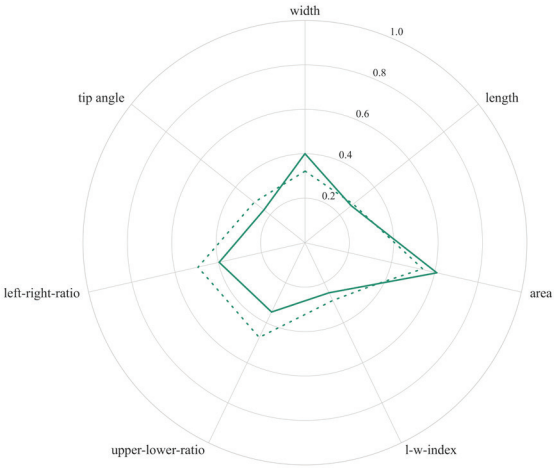



Figure 55: Coefficient of Variation (CV) of morphometric features for Late Gravettian assemblages dating in the section from the 27th to the 26th millennium BP (dotted line = average CV for the Late Gravettian assemblages).

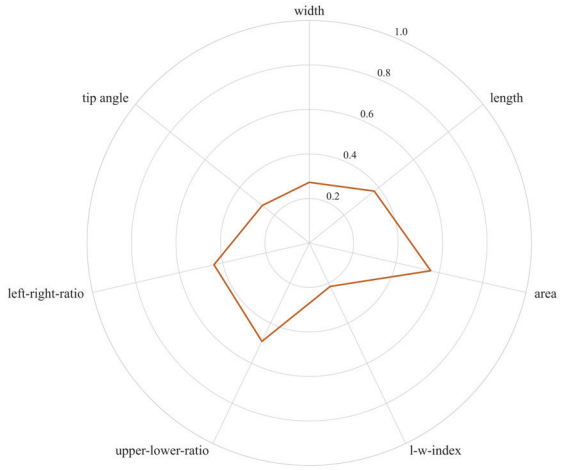



Figure 56: Coefficient of Variation (CV) of morphometric features for the entirety of the Upper Solutrean assemblages.

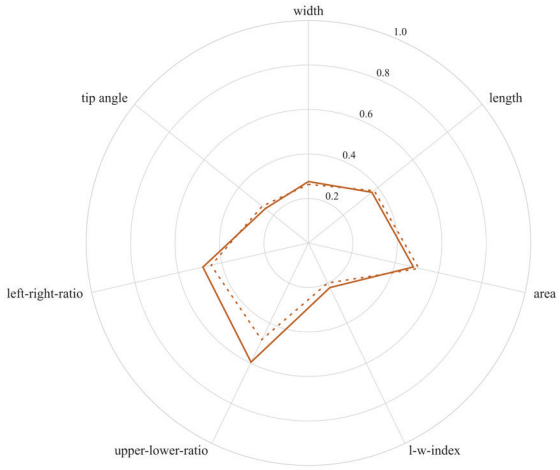



Figure 57: Coefficient of Variation (CV) of morphometric features for Upper Solutrean assemblages dating in the section from the 26th to the 25th millennium BP (dotted line = average CV for Upper Solutrean assemblages).

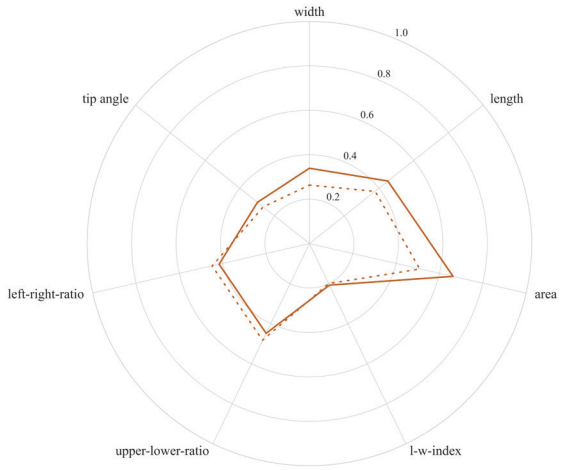



Figure 58: Coefficient of Variation (CV) of morphometric features for Upper Solutrean assemblages dating in the section from the 25th to the 24th millennium BP (dotted line = average CV for Upper Solutrean assemblages).

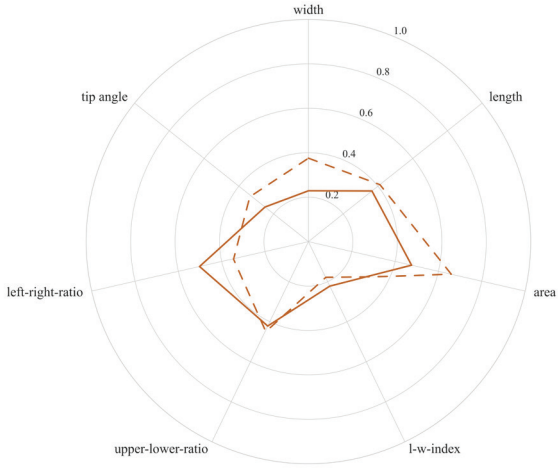



Figure 59: Coefficient of Variation (CV) of morphometric features of French and Iberian Upper Solutrean assemblages dating to the section from the 25th to the 24th millennium BP (solid line = French Upper Solutrean SPs; dashed line = Iberian Upper Solutrean SPs).

For the section ranging from the 25th to the 24th millennium BP, the weighting of the CV is shifted towards exceptional high variation in size-related features (area = 0.66, length = 0.45, width = 0.34), deriving from the exceptional sizes of the French Solutrean SPs. The CV for shape-related features are comparably low (l-w-index = 0.21, upper-lower-ratio = 0.45, left-right-ratio = 0.42, tip angle = 0.3). *(Figure 58)*

While the most pronounced differences between Iberian and French Upper Solutrean SPs appear in size-related features (see, for example, the comparison of area in *Figure 60*, upper plot), differences in shape-related characteristics are nonetheless evident. The French Upper Solutrean SPs exhibit slightly higher values for (Figure 60, middle plot) and notably more variation *(Figure 59)* in the l-w index and markedly lower values for the upper-lower ratio (*Figure 60*, lower plot). This indicates that the French SPs are generally slenderer and possess a more balanced proportion between the hafting and transformative parts, in contrast to the short-stemmed Iberian SPs.

If the French assemblages are analysed separately, some mayor differences are shown. The French assemblages yield a slightly lower, but nonetheless elevated CV ($\bar{x}$ = 0.35). While width (0.23), the l-w-index (0.22) and the tip angle (0.25) yield comparably low CV, the values for the other morphometric features are elevated (length = 0.37, area = 0.48, upper-lower-ratio = 0.42, left-right-ratio = 0.50). However, as the dataset for this subsample comprises SPs from only three assemblages, this result has to be interpreted with caution. The Iberian Upper Solutrean SPs of the section from the 25th to the 24th millennium BP are geographically widely distributed. Together, they yield elevated CV in all morphometric features (width = 0.38, length = 0.41, area = 0.67, upper-lower-ratio = 0.44, left-right-ratio = 0.35, tip angle = 0.33), except from the l-w-index /0.18), resulting in a comparably high average CV of 0.39. *(Figure 59 and 60)*

The weighting of the CV for the shape related features for the section ranging from the 24th to the 23rd millennium BP is almost similar to the previous section (upper-lower-ratio = 0.48, left-right-ratio = 0.41, tip angle = 0.3). The CV for the l-w-index (0.16) though, is exceptional low and differs a lot from the previous section. The CV for all size-related features are way lower than for the previous section (length = 0.34, area = 0.53), with width even remaining below the average CV for width for the entire Upper Solutrean. *(Figure 61)*

Inspecting the morphometric features individually again reveals pronounced differences in both size (with area as an example shown in *Figure 63*, upper plot) and in the upper-lower ratio (*Figure 63*, lower plot). Again, these results indicate that the French Upper Solutrean SPs are significantly larger than their Iberian counterparts and display a more balanced ratio between the hafting and transformative parts.

If again the dataset is subdivided into French and Iberian assemblages, further differences become observable. While the CV for the Iberian assemblages is almost identical to the CV for the entire section ($\bar{x}$ = 0.35, width = 0.31, length = 0.34, area = 0.54, l-w-index = 0.16, upper-lower-ratio = 0.44, left-right-ratio = 0.4, tip angle = 0.29), almost all values for the French assemblages are lower ($\bar{x}$ = 0.31, width = 0.12, length = 0.26, area = 0.33, l-w-index = 0.17, left-right-ratio = 0.34, tip angle = 0.33). The only exception is the remarkably high CV for the upper-lower-ratio (0.61). It is again emphasised that the limited sample size has some impact on this observation. *(Figure 52 and 63)*

For the section ranging from the 23rd to the 22nd millennium BP, almost all feature-specific CV remain below the respective average CV (width = 0.16, length = 0.23, area = 0.34, upper-lower-ratio = 0.41, tip angle = 0.24). The only exceptions are the values for the l-w-index (0.22), slightly above the average, and the left-right-ratio (0.48), equal to the average. *(Figure 64)*

#### *4.2.1.2.3 Non-Solutrean LGM Industries*

The variation within this aggregated dataset is notably low ($\bar{x}$ = 0.33). The morphometric features exhibiting the highest CV are area (0.45), the upper-lower-ratio (0.47) and the left-right-ratio (0.41). The other features yield remarkably low CV values (width = 0.24, length = 0.25, l-w-index = 0.26, tip angle = 0.25).

Breaking this dataset down into the underlying taxonomic units, the result can be diversified while, due to the low number of cases for each of the taxonomies, must be treated with caution. The Lower Magdalenian specimens show the least variation (0.22). The

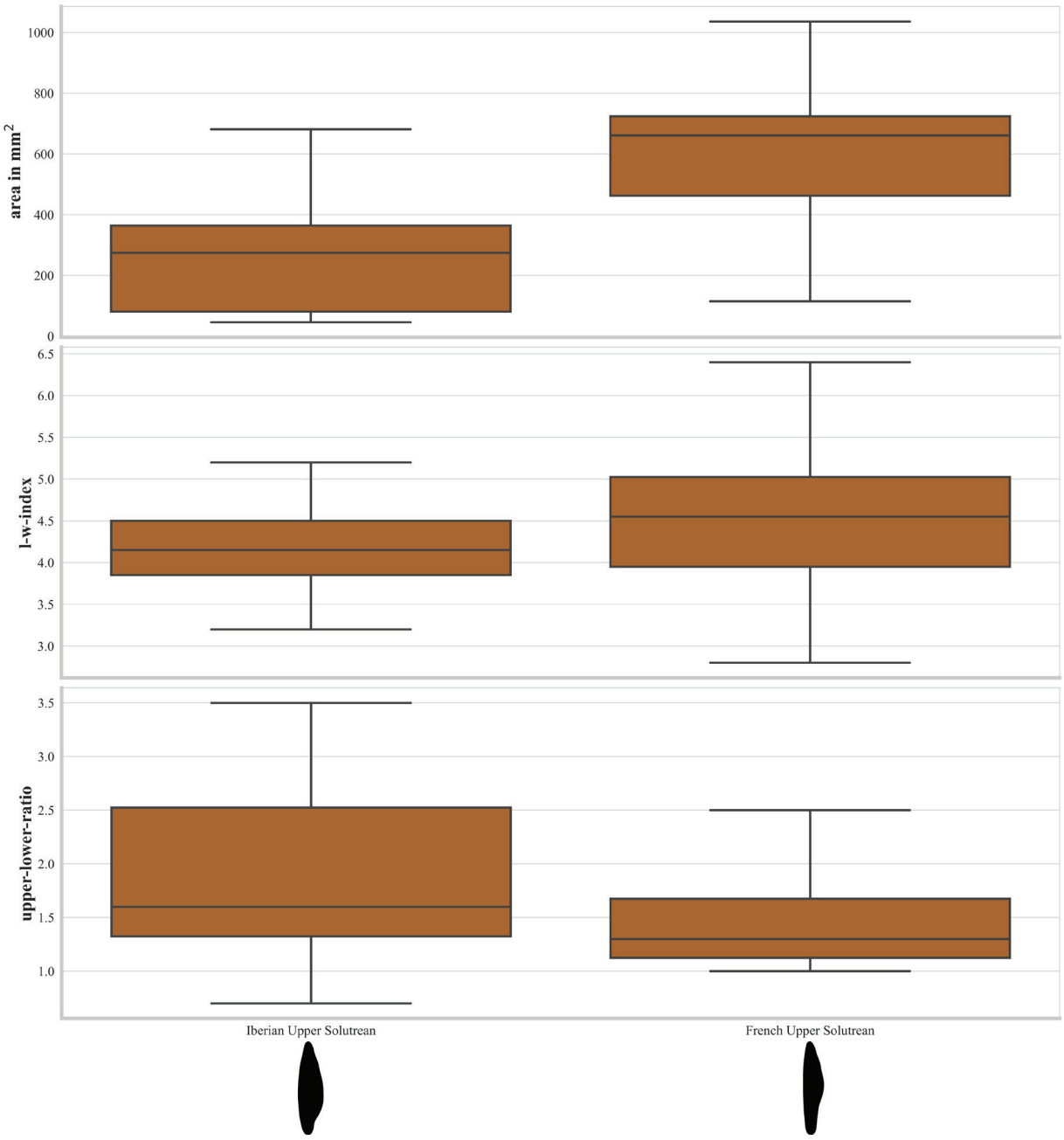



Figure 60: Comparison of area, l-w-index, and upper-lower-ratio between Iberian and French Upper Solutrean SPs dating to the section from the 25th to the 24th millennium BP (upper plot = area; middle plot = l-w-index; lower plot = upper-lower-ratio; left box = Iberian Upper Solutrean SPs; right box = French Upper Solutrean SPs; outliers excluded).

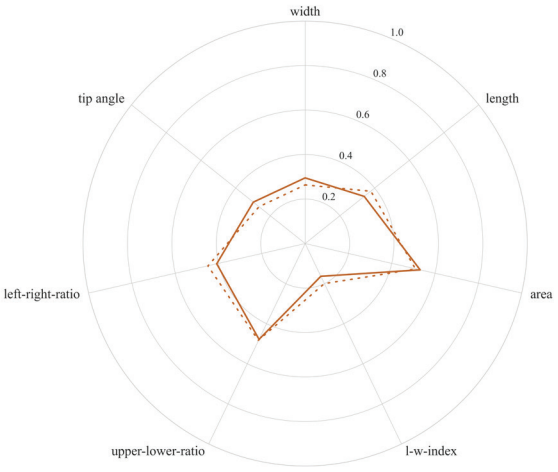



Figure 61: Coefficient of Variation (CV) of morphometric features for Upper Solutrean assemblages dating in the section from the 24th to the 23rd millennium BP (dotted line = average CV for Upper Solutrean assemblages).

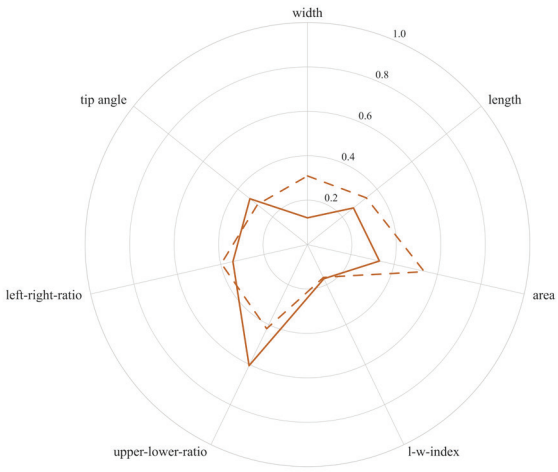



Figure 62: Coefficient of Variation (CV) of morphometric features of French and Iberian Upper Solutrean assemblages dating to the section from the 24th to the 23rd millennium BP (solid line = French Upper Solutrean SPs; dashed line = Iberian Upper Solutrean SPs).

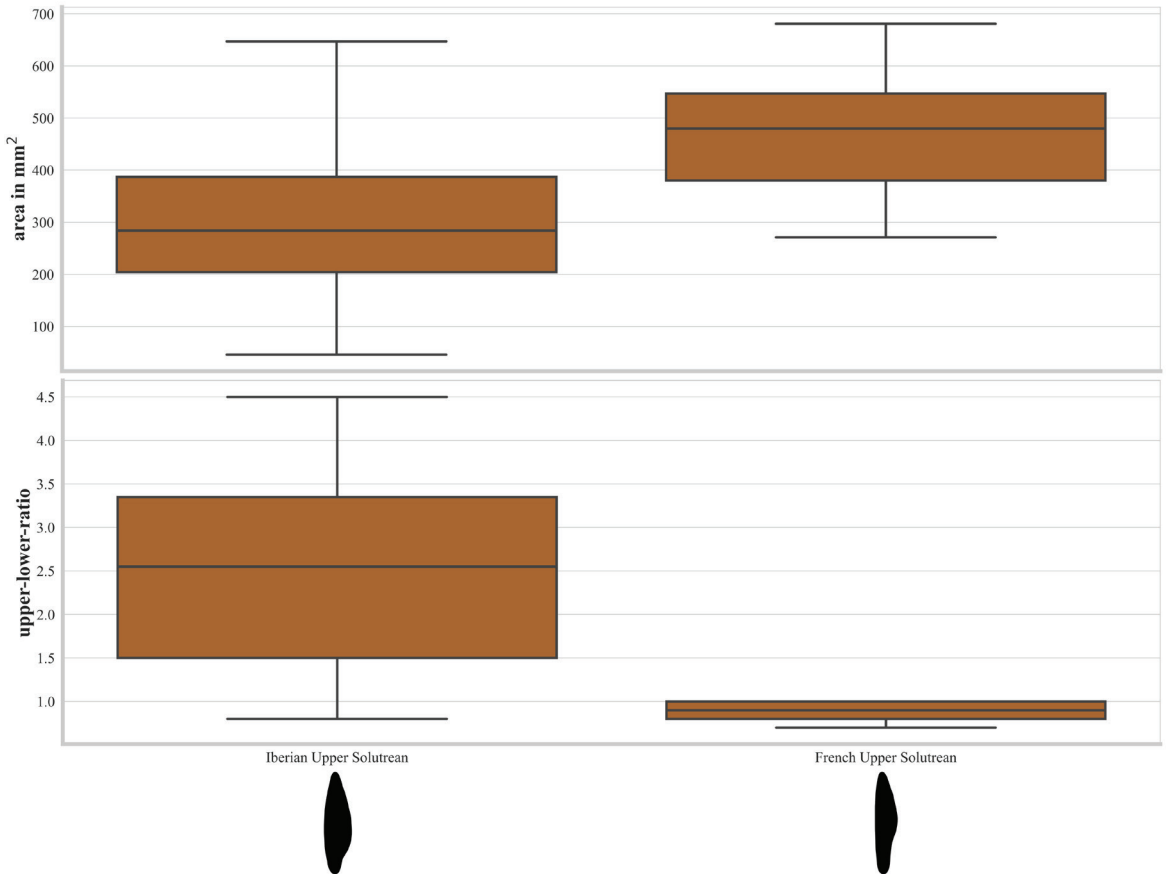



Figure 63: Comparison of area, and upper-lower-ratio between Iberian and French Upper Solutrean SPs dating to the section from the 24th to the 23rd millennium BP (upper plot = area; lower plot = upper-lower-ratio; left box = Iberian Upper Solutrean SPs; right box = French Upper Solutrean SPs; outliers excluded).

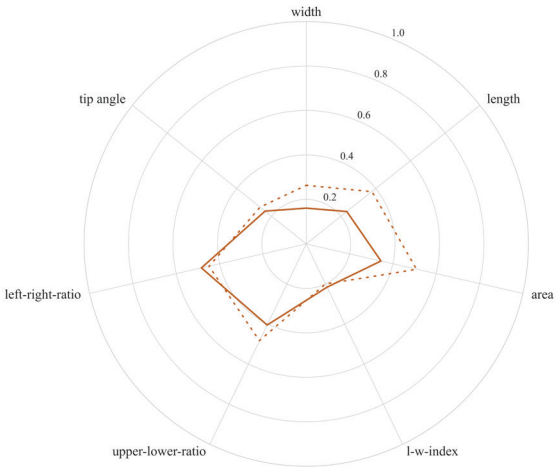



Figure 64: Coefficient of Variation (CV) of morphometric features for Upper Solutrean assemblages dating in the section from the 23rd to the 22nd millennium BP (dotted line = average CV for Upper Solutrean assemblages).

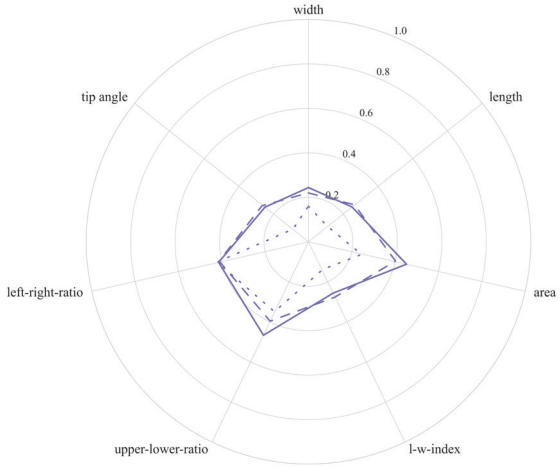



Figure 65: Coefficient of Variation (CV) of morphometric features of assemblages assigned to non-Solutrean LGM industries dating to the section from the 24th to the 20th millennium BP (solid line = entirety of the non-Solutrean LGM assembalges; dashed line = Epigravettian assemblages; dotted line = Lower Magdalenian assemblages).

feature-specific CV are particular low for all features (width = 0.16, length = 0.11, area = 0.25, l-w-index = 0.14, upper-lower-ratio = 0.35, tip angle = 0.09), with the exception of the left-right-ratio (0.42). The Epigravettian specimens have an average CV of 0.32. The variation in the upper-lower-ratio (0.40), the left-right-ratio (0.41) and the area (0.41) are quite pronounced but other than that, the variation is comparably low for all features (width = 0.22, length = 0.26, l-w-index = 0.28, tip angle = 0.26). As the other three taxonomic units are represented by only one assemblage each, no separate calculations were conducted. *(Figure 65)*

#### *4.2.1.2.4 Upper/Late–Final Magdalenian*

The average variation within this aggregated dataset is quite high ($\bar{x}$ = 0.37). The high average CV derives mostly from the exceptional high value for the left-right-ratio (0.67), that however, as already explained previously, is an artefact of PyREnArA struggling to properly orient some of the SPs from the last youngest three millennia, which are characterised by a straight back opposing the notch and a relatively straight base. Additionally, the values for the upper-lower-ratio (0.55) and the l-w-index (0.34) are comparable high. The CV for the size-related features however are not noticeable high (width = 0.28, length = 0.23, area = 0.38), neither is the CV for the tip angle (0.21). *(Figure 66)*

This elevated variation necessitated further investigation. Upon inspecting the images of the analysed assemblages, it becomes evident that two distinct types of SPs appear to coexist in the 16th and 15th millennium BP (for morphological validation see Chapter 6.3). The first type is elongated, as reflected in high l-w-indices (*Figure 68*, upper plot, left box), hence they are named 'pointes à cran allongé' (Langlais 2007; e.g., La Madeleine, layer B – Magdalenian V, B-7, Appendix Plate 109). This type features a relatively longer hafting part and a pronouncedly short transformative part, resulting in lower values for the upper-lower-ratio (*Figure 68*, lower plot, left box). The second type is shorter and more robust, indicated by lower values in the l-w-index (*Figure 68*, upper plot, right box). It has more or less equally proportioned hafting and transformative parts, leading to a more balanced upper-lower-ratio (*Figure 68*, lower plot, right box) (e.g., Appendix Plate 143, Petersfels, A-17). Type A is




Figure 66: Coefficient of Variation (CV) of morphometric features of Upper/Late and Final Magdalenian assemblages dating to the section from the 16th to the 15th millennium BP.

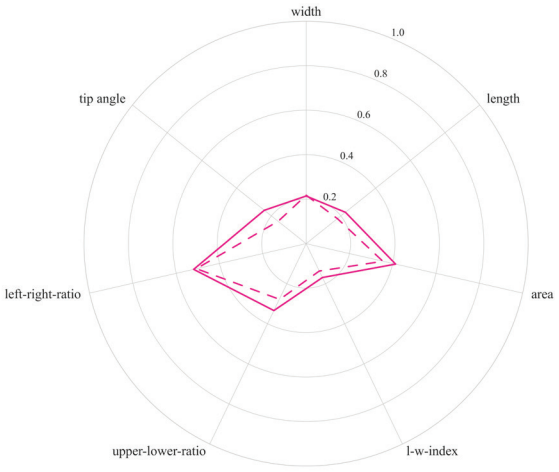



Figure 67: CV of morphometric features of the Upper/Late–Final Magdalenian assemblages differentiated by type (solid line = Type A, dashed line = Type B) dating in the section ranging from the 16th to the 15th millennium BP.

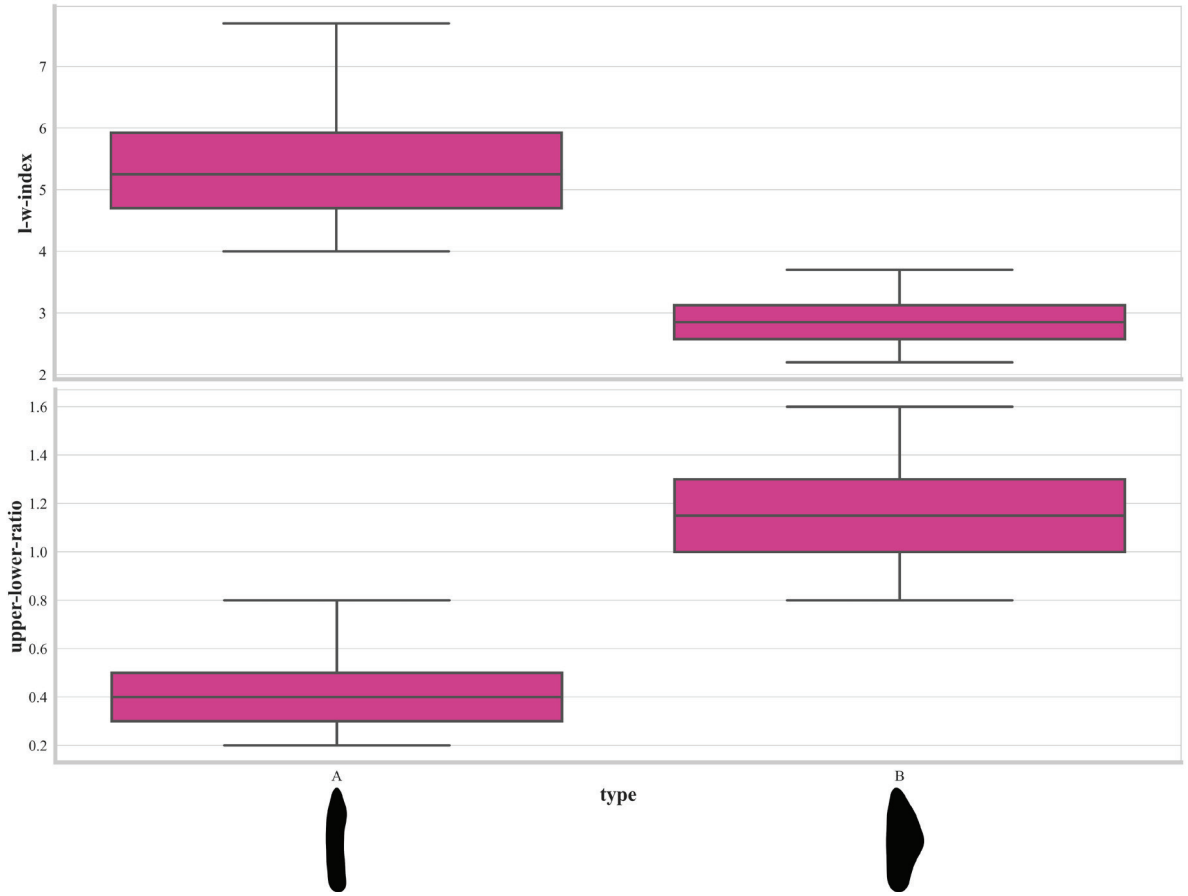



Figure 68: Comparison of l-w-index, and upper-lower-ratio between Type A and Type B of the Upper/Late–Final Magdalenian SPs dating to the section from the 16th to the 15th millennium BP (upper plot = l-w-index; lower plot = upper-lower-ratio; left box = Type A; right box = Type B; outliers excluded).

represented by 24 specimens, with 15 dating to the 16th millennium BP and nine to the 15th millennium BP. Type B is represented by 28 specimens, with 17 dating to the 16th millennium BP and 11 dating to the 15th millennium BP. Abri de Fontalès (A-20, Appendix Plate 2) is the only assemblage containing both types. However, no clear chronological or geographical separation between these two types is observable. The presence of these distinct forms likely accounts for the elevated variation in the upper-lower ratio and the l-w index, warranting a separate analysis.

The average variation within Type A SPs of the Upper/Late–Final Magdalenian assemblages from the 16th and 15th millennium BP is comparably low ($\bar{x}$ = 0.30). The highest variation is again observed in the left-right-ratio (0.52, *Figure 67*, solid line), though, as previously mentioned, this is likely an artefact of PyREnArA struggling to properly orient some of the SPs. The next highest CV is found in area (0.41). Other size-related features exhibit relatively low variation (width = 0.21, length = 0.23). The l-w-index shows a remarkably low CV (0.17), while both the upper-lower-ratio (0.33) and tip angle (0.24) also exhibit relatively low variation.

The average variation within Type B SPs of the Upper/Late–Final Magdalenian assemblages from the 16th and 15th millennium BP is even lower ($\bar{x}$ = 0.26). Once again, the highest variation is observed in the left-right ratio (0.51, *Figure 67*, dashed line), likely due to PyREnArA's difficulty in properly orienting certain SPs. The next highest CV values are found in area (0.36) and the upper-lower-ratio (0.28), though these remain relatively low. Beyond that, all other features display remarkably low CV values (width = 0.22, length = 0.18, l-w index = 0.14, tip angle = 0.16). *(Figure 67 and 68)*

#### *4.2.1.2.5 Hamburgian*

The CV for the entirety of the Hamburgian is exceptional low. The average CV is just 0.25, which is the lowest value calculated in this entire study. The most pronounced variation occurs in the left-right-ratio (0.51). The CV for Width (0.17), length (0.18), and the l-w-index (0.18) are extremely low. Also, the values for the upper-lower-ratio (0.26) and the tip angle (0.22) are among the lowest calculated for the respective feature in this study. *(Figure 69 and 70)*

In the Late Gravettian, shape-related features exhibit slightly higher variation ($\bar{x}$ = 0.39) than size-related features ($\bar{x}$ = 0.37). In contrast, this relationship is reversed in the Upper Solutrean, where size-related features show slightly greater variation ($\bar{x}$ = 0.37) compared to shape-related ones ($\bar{x}$ = 0.35). In both cases, this slight disparity can be explained by specific sample characteristics. For the Late Gravettian, the elevated average variation in shape-related features is largely driven by the distinct morphology of the SPs from Mitoc-Malu Galben, layer 4a (A-60, 29th millennium BP), which accounts for the peak in shape-related variation between the 30th and the 29th millennium BP *(Figure 71)*. In the Upper Solutrean, the increased variation in size-related features likely results from the size differences between Iberian and French SPs, explaining the peak in size-related variation observed between the 25th and the 24th millennium BP.

While variation in shape-related features declines steadily throughout the Late Gravettian, variation in size increases, peaking in the final section (27th–26th millennium BP). In the Upper Solutrean, variation in shape remains relatively stable, whereas size-related variation is pronounced primarily in the early phase, coinciding with the coexistence of Iberian and French SPs.

In non-Solutrean LGM industries, average variation in size-related features is relatively low ($\bar{x}$ = 0.31), while the slightly higher variation in shape-related features ($\bar{x}$ = 0.35) may reflect underlying morphological differences. The Upper Magdalenian SPs display low variation in size-related features ($\bar{x}$ = 0.30); however, due to the coexistence of two distinct SP designs, shape-related variation is notably high ($\bar{x}$ = 0.46). In the Hamburgian, both size ($\bar{x}$ = 0.22) and shape-related ($\bar{x}$ = 0.29) variation are notably low. *(Figure 71)*

For the Late Gravettian, the overall variation remains relatively consistent as well as high *(Figure 70)*, displaying pronounced size- and shape-related variation, particularly in the area, the upper-lower ratio and the left-right ratio. The analysis of the Upper Solutrean SPs reveals decreasing variation over time, with the most pronounced variation occurring in the first two sections. Regional comparisons highlight pronounced contrasts, with Iberian assemblages exhibiting substantially higher variation compared to French ones. Also, the




Figure 69: Coefficient of Variation (CV) of morphometric features of Hamburgian assemblages dating to the period between the 16th and the 14th millennium BP.

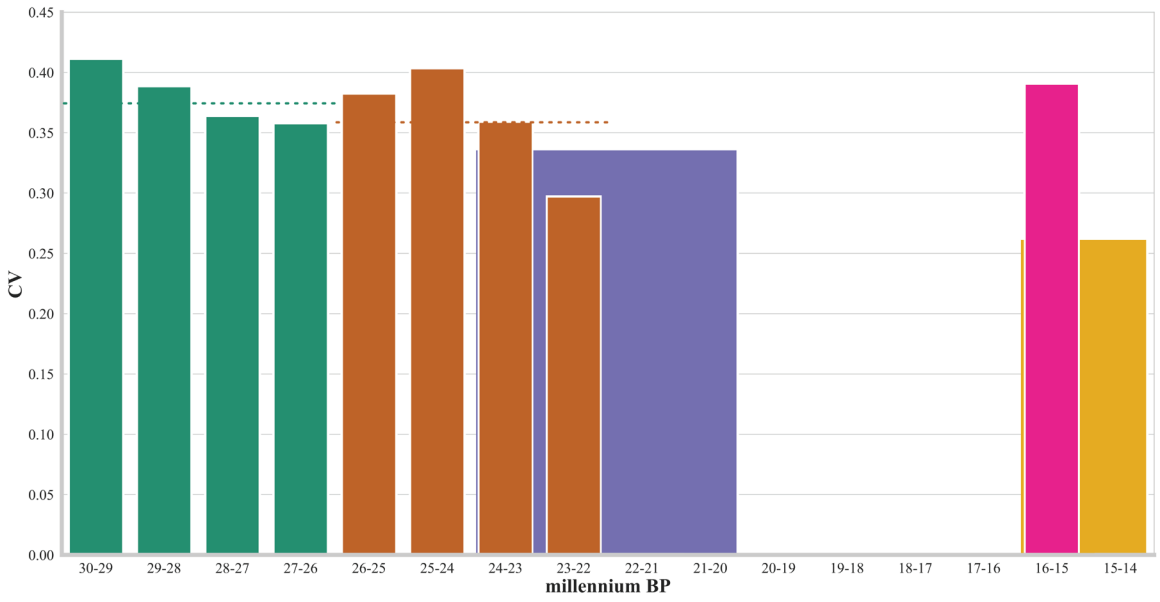



Figure 70: Averages (x̄) of Coefficient of Variation (CV) *per s*ection in millennium BP within taxonomic units (green = Late Gravettian; orange = Upper Solutrean; violet = non-Solutrean LGM industries; pink = Upper/Late–Final Magdalenian; yellow = Hamburgian).

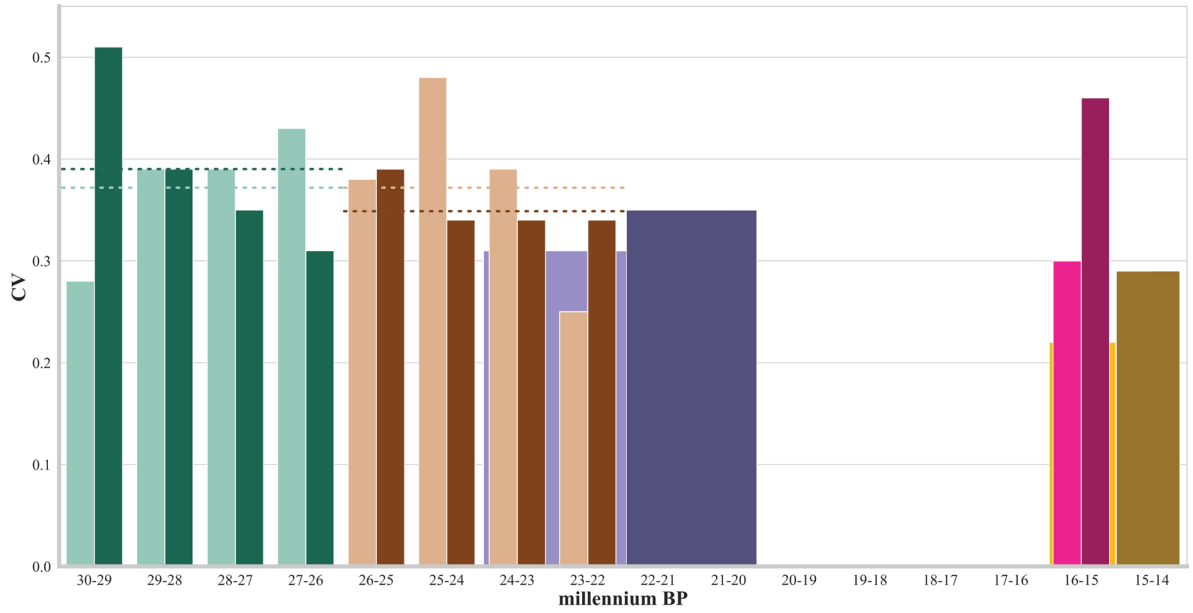



Figure 71: Averages ($\bar{x}$) of Coefficient of Variation (CV) *per se*ction in millennium BP within taxonomic units for features related to size and shape (size = light coloured; shape = dark coloured; dotted line = average CV for all sections; green = Late Gravettian; orange = Upper Solutrean; violet = non-Solutrean LGM industries; pink = Upper/Late–Final Magdalenian; yellow = Hamburgian).

high CV for the section from the 25th to the 24th millennium BP is most likely explained by the pronounced differences between the Iberian and the French Upper Solutrean SPs. The aggregated non-Solutrean LGM Industries exhibit a quite low overall variation, particularly expressed in low values for size-related features. However, the left-right ratio and the upper-lower-ratio show notable variation, indicating shape differentiation to some extent across the compiled taxonomies. For the Upper/Late–Final Magdalenian, elevated variation was calculated, reflecting pronounced shape-related differences, especially in the upper-lower-ratio and the left-right-ratio, deriving from two morphologically different types of SPs – an elongated and a stouter type. In contrast, size-related features seem to remain comparably stable. Within the Hamburgian assemblages, exceptional consistency is evident, with minimal variation across most morphometric features except for the left-right-ratio, emphasising a high level of standardisation in SP design. *(Table 22)*

### *4.2.1.3 Change Rates*

Having demonstrated that certain timeframes within specific taxonomic units exhibit higher morphological variation in SPs than others – and that, in some cases, this variation is more effectively explained by the passage of time (as detailed in Chapter 4.2.1) – the next step is again to systematically quantify the amount of change. This approach is applied across taxonomic units with sufficient granularity: the Late Gravettian, represented by four 2000 year sections; the Upper Solutrean, with three feasible sections; and the Upper/Late–Final Magdalenian, encompassing one section.

A preliminary examination of the calculated change rates *(Table 23)* again reveals extreme values for the centre of mass offsets (MP-CM-y-offset). Given that the values in this feature exert a significant influence on the averages, they are acknowledged but excluded from further calculations to ensure the integrity and relevance of the analysis.

Table 22: Coefficient of Variation (CV) for each morphometric feature, section, and taxonomic unit (green = Late Gravettian; orange = Upper Solutrean; violet = non-Solutrean LGM industries; pink = Upper/Late–Final Magdalenian; yellow = Hamburgian; highlighted in red = RDA significant sections; bold and underlined = highest change rate in feature/sections of respective taxonomic unit; faint = value below respective average).

| taxonomic unit | section m. BP | width | length | area | l-w-index | upper-lower-index | left-right-ratio | tip angle | $\bar{x}$ |
|---|---|---|---|---|---|---|---|---|---|
| Ham. | 15th–14th | 0.17 | 0.18 | 0.31 | 0.18 | 0.26 | 0.51 | 0.22 | 0.26 |
| Mag. | 16th–15th | 0.28 | 0.23 | 0.38 | 0.34 | 0.55 | 0.73 | 0.21 | 0.39 |
| | 17th–16th | | | | | | | | |
| | 18th–17th | | | | | | | | |
| | 19th–18th | | | | | | | | |
| | 20th–19th | | | | | | | | |
| non-Sol. LGM | 24th–20th | 0.24 | 0.25 | 0.45 | 0.26 | 0.47 | 0.41 | 0.25 | 0.33 |
| Upper Solutrean | 23rd–22nd | 0.16 | 0.23 | 0.34 | **0.22** | 0.41 | 0.48 | 0.24 | 0.30 |
| | 24th–23rd | 0.30 | 0.34 | 0.53 | 0.16 | 0.48 | 0.41 | **0.30** | 0.36 |
| | 25th–24th | **0.34** | **0.45** | **0.66** | 0.21 | 0.45 | 0.42 | **0.30** | **0.40** |
| | 26th–25th | 0.28 | 0.37 | 0.48 | **0.22** | **0.59** | **0.49** | 0.25 | 0.38 |
| | $\bar{x}$ | **0.27** | **0.35** | **0.51** | **0.20** | **0.48** | **0.45** | **0.27** | **0.36** |
| | complete | 0.27 | 0.37 | 0.56 | 0.22 | 0.49 | 0.44 | 0.27 | **0.38** |
| Late Gravettian | 27th–26th | **0.40** | 0.27 | **0.61** | 0.25 | 0.35 | 0.40 | 0.24 | 0.36 |
| | 28th–27th | 0.32 | **0.30** | 0.55 | 0.30 | 0.41 | 0.42 | 0.26 | 0.36 |
| | 29th–28th | 0.34 | **0.30** | 0.54 | **0.34** | 0.50 | 0.40 | 0.31 | **0.39** |
| | 30th–29th | 0.25 | 0.24 | 0.34 | *0.29* | **0.67** | **0.75** | **0.34** | **0.41** |
| | $\bar{x}$ | **0.33** | **0.28** | **0.51** | **0.29** | **0.48** | **0.49** | **0.29** | **0.38** |
| | complete | 0.36 | 0.29 | 0.58 | 0.29 | 0.46 | 0.52 | 0.27 | **0.40** |

Table 23: Change rates across successive millennia ($\bar{x}$ = averages for morphometric feature/section within respective taxonomic unit, calculated without MP–CM offsets; highlighted in red = RDA significant sections; bold and underlined = highest change rate in feature; faint = value below respective average).

| tax. unit | section m. BP | width | length | area | l-w-index | upper-lower-index | left-right-ratio | tip angle | MP-CM-x-offset | MP-CM-y-offset | $\bar{x}$ |
|---|---|---|---|---|---|---|---|---|---|---|---|
| | 15th–14th | | | | | | | | | | |
| Mag. | 16th–15th | -0.03 | -0.03 | -0.10 | 0.03 | -0.08 | -0.16 | -0.06 | -0.08 | *-0.25* | 0.07 |
| | 17th–16th | | | | | | | | | | |
| | 18th–17th | | | | | | | | | | |
| | 19th–18th | | | | | | | | | | |
| | 20th–19th | | | | | | | | | | |
| | 21st–20th | | | | | | | | | | |
| | 22nd–21st | | | | | | | | | | |
| Upper Solutrean | 23rd–22nd | 0.03 | 0.09 | 0.09 | 0.12 | 0.06 | 0.20 | **0.13** | -0.36 | *0.40* | 0.10 |
| | 24th–23rd | 0.16 | 0.18 | 0.27 | 0.03 | **0.25** | 0.02 | 0.11 | 0.14 | ***-1.89*** | 0.15 |
| | 25th–24th | **-0.23** | **0.34** | **0.48** | **0.13** | 0.01 | **0.32** | 0.06 | **0.38** | *-0.53* | 0.22 |
| | 26th–25th | | | | | | | | | | |
| | $\bar{x}$ | **0.14** | **0.20** | **0.28** | **0.09** | **0.11** | **0.18** | **0.10** | **0.29** | ***0.47*** | **0.16** |
| Late Gravettian | 27th–26th | **0.20** | 0.02 | **0.29** | -0.13 | -0.11 | 0.08 | 0.12 | **0.27** | *-2.26* | 0.14 |
| | 28th–27th | -0.08 | -0.14 | -0.24 | -0.09 | 0.09 | -0.12 | -0.01 | -0.14 | *1.55* | 0.11 |
| | 29th–28th | 0.12 | 0.03 | 0.30 | -0.12 | -0.32 | 0.14 | **0.44** | 0 | *1.03* | 0.21 |
| | 30th–29th | 0.14 | **0.26** | 0.29 | **0.21** | **0.58** | **-0.28** | -0.30 | -0.06 | ***-5.53*** | 0.30 |
| | $\bar{x}$ | **0.14** | **0.12** | **0.28** | **0.14** | **0.28** | **0.16** | **0.22** | **0.12** | ***2.59*** | **0.19** |

### 4.2.1.3.1 Change Rates for Sections

#### Late Gravettian

On average, the change rate between one millennium and the next during the Late Gravettian is 18% ($\bar{x}$ = 0.18). The first two sections of the Late Gravettian ranging from the 30th to the 29th and the 29th to the 28th millennium BP are characterised by higher average change rates ($\bar{x}$ = 0.29 and 0.19), as described in Chapter 4.1.3, responsible for the high average change rate of the Late Gravettian. Also inferable from that chapter is the comparable low change rate for the third section ranging from the 28th to the 27th millennium BP ($\bar{x}$ = 0.11), which actually is the lowest value within the entire Late Gravettian. For the 27th to the 26th millennium BP, the Late Gravettian assemblages resulted in a likewise low change rate ($\bar{x}$ = 0.12), below the average change rate for the entire Late Gravettian.

#### Upper Solutrean

The average change rate between one millennium and the next during the Upper Solutrean ($\bar{x}$ = 0.16) is a bit lower than for the Late Gravettian. The by far highest average change rate derives from the section ranging from the 25th to the 24th millennium BP ($\bar{x}$ = 0.24), driving the overall average change rate for the Upper Solutrean. The change rates for the subsequent two sections gradually decrease from quite low for the section from the 24th to the 23rd millennium BP ($\bar{x}$ = 0.15) to exceptional low for the section from the 23rd to the 22nd millennium BP ($\bar{x}$ = 0.10). The elevated change rates for the oldest section are largely driven by the morphological differences between the Iberian and French Upper Solutrean SPs. Notably, when excluding the French assemblage from the analysis, the average change rate between the SPs of the 25th and 24th millennium BP drops to just 0.18. However, the reliability of this result remains questionable due to the extremely low sample size, especially for the 25th millennium BP, where only six SPs from two assemblages are left. Conversely, for the section from the 24th to the 23rd millennium BP, the change rate increases when excluding the French assemblages ($\bar{x}$ = 0.26). This underscores the sensitivity of the method to both dataset selection and sample size, highlighting how variations in data composition can influence the calculated change rates and the resulting interpretations.

#### Upper/Late–Final Magdalenian

The average change rate for the Upper/Late–Final Magdalenian assemblages from the 16th to the 15th millennium BP is outstanding low ($\bar{x}$ = 0.07), implying almost no chronologically directed change between these two millennia within this taxonomic unit. While the datasets become quite *small* when conducting a type-specific analysis, the results provide a more nuanced perspective. They indicate that the overall change rates calculated for the entirety of the Upper/Late–Final Magdalenian dataset may be somewhat obscured by the interplay between the two types. The average change rate between the 15 SPs dating to the 16th and the nine SPs dating to the 15th millennium BP for Type A SPs is 11% ($\bar{x}$ = 0.106). For Type B SPs, the average change rate between the 17 SPs dating to the 16th and the 11 SPs dating to the 15th millennium BP is only at 4% ($\bar{x}$ = 0.04). *(Figure 72, Table 23)*

### 4.2.1.3.2 Change Rates for Morphometric Features

#### Late Gravettian

Besides the extreme high average for the MP-CM-y-offset ($\bar{x}$ = 2.59), which however is excluded from further calculations, the highest average change rates in the morphometric features are calculated for the area (0.28) and the upper-lower-ratio (both $\bar{x}$ = 0.28). An also quite high average change rate is calculated for the tip angle ($\bar{x}$ = 0.22), which however derives mostly from the oldest two sections. The averages for all size-related features apart from area (width = 0.14, length = 0.12) as well as for the l-w-index ($\bar{x}$ = 0.14), the left-right-ratio ($\bar{x}$ = 0.16) and the MP-CM-x-offset (0.2) are comparably low.

The oldest section of the Late Gravettian from the 30th to the 29th millennium BP is characterised by exceptional high change rates in both size- and shape-related features, comprising most of the peak values in the individual morphometric features (length = 0.26, l-w-index = 0.21, upper-lower-ratio = 0.58, left-right-ratio = -0.28 and MP-CM-y-offset = -5.53). The highest change rate in the tip angle is calculated for the section from the 29th to the 28th millennium BP (0.44), while most of the change rates for the other values remain

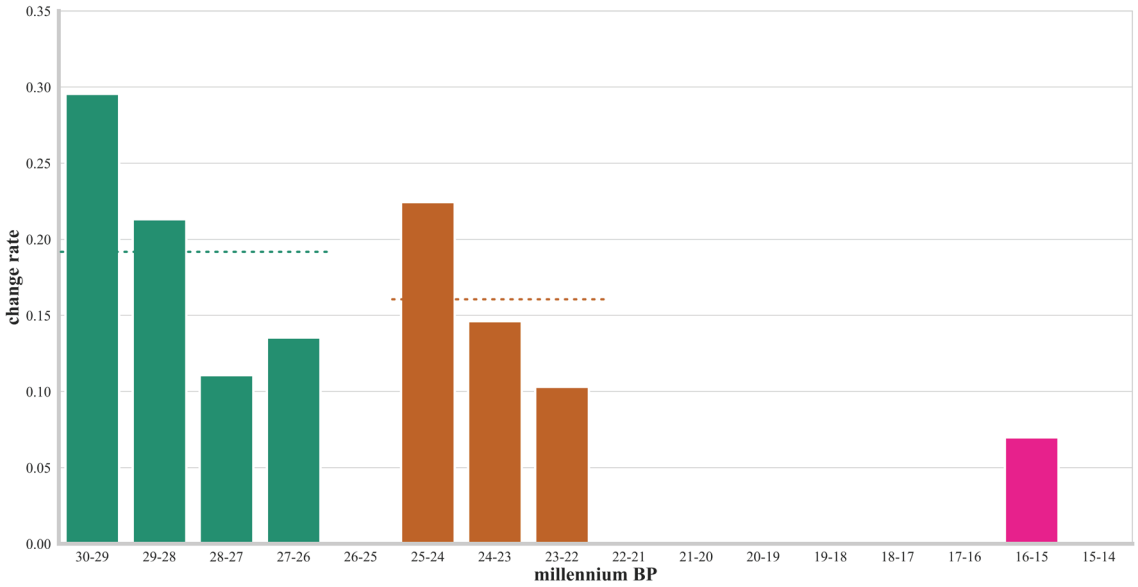



Figure 72: Averages ($\bar{x}$) of change rates *per section* in millennium BP within taxonomic units (green = Late Gravettian; orange = Upper Solutrean; pink = Upper/Late–Final Magdalenian; dotted line = average change rate for respective taxonomic unit, excluding MP–CM y-offset).

below their respective averages. Also, the change rates for almost all morphometric features remain below their respective averages in the section from the 28th to the 27th millennium BP. The youngest section of the Late Gravettian from the 27th to the 26th millennium BP, even though most of the change rates in the morphometric features and so the average of this section are below the respective averages, yield two peak values too (width = 0.2 and area = 0.29).

Overall, the shape-related features yield a higher average change rate ($\bar{x}$ = 0.2) than the size-related features ($\bar{x}$ = 0.18). The most pronounced disparity between the features related to the size ($\bar{x}$ = 0.12) and to the shape ($\bar{x}$ = 0.26) occur for the section from the 29th to the 28th millennium BP *(Figure 73)*. Also for the oldest section (30th–29th millennium BP) the average change in shape-related ($\bar{x}$ = 0.34) features is much higher than for the size-related features ($\bar{x}$ = 0.24), both of which exceeding their respective averages. For the section from the 28th to the 27th millennium BP, the proportions are opposed with clearly more change in size-related ($\bar{x}$ = 0.15) features than in shape-related features ($\bar{x}$ = 0.08) while both remain below their respective overall averages. Even proportions can be observed for the youngest section of the Late Gravettian (27th–26th millennium BP) with both values (size: $\bar{x}$ = 0.13; shape: $\bar{x}$ = 0.11) remaining below their respective overall averages.

***Upper Solutrean***

The highest average change rates in the morphometric features are calculated for the MP-CM-x-offset ($\bar{x}$ = 0.29) and area ($\bar{x}$ = 0.28). Also length ($\bar{x}$ = 0.2) yields a comparably high average change rate. The shape-related features overall yield lower values, with the highest average change rate calculated for the left-right-ratio ($\bar{x}$ = 0.18). This observation is reflected in the pronounced difference between the average change rates for size- ($\bar{x}$ = 0.2) and shape-related ($\bar{x}$ = 0.12) features, implying changes tend to occur more in the size than in the shape of the SPs throughout the entire Upper Solutrean. This however does not apply to the youngest Upper Solutrean section (23rd–22nd millennium BP), where only minor changes are indicated for the size-related features while the average for the shape-related features exceeds its overall average *(Figure 73)*.

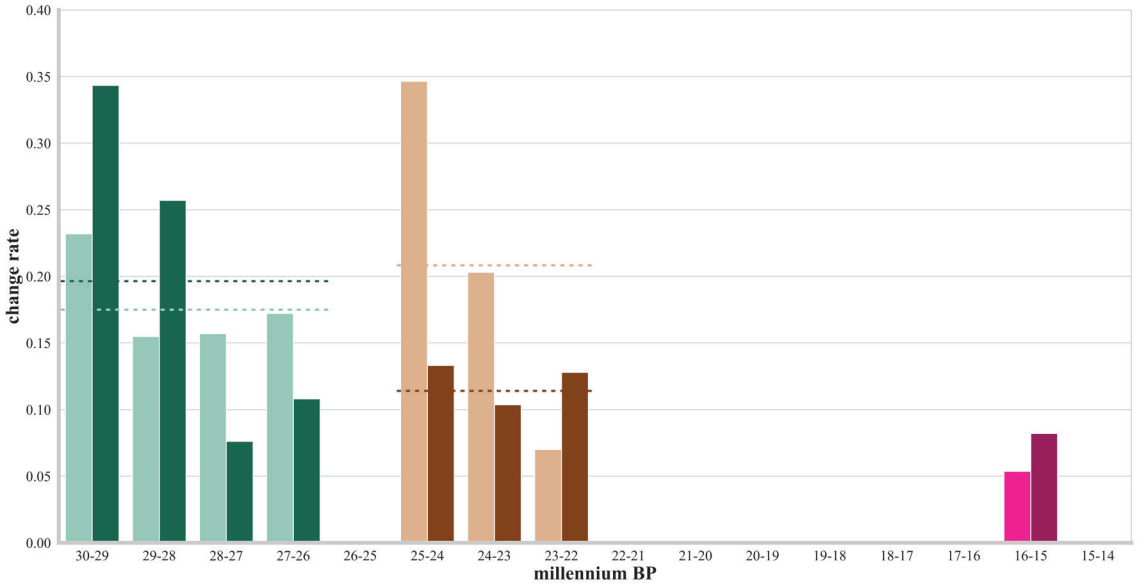



Figure 73: Averages ($\bar{x}$) of absolute change rates for features related to size and shape *per section* in millennium BP within taxonomic units (size = light coloured; shape = dark coloured; green = Late Gravettian; orange = Upper Solutrean; pink = Upper/Late–Final Magdalenian).

Almost all peak change rates in the morphometric features derive from the first section ranging from the 25th to the 24th millennium BP. This is especially true for the size-related features (width = -0.23, length = 0.34, are = 0.48), but applies also to the left-right-ratio (0.32). This high values for the size-related features again most likely derives from the exceptional sizes of the French Upper Solutrean SPs. Almost no change seems to happen in the upper-lower-ratio (0.01) and the tip angle (0.06). For the section ranging from the 24th to the 23rd millennium BP the peak change rate for the upper-lower-ratio (0.25) as well as comparably high change rates for length (0.18), area (0.27), width (0.16), and the tip angle (0.11) are calculated. The change rates for the left-right-ratio (0.03) and the l-w-index (0.02) are noticeable low. The change rates calculated for the section ranging from the 23rd to the 22nd millennium BP are even lower. With the exception of the peak change rate in the tip angle (0.13) and the comparably high change-rate in the left-right-ratio (0.2) and the l-w-index (0.12), all features yield change rates well below the respective averages (width = 0.03, length = 0.09, area = 0.09, upper-lower-ratio = 0.06).

### *Upper/Late – Final Magdalenian*

The change rates between the 16th and the 15th millennium BP in this taxonomic unit are remarkably low for all morphometric features. The highest change rates are calculated for the MP-CM-y-offset (-0.25), the left-right-ratio (-0.16) and area (-0.1). Almost no change seems to happen in width (-0.03), length (-0.03), the l-w-index (0.03) and the tip angle (-0.06). The average change rate for all size-related features is only 0.05, whereas the average change rate for shape-related features is just slightly higher (0.08).

For Type A the highest change rate is calculated for the MP-CM-x-offset (-0.31). The change rates for area (-0.19) width (-0.16), the tip angle (-0.14), the left-right-ratio (-0.13) and the l-w-index (0.12) are a bit elevated but not notably high. The other change rates remain remarkably low (length = -0.04, upper-lower-ratio = 0.02, MP-CM-y-offset = -0.04).

For Type B SPs, the highest change rate is observed in the MP-CM-y-offset (-0.8), though this value might be unreliable. The only other feature with a notably high change rate is the MP-CM-x-offset (0.28). All other morphometric features exhibit remarkably low change rates (width = 0.008, length = 0.07, area = 0.02, l-w-index = 0.07, upper-lower-ratio = 0.06, left-right-ratio = -0.009, tip angle = -0.06). *(Figure 73)*

### *4.2.1.3.3 Directedness of Change Rates*

***Late Gravettian***

Throughout the entire period a noticeable shift in size towards wider and overall bigger SPs is calculated. For length the values are increasing until the 28th millennium BP and slightly decreasing afterwards *(Figure 74)*. The most pronounced, constant trend in shape is the decreasing of the l-w-index from the 29th millennium BP on, indicating SPs become stouter throughout the Late Gravettian. After the high shift right at the beginning of the Late Gravettian and the significant subsequent drop, the upper-lower-ratio remains relatively stable at between approximately 1 and 0.6, indicating an almost even relation between hafting and transitional part. For the left-right-ratio, the values seem to oscillate around an 'optimum' of approximately 0.8 (almost perfectly axisymmetric), while no clear trend is visible. After an initial drop, the tip angle increases constantly throughout the Late Gravettian leading to more obtuse tips. The MP-CM-x-offset shows almost no change throughout the entire Late Gravettain, whereas the y-offset after the significant drop at the beginning, shows a comparably strong increasing trend until the 27th millennium BP, followed by another significant drop.

***Upper Solutrean***

Following the pronounced initial drop, linked to the notably big SPs of the French Upper Solutrean assemblage of Le Placard (A-46), dating within the 25th millennium BP, and comparably small specimens in the 24th millennium BP, the sizes of the Upper Solutrean SPs remain more or less stable *(Figure 74)*. Resulting from the slightly more pronounced changes in length, the l-w-index shows an almost constant decreasing trend towards stouter forms. Before and after a noticeable increase from the 23rd to the 22nd millennium BP, the values for the upper-lower-ratio remain more or less stable, indicating SPs with short hafting parts in relation to their transformative parts. The left-right-ratio shows a pronounced initial increase, highlighting a shift from extremely asymmetric SPs to less asymmetric pieces. This shift is followed by a phase of consistent decrease towards more asymmetric SPs again. The tip angle does not show a significant trend but rather an oscillation around a central value throughout the entire Upper Solutrean. The MP-CM-x-offset shows an increasing trend until the 23rd millennium BP, followed by a pronounced regression. The MP-CM-y-offset on the contrary undergoes an almost constant decreasing trend at the same time.

***Upper/Late–Final Magdalenian***

As described above, almost all values for the Magdalenian are very low so that the actual changes might not even be visible to the naked eye. The left-right-ratio however shows a noticeable decreasing shift *(Figure 74)*, indicating less asymmetric SPs in the Magdalenian assemblages dating to the 16th millennium BP.

The initial appearance of SPs during the Late Gravettian is marked by extreme change rates. However, it must be emphasised again that these elevated values primarily reflect the distinct SP design from Mitoc-Malu Galben, layer 4a (A-60, 29th millennium BP), rather than indicating broader chronologically directed changes. This interpretation is further supported by the absence of significant results in the RDA during the first two chronological sections. Thus, the Late Gravettian as a whole appears to be characterised by only minor morphometric shifts over time. Toward the end of the Late Gravettian (27th–26th millennium BP), however, a modest increase in change rates – corroborated by a significant signal from the RDA – suggests that chronologically driven transformations had begun to occur. The introduction of SPs into western Upper Solutrean assemblages is marked by elevated change rates. Yet once again, these are likely attributable to the morphological disparity between Iberian and French Upper Solutrean SPs rather than to internal temporal development. Throughout the Upper Solutrean, the extent of change steadily declines, culminating in minimal rates during the final phase




Figure 74: Added change rates for each morphometric feature per taxonomic unit (green = Late Gravettian; orange = Upper Solutrean; pink = Upper/Late–Final Magdalenian).

(23rd–22nd millennium BP). In contrast, the Upper/Late–Final Magdalenian period again shows no evidence of chronologically directed changes in SP morphometry. *(Figure 74)*

### *4.2.1.4 Combining Variation and Change*

When plotting values of variation against those of change for the analysable taxonomic units, the outcomes previously identified in the chronologically informed perspective (Chapter 4.1.4) are slightly revised. Beginning with the Late Gravettian, the three oldest sections remain unchanged in their positions. However, the section from the 27th to the 26th millennium BP – despite the RDA indicating the presence of directed changes – now plots in the lower left quadrant, indicative of both low variation and low change rates *(Figure 75)*. For the Upper Solutrean, the placement of sections within the plot remains largely consistent: the section from the 25th to the 24th millennium BP continues to exhibit elevated levels of both variation and change, placing it in the upper right quadrant, while the subsequent sections (24th–23rd and 23rd–22nd millennium BP) display relatively low values for both parameters, positioning them in the lower left quadrant. The only analysable representative of the Late Upper Palaeolithic – the Upper/Late–Final Magdalenian section from the 16th to the 15th millennium BP – plots differently compared to its position in the chronologically informed perspective. It is now situated in the upper left quadrant, reflecting elevated variation paired with a notably low rate of change. This distribution highlights the morphological disparity between Type A and Type B SPs, which may be interpreted as indicative of a speciation-like process. *(Figure 75–85)*

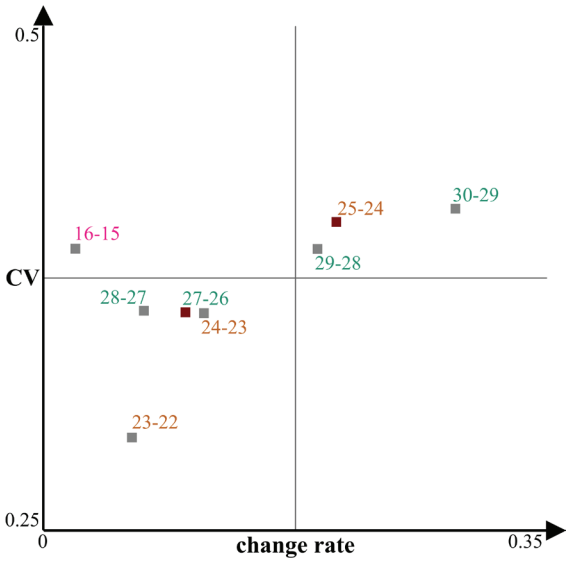



Figure 75: Scatterplot of Coefficient of Variation (CV) and change rate for analysable sections within taxonomic units (labels coloured by taxonomic unit: green = Late Gravettian; orange = Upper Solutrean; pink = Upper/Late–Final Magdalenian).

## 4.2.2 Between Taxonomic Units

The analyses in this chapter focus on transitional periods between major taxonomic units, further examining the strong signals identified in Chapter 4.1.3, which tend to appear within specific timeframes where major taxonomic changes are documented. Conversely, for periods that lacked strong signals despite taxonomic shifts, the analysis explores whether potential signals were obscured by specimens from minor taxonomic contexts or whether the taxonomic transition had no significant effect on SP morphometry. Although intra-taxonomic differences have been highlighted in the previous chapters – such as the disparity between the Iberian and French Upper Solutrean SPs, and the coexistence of two distinct SP design types (A and B) within the Upper/Late-Final Magdalenian – the following analyses do not incorporate this differentiation. Instead, they focus solely on the impact of taxonomic transitions as observed from a purely chronologically informed perspective. Through this approach, the importance of archaeo-stratigraphic developments in shaping the findings from the chronologically informed perspective is investigated. Four taxonomic transitions with potential influence on the chronological results are investigated here: between the Late Gravettian and the Upper Solutrean, the Upper Solutrean and the non-Solutrean LGM Industries, the Middle Magdalenian and the Upper/Late–Final Magdalenian, and the Upper/Late–Final Magdalenian and the Hamburgian. Mean-shapes are provided to visualise the results.

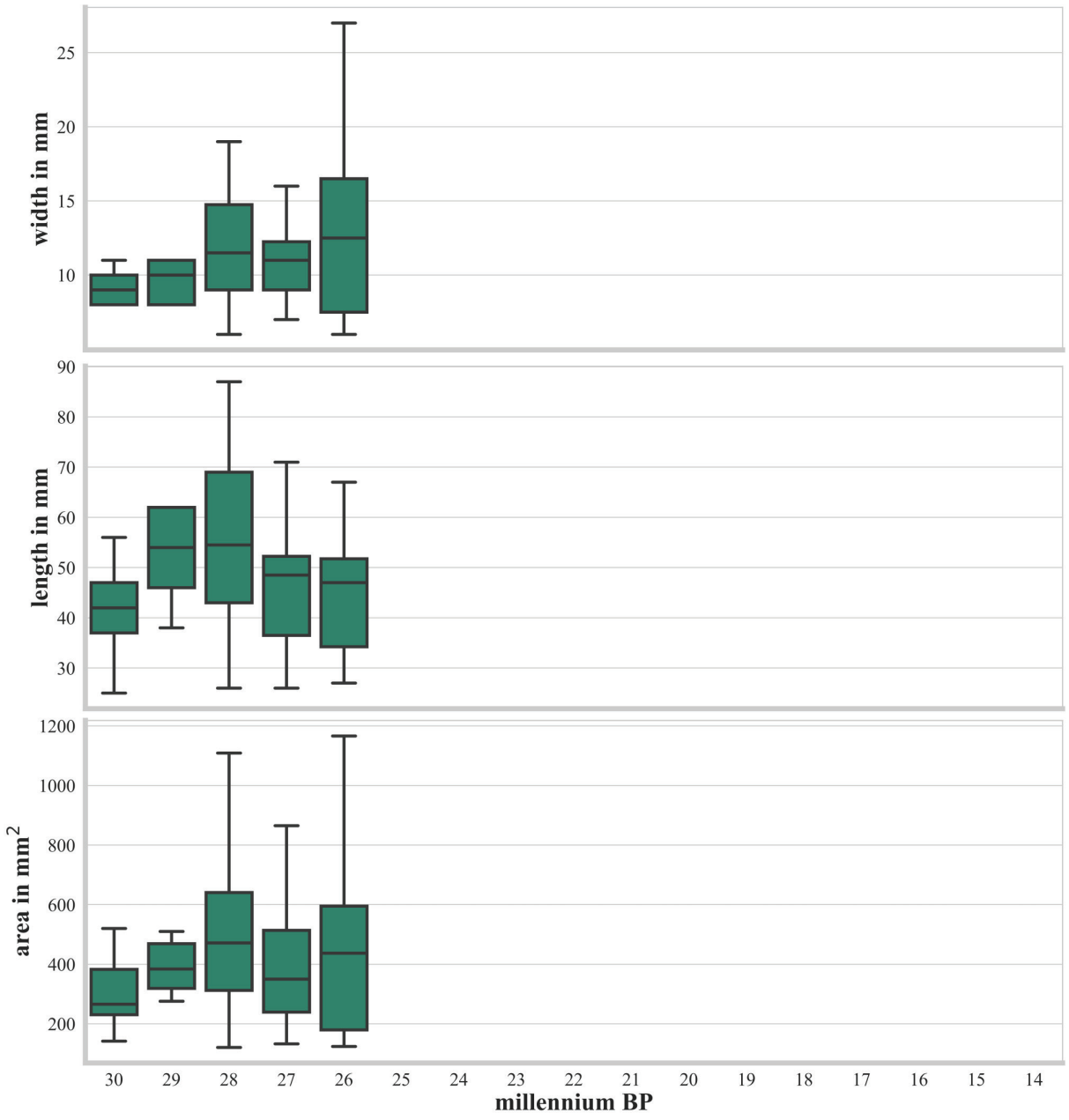



Figure 76: Box-plots of the real values of the size-related features for the Late Gravettian (outliers excluded).

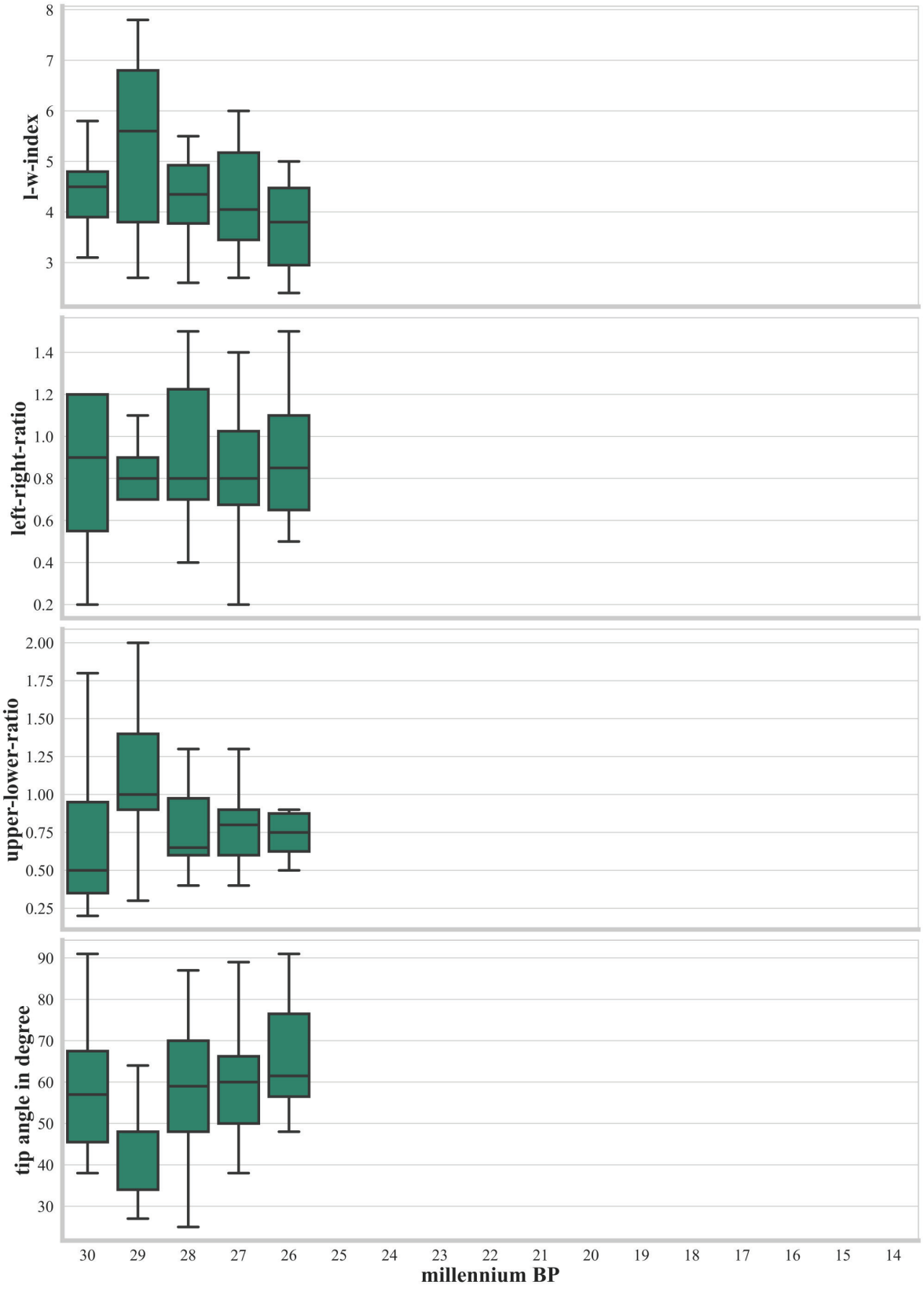



Figure 77: Box-plots of the real values of the shape-related features for the Late Gravettian (outliers excluded).

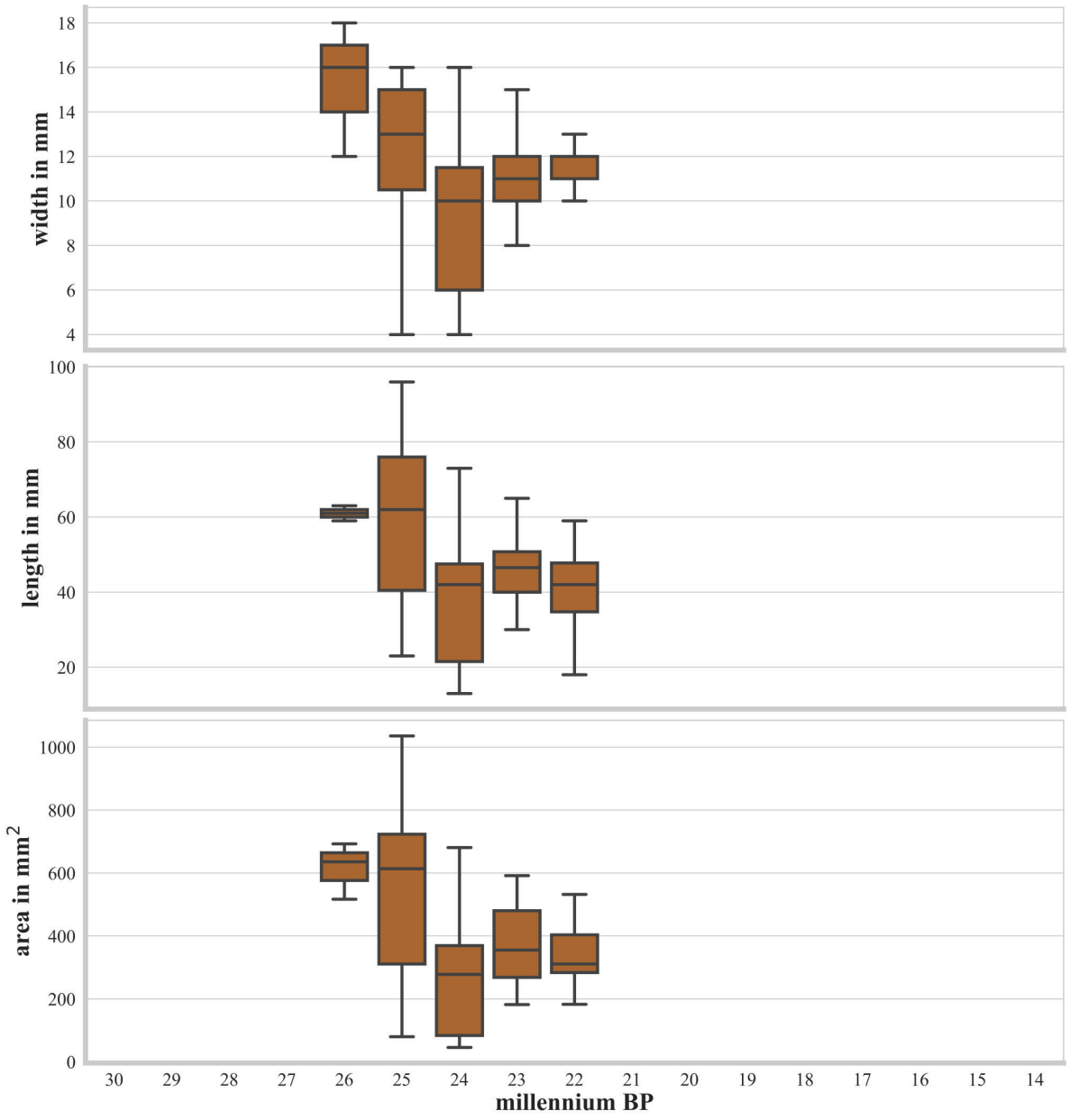



Figure 78: Box-plots of the real values of the size-related features for the Upper Solutrean (outliers excluded).

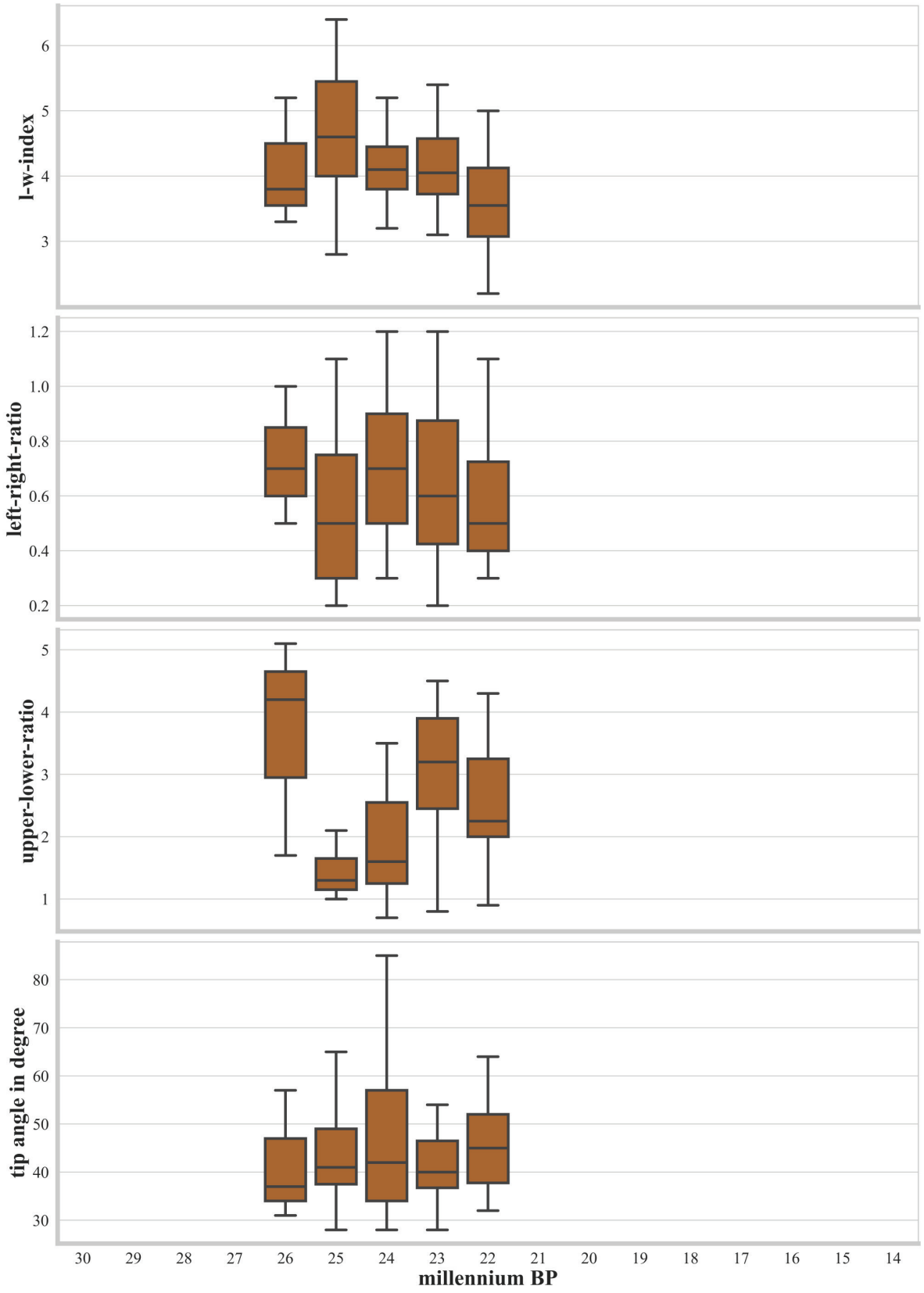



Figure 79: Box-plots of the real values of the shape-related features for the Upper Solutrean (outliers excluded).

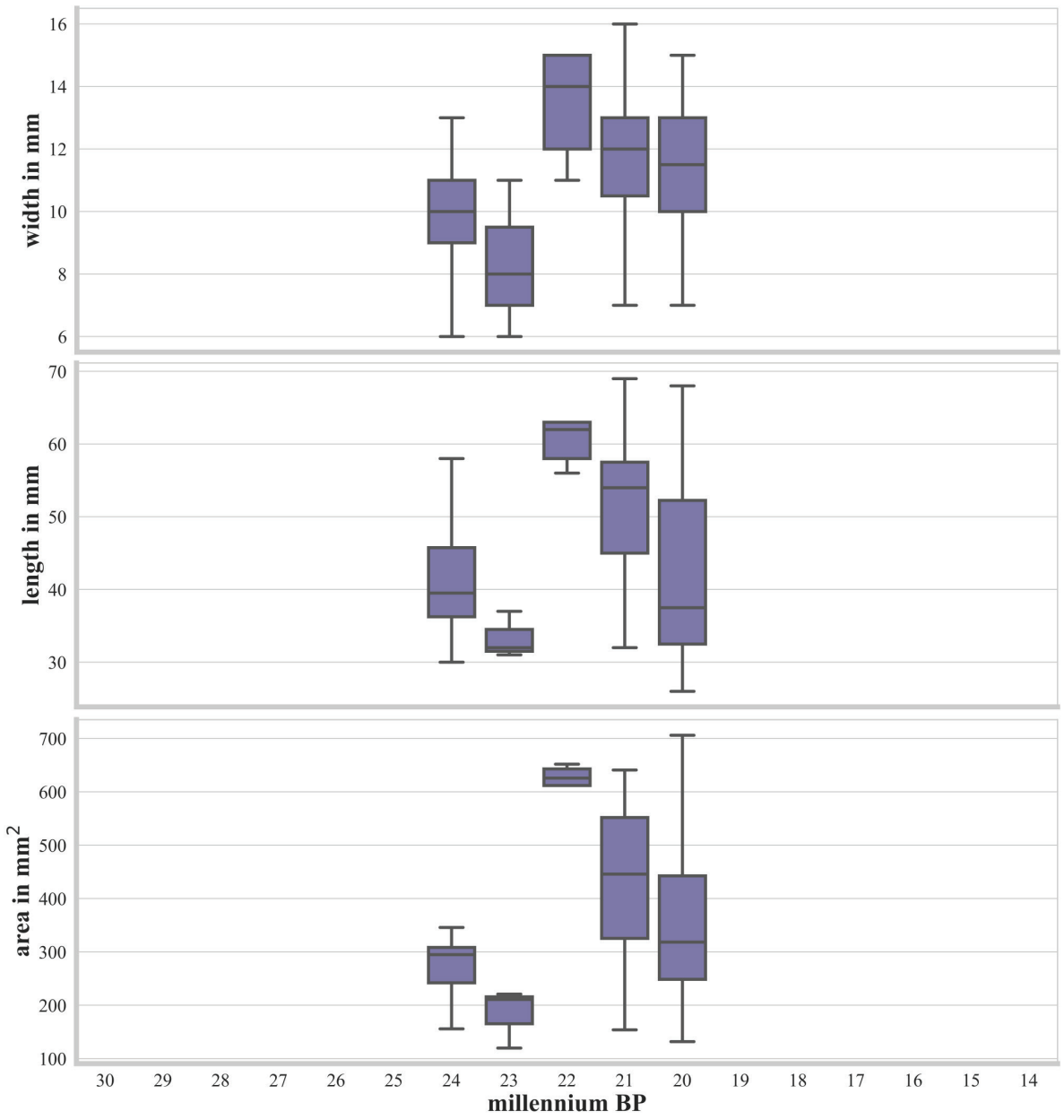



Figure 80: Box-plots of the real values of the size-related features for the non-Solutrean LGM industries (outliers excluded).

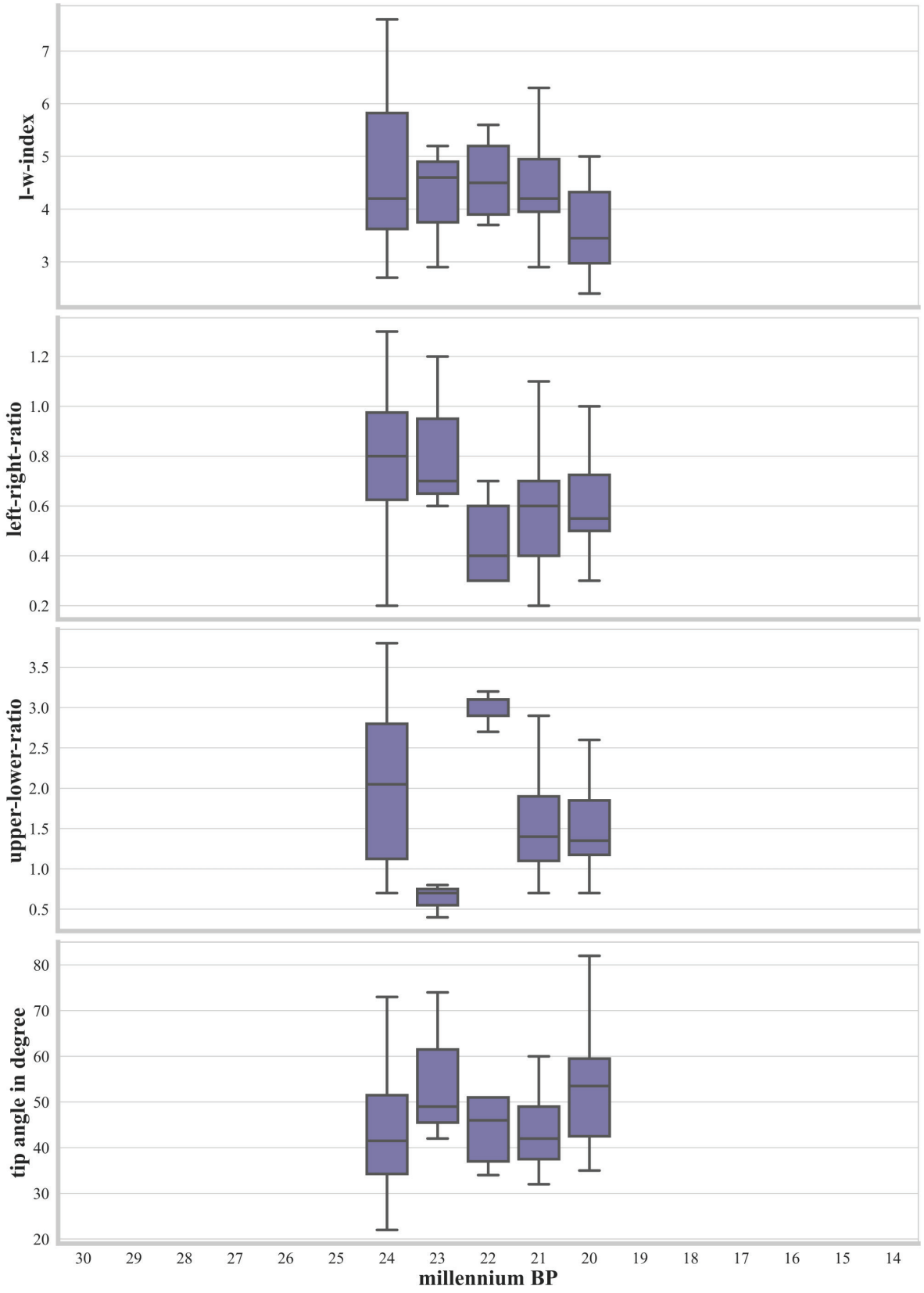



Figure 81: Box-plots of the real values of the shape-related features for the non-Solutrean LGM industries (outliers excluded).

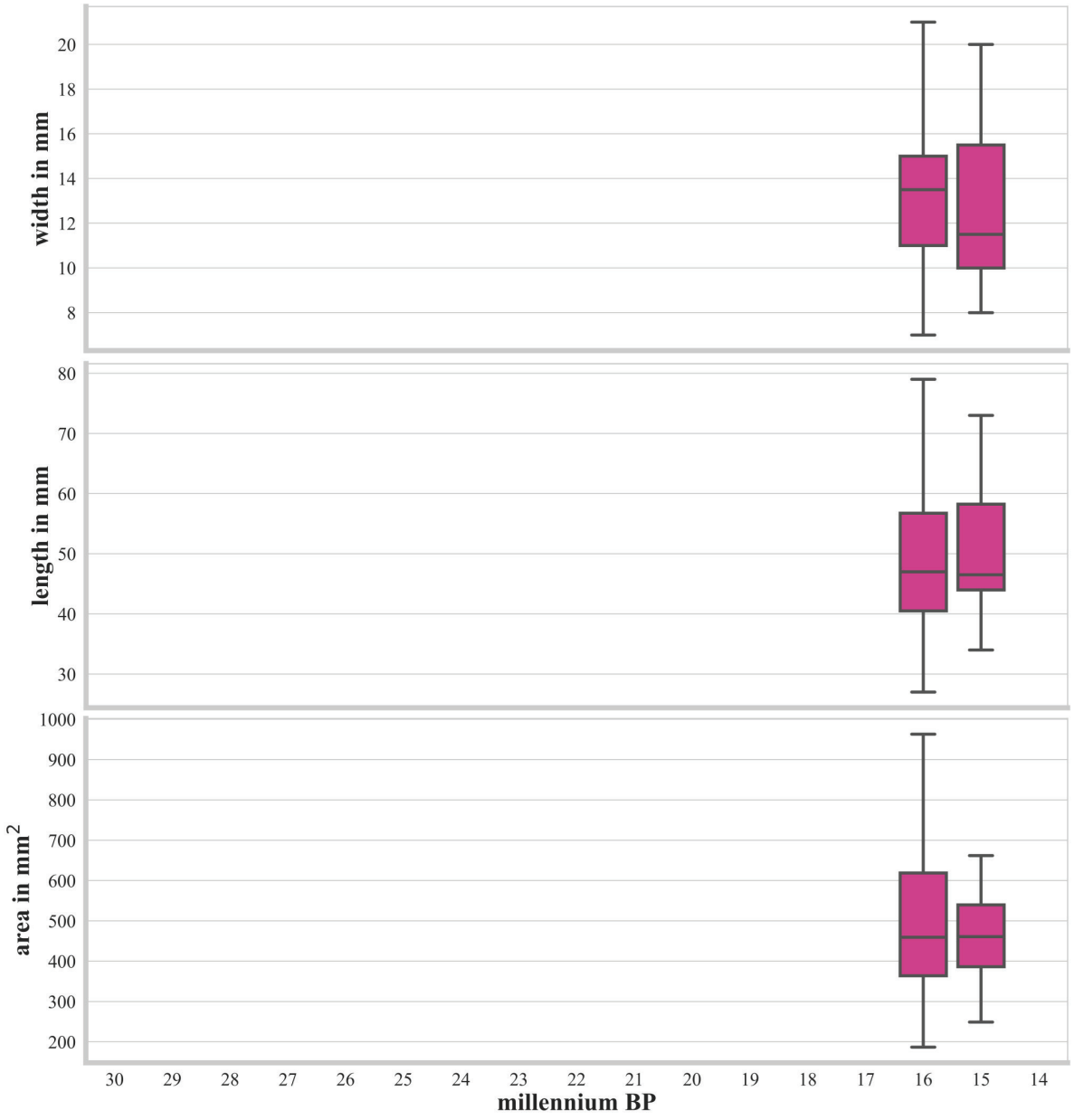



Figure 82: Box-plots of the real values of the size-related features for the Upper/Late–Final Magdalenian (outliers excluded).

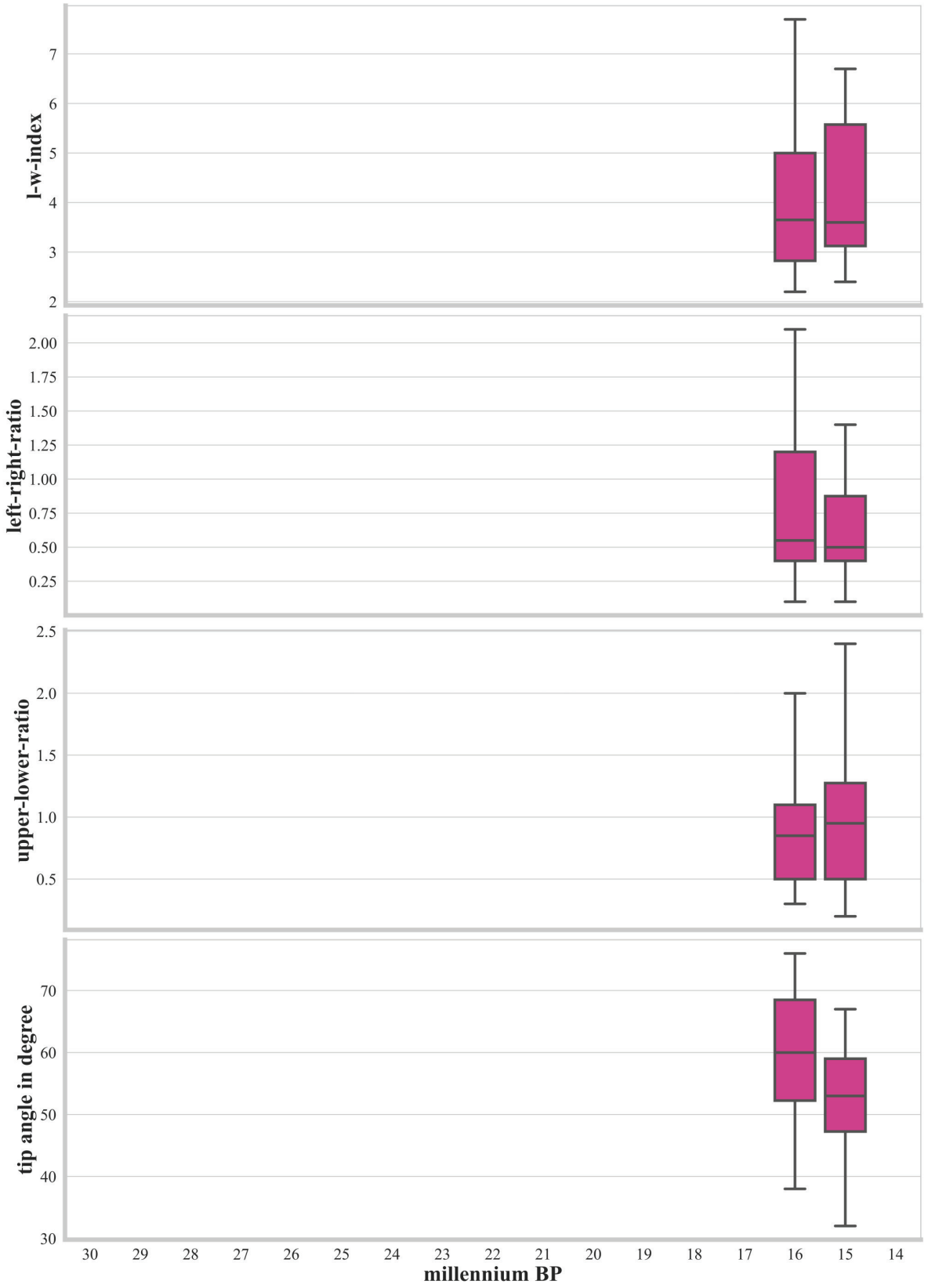



Figure 83: Box-plots of the real values of the shape-related features for the Upper/Late–Final Magdalenian (outliers excluded).

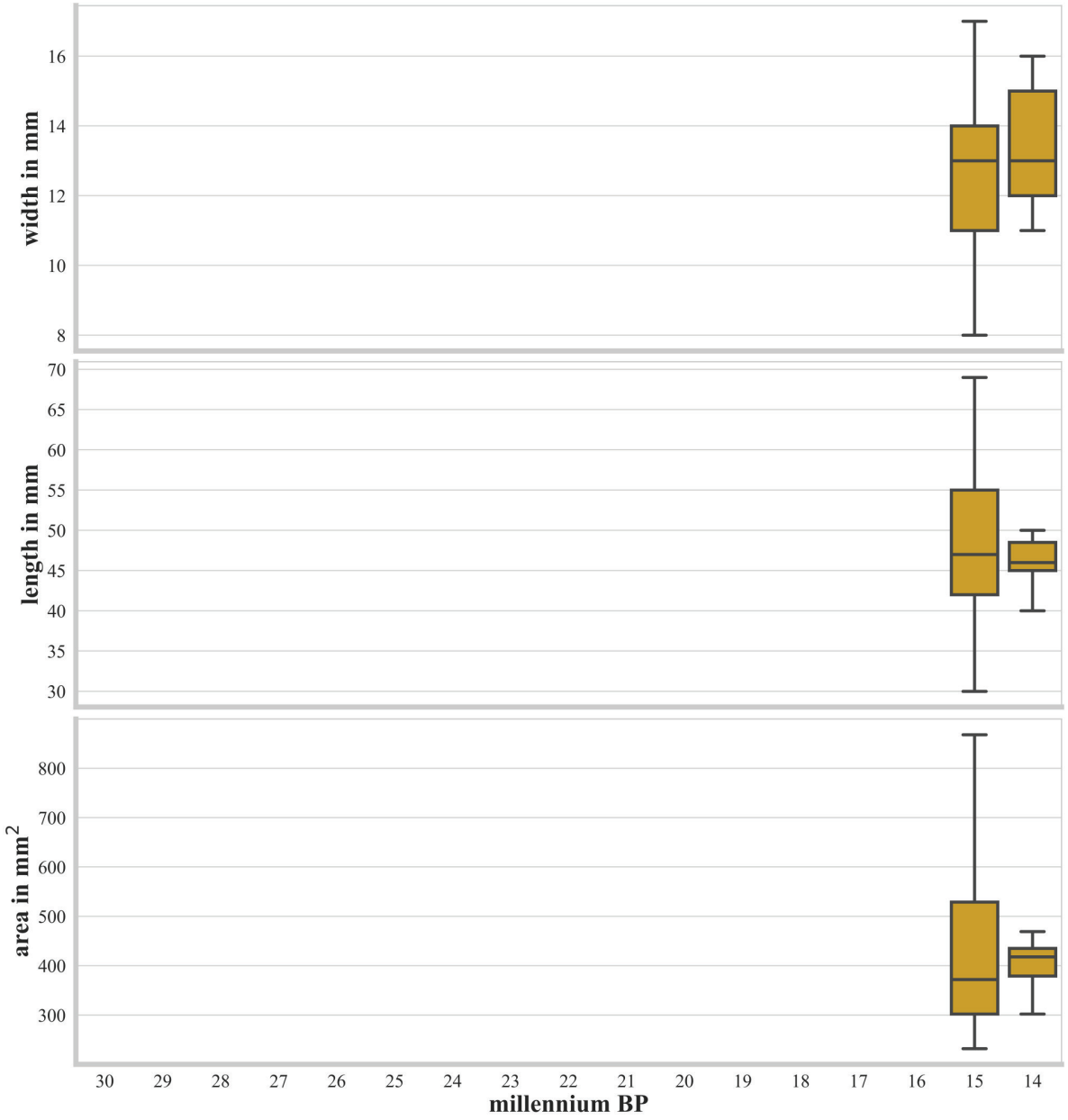



Figure 84: Box-plots of the real values of the size-related features for the Hamburgian (outliers excluded).

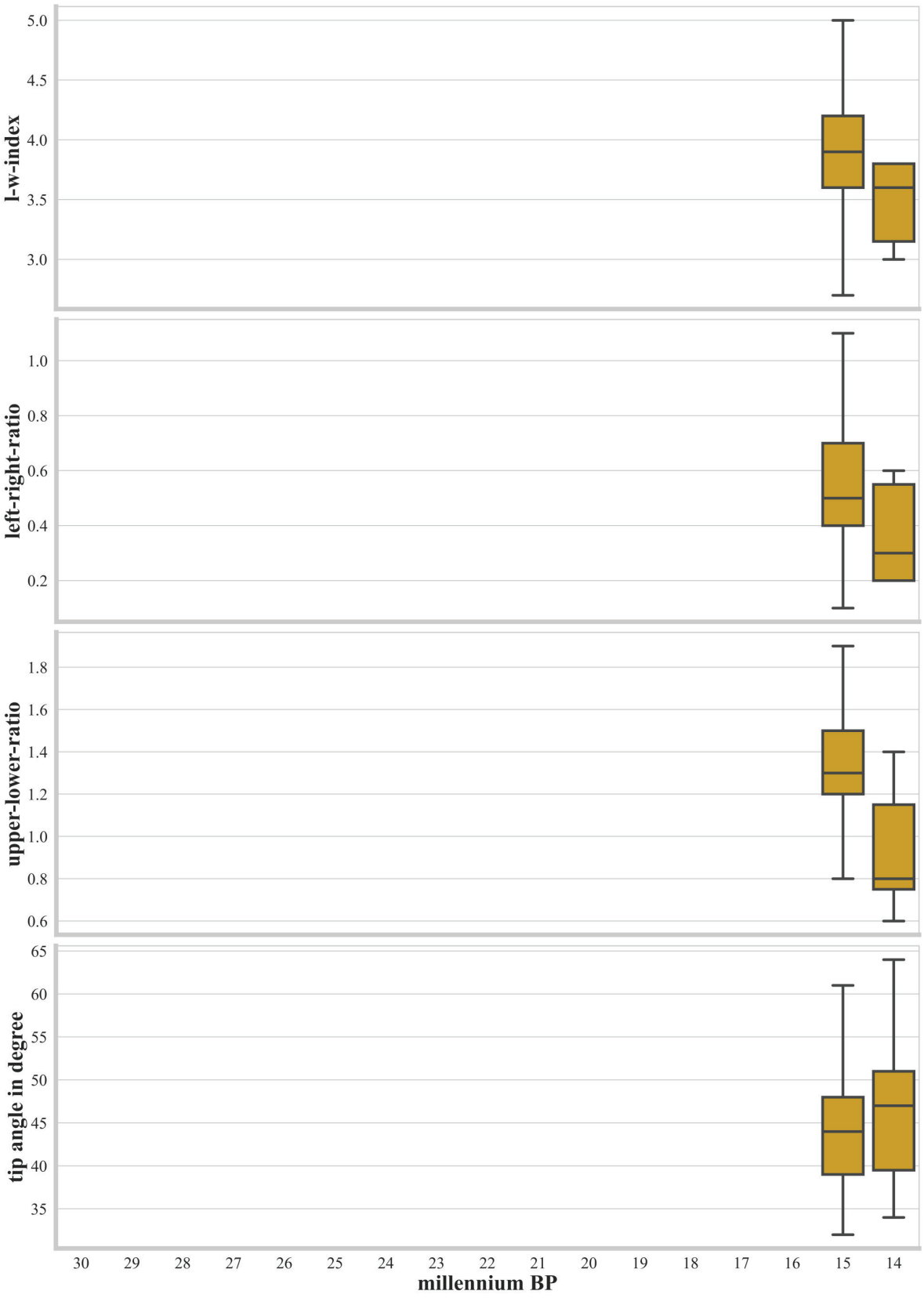



Figure 85: Box-plots of the real values of the shape-related features for the Hamburgian (outliers excluded).

### *4.2.2.1 Late Gravettian – Upper Solutrean*

As it has become obvious by the offset between the Late Gravettian and the Upper Solutrean curves in some features (see *Figure 74*), there are pronounced differences between SPs of these two taxonomic units. In order to analyse the transitional period in particular, the examined dataset here is reduced to the two key transitional sections – the section from the 27th to the 26th and from the 26th to the 25th millennium BP. The first section (27th–26th millennium BP) comprises 37 SPs from nine assemblages. With the exception of Abauntz (A-49), which is assigned to the Upper Solutrean, yielding only three SPs, all assemblages are attributed to the Late Gravettian. These assemblages derive predominantly from core area three – including Kostenki 21, layer III (A-54), Gagarino (A-50), and Avdeevo (A-48) – but also from core area one (Moravany nad Váhom-Podkovica (A-53), Banka-Horné farské role (B-21), and Petřkovice, layer 1a (A-51)), core area two (Dorotchivtsy III, layer 6 (A-52)), as well as from Italy (Grotta Paglicci, layer 20 (B-20)). The second section (26th–25th millennium BP) comprises 33 SPs from seven assemblages. Three of these represent the latest occurrences of Late Gravettian industries yielding SPs, all located in core area three (Gagarino (A-50), Avdeevo (A-48), and Pushkari (B-19)). The remaining four are widely distributed Upper Solutrean assemblages: Abauntz (A-49) and Cueva Morin, layer 5a (B-18), both situated along the northern Iberian coast; Vale Boi (A-47) on the Portuguese west coast; and Le Placard, located in central France.

#### *4.2.2.1.1 27th–26th millennium BP*

The change rates for the morphometric features between the Late Gravettian SPs and the Upper Solutrean SPs from Abauntz (A-49), within the section from the 27th to the 26th millennium BP, are notably high. The calculated average change rate ($\bar{x}$ = 0.73; *Table 24*) far exceeds both the average rate observed between two consecutive millennia across the entire dataset (as calculated in Chapter 4.1.3) and the section-wise significance threshold of 0.31. With the exception of the l-w-index (0.0), all features show change rates well above their

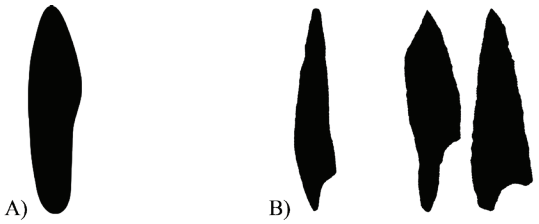



Figure 86: A) Meanshape of Late Gravettian SPs dating to the section from the 27th to the 26th millennium BP, and B) early Upper Solutrean SPs from Abauntz (A-49).

Table 24: Rates of change between the Late Gravettian SPs and the Upper Solutrean SPs of Abauntz for the section from the 27th to the 26th millennium BP ($\bar{x}$ = averages of the absolute values for change rates; bold = value exceeding the respective specific average change rate in Chapter 4.1.3; faint = value below the respective average change rate in Chapter 4.1.3; italic = extreme values excluded from the calculation of the averages; ! = value exceeding the respective significance threshold from Chapter 4.1.3).

| width | length | area | l-w-index | upper-lower-ratio |
|---|---|---|---|---|
| **0.29!** | **0.33!** | **0.47!** | 0.0 | **3.57!** |

| left-right-ratio | tip angle | MP-CM-x-offset | MP-CM-y-offset | $\bar{x}$ |
|---|---|---|---|---|
| -0.16 | **-0.32** | ***-1.11*** | ***-20.7*** | **0.73!** |

respective long-term averages for consecutive millennia. Moreover, aside from the left-right-ratio (-0.16), all values surpass their respective significance thresholds, highlighting the presence of substantial morphological shifts between the two taxonomic units. The most pronounced shifts are observed in the composition of the hafting and transformative parts *(Figure 86)*, resulting in a relatively shorter hafting part (upper-lower-ratio = 3.57) or respectively a relatively longer transformative part for the Upper Solutrean SPs. This change is also associated with significantly more acute tip angles (-0.32). *(Figure 86, Table 24)*

This exceptionally high average change rate further accounts for both the elevated variation values and the pronounced change rate observed on the chronologically informed perspective for the section spanning the 27$^{th}$ to the 26$^{th}$ millennium BP *(Chapter 4.1.3. Sections).*

#### *4.2.2.1.2 26$^{th}$–25$^{th}$ millennium BP*

The change rates for the morphometric features between the Late Gravettian SPs and the Upper Solutrean SPs within the section from the 26$^{th}$ to the 25$^{th}$ millennium BP are notably elevated *(Table 25)*. The average change rate between these two taxonomic units ($\bar{x}$ = 0.40) is much higher than the average change rate between two consecutive millennia and the section-wise significance threshold in the chronologically informed perspective (see Chapter 4.1.3). For all shape-related features, the change rates are particularly high, with the value for the upper-lower-ratio (1.4) exceeding the significance threshold established for this feature between two consecutive millennia. This again indicates a substantial change in the composition of the hafting and the transformative parts, resulting in a relatively shorter hafting part or respectively a relatively longer transformative part for the Upper Solutrean SPs *(Figure 87)*. This change is also associated with significantly more acute tip angles (-0.32). Additionally high change rates are observed for the left-right-ratio (-0.37), indicating a pronounced shift of both the tip and the base toward the left side of the SP. This shift results in a straighter appearance of the left side and a more pronounced right side (or countercut). In addition to these shape-related changes, length (0.29) also exhibits elevated change rates, suggesting the emergence of longer SPs in the Upper Solutrean. *(Figure 87, Table 25)*

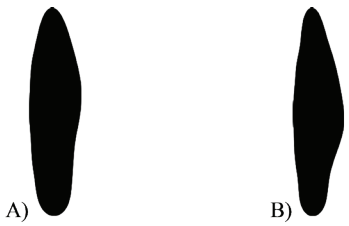



Figure 87: Meanshapes of A) Late Gravettian SPs, and B) Upper Solutrean SPs dating to the section from the 26$^{th}$ to the 25$^{th}$ millennium BP.

Table 25: Rates of change between the Late Gravettian and the Upper Solutrean SPs for the section from the 26$^{th}$ to the 25$^{th}$ millennium BP ($\bar{x}$ = averages of the absolute values for change rates; bold = value exceeding the respective specific average change rate in Chapter 4.1.3; faint = value below the respective average change rate in Chapter 4.1.3; italic = extreme values excluded from the calculation of the averages; ! = value exceeding the respective significance threshold from Chapter 4.1.3).

| width | length | area | l-w-index | upper-lower-ratio |
|---|---|---|---|---|
| -0.06 | **0.29** | 0.11 | **0.22** | **1.4!** |

| left-right-ratio | tip angle | MP-CM-x-offset | MP-CM-y-offset | $\bar{x}$ |
|---|---|---|---|---|
| **-0.37** | **-0.32** | ***0.96*** | ***0.70*** | **0.40!** |

Again, the high change rates calculated for between the Late Gravettian and the Upper Solutrean SPs within the section from the 26th to the 25th millennium BP accounts for both the elevated variation values and the pronounced change rate observed on the chronologically informed perspective. This is particularly true for the upper-lower-ratio, the left-right-ratio and the tip angle.

Although these results must be interpreted with caution given the limited dataset, the pronounced shift in both size and shape design of the SPs – as explained by the taxonomic transition – appears substantially more intense than would be expected from purely chronologically driven change. Rather than reflecting an incremental refinement of pre-existing forms, the observed morphological shift suggests a fundamental reconfiguration of SP design, which may point to significant technological innovation – or perhaps even to the independent (re)invention of SPs within the Upper Solutrean context.




Figure 88: Meanshapes of A) Upper Solutrean SPs, and B) Epigravettian SPs dating to the section from the 25th to the 24th millennium BP.

### 4.2.2.2 Upper Solutrean – Non-Solutrean LGM Industries

To gain a deeper understanding of the observations made for the period roughly spanning the late 25th to the 21st millennium BP, this section systematically analyses the impact of the interplay between the non-Solutrean LGM industries and the Upper Solutrean.

#### 4.2.2.2.1 25th–24th millennium BP

Within this section, three major taxonomic units are represented. In addition to the Upper Solutrean, the Salpetrian is present, though represented solely by a single assemblage from its eponymous site, Grotte de la Salpêtrière (A-38), dated to 23.0 ka calBP, yielding five SPs. The Epigravettian is likewise represented by a limited and geographically dispersed sample, comprising only five SPs in total, making it statistically weak. These originate from the assemblages of Grotta di Paina, layer 5 (B-16), and Ponte di Pietra (A-41) in Italy, dated to 23.6 and 23.4 ka calBP respectively, as well as from Kastrisa, layer 7 (A-42) in Greece, dated to 23.6 ka calBP. In contrast, the Upper Solutrean is represented more robustly in this section, with 42 SPs derived from nine assemblages, widely distributed across the Iberian Peninsula and central France.

Table 26: Rates of change between the Upper Solutrean and the Epigravettian SPs for the section from the 25th to the 24th millennium BP ($\bar{x}$ = averages of the absolute values for change rates; bold = value exceeding the respective specific average change rate in Chapter 4.1.3; faint = value below the respective average change rate in Chapter 4.1.3; italic = extreme values excluded from the calculation of the averages; ! = value exceeding the respective significance threshold from Chapter 4.1.3).

| width | length | area | l-w-index | upper-lower-ratio |
|---|---|---|---|---|
| **-0.21** | -0.10 | **-0.34** | **0.26** | 0.06 |

| left-right-ratio | tip angle | MP-CM-x-offset | MP-CM-y-offset | $\bar{x}$ |
|---|---|---|---|---|
| **0.38** | **-0.17** | ***-0.45*** | ***0.48*** | **0.22** |

### *Upper Solutrean – Epigravettian*

The change rates for the morphometric features between the Upper Solutrean and Epigravettian SPs within the section spanning the 25th to the 24th millennium BP are slightly higher than what would be expected for two consecutive millennia ($\bar{x}$ = 0.22; *Table 26*). The size-related features suggest primarily narrower SPs in the Epigravettian (width = -0.21), as well as slightly shorter forms (length = -0.10), resulting in overall smaller SPs (area = -0.34). Moreover, the elevated change rates for the l-w-index (0.26) and the left-right-ratio (0.38) point toward slenderer and more vertically-symmetric SPs in the Epigravettian compared to the Upper Solutrean *(Figure 88)*. Additionally, the tip angle shows a moderately elevated change rate (-0.17), suggesting more acute tips among the Epigravettian specimens. *(Figure 88, Table 26)*

### *Upper Solutrean – Salpetrian*

The change rates for the morphometric features between the Upper Solutrean SPs and the Salperian SPs from Grotte de la Salpêtrière, layer 6, within the section spanning the 25th to the 24th millennium BP, generally align with expectations for two consecutive millennia based on the chronologically informed perspective. The average change rate is 0.20 *(Table 27)* – only slightly higher than the overall average change rate between two successive millennia. While the value for length (-0.05) remains well below the average the change rates for width (-0.14) and area (-0.27) indicate more notable differences, suggesting that the Salpetrian SPs are narrower and thus overall *small*er. Among the shape-related features, the upper-lower-ratio (0.6) reflects a pronounced shift in the composition of the hafting and transformative parts, pointing to relatively shorter hafting respectively relatively longer transformative parts in the Salpetrian SPs *(Figure 89)*. In contrast, the l-w-index (0.14) shows only a slightly elevated change rate compared to the average. The left-right-ratio (0.13) and the tip angle (-0.10) both fall well below their respective averages for two consecutive millennia. *(Figure 89, Table 27)*

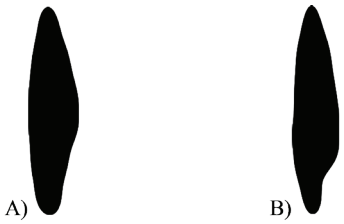



Figure 89: Meanshapes of A) Upper Solutrean SPs, and B) Salpetrian SPs from Grotte de la Salpêtrière, layer 6, dating to the section from the 25th to the 24th millennium BP.

Table 27: Rates of change between the Upper Solutrean SPs and the Salpetrian SPs from Grotta de la Salpêtriére, layer 6 for the section from the 25th to the 24th millennium BP ($\bar{x}$ = averages of the absolute values for change rates; bold = value exceeding the respective specific average change rate in Chapter 4.1.3; faint = value below the respective average change rate in Chapter 4.1.3; italic = extreme values excluded from the calculation of the averages; ! = value exceeding the respective significance threshold from Chapter 4.1.3).

| width | length | area | l-w-index | upper-lower-ratio |
|---|---|---|---|---|
| **-0.14** | -0.05 | **-0.27** | **0.14** | **0.6** |

| left-right-ratio | tip angle | MP-CM-x-offset | MP-CM-y-offset | $\bar{x}$ |
|---|---|---|---|---|
| 0.13 | -0.10 | ***-0.56*** | ***0.84*** | **0.20** |

***Epigravettian – Salpetrian***

The change rates for the morphometric features between the Epigravettian SPs and the Salpetrian SPs from Grotte de la Salpêtrière, layer 6, within the section from the 25th to the 24th millennium BP, are notably low. With the exception of the upper-lower-ratio (0.5), that indicates a shift towards relatively shorter hafting parts respectively relatively longer transformative parts from the Epigravettian to the Salpetrian *(Figure 90)*, the change rates for all features fall well below the average change rates observed between two consecutive millennia in the chronologically informed perspective *(Table 28)*. As a result, the calculated average change rate between these two taxonomic units is only 0.16 – slightly lower than the expected rate for two consecutive millennia. *(Figure 90, Table 28)*

The calculated impacts of the interplay between the taxonomic units on the patterns observed from the chronologically informed perspective within the section from the 25th to the 24th millennium BP are, despite isolated peaks in individual morphometric features, comparatively low, aligning well with the observed change rate for this section on the chronologically informed perspective. However, the isolated peaks especially in the upper-lower-ratio for between the Salpetrian and both the Upper Solutrean and the Epigravettian SPs, suggesting pronounced differences in the composition of the SPs, requires further investigation. *(Table 29)*

### *4.2.2.2.2 24th–23rd millennium BP*

Within the section from the 24th to the 23rd millennium BP, four major taxonomic units are represented. In addition to the Upper Solutrean, again the Salpetrian is present, though represented solely by a single assemblage from its eponymous site, Grotte de la Salpêtrière (A-38), dated to 23.0 ka calBP, yielding five SPs. The Epigravettian is represented by the same limited and geographically dispersed sample as for the section from the 25th to the 24th millennium BP, comprising only five SPs in total from three assemblages – Grotta di Paina, layer 5 (B-16), and Ponte di Pietra (A-41) in Italy, dated to 23.6 and 23.4 ka calBP respectively, as well as from Kastrisa, layer 7 (A-42) in Greece, dated to 23.6 ka calBP – making it statistically weak. Hence, the results from the previous section can be directly accepted.




Figure 90: Meanshapes of A) Epigravettian SPs, and B) Salpetrian SPs from Grotte de la Salpêtrière, layer 6, dating to the section from the 25th to the 24th millennium BP.

Table 28: Rates of change between the Epigravettian SPs and the Salpetrian SPs from Grotta de la Salpêtriére, layer 6 for the section from the 25th to the 24th millennium BP ($\bar{x}$ = averages of the absolute values for change rates; bold = value exceeding the respective specific average change rate in Chapter 4.1.3; faint = value below the respective average change rate in Chapter 4.1.3; italic = extreme values excluded from the calculation of the averages; ! = value exceeding the respective significance threshold from Chapter 4.1.3).

| width | length | area | l-w-index | upper-lower-ratio |
|---|---|---|---|---|
| 0.09 | 0.06 | 0.11 | -0.10 | **0.50** |

| left-right-ratio | tip angle | MP-CM-x-offset | MP-CM-y-offset | $\bar{x}$ |
|---|---|---|---|---|
| -0.18 | 0.08 | *-0.21* | *0.25* | 0.16 |

Table 29: Confusion matrix of the average change rates across the section from the 25th to the 24th millennium BP (! = value exceeding the respective significance threshold from Chapter 4.1.3; bold = value exceeding the average change rate for sections in Chapter 4.1.3; faint = value below the respective average change rate in Chapter 4.1.3).

| | Upper Solutrean | Epigravettian | Gr. de la Salpêtriére |
|---|---|---|---|
| **Upper Solutrean** | | **0.22** | **0.20** |
| **Epigravettian** | **0.22** | | 0.16 |
| **Gr. de la Salpêtriére** | **0.20** | 0.16 | |

Likewise limited represented is the Late Badegoulian by a single assemblage from Le Cuzoul de Vers, layers 21–16 (A-36), dating to 22.8 ka calBP and yielding three SPs. In contrast, the Upper Solutrean is represented more robustly in this section, with 37 SPs from eight assemblages, the majority of which – with the exception of three SPs from Combe-Saunière, layer IV (A-40) and two from Laugerie-Haute Ouest (A-43) – derive exclusively from the Iberian Peninsula.

### *Upper Solutrean – Epigravettian*

The change rates for the morphometric features between the Upper Solutrean SPs and the Epigravettian SPs within the section from the 24th to the 23rd millennium BP are just slightly elevated. Despite a peak in the l-w-index (0.33), indicating that Epigravettian SPs tend to be slenderer than their Upper Solutrean counterparts *(Figure 91)*, only a few features – width (-0.16), left-right-ratio (0.24), and tip angle (-0.16) – exceed the average change rates observed between two consecutive millennia. All other features fall well below their respective averages, resulting in an overall change rate that is slightly higher than expected for within a section ($\bar{x}$ = 0.18; *Table 30)*. *(Figure 91, Table 30)*

### *Upper Solutrean – Salpetrian*

The change rates for the morphometric features between the Upper Solutrean SPs and the Salpetrian SPs from Grotte de la Salpêtrière, layer 6, within the section from the 24th to the 23rd millennium BP, are notably low *(Table 31)*. With the exception of the l-w-index (0.20),




Figure 91: Meanshapes of A) Upper Solutrean SPs, and B) Epigravettian SPs dating to the section from the 24th to the 23rd millennium BP.

Table 30: Rates of change between the Upper Solutrean and the Epigravettian SPs for the section from the 24th to the 23rd millennium BP ($\bar{x}$ = averages of the absolute values for change rates; bold = value exceeding the respective specific average change rate in Chapter 4.1.3; faint = value below the respective average change rate in Chapter 4.1.3; italic = extreme values excluded from the calculation of the averages; ! = value exceeding the respective significance threshold from Chapter 4.1.3).

| width | length | area | l-w-index | upper-lower-ratio |
|---|---|---|---|---|
| **-0.16** | 0.03 | -0.16 | **0.33** | -0.20 |

| left-right-ratio | tip angle | MP-CM-x-offset | MP-CM-y-offset | $\bar{x}$ |
|---|---|---|---|---|
| **0.24** | **-0.16** | *-0.25* | *-0.27* | **0.18** |

that indicates slightly slenderer forms in the Salpetrian, the change rates for all features fall well below the average change rates observed between two consecutive millennia in the chronologically informed perspective. As a result, the calculated average change rate between these two taxonomic units is only 0.11 – significantly lower than the expected rate for comparable temporal intervals. *(Figure 92, Table 31)*

***Upper Solutrean – Late Badegoulian***

The change rates for the morphometric features between the Upper Solutrean SPs and the Late Badegoulian SPs from Le Cuzoul de Vers, layers 21–16, within the section from the 24th to the 23rd millennium BP, are notably high. In addition to elevated change rates across all size-related features *(Table 32)*, a substantial shift in the composition of the hafting and transformative parts is indicated by the pronounced change rate in the upper-lower-ratio (-0.73). This suggests relatively longer hafting parts respectively relatively shorter transformative parts for the Badegoulian SPs compared to their Upper Solutrean counterparts. These shorter transformative parts likely contribute to the more obtuse tip angles observed in the Badegoulian SPs, as reflected in the elevated change rate (0.23). The average change rate between the Upper Solutrean SPs and the Late Badegoulian SPs from Le Cuzoul de Vers, layers 21–16, is correspondingly elevated (0.28), underscoring the pronounced morphometric differences between these two taxonomic units. *(Figure 93, Table 32)*

***Epigravettian – Salpetrian***

The change rates for the morphometric features between the Epigravettian SPs and the Salpetrian SPs from Grotte de la Salpêtrière, layer 6, within the section from the 24th to the 23rd millennium BP, are notably low. With the exception of the upper-lower-ratio (0.50), that indicates relatively shorter hafting parts in the Salpetrian, the change rates for all features fall well below the average change rates observed between two consecutive millennia in the chronologically informed perspective (see Chapter 4.1.3). As a result, the calculated average change rate between these two taxonomic units is only 0.16 (Table 33) – slightly lower than the expected rate for comparable temporal intervals. *(Figure 94, Table 33)*

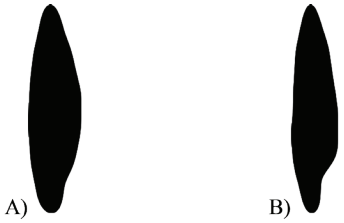



Figure 92: Meanshapes of A) Upper Solutrean SPs, and B) Salpetrian SPs from Grotte de la Salpêtrière, layer 6, dating to the section from the 24th to the 23rd millennium BP.

Table 31: Rates of change between the Upper Solutrean SPs and the Salpetrian SPs from Grotta de la Salpêtriére, layer 6 for the section from the 24th to the 23rd millennium BP ($\bar{x}$ = averages of the absolute values for change rates; bold = value exceeding the respective specific average change rate in Chapter 4.1.3; faint = value below the respective average change rate in Chapter 4.1.3; italic = extreme values excluded from the calculation of the averages; ! = value exceeding the respective significance threshold from Chapter 4.1.3).

| width | length | area | l-w-index | upper-lower-ratio |
|---|---|---|---|---|
| -0.08 | 0.09 | -0.07 | **0.20** | 0.20 |

| left-right-ratio | tip angle | MP-CM-x-offset | MP-CM-y-offset | $\bar{x}$ |
|---|---|---|---|---|
| 0.01 | -0.09 | ***-0.41*** | -0.09 | 0.11 |




Figure 93: Meanshapes of A) Upper Solutrean SPs, and B) Late Badegoulian SPs from Le Cuzoul de Vers, layers 21–16, dating to the section from the 24th to the 23rd millennium BP.




Figure 94: Meanshapes of A) Epigravettian SPs, and B) Salpetrian SPs from Grotte de la Salpêtrière, layer 6, dating to the section from the 24th to the 23rd millennium BP.

Table 32: Rates of change between the Upper Solutrean SPs and the Badegoulian SPs from Le Cuzoul de Vers, layers 21–16 for the section from the 24th to the 23rd millennium BP.

| width | length | area | l–w–index | upper–lower–ratio |
|---|---|---|---|---|
| **–0.18** | **–0.20** | **–0.42** | 0.03 | **–0.73** |

| left–right–ratio | tip angle | MP–CM–x–offset | MP–CM–y–offset | x̄ |
|---|---|---|---|---|
| 0.17 | **0.23** | *–0.02* | ***–1.84*** | **0.28** |

Table 33: Rates of change between the Epigravettian SPs and the Salpetrian SPs from Grotta de la Salpêtriére, layer 6 for the section from the 24th to the 23rd millennium BP.

| width | length | area | l–w–index | upper–lower–ratio |
|---|---|---|---|---|
| 0.09 | 0.06 | 0.11 | –0.1 | **0.5** |

| left–right–ratio | tip angle | MP–CM–x–offset | MP–CM–y–offset | x̄ |
|---|---|---|---|---|
| –0.18 | 0.08 | *–0.21* | *0.25* | 0.16 |

Signs/Markings: x̄ = averages of the absolute values for change rates; bold = value exceeding the respective specific average change rate in Chapter 4.1.3; faint = value below the respective average change rate in Chapter 4.1.3; italic = extreme values excluded from the calculation of the averages; ! = value exceeding the respective significance threshold from Chapter 4.1.3.

### *Epigravettian – Late Badegoulian*

The change rates for the morphometric features between the Epigravettian SPs and the Late Badegoulian SPs from Le Cuzoul de Vers, layers 21–16, within the section from the 24th to the 23rd millennium BP, are notably high as well. In addition to elevated change rates across all size-related features except from width *(Table 34)*, again a substantial shift in the composition of the hafting and transformative parts is indicated by the pronounced change rate in the upper-lower-ratio (-0.66). This suggests relatively longer hafting parts respectively relatively shorter transformative parts for the Badegoulian SPs compared to their Upper Solutrean counterparts. These shorter transformative parts likely contribute to the more obtuse tip angles observed in the Badegoulian SPs, as reflected in the elevated change rate (0.46). Additionally, the elevated change rate for the l-w-index (-0.22) indicates a stouter appearance of the Badegoulian SPs. The average change rate between the Epigravettian SPs and the Late Badegoulian SPs from Le Cuzoul de Vers, layers 21–16, is correspondingly elevated (0.28), underscoring the pronounced morphometric differences between these two taxonomic units. *(Figure 95, Table 34)*

### *Salpetrian – Late Badegoulian*

The change rates for the morphometric features between the Salpetrian SPs from Grotta de la Salpêtriére, layer 6 and the Late Badegoulian SPs from Le Cuzoul de Vers, layers 21–16, within the section from the 24th to the 23rd millennium BP, are notably high as well. In addition to elevated change rates across all size-related features *(Table 35)*, again a substantial shift in the composition of the hafting and transformative parts is indicated by the pronounced change rate in the upper-lower-ratio (-0.78). This suggests relatively longer hafting parts respectively relatively shorter transformative parts for the Badegoulian SPs compared to their Upper Solutrean counterparts. These shorter transformative parts likely contribute to the more obtuse tip angles observed in the Badegoulian SPs, as reflected in the elevated change rate (0.35). The average change rate between the Salpetrian SPs from Grotta de la Salpêtriére, layer 6, and the Late Badegoulian SPs from Le Cuzoul de Vers, layers 21–16, is correspondingly elevated (0.31), almost reaching the significance threshold for

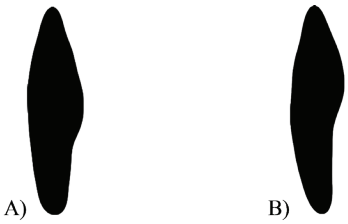



Figure 95: Meanshapes of A) Epigravettian SPs, and B) Late Badegoulian SPs from Le Cuzoul de Vers, layers 21–16, dating to the section from the 24th to the 23rd millennium BP.

Table 34: Rates of change between the Epigravettian SPs and the Badegoulian SPs from Le Cuzoul de Vers, layers 21–16 for the section from the 24th to the 23rd millennium BP ($\bar{x}$ = averages of the absolute values for change rates; bold = value exceeding the respective specific average change rate in Chapter 4.1.3; faint = value below the respective average change rate in Chapter 4.1.3; italic = extreme values excluded from the calculation of the averages; ! = value exceeding the respective significance threshold from Chapter 4.1.3).

| width | length | area | l-w-index | upper-lower-ratio |
|---|---|---|---|---|
| -0.03 | **-0.23** | **-0.31** | **-0.22** | **-0.66** |

| left-right-ratio | tip angle | MP-CM-x-offset | MP-CM-y-offset | $\bar{x}$ |
|---|---|---|---|---|
| -0.05 | **0.46** | *0.32* | ***-2.17*** | **0.28** |

two consecutive millennia (0.31, Chapter 4.1.3), underscoring the pronounced morphometric differences between these two taxonomic units. *(Figure 96, Table 35)*

The calculated impacts of the interplay between the taxonomic units on the patterns observed from the chronologically informed perspective within the section from the 24th to the 23rd millennium BP are again comparatively low. While this result must be treated with caution, given the low sample size, a clear exception are the interplays involving the Late Badegoulian SPs from Le Cuzoul de Vers (layers 21–16), which show pronounced differences across most morphometric dimensions to all other taxonomic units respectively assemblages. These differences suggest that a close morphometric relationship between any of the coexisting taxonomic units and the Late Badegoulian SPs is unlikely. It is presumably due to the small sample size and the exceptional low change rates between the other taxonomic units that these elevated change rates do not significantly affect the low average change rate observed for this section in the chronologically informed perspective. Drawing from the exceptional low change rates for between the other taxonomic units, it can be stated that the Upper Solutrean SPs, the Epigravettian SPs, and the Salpetrian SPs from Grotte de la Salpêtrière now share notable morphometric similarities. *(Table 36)*




Figure 96: Meanshapes of A) Salpetrian SPs from Grotta de la Salpêtriére, layer 6, and B) Late Badegoulian SPs from Le Cuzoul de Vers, layers 21–16, dating to the section from the 24th to the 23rd millennium BP.

Table 35: Rates of change between the Salpetrian SPs from Grotta de la Salpêtriére, layer 6 and the Badegoulian SPs from Le Cuzoul de Vers, layers 21–16 for the section from the 24th to the 23rd millennium BP ($\bar{x}$ = averages of the absolute values for change rates; bold = value exceeding the respective specific average change rate in Chapter 4.1.3; faint = value below the respective average change rate in Chapter 4.1.3; italic = extreme values excluded from the calculation of the averages; ! = value exceeding the respective significance threshold from Chapter 4.1.3).

| width | length | area | l-w-index | upper-lower-ratio |
|---|---|---|---|---|
| **-0.11** | **-0.27** | **-0.38** | -0.14 | **-0.78** |

| left-right-ratio | tip angle | MP-CM-x-offset | MP-CM-y-offset | $\bar{x}$ |
|---|---|---|---|---|
| 0.16 | **0.35** | 0.67 | ***-1.93*** | **0.31** |

Table 36: Confusion matrix of the average change rates across the section from the 24th to the 23rd millennium BP (! = value exceeding the respective significance threshold from Chapter 4.1.3; bold = value exceeding the average change rate for sections in Chapter 4.1.3; faint = value below the respective average change rate in Chapter 4.1.3).

| | Upper Solutrean | Epigravettian | Gr. de la Salpêtriére | Le Cuzoul de Vers |
|---|---|---|---|---|
| **Upper Solutrean** | | 0.18 | 0.11 | **0.278** |
| **Epigravettian** | 0.18 | | 0.16 | **0.28** |
| **Gr. de la Salpêtriére** | 0.11 | 0.16 | | **0.31** |
| **Le Cuzoul de Vers** | **0.28** | **0.28** | **0.31** | |

#### *4.2.2.2.3 23rd–22nd millennium BP*

Within the section from the 23rd to the 22nd millennium BP, three major taxonomic units are represented. In addition to the Upper Solutrean, again the Late Badegoulian is present, though represented solely by a single assemblage from Le Cuzoul de Vers, layers 21–16 (A-36), dating to 22.8 ka calBP and yielding three SPs. Likewise limited represented is the Tardigravettian by a single assemblage from Chinchon 1, layer C (A-33), dating to 21.6 ka calBP and yielding five SPs. In contrast, the Upper Solutrean is again represented more robustly in this section, with 34 SPs from five assemblages, all of which derive exclusively from the northern coast of the Iberian Peninsula.

***Upper Solutrean – Late Badegoulian***

The change rates for the morphometric features between the Upper Solutrean SPs and the Late Badegoulian SPs from Le Cuzoul de Vers, layers 21–16, within the section from the 23rd to the 22nd millennium BP, are again notably high. In addition to elevated change rates across all size-related features *(Table 37)*, a substantial shift in the composition of the hafting and transformative parts is indicated by the pronounced change rate in the upper-lower-ratio (-0.77), exceeding the significance threshold of this feature for two consecutive millennia. This suggests relatively longer hafting parts respectively relatively shorter transformative parts for the Badegoulian SPs compared to their Upper Solutrean counterparts. These shorter transformative parts likely contribute to the more obtuse tip angles observed in the Badegoulian SPs, as reflected in the elevated change rate (0.23). Additionally, the elevated change rate for the left-right-ratio (0.35) testifies more y-axisymmetric shapes for the Late Badegoulian SPs, compared to their Upper Solutrean counterparts. The average change rate between the Upper Solutrean SPs and the Late Badegoulian SPs from Le Cuzoul de Vers, layers 21–16, is correspondingly elevated (0.33), exceeding the significance threshold for change rates between two consecutive millennia (Chapter 4.1.3), again underscoring the pronounced morphometric differences between these two taxonomic units. *(Figure 97, Table 37)*

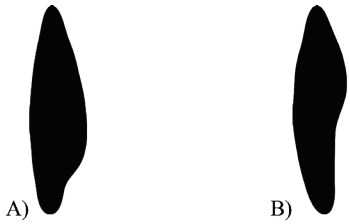



Figure 97: Meanshapes of A) Upper Solutrean SPs, and B) Late Badegoulian SPs from Le Cuzoul de Vers, layers 21–16, dating to the section from the 23rd to the 22nd millennium BP.

Table 37: Rates of change between the Upper Solutrean SPs and the Badegoulian SPs from Le Cuzoul de Vers, layer 21-16 for the section from the 23rd to the 22nd millennium BP ($\bar{x}$ = averages of the absolute values for change rates; bold = value exceeding the respective specific average change rate in Chapter 4.1.3; faint = value below the respective average change rate in Chapter 4.1.3; italic = extreme values excluded from the calculation of the averages; ! = value exceeding the respective significance threshold from Chapter 4.1.3).

| width | length | area | l-w-index | upper-lower-ratio |
|---|---|---|---|---|
| **-0.26** | **-0.24** | **-0.47** | 0.09 | **-0.77!** |

| left-right-ratio | tip angle | MP-CM-x-offset | MP-CM-y-offset | $\bar{x}$ |
|---|---|---|---|---|
| **0.35** | **0.23** | -0.11 | ***-1.66*** | **0.34!** |

### *Upper Solutrean –Tardigravettian*

The change rates for the morphometric features between the Upper Solutrean SPs and the Tardigravettian SPs from Chinchon I, layer C, within the section from the 23rd to the 22nd millennium BP, are notably high. This is particularly evident in all size-related features, with length (0.38) and area (0.75) exceeding their respective significance thresholds for two consecutive millennia, thereby driving the elevated average change rate of 0.27 (Table 38). These values suggest that the Tardigravettian SPs from Chinchon I are markedly longer and overall larger than their Upper Solutrean counterparts. In addition, the elevated change rates observed in the l-w-index (0.18), and even more so in the left-right-ratio (-0.26), indicate notable shape differences – specifically, that the Chinchon I SPs are both slenderer and more asymmetric. *(Figure 98, Table 38)*




Figure 98: Meanshapes of A) Upper Solutrean SPs, and B) Tardigravettian SPs from Chinchon I, layer C, dating to the section from the 23rd to the 22nd millennium BP.

### *Tardigravettian – Late Badegoulian*

The change rates for the morphometric features between the Tardigravettian SPs from Chinchon I, layer C, and the Late Badegoulian SPs from Le Cuzoul de Vers, layers 21–16 (A-36), within the section from the 23rd to the 22nd millennium BP, are extremely high. Except from the l-w-index (-0.08), all features surpass their respective average change rate for between two consecutive millennia *(Table 39)*. Additionally, with the exception of the tip angle (0.26), all of these features exceed their respective significance threshold, driving the average change rate (0.49), which in turn exceeds the significance threshold also. These findings, although build on very small sample sizes, highlight the marked differences between the SPs from Chinchon I and Le Cuzoul de Vers. Not only are the Badegoulian SPs much *small*er, their shape design is totally different. Their hafting parts are relatively much longer respectively their transformative part much shorter, and they are much more axisymmetric than their counterparts from Chinchon I. *(Figure 99, Table 39)*

Table 38: Rates of change between the Upper Solutrean SPs and the Tardigravetian SPs from Chinchon I, layer C for the section from the 23rd to the 22nd millennium BP ($\bar{x}$ = averages of the absolute values for change rates; bold = value exceeding the respective specific average change rate in Chapter 4.1.3; faint = value below the respective average change rate in Chapter 4.1.3; italic = extreme values excluded from the calculation of the averages; ! = value exceeding the respective significance threshold from Chapter 4.1.3).

| width | length | area | l-w-index | upper-lower-ratio |
|---|---|---|---|---|
| **0.18** | **0.38!** | **0.75!** | **0.18** | 0.10 |

| left-right-ratio | tip angle | MP-CM-x-offset | MP-CM-y-offset | $\bar{x}$ |
|---|---|---|---|---|
| **-0.26** | -0.02 | **-0.27** | ***0.61*** | **0.27** |

The calculated impact of the interplay between taxonomic units within the section from the 23rd to the 22nd millennium BP is notably high and does not align with the very low average change rate and CV observed in the chronologically informed perspective. This discrepancy is likely attributable to the low sample sizes of the non-Solutrean industries, which limit their influence on the overall results despite the elevated individual change rates. *(Table 40)*

#### *4.2.2.2.4 22nd–21st millennium BP*

Within the section from the 22nd to the 21st millennium BP, four major taxonomic units are represented. In addition to the Upper Solutrean, which is still well represented by three assemblages (A-34, A-32, A-31) yielding a total of 20 SPs, the Epigravettian is represented by the extensive assemblage from Grotta Paglicci, layers 18a–10 (A-29), dating to 20.3 ka calBP. Again, the Tardigravettian is represented by the single assemblage from Chinchon 1, layer C (A-33), dating to 21.6 ka calBP and yielding five SPs. Additionally, the Lower Magdalenian SPs makes its first appearance, represented by five SPs from two assemblages (A-30, A-28), dating to 20.5 and 20.2 ka calBP. The Upper Solutrean is represented by 20 SPs from three assemblages (A-34, A-32, A-31), all of which derive exclusively from the northern coast of the Iberian Peninsula.




Figure 99: Meanshapes of A) Tardigravettian SPs from Chinchon I, layer C, and B) Late Badegoulian SPs from Le Cuzoul de Vers, layers 21–16, dating to the section from the 23rd to the 22nd millennium BP.

Table 39: Rates of change between the Tardigravettian SPs from Chinchon I, layer C and the Badegoulian SPs from Le Cuzoul de Vers, layer 21-16 for the section from the 23rd to the 22nd millennium BP ($\bar{x}$ = averages of the absolute values for change rates; bold = value exceeding the respective specific average change rate in Chapter 4.1.3; faint = value below the respective average change rate in Chapter 4.1.3; italic = extreme values excluded from the calculation of the averages; ! = value exceeding the respective significance threshold from Chapter 4.1.3).

| width | length | area | l-w-index | upper-lower-ratio |
|---|---|---|---|---|
| **-0.38!** | **-0.45!** | **-0.70!** | -0.08 | **-0.79!** |

| left-right-ratio | tip angle | MP-CM-x-offset | MP-CM-y-offset | $\bar{x}$ |
|---|---|---|---|---|
| **0.81!** | **0.26** | 0.22 | ***1.41*** | **0.49!** |

Table 40: Confusion matrix of the average change rates across the section from the 23rd to the 22nd millennium BP (! = value exceeding the respective significance threshold from Chapter 4.1.3; bold = value exceeding the average change rate for sections in Chapter 4.1.3; faint = value below the respective average change rate in Chapter 4.1.3).

| | Upper Solutrean | Tardigravettian | Le Cuzoul de Vers |
|---|---|---|---|
| **Upper Solutrean** | | **0.27** | **0.33!** |
| **Tardigravettian** | **0.27** | | **0.49!** |
| **Le Cuzoul de Vers** | **0.33!** | **0.49!** | |

### *Upper Solutrean – Tardigravettian*

The average change rate for between the Upper Solutrean SPs and the Tardigravettian SPs from Chinchon, layer C, within the section from the 22nd to the 21st millennium BP, is notably high ($\bar{x}$ = 0.3). The average change rate, however, is driven by the elevated values for the size-related features only, two of which exceeding their respective significance threshold (length = 0.44, area = 0.82). None of the shape-related features shows a notable high value exceeding the respective average change rate for between two consecutive millennia *(Table 41)*. This indicates that, while the Tardigravettian SPs are substantially larger, they share notable shape characteristics with Upper Solutrean counterparts. *(Figure 100, Table 41)*




Figure 100: Meanshapes of A) Upper Solutrean SPs, and B) Tardigravettian SPs from Chinchon I, layer C, dating to the section from the 22nd to the 21st millennium BP.

Table 41: Rates of change between the Upper Solutrean and the Tardigravettian SPs from Chinchon, layer C, for the section from the 22nd to the 21st millennium BP

| width | length | area | l-w-index | upper-lower-ratio |
|---|---|---|---|---|
| **0.17** | **0.44!** | **0.82!** | **0.24** | 0.18 |

| left-right-ratio | tip angle | MP-CM-x-offset | MP-CM-y-offset | $\bar{x}$ |
|---|---|---|---|---|
| -0.18 | -0.07 | *-0.35* | *1.05* | **0.3** |

### *Upper Solutrean – Lower Magdalenian*

The average change rate for between the Upper Solutrean SPs and the Lower Magdalenian SPs within the section from the 22nd to the 21st millennium BP, is notably high ($\bar{x}$ = 0.27). The average change rate, however, is driven by the elevated values for the size-related features only, three of which exceeding their respective significance threshold (length = 0.38, area = 0.78). None of the shape-related features shows a notable high value exceeding the respective average change rate for between two consecutive millennia *(Table 42)*. This indicates that, while the Lower Magdalenian SPs are substantially larger, they share notable shape characteristics with Upper Solutrean counterparts. *(Figure 101, Table 42)*




Figure 101: Meanshapes of A) Upper Solutrean SPs, and B) Lower Magdalenian SPs dating to the section from the 22nd to the 21st millennium BP.

Table 42: Rates of change between the Upper Solutrean and the Lower Magdalenian SPs for the section from the 22nd to the 21st millennium BP

| width | length | area | l-w-index | upper-lower-ratio |
|---|---|---|---|---|
| **0.22** | **0.38!** | **0.78!** | 0.14 | -0.17 |

| left-right-ratio | tip angle | MP-CM-x-offset | MP-CM-y-offset | $\bar{x}$ |
|---|---|---|---|---|
| -0.14 | -0.03 | *-0.17* | *1.74* | **0.27** |

Signs/Markings: $\bar{x}$ = averages of the absolute values for change rates; bold = value exceeding the respective specific average change rate in Chapter 4.1.3; faint = value below the respective average change rate in Chapter 4.1.3; italic = extreme values excluded from the calculation of the averages; ! = value exceeding the respective significance threshold from Chapter 4.1.3.

### *Upper Solutrean – Epigravettian*

The average change rate for between the Upper Solutrean SPs and the Epigravettian SPs from Grotta Paglicci, layers 18a–10, within the section from the 22nd to the 21st millennium BP, is just slightly higher ($\bar{x}$ = 0.18) than what would be expected for between two consecutive millennia. The average change rate is mostly driven by elevated change rates in length (0.19), the l-w-index (0.22) and the upper-lower-ratio (-0.44), indicating that the Epigravettian SPs tend to be longer and thereby slightly slenderer than their Upper Solutrean counterparts and exhibit a shifted relation between the hafting and the transformative part towards a more pronounced hafting part. *(Figure 102, Table 43)*

### *Tardigravettian – Epigravettian*

The average change rate between the Tardigravettian SPs from Chinchon, layer C, and the Epigravettian SPs from Grotta Paglicci, layers 18a–10, within the section from the 22nd to the 21st millennium BP, is slightly elevated ($\bar{x}$ = 0.23). This is driven by changes in both size- and shape-related features *(Table 44)*. In terms of size, the most pronounced difference lies in area (-0.36), indicating that the Epigravettian SPs are substantially smaller than their Tardigravettian counterparts. Regarding shape, the two groups differ in the ratio between the hafting and transformative parts – Epigravettian SPs tend to have relatively longer hafting parts compared to the very short hafting parts of the Tardigravettian SPs – as well as in y-axis symmetry, with the Epigravettian SPs being more axis-symmetric than the distinctly asymmetric Tardigravettian SPs, *(Figure 103, Table 44)*




Figure 102: Meanshapes of A) Upper Solutrean SPs, and B) Epigravettian SPs from Grotta Paglicci, layers 18a–10, dating to the section from the 22nd to the 21st millennium BP.

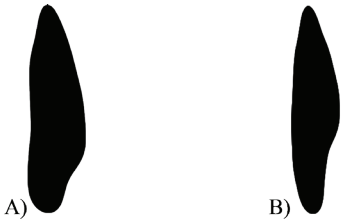



Figure 103: Meanshapes of A) Tardigravettian SPs from Chinchon, layer C, and B) Epigravettian SPs from Grotta Paglicci, layers 18a–10, dating to the section from the 22nd to the 21st millennium BP.

Table 43: Rates of change between the Upper Solutrean and the Epigravettian SPs from Grotta Paglicci, layers 18a–10, for the section from the 22nd to the 21st millennium BP.

| width | length | area | l-w-index | upper-lower-ratio |
|---|---|---|---|---|
| -0.02 | **0.19** | **0.16** | **0.22** | **-0.44** |

| left-right-ratio | tip angle | MP-CM-x-offset | MP-CM-y-offset | $\bar{x}$ |
|---|---|---|---|---|
| 0.13 | -0.09 | *0.03* | *-0.23* | **0.18** |

Table 44: Rates of change between the Tardigravettian SPs from Chinchon, layer C, and the Epigravettian SPs from Grotta Paglicci, layers 18a–10, for the section from the 22nd to the 21st millennium BP.

| width | length | area | l-w-index | upper-lower-ratio |
|---|---|---|---|---|
| **-0.16** | **-0.17** | **-0.36** | -0.02 | **-0.52** |

| left-right-ratio | tip angle | MP-CM-x-offset | MP-CM-y-offset | $\bar{x}$ |
|---|---|---|---|---|
| **0.37** | -0.02 | *0.57* | *-0.62* | **0.23** |

Signs/Markings: $\bar{x}$ = averages of the absolute values for change rates; bold = value exceeding the respective specific average change rate in Chapter 4.1.3; faint = value below the respective average change rate in Chapter 4.1.3; italic = extreme values excluded from the calculation of the averages; ! = value exceeding the respective significance threshold from Chapter 4.1.3.

### *Epigravettian – Lower Magdalenian*

The average change rate between the Epigravettian SPs from Grotta Paglicci, layers 18a–10, and the Lower Magdalenian SPs, within the section from the 22nd to the 21st millennium BP, is slightly elevated ($\bar{x}$ = 0.25). This is driven by changes in both size- and shape-related features *(Table 45)*. In terms of size, the most pronounced difference lies in area (-0.36), indicating that the Epigravettian SPs are substantially smaller than their Lower Magdalenian counterparts. Regarding shape, the two groups differ in the ratio between the hafting and transformative parts – Epigravettian SPs tend to have relatively longer hafting parts compared to the very short hafting parts of the Lower Magdalenian SPs – as well as in y-axis symmetry, with the Epigravettian SPs being more axis-symmetric than the distinctly asymmetric Lower Magdalenian SPs. *(Figure 104, Table 45)*

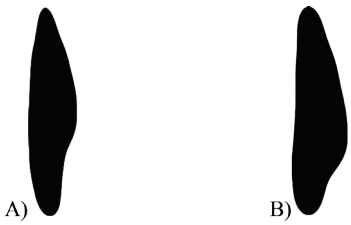



Figure 104: Meanshapes of A) Epigravettian SPs from Grotta Paglicci, layers 18a–10, and B) Lower Magdalenian SPs dating to the section from the 22nd to the 21st millennium BP.

Table 45: Rates of change between the Epigravettian SPs from Grotta Paglicci, layers 18a–10, and the Lower Magdalenian SPs for the section from the 22nd to the 21st millennium BP .

| width | length | area | l-w-index | upper-lower-ratio |
|---|---|---|---|---|
| **0.24** | **0.16** | **0.54** | -0.07 | **0.47** |

| left-right-ratio | tip angle | MP-CM-x-offset | MP-CM-y-offset | $\bar{x}$ |
|---|---|---|---|---|
| **-0.24** | 0.06 | *-0.19* | *2.53* | **0.25** |

### *Tardigravettian – Lower Magdalenian*

The average change rate for between the Tardigravettian SPs from Chinchon, layer C and the Lower Magdalenian SPs within the section from the 22nd to the 21st millennium BP is remarkably low ($\bar{x}$ = 0.08). None of the features shows a notable high value exceeding the respective average change rate for between two consecutive millennia. *(Figure 105, Table 46)*




Figure 105: Meanshapes of A) Tardigravettian SPs from Chinchon, layer C, and B) Lower Magdalenian SPs dating to the section from the 22nd to the 21st millennium BP.

Table 46: Rates of change between the Tardigravettian SPs from Chinchon, layer C, and the Lower Magdalenian SPs for the section from the 22nd to the 21st millennium BP.

| width | length | area | l-w-index | upper-lower-ratio |
|---|---|---|---|---|
| 0.04 | 0.04 | -0.02 | -0.08 | -0.3 |

| left-right-ratio | tip angle | MP-CM-x-offset | MP-CM-y-offset | $\bar{x}$ |
|---|---|---|---|---|
| 0.04 | 0.04 | 0.26 | *0.33* | **0.08** |

Signs/Markings: $\bar{x}$ = averages of the absolute values for change rates; bold = value exceeding the respective specific average change rate in Chapter 4.1.3; faint = value below the respective average change rate in Chapter 4.1.3; italic = extreme values excluded from the calculation of the averages; ! = value exceeding the respective significance threshold from Chapter 4.1.3.

Table 47: Confusion matrix of the average change rates across the section from the 22nd to the 21st millennium BP (! = value exceeding the respective significance threshold from Chapter 4.1.3; bold = value exceeding the average change rate for sections in Chapter 4.1.3; faint = value below the respective average change rate in Chapter 4.1.3).

| | Upper Solutrean | Tardigravettian | Epigravettian | Lower Magdalenian |
|---|---|---|---|---|
| **Upper Solutrean** | | **0.3** | **0.18** | **0.27** |
| **Tardigravettian** | **0.3** | | **0.23** | **0.08** |
| **Epigravettian** | **0.18** | **0.23** | | **0.25** |
| **Lower Magdalenian** | **0.27** | **0.08** | **0.25** | |

Although the calculated average change rates between the Upper Solutrean and the Epigravettian SPs, as well as between the Epigravettian and the Lower Magdalenian SPs within the section from the 22nd to the 21st millennium BP, exceed the expected values for two consecutive millennia and are higher than the average change rate for this section on the chronologically informed perspective, they remain comparatively low. However, the notably high change rate between the Upper Solutrean and the Lower Magdalenian SPs does not align with the generally low change rate and low CV observed on the chronologically informed perspective, suggesting more pronounced differences between these units. As the average change rates are predominantly, and in some cases exclusively, driven by differences in size-related features, it is suggested that the SPs within this section largely share common morphological characteristics, expressed primarily through points of differing sizes, thereby emphasising a consistent underlying shape design. *(Table 47)*

The period between the 25th and the 20th millennium BP, characterised by the coexistence of multiple taxonomic units yielding SPs, returned surprisingly low change rates and CVs on the chronologically informed perspective. However, when comparing the individual taxonomic units, a more complex picture of divergent and convergent developments emerges, which does not always align with the patterns observed previously. For the oldest section (25th–24th millennium BP), it was shown that, despite some minor differences between the Upper Solutrean and Epigravettian SPs, no pronounced divergences existed between these units, in good agreement with the lowered average change rate observed on the chronologically informed perspective. In the subsequent section (24th–23rd millennium BP), pronounced differences were calculated between the Late Badegoulian SPs and those of all other taxonomic units, indicating a morphological secession from the widely shared shape design established within the Upper Solutrean and continued in the Salpetrian SPs. Within the sections from the 23rd to the 22nd and from the 22nd to the 21st millennium BP, further divergence is suggested by the Tardigravettian SPs, represented solely by the assemblage from Chinchon I, layer C. The Late Badegoulian SPs remain morphologically distinct, showing no alignment either with the Upper Solutrean or with the Epigravettian design. In the section spanning the 22nd to the 21st millennium BP, the change rates generally return to more average values, with the notable exception of the comparison between the Upper Solutrean and both the Tardigravettian and the Lower Magdalenian SPs, which show pronounced differences from the Upper Solutrean shape design while sharing notable similarities. The latter might suggest a continuation of the Chinchon-like SP design.

### *4.2.2.3 Middle Magdalenian – Upper/ Late Magdalenian*

For assessing the interplay between the Middle and the Upper/Late Magdalenian, only the section from the 17th to the 16th millennium BP is relevant. The Middle Magdalenian is represented by a limited sample of 11 SPs from the French site of Jaurias (A-23), dating to 16.4 ka calBP. In contrast, the Upper/Late Magdalenian is more robustly represented by 34 SPs derived from nine assemblages distributed across France as well as southern and eastern Germany (A-21–A-17, A-15 and B-10–B-8).

As shown in Chapter 4.2.1.2.4, Upper/Late–Final Magdalenian SPs do not constitute a coherent form group. Rather, two distinct types coexisted. This disparity, however, is not considered in the present analysis, which focuses on the influence of taxonomic units on chronological developments. Consequently, differentiation between these two types is not relevant here. However, this disparity would strongly affect visualisation, as calculating a meanshape would merge both types into a single, artificial form. For this reason, joined meanshapes are not provided in the following chapters.

The change rates for the morphometric features between the Middle and the Upper/Late Magdalenian SPs within the section from the 17th to the 16th millennium BP, are extremely high. Except from the l-w-index (-0.09) and length (0.01), all features surpass their respective average change rate for between two consecutive millennia, with the left-right-ratio (0.75) even exceeding its significance threshold *(Table 48)*. These findings, although build on very small sample sizes, highlight the marked differences between the Middle Magdalenian and the Upper/Late Magdalenian SPs. The Upper/Late Magdalenian SPs tend to be narrower and thereby smaller. Their shape design is totally different. The relative proportions of their hafting parts are much longer respectively the relative proportions of their transformative part much shorter. They are also much more axisymmetric than their counterparts from the Middle Magdalenain. However, as this is based on averages, the coexistence of two distinct SP types during the Upper/Late Magdalenian is not accounted for. *(Figure 106, Table 48)*

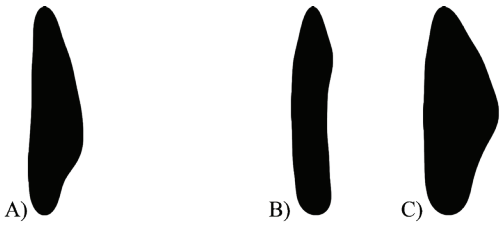



Figure 106: Meanshapes of A) Middle Magdalenia SPs from Jaurias of the 17th millennium BP, B) Upper/Late Magdalenian SPs of Type A, and C) of Type B, dating to the section from the 16th millennium BP.

Table 48: Rates of change between the Middle Magdalenian SPs from Jaurias and the Upper/Late Magdalenian SPs for the section from the 17th to the 16th millennium BP ($\bar{x}$ = averages of the absolute values for change rates; bold = value exceeding the respective specific average change rate in Chapter 4.1.3; faint = value below the respective average change rate in Chapter 4.1.3; italic = extreme values excluded from the calculation of the averages; ! = value exceeding the respective significance threshold from Chapter 4.1.3).

| width | length | area | l-w-index | upper-lower-ratio |
|---|---|---|---|---|
| **0.15** | 0.01 | **0.24** | -0.09 | **-0.58** |

| left-right-ratio | tip angle | MP-CM-x-offset | MP-CM-y-offset | $\bar{x}$ |
|---|---|---|---|---|
| **0.75!** | **0.37** | 0.06 | *-0.05* | **0.31** |

The elevated change rate calculated between the Middle and the Upper/Late Magdalenian SPs aligns well with the high values observed for the section from the 17th to the 16th millennium BP on the chronologically informed perspective, suggesting that this might be driven by the interplay between these two taxonomic units.

### 4.2.2.4 Late Upper Palaeolithic Industries

This section examines the impact of the interplay between SPs from the chronologically overlapping Late Upper Palaeolithic taxonomic units that yield SPs: the Upper/Late–Final Magdalenian, the Hamburgian, and the Creswellian. While most Upper/Late–Final Magdalenian assemblages date to the 17th and 16th millennia BP, some extend into the 15th millennium BP. The earliest Hamburgian assemblage in the dataset – Olbrachcice 8 (A-16) – dates to approximately 15.0 ka calBP, highlighting the chronological overlap between these cultural groups. The oldest Creswellian SPs in this study derive from layer B of Gough's Cave (A-12), dated to 14.8 ka calBP. In terms of geographical distribution, Upper/Late–Final Magdalenian assemblages are primarily located in France, with additional sites in Switzerland and Germany. In contrast, Hamburgian assemblages are confined to northern Germany and Poland, while Creswellian assemblages are found exclusively from Great Britain.

#### 4.2.2.4.1 17th–16th millennium BP

Within the section from the 17th to the 16th millennium BP, SPs from two additional taxonomic units – beyond the previously discussed Middle and Upper/Late–Final Magdalenian – are present: the Hamburgian and the Epigravettian. Both are represented by a single assemblage only: the Hamburgian by the assemblage from Olbrachcice 8 (A-16), and the Epigravettian by the assemblage from Riparo Tagliente, layer 15 (A-22). However, the latter yields only two complete SPs and was therefore excluded from the present analysis. Consequently, the analytical focus here lies on the interplay between the Upper/Late–Final Magdalenian and the Hamburgian SPs.

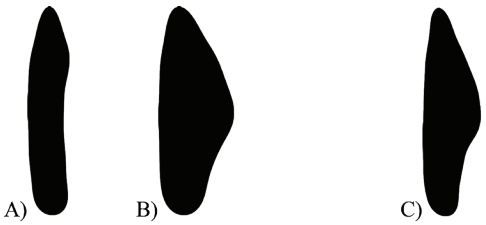



Figure 107: Meanshapes of Upper/Late Magdalenian SPs of Type A (A) and Type B (B), and C) Hamburgian SPs, dating to the section from the 17th to the 16th millennium BP.

Table 49: Rates of change between the Upper/Late–Final Magdalenian SPs and the Hamburgian SPs from Olbrachcice 8 for the section from the 17th to the 16th millennium BP ($\bar{x}$ = averages of the absolute values for change rates; bold = value exceeding the respective specific average change rate in Chapter 4.1.3; faint = value below the respective average change rate in Chapter 4.1.3; italic = extreme values excluded from the calculation of the averages; ! = value exceeding the respective significance threshold from Chapter 4.1.3).

| width | length | area | l-w-index | upper-lower-ratio |
|---|---|---|---|---|
| 0.12 | -0.04 | 0.02 | **-0.19** | 0.19 |

| left-right-ratio | tip angle | MP-CM-x-offset | MP-CM-y-offset | $\bar{x}$ |
|---|---|---|---|---|
| **-0.35** | -0.04 | 0.22 | -0.41 | 0.13 |

***Upper/Late–Final Magdalenian – Hamburgian***

The average change rate for between the Upper/Late–Final Magdalenian and the Hamburgian SPs from Olbrachcice 8 within the section from the 17th to the 16th millennium BP, is notably low (0.12). Among the morphometric features, only the l-w-index (-0.19) and the left-right-ratio (-0.35) exceed their respective average change rates observed between two consecutive millennia. These values indicate that the Hamburgian SPs tend to be slightly stouter and exhibit greater asymmetry along the y-axis than their Upper/Late–Final Magdalenian counterparts. Additionally, although remaining well below its average change rate for two consecutive millennia, the upper-lower-ratio yields a slightly elevated value (0.19), suggesting that the Hamburgian SPs tend to have relatively shorter hafting parts and correspondingly relatively longer transformative parts. Apart from these deviations, the change rates for all remaining morphometric features fall well below their respective averages, suggesting a comparatively high degree of morphometric similarity, especially in terms of size, between the Upper/Late–Final Magdalenian and Hamburgian SPs. *(Figure 107, Table 49)*

The low change rate between the Upper/Late–Final Magdalenian and the Hamburgian SPs confirms that the elevated change rates observed for the section from the 17th to the 16th millennium BP on the chronologically informed perspective are not significantly influenced by the interaction of these two taxonomic units, but rather by the transition from Middle to Upper/Late Magdalenian forms.

### *4.2.2.4.2 16th–15th millennium BP*

Within the section from the 16th to the 15th millennium BP, SPs from three taxonomic units are present. Again the Upper/Late–Final Magdalenian and the Hamburgian make most of the dataset. Additionally, the Creswellian, represented by two assemblages – Gough's Cave, layer B (A-12) and Mother Grundy´s Parlour, layers C/B and LB-SB (A-5) are present.

***Upper/Late–Final Magdalenian – Hamburgian***

The average change rate between the Upper/Late–Final Magdalenian and the Hamburgian SPs within the section from the 16th to the 15th millennium BP is notably low (0.17). This is primarily due to the extremely low change rates in all size-related features (Table 50), which pull down the overall average. In contrast, most shape-related features – except for the l-w-index – yield elevated values, indicating marked shape differences. As observed previously, Hamburgian SPs tend to exhibit relatively shorter hafting parts and correspondingly longer transformative parts, more acute tip angles, and greater asymmetry along the y-axis. *(Figure 108, Table 50)*

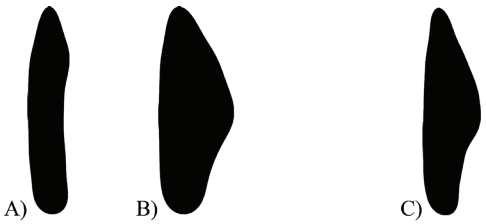



Figure 108: Meanshapes of Upper/Late Magdalenian SPs of Type A (A) and Type B (B), and C) Hamburgian SPs, dating to the section from the 16th to the 15th millennium BP.

Table 50: Rates of change between the Upper/Late–Final Magdalenian and the Hamburgian SPs for the section from the 16th to the 15th millennium BP ($\bar{x}$ = averages of the absolute values for change rates; bold = value exceeding the respective specific average change rate in Chapter 4.1.3; faint = value below the respective average change rate in Chapter 4.1.3; italic = extreme values excluded from the calculation of the averages; ! = value exceeding the respective significance threshold from Chapter 4.1.3).

| width | length | area | l-w-index | upper-lower-ratio |
|---|---|---|---|---|
| -0.03 | -0.02 | -0.10 | -0.04 | **0.51** |

| left-right-ratio | tip angle | MP-CM-x-offset | MP-CM-y-offset | $\bar{x}$ |
|---|---|---|---|---|
| **-0.32** | **-0.20** | 0.06 | -0.05 | 0.17 |

### *Upper/Late–Final Magdalenian – Creswellian*

The average change rate for between the Upper/Late–Final Magdalenian and the Creswellian SPs within the section from the 16th to the 15th millennium BP, is notably low (0.13; Table 51). Among the morphometric features, only the left-right-ratio (-0.25) exceeds its respective average change rates observed between two consecutive millennia. This indicates that the Creswellian SPs tend to exhibit greater asymmetry along the y-axis than their Upper/Late–Final Magdalenian counterparts. Additionally, although remaining well below its average change rate for two consecutive millennia, the upper-lower-ratio yields a slightly elevated value (0.21), suggesting that the Creswellian SPs tend to have relatively shorter hafting parts and correspondingly relatively longer transformative parts. Apart from these deviations, the change rates for all remaining morphometric features fall well below their respective averages, suggesting a comparatively high degree of morphometric similarity, especially in terms of size, between the Upper/Late–Final Magdalenian and Creswellian SPs. *(Figure 109, Table 51)*

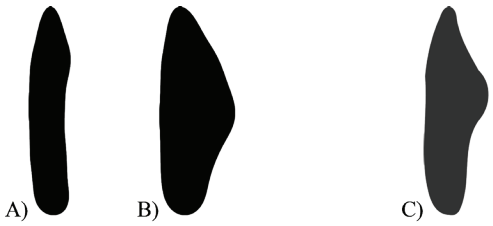



Figure 109: Meanshapes of Upper/Late Magdalenian SPs of Type A (A) and Type B (B), and C) Creswellian SPs, dating to the section from the 16th to the 15th millennium BP.

Table 51: Rates of change between the Upper/Late–Final Magdalenian and the Creswellian SPs for the section from the 16th to the 15th millennium BP ($\bar{x}$ = averages of the absolute values for change rates; bold = value exceeding the respective specific average change rate in Chapter 4.1.3; faint = value below the respective average change rate in Chapter 4.1.3; italic = extreme values excluded from the calculation of the averages; ! = value exceeding the respective significance threshold from Chapter 4.1.3).

| width | length | area | l-w-index | upper-lower-ratio |
|---|---|---|---|---|
| -0.03 | -0.12 | -0.16 | -0.13 | 0.21 |

| left-right-ratio | tip angle | MP-CM-x-offset | MP-CM-y-offset | $\bar{x}$ |
|---|---|---|---|---|
| **-0.25** | 0.01 | -0.01 | -0.46 | 0.13 |

### *Hamburgian – Creswellian*

The average change rate for between the Hamburgian and the Creswellian SPs within the section from the 16th to the 15th millennium BP, is notably low (0.12; *Table 52*). Among the morphometric features, only the tip angle (0.26) exceeds its respective average change rates observed between two consecutive millennia. This indicates that the Creswellian SPs tend to exhibit more obtuse tip angles than their Hamburgian counterparts. Additionally, although remaining well below its average change rate for two consecutive millennia, the upper-lower-ratio yields a slightly elevated value (-0.20), suggesting that the Creswellian SPs tend to have relatively longer hafting parts and correspondingly relatively shorter transformative parts. Apart from these deviations, the change rates for all remaining morphometric features fall well below their respective averages, suggesting a comparatively high degree of morphometric similarity between the Hamburgian and Creswellian SPs. *(Figure 110, Table 52)*

The low change rates calculated between the Late Upper Palaeolithic industries of the section from the 16th to the 15th millennium BP align well with the similarly low values observed on the chronologically informed perspective, indicating a period of only minor morphometric change in SPs. *(Table 53)*

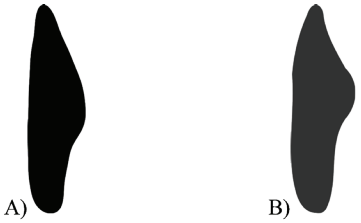



Figure 110: Meanshapes of A) Hamburgian SPs and B) Creswellian SPs dating to the section from the 16th to the 15th millennium BP.

Table 52: Rates of change between the Hamburgian and the Creswellian SPs for the section from the 16th to the 15th millennium BP ($\bar{x}$ = averages of the absolute values for change rates; bold = value exceeding the respective specific average change rate in Chapter 4.1.3; faint = value below the respective average change rate in Chapter 4.1.3; italic = extreme values excluded from the calculation of the averages; ! = value exceeding the respective significance threshold from Chapter 4.1.3).

| width | length | area | l-w-index | upper-lower-ratio |
|---|---|---|---|---|
| 0.0 | -0.11 | -0.06 | -0.09 | -0.20 |

| left-right-ratio | tip angle | MP-CM-x-offset | MP-CM-y-offset | $\bar{x}$ |
|---|---|---|---|---|
| 0.11 | **0.26** | -0.07 | -0.44 | 0.12 |

Table 53: Confusion matrix of the average change rates across the section from the 16th to the 15th millennium BP (! = value exceeding the respective significance threshold from Chapter 4.1.3; bold = value exceeding the average change rate for sections in Chapter 4.1.3; faint = value below the respective average change rate in Chapter 4.1.3).

| | Upper/Late–Final Magdalenian | Hamburgian | Creswellian |
|---|---|---|---|
| **Upper/Late–Final Magdalenian** | | 0.17 | 0.13 |
| **Hamburgian** | 0.17 | | 0.12 |
| **Creswellian** | 0.13 | 0.12 | |

### *4.2.2.4.3 15th–14th millennium BP*

Within the section from the 15th to the 14th millennium BP, SPs from five taxonomic units are present. As in the previous section, the Upper/Late–Final Magdalenian and the Hamburgian dominate the dataset, while the Creswellian is again represented by the same two assemblages. The Epigravettian, represented by only four SPs from two assemblages, is excluded from the analysis due to insufficient sample size. Similarly underrepresented is the Havelte Group, with just seven SPs derived from a single assemblage (Oldeholtwolde, A-1).

#### *Upper/Late–Final Magdalenian – Hamburgian*

The average change rate for between the Upper/Late–Final Magdalenian and the Hamburgian SPs from Olbrachcice 8 within the section from the 15th to the 14th millennium BP, is notably low (0.13). Among the morphometric features, only the upper-lower-ratio (0.3) and the left-right-ratio (-0.29) exceed their respective average change rates observed between two consecutive millennia. These values indicate that the Hamburgian SPs tend to exhibit greater asymmetry along the y-axis and relatively shorter hafting parts and correspondingly relatively longer transformative parts than their Upper/Late–Final Magdalenian counterparts. Apart from these deviations, the change rates for all remaining morphometric features fall well below their respective averages, suggesting a comparatively high degree of morphometric similarity, especially in terms of size, between the Upper/Late–Final Magdalenian and Hamburgian SPs. *(Figure 111, Table 54)*

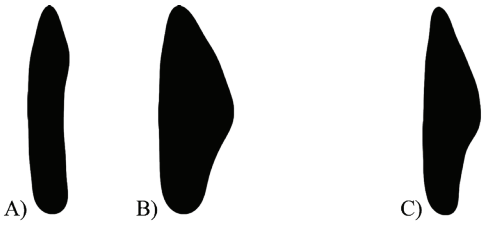



Figure 111: Meanshapes of Upper/Late Magdalenian SPs of Type A (A) and Type B (B), and C) Hamburgian SPs, dating to the section from the 15th to the 14th millennium BP.

Table 54: Rates of change between the Upper/Late–Final Magdalenian and the Hamburgian SPs for the section from the 15th to the 14th millennium BP ($\bar{x}$ = averages of the absolute values for change rates; bold = value exceeding the respective specific average change rate in Chapter 4.1.3; faint = value below the respective average change rate in Chapter 4.1.3; italic = extreme values excluded from the calculation of the averages; ! = value exceeding the respective significance threshold from Chapter 4.1.3).

| width | length | area | l-w-index | upper-lower-ratio |
|---|---|---|---|---|
| -0.01 | -0.04 | -0.10 | -0.09 | **0.30** |

| left-right-ratio | tip angle | MP-CM-x-offset | MP-CM-y-offset | $\bar{x}$ |
|---|---|---|---|---|
| **-0.29** | -0.15 | 0.09 | -0.28 | 0.14 |

### *Upper/Late–Final Magdalenian – Creswellian*

The average change rate for between the Upper/Late–Final Magdalenian and the Creswellian SPs within the section from the 15th to the 14th millennium BP, is notably low (0.12). Among the morphometric features, only the l-w-index (-0.24) and length (-0.14) exceed their respective average change rates observed between two consecutive millennia. These values indicate that the Creswellian SPs tend to be slightly stouter and shorter than their Upper/Late–Final Magdalenian counterparts. Apart from these deviations, the change rates for all remaining morphometric features fall well below their respective averages, suggesting a comparatively high degree of morphometric similarity, especially in terms of size, between the Upper/Late–Final Magdalenian and Creswellian SPs. *(Figure 112, Table 55)*

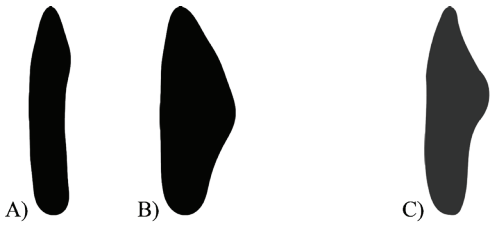



Figure 112: Meanshapes of Upper/Late Magdalenian SPs of Type A (A) and Type B (B), and C) Creswellian SPs, dating to the section from the 15th to the 14th millennium BP.

Table 55: Rates of change between the Upper/Late–Final Magdalenian and the Creswellian SPs for the section from the 15th to the 14th millennium BP ($\bar{x}$ = averages of the absolute values for change rates; bold = value exceeding the respective specific average change rate in Chapter 4.1.3; faint = value below the respective average change rate in Chapter 4.1.3; italic = extreme values excluded from the calculation of the averages; ! = value exceeding the respective significance threshold from Chapter 4.1.3).

| width | length | area | l-w-index | upper-lower-ratio |
|---|---|---|---|---|
| 0.07 | **-0.14** | -0.09 | **-0.24** | -0.01 |

| left-right-ratio | tip angle | MP-CM-x-offset | MP-CM-y-offset | $\bar{x}$ |
|---|---|---|---|---|
| -0.09 | 0.14 | -0.02 | -0.49 | 0.12 |

### *Hamburgian – Creswellian*

The average change rate for between the Hamburgian and the Creswellian SPs within the section from the 15th to the 14th millennium BP, is comparably low (0.15). The change rates for the individual morphometrical features are comparable to the values observed for the previous section. The tip angle (0.34) and the l-w-index (-0.16) exceed their respective average change rates observed between two consecutive millennia. This indicates that the Creswellian SPs tend to exhibit more obtuse tip angles and are slightly stouter than their Hamburgian counterparts. Additionally, although remaining well below its average change rate for two consecutive millennia, the upper-lower-ratio yields a slightly elevated value (-0.24), suggesting that the Creswellian SPs tend to have relatively longer hafting parts and correspondingly relatively shorter transformative parts. Apart from these deviations, the change rates for all remaining morphometric features fall well below their respective averages, suggesting a comparatively high degree of morphometric similarity between the Hamburgian and Creswellian SPs. *(Figure 113, Table 56)*

The low change rates calculated between the Late Upper Palaeolithic industries of the section from the 15th to the 14th millennium BP align well with the similarly low values observed on the chronologically informed perspective, indicating a period of only minor morphometric change in SPs. *(Table 57)*

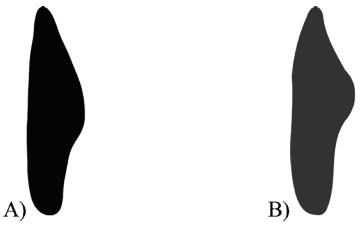



Figure 113: Meanshapes of A) Hamburgian SPs and B) Creswellian SPs dating to the section from the 15th to the 14th millennium BP.

Table 56: Rates of change between the Hamburgian and the Creswellian SPs for the section from the 15th to the 14th millennium BP ($\bar{x}$ = averages of the absolute values for change rates; bold = value exceeding the respective specific average change rate in Chapter 4.1.3; faint = value below the respective average change rate in Chapter 4.1.3; italic = extreme values excluded from the calculation of the averages; ! = value exceeding the respective significance threshold from Chapter 4.1.3).

| width | length | area | l-w-index | upper-lower-ratio |
|---|---|---|---|---|
| 0.08 | -0.11 | 0.02 | **-0.16** | -0.24 |

| left-right-ratio | tip angle | MP-CM-x-offset | MP-CM-y-offset | $\bar{x}$ |
|---|---|---|---|---|
| 0.14 | **0.34** | -0.10 | -0.29 | 0.15 |

Table 57: Confusion matrix of the average change rates across the section from the 15th to the 14th millennium BP (! = value exceeding the respective significance threshold from Chapter 4.1.3; bold = value exceeding the average change rate for sections in Chapter 4.1.3; faint = value below the respective average change rate in Chapter 4.1.3).

| | Upper/Late–Final Magdalenian | Hamburgian | Creswellian |
|---|---|---|---|
| **Upper/Late–Final Magdalenian** | | 0.14 | 0.12 |
| **Hamburgian** | 0.14 | | 0.15 |
| **Creswellian** | 0.12 | 0.15 | |

This chapter adds yet another layer to the deeper understanding of the patterns observed on the chronologically informed perspective. The high change rates calculated for the transitional period between the Late Gravettian and the Upper Solutrean (27th–25th millennium BP) is largely driven by the archaeo-stratigraphic change. While the period between the 24th and 20th millennium BP initially appeared to exhibit only low change rates in the chronological analysis, a more nuanced approach – calculating change rates between the Upper Solutrean and individual non-Solutrean LGM industries – reveals a more complex picture. Notably, the interplays involving the Late Badegoulian show relatively high change rates, whereas comparisons between other LGM industries yield lower values. A more detailed analysis of these patterns will however be conducted in the following Chapter (4.3) of this study, allowing for a deeper exploration of the morphometric relationships between the non-Solutrean LGM industries and the Upper Solutrean. The elevated change rates for the section from the 17th to the 16th millennium BP are likely driven by the pronounced differences between the Middle and the Upper/Late–Final Magdalenian. The low values seen for the period from the 17th to the 15th millennium BP are supported by the low amount of differences calculated between the Upper/Late–Final Magdalenian, the Hamburgian and the Creswellian, a high level of morphological uniformity in the SPs.

### 4.2.3 Summary of the Results on the 'Archaeo-Stratigraphically Informed' Perspective

The analysis in this chapter identified distinct patterns of morphological variation and change across different taxonomic units. While some datasets were too small for robust conclusions, RDA revealed chronologically directed changes within the youngest two sections of the Late Gravettian (27th–26th and 26th–25th millennium BP) and the oldest two sections of the Upper Solutrean (26th–25th and 25th–24th millennium BP). Additionally, significant chronologically directed changes were observed within the aggregated unit of the non-Solutrean LGM industries between the 24th and 20th millennium BP. In contrast, no significant chronologically directed trends were detected within the Upper/Late–Final Magdalenian or the Hamburgian.

Strong signals for variation are calculated for the entire Late Gravettian until the 26th millennium BP, as well as for the first three sections of the Upper Solutrean until the 23rd millennium BP. Similarly, high variation was detected within the Upper/Late–Final Magdalenian. In contrast, the non-Solutrean LGM industries and the Hamburgian exhibit lower morphological variation in their SPs.

Elevated variation within the Late Gravettian and the Upper Solutrean come along with higher change rates, which are most pronounced at the beginning of each taxonomic unit before declining afterwards over time. Within the Late Gravettian, the oldest two sections show that change was primarily driven by shape-related transformations, whereas the younger two sections were dominated by changes in size. Conversely, for the Upper Solutrean, the first two sections exhibit change rates primarily driven by size, while the youngest section is characterised by changes in shape. Although the variation within the Upper/Late–Final Magdalenian assemblages is relatively high, the change rate does not indicate strong chronologically directed transformations within this taxonomic unit. In fact, the elevated variation is due to two different types of SPs coexisting within this unit.

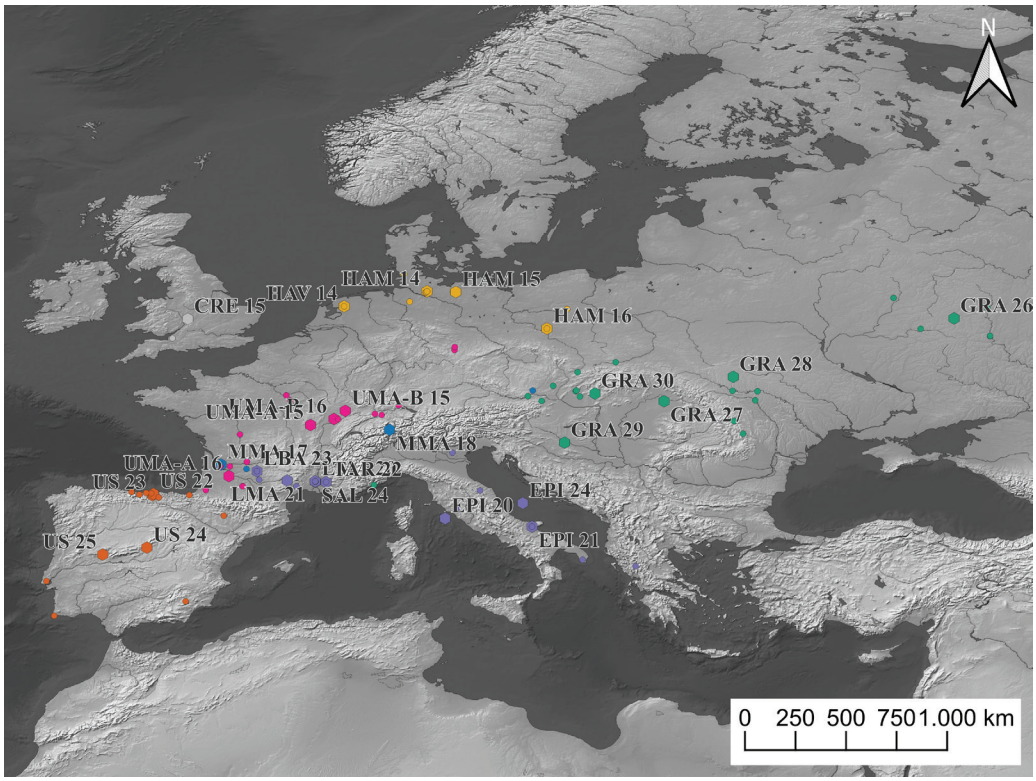
Within the Late Gravettian, size-related features show a clear trend towards larger SPs. The decreasing trend in the l-w-index and an increasing trend in the tip angle suggest a shift towards stouter forms with more obtuse tips, while other morphometric features remain relatively stable. For the Upper Solutrean, trends in size are somewhat obscured by the exceptionally large French SPs from the 25th and 24th millennium BP. However, a clear trend in shape is visible in the l-w-index, indicating a latent tendency toward stouter forms.

The transition between major taxonomic units is most pronounced between the Late Gravettian and the Upper Solutrean between the 27th and 25th millennium BP, suggesting no morphological continuity between these units. In contrast, the differences between the Upper Solutrean and the non-Solutrean LGM industries between the 24th and 20th millennium BP are, on average, not pronounced. Howev-

er, when analysing individual taxonomic units rather than an aggregated dataset, a more nuanced picture emerges. The most pronounced differences, which may have influenced the chronologically informed change rates, occur between the Late Badegoulian assemblage of Cuzoul de Vers and the other LGM industries. Additionally, elevated differences between the Upper Solutrean and the Lower Magdalenian are calculated, emphasising a notable discontinuity in SP morphology. The transition between the Middle and the Upper/Late–Final Magdalenian led to elevated differences, which are even more pronounced when accounting for the Type A SPs of the Upper/Late–Final Magdalenian only. Finally, the difference between the Upper/Late–Final Magdalenian SPs and the Hamburgian SPs is relatively low, suggesting a degree of morphological continuity between these units. However, this continuity is only probable from the Type B SPs of the Upper/Late–Final Magdalenian.

## 4.3 CLUSTER ANALYSES

This chapter applies Hierarchical Cluster Analysis (HCA) to distance matrices based on average change rates between a selected set of samples that include all major taxonomic units. Within each taxonomic unit, assemblages were consolidated by the millennium BP in which they are dated. Excluded from the analysis are the French Upper Solutrean SPs due to their extreme sizes, potentially resulting in a distorted analyses. Also, the 26$^{th}$ millennium BP of the Upper Solutrean and the 25$^{th}$ millennium BP of the Late Gravettian are not represented due to small sample sizes. In total, 28 samples were analysed *(Map 8)*. Other than that, the analysed samples follow the datasets used in the archaeo-stratigraphically informed perspective.




Map 8: All assemblages used in the Clustering Analysis (circles) and the respective average coordinates of the samples (hexagons) (Colour-code inferred from the taxonomic units (non-Solutrean LGM units condensed). Abbreviations: GRA = Late Gravettian; US = Upper Solutrean; SAL = Salpetrian; LBA = Late Badegoulian; EPI = Epigravettian; TAR = Tardigravettian; LMA = Lower Magdalenian; MMA = Middle Magdalenian; UMA = Upper Magdalenian (Type -A and -B); HAM = Hamburgian; CRE = Creswellian; HAV = Havelte).

### 4.3.1 Unconstrained Clustering

A preliminary examination of the unweighted distance matrix *(Table 62)* already reveals several notable patterns. Three clusters of low change rates (i.e., minimal morphological differences) between samples stand out. In the upper left corner, the Late Gravettian samples display relatively low differences among each other, while remaining clearly distinct from the other samples. The central portion of the matrix is dominated by a large zone of low change rates, spanning the LGM sensu lato, from the Upper Solutrean of the 25th millennium BP to the Middle Magdalenian of the 17th millennium BP. Notably, the lower left, respectively the upper right margins of this zone, comprising younger LGM-samples, display elevated levels of morphological difference (higher change rates) compared to the older LGM-samples, with particularly pronounced divergence observed in the Tardigravettian sample (22nd millennium BP) and both Lower Magdalenian samples (21st and 20th millennium BP). These peripheral increases suggest greater dissimilarity in morphometric traits relative to the core continuity observed within the central sequence. In the lower right corner, another zone of low change rates is evident, circumscribing the later Upper Palaeolithic samples, particularly from the Upper/Late Magdalenian SPs of the stouter Type B from the 16th millennium BP on – with the notable exception of the elongated Type A SPs from the 15th millennium BP. Additional noteworthy patterns emerge upon closer inspection. The Late Badegoulian sample stands out due to its extreme change rates – particularly in relation to the samples from the Upper Solutrean sample of the 23rd millennium BP on. In contrast, the Late Badegoulian SPs appear to share certain morphological characteristics with earlier SPs, particularly those from the Late Gravettian. Two pronounced morphological discontinuities are also evident. The first – already discussed in Chapter 4.2.2.1 – is the marked divergence between the Late Gravettian and Upper Solutrean SPs. The second occurs after the Middle Magdalenian sample of the 17th millennium BP, where a comparable morphological shift is observed. Finally, several diachronous connections can be observed. Although the Late Gravettian samples show high morphological differences when compared to the subsequently following Upper Solutrean samples, they exhibit notably lower change rates to certain Epigravettian samples, some of the later Upper Solutrean assemblages, the Late Badegoulian sample, and to the samples within the later Upper Palaeolithic cluster, including the Type A samples of the Upper/Late Magdalenian. In contrast, samples from the LGM cluster, apart from the just documented exceptions, generally show limited similarity to the Late Gravettian. Additionally, the older half of the LGM cluster reveals minimal resemblance to the samples of the later Upper Palaeolithic cluster, with only a few isolated exceptions. The younger half – from the Upper Solutrean sample of the 23rd millennium BP on – however, tends to exhibit lower change rates to chronologically adjacent samples, excluding the Upper/Late Magdalenian Type A samples. They remain distinct from all other samples, with the notable exception of the Late Gravettian, to which they show some morphological similarity. The samples from the younger Upper Palaeolithic cluster, particularly those attributed to the Hamburgian, Creswellian, and Havelte Group, consistently show moderate to low morphological differences when compared across almost all other samples.

The results of the unconstrained HCA reveal five main clusters (I–V), with Cluster III being significantly larger than the other, enabling a further subdivision into distinct sub-clusters, which show high internal similarities. The clusters I and II are markedly distinct from the other clusters, with an approximate distance of 0.43. Cluster I exclusively comprises the Upper/Late Magdalenian SPs of the elongated Type A from both the 16th and 15th millennia BP only *(Figure 118)*. Despite forming a separate cluster, these SPs share key morphological characteristics with Cluster II, which includes the oldest SPs in the dataset – those from the Late Gravettian of the 30th millennium BP – and the Late Badegoulian SPs from Le Cuzoul de Vers dating to the 23rd millennium BP. These SPs share a relatively short transformative part and a comparatively long hafting part, while exhibiting an overall symmetry along the y-axis.

Cluster III is a diverse compilation of multiple taxonomic and chronological units. Within it, two closely associated sub-clusters emerge. Closely grouped in sub-cluster IIIa are the 25th and the 24th millennium BP Upper Solutrean samples, the Epigravettian samples of the

24th millennium BP and the Salpetrian sample from Grotta de la Salpêtrière, dating to the 24th millennium BP. These samples share distinctive morphological traits – namely, a short hafting part, y-axis symmetry and an overall slenderer appearance *(Figure 115)*. Also grouping together in sub-cluster IIIb are the Upper Solutrean sample of the 23rd and the 22nd millennium BP, the Epigravettian sample of the 21st and the 20th millennium BP, the Middle Magdalenian sample of the 18th and the 17th millennium BP, the Late Gravettian SPs sample of the 29th millennium BP, the Hamburgian SPs of the 15th millennium BP, and the Havelte Group SPs from Oldeholtwolde (14th millennium BP). SPs in this sub-cluster tend to be slightly larger *(Figure 114)*, asymmetric along the y-axis and, while the transformative part remains longer, they exhibit a more balanced ratio between the hafting and transformative parts as well as between the left and the right part *(Figure 115)*. Overall Cluster III expresses a high level of diversity, while distances within each sub-cluster a comparably short, indicating less differences.

Cluster IV is closer related to cluster V than to the other clusters. It includes Hamburgian SPs from the 16th and 14th millennia BP, Creswellian SPs from the 15th millennium BP, and the stouter Type B Upper/Late Magdalenian SPs from both the 16th and 15th millennia BP. These SPs typically exhibit a more balanced ratio between the transformative and the hafting part (upper-lower-ratio ≈ 1) and asymmetry along the y-axis, *(Figure 115)*. They are also among the widest *(Figure 114)*, which makes them comparatively stout. Within this cluster, the distances between the samples are notably low (max. 0.15), indicating a high level of morphometric similarity.

Cluster V comprises the Lower Magdalenian SPs from the 21st and 20th millennia BP, and the Tardigravettian SPs from Chinchon, dating to the 22nd millennium BP. The SPs in this group are generally characterised by a straight back and a short hafting part *(Figure 115)*. Also, they are among the widest and thereby largest SPs in the entire dataset *(Figure 114)*. Their close morphological relation is highlighted by the short distances between the individual units (max. 0.16).

### *4.3.1.1 Cluster Distribution and Diversity*

The clusters also exhibit distinct patterns in their chronological *(Table 58)* and taxonomical *(Table 59)* distribution. While the elements of Cluster I, IV, and V appear in sharply defined and relatively short-term intervals, Cluster III comprises elements of a more extended period. Cluster I only comprises specimens of the Upper/Late Magdalenian betwenn the 16th and 15th millenium, while SPs belonging to Cluster IV occur only at the very end of the observed timeframe from the 16th millennium BP on, including the Upper/Late Magdalenian, the Hamburgian, and the Creswellian. The occurrence of SPs from Cluster V is also chronologically and taxonomically concentrated, spanning only from the 22nd to the 20th millennium BP, taxonomically assigned to the Lower Magdalenian and the Tardigravettian. Cluster II is present at two separate points in time: at the very beginning of the dataset 30th–26th millennium BP (with the exception of the 29th millennium BP) within the Late Gravettian and in the 23rd millennium BP within the Late Badegoulian. Cluster III, by contrast, spans a broader chronological range. In addition to its brief presence during the Late Gravettian, it is primarily represented between the 24th and 21st millennia BP, particularly within the Upper Solutrean, Salpêtrien, and Epigravettian contexts. It reappears toward the younger end of the investigated period from the 18th millennium BP onwards, encompassing the Middle Magdalenian, the Hamburgian, and the Havelte Group, albeit with a notable absence during the 16th millennium BP. When the two sub-clusters are considered separately, sub-cluster IIIa shows a marked short-term presence during the 25th and the 24th millennium BP within Upper Solutrean and Epigravettian contexts. In contrast, Sub-cluster IIIb appears more widely distributed, primarily between the 23rd and the 20th millennium BP, with additional occurrences in the 29th millennium BP and at the end of the observed timeframe in the 15th and the 14th millennium BP.

Building on the chronological distribution of the clusters, a seriation allows them to be arranged sequentially according to their chronological occurrence *(Table 60)*. Although the resulting sequence is not entirely unambiguous, it can be inferred that Cluster II – charac-

terised by longer hafting than transformative parts – represents the oldest form-group, as SPs of this style are the oldest in the dataset and seem to largely disappear after 26th millennium BP. This is followed by Cluster III, with subgroup IIIa likely predating IIIb, both comprising asymmetric forms with short hafting sections. Cluster V – featuring forms with straight or concave backs and short hafting parts – emerges during the middle phase of IIIb. Cluster I and IV both appear at the end of the observed timeframe. While Cluster I – comprising elongated forms with extremely short transformative parts – disappears after a short phase, Cluster IV – including stouter forms with a balanced ratio between hafting and transformative parts – outlasts and represents the most recent SP form-group.

Cluster diversity peaks at two chronological stages: during the Last Glacial Maximum (LGM), between the 23rd and the 20th millennium BP, and again during the late Upper Palaeolithic, between the 16th and the 14th millennium BP. These peaks may indicate episodes of innovation of new SPs forms during these periods. When shifting the focus to taxonomic units, the Late Gravettian, the Upper Magdalenian and the Hamburgian exhibit the highest diversity, with two distinct morphotypes. While the diversity within the Late Gravettian and the Upper Magdalenian has previously been described (Chapter 4.2.1.2), the morphological variation in the Hamburgian remains to be discussed. *(Table 58 and 59)*

Additionally, a clear separation of clusters emerges, with the dividing line falling roughly around the 23rd millennium BP. Clusters II and IIIa occur exclusively before this chronological threshold, whereas the other clusters appear only afterward – apart from the 29th-millennium-BP sample assigned to Cluster IIIb *(Table 60).*

### *4.3.1.2 Variation within Clusters*

Cluster II exhibits the highest average CV ($\bar{x}$ = 0.40), primarily driven by high values for area (0.41) and the left-right-ratio (0.52). These reflect marked differences in symmetry and size between the larger, more y-axis-symmetric Late Gravettian SPs and the smaller, more asymmetric Late Badegoulian SPs. The second-highest average CV appears in Cluster IIIa ($\bar{x}$ = 0.37), which includes Upper Solutrean, Epigravettian, and Salpetrian SPs dating to the 25th and the 24th millennium BP. Here, despite an extreme value for area (0.60), the overall elevation results from moderately high

Table 58: Chronological distribution of the clusters from the unconstrained Hierarchical Cluster Analysis (HCA) (numbers = millennium BP; Clust. = Cluster; div. = cluster diversity).

| Clust. | 30th | 29th | 28th | 27th | 26th | 25th | 24th | 23rd | 22nd | 21st | 20th | 19th | 18th | 17th | 16th | 15th | 14th |
|---|---|---|---|---|---|---|---|---|---|---|---|---|---|---|---|---|---|
| I | | | | | | | | | | | | | | | | | |
| II | | | | | | | | | | | | | | | | | |
| IIIa | | | | | | | | | | | | | | | | | |
| IIIb | | | | | | | | | | | | | | | | | |
| IV | | | | | | | | | | | | | | | | | |
| V | | | | | | | | | | | | | | | | | |
| div. | 1 | 1 | 1 | 1 | 1 | 1 | 1 | 2 | 2 | 2 | 2 | 0 | 1 | 1 | 2 | 3 | 2 |

Table 59: Taxonomic distribution of the clusters from the unconstrained Hierarchical Cluster Analysis (HCA) (GRA = Late Gravettian; US = Upper Solutrean; SAL = Salpetrian; LBA = Late Badegoulian; EPI = Epigravettian; TAR = Tardigravettian; LMA = Lower Magdalenian; MMA = Middle Magdalenian; UMA = Upper Magdalenian; HAM = Hamburgian; CRE = Creswellian; HAV = Havelte; Clust. = Cluster; div. = cluster diversity).

| Clust. | GRA | US | SAL | LBA | EPI | TAR | LMA | MMA | UMA | HAM | CRE | HAV |
|---|---|---|---|---|---|---|---|---|---|---|---|---|
| I | | | | | | | | | ■ | | | |
| II | ■ | | | ■ | | | | | | | | |
| IIIa | | ■ | | | ■ | | | | | | | |
| IIIb | ■ | ■ | ■ | | ■ | | | ■ | | ■ | | ■ |
| IV | | | | | | | | | ■ | ■ | ■ | |
| V | | | | | | ■ | ■ | | | | | |
| div. | 2 | 1(2) | 1 | 1 | 1(2) | 1 | 1 | 1 | 2 | 2 | 1 | 1 |

Table 60: Seriation of the clusters from the unconstrained Hierarchical Cluster Analysis (HCA) (numbers = millennium BP; Clust. = Cluster; div. = csluster diversity).

| Clust. | 30th | 29th | 28th | 27th | 26th | 25th | 24th | 23rd | 22nd | 21st | 20th | 19th | 18th | 17th | 16th | 15th | 14th |
|---|---|---|---|---|---|---|---|---|---|---|---|---|---|---|---|---|---|
| IV | | | | | | | | | | | | | | | ■ | ■ | ■ |
| I | | | | | | | | | | | | | | | ■ | ■ | |
| V | | | | | | | | | ■ | ■ | ■ | | | | | | |
| IIIb | | ■ | | | | | | ■ | ■ | ■ | ■ | | ■ | ■ | | ■ | ■ |
| IIIa | | | | | | ■ | ■ | | | | | | | | | | |
| II | ■ | | ■ | ■ | ■ | | | ■ | | | | | | | | | |
| div. | 1 | 1 | 1 | 1 | 1 | 1 | 1 | 2 | 2 | 2 | 2 | 0 | 1 | 1 | 2 | 3 | 2 |

Table 61: Coefficient of Variation (CV) for each morphometric feature and Cluster from the unconstrained Hierarchical Cluster Analysis (HCA) (Clust. = Cluster; x̄ = average).

| Clust. | width | length | area | l-w-index | upper-lower-ratio | left-right-ratio | tip angle | x̄ |
|---|---|---|---|---|---|---|---|---|
| I | 0.21 | 0.23 | 0.41 | 0.17 | 0.33 | 0.52 | 0.24 | 0.30 |
| II | 0.37 | 0.30 | 0.61 | 0.28 | 0.43 | 0.52 | 0.26 | 0.40 |
| IIIa | 0.33 | 0.36 | 0.60 | 0.27 | 0.39 | 0.34 | 0.30 | 0.37 |
| IIIb | 0.19 | 0.22 | 0.35 | 0.22 | 0.49 | 0.47 | 0.24 | 0.31 |
| IV | 0.19 | 0.16 | 0.31 | 0.16 | 0.34 | 0.53 | 0.20 | 0.27 |
| V | 0.15 | 0.10 | 0.17 | 0.20 | 0.32 | 0.41 | 0.13 | 0.21 |

values across all features *(Table 61)*. The other sub-cluster, the chronologically and taxonomically diverse Cluster IIIb, yields the third-highest CV (x̄ = 0.31), with elevated variation in the upper-lower-ratio (0.49), left-right-ratio (0.47), and a slightly higher area CV (0.35), indicating substantial shape variation and minor size variation within this large group. In contrast, Clusters IV (x̄ = 0.27) and V (x̄ = 0.21) exhibit notably low average CVs. Cluster V is based on only four assemblages from a narrow chronological and geographic context, whereas Cluster IV spans the entire *Late Palaeolithic*. In both, the left-right-ratio shows the greatest variation (0.53 and 0.41 respectively), while all other features remain low.

When viewed chronologically, the clusters show a steady decrease in variation – from the highest CVs in the oldest cluster to the lowest CVs in the youngest – again strongly suggesting a long-term reduction in morphological variation. Interestingly, the clusters contributing to elevated overall diversity during the LGM display comparatively low internal variation. This supports findings from other approaches, indicating that while multiple SP design concepts coexisted during the LGM, each individual design was relatively standardised. In other words, overall diversity was high, but variation within each design concept remained low. *(Table 61)*

### *4.3.1.3 Morphometrics across chronologically sorted Clusters*

The analysis of morphometric features across the chronologically sorted clusters reveals patterns that broadly align with the chronologically informed perspective. However, due to the aggregation of multiple chronological samples in certain clusters, some patterns become more pronounced.

Size-related features *(Figure 114)* remain relatively stable between the oldest Cluster II – primarily associated with Late Gravettian SPs – and the subsequent, taxonomically diverse Cluster III. In cluster IIIa, however, which includes the briefly represented Upper Solutrean, Epigravettian, and Salpetrian SPs of the 25th and the 24th millennium BP, a slight reduction in width, length, and area is evident. By contrast, Cluster V – partially contemporaneous and containing Lower Magdalenian and Tarigravettian SPs – comprises some of the largest SPs in the dataset. From this Lower Magdalenian cluster onwards, a general decline in overall size is observable across Clusters I and IV, although Cluster IV – including Upper Magdalenian, Hamburgian and Creswellian SPs – contains some of the widest SPs.

Shape-related features *(Figure 115)* also reveal a dynamic pattern. While the l-w-index remains stable across Clusters II, III, and V, Cluster I – containing exclusively the elongated Upper Magdalenian SPs of Type A – is characterised by comparatively high values, indicating notably slender forms. In contrast, Cluster IV – which includes the youngest *Late Palaeolithic* SPs in the dataset – shows the lowest l-w-indices, indicating markedly stouter forms. The left–right-ratio displays a steady decline from Cluster II through clusters III and V, reflecting a continuous trend toward increasing asymmetry along the y-axis. This trend is interrupted by Cluster I, which shows notably high average values and extreme variance. The youngest cluster exhibits values similar to those of Clusters IIIb and V. The tip angle follows yet another trajectory: it decreases from the oldest Cluster II to Cluster IIIa, marking a shift toward more pointed forms, but then increases steadily from cluster IIIa onward, culminating in Cluster IV, which reflects a clear long-term trend toward more obtuse tip angles. *(Figure 114 and 115)*

#### *4.3.1.4 Chronological Distance and Morphometric Difference*

The analysis of morphometric differences between samples across chronological distances *(Figure 116)* reveals notable structure in the data. Morphometric differences observed between samples dating to the same millennium BP vary considerably but, on average, exhibit low rates of change *(Figure 116)*. It should be noted that only 18 such cases occur across the entire timeframe of the analysis, primarily involving the LGM samples as well as the Upper Magdalenian and Hamburgian samples. Notably, the Late Badegoulian and the Upper Magdalenian Type A samples display particularly high morphometric differences compared to their contemporaneous samples. Interestingly, despite some pronounced exceptions – such as the differences between the latest Gravettian and the earliest Upper Solutrean sample, and notable differences involving the Late Badegoulian and the Upper Magdalenian Type A samples – samples that are one millennium apart show the lowest average morphometric differences overall. For chronological distances of two to seven millennia, morphometric differences are generally higher and more variable than those observed for samples separated by just one millennium or none at all. At a distance of eight millennia, the highest morphometric differences are recorded, with similarly elevated differences also observed at a distance of nine millennia. Beyond this, up to a chronological distance of sixteen millennia, morphometric differences decline again, reaching levels comparable to those seen between samples separated by two to seven millennia. Overall, these results indicate that – although notable exceptions exist – samples tend to be morphometrically more similar the closer they are in time. Conversely, the more chronologically distant samples are, the more morphometrically different they generally tend to be. However, beyond a chronological distance of approximately 9000 years, this trend notably appears to reverse, with morphometric differences decreasing despite increasing chronological separation. *(Figure 116)*

### 4.3.2 Chronologically-Constrained Clustering

This chapter presents the results of two hierarchical cluster analyses (HCA), each incorporating chronological weighting to different degrees. In the first approach, time was weighted at 1% (0.01), resulting in a cluster pattern resembling the unconstrained HCA, with minimal influence from the chronological position. In the second approach, the chronological weighting was increased to 2% (0.02), thereby giving greater emphasis to the chronological position of the individual units within the clustering process.

#### *4.3.2.1 1% Time-weighting*

Applying a 1% temporal weighting (Appendix Table 10) to the distance matrix *(Table 62)* prior to clustering slightly alters the resulting pattern. The three clusters of low change rates observed in the unconstrained matrix (Appendix Table 12) become better defined in the weighted matrix, with more pronounced discontinuities indicated by elevated change rates along the edges. Moreover, the previous-

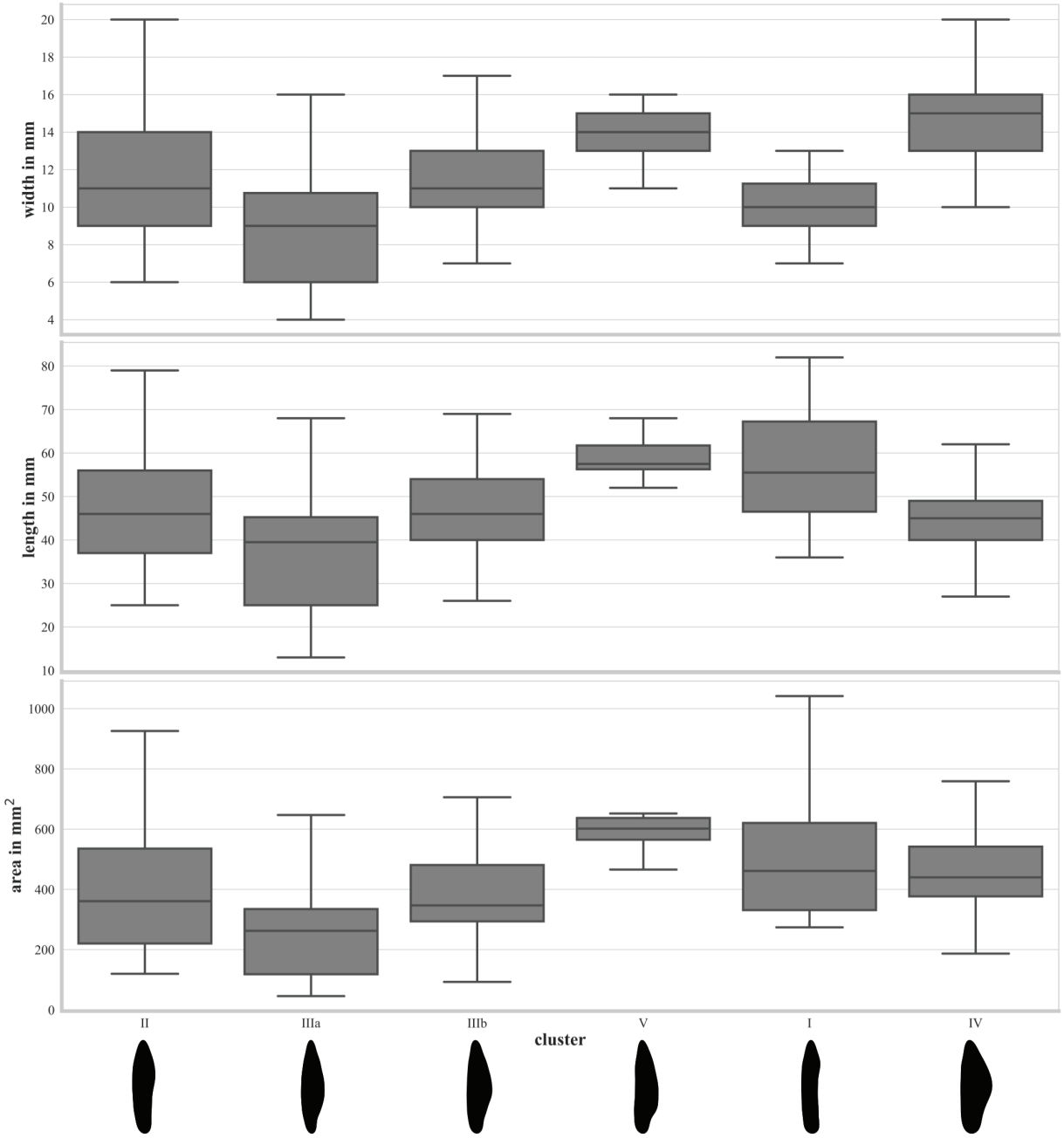



Figure 114: Box-plots of size-related features for chronologically sorted clusters from the unconstrained Hierarchical Cluster Analysis (HCA) (older to younger from left to right; outliers excluded).

Figure 115 (next page): Box-plots of shape-related features for chronologically sorted clusters from the unconstrained Hierarchical Cluster Analysis (HCA) (older to younger from left to right; outliers excluded).

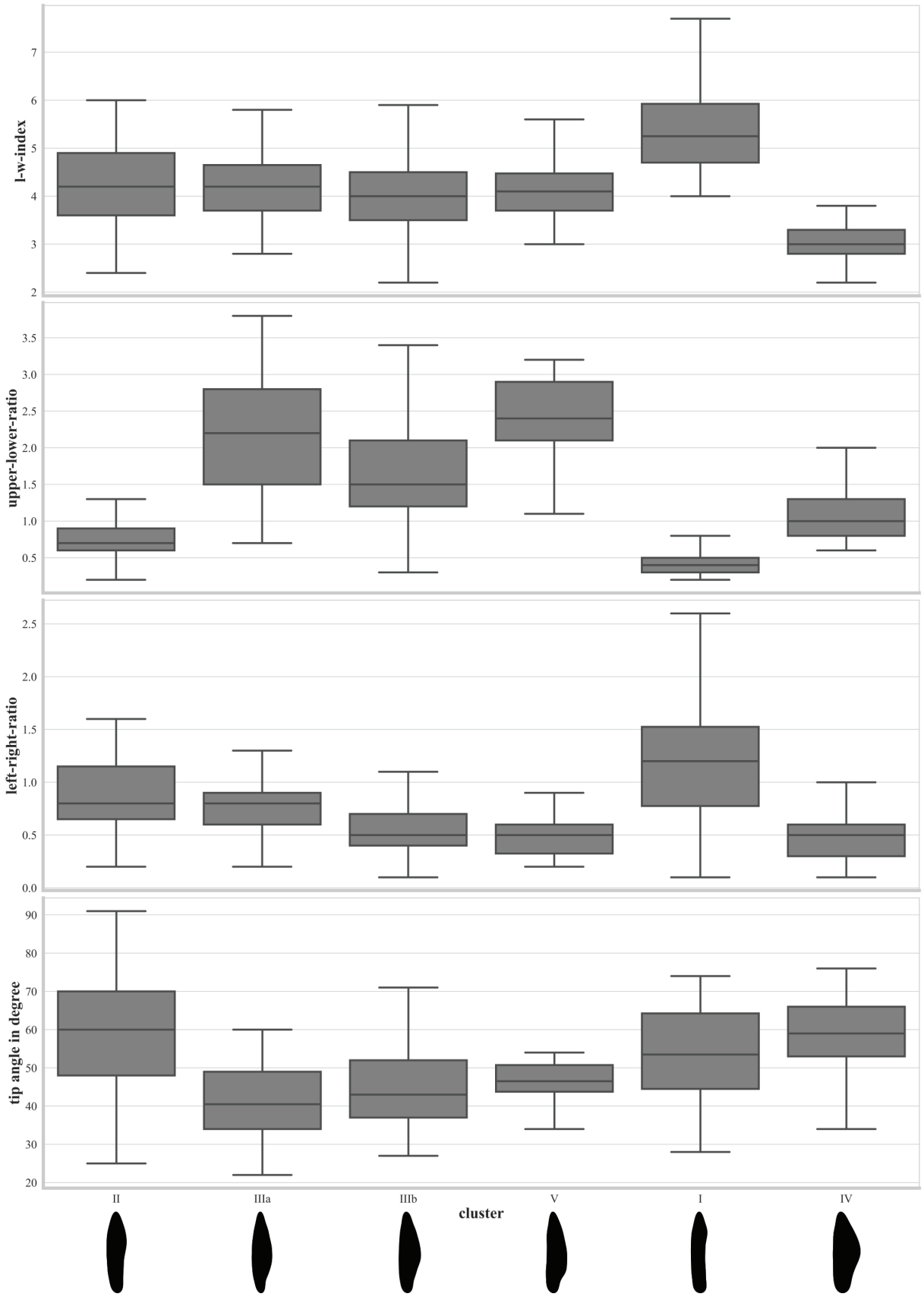



Figure 115,
explanation on previous page.

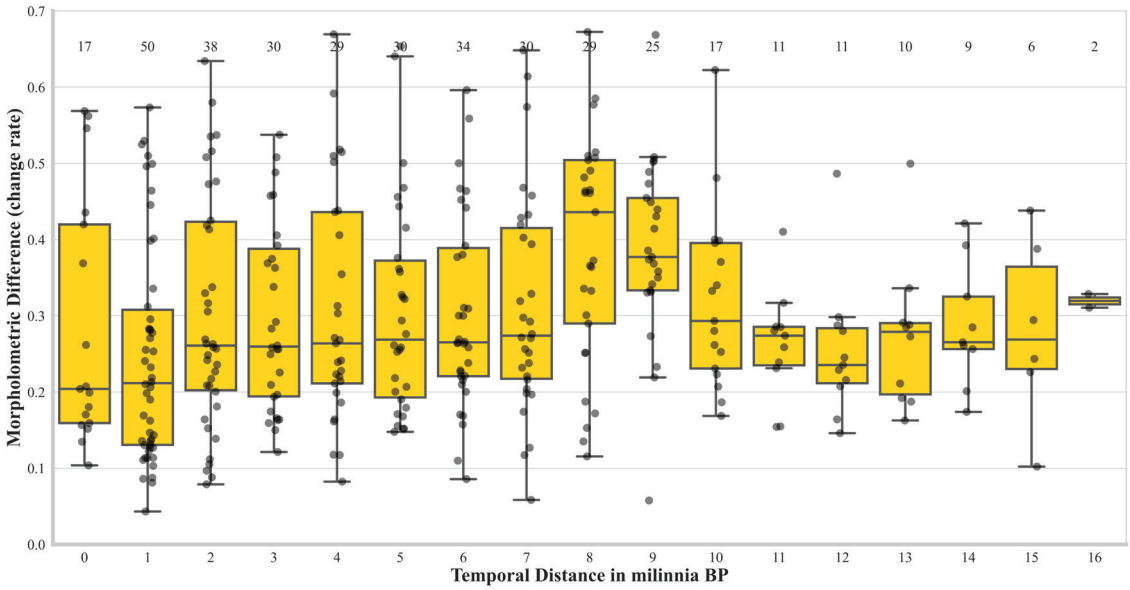



Figure 116: Change rates across chronological distances in millennia BP (numbers above boxes = number of distances between samples included in each box).

ly broad similarities between the Hamburgian, Creswellian, and Havelte samples and many of the older samples are now less apparent, reflecting a stronger chronological constraint on their placement. The same applies to the Late Gravettian samples, which are now more or less cut off the other samples by high change rates. The pronounced divergence of the Late Badegoulian sample from samples dating to the 23rd millennium BP and later is further accentuated, while its differences to older samples appear reduced. Further, the younger peripheral zone of the LGM cluster – again, particularly the Tardigravettian and Lower Magdalenian samples – continue to exhibit elevated change rates relative to the older LGM samples, suggesting greater morphological divergence in these periods. The morphological affinity between the younger LGM samples and those of the Late Upper Palaeolithic is less pronounced than observed in the unconstrained matrix. The Upper/Late Magdalenian samples of the elongated Type A remain clearly separated from the other later Upper Palaeolithic samples as well as across all other samples.

The dendrogram produced by the HCA, based on the time-weighted (0.01) distance matrix *(Figure 119)*, reveals a chronologically more structured pattern. Two major clusters emerge, each corresponding to distinct morphological form-groups: one predominantly characterised by SPs with relatively long hafting parts and short transformative parts, and the other by SPs with comparatively shorter hafting parts. Both major clusters further divide into secondary clusters with clear chronological coherence.

The first major cluster, representing SPs with elongated hafting parts, includes two sub-clusters: one composed of Upper Magdalenian SPs of the elongated Type A, dated to the 16th and 15th millennium BP, and another comprising all Late Gravettian samples (30th–26th millennium BP), forming a 'pre-LGM' cluster.

The second major form-group, defined by SPs with shorter hafting parts, is more extensive and subdivides into two secondary clusters of approximately equal morphological distance. The first sub-cluster of the first secondary cluster encompasses exclusively Late Upper Palaeolithic samples, including Upper/Late Magdalenian Type B SPs, the Hamburgian samples (16th and 14th millennium BP), and the Creswellian sample (15th millennium BP), together forming a coherent 'post-LGM' cluster. SPs in this cluster tend to be stouter and have a more or less even ratio between the hafting and the transformative part. The sec-

ond sub-cluster comprises younger LGM samples, including Upper Solutrean SPs from the 23rd and the 22nd millennium BP, Epigravettian samples from the 21st and the 20th millennium BP, and both Middle Magdalenian samples (18th and 17th millennium BP). Despite being chronological outliers, the Hamburgian and Havelte samples from the 15th and the 14th millennium BP also fall within this cluster. Additionally, the Lower Magdalenian and Tardigravettian samples (22nd–20th millennium BP) are included, albeit slightly separated.

The second secondary cluster within this same form-group clearly isolates the Late Badegoulian SPs of Cuzoul de Vers (layers 21–16), from a distinct grouping, reflecting a brief but morphometrically well-defined chronological phase. It includes the Upper Solutrean samples from the 25th and the 24th millennium BP, the Epigravettian sample from the 24th millennium BP, and the Salpêtrian sample from the same millennium – together forming an older LGM cluster. This cluster is morphologically characterised by a more pronounced transformative part and a tendency towards overall slenderer forms.

### *4.3.2.2 2% Time-weighting*

Applying a 2% temporal weighting to the distance matrix (Appendix Table 13) prior to clustering significantly alters the resulting pattern. While the three clusters of low change rates observed in the unconstrained matrix (Appendix Table 12) remain identifiable, they begin to dissolve in favour of a pattern more strongly aligned along the diagonal axis – reflecting increased chronological coherence. The previously broad morphological affinities between the Hamburgian, Creswellian, and Havelte samples and much older samples are now largely compensated, with low differences occurring primarily between chronologically proximate samples. The pronounced divergence of the Late Badegoulian sample from samples dating to the 23rd millennium BP and later is further accentuated, while its differences to older samples are now also more distinct, particularly where large chronological gaps exist. The younger members of the LGM cluster are more or less excluded from the central low-change-rate cluster, exhibiting higher change rates to their older LGM counterparts. Moreover, the previously noted affinities between the younger LGM samples and those from the Late Upper Palaeolithic are now barely visible and are limited primarily to the Middle Magdalenian. Despite the increased emphasis on chronological proximity, the Upper/Late Magdalenian samples of the elongated Type A remain clearly distinct from the other Late Upper Palaeolithic samples.

The dendrogram resulting from the HCA based on the time-weighted (0.02) distance matrix *(Figure 120)* thus also reveals a strongly chronological pattern. As in the previous analyses, the dendrogram initially divides into two major clusters, each of which further splits into two large secondary clusters. The first lower cluster of the first major cluster includes only Late Gravettian samples, forming a tight 'pre LGM' cluster. Within this cluster, the samples from the 30th and 29th millennium BP are morphologically more distinct from the younger Late Gravettian samples dated to the 28th through the 26th millennium BP.

The second lower sub-cluster of this major cluster comprises older LGM samples, specifically the Upper Solutrean samples of the 25th and 24th millennium BP, the Epigravettian and Salpetrian samples from the 24th millennium BP, and – despite a substantial distance of approximately 0.29 – the Late Badegoulian sample (23rd millennium BP).

In the second major cluster, the first lower cluster is clearly isolated from all other samples by a pronounced morphological distance. It contains only the Upper/Late Magdalenian SPs of the elongated Type A, dated to the 16th and 15th millennium BP.

The second lower cluster of this major cluster is considerably larger and divides into two distinct sub-clusters. The first of these contains all samples attributed to the Late Upper Palaeolithic, including the Upper/Late Magdalenian SPs of Type B (16th and 15th millennium BP), the Hamburgian samples (16th–14th millennium BP), the Creswellian sample (15th millennium BP), and the Havelte sample (14th millennium BP), forming a 'post LGM'. This sub-cluster itself divides into two further sub-groups: one comprising the older samples of the 16th and 15th millennium BP, including the Upper Magdalenian, and another containing the younger samples of the 15th and 14th millennium BP, which lack a Magdalenian component.

The second sub-cluster includes all younger LGM samples. Within it, the Lower Magdalenian and Tardigravettian samples (22nd–20th millennium BP) form a distinct grouping, while the Middle Magdalenian samples (18th and 17th millennium BP) constitute a separate sub-cluster. Finally, the Upper Solutrean samples of the 23rd and 22nd millennium BP cluster together with the Epigravettian samples of the 21st and 20th millennium BP, highlighting their close morphological affinities.

### 4.3.3 Adding Geographical Proximity

In this analysis, the 1% temporal-weighted distance matrix (Appendix Table 12) is further refined by incorporating geographical proximity as distance between the average coordinates of the samples (Map 8) (see Methods Chapter 3.3.4). The resulting geographical weight matrix (Appendix Table 14) was then added to the existing 1% temporal-weighted distance matrix, thereby modifying the results presented earlier in Chapter 4.3.2.1. It is acknowledged here that the chronologically driven distribution pattern of the assemblages may itself introduce an additional chronological signal into the analyses. For instance, the considerable distance observed between the Late Gravettian and Upper Solutrean samples is mirrored at the chronological level. Similarly, the spatial distribution from the Last Glacial Maximum (LGM) onward into the Late Upper Palaeolithic follows a predominantly south-to-north trajectory, further reinforcing the chronological structure in the dataset.

The combined matrix (Appendix Table 14) exhibits only minor deviations from the non-geographically weighted version. However, the boundary between Late Gravettian and Upper Solutrean samples becomes more pronounced, reflecting the considerable geographical separation between these groups. Similarly, Late Upper Palaeolithic samples exhibit further reduced similarity with older samples that originate from more southerly or easterly assemblages, thus reflecting the added influence of spatial distance on morphometric dissimilarity. The marked divergence of the Late Badegoulian sample from assemblages dating to the 23rd millennium BP and later remains evident. Furthermore, elevated change rates between older LGM samples and the younger, more peripheral members of the LGM cluster – particularly the Tardigravettian and Lower Magdalenian samples – are further emphasised by a slight geographical shift from the Iberian Peninsula (notably the Upper Solutrean samples) toward the Rhône Valley.

The HCA dendrogram shows subtle modifications compared to the dendrogram based solely on temporal weighting. The analysis initially separates into two major clusters. The first major cluster contains a larger number of samples and further subdivides into five archaeologically meaningful sub-clusters, both chronologically and geographically. The first sub-cluster includes younger LGM samples such as the Lower (21st–20th millennium BP) and the Tardigravettian (22nd millennium BP) as well as the Middle Magdalenian samples (18th and 17th millennium BP), forming a late 'LGM/early post-LGM' cluster centred in southern France. The second sub-cluster comprises all Late Upper Palaeolithic samples, including Upper Magdalenian Type B (16th and 15th millennium BP), Hamburgian (16th–14th millennium BP), Havelte (14th millennium BP), and Creswellian samples (15th millennium BP), forming a distinct 'post-LGM' cluster. This cluster subdivides into a more southern cluster, represented by the Upper Magdalenian and Creswellian samples, and a more northern cluster, comprising the Hamburgian and Havelte samples. The Hamburgian sample from the 16th millennium BP is excluded from this northern sub-cluster, likely due to its more easterly geographic origin. The third and fourth sub-clusters contain LGM samples: one is composed of all Upper Solutrean samples and the Salpetrian sample (24th millennium BP), representing a slightly older and more western grouping with geographical focus in the Iberian Peninsula and southern France. The final sub-cluster groups more easterly Epigravettian samples from the 24th, the 21st and the 20th millennium BP alongside the 29th millennium BP Late Gravettian sample.

The second major cluster groups all Late Gravettian samples, except for the 29th millennium BP sample, which now clusters with the younger Epigravettian (21st and 20th millennium BP) samples, again forming a 'pre LGM' cluster. Also included in this major cluster – though clearly distinct – is the Late Badegoulian sample (23rd millennium BP), which remains highly divergent. Even more divergent are the Up-

per Magdalenian samples of Type A (16th and 15th millennium BP), which cluster tightly and distinctly, *setting* them apart from the other sub-clusters.

The cluster analyses revealed distinct morphological patterns in SPs that align closely with both chronological and geographical frameworks, thereby reinforcing interpretations of their taxonomic relationships. Even the unconstrained clustering approach produced several taxonomically and chronologically plausible clusters. It identified strong morphological affinities – particularly between the Lower Magdalenian and the Tardigravettian (22nd–20th millennium BP), as well as within the Late Upper Palaeolithic – and pronounced discontinuities – most notably between the Late Gravettian and the Upper Solutrean but also between older and younger LGM samples. Notably, five morphological clusters emerged, each varying in their chronological and taxonomic distribution. While some clusters (e.g., Cluster III) span a broader chronological range, others (e.g., Cluster I and V) are confined to shorter chronological phases. Furthermore, the analysis showed that, across most of the studied timeframe, typically only one morphological cluster is present at a time. However, during the LGM, multiple clusters co-occur, suggesting a period of morphological diversification. A similar pattern is observed during the 16th and 15th millennia BP, where the elongated Type A Upper Magdalenian SPs shortly coexist with and eventually got replaced by stouter forms. Additionally, a continuous decrease in variation across the clusters was observed, indicating a progressive increase in standardisation. This finding aligns with the results from the chronologically informed perspective. Furthermore, the analysis of individual morphometric features within the clusters revealed patterns that are chronologically significant.

The chronologically constrained clustering produced chronologically coherent and meaningful groups. Overall, the morphometric data support the existence of three major groupings with higher internal similarity: a 'pre-LGM' group, two phases within the LGM ('older' and 'younger'), and a 'post-LGM' group. The 'pre-LGM' cluster is clearly associated with the Late Gravettian, whereas both LGM clusters are more taxonomically diverse. The older LGM cluster appears to be primarily linked with an older Iberian Upper Solutrean SP tradition, while the younger cluster is dominated by forms associated with the younger Upper Solutrean, the Lower Magdalenian and the morphologically closely related Tardigravettian assemblages. In the later periods, SP forms from the Late Upper Palaeolithic tend to cluster together, although the Type A SPs of the Upper Magdalenian stand out as a distinct morphological group. The same applies to the Late Badegoulian SPs, which show limited morphological affinity with other contemporaneous forms.

Incorporating geographical proximity into the analysis further refined the results. It subdivided the LGM cluster into more spatially coherent sub-clusters, distinguishing between eastern – including younger Epigravettian

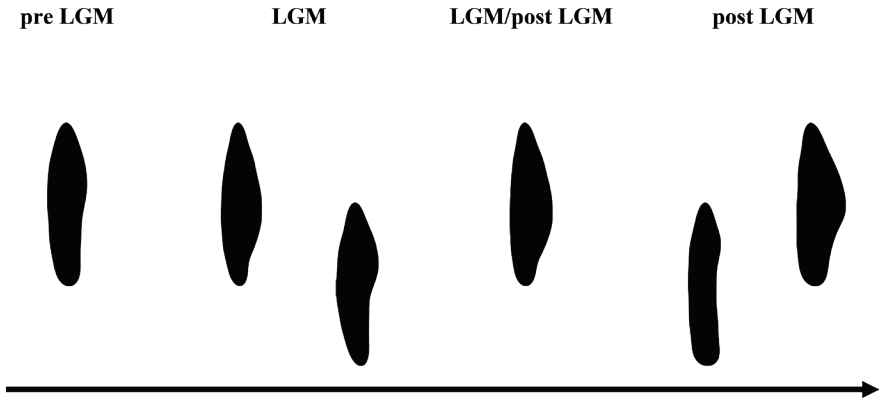



Figure 117: Coarse chronological sequence of the morphological development of SPs (lowered shapes = short-term occurences).

Table 62: Distance-Matrix for Hierarchical Cluster Analysis (HCA) based on the average change rates between averages of samples (Colour scale: dark – light = pronounced morphometric differences – moderate differences – notable morphometric similarities (1.15 – 0.32 – 0.00); GRA = Late Gravettian; US = Upper Solutrean; SAL = Salpetrian; LBA = Late Badegoulian; EPI = Epigravettian; TAR = Tardigravettian; LMA = Lower Magdalenian; MMA = Middle Magdalenian; UMA = Upper Magdalenian; HAM = Hamburgian; CRE = Creswellian; HAV = Havelte; numbers = millennium BP).

| | GRA 30 | GRA 29 | GRA 28 | GRA 27 | GRA 26 | US 25 | US 24 | SAL 24 | EPI 24 | US 23 | LBA 23 | US 22 | TAR 22 | EPI 21 | LMA 21 | EPI 20 | LMA 20 | MMA 18 | MMA 17 | UMA-A 16 | UMA-B 16 | HAM 16 | UMA-A 15 | UMA-B 15 | HAM 15 | CRE 15 | HAM 14 | HAV 14 |
|---|---|---|---|---|---|---|---|---|---|---|---|---|---|---|---|---|---|---|---|---|---|---|---|---|---|---|---|---|
| GRA 30 | | 0,30 | 0,23 | 0,15 | 0,24 | 0,50 | 0,45 | 0,56 | 0,39 | 0,39 | 0,17 | 0,37 | 0,86 | 0,35 | 0,67 | 0,28 | 0,62 | 0,49 | 0,50 | 0,28 | 0,42 | 0,39 | 0,24 | 0,44 | 0,39 | 0,29 | 0,33 | 0,31 |
| GRA 29 | 0,30 | | 0,21 | 0,15 | 0,28 | 0,30 | 0,32 | 0,32 | 0,22 | 0,17 | 0,30 | 0,24 | 0,47 | 0,12 | 0,36 | 0,23 | 0,36 | 0,32 | 0,24 | 0,29 | 0,34 | 0,29 | 0,20 | 0,33 | 0,17 | 0,26 | 0,23 | 0,10 |
| GRA 28 | 0,23 | 0,21 | | 0,11 | 0,10 | 0,54 | 0,51 | 0,59 | 0,44 | 0,36 | 0,26 | 0,38 | 0,60 | 0,28 | 0,43 | 0,33 | 0,37 | 0,48 | 0,41 | 0,15 | 0,30 | 0,22 | 0,19 | 0,29 | 0,27 | 0,21 | 0,26 | 0,27 |
| GRA 27 | 0,15 | 0,15 | 0,11 | | 0,14 | 0,41 | 0,41 | 0,49 | 0,36 | 0,24 | 0,20 | 0,28 | 0,64 | 0,20 | 0,47 | 0,23 | 0,42 | 0,39 | 0,33 | 0,26 | 0,29 | 0,23 | 0,25 | 0,28 | 0,23 | 0,16 | 0,19 | 0,16 |
| GRA 26 | 0,24 | 0,28 | 0,10 | 0,14 | | 0,53 | 0,51 | 0,63 | 0,48 | 0,37 | 0,26 | 0,35 | 0,67 | 0,33 | 0,47 | 0,31 | 0,38 | 0,46 | 0,45 | 0,25 | 0,23 | 0,19 | 0,29 | 0,24 | 0,27 | 0,15 | 0,21 | 0,29 |
| US 25 | 0,50 | 0,30 | 0,54 | 0,41 | 0,53 | | 0,13 | 0,11 | 0,21 | 0,11 | 0,31 | 0,12 | 0,34 | 0,16 | 0,31 | 0,16 | 0,36 | 0,12 | 0,17 | 0,49 | 0,38 | 0,37 | 0,40 | 0,37 | 0,21 | 0,29 | 0,28 | 0,15 |
| US 24 | 0,45 | 0,32 | 0,51 | 0,41 | 0,51 | 0,13 | | 0,19 | 0,17 | 0,22 | 0,20 | 0,22 | 0,54 | 0,29 | 0,46 | 0,21 | 0,52 | 0,21 | 0,29 | 0,59 | 0,50 | 0,51 | 0,45 | 0,50 | 0,33 | 0,41 | 0,40 | 0,26 |
| SAL 24 | 0,56 | 0,32 | 0,59 | 0,49 | 0,63 | 0,11 | 0,16 | | 0,14 | 0,14 | 0,31 | 0,21 | 0,34 | 0,19 | 0,37 | 0,23 | 0,44 | 0,22 | 0,22 | 0,47 | 0,46 | 0,44 | 0,34 | 0,44 | 0,27 | 0,37 | 0,34 | 0,17 |
| EPI 24 | 0,39 | 0,22 | 0,44 | 0,36 | 0,48 | 0,21 | 0,15 | 0,16 | | 0,19 | 0,28 | 0,24 | 0,52 | 0,25 | 0,46 | 0,26 | 0,50 | 0,26 | 0,27 | 0,48 | 0,51 | 0,51 | 0,33 | 0,50 | 0,33 | 0,43 | 0,40 | 0,22 |
| US 23 | 0,39 | 0,17 | 0,36 | 0,24 | 0,37 | 0,11 | 0,22 | 0,14 | 0,19 | | 0,31 | 0,10 | 0,34 | 0,08 | 0,25 | 0,17 | 0,26 | 0,15 | 0,11 | 0,40 | 0,33 | 0,30 | 0,34 | 0,30 | 0,14 | 0,25 | 0,22 | 0,06 |
| LBA 23 | 0,17 | 0,30 | 0,26 | 0,20 | 0,26 | 0,31 | 0,20 | 0,31 | 0,28 | 0,56 | | 0,52 | 1,17 | 0,54 | 0,94 | 0,39 | 0,89 | 0,65 | 0,71 | 0,57 | 0,65 | 0,61 | 0,46 | 0,67 | 0,58 | 0,49 | 0,51 | 0,47 |
| US 22 | 0,37 | 0,24 | 0,38 | 0,28 | 0,35 | 0,12 | 0,22 | 0,21 | 0,24 | 0,10 | 0,52 | | 0,39 | 0,14 | 0,28 | 0,09 | 0,26 | 0,08 | 0,15 | 0,50 | 0,26 | 0,26 | 0,43 | 0,26 | 0,13 | 0,20 | 0,19 | 0,15 |
| TAR 22 | 0,86 | 0,47 | 0,60 | 0,64 | 0,67 | 0,34 | 0,54 | 0,34 | 0,52 | 0,34 | 1,17 | 0,26 | | 0,23 | 0,08 | 0,33 | 0,20 | 0,22 | 0,15 | 0,46 | 0,30 | 0,26 | 0,46 | 0,27 | 0,20 | 0,32 | 0,25 | 0,29 |
| EPI 21 | 0,35 | 0,12 | 0,28 | 0,20 | 0,33 | 0,16 | 0,29 | 0,19 | 0,25 | 0,08 | 0,54 | 0,14 | 0,23 | | 0,25 | 0,15 | 0,25 | 0,20 | 0,12 | 0,38 | 0,29 | 0,26 | 0,31 | 0,27 | 0,09 | 0,22 | 0,20 | 0,06 |
| LMA 21 | 0,67 | 0,36 | 0,43 | 0,47 | 0,47 | 0,31 | 0,46 | 0,37 | 0,46 | 0,25 | 0,94 | 0,28 | 0,08 | 0,21 | | 0,28 | 0,13 | 0,16 | 0,12 | 0,44 | 0,25 | 0,21 | 0,44 | 0,22 | 0,16 | 0,27 | 0,22 | 0,25 |
| EPI 20 | 0,28 | 0,23 | 0,33 | 0,23 | 0,31 | 0,16 | 0,21 | 0,23 | 0,26 | 0,17 | 0,39 | 0,09 | 0,33 | 0,15 | 0,28 | | 0,33 | 0,16 | 0,26 | 0,51 | 0,27 | 0,27 | 0,46 | 0,26 | 0,17 | 0,19 | 0,23 | 0,17 |
| LMA 20 | 0,62 | 0,36 | 0,37 | 0,42 | 0,38 | 0,36 | 0,52 | 0,44 | 0,50 | 0,26 | 0,89 | 0,26 | 0,20 | 0,25 | 0,13 | 0,20 | | 0,21 | 0,21 | 0,41 | 0,21 | 0,16 | 0,42 | 0,18 | 0,17 | 0,20 | 0,23 | 0,24 |
| MMA 18 | 0,49 | 0,32 | 0,48 | 0,39 | 0,46 | 0,12 | 0,21 | 0,22 | 0,26 | 0,15 | 0,65 | 0,08 | 0,22 | 0,20 | 0,16 | 0,16 | 0,21 | | 0,13 | 0,58 | 0,26 | 0,26 | 0,51 | 0,26 | 0,16 | 0,23 | 0,19 | 0,22 |
| MMA 17 | 0,50 | 0,24 | 0,41 | 0,33 | 0,45 | 0,17 | 0,29 | 0,22 | 0,27 | 0,11 | 0,71 | 0,15 | 0,15 | 0,12 | 0,12 | 0,26 | 0,21 | 0,13 | | 0,50 | 0,27 | 0,26 | 0,43 | 0,24 | 0,11 | 0,26 | 0,17 | 0,16 |
| UMA-A 16 | 0,28 | 0,29 | 0,15 | 0,26 | 0,25 | 0,49 | 0,59 | 0,47 | 0,48 | 0,40 | 0,57 | 0,50 | 0,46 | 0,38 | 0,44 | 0,51 | 0,41 | 0,58 | 0,50 | | 0,51 | 0,39 | 0,11 | 0,51 | 0,50 | 0,40 | 0,42 | 0,47 |
| UMA-B 16 | 0,42 | 0,34 | 0,30 | 0,29 | 0,23 | 0,38 | 0,50 | 0,46 | 0,51 | 0,33 | 0,65 | 0,26 | 0,30 | 0,29 | 0,25 | 0,27 | 0,21 | 0,26 | 0,27 | 0,57 | | 0,11 | 0,57 | 0,04 | 0,21 | 0,13 | 0,18 | 0,32 |
| HAM 16 | 0,39 | 0,29 | 0,22 | 0,23 | 0,19 | 0,37 | 0,51 | 0,44 | 0,51 | 0,30 | 0,61 | 0,26 | 0,26 | 0,26 | 0,21 | 0,27 | 0,16 | 0,26 | 0,26 | 0,44 | 0,10 | | 0,46 | 0,09 | 0,17 | 0,09 | 0,14 | 0,27 |
| UMA-A 15 | 0,24 | 0,20 | 0,19 | 0,25 | 0,29 | 0,40 | 0,45 | 0,34 | 0,33 | 0,34 | 0,46 | 0,43 | 0,46 | 0,31 | 0,44 | 0,46 | 0,42 | 0,51 | 0,43 | 0,11 | 0,57 | 0,46 | | 0,57 | 0,47 | 0,42 | 0,40 | 0,45 |
| UMA-B 15 | 0,44 | 0,33 | 0,29 | 0,28 | 0,24 | 0,37 | 0,50 | 0,44 | 0,50 | 0,30 | 0,67 | 0,26 | 0,27 | 0,27 | 0,22 | 0,26 | 0,18 | 0,26 | 0,24 | 0,51 | 0,04 | 0,09 | 0,55 | | 0,18 | 0,13 | 0,16 | 0,28 |
| HAM 15 | 0,39 | 0,17 | 0,27 | 0,23 | 0,27 | 0,21 | 0,33 | 0,27 | 0,33 | 0,14 | 0,58 | 0,13 | 0,20 | 0,09 | 0,16 | 0,17 | 0,17 | 0,16 | 0,11 | 0,50 | 0,21 | 0,17 | 0,37 | 0,18 | | 0,16 | 0,14 | 0,11 |
| CRE 15 | 0,29 | 0,26 | 0,21 | 0,16 | 0,15 | 0,29 | 0,41 | 0,37 | 0,43 | 0,25 | 0,49 | 0,20 | 0,32 | 0,22 | 0,27 | 0,19 | 0,20 | 0,23 | 0,26 | 0,40 | 0,13 | 0,09 | 0,42 | 0,13 | 0,17 | | 0,12 | 0,24 |
| HAM 14 | 0,33 | 0,23 | 0,26 | 0,19 | 0,21 | 0,28 | 0,40 | 0,34 | 0,40 | 0,22 | 0,51 | 0,19 | 0,25 | 0,20 | 0,22 | 0,23 | 0,23 | 0,19 | 0,17 | 0,42 | 0,18 | 0,14 | 0,40 | 0,16 | 0,14 | 0,12 | | 0,29 |
| HAV 14 | 0,31 | 0,10 | 0,27 | 0,16 | 0,29 | 0,15 | 0,26 | 0,17 | 0,22 | 0,06 | 0,47 | 0,15 | 0,29 | 0,06 | 0,25 | 0,17 | 0,24 | 0,22 | 0,16 | 0,47 | 0,32 | 0,27 | 0,45 | 0,28 | 0,11 | 0,24 | 0,20 | |

samples – and western regions – represented by the Upper Solutrean on the Iberian Peninsula, the Salpetrian and older Epigravettian samples – as well as forming a geographically tighter group within southern France – including the Lower and Middle Magdalenian and the Tardigravettian. Additionally, it strengthened the cohesion of the Late Upper Palaeolithic cluster – again excluding the distinctive Type A SPs of the Upper Magdalenian.

Combining these results into a narrative of the chronological development of SP morphology, it can be stated that, after their initial appearance during the Late Gravettian, where they exhibit comparatively short transformative parts and relatively long hafting parts, SPs with longer transformative parts and shorter hafting parts emerged at the beginning of the LGM within Upper Solutrean contexts in western Europe and, with only two short-lived exceptions, remained the dominant form *(Figure 117)*. While the earliest SPs with short hafting parts were only slightly asymmetric along the y-axis, asymmetry became increasingly pronounced during the LGM, reaching its peak in the Tardigravettian/Lower–Middle Magdalenian realm and continuing into the Late Upper Palaeolithic. Toward the end of the Late Upper Palaeolithic, a trend toward longer hafting parts re-emerges, although they typically do not exceed 50% of the total SP length. Despite a notable chronological gap in the record, this reappearance of longer hafting parts may point to influences from eastern late-LGM traditions, where such proportions occasionally occur. *(Figure 117, Table 62; Figure 118–121)*

## 4.4 BRIDGING THE GAP? SCALENE BLADELETS AND SHOULDERED POINTS

During the period characterised by a near absence of classical SPs, between approximately 19,000 and 16,000 calBP, a type of triangular lithic implement referred to as scalene bladelets appears in central and western European assemblages *(Figure 122)*. Maier (2020) suggested that these bladelets represent a variant of SPs, potentially bridging the chronological gap between classical SP forms and being phylogenetically closely related to the SPs of the Late Badegoulian, ultimately giving rise to the Upper Magdalenian and Late Glacial SPs (ibid., 186).

To explore the possible relationships between scalene bladelets and SPs, morphometric analyses were conducted on a small sample of scalene bladelets (n = 10), which were compared with dated SPs from the Late Badegoulian, Upper/Late–Final Magdalenian SPs of Type A, and, as representatives of the Late Glacial, Hamburgian SPs of the 15th millennium BP. Given the limited sample sizes, this analysis does not aim to provide a comprehensive assessment of phylogenetic relationships but rather offers an initial perspective that may serve as a basis for future investigations in this field. *(Figure 122)*

The average change rate between the Late Badegoulian SPs from Le Cuzoul de Vers, layers 21–16, and the scalene bladelets ($\bar{x}$ = 0.32) is at the significance threshold for changes observed between two consecutive millennia (Chapter 4.1.3). This is primarily driven by elevated change rates in all size-related features *(Table 63)*, indicating that scalene bladelets are substantially smaller than the Late Badegoulian SPs. Additionally, the change rates for the left-right-ratio and the tip angle exceed what would be expected between two consecutive millennia, suggesting that scalene bladelets are markedly more asymmetrically shaped and possess considerably more obtuse points. While the upper-lower-ratio is slightly elevated, the difference does not exceed the significance threshold. Nonetheless, it suggests that the scalene bladelets possess relatively longer hafting parts, or respectively, relatively shorter transformative parts com-

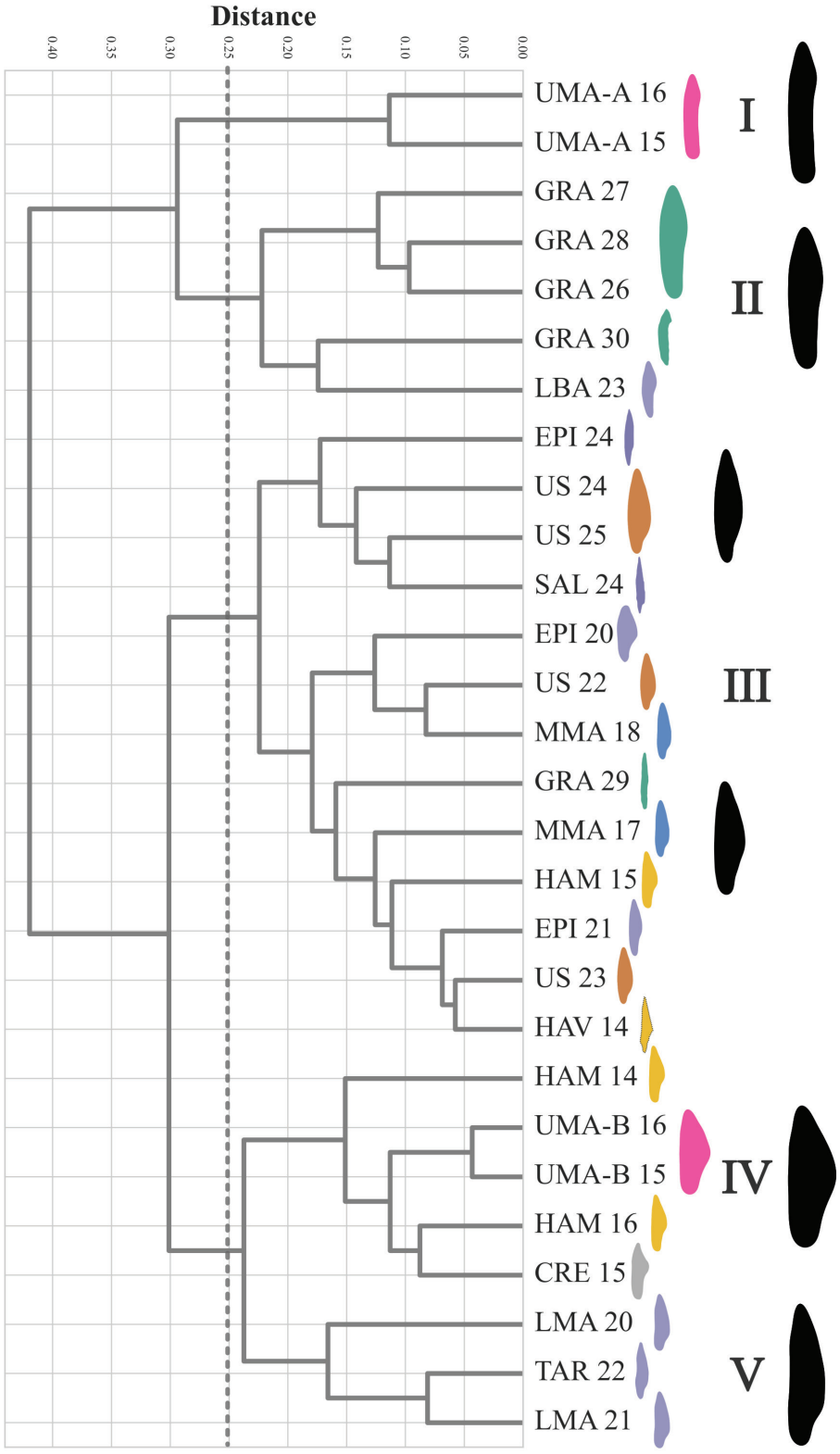



Figure 118: Dendrogram of unconstrained Hierarchical Cluster Analysis (HCA) based on distance matrix of average morphometric features. Roman numerals = morphotypes inferred from HCA: I = elongated forms, upper–lower ratio < 1; II = forms with upper–lower–ratio ≤ 1; III = asymmetric, shorter–stemmed forms; IV = stouter forms, upper–lower–ratio ≈ 1; V = straight or concave–backed, short–stemmed forms (MP–CM–offsets exluded; dotted line = hierarchical grouping of clusters by linkage distance; shapes = meanshapes of respective unit/cluster; colour–coded by taxonomic unit).

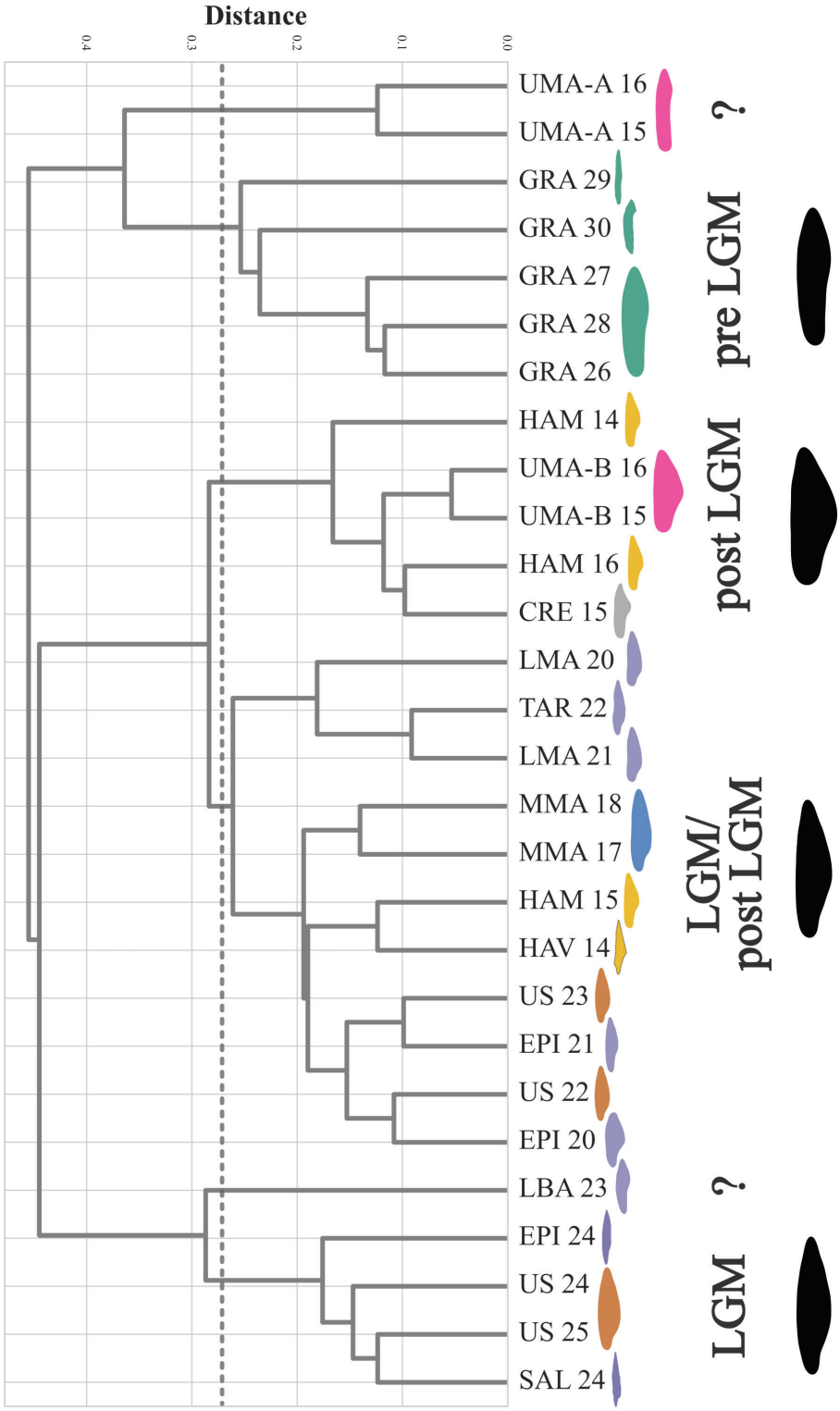



Figure 119: Dendrogram of a time-weighted (t = 0.01) Hierarchical Cluster Analysis (HCA) based on distance matrix of average morphometric features. Cluster: Late Gravettian samples forming a 'pre LGM' cluster; younger LGM samples mixed with post LGM samples; older LGM samples; Late Upper Palaeolithic samples forming a 'post LGM' cluster; non assigned ('?') samples/potential special forms (MP-CM-offsets exluded; dotted line = hierarchical grouping of clusters based on the linkage distance; shapes = meanshapes of the respective unit/cluster; colour-code inferred from the taxonomic units).

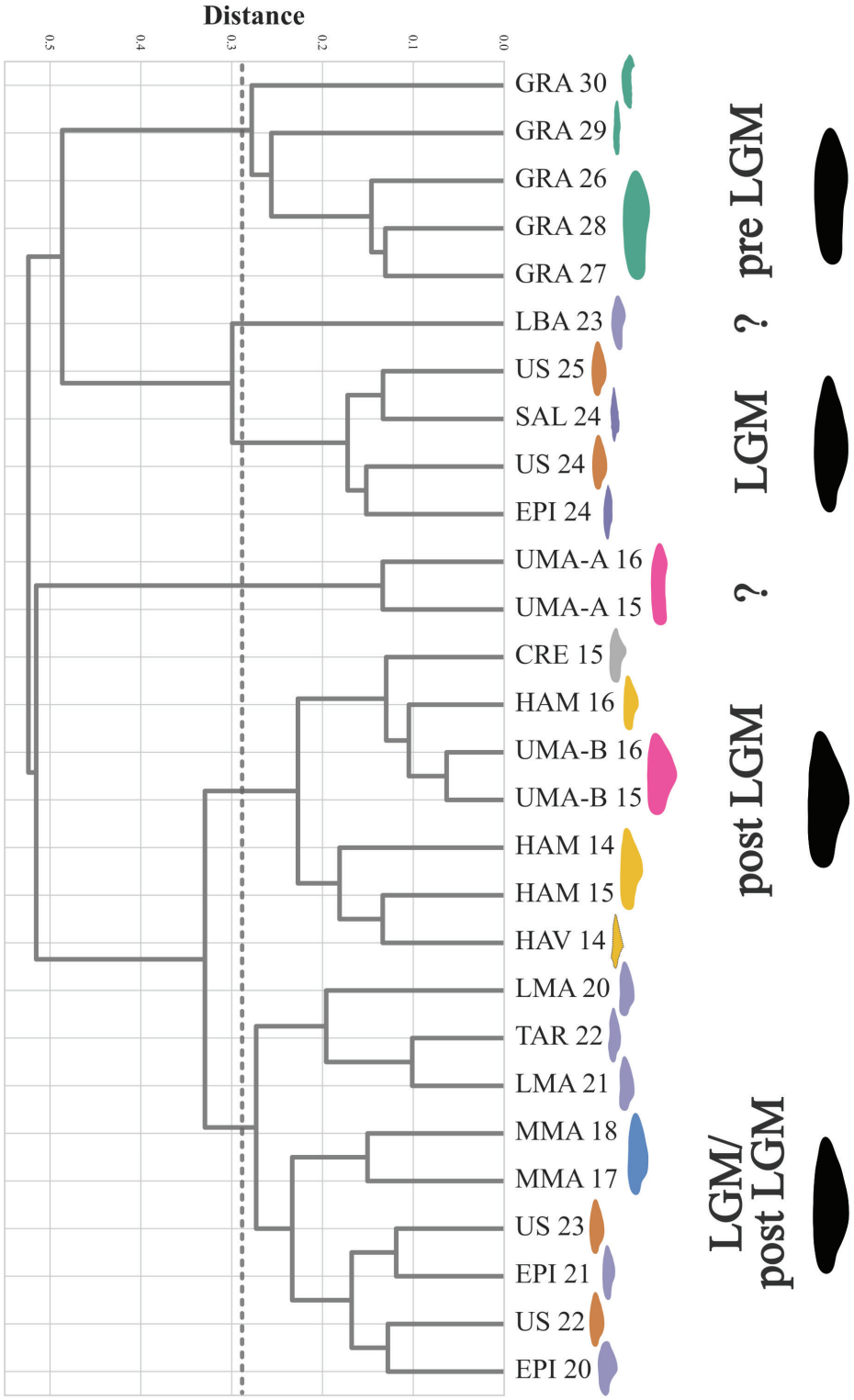



Figure 120: Dendrogram of a time-weighted (t = 0.02) Hierarchical Cluster Analysis (HCA) based on distance matrix of average morphometric features. Cluster: Late Gravettian samples forming a 'pre LGM' cluster; younger LGM samples mixed with post LGM samples; older LGM samples; Late Upper Palaeolithic samples forming a 'post LGM' cluster; non assigned ('?') samples/potential special forms (MP-CM-offsets exluded; dotted line = hierarchical grouping of clusters based on the linkage distance; shapes = meanshapes of the respective unit/cluster; colour-code inferred from the taxonomic units).

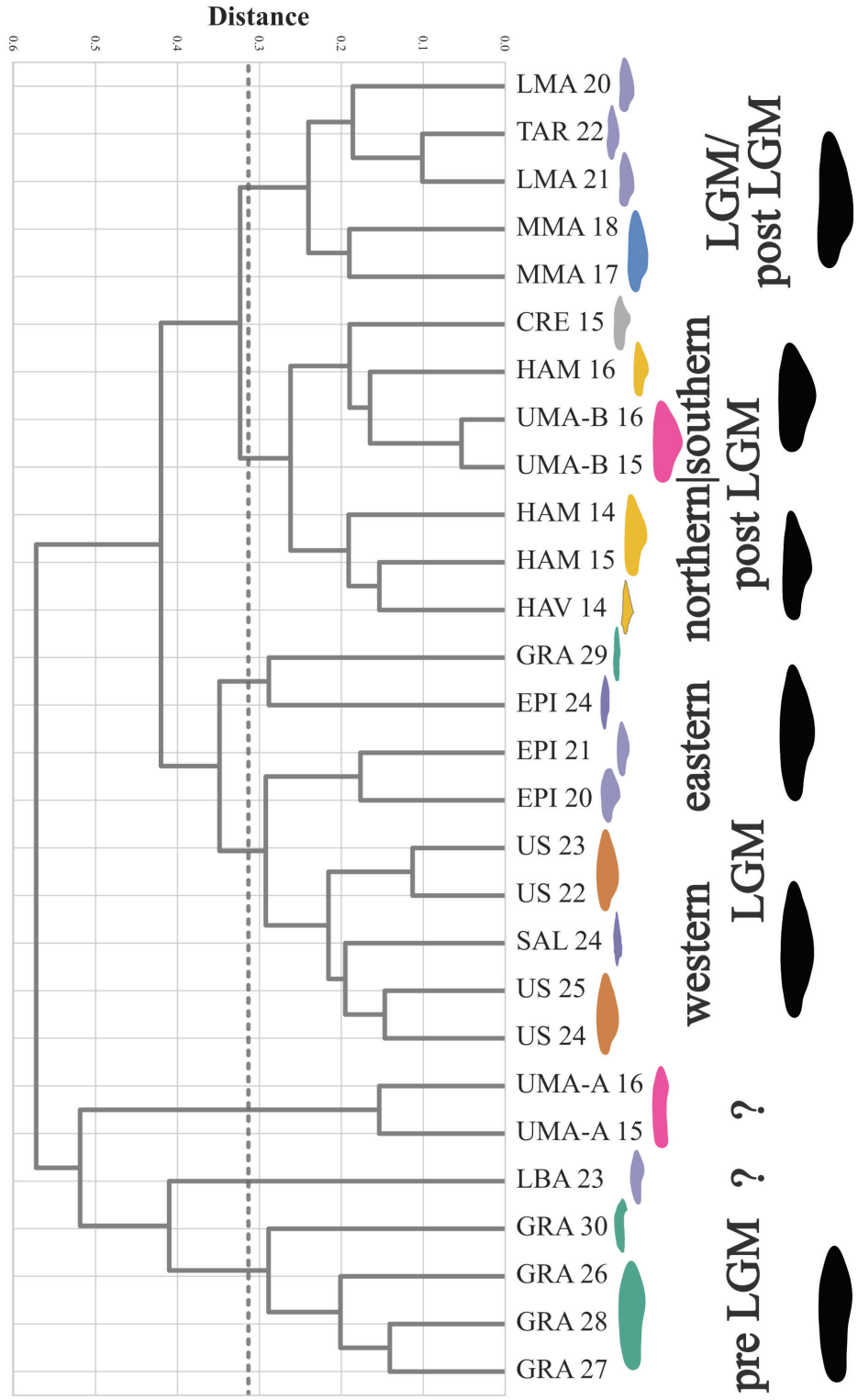



Figure 121: Dendrogram of a time- (t = 0.01) and geographical distance-weighted Hierarchical Cluster Analysis (HCA) based on distance matrix of average morphometric features. Late Gravettian samples forming a 'pre LGM' cluster; younger LGM samples mixed with post LGM samples; older LGM samples subdivided in eastern and western samples; Late Upper Palaeolithic samples forming a 'post LGM' cluster subdivided in northern and southern samples; non assigned ('?') samples/potential special forms (MP-CM-offsets exluded; dotted line = hierarchical grouping of clusters based on the linkage distance; shapes = meanshapes of the respective unit/cluster; colour-code inferred from the taxonomic units).

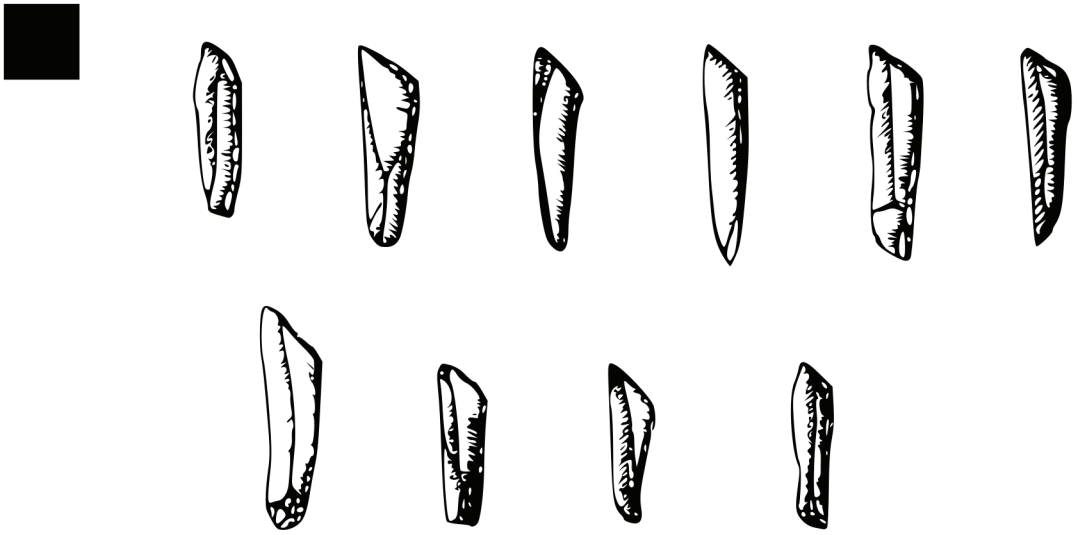


Figure 122: Scalene Bladelets / lamelles scalènes (modified after Langlais 2007 (Soler 1980); reference object = 1x1 cm).

pared to the Late Badegoulian SPs *(Figure 123)*. The latter is highlighted in a much lower centre of mass, indicated by the extreme high change rate for the MP-CM-y-offset. *(Figure 123, Table 63)*

The average change rate between the Upper Magdalenian SPs of the elongated Type A, dating to the 16th millennium BP, and the scalene bladelets ($\bar{x}$ = 1.17) by far exceeds the significance threshold for changes observed between two consecutive millennia (Chapter 4.1.3). This is primarily driven by extreme high change rates in all size-related features *(Table 64)*, indicating that scalene bladelets are substantially smaller than the Upper Magdalenian SPs of the elongated Type A. Additionally, scalene bladelets are slightly stouter, as indicated by the elevated change rate for the l-w-index. The extremely high value for the left-right-ratio once again underscores their pronounced asymmetry *(Figure 124)*. However, this is not accompanied by a corresponding shift in the centre of mass. The notably obtuse tip angle of the scalene bladelets also stands out. Interestingly, the upper-lower-ratio is virtually identical between the scalene bladelets and the elongated Type A Upper Magdalenian SPs *(Figure 124)*, suggesting comparable proportions between the hafting and transformative parts. *(Figure 124, Table 64)*

The average change rate between the Hamburgian SPs of the 15th millennium BP and the scalene bladelets ($\bar{x}$ = 1.08) by far exceeds the significance threshold for changes observed between two consecutive millennia (Chapter 4.1.3). This is not only driven by extremely high change rates across all size-related features *(Table 65)*, which indicate that scalene bladelets are substantially smaller than the Hamburgian SPs, but also by a remarkably high change rate for the upper-lower-ratio. This suggests pronounced differences in shape composition, with scalene bladelets exhibiting a relatively much longer hafting part, in contrast to the Hamburgian SPs, which tend to have a ratio slightly favouring a relatively longer transformative part *(Figure 125)*. *(Figure 125, Table 65)*

These results suggest a close morphological relationship between Late Badegoulian SPs and scalene bladelets. Although substantial size differences were identified between the elongated Upper Magdalenian SPs of Type A and the scalene bladelets, both align closely in the relative proportions of the hafting and transformative parts. However, notable differences in y-axis symmetry distinguish scalene bladelets from both SP representatives, indicating that the bladelets are significantly more asymmetric. In contrast, no close relationship to Hamburgian SPs – used here as a represen-




Figure 123: Meanshapes of A) Late Badegoulian SPs from Le Cuzoul de Vers, layers 21–16, and B) scalene bladelets.

Table 63: Rates of change between the scalene bladelets and the Late Badegoulian SPs from Le Cuzoul de Vers, layer 21–16 .

| width | length | area | l–w–index | upper–lower–ratio | left–right–ratio | tip angle | MP–CM–x–offset | MP–CM–y–offset | x̄ |
|---|---|---|---|---|---|---|---|---|---|
| **–0.24** | **–0.24** | **–0.30** | –0.05 | **–0.38** | **–0.54** | **0.48** | *–0.09* | ***–1.9!*** | **0.32** |

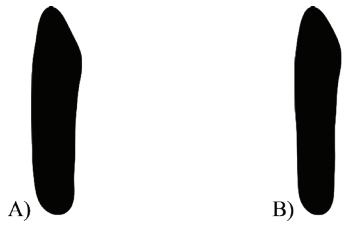



Figure 124: Meanshapes of A) Upper Magdalenian SPs of the elongated Type A, dating to the 16th millennium BP, and B) scalene bladelets.

Table 64: Rates of change between the scalene bladelets and the Upper Magdalenian SPs of Type A of the 16th millennium BP.

| width | length | area | l–w–index | upper–lower–ratio | left–right–ratio | tip angle | MP–CM–x–offset | MP–CM–y–offset | x̄ |
|---|---|---|---|---|---|---|---|---|---|
| **0.81** | **1.28!** | **3.13!** | **0.27** | 0.15 | **2.25!** | **–0.31** | *0.17* | ***0.29*** | **1.17!** |

Signs/Marks: x̄ = averages of the absolute values for change rates; bold = value exceeding the respective specific average change rate in Chapter 4.1.3; faint = value below the respective average change rate in Chapter 4.1.3; italic = extreme values excluded from the calculation of the averages; ! = value exceeding the respective significance threshold from Chapter 4.1.3.




Figure 125: Meanshapes of A) Hamburgian SPs, dating to the 15th millennium BP, and B) scalene bladelets.

Table 65: Rates of change between the scalene bladelets and the Hamburgian SPs of the 15th millennium BP ($\bar{x}$ = averages of the absolute values for change rates; bold = value exceeding the respective specific average change rate in Chapter 4.1.3; faint = value below the respective average change rate in Chapter 4.1.3; italic = extreme values excluded from the calculation of the averages; ! = value exceeding the respective significance threshold from Chapter 4.1.3).

| width | length | area | l-w-index | upper-lower-ratio | left-right-ratio | tip angle | MP-CM-x-offset | MP-CM-y-offset | $\bar{x}$ |
|---|---|---|---|---|---|---|---|---|---|
| **1.0!** | **0.94!** | **2.29!** | -0.02 | **2.46!** | **0.42** | **-0.45** | ***0.53*** | ***0.63*** | **1.08!** |

Figure 126 (next page): Comparison of width, length, the upper-lower-ratio, and the left-right-ratio between the Late Badegoulian SPs from Le Cuzoul de Vers, layer 21-16, scalene bladelets (grey, second from left), Upper Magdalenian SPs of Type A of the 16th millennium BP (pink, third from left), and Hamburgian SPs of the 15th millennium BP (yellow, right) (upper plot = width; second plot = length; third plot = upper-lower-ratio; lower plot = left-right-ratio; violet, left box = Late Badegoulian SPs; grey, second box = scalene bladelets; pink, third box = Upper Magdalenian SPs of Type A; yellow, right box = Hamburgian SPs; outliers excluded).

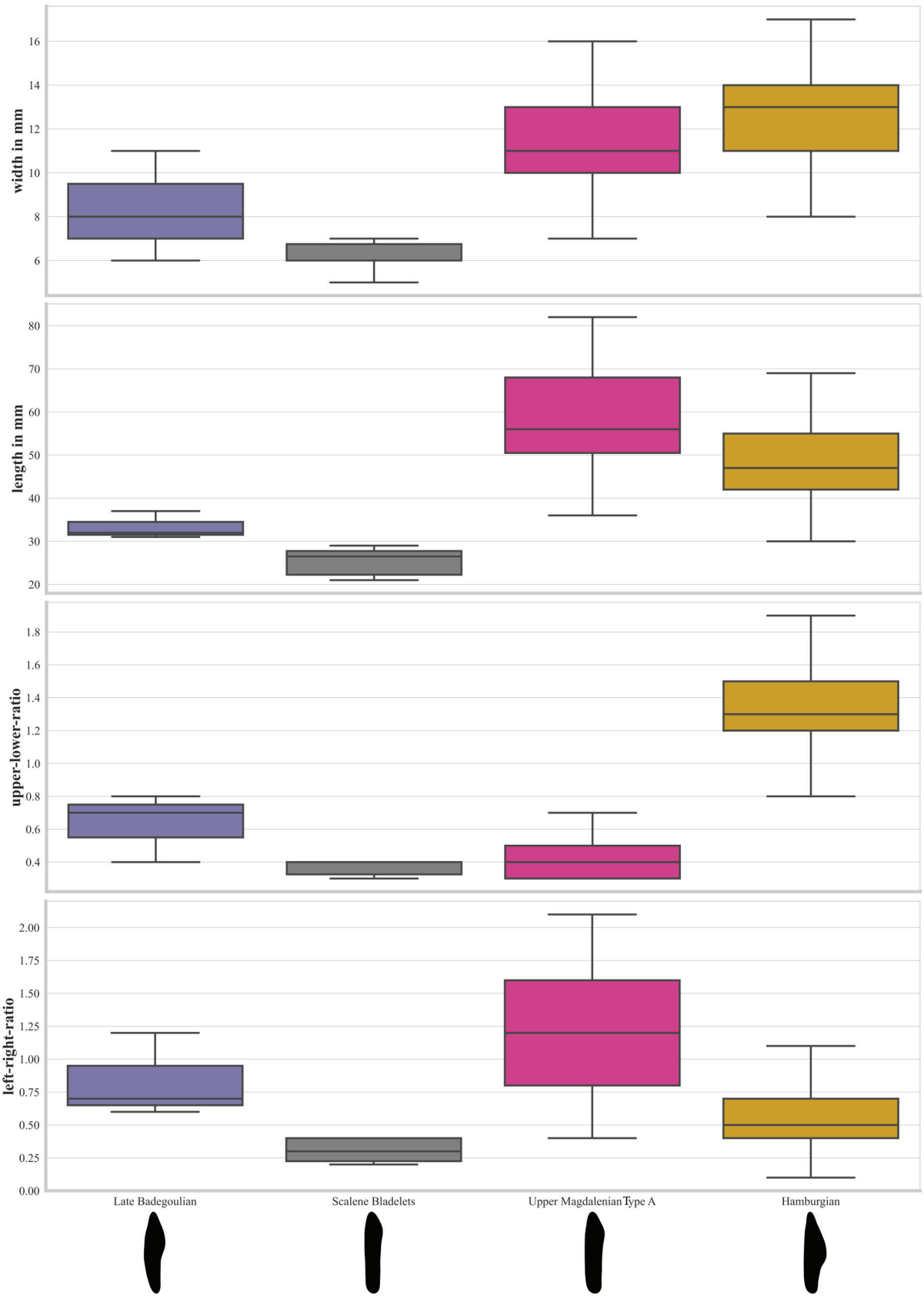



Fig. 126,
explanation on previous page.

## 5. DISCUSSION

The results of the RDA from the chronologically informed perspective are partially supported by those obtained from the archaeo-stratigraphically informed perspective. The significant findings for the period between the 27th and 24th millennium BP align with notable results in the youngest section of the Late Gravettian (27th–26th millennium BP) and the oldest two sections of the Upper Solutrean (26th–25th and 25th–24th millennium BP). This emphasises the presence of strong chronologically directed changes occurring independently within these two taxonomic units during this period. The significant results for the sections from the 22nd to the 21st and from the 21st to the 20th millennium BP are somewhat less directly supported by the results on the archaeo-stratigraphically informed perspective. However, pronounced chronologically directed changes are observed in the non-Solutrean LGM industries, dating between the 24th and the 20th millennium BP, likely underlying the signals detected in the chronologically informed perspective. When analysing the youngest three sections of the dataset within the respective taxonomic units with sufficient sample sizes, the significant results identified in the chronologically informed perspective for the sections from the 17th to the 16th and from the 16th to the 15th millennium BP cannot be supported. This discrepancy is most likely attributable to the influence of assemblages belonging to minor taxonomic units within the strictly chronological framework, such as the Epigravettian assemblage from Riparo Tagliente, layer 15 (A-22), and the Tardigravettian assemblage from Abri du Rouet, layer 9b (A-10). Additionally, the overlap between slightly older Upper/Late–Final Magdalenian and slightly younger Hamburgian assemblages may contribute to the lack of consistent signals.

Regarding morphometric variation, the results from the chronologically informed and archaeo-stratigraphically informed perspectives align well. The Late Gravettian begins with high variation, which gradually declines until its end in the 26th millennium BP. However, the chronologically informed perspective indicates exceptionally high variation for the section from the 27th to the 26th millennium BP. This is a first suggestion of the pronounced differences in the morphometry of SPs between the chronologically overlapping taxonomic units of the Late Gravettian and the Upper Solutrean. Variation in the Upper Solutrean begins at a high level for the older two sections (26th–25th and 25th–24th) and declines rapidly over the youngest two sections (24th–23rd and 23rd–22nd millennium BP). However, while the CV for the section from the 26th to the 25th millennium BP within the Upper Solutrean is relatively high, it remains significantly lower than the CV for the same section in the chronologically informed perspective. This again suggests major differences between the SPs of the Late Gravettian and the Upper Solutrean. The high value for the section from the 25th to the 24th millennium BP seen in both, the chronologically informed and the archaeo-stratigraphically informed perspective, is most likely driven by pronounced differences between the SPs of the Iberian and the French Upper Solutrean. The pattern of the subsequent decrease aligns well between both perspectives. Notably, the period between the 24th and 20th millennium BP stands out due to its low variation coefficients, despite the dataset for this period being aggregated from multiple taxonomic units – an observation that seems counterintuitive. The elevated variation calculated for the section from the 17th to the 16th millennium BP in the chronologically informed perspective can on the one hand be explained by the occurrence of two morphologically distinct SPs types within the Upper/Late–Final Magdalenian and on the other by the pronounced differences between the Middle and the Upper/Late–Final Magdalenian SPs of the elongated Type A. Additionally, although the sample size for this period is substantial, the variation within the youngest section is particularly low. The archaeo-stratigraphically informed perspective suggests that this is likely due to a high level of standardisation within the Hamburgian.

The comparison of change rates reveals several pronounced differences. For the first three sections (30th–29th, 29th–28th, and 28th–27th millennium BP), the results align, as the Late Gravettian is the only taxonomic unit yielding SPs during this period. The first divergence occurs in the section from the 27th to the 26th millennium BP. In the archaeo-stratigraphically informed perspective, this section returns very low values for the Late Gravettian, whereas the chronologically informed perspective calculates a peak value nearly twice as high.

This provides further evidence of the significant differences between the SPs of the Late Gravettian and the Upper Solutrean, which drive the change rate in this period (see Chapter 4.2.2.2.1). Probably due to the influence of assemblages from other taxonomic units, the change rate for the section from the 25th to the 24th millennium BP is slightly higher in the chronologically informed perspective than in the archaeo-stratigraphically informed perspective for the Upper Solutrean. In contrast, in the subsequent section (24th–23rd millennium BP), the change rate in the chronologically informed perspective is lower than in the archaeo-stratigraphically informed perspective for the Upper Solutrean. This suggests that the higher rate of change in the Upper Solutrean during this period is masked by the lower rate of change within the non-Solutrean LGM industries. For the section from the 23rd to the 22nd millennium BP, the results from both perspectives align once again. Unfortunately, for the period between the 22nd and the 17th millennium BP, no taxonomic unit provides a sufficient sample size for comparison. However, the low change rate observed for the section from the 16th to the 15th millennium BP is supported by an even lower change rate calculated for within the Upper/Late–Final Magdalenian assemblages.

The transitions between the major taxonomic units add to the patterns observed earlier. As previously suggested, the change rates – and consequently, the differences – between the latest Gravettian and the earliest Upper Solutrean SPs are substantial, explaining the high change rates in the chronologically informed perspective for the sections from the 27th to the 26th and from the 26th to the 25th millennium BP. Despite the pronounced differences calculated between the Late Badegoulian assemblage from Cuzoul de Vers and the other LGM industries, as well as some elevated signals for the Lower Magdalenian SPs, the overall low change rates observed between the 24th and 20th millennium BP are well reflected. The elevated change rate observed for the section form the 17th to the 16th millennium BP can be supported by the pronounced differences between Middle and Upper/Late–Final Magdalenian SPs of the elongated Type A. Finally, the change rate between the Type A SPs of the Upper/Late–Final Magdalenian and the Hamburgian assemblages probably accounts for the elevated change rates for the section from the 16th to the 15th millennium BP in the chronologically informed perspective, while change rates between Type B SPs of the Upper/Late–Final Magdalenian and the Hamburgian SPs are comparably low, suggesting a level of morphometrical continuity.

The cluster analysis, both in the unconstrained as well as the chronologically and geographically constrained approaches, well represented the marked dichotomy between the Late Gravettian and Upper Solutrean SPs (here only the Iberian), highlighting an apparent lack of morphological continuity between these two taxonomic units. The cluster analyses also suggest that the LGM phase may be divisible into two distinct morphometric clusters: an older one, primarily associated with early Upper Solutrean forms, and a younger one linked to Lower Magdalenian and Tardigravettian SPs. However, the continuity between these two clusters remains questionable. The developmental shift observed for the Upper Solutrean is reflected as earlier specimens tend to cluster within the older LGM group, while later specimens show affinities with the younger LGM cluster. Similarly, the Epigravettian does not emerge as a coherent unit, instead displaying a distribution pattern comparable to that of the Upper Solutrean. The younger LGM cluster appears to be more closely linked to Middle Magdalenian forms, which themselves show strong affinities to Upper Magdalenian SPs of Type B. These Type B forms, in turn, cluster closely with Hamburgian and Creswellian SPs. By contrast, both the Late Badegoulian SPs and the Upper Magdalenian SPs of Type A tend to cluster in isolation, underlining their distinct morphologies.

The results of this study enable the discussion of two main topics: first, the general evolutionary dynamics of SPs and the reasons underlying their patterns of variation and change; and second, the ancestral history of SPs, covering hypothesis on how SPs could be related. While the chronologically and the archaeo-stratigraphic informed perspectives initially presented separate results, Chapter 4.4 demonstrated that they are, in fact, complementary. Some dynamics observed from the chronologically informed perspective could be further clarified – or even explained – by incorporating archaeo-stratigraphic information.

## 5.1 EVOLUTIONARY DYNAMICS

The results of this study so far revealed dynamics of variation and distinct trajectories of variation and change through time, which are difficult to capture using typological approaches and can not be quantified by them. It was observed that morphometric variation in SPs repeatedly decreases over time in a kind of cyclical pattern at different scales. This trend is most evident within the larger taxonomic units – particularly the Late Gravettian and the Upper Solutrean – but can also be inferred for the entire observed timeframe, if the elevated variation associated with the disparity between the French and the Iberian Upper Solutrean SPs as well as the emergence of elongated Upper Magdalenian SPs are set aside. Interestingly, the observed pattern of gradually decreasing variation following the introduction of SPs into new geographical and taxonomical contexts aligns notably with what Rosa (1903) termed the 'law of progressive reduction in variability' for biological species. He argued that, over the course of a lineage's evolution, characteristics become more constant and more organised, leading to a decrease in variability. As a result, further change becomes progressively constrained by the reduction of developmental possibilities. In biological species, this pattern is largely explained by Dollo's Law of Irreversibility (Dollo 1893), which posits that evolution cannot revert to earlier states. This principle, however, does not apply straightforwardly to human material culture, as, for instance, fashion trends tend to periodically reappear over time. Nevertheless, a clear reversion to the SP forms characteristic of the earliest SPs is not observable. The observed pattern instead appears to reflect repeated processes of introduction to new geo-taxonomic contexts accompanied by what probably can be translated to experimentation, followed by refinement and, ultimately, maintenance of desired features.

Cultural transmission is thought to exert a strong influence on this through 'morphological norms' governing how SPs are produced within a given geo-taxonomic context. Although individual knappers may refine existing characteristics once SPs have been introduced into their social milieu, they are highly likely to continue producing SPs that adhere to the prevailing major characteristics – a tendency known as 'conformist *bias*' (Acerbi & Bentley 2014). It is therefore unlikely that they would reproduce forms resembling morphological states from several millennia earlier, which they have never encountered. However, changes in individual production techniques, skill transmission, social hierarchy, or greater individual specialisation can also result in patterns of increased standardisation (Roux 2003 and 2015). Such a discussion, however, necessitates a broader discussion of demographic and social structures, the former of which will be conducted in Chapter 5.1.3 and the latter which will only be touched in Chapter 5.2.4 but otherwise goes beyond the scope of this study.

While considerable variation exists in the amount of change between successive millennia, the average morphometric change of SPs from one millennium to the next is calculated at 17% when viewed from a purely chronological perspective. Given the physiological limits of human perceptual discrimination (Coren 1994), it is initially questionable how perceptible these amounts of change over time actually are. In two-dimensional length discrimination, the human eye can reliably detect differences in length within a range of approximately 1–3%, known as the "Just Noticeable Difference" or "Weber fraction" (Fechner 1889, 211–217). In three-dimensional contexts, studies have shown that differences in length are typically detected at thresholds between 11.1% and 14.6% (Norman et al. 1996). Therefore, the observed average change rate of 17% exceeds both perceptual thresholds, suggesting that the diachronic changes in SP morphometry – especially those occurring between the 27$^{th}$ and 24$^{th}$ millennium BP as well as between the 17$^{th}$ and 16$^{th}$ millennium BP – were likely perceptible and thereby potentially functionally relevant. In contrast, the comparatively low change rates calculated for the period from the 16$^{th}$ to the 14$^{th}$ millennium BP, which were also supported by the archaeo-stratigraphically informed perspective, likely fall below perceptual thresholds, implying that these changes were probably functionally negligible and might have been the result of stochastic variation, potentially induced by minute copying/transmission errors (Eerkens & Lipo 2005) or altering raw material quality, and drift rather than deliberate morphological development.

Taken together, the results demonstrate that diachronic morphometric variation in SPs cannot be adequately captured by a model of

steady, linear change. Rather, the evidence indicates a dynamic evolutionary pattern, in which periods of stochastic variation or even stasis are interspersed by abrupt episodes of directed morphological change indicative of selective pressure. This pattern is characteristic of a punctuated mode of evolution (Eldredge 1971; Eldredge & Gould 1972). However, as these bursts of directed change are not evident across all features simultaneously – although some clearly do coincide – the results are consistent with the concept of 'mosaic change' (Martin & Barnosky 1993).

Episodes of rapid morphological change coincide with taxonomic transitions and the associated emergence of innovative morphological traits. Three such bursts are evident from a chronologically informed perspective and are further supported by archaeo-stratigraphic evidence: the transition from the Late Gravettian to the Upper Solutrean; the shift from older to younger LGM samples – particularly associated with the emergence of the Magdalenian; and the development of elongated Upper/Late Magdalenian SPs, contrasting with the stouter variants of the Middle and Upper Magdalenian. Notably, the burst of change linked to the Late Gravettian–Upper Solutrean transition is not solely driven by this dissimilarity. Rather, it appears to have begun during the terminal phase of the Late Gravettian and continued into the Upper Solutrean. While the latter is clearly defined by the distinctive morphology of French Upper Solutrean SPs absent in the subsequent millennia, no equally clear typological distinction can be identified for the Late Gravettian.

Phases of stochastic variation are most evident during the early millennia of the Late Gravettian (30$^{th}$–28$^{th}$ millennium BP), as indicated by the absence of chronologically directed change alongside elevated variation. The high rates of observed change are clearly associated with the distinctive morphology of the Mito Malu-Galben SPs, which dominate the 29$^{th}$ millennium BP and most likely reflect a highly regional and short-lived invention.

Two phases produced results indicative of apparent stasis, characterised by low variation and change rates combined with an absence of chronologically directed change. These periods encompass the interval between the 24$^{th}$ and the 22$^{nd}$ millennium BP, spanning both the later phase of the Upper Solutrean and the non-Solutrean LGM industries, as well as the Late Upper Palaeolithic (16$^{th}$–14$^{th}$ millennium BP) following the transition from the Middle to the Upper/Late Magdalenian in the section from the 17$^{th}$ to the 16$^{th}$ millennium BP. The section covering the 16$^{th}$ and the 15$^{th}$ millennium BP may represent an exception, as it yielded a statistically significant – albeit comparatively weak – result in the RDA, suggesting minor chronologically directed changes. However, since this outcome is most likely attributable to the absence of elongated SPs in the 15$^{th}$ millennium BP (see Chapter 4.2.2.4.2), the apparent significance should be treated with caution.

When selective pressure is intense, traits under pressure are expected to exhibit directional, non-stochastic trends or remain stable. In contrast, weak selective pressure allows traits to evolve in a more random manner, producing little to no clear directional patterns. Therefore, shifts in the trend dynamics of morphological traits can serve as indicators of changes in selective pressure (Dunnelll 1978a; Neiman 1995; Rogers & Ehrlich 2008; Brantingham & Perrault 2010; Creanza et al. 2017).

It is crucial to note that selection here should not be mistaken for personal decision-making or deliberate choice. Instead, it refers to a macroevolutionary process, in which competing variants, differing in effectiveness, are subjected to selective pressures, which results in unequal transmission and persistence of these variants within a group across successive generations (e.g., O'Brien & Lyman 2000).

The calculation of feature-specific correlations with the passage of time (Chapter 4.1.3.1, Table 11) provides insights into the dynamics of trends within individual features. Millennia with higher counts of significant correlations correspond closely to the RDA-significant millennia (Chapter 4.1.1.4.2, *Figure 19*), outlining a pattern of alternating intensity of selective forces. The first three millennia yield little evidence for directed change in morphometric features, while variation within them is notably high. Thus, features appear to behave in a largely random manner – at least not chronologically driven, though possibly influenced by regional traditions. Selective pressure during this period was likely comparatively weak at the target scale of this study.

Between the 27$^{th}$ and the 24$^{th}$ millennium BP, however, the evidence for chronologically directed change is striking. This pattern, not solely driven by the dissimilarity between

the taxonomic units, is indicated by high RDA values and an elevated number of significant correlations among individual morphometric features. It therefore seems that selective pressure was relatively strong during the terminal Late Gravettian and into the Upper Solutrean, acting strong on shape-related features, or that the Upper Solutren specimens represent an independent and morphologically different invention causing the peak in change observed (see Chapter 5.2.1).

Subsequently, between the 24th and the 22nd millennium BP, chronologically directed change appears absent, as reflected by low and non-significant RDA values and the lack of significant correlations of individual features with the ongoing of time as well as the low change rates. In addition, variation is notably reduced during this period, suggesting that selective forces were acting to maintain established morphological characteristics.

From the 22nd to the 21st millennium BP, selective pressure again seems to force change into a specfifc direction, though limited to a single feature – the upper-lower-ratio. In the following millennia, another interval of intensified selective pressure is indicated by the RDA results and by multiple significant correlations across morphometric features.

After the two poorly represented millennia (19th and 18th), for which no results could be calculated, another peak of chronologically directed change is suggested by the RDA and several significantly correlated features, which, however, marks a phase of two competing types – the elongated and the stout SP type. After the disappearance of the elongated type and the "survival" of the apparently fitter stouter type, selective pressure again acted to maintain overarching characteristics of this type during the most recent two millennia.

### 5.1.1 What is Changing?

It was shown that throughout the entire period – despite some exceptions – shape-related features underwent more frequent and pronounced changes than size-related features allowing inferences on the blanks on which the points were made (see Chapter 3.2.2). Thus, shape-related features provide the chronologically most sensitive information on the morphometry of SPs.

The general trends in the morphometry of the SPs across the entire observed timeframe can be summarised as follows. At the beginning of the observed timeframe, during the Late Gravettian, SPs tend to be largely y-axis symmetric, resulting in an even ratio between what is termed here the primary and secondary cutting edges within the transformative part – even though these edges may bear retouches and therefore do not necessarily possess cutting properties. Thereafter, SPs follow a general trend towards more asymmetry until around the 22nd millennium BP, after which they remain predominantly asymmetric for the rest of the observed timeframe *(Figure 42)*. This reduces the prominence of the primary cutting edge within the transformative part and thereby increases the relative importance of the secondary cutting edge. It is important to stress that by 'importance' it is solely referred to the proportional contribution to the composition of the tip, without implying any enhanced functional role in penetration.

Furthermore, after the Late Gravettian, SPs with an approximately balanced ratio between hafting and transformative parts reappear only at the very end of the observed timeframe. The absolute length of the transformative part and thus the cutting edges, however, appears less affected *(Figure 127)*. Also, length does not follow a directed long-term trend *(Figure 41)*. Consequently, after the Late Gravettian, the dominant SP form is characterised by relatively long transformative parts. This suggests that the available edges on the blanks were more intensively utilised as functional cutting edges for the projectile points, while the overall dimensions of the penetrating transformative part remained unchanged. At the end of the observed timeframe – within Upper Magdalenian, Hamburgian and Creswellian contexts – the relative length of the transformative parts slightly decreases again. Nonetheless, between the 24th and the 21st millennium BP, a distinct trend towards longer SPs with correspondingly longer cutting edges is observable – although this is not observable in the datasets for the Upper Solutrean and the non-Solutrean LGM industries. In light of this, it can be argued that while no strong selective pressure appears to have acted on increasing the size of the penetrating part of the projectile point – in other words, on producing larger tips – selective forces did act on the exploitation of blank

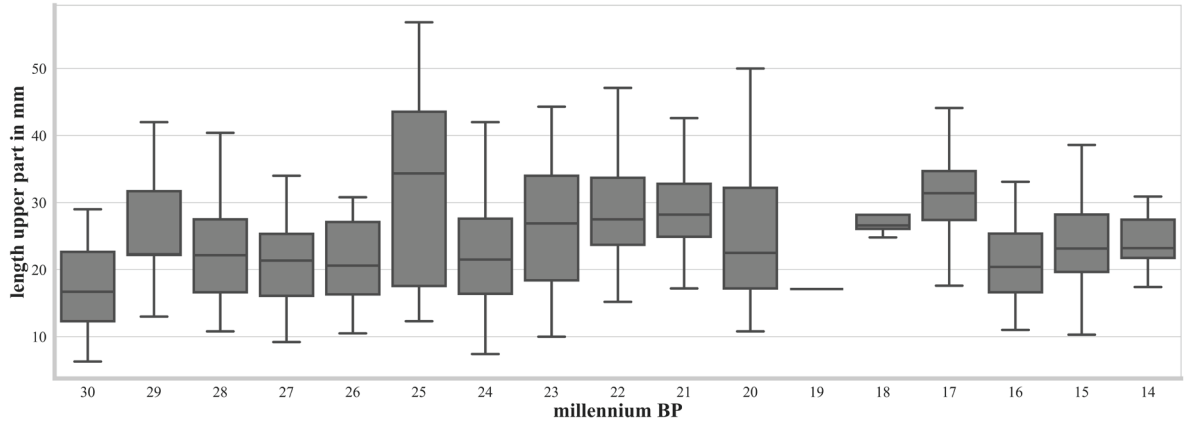



Figure 127: Absolute length of the transformative (upper) part across the millennia (in mm).

dimensions in favour of the penetrating part to maximise the penetrating functionality of the resulting points. This trend, however, appears to be somewhat inverted in the Upper Magdalenian, Hamburgian, and Creswellian – an observation that may be explained by differences in production and hafting techniques (see below). *(Figure 127)*

Importantly, discussions of evolutionary trends must grapple with the challenge of the distinction between variation that arises due to differences in functional roles and that which results from competing design alternatives serving the same function (Dunell 1978b). This distinction bears heavily on evolutionary interpretation. According to Mesoudi et al. (2004), when multiple functionally equivalent variants in material culture coexist, selection tends to favour those with superior performance or adaptability, leading to the gradual decline or extinction of less advantageous alternatives, mirroring what Darwin found for biological terms. This dynamic underscores the importance of understanding the functional context of artefact variation when reconstructing evolutionary pathways. However, gaining such understanding requires detailed insights into how these artefacts were used in practice – insights that are discussed here but clearly go beyond the scope of the present study. Approaches such as use-wear analysis and experimental archaeology may provide the necessary data to explore these functional aspects more thoroughly in future research.

Changes in size, symmetry and the length of the hafting part may reflect shifts in hafting techniques. Hafting propositions, however, cannot be derived from morphometrics alone. Rather, they depend largely on technological information, particularly the position and character of retouch as well as on use-wear analysis (e.g. Rots 2016). Accordingly, different hafting techniques have been suggested for distinct SP subtypes. Muñoz Ibáñez et al. (2017, 50), for example, identified three probable hafting methods for Upper Solutrean SPs, which frequently exhibit abruptly retouched straight backs, that best replicated the use-wear observed on archaeological specimens while also performing effectively in penetration tests: a) hafting at the distal end with the notch facing inward, b) hafting at the distal end with the notch facing outward – a method as well proposed by Beckhoff (1967) for Hamburgian SPs – and c) (pairwise/partially) lateral hafting with the notch facing outward *(Figure 127)*. The latter, in turn, is only viable for SPs with abruptly retouched primary cutting edges, respectively backs, which would provide surface to be inserted in the shaft. Proposition b) however, is thought to be not practical. Weber (2009) state that positioning the projectile outside of the longitudinal axis of the projectile is a disadvantage, and parts of the point laterally protruding the shaft "creates a circular motion around the axis of the projectile during flight and thus reduces the precision of the shot" (ibid., 40). Another proposition, specifically suggested for hating the asymmetric Ham-

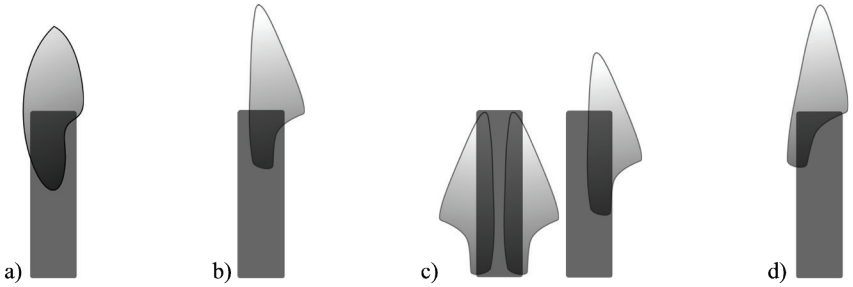



Figure 128: Schematic illustration of hafting propositions for symmetric (a = after Plisson & Geneste 1989, 91, Fig. 21) and asymmetric SPs (b = after Beckhoff 1967 and Muñoz Ibáñez et al. 2017, 48–49, Fig. 2, 6; c = after Muñoz Ibáñez et al. 2017, 48–49, Fig. 2, 4a and 5a; d = after Lund 1993, 408, Fig. 3).

burgian and SPs, which are largely produced by a steep truncation forming what is here called the secondary cutting edge, ensuring effective force transmission along the central axis of the projectile and that sharp edges make first contact with the prey instead of blunt retouched parts has been proposed by Lund (1993). In this, the point is hafted at a slight angle with the notch facing inward, thereby realigning the tip with the centre of the shaft *(Figure 128, d)*. *(Figure 128)*

Since this study focusses on metrical rather than retouch features, it provides limited insights into hafting techniques. Nevertheless, some implications derived from the morphometric results can be discussed here as different hafting techniques require distinct morphological preconditions. Hafting a SP latero-frontally at the distal end of a shaft with the notch facing inward (a) demands the point to be largely y-axis symmetric to ensure that the tip aligns with the centre of the shaft, enabling maximum force transmission, while it could accommodate SPs with longer hafting parts. On the contrary, hafting SPs (pairwise) laterally with the notch facing outward (c), while it has no particular demands on hafting part lengths, is only viable with more or less straight backed asymmetric SPs. SPs with longer hafting parts would probably also not be suited to be hafted in the way suggested for the Hamgurgian SPs (d), as the long hafting part would protrude far outside the projectile and the tip would hardly align with the centre of the shaft. While a latero-frontally hafting mode could accommodate larger SPs, laterally hafting – at least pairwise – is restricted to smaller specimens Muñoz Ibáñez et al. (2017, 51).

The abrupt shift in the importance of the hafting part – from the Late Gravettian SPs with comparatively long hafting parts to post-Gravettian SPs with relatively short hafting parts – implies, without regarding for retouches, a radical shift in hafting technique, that could have proceeded as follows: during the Late Gravettian, SPs were largely hafted latero-frontally at the distal end with the notch facing inward (a); in Upper Solutrean contexts – especially on the Iberian Peninsula – where SPs frequently show steep retouches on comparably straight primary cutting edges respectively backs, a lateral hafting with the notch facing outwards is most probable, aligning the tip with the centre of the shaft *(Figure 128, c)*. Some specimens with unretouched cutting edges and slightly more symmetric shapes might as well have been hafted latero-frontally. Apart from the Upper Solutrean SPs, however, abrupt retouch along the primary cutting edge is uncommon during the LGM and thereafter, making lateral hafting an unlikely option for most non-Solutrean SPs. Thus, latero-frontal hafting is expected to have been the dominant mode of attachment until the disappearance of SPs from the archaeological record.

An elongated transformative part – and thus an extended penetrating part – would provide a longer cutting surface, potentially enhancing penetration depth. A long, proximally protruding tip would, however, be subject to considerable mechanical stress and is more prone to breakage upon impact or bending than the shorter, more robust tips characteristic of Late Gravettian SPs. While the SPs of the Late Gravettian might had a tendency to break below or close to the widest part, the SPs with rel-

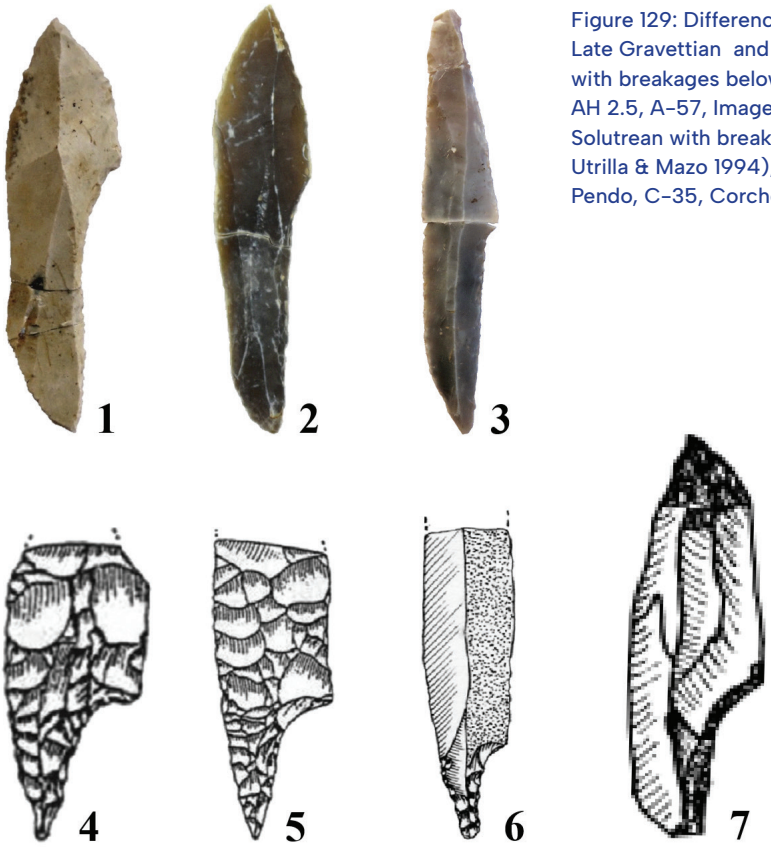



Figure 129: Differences in likely position of breakage between Late Gravettian and Upper Solutrean SPs. Late Gravettian SPs with breakages below shoulder (1–3: from Bistricioara-Lutărie III, AH 2.5, A-57, Images kindly prov. by Anghelinu & Niţă); Upper Solutrean with breakages above shoulder (4–6: Abauntz, A-49, Utrilla & Mazo 1994); 7: reworked tip on Upper Solutrean SP (El Pendo, C-35, Corchon 1971). Images not scaled.

atively longer transformative parts might show more breakages above the widest part *(Figure 129)*, due to shifted leverage forces. Breakages of the transformative part might have been fixed more easily by overworking than a broken hafting part, giving this SP design further practical advantages. Hypothesis on performance and durability advanteges, however, require verification, as previous studies have reported notable frequencies of fragmented hafting parts in contexts containing SPs with short hafting parts (Boccaccio 2021). Such an investigation, however, lies beyond the scope of the present study, but is planned to be conducted soon.

Some of the early SPs (30$^{th}$, 28$^{th}$, 27$^{th}$, 26$^{th}$ millennium BP), associated with the Late Gravettian, and some SPs of the 17$^{th}$ millennium BP – the Upper Magdalenian SPs of the elongated Type A, frequently exhibit tip angles exceeding a functional viable tip angle of 55°, suggested by Beckhoff (1966). Almost all SPs in the dataset however align with findings from other case studies ($\bar{x}$ = 51°; excluding Late Gravettian SPs and Upper Magdalenian SPs of Type A: $\bar{x}$ = 47°). Sahle & Brooks (2019), for example, report tip angles ranging between 53° and 64° in Late Pleistocene point assemblages from Ethiopia – values that overlap with those observed in projectiles from the French Upper Palaeolithic (Peterkin 1993). Dev and Riede (2012) identified a mean tip angle of 39° for *Late Palaeolithic* projectiles from the Federmesser-Gruppen and Ahrensburgian. The most effective tip angle of 20°–40°, as demonstrated by Friis-Hansen (1990) is met by numerous specimens from various taxonomic units, including the Late Gravettian, the Upper Solutrean, the non-Solutrean LGM industries and the Magdalenian. *(Figure 129)*

The change in tip angle *(Figure 42)* shows a clear trend toward increasingly acute values from the earliest periods onward, which might indicate a selective process acting on penetration properties taking place. They stabilise at comparatively low levels between the 25$^{th}$ and 20$^{th}$ millennium BP – potentially reflecting convergence on an 'optimal' functional

range, balancing penetration effectiveness and robustness. Although a brief resurgence of more obtuse tip angles is observable in the 16th millennium BP – which, again, is linked to the elongated Upper Magdalenian forms, highlighting a phase, where lateral cutting edge gains importance, rather than penetrating tips – tip angles remain consistently low throughout the younger periods as well. In contrast, the development observed in the relative length of the hafting part respectively length of the transformative part likely reflects an intentional decision by the knappers.

Overall, this suggests that changes in the functional design of the points were likely under more selective pressure and thus object to more adaptive change, than those in blank production techniques.

### 5.1.2 Morphometrics and Dynamics in Palaeodemography and Enviromental Conditions

Numerous studies have demonstrated a correlation between population size and density, the level of connectivity among learning individuals, and cultural evolutionary dynamics (e.g., Collard et al. 2013a and 2013b; Deffner et al. 2022; Derex et al. 2013; Derex et al. 2018; Derex & Boyd 2016; Derex & Mesoudi 2020; Edinborough 2009; Grove 2016; Henrich 2004; Kempe & Mesoudi 2014; Kline & Boyd 2010; Lycett & Norton 2010; Powell et al. 2010; Richerson et al. 2009; Shennan 2001; Sterelny 2021; Walker et al. 2021). These studies suggest that larger and more connected populations are more likely to foster and maintain complex cultural traits. However, other research challenges this hypothesis, highlighting alternative drivers such as risks of resource failure (Collard et al. 2005) and the role of social conformity (Nelson et al. 2011). It is, however, broadly excepted that successful cultural transmission and innovations should be more frequently in larger population (e.g., Derex et al. 2013) and well-connected populations will have more diverse and complex tool kits than small, isolated populations (e.g., Kline & Boyd 2010; Kempe & Mesoudi 2014; Sterelny 2021). It is further suggested – although this study has been heavily criticised (Read 2006; Collard et al. 2016) – that demographic bottlenecks or reductions in the effective population of social learners may lead to the loss of complex skills (Henrich 2004). This aligns with broader theoretical and empirical work (e.g., Shennan 2001; Powell et al. 2009), which emphasises that both the quantity and structure of interacting individuals determine a population's capacity to maintain and innovate culturally. Derex & Boyd (2016), Derex et al. (2018) and Derex & Mesoudi (2020), however, demonstrate that high connectivity in populations, while efficient at spreading information and mitigating cultural loss, can also homogenise cultural repertoires, thereby limiting the diversity that fuels innovation. Conversely, fragmented or inefficient networks, especially those with intermittent or weak links, are prone to cultural divergence and loss due to restricted information flow and increased isolation. Together, these findings suggest that neither size nor connectivity alone dictates cultural outcomes. Rather, cultural evolution emerges from a dynamic interplay between demographic factors and network structures, where intermediate levels of connectedness and robust, diverse populations may offer the optimal conditions for long-term cultural complexity.

Maier et al. (2022a) offer quantifiable palaeodemographic estimates for the Upper Palaeolithic of Europe, which serve here as a baseline for discussing the results of this study. Specifically, they provide data on both population size and density (numbers gathered in Figure 130), the latter of which will be used in the following discussion as a proxy for connectivity. This is conducted under the assumption that the more people living in close proximity and that mobility is constantly high throughout the investigated timeframe, the higher the level of interaction and connectedness.

SPs first emerge during what Maier et al. (2022a, 114) describe as a period of "network densification" between 33,000 and 29,000 years calBP. During this phase, population size nearly doubled compared to the preceding period from 43,000 to 33,000 years calBP (Maier & Zimmermann 2017). Alongside an expansion of inhabited areas, population density slightly declined. The distances between core areas – regional clusters that were spatially separated by areas which were only sporadically used or entirely uninhabited (Schmidt & Zimmermann 2019) – however, did not increase and

the overall large-scale network structure was maintained. High connectivity between regions is reflected in striking morphological similarities of female figurines (Gaudzinski-Windheuser & Jöris 2015). However, Baker et al. (2024) demonstrated notable differences in personal ornaments between central-eastern and western Europe during this time, indicating a marked regionaisation. This regionaisation is also evident in differences in osseous and lithic projectile technologies – notably to this study, the absence of SPs in western Europe. The emergence of SPs is part of a pronounced transformation in the lithic projectile point assemblage that marks the onset of the Late Gravettian or 'Willendorf-Kostenkian' (e.g., Svoboda 1996 and 2007), characterised by a replacement of axisymmetric projectile points with non-axisymmetric morphologies (Maier et al. 2021). This shift is accompanied by a slight reduction in projectile point diversity. The results of this study show a high amount variation in the morphometry of the SPs, which likely represents regional traditions. This is also displayed in the elevated change rate for the section from the 30$^{th}$ to the 29$^{th}$ millennium BP, that highlights the distinct morphology of the Mitoc-Malu Galben, layer 4a (Otte et al. 2007) SPs dating to the 29$^{th}$ millennium BP. These distinct SPs may also represent a short-lived innovation made possible by the presence of a sufficiently large and well-connected group of social learners. However, the population may not have been large and/or interconnected enough to sustain this innovation, leading to its eventual loss. Alternatively, it is possible that the innovation proved unsuitable within its technological or environmental context and was therefore abandoned.

The period between 29,000 and 25,000 years calBP is characterised by a decline in both population size and the extend of core areas (Maier et al. 2022a, 115). During this phase, the average population density within core areas decreased, as did the estimated average number of people living simultaneously, likely approaching the threshold of a minimal viable population (Maier & Zimmermann 2017). While core areas north of the Alps disappear from the archaeological record, Maier & Zimmermann (2017) do not interpret this as a southward migration. Instead, they suggest regional population collapses. These demographic declines resulted in the breakdown of the previously extensive large-scale interaction network and its fragmentation into two smaller structures: a western network, which contracted markedly, and an eastern network, referred to as the Willendorf-Kostenkian, which largely maintained its spatial extend. This fragmentation fostered the development of regional idiosyncrasies within each of these smaller networks. Interestingly, this demographic crisis coincides with low diversity and an absence of major changes in lithic and osseous projectile types (Maier et al. 2021). The results of this study highlight the disparity between east and west during the late phase of this period, as evidenced by the pronounced morphological differences between Late Gravettian and Upper Solutrean SPs. This east–west divergence largely accounts for the elevated overall variance observed. However, when the regions are analysed separately, the eastern region exhibits low variance, suggesting the presence of standardisation processes. In contrast, the western region reveals a marked disparity between the French and Iberian sub-regional traditions, reflecting distinct trajectories within the broader western sphere.

The subsequent period between 25,000 and 20,000 years calBP is described by Maier et al. (2022a, 116) as a phase of "network reorganisation". Although this period is marked by pronounced glacial climatic conditions – hence referred to as the Last Glacial Maximum (LGM; Mix et al. 2001) – it is characterised by a significant increase in both population size and the extend of core areas. Population density within these core areas also rises markedly. Notably, however, this demographic growth is observed primarily in Western Europe, whereas population numbers in Central Europe remain low (Maier et al. 2016). This demographic pattern coincides with the continued fragmentation of the large-scale interaction network identified in the preceding period, fostering the development of pronounced regional idiosyncrasies, coupled with contrasting environmental preferences: cool temperate conditions in the West versus colder and drier conditions in the East (Maier et al. 2016). These are exemplified by the emergence of the Upper Solutrean in Iberia and southern France, in contrast to what may be termed Epigravettian traditions – with local variations – north and east of the Alps. Both technocomplexes yield SP. From approximately 23,000 years calBP onward, however,

this separation between the two major networks may have begun to dissolve, suggested by the emergence of the Badegoulian technocomplex, which potentially reflects influences from eastern traditions (Ducasse et al. 2021; Händel et al. 2021). It is within this context that numerous taxonomic units, next to the Solutrean, Epigravettian and Badegoulian, were established by researchers – such as the Grubgrabian (Terberger 2003), and Salpetrian (Boccaccio 2005) – to name just those which include assemblages with SPs. During this time, the number of lithic projectile points appears to decline, while laterally retouched micro-bladelets gain prominence (Ducasse et al. 2021). The period between 25,000 and 20,000 BP exhibits very low variance as well as an almost complete absence of pronounced chronologically directed changes in the morphometry of the SPs, as indicated by the low rates of change. However, when examined separately, the individual taxonomic units reveal marked differences. Notably, the Late Badegoulian SPs as evidenced at Le Cuzoul de Vers, layers 21-16 (Ducasse et al. 2021) stand out due to their distinct morphology – an elongated hafting part and a very short transformative part – potentially reflecting an innovation (discussed in more detail in Chapter 5.2.2.3). Furthermore, the HCA underscores morphometric differences between older LGM assemblages – primarily associated with the Upper Solutrean, Epigravettian, and Salpetrian – and younger LGM assemblages, represented by the Lower Magdalenian and Tardigravettian. This period can thus be interpreted as a phase of modest diversification in SP designs, marked by the coexistence of multiple design concepts – four clusters (unconstrained HCA) occur between 25,000 and 20,000 BP. Some of these were short-lived while others had a more lasting influence (see Chapter 5.2.2).

The final period investigated by Maier et al. (2022a), spanning 20,000 to 15,000 years calBP, is termed "network reinvigoration" (ibid., 116). During this phase, previously abandoned areas were repopulated, and human groups expanded further north. Population sizes continued to grow, reaching their maximum levels within the Upper Palaeolithic (Kretschmer 2015). A similar trend is evident for population density within the core areas. Communication networks also appear to have been re-established, as indicated by pan-European overarching similarities in the material culture (Gaudzinski-Windheuser & Jöris 2015). Nonetheless, the two previously distinct networks remain discernible in mollusc transport patterns (Maier 2015), but also in the continued absence of SPs east of present-day Poland. From 19,000 years calBP onward, lithic projectile points remain relatively stable, whereas osseous projectile points become increasingly numerous and undergo notable transformations. Laterally retouched micro-bladelets gradually fall out of use, replaced by backed bladelets. Classical SPs are very rare, while scalene bladelets become common – considered a specialised form of SP with roots in the preceding Badegoulian (Maier 2020). Around 16,000 years calBP, Maier et al. (2021) document the highest rate of change in projectile point types, indicating a phase of major turnover in hunting equipment. During this period, SPs gain prominence and appear alongside lithic triangles (scalene triangles), which may have been used in composite barbed points (Maier et al. 2020; Maier 2020), as well as backed bladelets (Langlais et al. 2016). The dataset of this study begins in the second half of this period, where it reveals elevated variation and morphological change in SPs. This, however, is largely attributable to the coexistence of two distinct SP types within Upper Magdalenian contexts: one type that persisted and likely gave rise to the Late Upper Palaeolithic SPs, and another discontinued type characterised by elongated forms with a long hafting part and a short transformative part. In contrast, the subsequent millennia are marked by minimal change and low variation, indicating a standardisation of SP design that is consistent across the taxonomic units of the Late Upper Palaeolithic, namely the Hamburgian and the Creswellian.

The results of this study, when compared to palaeodemographic estimations, align closely with theoretical models on the interplay between population size, density, and dynamics in material culture. Empirical evidence supports that higher population size and density – implying increased connectedness – correlate with lower variance in SP morphometry. Elevated morphometric variation in SPs up to the 24$^{th}$ millennium BP corresponds with a demographic crisis marked by declining population size and density. This pattern underscores the loosely connected populations during the Late

Gravettian in Central and Eastern Europe, as well as during the initial emergence of SPs in Western European Upper Solutrean contexts. The breakdown of the previously extensive interaction network and its fragmentation into two smaller regional systems is reflected in the absence of SPs in western Late Gravettian contexts and in the morphological disparity between Late Gravettian and the earliest Upper Solutrean SPs. As SPs become restricted to southwestern and western Europe, variation declines sharply and remains consistently low – with the exception of a notable peak between the 17th and 16th millennium BP – coinciding with demographic recovery and the reorganisation of supra-regional networks. This low variance underscores the increased connectedness of populations during this phase.

Also, at the onset of each period as defined by Maier et al. (2022a), both the variation and the rate of change in SPs begin at elevated levels and that subsequently decline over the course of the period, only to rise again at the beginning of the next. An explanation for this progressive decrease in variation – and, consequently, in change – over time was discussed for the entire observed timeframe and for the major taxonomic units in Chapter 5.1.1. As the transitional points between Maier et al.'s (2022a) periods correspond with major taxonomic shifts – particularly the transition from the Late Gravettian to the Upper Solutrean, which coincides with the onset of the "network reorganisation" period – this reinforces the discussion by suggesting that the initiation of social network reorganisation or densification triggers processes that progressively reduce variation.

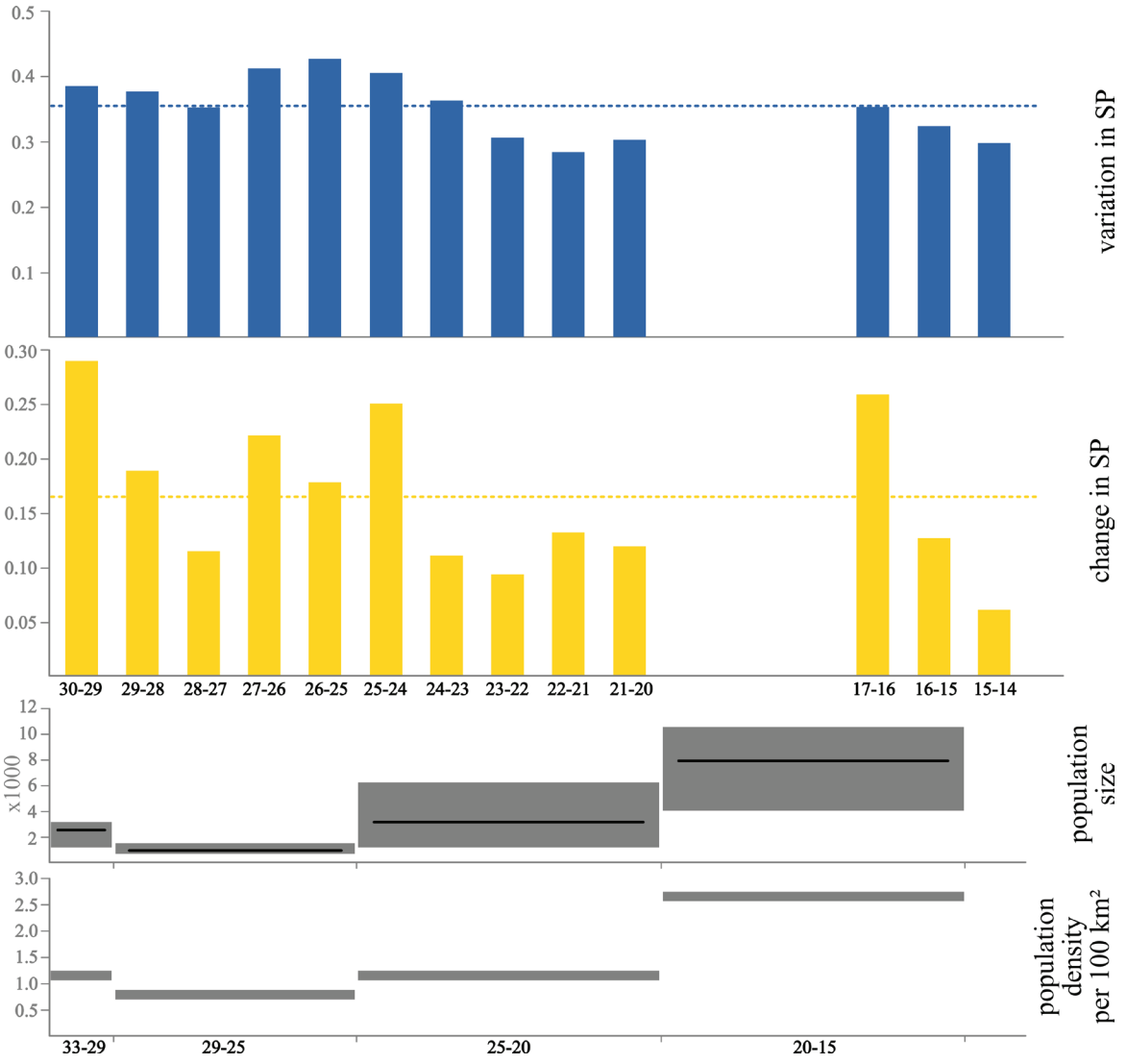



Figure 130: Comparison of dynamics in SP morphometry and population size and density (after Maier & Zimmermann 2017; Maier et al. 2022a).

Notably, periods of higher population size and density also tend to coincide with short-lived morphological inventions that hence not have an impact on the overall variation. One of such occurs during the recovery phase at around 23,000 years calBP, when a new, very distinct SP form appears in a Badegoulian context. This distinct, short-lived form may be the outcome of a phase of experimentation or technological testing occurring under conditions of increasing population size and density and network reorganisation.

According to Maier et al. (2022b), European ecosystems between 43,000 and 15,000 years calBP were highly responsive to fluctuations in solar energy, which may have influenced the timing of plant and animal life cycles. They further suggest an indirect causal link – mediated by shifts in animal populations – between reduced solar insolation and the decline of hunter-gatherer groups in Western and Central Europe between 29,000 and 25,000 years calBP (ibid., 45). Environmental pressures driven by shifts in animal populations up to around 25,000 years calBP, although this signal is more global than regional in character, may have contributed to the selective pressures observed between the 27$^{th}$ and the 24$^{th}$ millennium BP. Conversely, they connect increasing spring insolation, along with progressively earlier growing seasons, to the demographic expansion and territorial spread of hunter-gatherer populations after 23,500 years calBP (ibid., 45–46). With increasing spring insolation and earlier growing seasons, environmental stress was likely reduced, and the greater predictability of resources may have facilitated the maintenance of morphometric characteristics observed between the 24$^{th}$ and the 22$^{nd}$ millennium BP. Up to 15,000 years calBP, progressively earlier onsets of the growing season are observed, together with increased cumulative temperatures across the entire season (ibid., 47). During this later phase, adaptation to post-glacial conditions may once again have imposed selective pressures on SP morphology. *(Figure 130)*

## 5.2 SHOULDERED POINT LINEAGES

It must once again be highlighted that artefacts typologically assigned to the type SP are unlikely to represent a coherent unit. Consequently, the examination of phylogenetic relationships between individual designs (subtypes) faces a range of methodological and conceptual challenges, as outlined in Chapter 3.3.4. While the results clearly argue against a single evolutionary lineage, they instead indicate the presence of distinct lineages with geographical and taxonomic significance. The present study thus contributes to several ongoing debates on the relationships between taxonomic units by providing new insights into the degree of morphometric similarity among SPs from differing taxonomic and chronological contexts.

Furthermore, it must be emphasised again that, when assessing relationships between SP forms, these are not to be understood in a biological sense. Rather, it is the underlying ideas, specific design blueprints, concepts or "recipes" (Lyman & O'Brien 2003) – what might be considered the cultural equivalents of genes (Dawkins 1982) – that are shared among knappers or users through cultural interaction (see Chapter 3.3.4).

Shape-related features seem to be of more discriminant value than size-realted features. Since shape-related features tend to vary more dynamically over time, similarities in shape are consistent with Hennig's (1950) concept of complex similarity. According to Hennig, complex similarities outweigh even numerous simple ones, as simple similarities are more likely to result from convergent evolution. Similarities based on size-related features could be considered as such simple similarities. The focus in the following discussion thus lies on shape.

### 5.2.1 From the Late Gravettian to the Upper Solutrean: Heritable Continuity or Re-Innovation of Shouldered Points?

The results of this study highlight pronounced morphological differences, most notably in the configuration of the hafting and transformative parts. These differences are particularly evident in the SPs from the Iberian Peninsula, whereas the French Upper Solutrean SPs, despite some notable differences in size, appear more consistent but not identical with the configurations observed in the Late Gravettian. While Late Gravettian SPs typically show an even ratio or ratios in favour of the hafting part, (Iberian) Upper Solutrean SPs have much shorter hafting parts, resulting in a relative elongation of the transformative (penetrating) part of the projectile point and thereby lengthening the cutting edges, potentially increasing projectile efficiency. Not only did the transition between these two taxonomic units yield extreme values for morphological change on both the chronologically and the archaeo-stratigraphic informed perspective, but both the constrained and unconstrained cluster analyses also consistently separated them (Chapter 4.3.1).

Beyond these morphological contrasts, some Upper Solutrean SPs also differ technologically. Whereas Late Gravettian SPs are exclusively shaped by abrupt retouch – sometimes accompanied by basal retouch on the ventral side (e.g., Avdeevo, A-48, Appendix Plate 13), reminiscent of typical Gravette-Point retouch (e.g., Nuzhnyi 2009, Fig. 4) – Upper Solutrean SPs are frequently, though not exclusively, produced by both uni- and bifacial retouch. Those not shaped by facial retouch often show abrupt retouches. Ventral retouch on the base is common, especially (but not exclusively) among French specimens (e.g., Gruta de Salemas, A-45; El Pendo, C-35; Combe-Saunière, layer IV, A-40; Fourneau du Diable, Solutréen supérieur II, C-37; see Appendix Plates 59a and b). Whether these stylistic or technological features are homologous, i.e. carried over from Late Gravettian traditions (and potentially lacking direct practical purpose), or analogous, i.e. invented anew without any inherited basis (e.g. for offering a technological advantage), remains an open question. This brief paragraph already underscores the variability in technology and morphology of Upper Solutrean SPs, often following regional patterns, a topic long noted by researchers (e.g., Smith 1966; Geneste & Plisson 1989; Schmidt 2015), and captured in this study particularly through the marked disparity in size and in the proportions of the hafting and transformative parts between the Iberian and French Upper Solutrean specimens.

The long geographical distance and the chronological gap between the latest Gravettian assemblages yielding SPs in Eastern and Central Europe and the first Solutrean SPs on the Iberian Peninsula and in Southern France further complexify the question of whether they are related to each other. Specifically, are the first Solutrean specimens part of a tradition stemming from the latest Gravettian ones – descendants reflecting heritable continuity and homologous traits – or are they independent innovations showing merely analogous traits to the Late Gravettian SPs? Notably, at the Spanish site of Abauntz, dating to around 25.9 ka calBP, the first appearance of SPs in Western Europe is approximately contemporary with the latest assemblages in Eastern Europe, despite being separated by about 2000 km. However, most Upper Solutrean SPs derive from assemblages roughly 2000 years younger or more.

De Sonneville-Bordes & Perrot (1956, 547), report what they describe as "pointe à cran périgordienne, atypique" from French sites assigned to the Périgordian, which they argue are closely related to Gravettian SPs *(Figure 131)*. Taken seriously, these could serve as intermediate forms, potentially bridging the morphological and geographical gap. The Late Gravettian SPs from Central and Eastern Europe analysed in this study, while exhibiting chronologically directed changes toward larger forms, however, show no tendencies toward a relative shortening of the hafting part. *(Figure 131)*

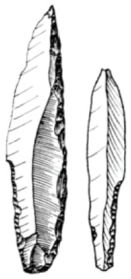


Figure 131: "Pointe à cran périgordienne, atypique" (de Sonneville-Bordes & Perrot 1956, 551, Fig. 2).

Adding to the chronological and especially the geographical separation between the Late Gravettian SPs and most Upper Solutrean SPs, Posth et al. (2023) identified a distinct genetic cluster, the so-called Fournol cluster, different from the Věstonice cluster associated with Central and Eastern European Gravettian populations (Fu et al. 2016). This Fournol cluster includes Gravettian individuals from Western and Southwestern Europe, related to earlier Aurignacian groups from Belgium, and persists into the Upper Solutrean as a refugial population during the LGM. Baker et al. (2024) additionally demonstrated that the Gravettian is initially not only genetically subdivided, but also exhibits differences in personal ornaments between central-eastern and western Europe. Posth et al. (2023) further propose that a population from Goyet (Belgium) was genetically intermediate between the Věstonice and Fournol clusters, and that by the time of the Late Gravettian, Věstonice ancestry had expanded westward, resulting in a genetic cline with the Fournol cluster. However, the sequenced genomes from Solutrean-associated individuals from southwestern France and northern Spain are more closely related to the Fournol and Goyet clusters than to the Věstonice cluster (Posth et al. 2023), highlighting a relative weak genetically input from Central and Eastern Europe.

Maier et al. (2016) additionally identified pronounced demographic differences between Western Europe and Eastern Central Europe between 25,000 and 20,000 calBP, which coincided with contrasting environmental preferences: cool temperate conditions in the West versus colder and drier conditions in the East. These findings, although they only marginally encompass the latest Gravettian assemblages examined in this study, may nonetheless suggest differing subsistence strategies and, potentially, distinct hunting equipment adapted to the respective environmental conditions between the Late Gravettian and the Upper Solutrean.

In light of the results of the present study and the insights gained from the literature reviewed above, two interpretations regarding the origin of the Upper Solutrean SPs appear plausible:

*1) No heritable continuity: There is no direct inheritance between the SPs of the Late Gravettian and those of the Upper Solutrean.* Instead, the SP was newly invented in the Upper Solutrean as an analogous solution to the same functional problem – hafting fronto-lateral projectile points to extend cutting edges. This interpretation draws on theories of convergent evolution, suggesting that the limited morphological options for creating such projectile points led to an independent innovation (McGhee 2011 and 2018). The observed differences in shape thus reflect this separate development. The stylistic differences, such as facial retouch on some specimens, could be seen as the integration of invention into the prevailing technological repertoire of facially retouched leaf points. The potential intermediate forms would be interpreted as exceptional phenomena outside the classic distribution area. This scenario assumes that, although Věstonice ancestry expanded westward, the knowledge of manufacturing SPs in the Late Gravettian style was lost 'en route' or was not part of a potentially transmitted knowledge-package. The development of the upper-lower-ratio in the SPs during the Late Gravettian does not indicate any tendency towards shorter hafting parts, respectively relatively longer transformative parts.

*2) Heritable continuity: There is indeed continuity between the Late Gravettian and Upper Solutrean SPs.* Heritable continuity between the Late Gravettian and the Upper Solutrean SPs is asserted by Tiffagom (2006, p. 215, Planche XIV), who suggests an east-to-west spread of SPs – an interpretation that has been adopted by other researchers (e.g., Cascalheira & Bicho 2015). The diffusion model suggests that information originating from a "Gravettian hearth" was filtered by the Solutrean groups of southwestern France, who adapted it to their own technological framework (pressure flaking/facial retouch), resulting in a so-called 'pointe à cran de type atlantique' (SPs of the Atlantic type). From there, SPs were further adapted and modified by the Cantabrian and Portuguese Solutrean. Likewise, the Andalusian Solutrean adopted the 'pointe à cran de type méditerranéen (PCM)' (SPs of the Mediterranean type), which originated from a southern diffusion route extending through northern Italy and the Rhône valley, thereby incorporating influences from Epigravettian, Arenian, and Salpetrian contexts.

The interpretation of a diffusion of SPs from Central and Eastern European Gravettian assemblages over French Upper Solutrean and Italian Epigravettian assemblages, and thereby a continuity between the Late Gravettian and the Upper Solutrean SPs first of all rests on the assumption that SPs constitute a coherent typological unit and thus a lineage, with internal differences representing typological subgroups or mere variation. However, the results of this study clearly demonstrate that SPs generally do not form a unified group. Rather, they comprise distinct entities – some more variable, others less – some more closely related, others less – that share certain morphological features. This also applies to the Late Gravettian SPs. The results of the RDA and the calculated change rates indicate subtle morphological dynamics, suggesting minor chronologically directed changes towards the end of the Late Gravettian. Additionally, the coefficient of variation (CV) results reveal notable variation throughout this period (Chapter 4.1.2), which may reflect loosely connected populations occupying geographically distant core areas across central and eastern Europe (Maier et al. 2021). The dynamics observed within the Upper Solutrean and the spatiotemporal segmentation of SP designs – particularly the pronounced differences between French and Iberian assemblages – identified in this study were already emphasised by Tiffagom (2006) in his diffusion model. Consequently, these generalisations about continuity warrant careful reconsideration. This may be particularly evident when comparing Upper Solutrean to Late Gravettian SPs, the latter of which frequently exhibit tip angles that far exceed the range considered functionally viable for projectile points (Beckhoff 1966), suggesting that some of them may not even have served as projectile points at all.

Furthermore, the diffusion model assumes staggered ages for Solutrean assemblages containing SPs, beginning with the oldest occurrences in France and in Italy represented by Epigravettian assemblages followed by assemblages in the Rhône valley as well as Cantabrian and Portuguese assemblages. Lastly, the Aquitanian assemblages should be the youngest. However, although the radiocarbon record for the entire Upper Solutrean remains far from sufficient in resolution, it is questionable whether such an assumption is supported by the actual ages of the assemblages. At least the dataset aggregated for this study (Appendix Table 14) draws a different pattern *(Figure 132)*. While the three French Upper Solutrean assemblages – Le Placard (24.2 ka calBP), Laugerie-Haute Ouest (23.6 ka calBP), and Combe-Saunière (23.4 ka calBP) – are indeed among the older Upper Solutrean contexts, there are several assemblages on the Iberian Peninsula that are either older or at least contemporary with the French sites. These include Abauntz (25.9 ka calBP), Vale Boi (24.7 ka calBP), Cueva Morín (24.3 ka calBP), Cueva de la Riera (23.9 ka calBP), Gruta de Salemas (23.7 ka calBP), and Cueva de Chaves (23.7 ka calBP). Two Italian Epigravettian assemblages – Grotta di Paina, layer 5 (23.6 ka calBP) and Ponte di Pietra (23.4 ka calBP) – are older than the only Aquitanian assemblage in the dataset, Cueva de Ambrosio, layer II (23.0 ka calBP), lending some support to a southern diffusion route. However, Grotta de la Salpêtrière, layer 6 (23.0 ka calBP) – the sole Salpetrian assemblage containing SPs – is approximately contemporaneous with Cueva de Ambrosio and thus cannot be interpreted as a chronological marker along this route.

The morphological differences between the Late Gravettian and the Upper Solutrean SPs as calculated in this study, however, seem unlikely to be the result of copying errors as the 'idea of the SP' was transmitted (by whatever mechanisms) from Central and Eastern Europe to Iberia and France alongside the Věstonice genomic ancestry. These differences clearly exceed the plausible range expected for transmission errors (Eerkens & Lipo 2005) as well as all thresholds for perceptible variation, thereby refuting such interpretations. Assuming heritable continuity, the differences would more likely be the result of conscious adaptations, either to suit a different already existing hafting system, potentially optimised for another kind of projectile composition or even propulsion system, or to improve the effectiveness or durability of the projectile points. The introduction of bow and arrow is frequently discussed for the Solutrean, especially in context of SPs and tanged and winged 'Parpalló-type' points (Muñoz Ibáñez 2000; Muñoz Ibáñez et al. 2017 and 2019; Ripoll López et al. 2015). Such a technological development could, in turn, represent an adaptation in subsistence strategy within an environmental refugium

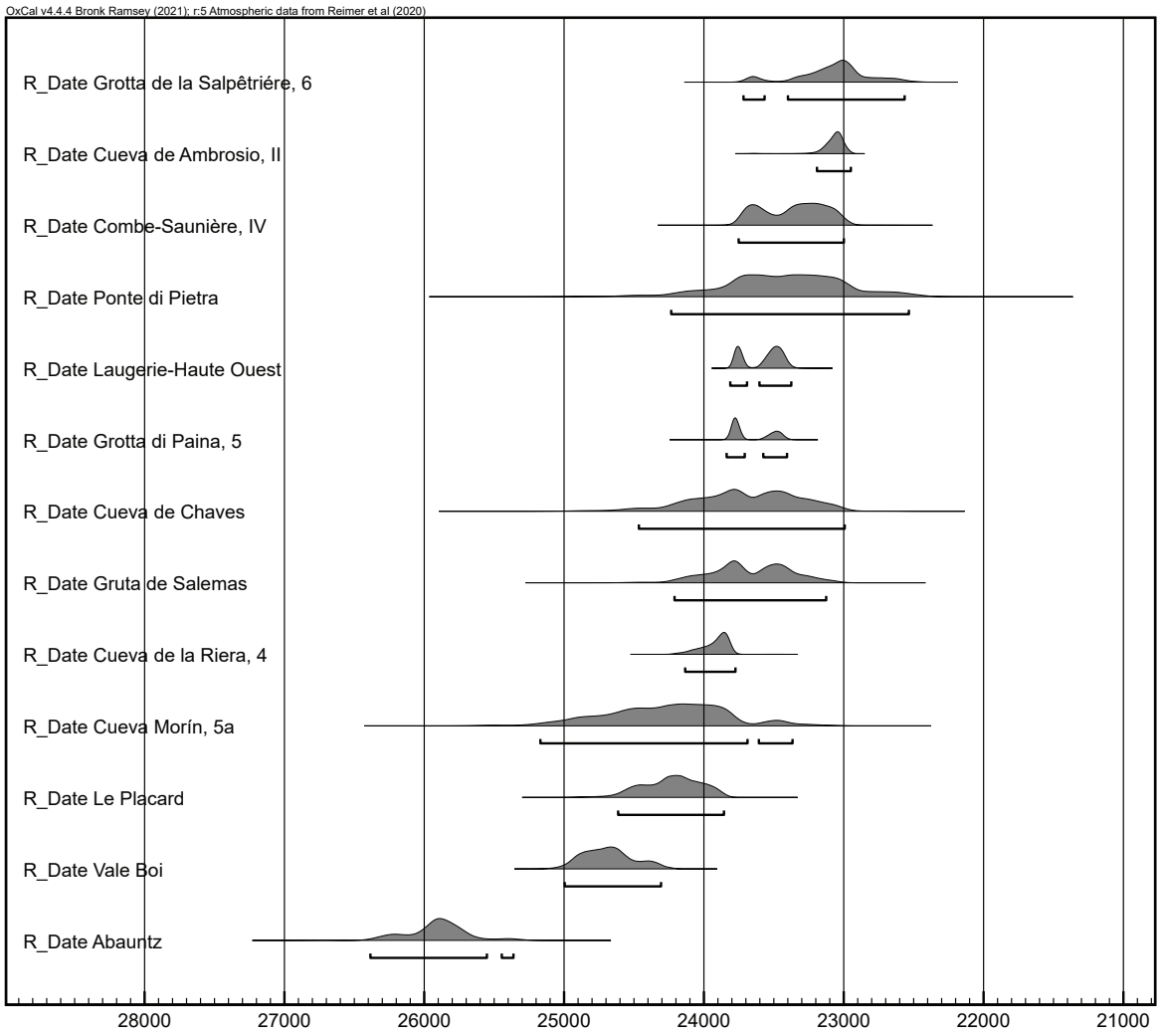



Figure 132: Weighted averages (WA) or single dates (calBP) for the earliest Upper Solutrean SPs (calibrated in CalPal (Weninger 2022) using IntCal20 (Reimer et al. 2020); see Appendix Table 14; figure produced in OxCal v4.4 (Bronk Ramsey 2021)).

in Western Europe (Straus 2015; Posth et al. 2023). In Central and Eastern Europe, humans were adapted to harsher conditions (Maier et al. 2016). Without overemphasising the significance of this observation for the presence of the bow and arrow, it is noteworthy that shouldered and tanged points disappear from the central and eatsern European record after the Late Gravettian. *(Figure 132)*

While this study cannot provide a definitive answer as to whether Upper Solutrean SPs are descendants of Late Gravettian SPs, it clearly highlights the pronounced morphological differences between these two units, casting doubt on a direct line of inheritance. These findings thereby align with recent publications reviewed above, pointing towards an east-west subdivision of populations before and during the LGM.

It thus also remains unclear – assuming heritable continuity – whether Upper Solutrean SPs represent a variation that emerged due to a different functional role – such as their potential use as arrow points in bow-and-arrow technology – or whether they constitute a competing design alternative for the same function. What can be stated with greater confidence is that the Upper Solutrean SP design

ultimately proved to be successful, indicating that it was likely the variant with greater functional performance or adaptive advantage in its specific techno-functional *setting*. This may have included a reduced likelihood of breakage in the hafting area, thereby allowing for the reuse or reworking of broken points. SPs featuring a short hafting element and an elongated transformative part became the predominant design throughout the remainder of the Upper Palaeolithic. Occasional reappearances of SPs with longer hafting parts probably do not indicate brief revivals of a Late Gravettian SP tradition, but rather fluctuations without cultural association.

### 5.2.2 Relationships during the Last Glacial Maximum

The taxonomic units during the LGM revealed a mosaic image of morphological relatedness between the SP designs. This aligns well with the complex image drawn by a wide field of publications that frequently report SPs with abrupt retouch as 'unifying' element. The results on the morphometric relationships between the SPs conducted here can further strengthen some of the hypotheses made by those researches while for others suspicions can be raised. The clustering results most notably reveal a division of the LGM period into an older and a younger morphological phase, with a clear break around 23,000 calBP.

#### *5.2.2.1 The Epigravettian and the West*

While the term Epigravettian was first coined for Franco-Cantabrian sites (Laplace 1964a), it is especially applied to the Italian Late Upper Palaeolithic (e.g., Broglio 1997). Today, the term is largely applied to all Eastern Central European sites from the LGM that post-date the Gravettian and exhibit neither Gravettian nor Magdalenian characteristics (Lengyel 2016, 2018; Lengyel et al. 2021). This wide-ranging uniformity in taxonomic association is applied to highlight the uniformity, which is thought to derive from one hunter-gatherer culture (ibid.). The classification also extends to the Eastern Adriatic, where SPs occur frequently (Vukosavljević & Karavanić 2017). The emergence of SPs in Early Epigravettian lithic assemblages of the Balkan and Apennine peninsulas has been interpreted as evidence of cultural influence – or even population movement – from central European Late Gravettian assemblages toward southern Europe during the LGM (Kozłowski 1999). Others argue that SPs have been part of an adaptational response of well-connected social networks to climatic deterioration during the LGM (Borić & Cristiani 2016, 82).

Despite certain divergences, the Epigravettian groups appear to have maintained connections with Western European groups (Fasser 2022). As the assemblages yielding SPs assigned to the Epigravettian scatter substantially both chronologically and geographically, and the morphological variability within this taxonomic unit is notable, a unified discussion does not seem to be sensible. The interpretation of contacts, however, is largely supported by the results of this study, with Epigravettian samples yielding low change rates to other taxonomic samples of the LGM and frequently clustering especially with Upper Solutrean samples. Particularly, the Epigravettian samples dated to the 24th millennium BP – including those from Grotta di Paina, layer 5 (B-16), Kastrisa, layer 7 (A-42), and Ponte di Pietra (A-41) – cluster closely with contemporary Upper Solutrean and Salpetrian samples.

Likewise, the assemblage from Chinchon 1, layer C (A-33), frequently classified as Tardigravettian (Brochier 2016), clusters closely with the Lower Magdalenian samples, indicating a close morphological relation and thereby aligning with broader suggestions on cultural relatedness (de Soneville-Bordes 1966; Escalon de Fonton 1966; Combier 2003).

A close relation between the Tardigravettian of Chinchon 1, layer C and the Salpetrian, as suggested by Laplace (1964b) and Combier (1967), in turn, cannot be supported by the results of this study. In none of the clustering approaches do both samples appear together, reflecting the observed division of the LGM into an older and a younger morphological phase. Although both share features such as a short hafting part, Salpetrian SPs are distinctly smaller, slenderer, and pointier than the Tardigravettian SPs from Chinchon 1, layer C. Moreover, the pronounced asymmetry characteristic of the Tardigravettian SPs is absent in the Salpetrian specimens.

The first reappearance of SPs in Central Europe is documented at Kammern-Grubgraben, layers 2 and 3 (A-39). At the current state of research, however, this assemblage remains an isolated case for another 6000 years, until SPs reappear in inventories north of the Alps. Ongoing research aims to clarify whether this assemblage should be attributed to the Badegoulian, the Epigravettian, or regarded as an independent taxonomic entity – the so-called 'Grubgrabian' (Terberger 2013). This study cannot contribute further to this classification. The SPs from Kammern-Grubgraben display comparatively high variability, with individual specimens showing little resemblance to contemporaneous SP forms.

### *5.2.2.2 The Salpetrian: A Regional Expression of the Solutrean?*

The Salpetrian, as a taxonomic unit, was originally defined based on layer 6 of the eponymous site, Grotta de la Salpêtrière (Boccaccio 2005). Its lithic industry is characterised by pronounced typological and technological homogeneity and exhibits strong affinities to the Upper Solutrean – thought to be particularly evident in SPs with abrupt retouch of the so-called 'Mediterranean type' (Boccaccio 2005; Bazile & Boccaccio 2008). Despite there being no complete stratigraphic sequence, the Salpetrian is believed to follow on the local Upper Solutrean (Boccaccio 2021) or to reflect a regional expression of the Upper Solutrean (Ducasse et al. 2021). The interpretation of a close relationship between the Upper Solutrean and the Salpetrian is strongly supported by the results of this study. The Salpetrian SPs display only minimal differences from the more or less contemporary Iberian Upper Solutrean samples dated to the 25th and the 24th millennium BP, indicating substantial shared morphological traits.

### *5.2.2.3 The Badegoulian Phenomenon*

The cultural classification of some distinct French post-Solutrean assemblages has been the subject of debate, involving both osseous and lithic artefacts, since they were first described (Peyrony 1908). Initially, they were regarded to as an early phase of the Magdalenian (Magdalenian I; Breuil 1913) – an interpretation revisited later by Bordes (Magdalenian 0 and I; 1958). Cheynier (1939) reinterpreted these assemblages and proposed the term 'Proto-Magdalenian' to emphasise their distinctiveness. Scholars ultimately recognised these assemblages as belonging to a separate archaeological taxonomic unit, named the 'Badegoulian' (Allain 1989) after the type-site at Badegoule in Dordogne, France (Vignard & Vacher 1965). Analysis of the stratified site of Abri Fritsch (Allain & Fritsch 1967) revealed a clear divergence between the Upper Solutrean and Badegoulian layers, as well as marked differences between the Badegoulian and Magdalenian layers. These findings suggest a cultural "discordance," with no clear developmental links to either the preceding or subsequent archaeological units (Bosselin & Djindjian 1988, 322). More recent studies further confirm a discontinuity between the Upper Solutrean and, in particular, the Early Badegoulian (Ducasse 2012). The results of this study largely support the proposed discordance, as Late Badegoulian SPs consistently show marked differences from Upper Solutrean SPs, indicating fundamentally distinct shape designs between these two taxonomic units. Hence, the Late Badegoulian SPs might reflect an innovation. Such an innovation, in turn, might have been driven by the arrival of new populations from east (as cited e.g. in Ducasse 2012; Ducasse et al. 2021).

The relationship between Badegoulian and Salpetrian has been the subject of broader debate. Bazile & Boccaccio (2008) and Boccaccio (2021) argue for partial synchrony between the two, citing, among other evidence, the presence of abruptly retouched shouldered lithic points – a diagnostic feature of the Salpetrian – within certain Badegoulian assemblages. In contrast, Ducasse et al. (2021) emphasise stratigraphic evidence from Petite Grotte Bize (C-45; Sacchi 1986), where Salpetrian layers succeed Badegoulian layers. They also stress differences in the lithic armatures themselves: whereas Badegoulian SPs are highly distinctive and morphologically variable, Salpetrian SPs adhere to stricter typo-technological standards. Although SPs occur in both, Salpetrian and Badegoulian assemblages – and despite Boccaccio's (2021) suggestion of contacts between Salpetrian groups and the

Badegoulian group at Cuzoul de Vers – the pronounced differences identified in this study between representatives of these two taxonomic units indicate that no shared underlying design concept is likely. Notably, the differences observed – particularly in the ratio between the transformative and hafting parts – have already been emphasised by Ducasse (2010) and Ducasse & Lelouvier (2012). This could, in turn, support hypotheses regarding the distinctiveness of Badegoulian populations.

#### *5.2.2.4 The Emergence of the Magdalenian*

In spite of the fact that a continuity between the Solutrean and Magdalenian has been emphasised for the Iberian Peninsula (e.g., Straus & Clark 1986), SPs disappear from the archaeological record south of the Pyrenees at around 21,000 calBP, the latest. While radiometric dates place the French Upper Solutrean SPs significantly earlier than the Lower Magdalenian, making a direct relationship between these units unlikely, this study identified weak affinities to younger Iberian Upper Solutrean SP samples. This could be interpreted as evidence for a very late Upper Solutrean origin of the Lower Magdalenian SPs, or as a convergence of SP morphologies during the late phase of the LGM.

By the time the first Lower Magdalenian SPs appeared, the Salpetrian phenomenon had likely already ended as well (Boccaccio 2021). This is well reflected in the results of the present study, as the Salpetrian and Lower Magdalenian SP samples display pronounced differences and do not cluster together in any analytical approach. It is therefore unlikely that the Salpetrian SP design exerted a direct influence on the emergence of the distinctive Lower Magdalenian SPs.

Despite certain notable differences – described by Ducasse (2012, 158, Fig. 7) as a case of "gradual change" – the lithic technological system of the Lower Magdalenian is considered to share substantial continuity with that of the Late Badegoulian (Ducasse and Langlais 2005; Primault et al. 2007; Langlais 2007; Ducasse 2010). However, in light of this study's results – showing that Late Badegoulian and Lower Magdalenian SPs often exhibit extreme differences and therefore not cluster together in any clustering approach – the proposed continuity or gradual change appears questionable for SP designs. Lower Magdalenian SPs exhibit an entirely different design, characterised by short hafting parts and straight backs. In contrast, Late Badegoulian SPs consistently feature long hafting parts – a trait that recurs even on fragmented specimens (Ducasse et al. 2021).

This study demonstrates a strong morphological affinity between the Lower Magdalenian samples and the Tardigravettian SPs of Chinchon 1, layer C (A-33; Paccard 1964; Paccard & Dumas 1977), which are roughly 1000 years older. This observation agrees with the suggestion that Chinchon represents an early stage of the Lower Magdalenian (Brochier 2016), supporting the view that this assemblage may signal the onset of the Lower Magdalenian SP tradition. This finding reflects early interpretations of the Chinchon 1 assemblage, which was long typologically regarded to as resembling an Upper Magdalenian inventory (Paccard 1961 and 1964; de Sonneville-Bordes 1966; Escalon de Fonton 1966; Combier 2003).

### 5.2.3 Magdalenian Shouldered Point Tradition?

Leaving the chronological gap aside, the design of Late Badegoulian SPs may have influenced the production of scalene bladelets – a type of triangular lithic implement occurring approximately between 19,000 and 16,000 calBP – to which they show a closer morphological affinity as shown by the results of this study (Chapter 4.5). Although scalene bladelets show clear shape differences from the Late Badegoulian and the elongated Upper Magdalenian SPs of Type A – primarily in terms of symmetry and tip angle – their ratios between the hafting and the transformative parts, are largely identical. These findings support the suggestion by Maier (2020) that scalene bladelets may represent a variant of SPs closely related to the Late Badegoulian SPs (ibid., 186), bridging the chronological gap between classical SP forms. The results on the size differences thus align with the observation of a decrease in size of projectile points between 19,000 and 16,000 calBP followed by an increase in size towards the elongated Upper Magdalenian SPs (Maier's (2020)).

In contrast, the Hamburgian SPs of the 15th millennium BP differ markedly, especially due to their relatively longer transformative parts. Consequently, a developmental sequence from the Late Badegoulian SPs through scalene bladelets and elongated Upper Magdalenian SPs to the Late Glacial SPs, as suggested by Maier (2020, 186) cannot be supported by these findings. Such a sequence likely ended with the disappearance of the elongated Upper Magdalenian SPs of Type A around 15,000 years ago.

While evidence for SPs in both the Lower and Middle Magdalenian is rare – occurring only sporadically in a few assemblages in southern France, with Kamegg in Lower Austria (B-11, Neugebauer-Maresch 1999) being a clear exception – more typical SPs appear in great numbers during the Upper, Late, and Final Magdalenian not only in southern France but also north the Alps (see Nielsen 2009; Maier 2015).

The results of this study suggest a morphological continuity from the Lower Magdalenian SPs to the Middle Magdalenian SPs, primarily distributed in southern France to the Upper Magdalenian SPs of the stouter Type B, occurring both in France and north of the Alps. This result aligns well with the insight from paleogenetic studies, suggesting that the diffusion of the Magdalenian after the LGM was associated with a northward and a north-eastward population expansions from western Europe (Posth et al. 2023). But also archaeological studies emphasised such a continuity. Langlais et al. (2015) concludes a that the Middle Magdalenian derived from a widely homogenic Lower Magdalenian (Langlais 2010). This continuity is nonetheless characterised by a developmental shift of the shoulder towards the tip – beginning with SPs featuring notably short hafting parts and culminating in the Upper Magdalenian Type B SPs, which display a more balanced ratio between the transformative and hafting parts.

### 5.2.4 The Late Upper Palaeolithic Shouldered Points

Weber (2009) highlights the morphological similarities between Magdalenian SPs from the Paris Basin (Cepoy-Marsangy facies), as published by Burdukiewicz & Schmider (2000), and the Hamburgian SPs from Poggenwisch and Teltwisch 1, originally published by Rust (1958) and Tromnau (1975b) – all included in the present study. A Magdalenian origin for the Hamburgian SPs is supported by this study's findings: Hamburgian samples frequently cluster with the stouter Type B Upper Magdalenian SPs. Also, the low variances and change rates during the later millennia of the study indicate the absence of major morphometrical shifts. Although this theory has been questioned (Djindjian 2000), these results align with broader interpretations of the Hamburgian as a cultural development rooted in the Magdalenian tradition (Rust 1937; Burdukiewicz 2001; Weber 2012, 197),

The Creswellian was first defined by Garrod (1926, 301) as a "semi-independent facies of the Magdalenian". While some recent scholars maintain this taxonomic distinction to emphasise a "distinct archaeological entity" and a "progressive cultural adaptation to new environmental circumstances in the re-colonised land north of the Channel River" (e.g., Cooper 2012, 31), others advocate for its reclassification as part of the Late Magdalenian (e.g., Pettitt 2008; Jacobi & Higham 2011), in recognition of the broader cultural continuities. The present study supports this latter view: the morphometric clustering of Creswellian SPs with Type B Upper/Late and Final Magdalenian as well as Hamburgian samples underscores their strong morphological similarities. This pattern suggests not only cultural relatedness, but also potentially shared subsistence strategies, as reflected in their comparable hunting technologies.

This study clearly demonstrates that the mere presence of SPs in the inventories of different taxonomic units – even when produced using the same technique, most notably abrupt retouch – does not necessarily indicate a close relationship, which is what Maier (2015, 41 ff.) already emphasised for types in general or e.g., Sauer & Riede (2019) found for large tanged

points in *Late Palaeolithic* contexts. On the contrary, the findings strongly suggest that greater caution is required and that morphological design may play a more significant role than it is currently given credit for. Thereby, the findings actually support and validate the distinction of certain taxonomic units based solely on SP morphology – most prominently the separation between the Late Gravettian and the Upper Solutrean as well as between the Badegoulian and other LGM industries.

In light of this, it remains uncertain whether Late Gravettian SPs directly gave rise to Upper Solutrean SPs, or whether the similarity – a lateral notch – reflects an independent innovation shaped by morphological and functional constraints and convergent developments.

The period of the LGM in a larger sense is characterised by the coexistence of multiple SP design concepts and comparably low differences between the individual regional expressions. Some of the LGM SP design concepts were short-lived – such as the French Upper Solutrean SPs, which disappeared shortly after their emergence – while others had a more lasting influence. The Upper Solutrean SP design probably have given rise to both the Salpetrian and the Lower Magdalenian SP designs, the latter persisting through the Middle and likely into the Upper Magdalenian. The stouter Upper Magdalenian SPs, in turn, show close affinities with contemporaneous and slightly younger SPs from *Late Palaeolithic* industries, such as the Hamburgian and Creswellian. This continuity supports Thévenin's (2000) proposal of a tradition extending from at least the earliest Lower Magdalenian SPs to those of the Hamburgian. Similarly, the Late Badegoulian SP design, for which the relationship to other LGM SPs is at least uncertain, most likely continued in the form of scalene bladelets into the elongated Upper Magdalenian SPs *(Figure 133)*.

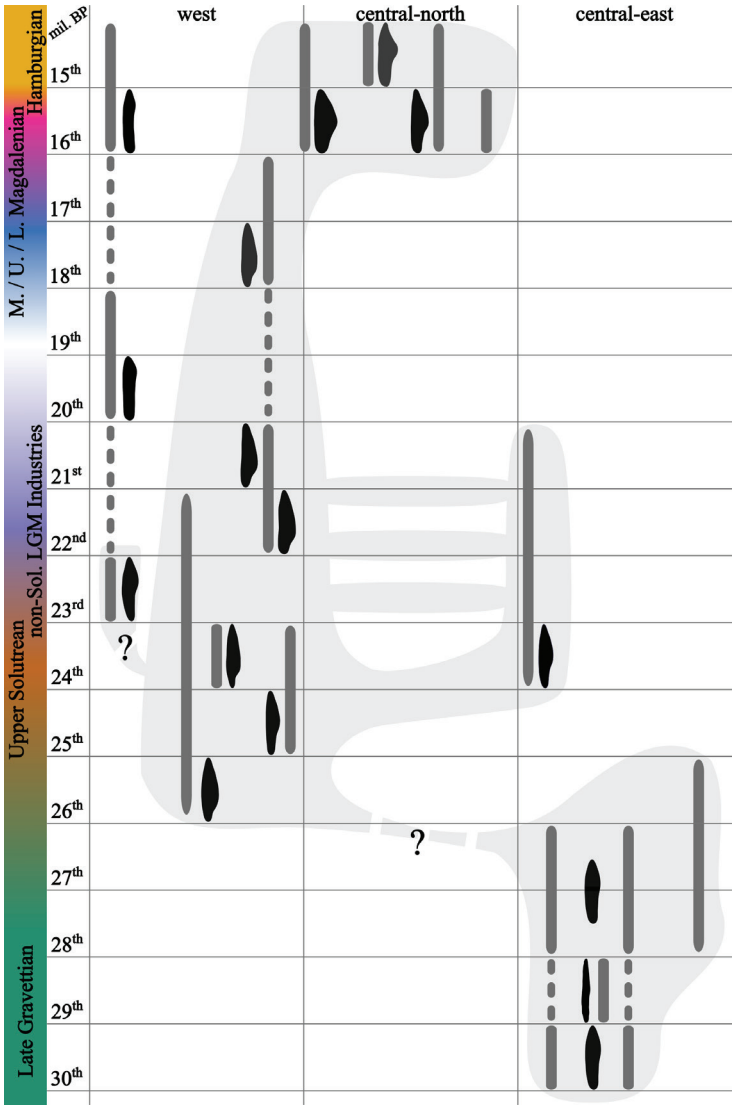



Figure 133: Phylogenetic proposition, coarse geographical distribution in Europe, taxonomic assignment, and shape of SPs (vertical lines = actual time ranges of SP shapes in millennia BP; shapes = representative meanshapes; ? = uncertain relationship; sorting within geographical bins prioritises phylogenetic relations over fine geographical distribution).

# 6. OUTLOOK: PREDICTIVE POTENTIAL OF MORPHOMETRICS

Building on the insights into morphological change over time, this experimental chapter explores whether these patterns can be applied in reverse to chronologically or at least taxonomically sort Class II SPs. As emphasised throughout this study, shape-related features provide the chronologically most sensitive information for SPs. However, individual morphometric features often overlap across millennia and identical values may occur in multiple periods. In contrast, the combined analysis of several features generates an almost unambiguous chronological signal. For example, SPs with upper-lower-ratios between 1 and 1.5 likely occur in the 29th, 25th, 24th, 23rd, 21st, 20th, 15th, and 14th millennia BP. SPs with a l-w-indices of around 3.5 are restricted to the 29th, 20th, 15th, and 14th millennia BP, thereby narrowing the possible chronological position of SPs with such morphometrics. Adding left-right-ratios below 0.5 excludes the 29th and 20th millennia BP, leaving only the 15th and 14th millennia BP as plausible associations. In this exemplary case – the Hamburgian assemblage of Deimern 42 (C-4) – it was possible to determine the most probable age – even though this result adds little to the refinement of broader research questions, as the resolution for Late Upper Palaeolithic contexts remains comparatively coarse – without recourse to geographic context or taxonomic assignment. In more ambiguous cases, however, such information could further refine the chronological attribution, drawing on insights from the archaeo-stratigraphically informed perspective.

This approach resembles early phylogenetic methods in evolutionary biology, before the advent of genetic and molecular techniques (see e.g. López-Antoñanzas et al. 2022). During this period, the position of a specimen within a lineage was inferred from morphological similarities to specimens from stratigraphic sequences, an approach commonly referred to as 'morphological phylogenetics' (Hennig 1950; 1965). In this context, the established morpho-chronology of SPs serves as an evolutionary sequence, comparable to what e.g., Simpson (1951) proposed for horses.

While one might argue that this approach represents yet another typology – albeit based on morphometrics – it overcomes some of the inherent limitations of traditional typologies, particularly their insufficiency in capturing variation (see Maier et al. 2023), and, at least to some degree, their subjectivity. However, this approach should be understood as an experiment. Its reliability is constrained by sample size and dataset composition, and further testing on independent material is required. The results presented here remain largely open to significant changes – particularly for the weaker datasets – as new or previously unavailable data are incorporated.

In most cases, the outcome of this approach may not substantially contribute to specific research questions on the fine-chronological position of the assemblages. Rather, this chapter should be understood as a showcase for its broader applicability in other fields, where morphometric analysis may indeed refine chronological resolution. Within the scope of this study, it primarily serves as a proof of concept, demonstrating that SP morphometrics change systematically over time and thus generate unambiguous chronological patterns.

## 6.1 PREDICTION METHOD

To integrate multiple morphometric features within a single analysis, Principal Component Analysis (PCA) is employed here as both an analytical and a visualisation tool. PCA is a statistical technique used for dimensionality reduction while preserving as much variance (information) in the data as possible (for all further descriptions of the PCA see original literature: Hotelling 1933 and Jolliffe 2002). It transforms a large set of correlated variables – here morphometric features – into a *small*er set of uncorrelated variables called principal components.

In archaeology in a wider sense, PCA is frequently applied in archaeology, especially in combination with Geometric Morphometrics (GMM) (e.g., Owen et al. 2014; Rossini et al. 2023) and genetic analysis (e.g., Charlton et al. 2022). However, since there is no guarantee that variables exhibiting group-level structures of interest will also be the ones contributing the most variance (MacLeod 2018), it is

acknowledged here that alternative statistical methods may offer greater power in detecting group-level structures – e.g., 'Random Forest' (Cole et al. 2022) or Nearest-Neighbour-Classification (Fix & Hodges 1951; Cover & Hart 1967). Such methods provide a promising approach, as they can account for complex, non-linear relationships between variables and may yield more robust classifications of archaeological assemblages. Future research could benefit from integrating such machine-learning-based approaches alongside traditional multivariate analyses to enhance the resolution of cultural and morphological distinctions.

The first step in PCA is to standardise the data so that each feature has an average of zero and a variance of one. This ensures that features with larger ranges do not dominate the analysis. A covariance matrix is calculated to understand how the variables in the dataset are correlated with each other. PCA then computes the eigenvalues and eigenvectors of the covariance matrix. The eigenvectors represent the directions (principal components), and the eigenvalues represent the magnitude of variance in each of those directions. The eigenvalues are sorted in descending order, and the top eigenvectors corresponding to the largest eigenvalues are selected. These eigenvectors form the new axes for the data. Finally, the original data is projected onto the new set of axes formed by the selected eigenvectors, resulting in a transformed dataset with reduced dimensionality, representing the shifted and turned original data distribution (Wickens 1995). A major advantage of PCA is that, while reducing dimensionality, it retains the ability to assess the influence of correlated variables on each principal component. This provides deeper insight into the underlying structure of the data and helps in interpreting the distribution patterns observed. Besides the shape-related features (l-w-index, upper-lower-ratio, left-right-ratio and tip-angle), area is integrated in the analysis as a proxy for size variation.

Additionally, confidence ellipses are applied to group-wise data distributions, encompassing 95% of the data distributions. These ellipses provide a visual representation of the variation within each group, helping to assess the degree of overlap and separation between different groups.

After dimensions have been reduced and features are decorrelated by PCA, Linear Discriminant Analysis (LDA) is applied on the PC scores to predict the group membership of the individual SPs. LDA is a supervised classification method introduced by Fisher (1936). It is used to separate two or more groups by finding linear combinations of predictor variables (called discriminant functions) that maximise the ratio of between-group variance to within-group variance. It computes within-group and between-group scatter matrices and then finds projection directions (linear discriminants) that maximise group separation. It can then assign new samples to the group with the closest discriminant score. PCA helps stabilise LDA in high-dimensional *setting*s by reducing dimensinality and hence noice in the data (e.g., Belhumeur et al. 1997).

Initially, for each analysis a model is trained using the scores of the first five PC axes for all Class I SPs, with the PCA conducted on both Class I and II SPs (Code in Appendix). This allows the model to learn and test the multidimensional distribution space of each group (Class I SPs only). In a first step, the model is validated on a training sub-dataset of Class I SPs, yielding an initial measure of accuracy. In a second step, Class II SPs are assigned to the most probable group based on their scores on the first five PC axes. Predictive accuracy can then be assessed as the proportion of correctly classified versus misclassified SPs. As there is currently no established benchmark for evaluating such models in archaeology, the values reported here should be understood as exploratory, and further research is required to refine both methodology and interpretative frameworks.

When evaluating the model, two key metrics are precision and recall. Precision measures the proportion of samples assigned to a given group that truly belong to it, while recall indicates the proportion of all true samples from that group that were correctly identified. Considering both is essential, as precision alone ignores missed cases, while recall alone ignores misclassifications, and only their balance provides a reliable picture of model performance (see e.g., Buckland & Gey 1994).

It should be emphasised that model accuracy could potentially be improved by removing outliers from the Class I assemblages prior to training or reducing the input training data

to, e.g. the first three PC axes. Developing and testing such methodological refinements, however, lies beyond the scope of this study and will be a matter for future research.

## 6.2 TAXONOMIC PREDICTION

The explorational excurse will start by showcasing the predictive potential of morphometrics on the level of taxonomic units. To begin, the two taxonomical units that yielded the most distinct morphometrics – the Late Gravettian and the Iberian Upper Solutrean – will be used as a case study. Afterwards, a more ambiguous test will compare the Upper Solutrean and the Salpetrian and test the predictive potential.

### 6.2.1 Late Gravettian – Upper Solutrean

As this study has demonstrated, Late Gravettian and Iberian Upper Solutrean SPs differ markedly in their overall shape composition. Consequently, the approach applied here should largely prevent Class II SPs from eastern Central Europe assigned to the Late Gravettian from clustering within the range of Class I Upper Solutrean SPs from the Iberian Peninsula, and *vice versa*.

Although slight overlaps between the confidence ellipses are observable, the two taxonomic units separate quite clearly along the first and second PC axes, with the Class II Late Gravettian SPs falling well within the confidence ellipse of the Class I Late Gravettian SPs *(Figure 134)*. The first axis (PC1) accounts for 37.4% of the variation in the data and is primarily driven by variation in tip-angle (0.63) and upper-lower-ratio (-0.48), while the second axis (PC2) accounts for 24.9% of the variance in the data and is dominated by l-w-index (0.8) and, again, upper-lower-ratio (-0.42) – a pattern fully consistent with the results presented earlier that highlighted the pronounced shape-differences between the Late Gravettian and the Upper Solutrean SPs.

This pattern is reproduced in the analysis of the Class II SPs of the Upper Solutrean *(Figure 135)*. Despite some overlap, both taxonomic units separate clearly, with the Class II SPs falling well within the range of the Class I Upper Solutrean SPs. Once again, variation along PC1, accounting for 35.5% of the variance in the data, is primarily driven by tip angle (0.6) and upper–lower ratio (-0.55), whereas PC2, capturing 27.2% of the variance in the data, is dominated by l–w index (0.8), with additional contributions from the tip angle (-0.4) and area (0.31).

PC scores can also be calculated for lower axes to further explore potential group separation. In this case, clear separation is observable not only on the first and second axes, as previously demonstrated, but also on the fourth axis (PC4; *Figure 137*). This additional evidence further underscores the robustness of the approach at a coarse chronological scale. *(Figure 134–137)*

A LDA conducted on the scores of the first five principal components from a joint PCA (Figure 136 and 137) yields an overall accuracy of 0.86 (0.87 cross-validation accuracy) with a 1.0 precision and 0.75 recall for Late Gravettian and a 0.75 precision and 1.0 recall for Upper Solutrean SPs. The model reliably assigned Class II SPs to their respective taxonomic units: out of 101 specimens, only 12 were misclassified, corresponding to a prediction accuracy of 88% *(Table 66)*.

The misclassified SPs include single specimens from Zamostya I (C-49; n = 1) and Baío (C-25; n = 1), as well as all or multiple SPs from Cueva del Parpalló (C-32–C-30; n = 4), Cueva del Reclau Viver (C-33; n = 3), El Pendo (C-35; n = 2), and Legintxiqui (D-21; n = 1). On average, the 96% correctly assigned Late Gravettian SPs were assigned to with a probability of 0.86, whereas Iberian Upper Solutrean SPs were classified to their correct unit with a slightly lower mean probability of 0.76.

This result once again underscores the pronounced shape differences between Late Gravettian and Upper Solutrean SPs, making them an especially suitable case for a first exploratory test. The resulting accuracy is remarkable: one could imagine placing 100 Late Gravettian and Upper Solutrean SPs randomly on a table – without considering raw material, origin or retouches at all – and still assigning them to their respective taxonomic units with almost 90% accuracy. *(Table 66)*

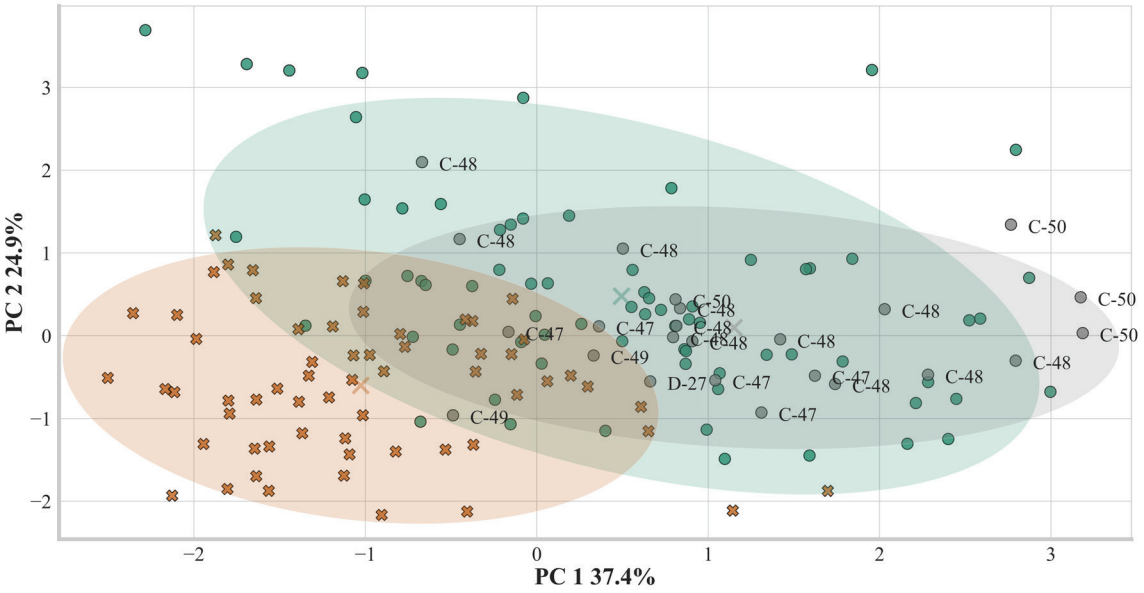



Figure 134: First two principal components of the Principal Component Analysis (PCA) for between Late Gravettian, Upper Solutrean, and Class II Late Gravettian SPs (Late Gravettian = green dots; Upper Solutrean = orange crosses; Class II Late Gravettian = grey dots; labels = IDs for the Class II assemblages).

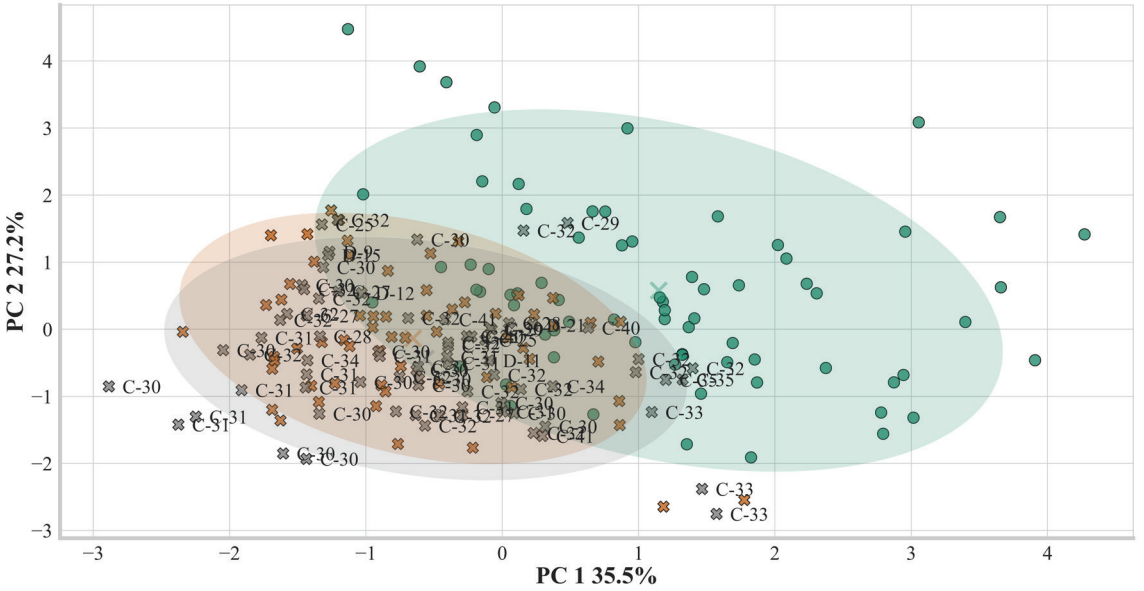



Figure 135: First two principal components of the Principal Component Analysis (PCA) for between Late Gravettian, Upper Solutrean and Class II Upper Solutrean SPs (Late Gravettian = green dots; Upper Solutrean = orange crosses; Class II Upper Solutrean = grey crosses; labels = IDs for the Class II assemblages).

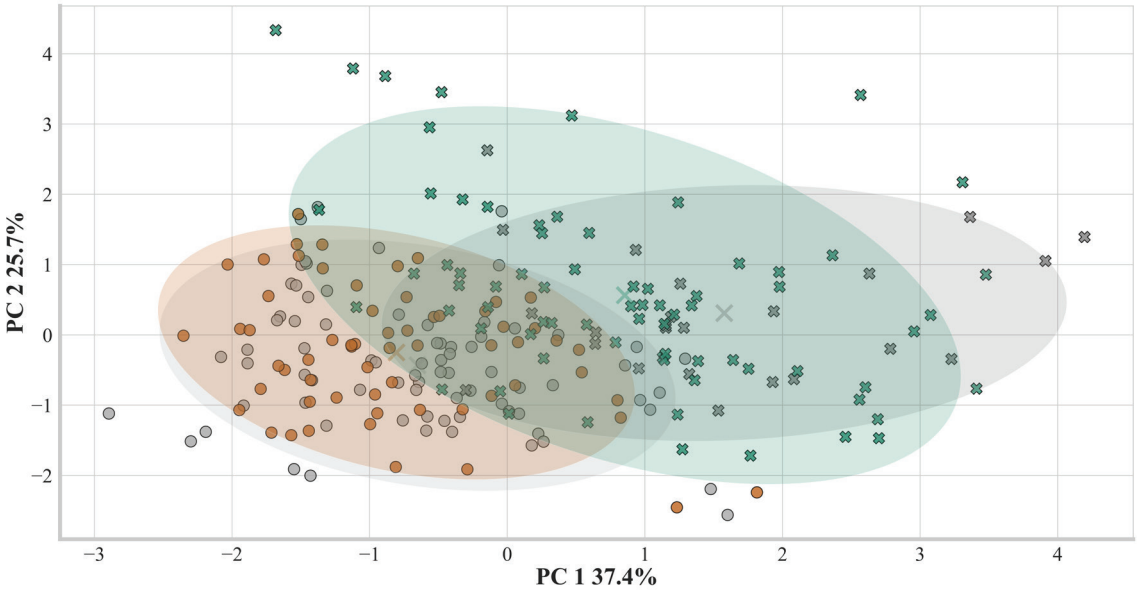



Figure 136: First two principal components of the Principal Component Analysis (PCA) for between Late Gravettian and Upper Solutrean Class I and II SPs (Late Gravettian = green crosses; Upper Solutrean = orange dots; Class II Late Gravettian = dark grey crosses; Class II Upper Solutrean = grey dots; labels = IDs for the Class II assemblages).

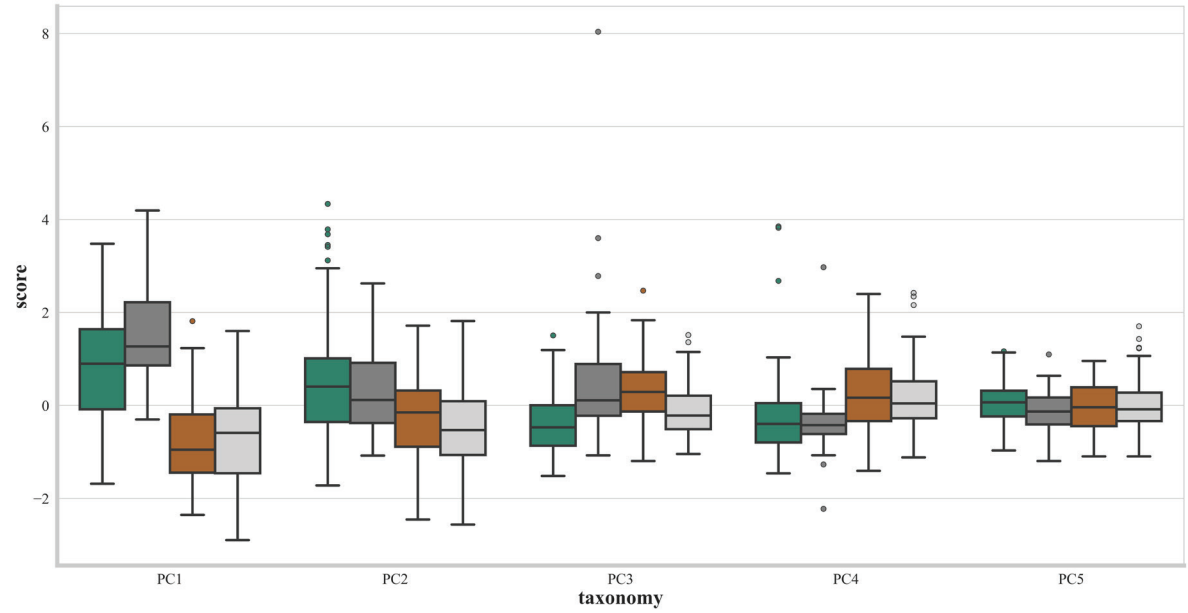



Figure 137: PC scores across the first five principal components of a joined Principal Component Analysis (PCA) for between Late Gravettia, Iberian Upper Solutrean and Class II Iberian Upper Solutrean SPs (Late Gravettian = green boxes; Class II Late Gravettian = grey boxes; Iberian Upper Solutrean = orange boxes; Class II Iberian Upper Solutrean = light grey boxes).

### 6.2.2 Upper Solutrean – Salpetrian

This study has so far revealed only minor morphometrical differences between Salpetrian SPs and Upper Solutrean SPs in general, and especially when compared with Iberian Upper Solutrean SPs (Chapter 4.2.2.2). Consequently, applying the present approach in this case is expected to yield more ambiguous results. This is further *compound*ed by the fact that the assemblages considered here are geographically closer to one another, or at least within overlapping distribution ranges, in contrast to the previous case study.

Iberian and French Upper Solutrean SPs overlap only very slightly on the first two PC axes – where PC1 accounts for 37.7% and PC2 for 24.1% of the data distribution – once more highlighting the pronounced morphometrical differences between the two regional expressions of this taxonomic unit *(Figure 138)*. The separation is almost without overlap on the PC2, which is primarily driven by the upper-lower-ratio (-0.75), area (0.47) and the tip angle (0.38). Both, the Class I and II SPs of the Salpetrian align clearly with the distribution of the Iberian Upper Solutrean, as well separating from the French Upper Solutrean SPs on the second axes.

The Class II SPs for the Upper Solutrean support the separation between the two regional expressions – Iberian and French Upper Solutrean – as they clearly align with the distribution of their respective Class I SPs and thereby solidify the result *(Figure 139)*. *(Figure 138–141)*

A LDA conducted on the scores of the first five principal components from a joint PCA *(Figure 140 and 141)* yields an overall accuracy of 0.88 (0.87 cross-validation accuracy) with a 0.92 precision and 0.92 recall for Iberian Upper Solutrean and a 0.8 precision and 1.0 recall for French Upper Solutrean SPs. No precision nor recall is calculatable for the Salpetrian, as there are too few SPs left after training the model. The model reliably assigned Class II SPs to their respective taxonomic units: out of 155 specimens, only 47 were misclassified, corresponding to a prediction accuracy of 0.7 *(Table 67)*.

The misclassified SPs include seven specimens from Cueva del Parpalló (C-32–C-30) that are assigned to the Salpetrian, both specimens from Cueva del Boquete Zafarraya (C-29) assigned to the French Upper Solutrean, two specimens from Baume d´Oullins (C-26) and a single SP from Pech de la Boissière (C-44) assigned to the Salpetrian, multiple French Upper Solutrean SPs assigned to the Iberian Upper Solutrean – including all specimens from Petite Grotte de Bize (C-45; n = 11), three specimens from each Baume d´Oullins (C-26) and Les Jean-Blancs (C-42), two SPs from each Pech de la Boissière (C-44) and Tourtoirac (C-46), a single SP from each Fourneau du Diable, layer Solutrean superior I (C-36) and Oreille-d´Enfer (C-43), the single specimens from Brassempouy (D-10), Grotte des Eyzies (D-14), La Pasiega (D-18), Noailles (D-23), Roc de Sers (D-25) and Saint-Front-de-Corgnac (D-26) – and a single specimen from each Cadenet (C-23) and La Rouviére (C-24) assigned to the Iberian Upper Solutrean as well as a single SP from La Rouviére (C-24) assigned to the French Upper Solutrean. *(Table 67)*

On average, the 84% of correctly classified Iberian Upper Solutrean SPs were assigned with a mean probability of 0.82, whereas only 56% of the French Upper Solutrean SPs were correctly classified, with a considerably lower mean probability of 0.57. For the Salpetrian, the very limited number of SPs likely proved insufficient to train the model adequately. The three correctly classified specimens yielded only a low mean probability of 0.52, underlining the limitations of the current dataset.

However, this outcome also reflects the genuinely minor morphometric differences between Salpetrian and Upper Solutrean SPs. By contrast, the pronounced differences between Iberian and French Upper Solutrean SPs are clearly mirrored in the comparatively low rates of cross-misclassification.

Despite the low probabilities for the Salpetrian and the greater ambiguity of the latter case, the results nonetheless demonstrate the potential of morphometric analysis as a predictive tool for taxonomic classification.

## 6.3 TYPOLOGICAL PREDICTION

Having shown previously that this method can assist in distinguishing between Iberian and French Upper Magdalenian SPs, the following case study turns to what is potentially an even clearer test case: the differentiation of Upper

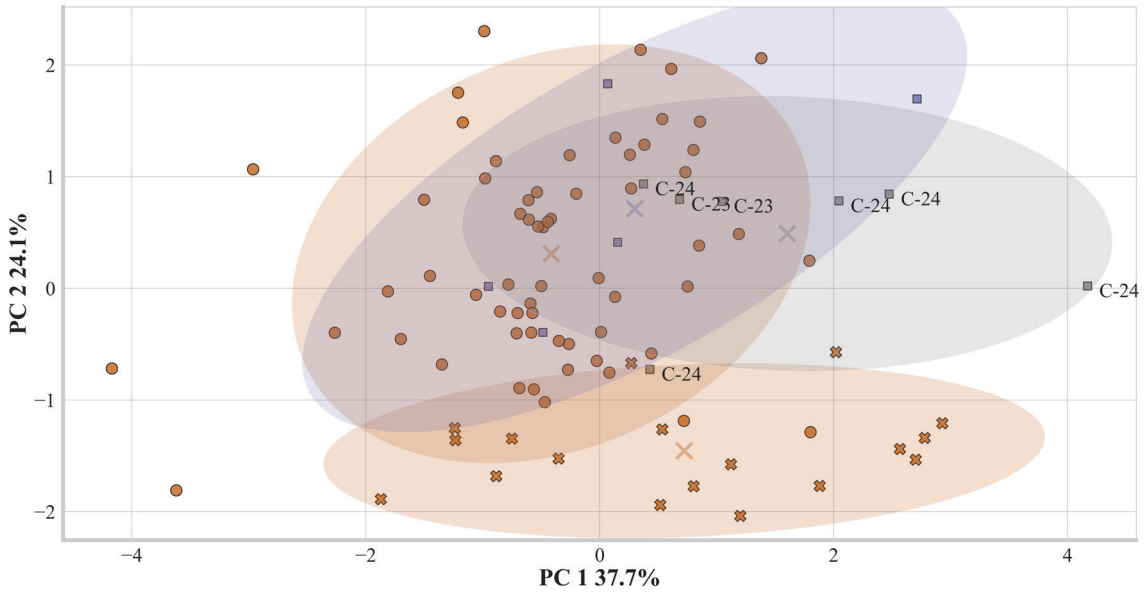



Figure 138: First two principal components of the Principal Component Analysis (PCA) for between Iberian and French Upper Solutrean, and Salpetrian Class I and II SPs (Iberian Upper Solutrean = orange dots; French Upper Solutrean = orange crosses; Salpetrian = violet squares; Class II Salpetrian = grey squares; labels = IDs for the Class II assemblages).

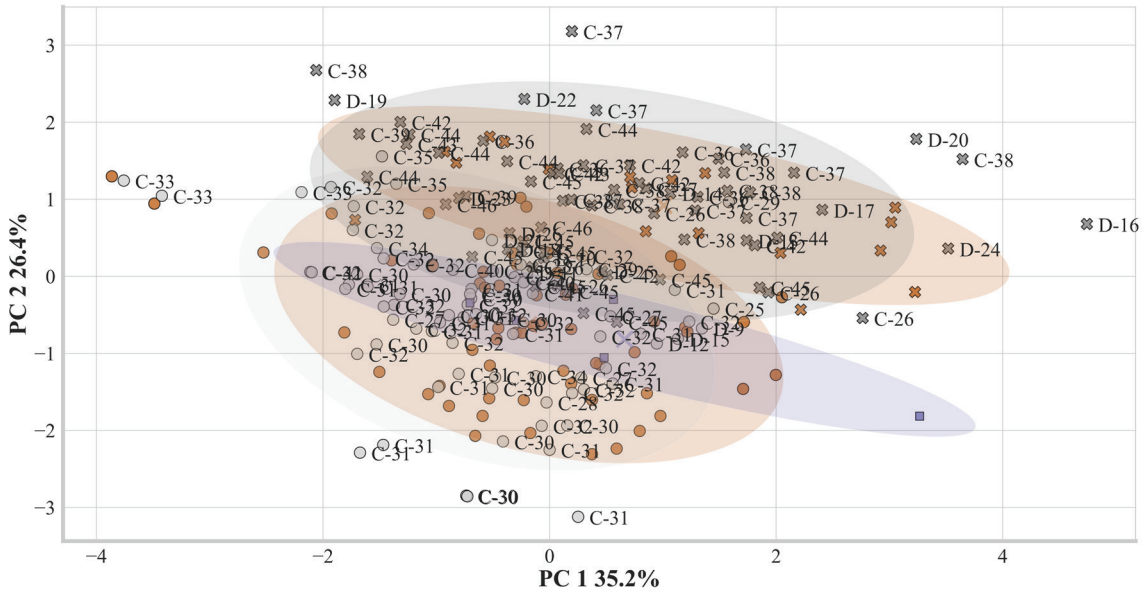



Figure 139: First two principal components of the Principal Component Analysis (PCA) for between Iberian and French Upper Solutrean Class I and II, and Salpetrian SPs (Iberian Upper Solutrean = orange dots; French Upper Solutrean = orange crosses; Salpetrian = violet squares; Class II Iberian Upper Solutrean = light grey dots; Class II French Upper Solutrean = grey crosses; labels = IDs for the Class II assemblages).

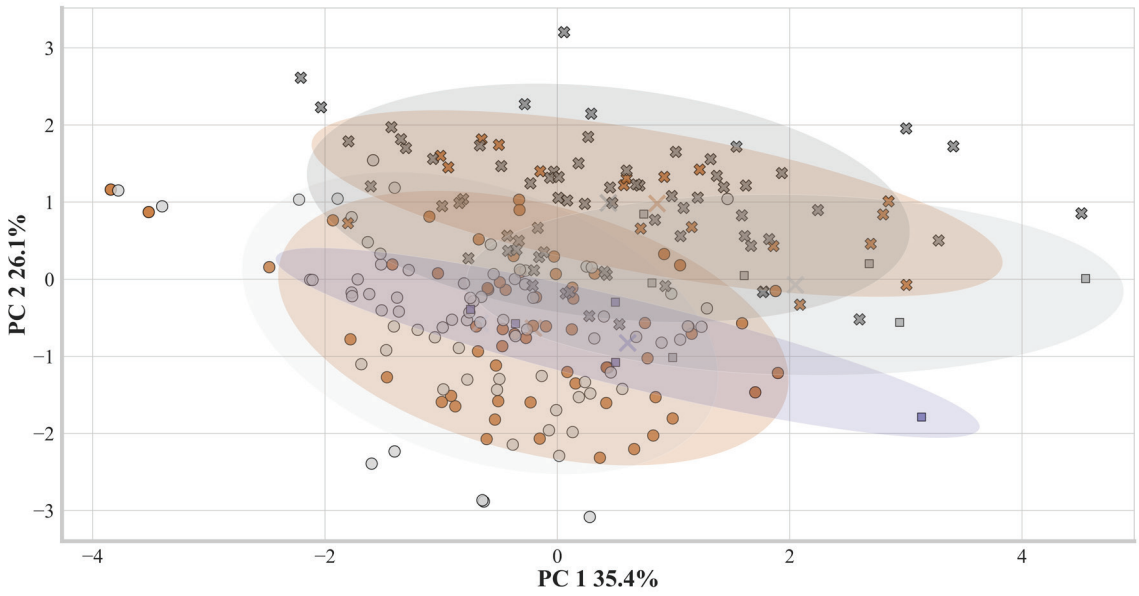



Figure 140: First two principal components of the Principal Component Analysis (PCA) for between Iberian and French Upper Solutrean Class I and II, and Salpetrian Class I and II SPs (Iberian Upper Solutrean = orange dots; French Upper Solutrean = orange crosses; Salpetrian = violet squares; Class II Iberian Upper Solutrean = grey dots; Class II French Upper Solutrean = dark grey crosses; Class II Salpetrian = grey squares).

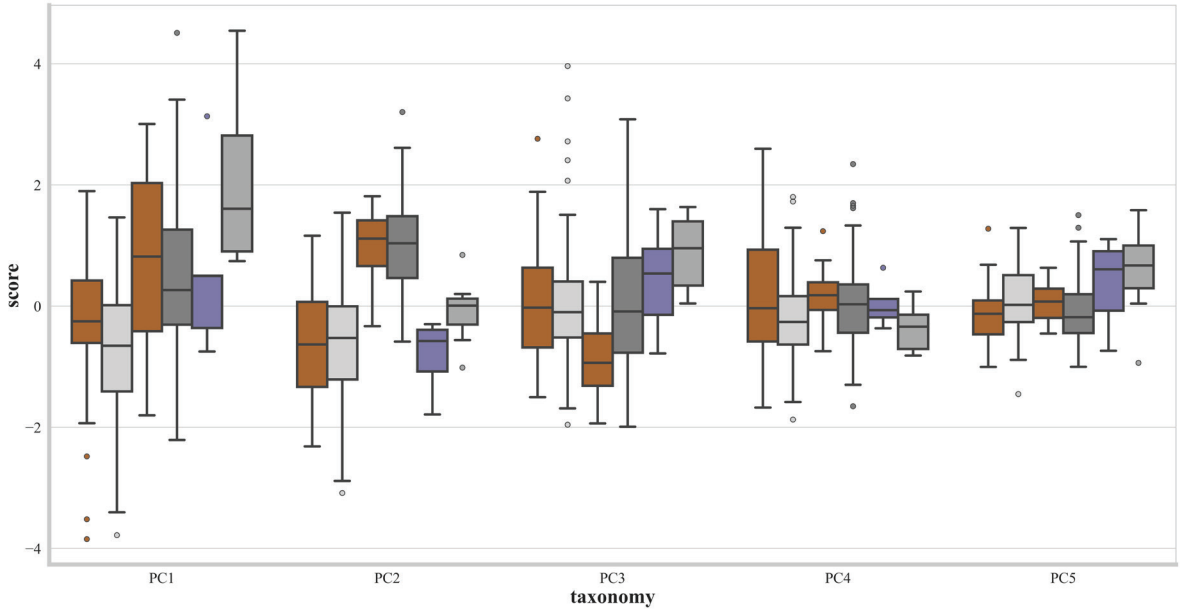



Figure 141: PC scores across the first five principal components of a joined Principal Component Analysis (PCA) for between Iberian Upper Solutrean, French Upper Solutrean, Salpetrian and the respective Class II SPs (Iberian Upper Solutrean = left orange boxes; Iberian Upper Solutrean = right orange boxes; Class II Iberian Upper Solutrean = light grey boxes; Class II French Upper Solutrean = dark grey boxes; Salpetrian = violet box; Class II Salpetrian = grey boxes).

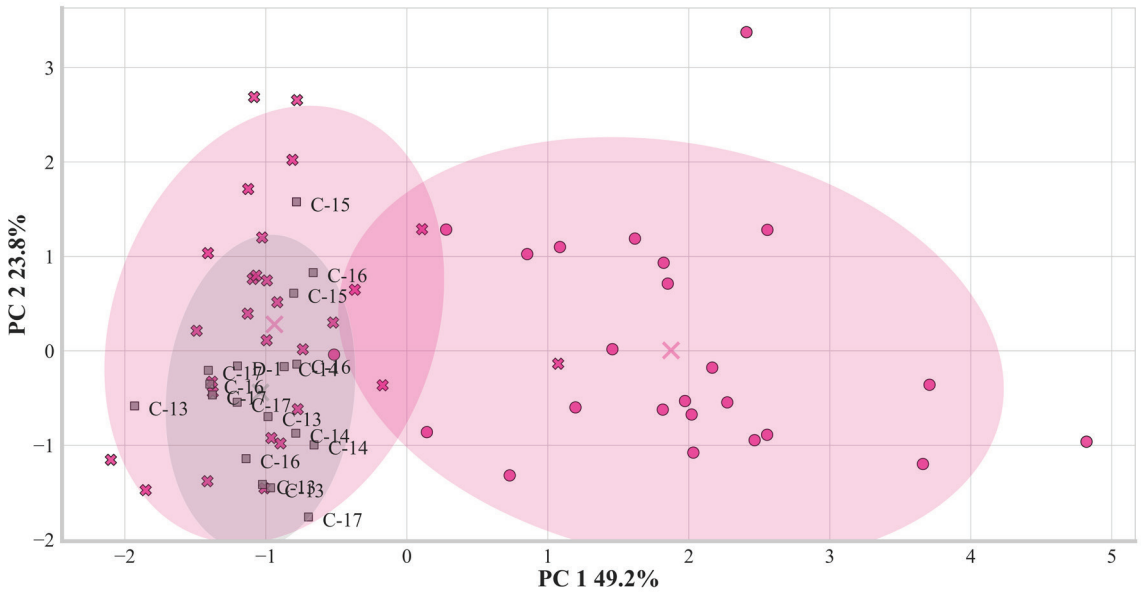



Figure 142: First two principal components of the Principal Component Analysis (PCA) for between Class I Upper Magdalenian SPs of Type A and B and Class II Upper Magdalenian SPs (Upper Magdalenian Type A = pink dots; Upper Magdalenian Type B = pink crosses; Class II Upper Magdalenian SPs = grey squares; labels = IDs for the Class II assemblages).

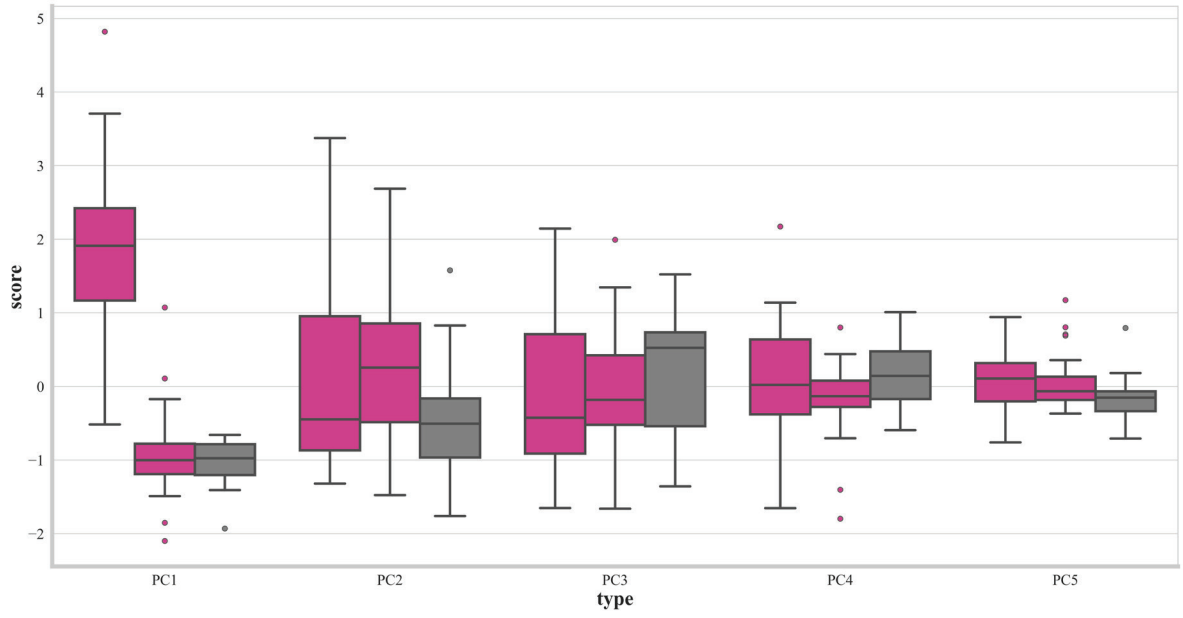



Figure 143: PC scores across the first five principal components of a joined Principal Component Analysis (PCA) for between Class I Upper Magdalenian SPs of Type A and B and Class II Upper Magdalenian SPs (Upper Magdalenian Type A = left pink boxes; Upper Magdalenian Type B = right pink boxes; Class II Upper Magdalenian SPs = grey boxes).

Table 66: Scores of the LDA for the Late Gravettian and the Iberian Upper Solutrean Class I and II.

| | misclassified | Class II total | accuracy | x̄ prob. | Late Gravettian | Upper Solutrean |
|---|---|---|---|---|---|---|
| **Late Gravettian** | 1 | 25 | 0.96 | 0.86 | 24 | 1 |
| **Upper Solutrean** | 11 | 77 | 0.86 | 0.76 | 11 | 66 |
| **total** | 12 | 101 | 0.88 | | | |

Table 67: Scores of the LDA for the Iberian and French Upper Solutrean Class I and II, and Salpetrian Class I and II SPs.

| | misclassified | Class II total | accuracy | x̄ prob. | Iberian Upper Solutrean | French Upper Solutrean | Salpetrian |
|---|---|---|---|---|---|---|---|
| **Iberian Upper Solutrean** | 12 | 77 | 0.84 | 0.82 | 55 | 5 | 7 |
| **French Upper Solutrean** | 31 | 71 | 0.56 | 0.57 | 28 | 40 | 3 |
| **Salpetrian** | 4 | 7 | 0.43 | 0.52 | 2 | 1 | 4 |
| **total** | 47 | 155 | 0.70 | | | | |

Magdalenian SP types. The Class II assemblages included in this case study originate from western Germany (C-13, C-14, D-1), Switzerland (C-15, C-17), and France (C-16), comprising a total of 18 SPs.

As emphasised repeatedly throughout this study, the two Upper Magdalenian SP types differ markedly (Chapter 4.2.1.2.4). This distinction is strongly reflected on the first PC axis *(Figure 139)*, which explains 49.2% of the total variation in the dataset and is primarily influenced by the l-w-index (0.59), the upper-lower-ratio (-0.53), and the left-right-ratio (0.54). The distribution of the Class II Upper Magdalenian SPs is confined to the negative side of PC1, showing a pronounced alignment with Type B SPs. This correspondence is further supported by the visual inspection of the individual SPs (Appendix Plates 61, 62, 7, 28, 102, 159), which exhibit clear morphological traits of the stouter type.

On the lower axes, this pronounced distinction between the types disappears *(Figure 142)*, as the first axis already captures a substantial proportion of the variation, leaving little explanatory power for the subsequent axes. This further underlines that PC1 is the most important axis for the morphological distinction.*(Figure 142 and 143)*

A LDA conducted on the scores of the first five principal components from a joint PCA *(Figure 143)* yields an overall accuracy of 91% (93% cross-validation accuracy) with a 1.0 precision and 0.8 recall for the Type and 0.86 precision and 1.0 recall for the Type B of the Class I Upper Magdalenian SPs. The model reliably assigned all Class II SPs to Type B Upper Magdalenian SPs (Table 68). On average, the Class 2 SPs were assigned with a mean probability of 0.996. *(Table 68)*

Table 68: Scores of the LDA for the Class I Upper Magdalenian SPs of Type A and B and Class II Upper Magdalenian SPs.

| | misclassified | Class II total | accuracy | x̄ prob. | Upper Magdalenian Type A | Upper Magdalenian Type B |
|---|---|---|---|---|---|---|
| **Upper Magdalenian Type A** | 0 | 0 | / | / | / | / |
| **Upper Magdalenian Type B** | 0 | 18 | 1.0 | 1.0 | 0 | 18 |
| **total** | 0 | 18 | 1.0 | | | |

This case study demonstrates the potential of this method for predicting the taxonomic affiliation of unassigned artefacts. At the same time, it must be regarded as a proof of concept: future studies will need to rigorously test and refine its applicability across other artefact categories and datasets before broader conclusions can be drawn.

## 6.4 CHRONOLOGICAL PREDICTION

Finally, the method is tested for its potential to predict the chronological position of SPs. This analysis draws on the complete set of Class I SPs and the morphometric developments outlined in the result Chapter 4.1.3. The two assemblages used as a case study here have been radiometrically dated but were excluded from the Class I dataset for specific reasons (*Table 2*; Appendix Table 17).

The LDA classification based on the scores of the first five principal components from a joint PCA with all Class I SPs yields an overall accuracy of only 25% (cross-validation accuracy is 25% as well). It shows a generally low performance across most centuries, largely due to sparse sample sizes, overlapping group structure and high within-group variation. Classes with very limited support (e.g., 14$^{th}$, 17$^{th}$, 18$^{th}$, 29$^{th}$, 30$^{th}$ millennium BP) were not successfully identified (precision and recall = 0) *(Table 69)*. Among groups with higher support, the 15$^{th}$ century achieved the best recall (0.67, support = 15) but low precision (0.27), while the 27$^{th}$ century showed the highest balance (F1 = 0.50, support = 5). The elevated f1-scores for the 27$^{th}$, the 25$^{th}$ and the 15$^{th}$ millennium BP highlights, that the model picks up many samples from these millennia and classifies them correctly but also misclassifies others as such. Overall, classification accuracy is poor, suggesting that finer chronological divisions tend to be difficult to separate reliably with the current dataset. *(Table 69)*

### 6.4.1 Berdyzh

Three radiometric dates are available for Berdyzh. However, it was not possible to calculate a WA, since two conventional dates with sufficient standard deviation are too far apart. The third date, obtained via AMS, shows a standard deviation exceeding the quality threshold of 1.5 applied in this study and is also much too young compared to the expected age of the site. The most recent date published by Demay et al. (2021) suggests an age of approximately 26.7 ka calBP, placing Berdyzh within the 27$^{th}$ millennium BP. The site, located in present-day Belarus, can thus only reasonably be associated with the Late Gravettian – an attribution that also aligns with the chronological evidence.

Nevertheless, the Late Gravettian is not an especially suitable case study for fine-scale chronological prediction of SPs based on morphometry, as this study has shown that it displays considerable internal variability and only weak signals of directed chronological development.

Table 69: Classification report for the LDA model trained on the scores of the first five principal components from a joint PCA with all Class I SPs (bold = millennia BP with sufficient support).

| | precision | recall | f1-score | support |
|---|---|---|---|---|
| **14th** | 0.00 | 0.00 | 0.00 | 1 |
| **15th** | 0.27 | 0.67 | 0.38 | 15 |
| **16th** | 0.29 | 0.25 | 0.27 | 8 |
| **17th** | 0.00 | 0.00 | 0.00 | 2 |
| **18th** | 0.00 | 0.00 | 0.00 | 1 |
| **19th** | / | / | | / |
| **20th** | 0.00 | 0.00 | 0.00 | 4 |
| **21st** | 0.00 | 0.00 | 0.00 | 6 |
| **22nd** | 0.14 | 0.2 | 0.17 | 5 |
| **23rd** | 0.00 | 0.00 | 0.00 | 3 |
| **24th** | 0.25 | 0.14 | 0.18 | 7 |
| **25th** | 0.50 | 0.25 | 0.33 | 4 |
| **26th** | 0.00 | 0.00 | 0.00 | 3 |
| **27th** | 0.67 | 0.40 | 0.50 | 5 |
| **28th** | 0.11 | 0.20 | 0.14 | 5 |
| **29th** | 0.00 | 0.00 | 0.00 | 1 |
| **30th** | 0.00 | 0.00 | 0.00 | 2 |

The distribution of the Berdyzh SP morphometrics on the first five PC axes *(Figure 144)* appears promising but also exposes a fundamental issue: the morphometric signatures of the last three millennia (16th, 15th, 14th) overlap considerably with those of the Late Gravettian millennia at the beginning of the dataset.*(Figure 144)*

It is therefore unsurprising that the LDA assigns three of the five Berdyzh SPs to the 15th millennium BP, as this portion of the dataset provides stronger statistical support for the model. Nonetheless, the average probability for an assignment to the 27th millennium BP ranks third (0.15; 15th = 0.25; 16th = 0.20), and one SP is indeed classified accordingly. Another specimen is assigned to the 30th millennium BP, which – while not chronologically precise – still situates it within a Late Gravettian context. This underlines both the potential and the current limitations of the method: while broad taxonomic affiliations can be captured, fine-scale chronological placement remains problematic when morphometric overlap exists across distant time periods.

However, if the chronological frame of this case study is constrained to plausible ranges for the specific geographical *setting* – here, the Late Gravettian millennia only *(Figure 145)* – the predictive performance improves considerably. Under these conditions, the LDA assigns four of the Berdyzh SPs to the 27th millennium BP, with a mean probability of 45%. The fifth specimen is classified to the 28th millennium BP with a probability of 37%, only marginally higher than the 31% probability for an assignment to the 27th millennium BP. This demonstrates that narrowing the chronological frame to archaeologically reasonable ranges can substantially enhance the predictive value of the method, while also underscoring that probabilistic uncertainty remains inherent in borderline cases. *(Figure 145)*

### *6.4.2 Baume d'Oullins, layer D*

For Baume d'Oullins, three radiometric dates were published by Bazile (1990). Due to the elevated standard deviation of two dates – exceeding the quality threshold applied in this study – a weighted average could only be partially relied upon, yielding 24.7 ka calBP and placing the assemblage within the 25th millennium BP. While the assemblage is generally assigned to the French Upper Solutrean, a purely chrono-geographical perspective would also allow a possible assignment to the Salpetrian.
The distribution of the Baume d'Oullins SPs across the first five PC axes is already highly informative *(Figure 146)*. In particular, on the first axis, the SPs align closely with the Solutrean-driven millennia (especially the 25th and 24th millennium BP), despite some overlaps with younger periods.

The LDA assigns two SPs from Baume d'Oullins to the 24th millennium BP with a mean probability of 30%. Another specimen is classified as belonging to the 25th millennium BP

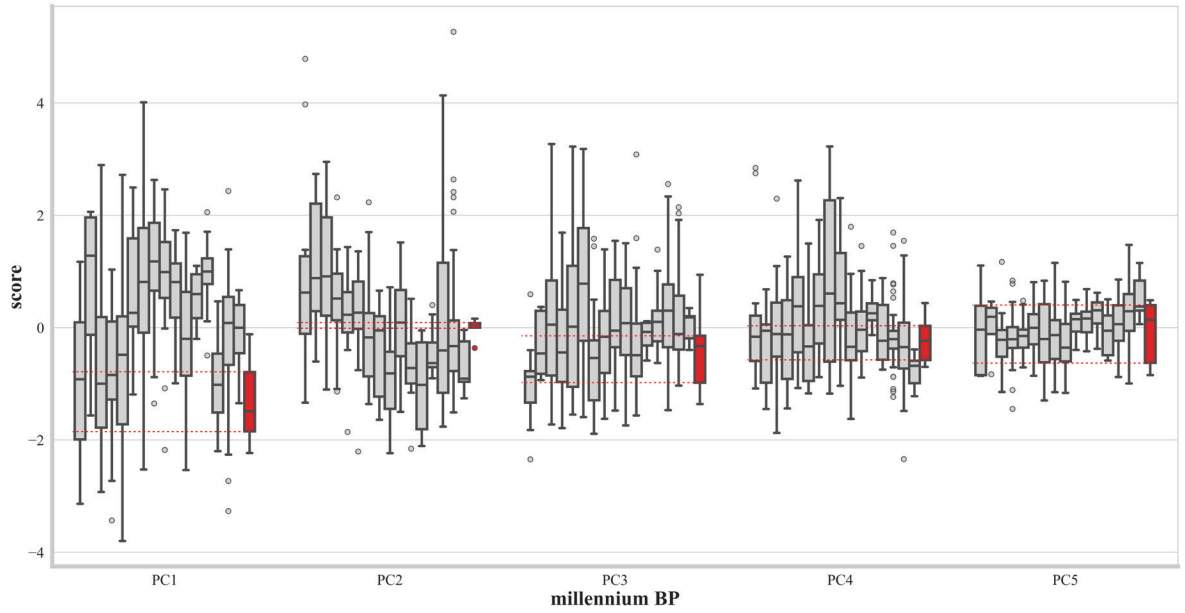



Figure 144: PC scores across the first five PC axes for all millennia BP and Berdyzh (older to younger from left to right; 30th–14th millennium BP; millennia BP = light grey; Berdyzh = red).

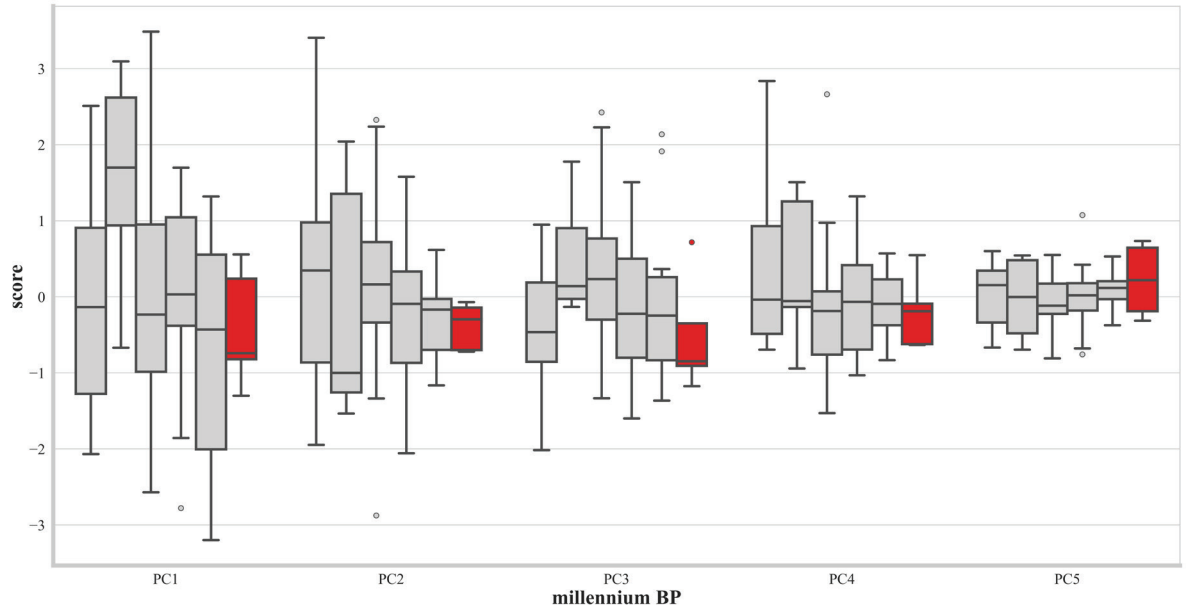



Figure 145: PC scores across the first five PC axes for Late Gravettian millennia BP (30th–26th millennium BP) and Berdyzh (older to younger from left to right; millennia BP = light grey; Berdyzh = red).

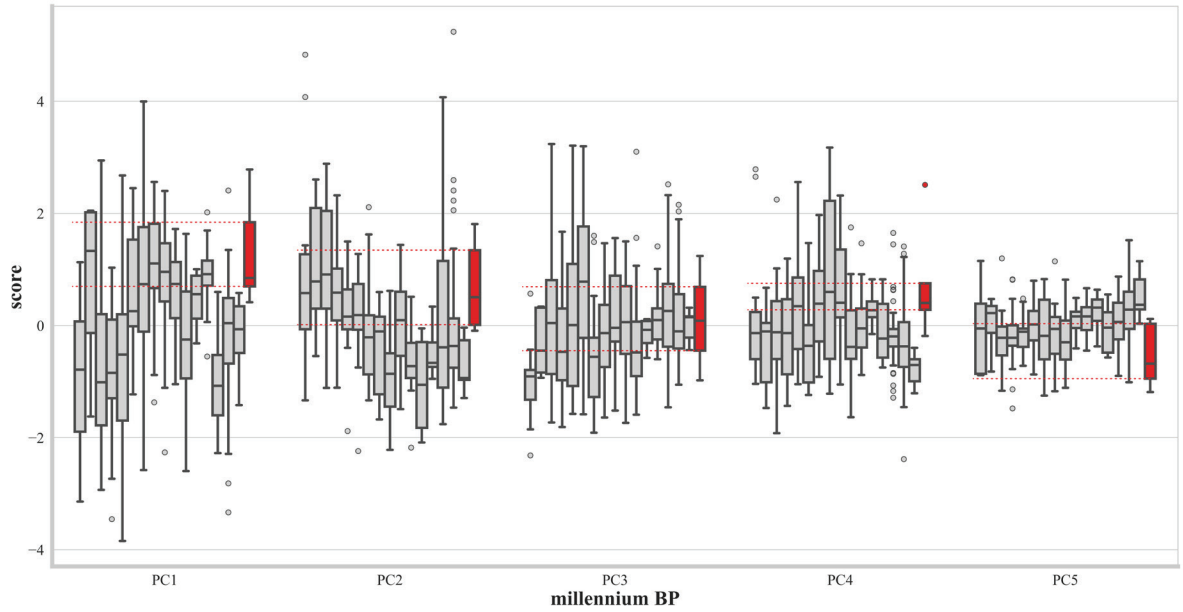



Figure 146: PC scores across the first five PC axes for all millennia BP and Baume d'Oullins, layer D (older to younger from left to right; millennia BP = light grey; Berdyzh = red).

with a probability of 38%. One SP is assigned to the 22nd millennium BP with a probability of 70%, reflecting the overlap with younger millennia noted above. The final SP is placed in the 15th millennium BP, which likely represents an artefact of the elevated recall for this later millennium. Overall, these results align comparatively well with the WA, as three of the five SPs are confidently placed close to it, supporting the effectiveness of the morphometric approach in approximating the chronological position of the Baume d'Oullins assemblage. *(Figure 146)*

The exploratory approach conducted here, while not yet fully developed, yielded notably reliable predictions. It demonstrated considerable potential for both taxonomic and chronological assignments, though certain limitations remain – some of which may be specific to SPs, where particular morphometric characteristics tend to reappear. Furthermore, the results highlighted the potential for typological prediction, underscoring the need for further studies in this direction.

# 7. SUMMARY

This study has presented the most comprehensive collection of shouldered points and associated radiocarbon data compiled to date. By bringing together an unprecedented breadth of depictions, metric data, and chronological evidence – spanning approximately 16.000 years – it has created a unique foundation for addressing questions about long-term cultural dynamics during the Late Pleistocene. The dataset not only enables fine-grained analyses of morphological variation but also provides the chronological anchors required to trace cultural macro-evolutionary trajectories across space and time. This scale of integration marks a significant advance in research on shouldered points, which has previously been dominated by regional case studies detached from broader chronological frameworks (e.g., Demars & Laurent 1992; Boccacio 2005; Livache & Brochier 1976; Lenoir 1975) or restricted to typo-technological comparisons (e.g., de Sonneville-Bordes & Perrot 1956; Monmejan et al. 1964; Leroi-Gourhan 1964; Bordes 1965; Brézillon 1971).

At the same time, this study introduces a methodological toolkit explicitly designed for the analysis of chronological developments in the morphology of cultural objects. Borrowing concepts and methods from (palaeo-) biology and ecology, it adapts methods such as Redundancy Analysis (RDA), Coefficient of Variation (CV) and change rates to the archaeological record. These approaches allow for the systematic quantification of size and shape variation, and the identification of structured chronological patterns. By framing material culture as a dynamic system subject to measurable variation and change, this study demonstrates the benefits of methodological cross-pollination between the natural sciences and archaeology.

Initially, two separate approaches were undertaken: one focusing exclusively on chronological changes, and the other incorporating both taxonomic units and, where feasible, geographical position. The morphometric analyses on both perspectives revealed meaningful patterns of variation and change, which clearly showed that shouldered points are not static artefacts but evolve in ways that can be quantified and chronologically situated. Several key themes emerged:

### *Duration and Timing*

Trends could be identified across different chronological scales of periodisation. Although relatively weak, some patterns were still discernible over a span of 5000 years. At finer scales, the occasionally limited availability of data reduced the significance of observable trends, but returned stronger signals for chronologically directed change. The 2000-year scale was selected for subsequent analysis as a compromise between granularity and over-refinement, as well as because it offered strong data support for most of the 2000-year intervals.

Morphological change is not constant but clusters within particular periods, most notably between the 27$^{th}$ and the 25$^{th}$ millennium BP, as well as between the 22$^{nd}$ and the 20$^{th}$ millennium BP and between the 17$^{th}$ and the 15$^{th}$ millennium BP. These periods tend to correlate with major taxonomic transitions. However, trends were also observable within individual taxonomic units. Notably, in cases with sufficient data, such trends likely occurred at the end and at the beginning of the respective taxonomic unit.

### *Variation*

Variation itself appears to be historically meaningful, potentially reflecting phases of experimentation, consolidation, or regional differentiation. From a purely chronological perspective, a cyclical pattern of variation was observed. This is characterised by an initial high degree of variation, followed by a decline until approximately the 27$^{th}$ millennium BP. Variation then increased, reaching a peak around the 25$^{th}$ millennium BP, before declining again and remaining notably low between the 24$^{th}$ and the 20$^{th}$ millennium BP. Finally, after shouldered points have virtually been absent for roughly 2000 years, in the 17$^{th}$ millennium BP, variation is elevated once more before undergoing a final decrease.

Internal variation within taxonomic units is uneven. The Late Gravettian, for instance, exhibits considerable internal variation, whereas the Upper Magdalenian and Hamburgian demonstrate tendencies towards standardisation. The larger taxonomic units – the Late Gravettian and the Upper Solutrean – also display elevated variation at the onset of the

introduction of shouldered points, which subsequently declines over the duration of the respective taxonomic unit. This further reinforces the notion of consolidation occurring over several millennia following the introduction of shouldered points into a given geographical region or technological spectrum, aligning with Rosa's 'law of progressive reduction in variability' (1903).

### *Change*

Not all chronological phases are equally transformative. Certain periods show minor adjustments, while others reveal profound reconfigurations of size and shape. The most pronounced changes were observed between the 26$^{th}$ and the 24$^{th}$ millennium BP, corresponding to the transition from the Late Gravettian to the Upper Solutrean, as well as to the differentiation between Iberian and French Upper Solutrean shouldered points. By contrast, the period between the 24$^{th}$ and the 20$^{th}$ millennium BP, along with the final two millennia (15$^{th}$ and 14$^{th}$ millennium BP), shows comparatively low levels of change. While some of the signals may be attributed to inventions – such as the short-lived Late Badegoulian shouldered points – others are likely to reflect selective pressures at work – e.g., between the 22$^{nd}$ and the 21$^{st}$ or between the 16$^{th}$ and the 15$^{th}$ millennium BP.

The observed alternation between phases of random walk or stasis and episodes of abrupt directional change corresponds closely to the concept of punctuated equilibrium (e.g. Eldredge 1971; Eldredge & Gould 1972).

Morphometric features do not all display the same degree of dynamism. In general, shape-related traits change more markedly over time than size-related ones, suggesting that shape characteristics were subject to more intense adaptive processes.

### *Alignment with Palaeodemographic Studies*

The uncovered morphometric patterns align closely with recent palaeodemographic studies (Maier et al. 2022). High levels of variation are associated with periods of demographic decline and the disruption of social networks. Conversely, reductions in variation, or the persistence of conservative morphologies, appear to coincide with increases in population size and density and the reorganisation of social networks. This correlation suggests that shouldered points, as key components of hunting weaponry, were directly responsive to the pressures and opportunities created by demographic dynamics.

### *Taxonomic Relations and the Limits of Typology*

While the results generally support taxonomic distinctions, they also advance the debate on relations between archaeological taxonomic units in respect to the associated shouldered points. By quantifying morphology rather than relying solely on typological labels, this study demonstrates that some distinctions are actually meaningful. The morphometric signal consistently separates Late Gravettian from Upper Solutrean shouldered points, validates the distinction of the Badegoulian from other LGM units, and clarifies the placement of shouldered points associated with early Magdalenian contexts. However, the analysis also highlights that not all taxonomic units exhibit equally clear signatures: some, such as the Salpetrian, overlap significantly with their neighbours, revealing the limits of typological clarity.

A particularly important finding is that the mere presence of pointed artefacts with one lateral notch, regardless of their shape, does not necessarily indicate cultural continuity or contact. Although such artefacts are conventionally classified as 'shouldered points,' morphometric analysis may support the interpretation that such forms could arise independently in different traditions as a convergent technological solution. This insight cautions against overly direct readings of typology and underlines the need to disentangle morphological and potentially functional similarity from historical relatedness.

### *Predictive Potential of Morphometrics*

Finally, this study has shown the predictive potential of morphometric approaches. It was able to assign shouldered points solely based on their morphological characteristics to taxonomic units with high accuracy. Additionally, exploratory applications demonstrated that chronological placement can be approximated based solely on morphometric data, albeit with limitations. While the models are not yet re-

fined enough for routine chronological attribution, they provide proof of concept for future predictive approaches.

This predictive capacity showed that morphometrics can move beyond post-hoc description to become a forward-looking tool capable of generating probabilistic assignments for new or ambiguous artefacts. Such an approach holds particular promise in cases where stratigraphic or radiocarbon data are absent or ambiguous, opening new avenues for the integration of statistical modelling into archaeological interpretation.

This study contributes to a broad range of central topics in Evolutionary Archaeology, including the analysis of variation and change in SPs, as well as the investigation of phylogenetic relationships among them. Together, these contributions highlight that material culture, when analysed systematically and quantitatively, encodes chronological and cultural signals that extend far beyond descriptive typology. It thereby underlined the importance of macro-scale approaches on traditional archaeological types for the uncovering and understanding of large-scale dynamics of human cultural evolution. Shouldered points emerge not as static typological markers but as dynamic artefacts that vary and change over time. This shows that variation in artefact types is not simply statistical noise to be acknowledged and set aside. Instead, it represents valuable information which, when quantified using appropriate methods, provides broader insights into past processes and dynamics. The integration of morphological perspectives therefore offers a powerful framework for future research into cultural change during this crucial period of human prehistory. This study proposes a methodological framework suitable for application to further case studies and presents unprecedented quantifications and comparative values.

# REFERENCES


Abdolahzadeh, A., Olszewski, D. I. & Ranhorn, K. L. (2025). To What Extent Are Similarities in Lithic Artifacts Due to Convergence? *Journal of Paleolithic Archaeology 8(17)*, 2025. https://doi.org/10.1007/s41982-025-00218-1

Abramova, Z. A., Grigorieva, G. V. & Zaitseva, G. I. (2001). The age of Upper Paleolithic Sites in the Middle Dnieper River Basin of Eastern Europe. *Radiocarbon 42*, 2001, 1077–1084. https://doi.org/10.1017/S0033822200041734

Absolon, K. & Klíma, B. (1977). *Předmostí: ein Mammutjägerplatz in Mähren*. Fontes Archaeologiae Moravicae 8 (Brno 1977).

Acerbi, A. & Bentley, A. (2014). Biases in cultural transmission shape the turnover of population traits. *Evolution and Human Behavior 35*, 2014, 228–236. https://doi.org/10.1016/j.evolhumbehav.2014.02.003

Adam, E. (2007). Looking out for the Gravettian in Greece. *PALEO 19*, 2007. https://doi.org/10.4000/paleo.579

Aleo, A., Duches, R., Falcucci, A., Rots, V. & Peresani, M. (2021). Scraping hide in the early Upper Paleolithic: Insights into the life and function of the Protoaurignacian endscrapers at Fumane Cave. *Archaeological and Anthropological Science 13, 137*, 2021. https://doi.org/10.1007/s12520-021-01367-4

Alexandrowicz, W.S., Kaminská, Ľ., Kazior, B., Kozlowski, J. K., Pawlikowski, M. & Sobczyk, K. (2000). Excavations at Banka-Horné farské role site. In: Kozłowski, J. K. (ed.), *Complex of Upper Palaeolithic Sites Near Moravany,Western Slovakia, Late Gravettian Shouldered Points Horizon Sites in the Moravany-Banka Area* (Krakow 2000), vol. III, 121–152.

Allain, J. (1974). Circonscription du Centre. *Gallia Préhistoire 17*, 1974, 465–485.

Allain, J. (1989). La fin du Paléolithique supérieur en région Centre, In: Rigaud, J.-P. (ed.), *Le Magdalénien en Europe*, Actes du Colloque du Mayence 1987, ERAUL 38 (Mayence 1989), 193–217.

Allain, J. & Fritsch, R. (1967). Le Badegoulien de l'abri Fritsch aux Roches de Pouligny Saint-Pierre (Indre). *Bulletin de la Société Préhistorique Française 64*, 1967, 83–93.

Alshahrani, N. D. (2026). Statistical reproducibility of correlation tests: Pearson, Spearman, and Kendall. *AIMS Mathematics 11(1)*, 2026, 957–976. https://doi.org/10.3934/math.2026042

Amirkhanov, K. A. (2000). *Zarajskaja stojanka*. (Moscow 2000).

Amirkhanov, K. A. (ed.) (2009). *Issledovaniia paleolita v Zaraiske 1999–2005* (Moscow 2009).

Anghelinu, M., Händel, M., Niță, L., Cordoș, C., Veres, D., Hambach, U., Murătoreanu, G., Ciornei, A., Schmidt, C., Sava, T., Mănăilescu, C., Ilie, M., Demay, L. & Georgescu, V. (2021). From Gravettian to Epigravettian in the Eastern Carpathians: Insights from the Bistricioara-Lutărie III archaeological site. *Quaternary International 587–588*, 2021, 210–229.

Antl-Weiser, W., Fladerer, F. A., Nigst, P. R. & Verpoorte, A. (2010). Grub/Kranawetberg (Lower Austria) – Insights into a Gravettian Micro-region in Eastern Austria. In: Neugebauer-Maresch, C. & Owen, L. (Eds), *New aspects of the Central European Upper Palaeolithic – Methods, Chronology, Technology and Subsistence. Symposium by the Prehistoric Commission of the Austrian Academy of Sciences, Vienna, November 9–11, 2005*. Mitteilungen der Prähistorischen Kommission 72 (Wien 2010), 231–143.

Arambourou, R., Delpech, F., Evin, J., Laurent, P. & Paquereau, M. M. (1978). *Le gisement préhistorique de Duruthy à Sorde-l'Abaye (Landes). Bilan des recherches de 1958 à 1975*. Mém. SPF 13 (Paris 1978).

Archer, W., Pop, C. M., Gunz, P. & McPherron, S. P. (2016). What is Still Bay? Human biogeography and bifacial point variability. *Journal of Human Evolution 97*, 2016, 58–72. https://doi.org/10.1016/j.jhevol.2016.05.007

Arppe, L. & Karhu, J. A. (2010). Oxygen isotope values of precipitation and the thermal climate in Europe during the

middle to late Weichselian ice age. *Quaternary Science Reviews 29*, 2010, 1263–1275. https://doi.org/10.1016/j.quascirev.2010.02.013

Arslanov, K. A. & Svezhentsev, Y. S. (1993). An improved method for radiocarbon dating fossil bones. *Radiocarbon 35(3)*, 1993, 387–391. https://doi.org/10.1017/S0033822200060392

Auffermann, B., Burkert, W., Hahn, J., Pasda, C. & Simon, U. (1990). Ein Merkmalsystem zur Auswertung von Steinartefaktinventaren. *Archäologisches Korrespondenzblatt 20*, 1990, 259–268.

Baker, J., Rigaud, S., Pereira, D. et al. (2024). Evidence from personal ornaments suggest nine distinct cultural groups between 34,000 and 24,000 years ago in Europe. *Nature Human Behaviour 8*, 2024, 431–444. https://doi.org/10.1038/s41562-023-01803-6

Bárta, J. (1965). *Slovensko v staršej a strednej dobe kamennej* (Bratislava 1965).

Bárta, J. (1966). Paläolithische Besiedlung von Nitra. In: Bárta, J. (ed.), *Eine beachtenswerte paläolithische Funde in der Westslowakei.* Actes du VIIe Congrès UISPP. Ex cursion en Slovaquie. Nitra (Prague 1966), 3–9.

Barshay-Szmidt, C., Costamagno, S., Henry-Gambier, D., Laroulandie, V., Pétillon, J. M., Boudadi-Maligne, M., Kuntz, D., Langlais, M. & Mallye, J. B. (2016). New extensive focused AMS 14C dating of the Middle and Upper Magdalenian of the western Aquitaine/Pyrenean region of France (ca. 19–14 ka cal BP): Proposing a new model for its chronological phases and for the timing of occupation. *Quaternary International 414*, 2016, 62–91. https://doi.org/10.1016/j.quaint.2015.12.073

Barton, R. N. E. (1992). *Hengistbury Head, Dorset. Volume 2: The Late Upper Palaeolithic & Early Mesolithic Sites* (Oxford 1992).

Baxter, M. J. (2003). *Statistics in Archaeology* (London 2003).

Bazile, F. (1990). Le Solutreen et l'Episolutreen dans le Sud-Est de la France. In: Kozłowski, J. K. (ed.), *Feuilles de pierre. Les industries à pointes foliacées du Paléolithique supérieur européen. Actes du Colloque de Cracovie 1989*. E.R.A.U.L. 42 (Liege 1990), 393–423.

Bazile, F. (1999). Fontgrasse, gisement Magdalénien moyen (?) en Languedoc oriental. In: Sacchi D. (ed.), *Les faciès leptolithiques du nord-ouest méditerranéen*. Société préhistorique française (Congrès préhistorique de France 24/Colloque international; Carcassonne; septembre 1994) (Paris 1999), 229–236.

Bazile, F. (2006). Datations du site de Fontgrasse (Vers-Pont-Du-Gard, Gard.) Implications sur la phase ancienne du Magdalénien en France Méditerranéenne. *Bulletin de la Société Préhistorique Française 103(3)*, 2006, 597–602.

Bazile, F. (2011). De l'Epigravettien à l'Ouest du Rhone? *PALEO 22*, 2011, 27–52. https://doi.org/10.4000/paleo.2061

Bazile, F. & Boccaccio, G. (2008). Le Salpêtrien ancien: un technocomplexe épisolutréen redéfini. *Gallia Préhistoire 50*, 2008, 103–141. https://doi.org/10.3406/galip.2008.2459

Beckhoff, K. (1966). Zur Morphogenese der steinzeitlichen Pfeilspitze. *Die Kunde N.F. 17*, 1966, 34–65.

Beckhoff, K. (1967). Zur jungpaläolithischen Kerbspitze. *Die Kunde N.F. 18*, 1967, 8–15.

Belyaeva, V. I. (2002). Pushkari I lithic industry. In: Praslov, N. D. (ed.), *Upper Paleolithic-Upper Pleistocene: Dynamics of Natural Events and Archaeological Cultures/International Congress, in Honour to Rogatchev A.N.* (St.-Petersburg 2002), 133–137.

Belhumeur, P. N., Hespanha, J. P. & Kriegman, D. J. (1997). Eigenfaces vs. Fisherfaces: Recognition using class specific linear projection. *IEEE Transactions on Pattern Analysis and Machine Intelligence 19(7)*, 1997, 711–720.

Bentley, R. A., Hahn, W. & Shennan, S. J. (2004). Random drift and culture change. *Proceedings of the Royal Society B: Biological Sciences 271*, 2004, 1443–1450. https://doi.org/10.1098/rspb.2004.2746

Bettinger, R. L., Boyd, R. & Richerson, P. J. (1996). Style, function and cultural evolutionary processes. In: Maschner, H. D. G. (ed.), *Darwinian archaeologies* (New York 1996), 133–164.

Beyries, S. & Cattin, M.-I. (2015). Resharpening and recycling: Different conceptions of the Magdalenian tools. *Quaternary International 361*, 2015, 260–268. https://doi.org/10.1016/j.quaint.2014.07.042

Bietti, A. (1979). Le gisement paléolithique supérieur de Taurisano (Lecce, Italie) et sa position chronologique et culturelle dans l'Epigravettien Italien. In: de Sonneville-Bordes, D. (ed.), *La Fin des Temps Glaciares in Europe*. Proceedings of the CNRS colloquium 271 (Paris 1979), 333–344.

Bietti, A., Martini, F. & Tozzi, C. (1983). L'Epigravettien evolue et final de la zone moyenne et basse tyrrhenienne. *Rivista di Scienze Preistoriche 38*, 1983, 319–349.

Binford, L. R. (1972). *An archaeological perspective* (New York 1972),

Bischoff, R. (2023). Geometric morphometric analysis of projectile points from the Southwest United States. *Peer Community Journal 3*, 2023, e80. https://doi.org/10.24072/pcjournal.312

Bitiri-Ciortescu, M., Căpitanu, V. & Cârciumaru, M. (1989). Paleoliticul din sectorul subcarpatic al Bistriţei în luminacercetărilor de la Lespezi-Bacău. *Carpica XX*, 1989, 7–52.

Blanc, A. C. (1953). Il riparo Mochi ai Balzi Rossi di Grimaldi: Le industrie. *Paleontographia Italica, Paleontologia e Ecologia del Quaternario, III* (Pise 1953), 1–43.

Boccacio, G. (2005). *Les industries lithiques du Solutréen supérieur et du Salpêtrien ancien en Languedoc: ruptures et continuités des traditions techniques*. PhD Thesis at Université Aix-Marseille I.

Boccacio, G. (2021). The Salpetrian culture toward the end of the Solutrean around 23 ka cal BP in the Rhône Valley (France). *Quaternary International 581–582*, 2021, 84–98. https://doi.org/10.1016/j.quaint.2020.12.005

Boëda, E. (2018). *Techno-logique & Technologie. Une Paléo-histoire des objets lithiques tranchants* (Paris 2018).

Bofinger, E. & Davidson, I. (1977). Radiocarbon age and depth: a statistical treatment of two sequences of dates from Spain. *Journal of Archaeological Science 4*, 1977, 231–243.

Bohmers, A. (1947). Jong-Palaeolithicum en Vroeg-Mesolithicum. In: van Gelder, H. E., Glazema, P., Bontekoe, G. A., Halbertsma, H. & Glasbergen, W. (eds.), *Oudheidkundig bodemonderzoek in Nederland. Gedenkboek A. E: van Giffen* (Meppel 1947), 129–201.

Bonhomme, V., Picq, S. & Gaucherel, C. (2014). Momocs: Outline Analysis Using R. *Journal of Statistical Software*, Volume 56(13), 2014, 1–24. https://doi.org/10.18637/jss.v056.i13

Borcard, D., Gillet, F. & Legendre, P. (2011). *Numerical Ecology with R* (New York, Dordrecht, London, Heidelberg 2011).

Bordes, F. (1958). Nouvelles fouilles à Laugerie-Haute Est: premiers résultats. *L'Anthropologie 62*, 1958, 205–244.

Bordes, F. (1965). A propos de typologie. *L'Anthropologie 69*, 1965, 369–377.

Borić, D. & Cristiani, E. (2016). Social Networks and Connectivity among the Palaeolithic and Mesolithic Foragers of the Balkans and Italy. In: Krauß, R. & Floss, H. (eds.), *Southeast Europe before Neolithisation (Proceedings of the Workshop held in Tübingen, Germany, May 9th, 2014)* (Tübingen 2016), 72–112.

Borić, D., Cristiani, E., Vušović-Lučić, Z., Borovinić, N. & Mihailović, D. (2014). LGM Marmot Hunting at Vrbička Cave in the Dinaric Alps. *Poster Presented at the Conference 'Where the Wild Things Are', University of Durham, January 8th to 9th, 2014*.

Boschin, F., Boscato, P., Berto, C., Crezzini, J. & Rontichelli, A. (2018). The palaeoecological meaning of macromammal remains from archaeological sites exemplified by the case study of Grotta Paglicci (Upper Palaeolithic, southern Italy). *Quaternary Research 90(3)*, 470–482. https://doi.org/10.1017/qua.2018.59

Bosselin, B. & Djindjian, F. (1988). Un essai de structuration du Magdalénien français à partir de l'outillage lithique. *Bulletin de la Société Préhistorique Française 85*, 1988, 304–331.

Boyd, R. & Richerson, P. (1985). *Culture and the evolutionary process* (Chicago 1985).

Boyd, R. & Richerson, P. (2024). Cultural evolution: Where we have been and where we are going (maybe). *Proceedings of the National Academy of Sciences 121*, 2024, e2322879121. https://doi.org/10.1073/pnas.2322879121

Boyd, R., Richerson, P. J. & Henrich, J. (2013). The cultural evolution of technologies: Facts and theories. In: Richerson, P. J. & Christiansen, M. H. (eds.), *Cultural evolution: Society, technology, language, and religion* (Cambridge, Massachusetts 2013), 119–142.

Brasser, M. (2013). Die Struktur 5 der Magdalénien-Fundstelle Oelknitz – Befundanalyse, faunistische und lithische Untersuchungen zum Jungpaläolithikum in Thüringen. *Alt-Thüringen 42, 2010/2011*, 2013, 5–78.

Brantingham, P. J. (2007). A Unified evolutionary model of archaeological style and function based on the Price equation. *American Antiquity 42*, 2007, 395–416. https://doi.org/10.2307/40035853

Brantingham, P. J. & Perreault, C. (2010). Detecting the effects of selection and stochastic forces in archaeological assemblages. *Journal of Archaeological Science 37*, 3211–3225. https://doi.org/10.1016/j.jas.2010.07.021

Breuil, H. (1913). Les subdivisions du Paléolithique supérieuret leur signification. In: *Congrés International d'Anthropologie et d'Archéologie Préhistoriques. Compte rendu de la XIVéme session* (Genève 1912), 165–238.

Breuil, H. & Obermaier, H. (1935). *The Cave of Altamira at Santillana de Mar, Spain*. (Madrid 1935).

Brézillon, M. (1971). *La dénomination des objets de pierre taillée*. IVe suppl. à Gallia Préhistoire, C.N.R.S. (Paris 1971).

Bridault, A., Lang, L. & Rieu, J.-L. (1997). Les sites magdaléniens de Marolles-sur-Seine: Le Tureau des Gardes et Le Grand Canton (Seine-et-Marne). In: Thévenin, A. (ed.), *Le Paléolithique supérieur de l'est de la France*. Actes du Colloque de Chaumont, 1994, vol. 13. Mémoire de la Société archéologique champenoise (Chaumont 1997), 119–128.

Brochier, J. E. (2016). Radiocarbon dates for the early shouldered Tardigravettian from the rockshelter of Chinchon 1 at Saumane-de-Vaucluse and the chronology of the recent Provençal Upper Palaeolithic. *Gallia Préhistoire 56*, 2016, 1–7. https://doi.org/10.4000/galliap.277

Brochier, J. E. & Livache, M. (2003a). Les niveaux à crans de l'abri du Rouet (Carry-Le-Rouet, Bouches-du-Rhône) et les industries pléni-tardiglaciaires du bassin bas-rhodanien. In: Ladier, E. (ed.), *Les pointes à cran dans les industries lithiques du Paléolithique supérieur récent de l'oscillation de Lascaux à l'oscillation de Bölling, Table ronde de Montauban*, Préhist. du Sud-Ouest suppl. n°6 (Montauban 2003), 47–66.

Brochier, J. E. & Livache, M. (2003b). L'évolution des industries pléni- et tardiglaciaires en Provence et dans le bassin bas Rhodanien, lignée évolutive et convergences. *Rivista di Scienze Preistoriche 53*, 2003, 37–54.

Brodar, M. (1986). Jama v Lozi. *Arheološki vestnik 37*, 1986, 23–76.

Broglio, A. (1997). Considérations sur l'Epigravettien italique. In: Fullola, J. M. & Soler, N. (eds.), *El mòn mediterrani després del Pleniglacial (18.000-12.000 BP)* (Girona 1997), 147–157.

Broglio, A. & Improta, S. (1995). Nuovi dati di cronologia assoluta del Paleolitico superiore e del Mesolitico del Veneto, del Trentino e del Friuli. Atti Istituto Veneto Scienze. *Lettere e Arti 153*, 1995, 1–45.

Broglio, A. & Lollini, D. (1982). *I ritovamenti Marchigiani del Paleolitico Superiore e del Mesolitico*. Atti I Convegno Beni Culturali e Ambientali delle Marche (Rome 1982).

Broglio, A., Chelidonio, G. & Longo, L. (1993). Analyse morphologique et fonctionnelle des pointes à cran de l'Épigravettien ancien. In: Anderson, P. C., Beyries, S., Otte, M. & Plisson, H. (eds.), *Actes du Colloque International Traces et fonction: les gestes retrouvés*. ERAUL (Liége 1993), 31–39.

Broglio, A., Bertola, S., de Stefani, M. & Gurioli, F. (2009). The Shouldered Points of the Early Epigravettian of the Berici Hills (Venetian Region, North Italy). Materials, Blanks, Typology, Exploitation. In: Burdukiewicz, J. M., Cyrek, K., Dyczek, P. & Szymczak, K. (eds.), *Understanding the Past. Center for Research on the Antiquity of Southeastern Europe* (Warsaw 2009), 59–68.

Bronk Ramsey, C. (2021). OxCal v.4.4.4 [software]. URL: https://c14.arch.ox.ac.uk/oxcal.html

Buchanan, B. (2006). An analysis of Folsom projectile point resharpening using quantitative comparisons of form and allometry. *Journal of Archaeological Science 33(2)*, 2006, 185–199. https://doi.org/10.1016/j.jas.2005.07.008

Buchanan, B. & Collard, M. (2008). Testing models of early Paleoindian colonization and adaptation using cladistics. In: O'Brien, M. J. (ed.), *Cultural transmission and archaeology: issues and case studies* (Washington, DC 2008), 59–76.

Buchanan, B. & Collard, M. (2010). An Assessment of the Impact of Resharpening on Paleoindian Projectile Point Blade Shape Using Geometric Morphometric Techniques. In: Lycett, S. J. & Chauhan, P. R. (eds.), *New Perspectives on Old Stones: Analytical Approaches to Paleolithic Technologies* (New York 2010), 255–273.

Buckland, M. & Gey, F. (1994). The Relationship between Recall and Precision. *Journal of the American Society for Information Science 45(1)*, 1994, 12–19. https://doi.org/10.1002/(SICI)1097-4571(199401)45:1<12::AID-ASI2>3.0.CO;2-L

Burdukiewicz, J. M. (1981). The flint technology of the Hamburgian Culture (Olbrachcice, S.W. Poland). In: Engelen, F. H. G. (ed.), *3rd International Symposium on Flint*. Staringa 6. Nederlandse Geologische Verenigung, Sittard (Maastricht 1979), 67–70.

Burdukiewicz, J. M. (1986). *The late pleistocene shouldered point assemblages in Western Europe* (Leiden 1986).

Burdukiewicz, J. M. (1987). Late paleolithic settlements in the Kopanica valley. In: Burdukiewicz, J. M. & Kobusiewicz, M. (eds.), *Late Glacial in Central Europe. Culture and Environment* (Wroclaw, Warszawa, Kraków, Gdansk, Lódz 1987), 183–213.

Burdukiewicz, J. M. (2001). The last ice age and settlement break in the northern part of Central Europe. *Fontes Archaeologici Posnanienses 39*, 2001, 15–29.

Burdukiewicz, J. M. & Schmider, B. (2000). Analyse comparative des pointes a' cran hambourgiennes du Bassin de l'Oder et des pointes a' cran magdale·niennes du Bassin parisien.

In: Valentin, B., Bodu, P. & Christensen, M. (eds.), *L'Europe centrale et septentrionale au Tardiglaciaire: Confrontation desmode'les re·gionaux de peuplement. Actes de la Table-ronde internationale de Nemours,14–16 Mai 1997* (Nemours 2000), 97–108.

Cabrera, V. & Bernaldo de Quirós, F. (1977). The Solutrean site of Cueva Chufín (Santander, Spain). *Current Anthropology 18*, 1977, 780–781.

Calcagnile, L., Sardella, R., Mazzini, I., Giustini, F., Brilli, M., D'Elia, M., Braione, E., Conti, J., Mecozzi, B., Bona, F., Iurino, D. A., Lembo, G., Muttillo, B. & Quarta, G. (2019). New Radiocarbon Dating Results from the Upper Paleolithic–Mesolithic Levels in Grotta Romanelli (Apulia, Southern Italy). *Radiocarbon 61(5)*, 2019, 1211–1220. https://doi.og/10.1017/RDC.2019.8

Campbell, J. B. (1977). *The Upper Paleolithic of Britain. A study of Man and nature in the late Ice Age* (Oxford 1977).

Cancellieri, E. (2018). An overview of early Epigravettian techno-economic behaviour in northern and western Adriatic area. In: Borgia, V. & Cristiani, E. (eds.), *Paleolithic Italy. Advanced Studies on Early Human Adaptations in the Apennine Peninsula* (Leiden 2018), 265–285.

Cardillo, M. & Charlin, J. (2018). Phylogenetic analysis of stemmed points from Patagonia: shape change and morphospace evolution. *Journal of Lithic Studies 5(2)*, 2018, 1–31. https://doi.org/10.2218/jls.2797

Cascalheira, J. & Bicho, N. (2015). On the Chronological Structure of the Solutrean in Southern Iberia. *PLoS ONE 10(9)*, 2015, e0137308. https://doi.org/10.1371/journal.pone.0137308

Cascalheira, J., Bicho, N., Marreiros, J., Pereira, T., Évora, M., Cortés Sánchez, M., Gibaja, J., Manne, T., Regala, F., Gonçalves, C. & Monteiro, P. (2012). Vale Boi (Algarve, Portugal) and the Solutrean in Southwestern Iberia. Espacio. *Tiempo y Forma 5*, 2012, 455–67. https://doi.org/10.5944/etfi.5.2012.5376

Castel, J. C. (1999). *Comportements de subsistance au Solutréen et au Badegoulien d'après les faunes de Combe-Saunière (Dordogne) et du Cuzoul-de-Vers (Lot)*. Ph.D thesis, University of Bordeaux I.

Cavalli-Sforza, L. L. (1986). Cultural Evolution. *American zoologist 26(3)*, 1986, 845–856.

Cavalli-Sforza, L. L. & Feldman, M. W. (1981). *Cultural transmission and evolution* (Princeton 1981).

Charbonneau, M. (2018). Technical constrains on the convergent evolution of technologies. In: O'Brien, M. J., Buchanan, B. & Eren, M. I. (eds.), *Convergent evolution in stone-tool technology* (Cambridge, Massachusetts 2018), 73–89.

Charlesworth, B. (2009). Fundamental concepts in genetics: Effective population size and patterns of molecular evolution and variation. *Nature Reviews Genetics 10*, 2009, 195–205.

Cheynier, A. (1939). Le Magdalénien primitif de Badegoule, niveaux à raclettes. *Bulletin de la Société Préhistorique Française 36*, 1939, 334–396.

Chernysh, O. P. (1961). *The Paleolithic site of Molodova V* (Kiev 1961) (in Ukrainian).

Childe, V. G. (1951). *Social Evolution* (London 1951).

Chłodnicki, M. & Kabaciński, J. (1997). Mirkowice–another settlement of the Hamburgian Culture at the Polish Plain. *Przegląd Archeologiczny 45*, 1997, 5–23.

Chmielewski, W., Schild, R. & Wieckowska, H. (1975). *Prahistoria ziem Polskich. Paleolit i Mezolit*. Polska Akademia Nauk, Instytut Historii Kultury Materialnej (Wrocław 1975).

Chollet, A. & Dujardin, V. (2005). *La grotte du Bois-Ragot á Gouex (Vienne) Magdalénien et Azilien. Essais sur les hommes et leur environnement*. Mémoire XXXVIII de la Société Préhistorique Française (Joué-lès-Tours 2005).

Claude, J. (2008). (ed.), *Morphometrics with R* (New York 2008).

Clausen, I. (1998). Neue Untersuchungen an späteiszeitlichen Fundplätzen der Hamburger Kultur bei Ahrenshöft, Kr. Nordfriesland. *Archäologische Nachrichten aus Schleswig-Holstein, 8 (1997)*, 1998, 8–49.

Clottes, J. (1994). L'art pariétal paléolithique en France: dernières découvertes. *Complutum 5*, 1994, 221–233.

Clottes, J., Duport, L. & Feruglio, V. (1991). Derniersléléments sur les signes du Placard. *Préhistoireariégeoise, Bulletin de la Société préhistorique Ariège-Pyrénées XLVI*, 1991, 119–132.

Clottes, J., Duport, L. & Feruglio, V. (1994). Vilhonneur. Grotte du Placard. *Bilan scientifique régional Poitou-Charentes 1993*, 24–25.

Cowgill, G. L. (1972). Models, methods and techniques for seriation. In: Clarke, D. L. (ed.), *Models in archaeology* (London 1972), 381–424.

Collard, M., Kemery, M. & Banks, S. (2005). Causes of Toolkit Variation Among Hunter-Gatherers: A Test of Four Competing Hypotheses. *Canadian Journal of Archaeology 29*, 2005, 1–19.

Collard, M., Ruttle, A., Buchanan, B. & O'Brien, M. J. (2013a). Population Size and Cultural Evolution in Nonindustrial Food-Producing Societies. *PLoS ONE 8(9)*, 2013, e72628. https://doi.org/10.1371/journal.pone.0072628

Collard, M., Buchanan, B. & O'Brien, M. J. (2013b). Population size as an explanation for patterns in the Paleolithic archaeological record: More Caution is needed. *Current Anthropology 54*, 2013, 388–396. https://doi.org/10.1086/673881

Collard, M., Vaesen, K., Cosgrove, R. & Roebroeks, W. (2016). Population size does not explain past changes in cultural complexity, *PNAS 113(16)*, 2016, E2241-E2247. https://doi.org/10.1073/pnas.1520288113

Combier, J. (1967). *Le Paléolithique de l'Ardèche dans son cadre paléoclimatique* (Bordeaux 1967).

Combier, J. (2002). Pointes à cran du Sud-Est de la France (du Gravettien au Magdalénien final). In: Ladier, E. (ed.), *Les pointes à cran dans les industries lithiques du Paléolithique supérieur récent de l'oscillation de Lascaux à l'oscillation de Bölling, Table ronde de Montauban*, Préhist. du Sud-Ouest suppl. n°6 (Montauban 2003), 129–143.

Cooper, L.P. (2012). An open-air Creswellian site at Bradgate Park, Newtown Linford, Leicestershire. *Lithics: the Journal of the Lithic Studies Society 33*, 2012, 30–39.

Corchon, M. S. (1971). *El solutrense en Santander* (Santander 1971).

Coren, S., Ward, L. M. & Enns, J. T. (1994). *Sensation and perception* (San Diego 1994).

Cover, T. M. & Hart, P. E. (1967). Nearest Neighbor Pattern Classification. I*EEE Transactions on Information Theory 13(1)*, 1967, 21–27.

Creanza, N., Kolodny, O. & Feldman, M. W. (2017). How culture evolves and why it matters. *Proceedings of the National Academy of Sciences 114*, 7782–7789. https://doi.org/10.1073/pnas.1620732114

Crema, E. R., Kandler, A. & Shennan, S. (2016). Revealing patterns of cultural transmission from frequency data: equilibrium and non-equilibrium assumptions. *Scientific Reports 6(1)*, 2016, 1–10. https://doi.org/10.1038/srep39122

Crema, E. R., Bortolini, E. & Lake, M. (2024). How Cultural Transmission Through Objects Impacts Inferences About Cultural Evolution. *Journal of Archaeological Method and Theory 31*, 2024, 202–226. https://doi.org/10.1007/s10816-022-09599-x

Cristiani, E. (2013). Prehistoric Foragers of Montenegro. *Archaeology at Cambridge 27*, 2011–2012.

Cristiani, E. (2014). Late Pleistocene and Early Holocene Foragers of Montenegro. *Archaeology at Cambridge 41*, 2012–2013.

Damblon, F, Hasaerts, P. & van der Plicht, J. (1996). New datings and considerations on the chronology of Upper Palaeolithic sites in the Great Eurasiatic plain. *Préhistoire Européenne 9*, 1996, 177–231.

Darasse, P. & Guffroy, S. (1960). Le Magdalénien supérieur de l'abri Fontalès près Saint-Antonin (Tarn-et-Garonne). *L'Anthropologie 64*, 1960, 1–34.

Darwent, J. & O'Brien, M. J. (2006). Using cladistics to construct lineages of projectile points from northeastern Missouri. In: Lipo, C. P, O'Brien, M. J., Collard, M. & Shennan, S. J. (eds.), *Mapping our ancestors: Phylogenetic Approaches in Anthropology and Prehistory* (New York 2006), 185–208.

Darwin, C. (1859). *On the Origin of Species by Means of Natural Selection, or the Preservation of Favoured Races in the Struggle for Life* (London 1859).

David, S. (1996). La fin du Paléolithique supérieur en Franche-Comté. Environnement, cultures, chronologie. *Gallia Préhistoire 38*, 1996, 111–248.

Dawkins, R. (1976). *The selfish Gene* (Oxford 1976).

Dawkins, R. (1982). *The Extended Phenotype: The Long Reach of the Gene* (Oxford 1982).

Debénath, A. & Dibble, H. L. (1994). *Handbook of Paleolithic Typology, Volume 1: Lower and Middle Paleolithic of Europe.* (Philadelphia 1994).

Deffner, D., Kandler, A. & Fogarty, L. (2022). Effective population size for culturally evolving traits. *PLoS Computational Biology 18(4)*, 2022, e1009430. https://doi.org/10.1371/journal.pcbi.1009430

Delage, C. (2018). Revisiting Le Placard Radiometric Chronology. In: Delage, C. (ed.), *The Grotte du Placard at 150: New Considerations on an Exceptional Prehistoric Site* (Oxford 2018), 105–111.

De Lisle, S. P. & Svensson, E. I. (2026). Revisiting evolutionary rate-time relationships. *Evolution 80(1)*, 2026, 28–39. https://doi.org/10.1093/evolut/qpaf222

Delpiano, D. & Uthmeier, T. (2020). Techno-functional and 3D shape analysis applied for investigating the variability of backed

tools in the Late Middle Paleolithic of Central Europe. *PLoS ONE 15(8)*, 2020, e0236548. https://doi.org/10.1371/journal.pone.0236548

Demars, P.-Y. & Laurent, P. (1992). *Types d'outils lithiques du Paléolithique supérieur en Europe* (Paris 1992).

Demay, L., Péan, S., Belyaeva, V. I., Vasilev, P. M. & Patou-Mathis, M. (2015). Zooarchaeological study of an Upper Palaeolithic site with mammoth remains, Pushkari I – excavation VII (Chernigov oblast, Ukraine). *Quaternary International 406(B)*, 2015, 1–19. https://doi.org/10.1016/J.QUAINT.2015.08.014

Demay, L., Vasyliev P. M. & Belyaeva, V. I. (2021). Subsistence activities in the gravettian occupations of the Pushkari group: Pushkari I and Pushkari VIII (Pogon) (Ukraine), *Quaternary International 587–588*, 2021, 291–309. https://doi.org/10.1016/j.quaint.2020.08.011

Derex, M. & Boyd, R. (2016). Partial connectivity increases cultural accumulation within groups. *PNAS 113(11)*, 2016, 2982–2987. https://doi.org/10.1073/pnas.1518798113

Derex, M. & Mesoudi, A. (2020). Cumulative Cultural Evolution within Evolving Population Structures. *Trends in Cognitive Sciences 24(8)*, 2020, 654–667. https://doi.org/10.1016/j.tics.2020.04.005

Derex, M., Beugin, M.-P., Godelle, B. & Raymond, M. (2013). Experimental evidence for the influence of group size on cultural complexity. *Nature 503*, 2013, 389–391. https://doi.org/10.1038/nature12774

Derex, M., Perreault, C. & Boyd, R. (2018). Divide and conquer: intermediate levels of population fragmentation maximize cultural accumulation. *Philosophical Transactions of the Royal Society B: Biological Sciences 373(1743)*, 2018, 20170062. https://doi.org/10.1098/rstb.2017.0062

Dev, S. & Riede, F. (2012). Quantitative functional analysis of Late Glacial projectile points from northern Europe. *Lithics 33*, 2012, 40–55.

Diachenko, A., Rivers, R. J. & Sobkowiak-Tabaka, I. (2023). Convergent Evolution of Prehistoric Technologies: the Entropy and Diversity of Limited Solutions. *Journal of Archaeological Method and Theory 30*, 2023, 1168–1199. https://doi.org/10.1007/s10816-023-09623-8

Dinnis, R., Bessudnov, A. A., Reynolds, N., Khlopachev, G. A., Sablin, M., Sinitsyn, A., Thomas, H. & Douka, K. (2021). The Tempo of cultural change in the Kostenki Upper Paleolithic: further insights. *Radiocarbon 163(3)*, 2021, 785–803. https://doi.org/10.1017/RDC.2021.20

Djindjan, F. (2000). Identité, chronologie et territoires du Magdalénien en Europe occidentale: questions posées. In: Pion, G. (ed.), *Le Paléolithique Supérieur récent: nouvelles données sur le peuplement et l'environnement, Actes de la table ronde de Chambéry, 13–14 mars 1999*, Société Préhistorique Française, Mémoire XXVIII (Chambéry 2000), 95–112.

Djindjian F., Kozlowski, J. & Otte, M. (1999). *Le Paleolithique superieur en Europe* (Paris 1999).

Dollo, L. (1893). Les lois de l'évolution. *Bulletin de la Société Belge de Géologie de Paléontologie et d'Hydrologie 7*, 1893, 164–166.

Douka, K., Grimaldi, S., Boschian, G., Del Lucchese, A. & Higham, T. F. G. (2011). A new chronostratigraphic framework for the Upper Palaeolithic of Riparo Mochi (Italy). *Journal of Human Evolution 62(2),* 2011, 286–299. https://doi.org/10.1016/j.jhevol.2011.11.009

Ducasse, S. (2010). *La "parenthèse" badegoulienne: fondements et statut d'une discordance industrielle au travers de l'analyse techno-économique de plusieurs ensembles lithiques méridionaux du Dernier Maximum Glaciaire*. University of Toulouse 2, unpublished PhD dissertation. https://tel.archives-ouvertes.fr/tel-00565784/fr/

Ducasse, S. (2012). What is left of the Badegoulian "interlude"? New data on cultural evolution in southern France between 23,500 and 20,500 cal. BP. *Quaternary International 272–273*, 2012, 150–165. https://doi.org/10.1016/j.quaint.2012.05.018

Ducasse, S. & Langlais, M. (2005). Badegoulien versus Magdalénien inférieur: comparaison des systèmes de production lithique, l'exemple quercinois au sein du Sud-Ouest européen. In: Jarry, M., Brugal, J.-Ph. & Ferrier, C. (ed.), *Modalités d'occupation et exploitation des milieux au Paléolithique dans le Sud-Ouest de la France : l'exemple du Quercy. Actes de la session C67, XVème Congrès de l'UISPP, Lisbonne, septembre 2006* (Lisbonne 2013), 379–394.

Ducasse, S. & Lelouvier, L. A. (2012). Les industries lithiques du Badegoulien: Technoéconomie des équipements en silex, une première approche diachronique. In: Clottes, J., Giraud, J. P. & Chalard, P. (eds.), *Solutréen et Badegoulien au Cuzoul de Vers. Des chasseurs de rennes en Quercy*, ERAUL, 131 (Liège 2012), 145–197.

Ducasse, S., Pétillon, J.-M. & Renard, C. (2014). Le cadre radiométrique de la séquence solutréo-badegoulienne du Cuzoul de Vers: lecture critique et compléments. *PALEO 25, 2014*, 37–58.

Ducasse, S., Chauvière, F.-X. & Pétillon, J.-M. (2021). Breaking bad? Discarding the Solutrean norms: Chronology, evolution and geographical extent of the badegoulian phenomenon in Western Europe. *Quaternary International 581–582*, 2021, 61–83. https://doi.org/10.1016/j.quaint.2020.10.063

Dujardin, V. & Oberlin, C. (2005). Les datations sur os du Bois-Ragot. In : Chollet, A. & Dujardin, V. (eds.), *La grotte de Bois-Ragot à Gouex (Vienne), Magdalénien et Azilien*. Essais sur les hommes et leur environnement, Société préhistorique française, Mémoire XXXVIII (Paris 2005), 401–404.

Dujardin, V. & Pinçon, G. (2000). Le Magdalénien dans la Vienne et la Charente. In: Pion, G. (ed.), *Le Paléolithique Supérieur récent: nouvelles don-nées sur le peuplement et l'environnement, Actes de la table ronde de Chambéry, 13–14 mars 1999*, Société Préhistorique Française, Mémoire XXVIII (Chambéry 2000), 213–222.

Dunnelll, R. C. (1970). Seriation method and its evaluation. *American Antiquity 35*, 1970, 305–319.

Dunnell, R. C. (1978a). *Natural Selection, Scale, and Cultural Evolution : Some Preliminary Considerations*. Paper presented at the 77th Annual Meeting of the American Anthropological Association. Los Angeles. [published in O'Brien 1996]

Dunnell, R. C. (1978b). Style and Function: A Fundamental Dichotomy. *American Antiquity 43*, 1978, 192–202.

Dunnell, R. C. (1980). Evolutionary Theory and Archaeology. In: Schiffer, M. B. (ed.), *Advances in Archaeological Method and Theory*, vol. 3 (New York 1980), 35–99.

Duran-Nebreda, S., Vidiella, B., Spiridonov, A., Eldredge, N., O'Brien, M. J., Bentley, R. A. & Valverde S. (2024). The many ways toward punctuated evolution. *Palaeontology 67(5)*, 2024, e12731. https://doi.org/10.1111/pala.12731

Edinborough, K. (2009). Population history and the evolution of Mesolithic arrowhead technology in South Scandinavia. In: Shennan, S. J. (ed.), *Pattern and process in cultural evolution* (Berkeley 2009), 191–202.

Eerkens, J. W. & Lipo, C. P. (2005) Cultural transmission, copying errors, and the generation of variation in material culture and the archaeological record. *Journal of Anthropological Archaeology 24*, 2005, 316–334. https://doi.org/10.1016/j.jaa.2005.08.001

Eerkens, J. W. & Lipo, C. P. (2007). Cultural transmission theory and the archaeological record: providing context to understanding variation and temporal changes in material culture. *Journal of Archaeological Research 15(3)*, 2007, 239–274.

Efimienko, P. P. (1958). *Kostienki I*. Académie des Sciences de l'U.R.S.S. Institut de la culture matérielle (Moscow 1958).

Eldredge, N. & Gould, S. J. (1972). Punctuated Equilibria: an alternative to phyletic gradualism. In: Schopf, T. J. M. (ed.), *Models in paleobiology* (San Francisco 1972), 82–115.

Eren, M. I., Buchanan, B. & O'Brien, M. J. (2018). Why convergence should be a potential hypothesis for the emergence and occurrence of stone-tool form and production processes: An illustration using replication. In: O'Brien, M. J., Buchanan, B. & Eren, M. I. (eds.), *Convergent evolution in stone-tool technology* (Cambridge, Massachusetts 2018), 61–71.

Escalon de Fonton, M. (1966). Du Paléolithique supérieur au Mésolithique dans le Midi méditerranéen. *Bulletin de la Société Préhistorique Française LXIII(1)*, 1966, 66–180.

Evin, J., Marien, G. & Pachiaudi, C. (1976). Lyon Natural Radiocarbon Measurements IV. *Radiocarbon 18,1*, 1976, 60–88.

Fagnart, J.-P. (1984). *Le Paleolithique superieur dans le Nord de la France et le Bassin de la Somme*. PhD-Thesis at Universite des Sciences et Techniques de Lille/U.E.R. de Geographie et D'Amenagement Spatial 1984.

Fagnart, J.-P. (1988). *Les Industries lithiques du Paléolithique supérieur dans le Nord de la France*. Revue Archéologique de Picardie, Numéro Spécial 7 (Laon 1988).

Fajardo, A. & Piper, F. I. (2011). Intraspecific trait variation and covariation in a widespread tree species (Nothofagus pumilio) in southern Chile. *New Phytologist 189*, 2011, 259–271. https://doi.org/10.1111/j.1469-8137.2010.03468.x

Falcucci, A. & Peresani, M. (2022) The contribution of integrated 3D model analysis to Protoaurignacian stone tool design. *PLoS ONE 17(5)*, 2022, e0268539. https://doi.org/10.1371/journal.pone.0268539

Falcucci, A., Karakostis, F. A., Göldner, D. & Peresani, M. (2022). Bringing shape into focus: Assessing differences between blades and bladelets and their technological significance in 3D form. *Journal of Archaeological Science: Reports 43*, 2022, 103490. https://doi.org/10.1016/j.jasrep.2022.103490

Fasser, N. (2022). Lithic armatures manufacture during the Late Glacial and the beginning of the Early Holocene between North-Eastern Italy and South-Western France: production methods and techniques. Ph.D. Thesis Université Toulouse 2.

Fechner, G. T. (1889). *Elemente der Psychophysik Vol. 1* (Leipzig 1889).

Feldman, M. W. & Laland, K. N. (1996). Gene–culture co-evolutionary theory. *Trends in Ecology & Evolution 11*, 1996, 453–457. https://doi.org/10.1016/0169-5347(96)10052-5

Felgenhauer, F. (1956). *Willendorf in der Wachau: Monographie d. Paläolith-Fundstellen 1–7. Inventar.* Mitteilungen der Prähistorischen Kommission der Österreichischen Akademie der Wissenschaften (Wien 1957).

Feustel, R. (1974). *Die Kniegrotte. Eine Magdalénien-Station in Thüringen* (Weimar 1974).

Fischer, A. & Tauber, H. (1986). New 14C-datings of the late Palaeolithic cultures from northwestern Europe. *Journal of Danish Archaeology 5*, 1986, 7–13. https://doi.org/10.1080/0108464X.1986.10589955

Fisher, R. A. (1925). *Statistical Methods for Research Workers* (Edinburgh 1925).

Fisher, R. A. (1936). The use of multiple measurements in taxonomic problems. *Annals of Eugenics 7(2)*, 179–188.

Fix, E. & Hodges, J. L. (1951). *Discriminatory analysis. Nonparametric discrimination: consistency properties*. Report No. 4, Project 21-49-004, USAF School of Aviation Medicine (Randolph Field 1951).

Floss, H. (1994). La redécouverte d'un grand inconnu: Varennes-lès-Mâcon, important gisement à pointes à dos dans la basse vallée de la Saône au sud de Mâcon (Saône-et-Loire, France). *Bulletin de la Société préhistorique française 94(3)*, 1994, 327–330.

Floss, H. (2012). Lithische Spitzen des Jungpaläolithikums. In: Floss, H. (ed.), *Steinartefakte vom Altpaläolithikum bis in die Neuzeit* (Tübingen 2012), 399–413.

Fogarty, L., Creanza, N. & Feldman, M. W. (2015). Cultural evolutionary perspectives on creativity and human innovation. *Trends in Ecology & Evolution 30*, 2015, 736–754. https://doi.org/10.1016/j.tree.2015.10.004

Fogarty, L., Kandler, A., Creanza, N. & Feldman, M. W. (2024). Half a century of quantitative cultural evolution. *Proceedings of the National Academy of Sciences 121*, 2024, e2418106121. https://doi.org/10.1073/pnas.2418106121

Ford, J. K. B. & Fisher, H. D. (1983). Group-specific dialects of killer whales (*Orcinus orca*) in British Columbia. In: Payne, R. (ed.), *Communication and Behavior of Whales*, Vol. 76 (Boulder 1983), 129–161.

Fortea Pérez, J. & Jordá Cerda, F. (1976). La Cueva de Les Mallaetes y los Problemas del Paleolítico Superior del Mediterráneo Español. *Zephyrvs XXVI-XXVII*, 1976, 129–166.

Fracchia, J. & Lewontin, R. (1999). Does culture evolve? *History and Theory 38*, 1999, 52–78. https://doi.org/10.1111/0018-2656.00104

Friis-Hansen, J. (1990). Mesolithic cutting arrows: functional analysis of arrows used in the hunting of large game. *Antiquity 64*, 1990, 494–504. https://doi.org/10.1017/S0003598X0007839X

Fu, Q. Posth, C., Hajdinjak, M. et al. (2016). The genetic history of Ice Age Europe. *Nature 534*, 2016, 200–205. https://doi.org/10.1038/nature17993

Futuyma, D. J. (2013). *Evolution*. 3rd ed. (Massachuset 2013).

Galanidou, N. & Tzedakis, C. (2001). New AMS dates from Upper Palaeolithic Kastritsa. *Proceedings of the Prehistoric Society 67*, 2001, 271–278. https://doi.org/10.1017/S0079497X00001699

Gallet, M. (1973). Les pièces à cran de la Rouvière, Gisement du Paléolithique supérieur de Vallon. *Études Préhistoriques, 5*, 1973, 8–14.

Garrod, D. (1926). The Upper Palaeolithic Age in Britain. *Proceedings of the University of Bristol Spelaeological Society 2(3)*, 1936, 299–301.

Gaudzinski-Windheuser, S. & Jöris, O. (2015). Contextualising the female image – symbols for common ideas and communalidentity in Upper Palaeolithic Societies. In: Coward, F., Hosfield, R., Pope, M. & Wenban-Smith, F. (eds.), *Settlement, Society and Cognition in Human Evolution: Landscapes in Mind* (Cambridge 2015), 288–314.

Gavrilov, K. N., Voskrenskaya, E. V., Maschenko, E. N. & Douka, K. (2015). East Gravettian Khotylevo 2 site: Stratigraphy, archeozoology, and spatial organization of the cultural layer at the newly explored area of the site. *Quaternary International 359–360*, 2015, 335–346. https://doi.org/10.1016/j.quaint.2014.08.020

Gelhausen, F. (2015). Das lithische Fundmaterial der Magdalenien-Station Oelknitz (Saale-Holzland-Kreis), Grabungen 1957–1967 – Eine Übersicht. *Archäologisches Korrespondenzblatt 45(2)*, 2015, 161–176.

Geneste, J.-M. & Plisson, H. (1986). Le Solutréen de la grotte de Combe Saunière 1 (Dordogne). Première approche palethnologique. *Gallia préhistoire, tome 29, fascicule 1*, 1986, 9–27.

Geneste, J.-M. & Plisson, H. (1989). Analyse technologique des pointes à cran solutréennes du Placard (Charente), du Fourneau du Diable, du Pech de la Boissiere et de Combe-Saunière (Dordogne). *Paléo 1*, 1989, 65–106. https://doi.org/10.3406/pal.1989.954

Gilot, E. (1997). *Index général des dates Lv. Laboratoire du Carbone 14 de Louvain/Louvain-la-Neuve*. Studia Praehistorica Belgica 7 (Liège 1997).

Gingerich, P. D. (1980). Evolutionary Patterns in Early Cenozoic Mammals. *Annual Review of Earth and Planetary Science 8*, 1980, 407–424. https://doi.org/10.1146/annurev.ea.08.050180.002203

Gingerich, P. D. (1983). Rates of evolution: Effects of time and temporal scaling. *Science 222(4620)*, 1983, 159–161. https://doi.org/10.1126/science.222.4620.15

Gingerich, P. D. (1993). Quantification and comparison of evolutionary rates. *American Journal of Science 293A*, 1993, 453–478. https://doi.org/10.2475/ajs.293.A.453

Gingerich, P. D. (2009). Rates of evolution. *Annual Review of Ecology, Evolution and Systematics 40*, 2009, 657–675. https://doi.org/10.1146/annurev.ecolsys.39.110707.173457

Gingerich, P. D. (2011). Rates of evolution on the time scale of the evolutionary process. *Genetica 112–113(1)*, 2011, 127–144. https://doi.org/10.1007/978-94-010-0585-2_9

González Echegaray, J. & Freeman, L. (1978). *Vida y muerte en Cueva Morín* (Santander 1978).

Gould, S. J. (1982). The Meaning of Punctuated Equilibrium and its Role in Validating a Hierarchical Approach to Macroevolution. In: Milkman, R. (ed.), *Perspectives in Evolution* (Sunderland 1982), 83–104.

Gribchenko, Yu. N., Belyaeva, V. I. & Kurenkova, E. I. (2011). Arkeologie i paleogeografie Pushkarevskich stoienak bassenia Desnu. *Vestnik antropologii 15*, 2011. (in Russian).

Griffiths, A. J. F., Wessler, S. R., Carroll, S. B. & Doebley, J. (2020). *Introduction to Genetic Analysis*. 12th edition (New York 2020).

Grimm, S. B. & Weber, M. J. (2008). The Chronological Framework of the Hamburgian in the Light of Old and New C14 Dates. *Quartär 55*, 2008, 17–40. https://doi.org/10.7485/QU55_02

Grosman, L. (2016). Reaching the Point of No Return: The Computational Revolution in Archaeology. *Annual Review of Anthropology 45(1)*, 2016, 129–145. https://doi.org/10.1146/annurev-anthro-102215-095946

Grove, M. (2016). Population density, mobility, and cultural transmission. *Journal of Archaeological Science 74*, 2016, 75–84. https://doi.org/10.1016/j.jas.2016.09.002

Guerreschi, A. & Leonardi, P. (1884). La fine del Paleolithico superiore (Epigravettiano finale). In: Aspes, A. (ed.), *Il Veneto nell´antichità, Preistoria e Protostoria*, vol. I (Verona 1984).

Gunasekaram, C., Battiston, F., Sadekar, O., Padilla-Iglesias, C., van Noordwijk, M. A., Furrer, R., Manica, A., Bertranpetit, J., Whiten, A., van Schaik, C. P., Vinicius, L. & Bamberg Migliano, A. (2024). Population interconnectivity shapes the distribution and complexity of chimpanzee cumulative culture. *Science 386*, 2024, 920–925. https://doi.org/10.1126/science.adk338

Gvozdover, M. (1995). *Art of the Mammoth Hunters: The Finds from Avdeevo* (Oxford 1995).

Haesaerts, P., Damblon, F., Bachner, M. & Trnka, G. (1996). Revised stratigraphy and chronology of the Willendorf II sequence, Lower Austria. *Archaeologica Austriaca 80*, 1996, 25–42.

Haesaerts, P., Borziac, I., Chekha, V. P.,Chirica, V., Drozdov, N. I., Koulakovska, L., Orlova, L. A., van der Plicht, J. & Damblon, F. (2010). Charcoal and wood remains for radiocarbon dating Upper Pleistocene loess sequences in Eastern Europe and Central Siberia. *Palaeogeography, Palaeoclimatology, Palaeoecology 291(1–2)*, 2010, 106–127. https://doi.org/10.1016/j.palaeo.2010.03.034

Haesaerts, P., Damblon, F., Neugebauer-Maresch, C. & Einwögerer T. (2016). Radiocarbon Chronology of the Late Palaeolithic Loess Site of Kammern-Grubgraben (Lower Austria). *Archaeologia Austriaca 100*, 2016, 271–277.

Hahn, J. (1996). *Le Paléolithique supérieur en Allemagne Méridionale (1991-1995)*. Le Paléolithique supérieur européen: Bilan quinquennal. 1991-1996 (Liège 1996).

Haldane, J. B. S. (1949). Suggestions as to Quantitative Measurement of Rates of Evolution. *Evolution 3(1)*, 1949, 51–56. https://doi.org/10.1111/j.1558-5646.1949.tb00004.x

Hansen, T. F. (2006). The Evolution of Genetic Architecture. *Annual Review of Ecology, Evolution, and Systematics 37*, 2006, 123–157. https://doi.org/10.1146/annurev.ecolsys.37.091305.110224

Hansen, T. F. (2015). Evolutionary constraints. In: Losos, J. (ed.), *Oxford Bibliographies in Evolutionary Biology* (Oxford 2015), 1–28. https://doi.org/10.1093/obo/9780199941728-0061

Hauck, T. C., Nolde, N., Ruka, R., Gjipali, I., Dreier, J. & Mayer, N. (2017). After the cold: Epigravettian hunter-gatherers in Blazi Cave (Albania). *Quaternary International 450*, 2017, 150–163. https://doi.org/10.1016/j.quaint.2016.11.045

Händel, M., Simon, U., Maier, A., Brandl, M., Groza-Săcaciu, S. M., Timar-Gabor, A. & Einwögerer, T. (2021). Kammern-Grubgraben revisited – first results from renewed investigations at a well-known LGM site in east Austria. *Quaternary International 587–588*, 2021, 137–157. https://doi.org/10.1016/j.quaint.2020.06.012

Hedges, R. E. M., Housley, R. A., Bronk, C. R. & van Klinken, G. J. (1992). Radiocarbon dates from the Oxford AMS system: Archaeometry datelist 15. *Archaeometry 34*, 1992, 337–357. https://doi.org/10.1111/j.1475-4754.1992.tb00507.x

Hedges, R. E M., Pettitt, P. B., Bronk-Ramsey, C. & Klinken, van, G. J. (1996). Radiocarbon dates from the Oxford AMS system: Archaeometry datelist 22. *Archaeometry 38(2)*, 1996, 391–415. https://doi.org/10.1111/j.1475-4754.1996.tb00785.x

Hennig, D. W. (1950). *Grundzüge einer Theorie der phylogenetischen Systematik* (Berlin 1950).

Henrich, J. (2004). Demography and cultural evolution: why adaptive cultural processes produced maladaptive losses in Tasmania. *American Antiquity 69(2)*, 2004, 197–214. https://doi.org/10.2307/4128416

Henrich, J. (2016). *The Secret of Our Success: How Culture Is Driving Human Evolution, Domesticating Our Species, and Making us Smarter* (Princeton 2016).

Hendry, A. P. & Kinnison, M. T. (1999). The Pace of Modern Life: Measuring Rates of Contemporary Microevolution. *Evolution 53*, 1999, 1637–1653. https://doi.org/10.1111/j.1558-5646.1999.tb04550.x

Heras, C. de las, Montes, R. & Lasheras, J. A. (2013). Altamira: nivel gravetiense y cronología de su arte rupestre. In: de las Heras, C., Lasheras, J. A., Arrizabalaga, A. & de la Rasilla, M. (eds.), *Pensando el Gravetiense: nuevos datos para la Región cantábrica en su contexto peninsular y pirenaico*. Monografía 23 (Madrid 2013), 476–491.

Hill, K., Barton, M. & Hurtado, A. M. (2009). The emergence of human uniqueness: characters underlying behavioral modernity. *Evolutionary Anthropoogy. Issues, News and Reviews 18*, 2009, 187–200. https://doi.org/10.1002/evan.20224

Höneisen, M. & Peyer, S. (1994). *Schweizersbild – ein Jägerleben der Späteiszeit. Beiträge und Dokumente zur Ausgrabung vor 100 Jahren*. Mit Beiträgen von Rudolf Glutz, Tina Grütter, Franz Hofmann, Karl Alban Hünermann, Elisabeth Langenegger und Hans Ulrich Wipf (Schaffhausen 1994).

Hromada, J. (2000). *Moravany nad Váhom Táboriská lovcov mamutov na Považí* (Bratislava 2000).

Hromada, J.& Žemla, M. (2000). Gravettienske sídliská v Hubine. *AVANS* 1998, 2000, 88–90.

Hodder, I. (2012). *Entangled: An Archaeology of the Relationships between Humans and Things* (Hoboken 2012).

Hoggard, C. S., McNabb, J. & Cole, J. N. (2019). The Application of Elliptic Fourier Analysis in Understanding Biface Shape and Symmetry Through the British Acheulean. *Journal of Paleolithic Archaeology 2*, 2019, 115–133. https://doi.org/10.1007/s41982-019-00024-6

Houle, D. (1992). Comparing evolvability and variability of quantitative traits. *Genetics 130*, 1992, 195–204. https://doi.org/10.1093/genetics/130.1.195

Höneisen, M. & Preyer, S. (1994). *Schweizerbild – Ein Jägerlager der Späteiszeit. Beiträge un Dokumente zur Ausgrabung vor 100 Jahren*. Schaffhauser Archäologie 2. Schaffhausen: Veröffentlichungen der Kantonsarchäologie, des Museums zu Allerheiligen und Pro Juliomago, Gesellschaft für Archäologie im Kanton Schaffhausen (Schaffhausen 1994).

Hunt, G. (1996). Manufacture and use of hook-tools by New Caledonian crows. *Nature 379*, 1996, 249–251. https://doi.org/10.1038/379249a0

Hunt, G. (2010). Evolution in fossil lineages: paleontology and the origin of species. *American Naturalist 176*, 2010, 61–76. https://doi.org/10.1086/657057

Hunt, G. (2012). Measuring rates of phenotypic evolution and the inseparability of tempo and mode. *Paleobiology 38*, 2012, 351–373. https://doi.org/10.1666/11047.1

Hussain, S. T., Riede, F. & Plutniak, S. (2024). The "Beast Within" – Querying the (Cultural Evolutionary) Status of Types in Archaeology. *Peer Community in Archaeology,* 2024, 100318. https://doi.org/10.24072/pci.archaeo.100318

Jacobi, R. M. (2004). The Later Upper Palaeolithic lithic collection from Gough's Cave, Cheddar, Somerset and human use of the cave. *Proceedings of the Prehistoric Society 70*, 2004, 1–92. https://doi.org/10.1017/S0079497X00001110

Jacobi, R. & Higham, T. (2011). The Later Upper Palaeolithic Recolonisation of Britain: New Results from AMS Radiocarbon Dating. *Developments in Quaternary Science 14*, 2011, 223–

247. https://doi.org/10.1016/B978-0-444-53597-9.00012-1

Johansen, L. & Stapert, D. (2004). *Oldeholtwolde: A Hamburgian family encampment around a hearth* (Lisse 2004).

John, R., Linsel, F., Roth, G. & Maier, A. (2023). PyREnArA (Python-R-Enviroment-for-Artefact-Analysis) (1.1). *Zenodo*. https://doi.org/10.5281/zenodo.7778071

Johnson, S. C. (1967). Hierarchical clustering schemes. *Psychometrika 32(3)*, 1967, 241–254. https://doi.org/10.1007/BF02289588

Jolliffe, I. T. (2002). *Principal Component Analysis*. Springer Series in Statistics (New York, Berlin, Hong Kong 2002).

Jones, A. M., Brown, C. & Gardner, S. (2011). Tool use in the tuskfish Choerodon schoenleinii? *Coral Reefs 30*, 2011, 865. https://doi.org/10.1007/s00338-011-0790-y

Jordá Cerdá, F. (1955). *El Solutrense en España y sus problemas*. Diputación provincial de Asturias. Servicio de Investigaciones Arqueológicas (Oviedo 1955).

Jordá Cerdá, F., Carral, P., Ripoll, S. & Muñoz Ibañez, F. J. (2012). Geoarqueología, radiocarbono y cronoestratigrafia del yacimiento solutrense de la Cueva de Ambrosio (Vélez-Blanco, Almería, España). Espacio. *Tiempo y Forma 5*, 2012, 63–74.

Jöris, O. (2012). Keilmesser. In: Floss, H. (ed.), *Steinartefakte vom Altpaläolithikum bis in die Neuzeit* (Tübingen 2012), 297–308.

Kabaciński, J. & Schild, R. (2005). The Hamburgian site at Mirkowice: a chronological framework. *Fontes Archaeologici Posnanienses 41*, 2005, 15–18.

Kaletchitz, E. G. (1984). *The initial settlement of the territory of Belarus* (Minsk 1984). In Russian.

Kandler A. & Shennan, S. (2015). A generative inference framework for analysing patterns of cultural change in sparse population data with evidence for fashion trends in LBK culture. *J. R. Soc. Interface 12*, 20150905. http://dx.doi.org/10.1098/rsif.2015.0905

Kaminská, L. (2015). Gravettian and Epigravettian lithics in Slovakia. *Quaternary International 406a,* 2015. http://dx.doi.org/10.1016/j.quaint.2015.08.083

Kaufman, L. & Rousseeuw, P. J. (2005). *Finding Groups in Data: An Introduction to Cluster Analysis*. Wiley Series in Probability and Statistics (New Jersey 2005).

Kempe, M. & Mesoudi, A. (2014). An experimental demonstration of the effect of group size on cultural accumulation. *Evolution and Human Behavior 35*, 2014, 285–290. https://doi.org/10.1016/j.evolhumbehav.2014.02.009

Kempe, M., Lycett, S. & Mesoudi, A. (2012). An experimental test of the accumulated copying error model of cultural mutation for Acheulean handaxe size. *PLoS One 7*, 2012, e48333. https://doi.org/10.1371/journal.pone.0048333

Kendall, M. G. (1938). A New Measure of Rank Correlation. *Biometrika 30(1/2)*, 1938, 81–93.

Kendall, D. (1989). A Survey of the Statistical Theory of Shape. *Statistical Science 4(2)*, 1989, 81–120.

Klaric, L. (2003). *L'unité technique des industries à burins du Raysse dans leur contexte diachronique. Réflexions sur la diversité culturelle au Gravettien à partir des données de la Picardie, d'Arcy-sur-Cure, de Brassempouy et du Cirque de la Patrie*. Ph.D. Dissertation, Université Paris I, Panthéon-Sorbonne (Paris 2003).

Klejn, L.S. (1982). *Archaeological typology*. BAR International Series 153 (Oxford 1982).

Klein, R. G. (1994). The problem of modern human origins. In: Nitecki, M. H. & Nitecki, D.V. (eds.), *Origins of Anatomically Modern Humans* (New York 1994), 3–17.

Klima, B. (1997). Zur Frage der Mikrolithindustrie aus Pavlov. In: Klima, B., Vlček, E., Adovasio, J. M., Damblon, F., Hyland, D. C., Jarošová, L., Musil, R., van der Pflicht, J., Soffer, O., Svoboda, J., Škrdla, P., Trinkaus, E., Vandiver, P. & Verpoorte, A. (eds.), *Pavlov I – Northwest. The Upper Paleolithic burial and it´s settlement context* (Brno 1997), 289–312.

Kline, M. A. & Boyd, R. (2010). Population size predicts technological complexity in Oceania. *Proceedings of the Royal Society B 277*, 2010, 2559–2564. https://doi.org/10.1098/rspb.2010.0452

Kobusiewicz, M. (1975). Stanowisko kultury hamburskiej w Linach, pow. Wolsztyn. *Światowit: rocznik poświęcony archeologii przeddziejowej i badaniom pierwotnej kultury polskiej i słowiańskiej 34* (Warszawa 1975), 213–237.

Kolodny, O., Creanza, N. & Feldman, M. W. (2015). Evolution in leaps: The punctuated accumulation and loss of cultural innovations. *PNAS 112*, 2015, E6762–E6769. https://doi.org/10.1073/pnas.1520492112

Kolodny, O., Creanza, N. & Feldman, M. W. (2016). Game-changing innovations: How culture can change the parameters of its

own evolution and induce abrupt cultural shifts. *PLOS Computational Biology 12*, 2016, e1005302. https://doi.org/10.1371/journal.pcbi.1005302

Kozłowski, J. K. (1999). Gravettian/Epigravettian sequences in the Balkans: environment, technologies, hunting strategies and raw material procurement. In: Bailey, G. N., Adam, E. Panagopoulou, E., Perlès, C. & Zachos, K. (eds.), *The Palaeolithic Archaeology of Greece and adjacent areas*. Proceedings of the ICOPAG Conference, Ioannina 1994. British School at Athens Studies 3 (London 1999), 319–329.

Kozłowski, J. K. (ed.) (1998). *Complex of Upper Palaeolithic Sites Near Moravany, Western Slovakia. Moravany-Lopata II (Excavations 1993-1996)* (Kraków 1998), vol. II.

Kozłowski, J. K. (2008). The shouldered point horizon and the impact of the LGM on human settlement distribution in Europe. In: Svoboda, J. (ed.), *Petřkovice: on shouldered points and female figurines, The Dolní Věstonice Studies Vol 15*, Institute of Archaeology at Brno, Academy of Sciences of the Czech Republic (Brno 2008), 181–192.

Kozłowski, J. K., Van Vliet, B., Sachse-Kozlowska, E., Kubiak, H. & Zakrzewska, G. (1974). Upper paleolithic site with dwellings of mammoth bones e Cracow, Spadzista street B. *Folia Quaternaria 44,* 1974, 1–110.

Kretschmer, I. 2015. *Demographische Untersuchungen zu Bevölkerungsdichten, Mobilität und Landnutzungsmustern im späten Jungpaläolithikum*. KSPA 6 (Rahden/Westf. 2015).

Kufel-Diakowska, B., Wilczyński, J., Wojtal. P. & Sobczyk, K. (2016). Mammoth hunting – Impact traces on backed implements from a mammoth bone accumulation at Kraków Spadzista (southern Poland). *Journal of Archaeological Science 65*, 2016, 122–133. https://doi.org/10.1016/j.jas.2015.11.008

Kulakovska, L., Usik, V. & Haesaerts, P. (2012). Dorochivtsi III e Gravettian site in the Dniester Valley (Ukraine). *Stratum plus 1*, 2012, 131–150. (in Russian).

Kulakovska, L., Usik, V., Haesaerts, P., Ridush, B., Uthmaier, Th. & Hauk, Th. (2014). Upper Paleolithic of Middle Dniester: Doroshivtsi III site. *Quaternary International 359–360*, 2014. http://dx.doi.org/10.1016/j.quaint.2014.10.034

Ladier, E. (2000). Le Magdalénien ancien à lamelles à dos de l'abri Gandil à Bruniquel (Tarn et Garronne): étude préliminaire de l'industrie de la C20. In: Pion, G. (ed.), *Le Paléolithique Supérieur récent: nouvelles don-nées sur le peuplement et l'environnement, Actes de la table ronde de Chambéry, 13–14 mars 1999*, Société Préhistorique Française, Mémoire XXVIII (Chambéry 2000), 191–200.

Lala, K. N. & O'Brien, M. J. (2023). The cultural contribution to evolvability. *Paleoanthropology 2023(2), Special Issue: Niche Construction, Plasticity, and Inclusive Inheritance:Rethinking Human Origins with the Extended Evolutionary Synthesis, Part 1*, 2023, 164–180. https://doi.org/10.48738/2023.iss2.115

Lamb, D. S., Downs, J. & Reader, S. (2020). Space-Time Hierarchical Clustering for Identifying Clusters in Spatiotemporal Point Data. *ISPRS International Journal of Geo-Information 9 (2)*, 2020, 85. https://doi.org/10.3390/ijgi9020085

Lance, G. N. & Williams, W. T. (1967). A general theory of classificatory sorting strategies: 1. Hierarchical systems. *The Computer Journal 9(4)*, 1967, 373–380. https://doi.org/10.1093/comjnl/9.4.373

Langlais, M. (2007). *Dynamiques culturelles des sociétés magdaléniennes dans leurs cadres environnementaux. Enquête sur 7000 ans d'évolution de leurs industries lithiques entre Rhône et Èbre*. Dissertation at University of Toulouse and University of Barcelona.

Langlais, M. (2009). Chronology and territories in the Magdalenian between the Rhone and Ebro Rivers: The example of lithic points. In: Pétillon, J.-M., Dias-Meirinho, M.-H., Cattelain, P., Honegger, M., Normand, C. & Valdeyron, N. (eds.), Projectile weapon elements from the Upper Palaeolithic to the Neolithic. Proceedings of session C83, XVth World Congress UISPP, Lisbon, September 4-9, 2006 (Toulouse 2009), *Palethnologie 1*, 211–240.

Langlais, M., Costamagno, S., Laroulandie, V., Pétillon, J.-M., Discamps, E., Mallye, J.-B., Cochard, D. & Kuntz, D. (2012). The evolution of Magdalenian societies in South-West France between 18,000 and 14,000 calBP: Changing environments, changing tool kits. *Quaternary International 272–273*, 2012, 138–149. https://doi.org/10.1016/j.quaint.2012.02.053

Langlais, M., Secher, A., Caux, S., Delvigne, V., Gourc, L., Normand, C. & Sanchez de la Torre, M. (2016). Lithic tool kits: a Metronome of the evolution of the Magdalenian in southwest France (19,000–14,000 cal BP). *Quaternary International 414*, 2016, 92–107. https://doi.org/10.1016/j.quaint.2015.09.069

Lanting, J. N. & van der Plicht, J. (1996). De 14 C-Chronologie van de Nederlandse Pre-en Protohistorie, I: Laat-Palaeolithicum. *Palaeohistoria 37/38*, 1996, 71–125.

Lanting, J., Niekus, M. & Stapert, D. (2002). Dateringen aan gecremeerd bot uit het Paleolithicum en Vroeg-Mesolithicum: een overzicht van de stand van zaken. *Paleo-aktueel 13*, 2002, 30–36.

Laplace, G. (1964a). Essai de Typologie Systématique. *Annali Dell'Università Di Ferrara, Sezione Paleontologia Umana e Paletnologia, Supplemento II, Volume I*, 1964, 1–85.

Laplace, G. (1964b). Les subdivisions du Paléolithique italien. Étude de typologie analytique. *Bullettino di Paletnologia Italiana. Nuova serie 73*, 1964, 25–63.

Laplace, G. (1972). La Typologie analytique et structurale: Base rationelle d'étude des industries lithiques et osseuses. In: CNRS (ed.), *Banques de données archéologiques. Colloques nationaux CNRS 932* (Paris 1972), 92–143.

Leesch, D. & Müller, W. (2012). Neue Radiokarbondaten an Knochen, Zähnen und Geweih aus einigen Magdalénien-Fundstellen der Schweiz, und ihre Bedeutung für die Stellung des Magdalénien innerhalb des Spätglazials. *Jahrbuch Archäologie Schweiz 95*, 2012, 117–126.

Legendre, P. & Legendre, L. (2012). *Numerical ecology* (Amsterdam 2012). 24th Vol.

Legendre, P., Dallot, S. & Legendre, L. (1985). Succession of Species within a Community: Chronological Clustering, with Applications to Marine and Freshwater Zooplankton. *The American Naturalist 125 (2)*, 1985, 257–288.

Lengyel, G. (2016). Reassessing the middle and late upper palaeolithic in Hungary. *Acta Archaeologica Carpathica 51*, 2016, 47–66.

Lengyel, G. (2018). Lithic analysis of the Middle and Late Upper Palaeolithic in Hungary. *Folia Quaternaria 86*, 2018, 5–157. https://doi.org/10.4467/21995923FQ.18.001.9819

Lengyel, G. (2021). The Epigravettian chronology and the human population of eastern Central Europe during MIS2. *Quaternary Science Reviews 271*, 2021, 107187. https://doi.org/10.1016/j.quascirev.2021.107187

Lenoir, M. (2000). La fin des temps glaciaires dans les basses vallées de la Dordogne et de la Garonne, In: Pion, G. (ed.), *Le Paléolithique Supérieur récent: nouvelles don-nées sur le peuplement et l'environnement, Actes de la table ronde de Chambéry, 13–14 mars 1999*, Société Préhistorique Française, Mémoire XXVIII (Chambéry 2000), 81–87.

Lenoir, M. (2003). Le Magdalénien à pointes à cran de Gironde. In: Ladier, E. (ed.), *Les pointes à cran dans les industries lithiques du Paléolithique supérieur récent de l'oscillation de Lascaux à l'oscillation de Bölling, Table ronde de Montauban*, Préhist. du Sud-Ouest suppl. n°6 (Montauban 2003), 73–83.

Lenoir, M. & Terraza, S. (1971). Le Magdalénien supérieur de l'abri Faustin, commune de Cessac (Gironde). *Bulletin de la Société préhistorique française. Études et travaux 68(1),* 1971, 311–327.

Leplongeon, A., Ménard, C., Bonhomme, V. & Bortolini, E. (2020). Backed Pieces and Their Variability in the Later Stone Age of the Horn of Africa. *African Archaeolgical Review 37*, 2020, 437–468. https://doi.org/10.1007/s10437-020-09401-x

Leroi-Gourhan, A. (1964). *Notes de morphologie descriptive. Cours de Préhistoire* (Paris 1964).

Le Tensorer, J.-M. (1981). *Le Paléolithique de l'Agenais*. Cahiers du Quaternaire 3 (Paris 1981).

Lipo, C., Madsen, M., Dunnelll, R. C. & Hunt, T. (1997). Population structure, cultural transmission, and frequency seriation. *Journal of Anthropological Archaeology 16*, 1997, 301–333.

Lisitsyn, S. & Dudin, A. E. (2019). The Gravettian / Epigravettian in the Kostenki-Borshevo locality on the Don – the division criteria, cultural interpretation and periodisation. *Camera praehistorica 1(2)*, 2019, 70–107. (in Russian) https://doi.org/10.31250/2658-3828-2019-1-70-107

López-Antoñanzas, R., Mitchell, J., Simões, T. R., Condamine, F. L., Aguilée, R., Peláez-Campomanes, P., Renaud, S., Rolland, J. & Donoghue, P. C. J. (2022). Integrative phylogenetics: tools for palaeontologists to explore the tree of life. *Biology 11*, 2022, 1185. https://doi.org/10.3390/biology11081185

Lucas G. (1997). Les lamelles Dufour du Flageolet 1 (Bézenac, Dordogne) dans le contexte aurignacien. *PALEO 9(1)*, 191–219. https://doi.org/10.3406/pal.1997.1233

Lund, M. (1993). Vorschäfte für Kerbspitzen der Hamburger Kultur. Archäologisches *Korrespondenzblatt 23*, 1993, 405–411.

Lycett, S. J. & Norton, C. J. (2010). A demographic model for Paleolithic technological evolution: The case of East Asia and the Movius line. *Quaternary International 211(1)*, 2010, 55–65. https://doi.org/10.1016/j.quaint.2008.12.001

Lyman, R. L. & O'Brien, M. J. (2000). Measuring and Explaining Change in Artifact Variation with Clade-Diversity Diagrams. *Journal of Anthropological Archaeology 19*, 2000, 39–74. https://doi.org/10.1006/jaar.1999.0339

Lyman, R. L. & O'Brien, M. J. (2003). Cultural traits: units of analysis in early twentieth-century anthropology. *Journal of Anthropological Research 59*, 2003, 225–250. https://doi.org/10.1086/jar.59.2.3631642

Lyman, R. L., O'Brien, M. J. & Dunnelll, R. C. (1997). *The rise and fall of culture history* (New York 1997).

Machado, R. S. R., Bonhomme, V., Soteras, R., Jeanty, A., Bouby, L., Evin, A., Martins, M. J. F., Gonçalves, S., Antolín, F., Salavert, A. & Oliveira, H. R. (2025). The origins and spread of the opium poppy (Papaversomniferum L.) revealed by genomics and seed morphometrics. *Philosophical Transactions of the Royal Society B 380*, 2025, 20240198. https://doi.org/10.1098/rstb.2024.0198

MacFadden, B. J. (1988). Fossil horses from "Eohippus" (Hyracotherium) to Equus, 2: rates of dental evolution revisited. *Biological Journal of the Linnean Society 35*, 1988, 37–48. https://doi.org/10.1111/j.1095-8312.1988.tb00457.x

Mahalanobis, P. C. (1936). On the generalized distance in statistics. *Proceedings of the National Institute of Sciences of India 2(1)*, 1936, 49–55.

Maier, A. (2020). On the morphology, chronology, and phylogeny of triangular lithic insets between 20 and 14 ka calBP. *Anthropologie LVIII/2–3*, 167–190. https://doi.org/10.26720/anthro.20.03.30.1

Maier, A. & Zimmermann, A. (2017). Populations headed south? The Gravettian from a palaeodemographic point of view. *Antiquity 91*, 2017, 573–588. https://doi.org/10.15184/aqy.2017.37

Maier, A. (2015). *The Central European Magdalenian. Regional Diversity and Internal Variability* (Dordrecht 2015).

Maier, A., Lehmkuhl, F., Ludwig, P., Melles, M., Schmidt, I., Shao, Y., Zeeden, Ch. & Zimmermann, A. (2016). Demographic estimates of hunter-gatherers during the Last Glacial Maximum in Europe against the background of palaeoenvironmental data. *Quaternary International 425*, 2016, 49–61. https://doi.org/10.1016/j.quaint.2016.04.009

Maier, A., Liebermann, C. & Pfeifer, S. (2020). Beyond the Alps and tatra mountains – the 20–14 ka repopulation of the northern mid-latitudes as inferred from palimpsests deciphered with keys from western and central Europe. *Journal of Paleolithic Archaeology 3(1)*, 2020, 398–452. https://doi.org/10.1007/s41982-019-00045-1

Maier, A., Stojakowits, P., Mayr, C., Pfeifer, S., Preusser, F., Zolitschka, B., Anghelinu, M., Bobak, D., Duprat-Oualid, F., Einwögerer, T., Hambach, U., Händel, M., Kaminská, L., Kämpf, L., Łanczont, M., Lehmkuhl, F., Ludwig, P., Magyari, E., Mroczek, P., Nemergut, A., Nerudová, Z., Niţă, L., Polanská, M., Połtowicz-Bobak, M., Rius, D., Römer, W., Simon, U., Škrdla, P., Újvári, G. & Veres, D. (2021). Cultural evolution and environmental change in Central Europe between 40 and 15 ka. *Quaternary International 581–582*, 2021, 225–240. https://doi.org/10.1016/j.quaint.2020.09.049

Maier, A., Schmidt, I. & Zimmermann, A. (2022a). A large-scale view on 'small-scale societies'. In: Widlok, T. & Cruz, M. D. (eds.), *Scale Matters. The Quality of Quantity in Human Culture and Sociality* (Bielefeld 2022), 111–130.

Maier, A., Ludwig, P., Zimmermann, A. & Schmidt, I. (2022b). The Sunny Side of the Ice Age: Solar Insolation as a Potential Long-Term Pacemaker for Demographic Developments in Europe Between 43 and 15 ka Ago. *PaleoAnthropology 2022(1), Special Issue: The Impact of Upper Pleistocene Climatic and Environmental Change on Hominin Occupations and Landscape Use, Part 1*, 35–51. https://doi.org/10.48738/2022.iss1.100

Maier, A., John, R., Linsel, F., Roth, G., Antl-Weiser, W., Bauer, L., Buchinger, N., Cavak, N., Hoffmann, H., Puschmann, J., Schemmel, M., Schmid, V. C., Simon, U. & Thomas, R. (2023). Analyzing trends in material culture evolution – a case study of Gravettian points from Lower Austria and Moravia. *Journal of Paleolithic Archaeology 6(15)*, 2023. https://doi.org/10.1007/s41982-023-00145-z

Malafouris, L. (2013). *How Things Shape the Mind: A Theory of Material Engagement Unavailable* (Cambridge, Massachusetts 2013).

Malez M. (1987). Pregled paleolitičkih i mezolitičkih kulturana području Istre. *Izdanja Hrvatskog Arheološkog Društva 11*, 1986, 3–47.

Martin, R. A. & Barnosky, A. D. (1993). Quaternary Mammals and Evolutionary Theory: Introductory Remarks and Historical Perspective. In: Martin, R. A. & Barnosky, A. D. (eds.), *Morphological Change in Quaternary Mammals of North America* (Cambridge 1993), 1–12.

Martini, F. (1978). L´Epigravettiano di Grotta della Cala a Marina di Camerota (Salerno). I: l´industria litica e ossea e la cronologia assoluta dell´Epigravettiano evoluto. *Rivista di Scienze Preistoriche 36*, 1978, 57–126.

Maschner, H. D. G. (1998). Review of "Evolutionary Archaeology: Theory and Application". *Journal of the Royal Anthropological Institute 4*, 1998, 354–355.

Matzig, D. N., Hussain, S. T. & Riede, F. (2021). Design Space Constraints and the Cultural Taxonomy of European Final Palaeolithic Large Tanged Points: A Comparison of Typological, Landmark-Based and Whole-Outline Geometric Morphometric Approaches. *Journal of Paleolithic Archaeology 4*, 2021. https://doi.org/10.1007/s41982-021-00097-2

Matzig, D. N., Marwick, B., Riede, F. & Warnock, R. C. M. (2024). A macroevolutionary analysis of European Late Upper Palaeolithic stone toolshape using a Bayesian phylodynamic framework. *Royal Society Open Science 11(8)*, 2024, 240321. https://doi.org/10.1098/rsos.240321

McBrearty, S. & Brooks, A. S. (2000). The revolution that wasn't: A new interpretation of the origin of modern human behaviour. *Journal of Human Evolution 39(5)*, 2000, 453–563. https://doi.org/10.1006/jhev.2000.0435

McGhee, G. R. (2011). *Convergent evolution: Limited form most beautiful* (Cambridge, Massachusetts 2011).

McGhee, G. R. (2018). Limits on the possible forms of stone tools: A perspective from convergent biological evolution. In: O'Brien, M. J., Buchanan, B. & Eren, M. I. (eds.*), Convergent evolution in stone-tool technology* (Cambridge, Massachusetts 2018), 23–46.

Mellars, P. (1994). *The Upper Paleolithic Revolution. The Oxford Illustrated Prehistory of Europe* (Oxford 1994).

Mercier, N., Rink, W. J., Rodriguez, K., Morley, M. W., Vander Linden, M. & Whallon, R. (2018). Radiometric Dating of the Crvena Stijena Sequence. In: R. Whallon (ed.), *Crvena Stijena in cultural and ecological context: Multidisciplinary archaeological research in Montenegro, Vol. 18* (Cetinje 2018), 140–149.

Mesoudi, A., Whiten, A. & Laland, K. N. (2004) Perspective: is human cultural evolution Darwinian? Evidence reviewed from the perspective of the Origin of Species. *Evolution 58*, 2004, 1–11. https://doi.org/10.1111/j.0014-3820.2004.tb01568.x

Mezzena, F. & Palma di Cesnola, A. (1967). L'Epigravettiano della Grotta Paglicci nel Gargano. *Rivista di Scienze Preistoriche 22*, 1967, 23–156.

Mihailovic, D. & Mihailovic, B. (2007). Considérations sur le Gravettien et l'Épigravettien ancien des Balkans de l'ouest. In: Rigaud, J.-Ph. (ed.), *Spécial table ronde (1ère partie): Le Gravettien: entités régionales d'une paléoculture européenne, Les Eyzies, juillet 2004*, Paleo 19 (Lyon 2007), 115–130.

Milliken, S. (1998). Hunter-gatherer land use in Late Glacial southeast Italy. *Oxford Journal of Archaeology 17(3)*, 1998, 269–286. https://doi.org/10.1111/1468-0092.00063

Mix, A. C., Bard, E. & Schneider, R. (2001). Environmental processes ofthe ice age: land, ocean, glaciers (EPILOG). *Quaternary Science Reviews 20*, 2001, 627–657. https://doi.org/10.1016/S0277-3791(00)00145-1

Monge Soares, A. M., Gutiérrez-Zugasti, I., González-Morales, M., Matos Martins, J. M., Cuenca-Solana, D. & Bailey, G. N. (2016). Marine Radiocarbon Reservoir Effect in Late Pleistocene and Early Holocene coastal waters off Northern Iberia. *Radiocarbon 58(4)*, 2016, 869–883. https://doi.org/10.1017/RDC.2016.71

Monmejan, E., Bordes, F. & de Sonneville-Bordes, D. (1964). Le Périgordien supérieur à burins de Noailles du Roc de Gavaudun (Lot-et-Garonne). *L'Anthropologie 68*, 1964, 253–316.

Montelius, G. O. A. (1903). *Die Methode: Der vergleichenden Untersuchung alterthümlicher Geräthe* (Stockholm 1903).

Morgan, L. H. (1877). *Ancient Society* (New York 1877).

Muñoz Ibáñez, F. J. (2000). *Las Puntas Ligeras de Proyectil Del Solutrense Extracantábrico. Análisis Tecnomorfológico E Implicaciónes Funciónales* (Madrid 2000).

Muñoz Ibáñez, F., Sanchez, J. A. M., de Espinosa Marquez, B., Lerma, M. I. & Sintes, J. (2017). The Solutrean shouldered point with abrupt retouch: hafting and propulsion systems. In: Alonso, R., Baena, J. & Canales, D. (eds.), *Playing with the Time. Experimental Archaeology and the Study of the Past. 4th International Experimental Archaeology Conference, 8-11 may 2014, Museo de la Evolución Huma. Burgos, Spain.* (Madrid 2017), 47–52.

Muñoz Ibáñez, F., de Espinosa Sánchez, J. A. M., Martín-Lerma, I., Márquez Mora, B. & Sánchez-Martínez, N. (2019). Solutrean Archers? The Shouldered Points from the End of the Outer-Cantabrian Solutrean Period. In: Schmidt, I., Cascalheira, J., Bicho, N. & Weniger, G.-W. (eds.), *Human adaptations to the Last Glacial Maximum: the Solutrean and its Neighbors* (Cambridge 2019), 283–301.

Münnich, K. O. (1957). Heidelberg Natural Radiocarbon Measurements I. *Science 126*, 1957, 194–199. https://doi.org/10.1126/science.126.3266.194

Murtagh, F. & Contreras, P. (2012). Algorithms for hierarchical clustering: an overview. *WIREs Data Mining and Knowledge Discovery 2(1)*, 2012, 86–97. https://doi.org/10.1002/widm.53

Murtagh, F. & Legendre, P. (2014). Ward's hierarchical agglomerative clustering method: which algorithms implement Ward's criterion? *Journal of Classification 31*, 2014, 274–295. https://doi.org/10.1007/s00357-014-9161-z

Musil, R. (1985). *Die Fauna der Magdalénien-Siedlung Oelknitz*. Weimarer Monographien zur Ur- und Frühgeschichte. Museum für Ur- und Frühgeschichte Thüringens (Weimar 1985).

Mussi, M. (2002). *Earliest Italy. An Overview of the Italian Paleolithic and Mesolithic* (New York, Boston, Dodrecht, London, Moskow 2002).

Neiman, F. D. (1995). Stylistic variation in evolutionary perspective: inferences from decorative diversity and interassemblage distance in Illinois woodland ceramic assemblages. *American Antiquity 60*, 1995, 7–36. https://doi.org/10.2307/282074

Nelson, M. C., Hegmon, M., Kulow, S. R., Peeples, M. A., Kintigh, K. W. & Kinzig A. P. (2011). Resisting Diversity: a Long-Term Archaeological Study. *Ecology and Society 16(1)*, 2011, 25. http://www.jstor.org/stable/26268840

Neugebauer-Maresch, C. (1999). *Le Paléolithique en Autriche* (Grenoble 1999).

Nielsen, E. H. (2009). *Paläolithikum und Mesolithikum in der Zentralschweiz. Mensch und Umwelt zwischen 17000 und 5500 v. Chr.* Archäologische Schriften Luzern 13 (Luzern 2009).

Nigst, P. R. (2012). *The Early Upper Palaeolithic in the Middle Danube region* (Leiden 2012).

Nigst, P., Libois, T., Haesaerts, P., Bosch, M. D., Branscombe, T., Chirica, V. & Noiret, P. (2021). The mid Upper Palaeolithic (Gravettian) sequence of Mitoc-Malu Galben (Romania): New fieldwork between 2013 and 2016 – Preliminary results and perspectives. *Quaternary International 587–588*, 2021, 189–209. https://doi.org/10.1016/j.quaint.2020.10.046

Niţă, L., Anghelinu, M. & Cordoş, C. (2021). The shouldered points and the Gravettian of the Eastern Carpathian area: insights from Bistricioara-Lutărie III (Ceahlău Basin, Northeastern Romania. In: Dobrescu, R., Boroneanţ, A. & Doboş, A. (eds), *Materiale şi cercetări arheologice (Serie nouă), H-S 2021. Scripta praehistorica. Miscellanea in honorem Mariae Bitiri dicata,* 291-311. https://doi.org/10.3406/mcarh.2021.2213

Noiret, P. (2007). Le Gravettien de Moldavie (30.000-23.000 BP). In: Rigaud, J.-Ph. (ed.), *Spécial table ronde (1ère partie): Le Gravettien: entités régionales d'une paléoculture européenne, Les Eyzies, juillet 2004*, Paleo 19 (Lyon 2007), 159–180.

Norman, J. F., Todd, J. T., Perotti, V. J. & Tittle, J. S. (1996). The Visual Perception of Three-Dimensional Length. *Journal of Experimental Psychology: Human Perception and Performance 22(1)*, 1996, 173–186.

Novák, M. (2008). Flint and radiolarite assemblages: Technology and typology. In: J. A. Svoboda (ed.), *Petřkovice. On shouldered points and female figurines*. DVS 15 (Brno 2008), 70–142.

Nuin, J. (1988-89) Paleolítico Superior Final en Leginpea (Etxauri, Navarra). Un yacimiento al aire libre. *Zephyrus XLI-XLII*, 1988/1989, 123–153.

Nuzhnyi, D. Yu. (2009). The industrial variability of the eastern Gravettian assemblages of Ukraine. *Quartär 56*, 2009, 159–174. https://doi.org/10.7485/QU56_09

Nuzhnyi, D. Yu. (2015). *Upper Paleolithic of the western and northern Ukraine (Techno-TypologicalVariability and Periodization)* (Kyiv 2015).

Oberlin, Ch. & Valladas, H. (2012). Datations par la méthode du carbone 14 des niveaux solutréens et badegouliens de l'abri sous roche du Cuzoul. In: Clottes, J., Giraud, J.-P. & Chalard, P. (eds.), *Solutréen et Badegoulien au Cuzoul de Vers. Des chasseurs de rennes en Quercy*. ERAUL 131 (Liège 2012), 79–84.

O'Brien, M. J. (ed.) (1996). *Evolutionary Archaeology: Theory and Application* (Salt Lake City 1996).

O'Brien, M. J. & Holland, T. D. (1990). Variation, Selection, and the Archaeological Record. *Archaeological Method and Theory 2*, 1990, 31–79.

O'Brien, M. J. & Holland, T. D. (1995). Behavioral archaeology and the extended phenotype. In: Skibo, J. M., Walker, W. H. & Nielsen, A. E. (eds.), *Expanding archaeology* (Salt Lake City 1995), 143–161.

O'Brien, M. & Lyman, R. L. (2000). *Applying Evolutionary Archaeology. A Systematic Approach* (New York 2000).

O'Brien, M. & Lyman, R. L. (2003a). Style, Function, Transmission. An Introduction. In: O'Brien, M. & Lyman, R. L. (eds.), *Style, Function, Transmission. Evolutionary Archaeology Perspective* (Salt Lake City, 2003) 1–32.

O'Brien, M. & Lyman, R. L. (2003b). *Cladistics and archaeology* (Salt Lake City 2003).

O'Brien, M. J. & Lala, K. N. (2023). Culture and Evolvability: a Brief Archaeological Perspective. *Journal of Archaeological Method and Theory 30*, 2023, 1079–1108. https://doi.org/10.1007/s10816-023-09624-7

O'Brien, M. J. & Leonard, R. D. (2001). Style and Function: An Introduction. In: Hurt, T. D. & Rakita, G. F. M. (eds.), *Style and Function. Conceptual Issues in Evolutionary Archaeology* (London 2001), 1–24.

O'Brien, M. J., Darwent, J. & Lyman, R. L. (2001). Cladistics is useful for reconstructing archaeological phylogenies: Palaeo-

indian points from the southeastern United States. *Journal of Archaeological Science 28*, 2001, 1115–1136. https://doi.org/10.1006/jasc.2001.0681

O'Brien, M. J., Collard, M., Buchanan, B. & Boulanger, M. T. (2012). Cultural Cladistics and the Early Prehistory of North America. In: Pontarotti, P. (ed.), *Evolutionary Biology: Mechanisms and Trends* (Berlin, Heidelberg 2012).

O'Brien, M. J., Boulanger, M. T., Buchanan, B., Collard, M., Lyman, R. L. & Darwent, J. (2014). Innovation and cultural transmission in the American Paleolithic: Phylogenetic analysis of eastern Paleoindian projectile-point classes. *Journal of Anthropological Archaeology 34*, 2014, 100–119. https://doi.org/10.1016/j.jaa.2014.03.001

O'Brien, M. J., Buchanan, B. & Eren, M. I. (2016). Clovis colonization of Eastern North America: A phylogenetic approach. *STAR: Science & Technology of Archaeological Research 2(1)*, 2016, 67–89. https://doi.org/10.1080/20548923.2016.1183920

Oksanen, J., Simpson, G. L., Blanchet, F. G., Kindt, R., Legendre, P., Minchin, P. R., O'Hara, R.B., Solymos, P., Stevens, M. H. H., Szoecs, E., Wagner, H., Barbour, M., Bedward, M., Bolker, B., Borcard, D., Carvalho, G., Chirico, M., De Caceres, M., Durand, S., Evangelista H. B. A., FitzJohn, R., Friendly, M., Furneaux, B., Hannigan, G., Hill, M. O., Lahti, L., McGlinn, D., Ouellette, M.-H., Ribeiro Cunha, E., Smith, T., Stier, A., Ter Braak, C. J. F., Weedon, J. & Borman, T. (2020). *vegan: Community Ecology Package*. URL: https://CRAN.R-project.org/package=vegan

Oliva, M. (1999). Some thoughts on pavlovian adaptations and their alternatives. In: Roebroeks, W., Mussi, M., Svoboda, J. & Fennema, K. (eds.), *Hunters of the Golden Age. The Mid Upper Palaeolithic of Eurasia 30.000 – 20.000 BP*. Analecta Praehistorica Leidensia 31 (Leiden 1999), 219–230.

Oliva, M. (2009). Štípaná Industrie Sektoru G. In: Oliva, M. (ed.), *Sídliště mamutího lidu u Milovic pod Pálavou. Otázka struktur s mamutími kostmi/Milovice: Site of a Mammoth People below the Pavlov Hills. The question of Mammoth bone structures*. Anthropos 27, N.S. 19 (Brno 2009), 161–211.

Onoratini, G. (1978). Un nouveau type de pointe à cran : la pointe de La Bouverie dans le complexe général des pointes à cran. *Bulletin de la Société préhistorique française 75(11–12)*, 1978, 522–542.

Onoratini, G. (1982). *Préhistoire, sédiments, climats du Würm III à l'holocène dans le sud-est de la France*. PhD-Thesis, Université d'Aix-Marseille.

Onoratini, G. & Renault-Miskovsky, J. (1999). Préhistoire et environnement du Paléolithique supérieur du Sud-Est de la France. In: Vermeersch, P. M. & Renault-Miskovsky, J. (eds.), *European late pleistocene, isotope stages 2 and 3: humans, their ecology & cultural adaptations*. (INQUA Congress in Durham South Africa, 1999), Proceedings of a Conference Held at the Katholieke Universiteit Leuven 5. September 1998, ERAUL 90 (Leuven 1999), 131–165.

Onoratini, G., Defleur, A., Fontugne, M. & Thinon, M. (1994). Le niveau du Paléolithique supérieur terminal de la Baume de Colle Rousse (Le Muy, Var). *Bulletin de la Société préhistorique française 91(1)*, 1994, 56–60.

Oros Sršen, A., Brajković, D., Radović, S., Mauch Lenardić, J. & Miracle, P. T. (2014). The Avifauna of Southern Istria (Croatia) During the Late Pleistocene: Implicationsfor the Palaeoecology and Biodiversity ofthe Northern Adriatic Region. *International Journal of Osteoarchaeology 24*, 2014, 289–299. https://doi.org/10.1002/oa.2364

Otte, M. (1981). *Le Gravettien en Europe central* (Brugge 1981).

Otte, M., Noiret, P., Chirica, V. & Borziac, I. A. (2007). *L'Aurignacien et le Gravettien de Mitoc-Malu Galben (Moldavie Roumaine)* (Liège 2007).

Paccard, M. (1961). L'abri n° 1 de Chinchon (commune de Saumanes de Vaucluse). *Bulletin de la Société Préhistorique Française 58(1-2)*, 1961, 40–44.

Paccard, M. (1964). L'abri n°1 de Chinchon (commune de Saumanes, Vaucluse). *Cahiers Ligures de Préhistoire et d'Archéologie 13(1)*, 1964, 3–67.

Paccard, M. & Dumas, C. (1977). Nouvelles recherches dans l'abri n/1 de Chinchon à Saumanes (Vaucluse). *Gallia Préhistoire 20-1*, 1977, 45–81.

Palma di Cesnola, A. (1976). Il Gravettiano della Grotta Paglicci nel Gargano. I: L´industria litica e la cronologia assoluta. *Rivista di Scienze Preistoriche 30*, 1976, 1–121.

Palma di Cesnola, A. (1979). La serie epigravettiana della Grotta del Fanciulli (Grimaldi) nel quadro del Paleolitico superiore ligure, *Rivista di Scienze Preistoriche 34*, 1979, 3–44.

Palma di Cesnola, A. (1985). L'Epigravettien evolue et final de la region haute-tyrrhenienne. Actes du Colloque International: La position taxonomique et chronologique des industries à pointes à dos autor de la Méditerranée européenne, Sienna, Novembre 1983, *Rivista di Scienze Preistoriche 38*, 1985, 301–318.

Patterson, C. (1982). Morphological characters and homology. In: Joysey, K. A. & Friday, A. E. (eds.), *Problems of phylogenetic reconstruction* (London 1982), 2 I–74.

Patterson, C. (1988). Homology in Classical and Molekular Biology. *Molecular Biology and Evolution 5*, 1988, 603–625. https://doi.org/10.1093/oxfordjournals.molbev.a040523

Păunescu, A. (1998). *Paleoliticul şi epipaleoliticul de pe teritoriul Moldovei cuprins între Carpaţi şi Siret*. Vol. I, 1. (Bucureşti 1998).

Pearson, K. (1895). Note on Regression and Correlation. *The Royal Society Proceedings 58*, 1895, 240–242.

Pedersen, J., Maier, A. & Riede, F. (2019). A punctuated model for the colonisation of the late glacial margins of northern Europe by Hamburgian hunter-gatherers. *Quartär 65*, 85–104.

Penacchioni, M. & Tozzi, C. (1984). L'Epigravettiano di Cenciano Diruto (Viganello, Viterbo). In: Palma di Cesnola, A., Geniola, A. & Biancofiore, F. (eds.), *Atti della XXIV Riun. Scient. dell´Istituto Italiano di Preist. e Protostoria* (Firenze 1984), 183–193.

Penacchioni, M. & Tozzi, C. (1986). L´industria epigravettiana del Riparo Biedano a Norchia (Viterbo). In: Liverani, M., Palmieri, A. & Peroni, R. (eds.), *Studi di Paletnologia in onore di S. M. Puglisi, Università di Roma "La Sapienza"* (Rome 1986).

Perrier, C. & Charmantier, A. (2018). On the importance of time scales when studying adaptive evolution. *Evolution Letters 2018(3)*, 2018, 240–247. https://doi.org/10.1002/evl3.86

Perry, S., Carter, A., Smolla, M., Akçay, E., Nöbel, S., Foster, J. G. & Healy, S. D. (2021). Not by transmission alone: the role of invention in cultural evolution. *Philosophical Transactions B of the Royal Society 376(1828)*, 2021, 20200049. https://doi.org/10.1098/rstb.2020.0049

Peterkin, G. L. (1993). Lithic and organic hunting technology in the French Upper Palaeolithic. *Archeological Papers of the American Anthropological Association 4(1)*, 1993, 49–67. https://doi.org/10.1525/ap3a.1993.4.1.49

Pétillon, J.-M., Barshay-Szmidt, C., Laroulandie, V., Sécher, A., Boudadi-Maligne, M., Brou, L., Castel, J.-C., Chauvière, F.-X., Costamagno, S., Ducasse, S., Grubert, M., Ladier, E:, Langlais, M., Mallye, J.-B. & Primault, J. (2023). Continuities and Discontinuities in the Human Settlement of the Aquitaine Basin between 19.5 cal. ka BP and 13.5 cal. ka BP: The Radiocarbon Evidence. In: Vanmoerkerke, J., Marcigny, C. & Riquier V. (eds.), *Hiatus, lacunes et absences: identifier et interpréter les vides archéologiques*. Actes du 29e Congrès préhistorique de France, 31 mai–4 juin 2021, Toulouse, Session Les espaces vides: preuves d'absences ou absences de preuves?, Société préhistorique française (Toulouse 2024), 47–64.

Pettitt, P. 2008. The British Upper Palaeolithic. In: Pollard, J. (ed.), *Prehistoric Britain* (Oxford 2008), 18–57.

Pettitt, P. B., Davies, W., Gamble, C.S. & Richards, M. B. (2003). Palaeolithic radiocarbon chronology: quantifying our confidence beyond two half-lives. *Journal of Archaeological Science 30*, 2003, 1685–1693. https://doi.org/10.1016/S0305-4403(03)00070-0

Peyrony, D. (1908). Nouvelles fouilles à Badegoule (Dordogne). Solutréen supérieur et transition du Solutréen au Magdalénien. *Revue Préhistorique 4*, 1908, 97–116.

Pinson, A., Xing, L., Namba, T., Kalebic, N., Peters J., Eugster Oegema, C., Traikov, S., Reppe, K., Riesenberg, S., Maricic, T., Derihaci, R., Wimberger, P., Pääbo, S. & Huttner, W. B. (2022). Human TKTL1 implies greater neurogenesis in frontal neocortex of modern humans than Neanderthals. *Science 377*, 2022. https://doi.org/10.1126/science.abl6422

Plisson, H. & Geneste, J.-M. (1989). Analyse technologique des pointes à cran solutrénnes du Placard (Charente), du Fourneau du Diable, du Pech de la Boissière et de Combe Saunière (Dordogne), *Paléo 1*, 1989, 65–106.

Polanská, M., Novák, M. & Klaric, L. (2021). Fossiles directeurs variability in Late and Final Stages of the Gravettian of Central Europe. *Študijné zvesti Archeologického ústavu SAV – Supplementum 2*, 2021, 145–162.

Powell, A., Shennan, S. & Thomas, M. G. (2009). Late Pleistocene demography and the appearance of modern human behavior. *Science 324(5932)*, 2009, 1298–1301. https://doi.org/10.1126/science.1170165

Powell, A., Shennan, S. J. & Thomas, M. G. (2010). Demography and variation in the accumulation of culturally inherited skills. In: O'Brien, M. J. & Shennan, S. J. (eds.), *Innovation in cultural systems: Contributions from evolutionary anthropology* (Cambridge, Massachusetts 2010), 137–160.

Praslov, N. D. & Ivanova, M. A. (1982). Kostënki 21 (Gmelinskaia stoianka). In: Praslov, N. D. & Rogachëv, A. N. (eds.), *Paleolit kostënkovsko-borshchëvskogo raiona na Donu 1879–1979: Nekotorye itogi polevykh issledovanii* (Leningrad 1982), 198–210.

Praslov, N. D. & Rogachev, A. N. (1982). Palaeolithic of the Kostenki-Borshchevo area on the river Don. 1879–1979. Results of

field investigations (Leningrad 1982).

Prentiss, A. M., Kuijt, I. & Chatters, J. C. (2009). *Macroevolution in human prehistory* (Dodrecht, Heidelberg, London 2009).

Prentiss, A. M., Walsh, M. J., Gjesfjeld, E., Denis, M. & Foor, T. A. (2022). Cultural macroevolution in the middle to late Holocene Arctic of east Siberia and north America. *Journal of Anthropological Archaeology 65*, 2022, 101388. https://doi.org/10.1016/j.jaa.2021.101388

Preucel, R. W. (1999). Review of "Evolutionary Archaeology: Theory and Application". *Journal of Field Archaeology 26*, 1999, 93–99.

Primault, J., Gabilleau, J., Brou, L., Griggo, C., Henry-Gambier, D., Houmard, C., Laroulandie, V., Lebrun-Ricalens, L., Liolios, D., Mistrot, V., Rambaud, D., Schmitt, A., Langlais, M., Guérin, S., Berthet, A.-L., Soler, L. & Taborin, Y. (2007). Le Magdalénien inférieurà microlamelles à dos de la grotte du Taillis des Coteaux à Antigny (Vienne, France). *Bulletin dela Société préhistorique de France 104(1)*, 2007, 5–30.

R Core Team (2021). *R: A language and environment for statistical computing*. R Foundation for Statistical Computing, Vienna, Austria. URL: https://www.R-project.org/

Reade, H., Tripp, J. A., Charlton, S., Grimm, S. B., Leesch, D., Müller, W., Sayle, K. L., Fensome, A., Higham, T. F. G., Barnes, I. & Stevens R. E. (2020). Deglacial landscapes and the Late Upper Palaeolithic of Switzerland. *Quaternary Science Reviews 239*, 2020, 106372. https://doi.org/10.1016/j.quascirev.2020.106372

Read, D. (2006). Tasmanian Knowledge and Skill: Maladaptive Imitation or Adequate Technology? *American Antiquity 71(1)*, 2006, 164-184. https://doi.org/10.2307/40035327

Reimer, P. J., Austin, W E. N., Bard, E., Bayliss, A., Blackwell, P. G., Bronk Ramsey, C., Butzin, M., Cheng, H., Edwards, R. L., Friedrich, M., Grootes, P. M., Guilderson, T. P., Hajdas, I., Heaton, T. J., Hogg, A. G., Hughen, K. A., Kromer, B., Manning, S. W., Muscheler, R., Palmer, J. G., Pearson, C., van der Plicht, J., Reimer, R. W., Richards, D. A., Scott, E. M., Southon, J. R., Turney, C. S. M., Wacker, L., Adolphi, F., Büntgen, U., Capano, M., Fahrni, S. M., Fogtmann-Schulz, A., Friedrich, R., Köhler, P., Kudsk, S., Miyake, F., Olsen, J., Reinig, F., Sakamoto, M., Sookdeo, A. & Talamo, S. (2020). The Intcal20 Northern Hemisphere Radiocarbon Age Calibration Curve (0–55 cal kBP*). Radiocarbon 62(4)*, 2020, 725–757. https://doi.org/10.1017/RDC.2020.41

Reynolds, N. (2014). *The Mid Upper Palaeolithic of European Russia: chronology, culture history and context. A study of five Gravettian backed lithic assemblages.* PhD at Wolfson College, School of Archaeology, University of Oxford (submitted 2014).

Reynolds , N. & Riede, F. (2019). House of cards: cultural taxonomy and the study of the European Upper Palaeolithic. *Antiquity 93(371)*, 2019, 1350–1358. https://doi.org/10.15184/aqy.2019.49

Richerson, P. J., Boyd, R. & Bettinger, R. L. (2009). Cultural innovations and demographic change. *Human Biology 81(3)*, 2009, 211–235. https://doi.org/10.3378/027.081.0306

Richter, J. (1997). *Sesselfelsgrotte III. Der G-Schichten-Komplex der Sesselfelsgrotte. Zum Verständnis des Micoquien* (Saarbrücken 1997).

Riede, F. & Edinborough, K. (2012). Bayesian radiocarbon models for the cultural transition during the Allerød in southern Scandinavia. *Journal of Archaeological Science 39*, 2012, 744–756. https://doi.org/10.1016/j.jas.2011.11.008

Riede, F., Matzig, D. N., Biard, M., Crombé, P., de Pablo, J. F.-L., Fontana, F, Groß, D., Hess, T., Langlais, M., Mevel, L., Mills, Wi., Moník, M., Naudinot, N., Posch, C., Rimkus, T., Stefański, D., Vandendriessche, H. & Hussain, S. T. (2024). A quantitative analysis of Final Palaeolithic/earliest Mesolithic cultural taxonomy and evolution in Europe. *PLOS ONE 19*, 2024, e0299512. https://doi.org/10.1371/journal.pone.0299512

Ripoll López, S. (1988). *La Cueva de Ambrosio (Almería, España) y su posición cronoestratigrafía en el Mediterráneo Occidental*, BAR International Series 462 (Oxford 1988).

Ripoll Lopez, S. & Cacho Ouesada, C. (1990). Le Solutréen dans le Sud de la Peninsule Iberique. In: Kozłowski, J. K. (ed.), *Feuilles de pierre. Les industries à pointes foliacées du Paléolithique supérieur européen. Actes du Colloque de Cracovie 1989*. E.R.A.U.L. 42 (Liege 1990), 449–465.

Ripoll López, S., Muñoz Ibañez, F. J. & Lerma, I. M. (2015). The Solutrean Site of Ambrosio Cave (Almería, Spain). New Perspectives from Andalucia. *Journal of Anthropological Research 71(4)*, 2015, 509–522. https://doi.org/10.3998/jar.0521004.0071.403

Rindos, D. (1980). Symbiosis, Instability, and the Origins and Spread of Agriculture: A New Model. *Current Anthropology 21*, 1980, 751–772.

Rogachev, A. N., Praslov, N. D., Anikovich, M. V., Belyaeva, V. I. & Dmitrieva, T. N. (1982). Kostenki 1. In: Praslov, N. D & Rogachev, A. N. (eds.), *Paleolit Kostenkovsko-Borshchevskogo raiona na Donu 1879-1979* (Leningrad 1982), 42–66.

Rogers, D. S. & Ehrlich, P. R. (2008). Natural selection and cultural rates of change. *Proceedings of the National Academy of Sciences 105*, 2008, 3416–3420. https://doi.org/10.1073/pnas.0711802105

Rohlf, F. J. & Marcus, L. F. (1993). A revolution in morphometrics. *Trends in Ecology & Evolution 8(4)*, 1993, 129–132. https://doi.org/10.1016/0169-5347(93)90024-J

Rosa, D. (1903). *Die progressive Reduktion der Variabilität und ihre Beziehungen zum Aussterben und zur Entstehung der Arten* (Jena 1903).

Rossini, M., Falcucci, A., Dominici, C., Ronchitelli, A., Tomasso, A. & Boschin, F. (2023). Application of 2D shape analysis to study Epigravettian lithic assemblages: assessing its analytical potential. *Acta IMEKO 12(4)*, 2023, 1–8. https://doi.org/10.21014/actaimeko.v12i4.1539

Rossini, M., Tomasso, A., Boschin, F., Martini, I., Crezzini, J., Dominici, C. & Moroni, A. (2025). Early Epigravettian backed pieces from layer O of Grotta della Cala (Southern Italy). A techno-typological and use-wear integrated approach. *Journal of Archaeological Science: Reports 62*, 2025. https://doi.org/10.1016/j.jasrep.2025.105046

Roth, G. (2022). Überflüssige Information? Zum Verständnis moderner Deutung archäologischer Zusammensetzungsdaten mit transformationsbasierter Redundanzanalyse (tb-RDA). In: Kaiser, E., Meyer, M., Scharl, S. & Suhrbier, St. (eds.), *Wissensschichten. Festschrift für Wolfram Schier zu seinem 65. Geburtstag*. Studia honoraria 41 (Rahden/Westf. 2022), 28–42.

Rothert, L. (1936). *Die mittlere Steinzeit in Schlesien* (Leipzig 1936).

Rots, V. (2016). Projectiles and Hafting Technology. In: Iovita, R. & Sano, K. (eds.), *Multidisciplinary Approaches to the Study of Stone Age Weaponry. Vertebrate Paleobiology and Paleoanthropology* (Dordrecht 2016), 167–185.

Roque, C., Guibert, P., Vartanian, E., Bechtel, F., Oberlin, C., Evin, J., Mercier, N., Valladas, H., Texier, J. & Rigaud, J.-Ph (2001). Une expérience de croisement de datations TL/14C pour la séquence solutréenne de Laugerie-Haute, Dordogne. In: Barrandon, J.-N., Guibert, P. & Michel, V. (eds.), *Datation* (Antibes 2001), 217–232.

Roux, V. (2003). Ceramic standardization and intensity of production: Quantifying degrees of specialization. *American Antiquity 68(4)*, 2003, 768–782. https://doi.org/10.2307/3557072

Roux, V. (2015). Standardization of ceramic assemblages: Transmission mechanisms and diffusion of morpho-functional traits across social boundaries. *Journal of Anthropological Archaeology 40*, 2015, 1–9. https://doi.org/10.1016/j.jaa.2015.04.004

Rubin, M. & Suess, H. E. (1956). U.S. Geological Survey Radiocarbon Dates III. *Science 123*, 1956, 442–448.

Rust, A. (1937). *Das altsteinzeitliche Rentierjägerlager Meiendorf* (Neumünster 1937).

Rust, A. (1943). *Die Alt- und Mittelsteinzeitlichen Funde von Stellmoor* (Neumünster 1943).

Rust, A. (1958). *Die jungpaläolithischen Zeltanlagen von Ahrensburg* (Neumünster 1958).

Sacchi, D. (1986). *Le Paléolithique supérieur du Languedoc occidental et du Roussillon*. Gallia Préhistoire, Suppl. 21 (Paris 1986).

Sackett, J. R. (1977). The meaning of style in archaeology: A general model. *American Antiquity 42*, 1977, 369–380.

Sahle, Y. & Brooks, A.S. (2019). Assessment of complex projectiles in the early Late Pleistocene at Aduma, Ethiopia. *PLoS ONE 14(5)*, 2019, e0216716. https://doi.org/10.1371/journal.pone.0216716

Santamaría Álvarez, D. & de la Rasilla Vives, Marco (2013). Datando el final del Paleolítico medio en la Península Ibérica. Problemas metodológicos y límites de la interpretación. *Trabajos de Prehistoria 70(2),* 2013, 241–263. https://doi.org/10.3989/tp.2013.12111

Sanz, C. M. & Morgan, D. B. (2009). Flexible and Persistent Tool-using Strategies in Honey-gathering by Wild Chimpanzees. *International Journal of Primatology 30(3)*, 2009, 411–427. https://doi.org/10.1007/s10764-009-9350-5

Sardella, R., Mazzini, I., Giustini, F., Mecozzi, B., Brilli, M., Iurino, D.A., Lembo, G., Muttilllo, B., Massussi, M., Sigari, D., Tucci, S. & Voltaggio, M. (2018). Grotta Romanelli (Southern Italy, Apulia): legacies and issues in excavating a key site for the pleistocene of the Mediterranean. *Rivista Italiana di Paleontologia e Stratigrafia [Research in Paleontology and Stratigraphy] 124(2)*, 2018, 247–264. https://doi.org/10.13130/2039-4942/9983

Sauer, F. & Riede, F. (2019). A Critical Reassessment of Cultural Taxonomies in the Central European Late Palaeolithic. *Journal of Archaeological Method and Theory 26*, 2019, 155–184. https://doi.org/10.1007/s10816-018-9368-0

Scerri, E. M. L. & Will, M. (2023). The revolution that still isn't: The origins of behavioral complexity in Homo sapiens. *Journal of Human Evolution 179*, 2023, 103358. https://doi.org/10.1016/j.jhevol.2023.103358

Scharl, S. (2017). Organisationsformen von Tausch im Neolithikum – Eine Fallstudie aus Nordwestbayern. *Der Anschnitt, Beih. 34*, 2017, 111–123, https://doi.org/10.46586/DBM139

Schmider, B. (1992). *Marsangy: Un campement des derniers chasseurs magdaleniens, sur les bords del'Yonne*. ERAUL 55 (Liège 1992).

Schmidt, I., Bradtmöller, M., Kehl, M., Pastoors, A., Tafelmaier, Y., Weninger, B. & Weniger, G.-C. (2012). Rapid climate change and variability of settlement patterns in Iberia during the Late Pleistocene. *Quaternary International 274*, 2012, 179–204. https://doi.org/10.1016/j.quaint.2012.01.018

Schmidt, I. (2015). *Solutrean Points of the Iberian Peninsula. Tool making and using behaviour of hunter-gatherers during the Last Glacial Maximum*. BAR International Series 2778 (Oxford 2015).

Schmidt, I. & Mom, V. (2015). Shape and technological organization of lithic Solutrean points from Iberia: A computational approach for exploring the diversity of shapes. In: Traviglia, A. (ed.), *Across Space and Time. Papers from the 41st Conference on Computer Applications and Quantitative Methods in Archaeology. Perth, 25-28 March 2013* (Amsterdam 2015), 475–481.

Schmidt, I. & Zimmermann, A. (2019). Population dynamics and socio-spatial organization of the Aurignacian: Scalable quantitative demographic data for western and central Europe. *PLoS ONE 14(2)*, 2019, e0211562. https://doi.org/10.1371/journal.pone.0211562

Shimelmitz, R., Bisson, M., Weinstein-Evron, M. & Kuhn S. L. (2017). Handaxe manufacture and re-sharpening throughout the Lower Paleolithic sequence of Tabun Cave, *Quaternary International 428(A)*, 2017, 118–131. https://doi.org/10.1016/j.quaint.2015.12.076

Schuler, A. (1994). *Die Schussenquelle. Eine Freilandstation des Magdalénien in Oberschwaben*. Materialhefte zur Archäologie in Baden-Württemberg 27 (Stuttgart 1994).

Sharon, G. (2007). *Acheulian Large Flake Industries: Technology, Chronology, and Significance* (Oxford 2007).

Shennan, S. J. (1997). *Quantifying Archaeology*. 2nd ed. (Edinburgh 1997).

Shennan, S. J. (2001). Demography and Cultural Innovation: a Model and its Implications for the Emergence of Modern Human Culture. *Cambridge Archaeological Journal 11(1)*, 2001, 5–16. https://doi.org/10.1017/S0959774301000014

Shott, M. J. & Ballenger, J. (2007). Biface reduction and the measurement of Dalton curation: a southeastern case study. *American Antiquity 72(1)*, 2007, 153–175. https://doi.org/10.2307/40035302

Siemssen, T., John, R. & Wurz, S. (in prep.). Morphometric Analysis of the Post-Howiesons Poort points from Klasies River Mouth, South Africa.

Silvestrini, M., Cancellieri, E. & Peresani, M. (2008). Madonna dell'Ospedale, un sito Epigravettiano antico al margine dell'Appenino marchigiano: osservazioni sulla produzione litica. In: Mussi, M. (ed.), *Il Tardiglaciale in Italia: lavori in corso*. B.A.R. International Series 1859 (Oxford 2008), 81–102.

Simon, U. & Moreau, L. (2012). Ein Aufnahmesystem zur merkmalanalytischen Erfassung jungpaläolithischer Kerntechnologie. In: Beier, H.-J., Ostritz, S., Küßner, M., Schäfer, D., Schimpff, V., Wagner, K. & Zimmermann, A. (eds.), *Finden und Verstehen. Festschrift für Thomas Weber zum sechzigsten Geburtstag* (Langenweißbach 2012), 105–110.

Simpson, G. G. (1940). Types in Modern Taxonomy. *American Journal of Science 238(6)*, 1940, 413–431.

Simpson, G. G. (1944). *Tempo and Mode in Evolution* (New York 1944).

Simpson, G. G. (1951). *Horses: the story of the horse family in the modern world and through sixty million years of history* (Oxford 1951).

Sinitsyn, A. A. (2007). Variabilité du Gravettien de Kostienki (Bassin moyen du Don) et des territoires associés. In: Rigaud, J.-Ph. (ed.), *Spécial table ronde (1ère partie): Le Gravettien: entités régionales d'une paléoculture européenne, Les Eyzies, juillet 2004*, Paleo 19 (Lyon 2007), 181–201. https://doi.org/10.4000/paleo.599

Sinitsyn, A. A., Praslov, N. D., Svezhentsev, I. S. & Sulerzhitskii, L. D. (1997). Radiouglerodnaiakhronologiia verkhnego paleolita Vostochnoi Evropy. In: Sinitsyn, A. A. & Praslov, N. D. (eds.), *Radiouglerodnaia khronologiia paleolita Vostochnoi Evropy i Severnoi Azii. Problemy i perspektivy* (Saint Petersburg 1997), 21–66.

Sneath, P. H. A. & Sokal, R. R. (1973). *Numerical Taxonomy: The Principles and Practice of Numerical Classification* (San Francisco 1973).

Snyder, W. D., Reeves, J. S. & Tennie, C. (2022). Early knapping techniques do not necessitate cultural transmission. *Science Advances 8(27)*. https://doi.org/10.1126/sciadv.abo2894

Small, C. G. (1996). *The Statistical Theory of Shape. Springer Series in Statistics* (New York 1996).

Smith, Ph. (1966). *Le Solutréen en France* (Bordeaux 1966).

de Sonneville-Bordes, D. (1966). Évolution du Paléolithique supérieur en Europe occidentale et sa signification. *Bulletin de la Société Préhistorique Française LXIII(1)*, 1966, 3–34.

de Sonneville-Bordes, D. (1969). Pointes à cran (Kerbspitzen) du Magdalénien supérieur du Petersfels. *Quartär 20*, 1969, 175–188. https://doi.org/10.7485/QU20_08

de Sonneville-Bordes, D. & Perrot, J. (1954). Lexique typologique du Paléolithique supérieur. Outillage lithique: I Grattoirs – II Outils solutréens. *Bulletin de la Société Préhistorique Française 51*, 1954, 327–355.

de Sonneville-Bordes, D. & Perrot, J. (1955). Lexique typologique du Paléolithique supérieur. Outillage lithique – III Outils composites – Percoirs. *Bulletin de la Société Préhistorique Française 52*, 1955, 76–79.

de Sonneville-Bordes, D. & Perrot, J. (1956b). Lexique typologique du Paléolithique supérieur. Outillage lithique. *Bulletin de la Société Préhistorique Française 53*, 1956, 408–559.

Soto-Barreiro, M. J. (2003). *Cronología radiométrica, ecología y clima del Paleolítico Cantábrico*. Altamira Monographia 19 (Madrid 2003).

Spaulding, A.C. (1953). Statistical techniques for the discovery of artefact types. *American Antiquity 18*, 1953, 305–313.

Spaudling, A. (1960). The Dimensions of Archaeology. In: Dole, G. E. & Carneiro, R. L. (eds.), *Essays in the Sience of Culture in Honor of Leslie A. White* (New York 1960), 437–456.

Srdoč, D., Sliepčević, A., Planinić, J., Obelić, B., Breyer, B. (1973). Rudjer Bošković radiocarbon measurements II. *Radiocarbon 15, 2*, 1973, 435–441.

Sterelny, K. (2021). Demography and cultural complexity. *Synthese 198*, 2021, 8557–8580. https://doi.org/10.1007/s11229-020-02587-2

Stodiek, U. (1987). Fußgönheim – zwei jungpaläolithische Fundplätze in der Vorderpfalz. *Archäologisches Korrespondenzblatt 17*, 1987, 31–41.55

Straus, L. G. (1983). *El Solutrense Vasco-Cantábrico: una Nueva Perspectiva*, vol. 10 (Altamira 1983).

Straus, L. G. (1990). The Original Arms Race: Iberian Perspective on the Solutrean Phenomenon. In: Kozłowski, J. K. (ed.), *Feuilles de pierre. Les industries à pointes foliacées du Paléolithique supérieur européen. Actes du Colloque de Cracovie 1989*. E.R.A.U.L. 42 (Liege 1990), 425–447.

Straus, L. G. (2015). The human occupation of southwestern Europe during the Last Glacial Maximum: Solutrean cultural adaptations in France and Iberia. *Journal of Anthropological Research 71*, 2015, 465–492.

Straus, L. G. & Clark, G. A. (1986). *La Riera Cave: stone age hunter-gatherer adaptations in northern Spain, vol. 36 of Anthropological research papers* (Tempe 1986).

Straus, L. G. & González Morales, M. R. (2007). Further Radiocarbon Dates for the Upper Paleolithic of El Mirón Cave (Ramales De La Victoria, Cantabria, Spain). *Radiocarbon 49(3)*, 2007, 1205–1214. https://doi.org/10.1017/S0033822200043113

Straus, L. G. & González Morales, M. R. (2009). A preliminary description of Solutrean occupations in El Mirón cave (Ramales de la Victoria, Cantabria). *Munibe 60*, 2009, 117–137.

Straus, L. G., González Morales, M. R., Martínez, M. A. F. & García-Gelabert, M. P. (2002). Last Glacial Human Settlement in Eastern Cantabria (Northern Spain). *Journal of Archaeological Science 29*, 2002, 1403–1414. https://doi.org/10.1006/jasc.2001.0800

Street, M. & Höck, C. (1998). Comments on the dating of the Kniegrotte. In: Hedges, R. E. M., Pettitt, P. B., Bronk Ramsey, C. & van Klinken, G. J. (eds.), *Radiocarbon dates from the Oxford AMS system: Archaeometry Datelist 25*. Archaeometry 40 (Oxford 1998), 231–232.

Stuart, A. J., Sulerzhitsky, L. D., Orlova, L. A., Kuzmin, Y. V. & Lister, A. M. (2002). The latest woolly mammoths (Mammuthus primigenius Blumenbach) in Europe and Asia: a review of the current evidence. *Quaternary Science Reviews 21*, 2002, 1559–1569. https://doi.org/10.1016/S0277-3791(02)00026-4

Svezhentsev, Y. S. (1993). Radiocarbon Chronology for the Upper Paleolithic Sites on the East European Plain. In: Soffer, O. & Praslov, N. D. (eds.), *From Kostenki to Clovis: Upper Paleolithic – Paleo-Indian Adaptations* (New York 1993), 23–30.

Svezhentsev, Y. S. & Popov, S. G. (1993). Late Paleolithic Chronology of the East European Plain. *Radiocarbon 35*, 1993, 495–501. https://doi.org/10.1017/S0033822200060525

Svoboda, J. (1996). Gravettian and Epigravettian chronologies in the Middle Danube area. *Přehled výzkumů 1992*, 1996, 9–19.

Svoboda, J. (2007). The Gravettian on the Middle Danube. *PALEO 19*, 2007, 203–220. https://doi.org/10.4000/paleo.607

Svoboda, J. (2008). Formation of the archaeological layers, structure of the site and features. In: J. Svoboda (ed.), *Petřkovice. On shouldered points and female figurines*. DVS 15 (Institute of Archaeology Brno 2008), 31–45.

Svoboda, J. (2013). Location and history of Předmostí, spatial structure and overall stratigraphy. In: J. Svoboda (ed.), *Předmostí*. DVS 19 (Institute of Archaeology Brno 2013), 9–18.

Szmidt, C., Laroulandie, V., Dachary, M., Langlais, M. & Costamagno, S. (2009). Harfang, Renne et Cerf: nouvelles dates 14C du Magdalénien supérieur du Bassin aquitain au Morin (Gironde) et Bourrouilla (Pyrénées-Atlantiques). *Bulletin de la Société préhistorique française 106(3)*, 2009, 583–587.

Tarasov, L. M. (1979). *Gagarinskaia stoianka i e mesto v paleolite Evropy* (Leningrad 1979). (in Russian)

Taute, W. (1968). *Die Stielspitzengruppen im nördlichen Mitteleuropa: Ein Beitrag zur Kenntnis der späten Altsteinzeit* (Köln 1968).

Taylor, A. (2012). Armatures et pièces à dos du Magdalénien supérieur de La Madeleine (Tursac, Dordogne), nouvelles données de la technologie lithique. *PALEO 23*, 2012, 277–312. https://doi.org/10.4000/paleo.2402

Terberger, T. (2003). Vom Gravettien zum Magdalénien in Mitteleuropa – Aspekte der menschlichen Besiedlungsgeschichte in der Zeit um das zweite Kältemaximum der letzten Eiszeit. *Archäologisches Nachrichtenblatt 8*, 2003, 55–62.

Terberger, T. (2013). Le Dernier Maximum glaciaire entre le Rhin et le Danube, un réexamen critique. Le paléolithique superieur ancien de l'Europe du Nord-Ouest. *Mémoire de la Société Préhistorique française 56*, 2013, 415–443.

Terlato, G., Bocherens, H., Romandini, M., Nannini, N., Hobson, K. A. & Peresani, M. (2019). Chronological and Isotopic data support a revision for the timing of cave bear extinction in Mediterranean Europe. *Historical Biology 31*, 2019, 474–484. https://doi.org/10.1080/08912963.2018.1448395

Thévenin, A. (2000). Géographie et cultures au Tardiglaciaire. L'impact de l'axe Rhône-Saône. In: Pion, G. (ed.), *Le Paléolithique Supérieur récent: nouvelles don-nées sur le peuplement et l'environnement, Actes de la tableronde de Chambéry, 13–14 mars 1999*, Société Préhistorique Française, Mémoire XXVIII (Chambéry 2000), 67–79.

Tiffagom, M. (2006). *De la pierre à l'homme: essai sur une paléoanthropologie solutréenne*. ERAUL 113 (Liège 2006).

Timbrell, L., de la Peña, P., Way, A., Hoggard, C., Backwell, L., d'Errico, F., Wadley, L. & Grove, M. (2022). Technological and geometric morphometric analysis of 'post-Howiesons Poort points' from Border Cave, KwaZulu-Natal, South Africa. *Quaternary Science Reviews 297*, 2022, 107813. https://doi.org/10.1016/j.quascirev.2022.107813

Thommeret, J. & Thommeret, Y. (1973). Monaco radiocarbon measurements IV. *Radiocarbon, 15(2)*, 1973, 321–344. https://doi.org/10.1017/S0033822200001247

Thompson, D. A. W. (1945). *On Growth and Form* (Cambridge 1945).

Tomasso, A. & Rots, V. (2021). Looking into Upper Palaeolithic gear: The potential of an integrated techno-economic approach. *Journal of Anthropological Archaeology 61 (101240)*, 2021. https://doi.org/10.1016/j.jaa.2020.101240

Tostevin, G. (2003). Attribute Analysis of the Lithic Technologies of Stránská skála IIIc and IIId in Regional and Interregional Context. In: Svoboda, J. & Bar-Yosef, O. (eds.), *Origins of the Upper Paleolithic in the Brno Basin Moravia, Czech Republic* (Harvard 2003), 77–118.

Tromnau, G. (1975a). Die Fundplätze der Hamburger Kultur von Heber und Deimern, Kreis Soltau. *Materialhefte zur Ur- und Frühgeschichte Niedersachsens 9*, 1975, 1–46.

Tromnau, A. V. (1975b). *Neue Ausgrabungen im Ahrensburger Tunneltal. Ein Beitrag zur Erforschung des Jungpaläolithikums im nordwestlichen Flachland* (Neumünster 1975).

Troussov A.V. (1998). The lithic assemblage from the Palaeolithic site of Zaraisk. In: Amirkhanov. Kh. A. (ed.). *Gravettien oriental* (Moscow 1998), 279–298.

Tsanova, T., Delvigne, V., Sirakova, S., Anastasova, E., Horta, P., Krumov, I., Marreiros, J., Nacheva, E., Rezek, Z., Hublin, J.-J. & Sirakov, N. (2024). Curated character of the Initial Upper Palaeolithic lithic artefact assemblages in Bacho Kiro Cave (Bulgaria). *PLoS ONE 19(9)*, 2024, e0307435. https://doi.org/10.1371/journal.pone.0307435

Tsirintoulaki, K., Matzig, D. N. & Riede, F. (2023). A 2D Geometric Morphometric Assessment of Chrono-Cultural Trends in Osseous Barbed Points of the European Final Palaeolithic and Early Mesolithic. *Open Archaeology 9(1)*, 2023, 20220276. https://doi.org/10.1515/opar-2022-0276

Tuffreau, A., Dobrescu, R., Ciornei, A., Niţă, L. & Kostek, A. (2018). Le Paléolithique supérieur de la basse vallée de la Bistriţa (Moldavie roumaine): Buda et Lespezi, nouvelles recherches. The Upper Palaeolithic of the Lower Bistriţa Valley (Romanian Moldavia): Buda and Lespezi, new researches. *L'Anthropolgie 122*, 2018, 129–165. https://doi.org/10.1016/j.anthro.2018.02.003

Tyler, E. G. (1871). *Primitive Culture* (London 1871).

Ucelli Gnesutta, P. & Cristiani, E. (2002). Analisi stilistica e tecnologica di frammenti di osso decorato dai livelli epigravettiani della Grotta di Settecannelle (Viterbo). *Rivista di Scienze Preistoriche 52*, 2002, 143–160.

Uller, T., Moczek, A. P., Watson, R. A., Brakefield, P. M. & Laland, K. N. (2018). Developmental bias and evolution: A regulatory network perspective. *Genetics 209*, 2018, 949–966. https://doi.org/10.1534/genetics.118.300995

Uthmeier, T. (2016). Neanderthal Utilitarian Equipment and Group Identity: The Social Context of Bifacial Tool Manufacture and Use. In: Haidle, M., Conard, N. & Bolus, M. (eds.), *The nature of culture, vertebrate paleo-biology and paleoanthropology* (Dordrecht 2016), 65–77. https://doi.org/10.1007/978-94-017-7426-0_7

Utrilla, P. (1995). El Valle del Ebro durante el Tardiglaciar y comienzos del Holocenolas. relaciones con el Magdaleniense cantábrico. In: Romanillo, J. A. M. & Sainz, C. G. (eds.), *El final del Paleolítico cantábrico: transformaciones ambientales y culturales durante el Tardiglacial y comienzos del Holoceno en la* Región *Cantábrica* (Santander 1995), 281–312.

Utrilla, P. & Mazo, C. (1994). El Solutrense en el valle medio del Ebro. *Férvedes 1*, 1994, 89–104.

Utrilla, P. & Montes, L. (2007). La période 19000-14000 BP dans le bassin de l'Èbre. *Bulletin de la Société préhistorique française 104(4)*, 2007, 797–807.

Vaesen, K., Collard, M., Cosgrove, R. & Roebroeks, W. (2016). Population size does not explain past changes in cultural complexity. *PNAS 2016,* E2241–E2247. https://doi.org/10.1073/pnas.1520288113

Valentin, B. & Pigeot, N. (2000). Eléments pour une chronologie des occupations magdaléniennes dans le Bassin parisien. In : Valentin, B., Bodu, P. & Christensen, M. (eds.), *L'Europe centrale et septentrionale au Tardiglaciaire: Confrontation desmode'les re·gionaux de peuplement. Actes de la Table-ronde internationale de Nemours,14–16 Mai 1997* (Nemours 2000), 129–138.

Vasyliev, P. M. (2019). *ПАМ'ЯТКИ ПУШКАРІВСЬКОГО ТИПУ У ВЕРХНЬОМУ ПАЛЕОЛІТІ ПІВНІЧНОЇ УКРАЇНИ*. PhD (Kiev 2019).

Vaughan, C. D. (2001). A Million Years of Style and Function: Regional and Temporal Variation in Acheulean Handaxes In: Hurt, T. D. & Rakita, G. F. M. (eds.), *Style and Function. Conceptual Issues in Evolutionary Archaeology* (London 2001), 141–164.

Vega del Sella, C. d. l. (1916*). Paleolítico de Cueto de la Mina (Asturias)*. vol. 13 of Memoria / Comisión de Investigaciones Paleontológicas y Prehistóricas (Madrid 1916).

Vega del Sella, C. d. l. (1930). *Las Cuevas de la Riera y Balmori (Asturias), vol. 38 of Memoria / Comisión de Investigaciones Paleontológicas y Prehistóricas* (Madrid 1930).

Velichko, A. A. & Zelikson, E. M. (2005). Landscape, climate and mammoth food resources in the East European Plain during the Late Paleolithic epoch. *Quaternary International 126–128*, 2005, 137–151. https://doi.org/10.1016/j.quaint.2004.04.019

Vermeersch, P. M. (2023). *Radiocarbon Palaeolithic Europe Database, Version 30*. Available at: https://www.researchgate.net/project/Radiocarbon-Palaeolithic-Europe-Database

Verpoorte, A. (2002). Radiocarbon dating the Upper Palaeolithic of Slovakia: results, problems and prospects. *Archäologisches Korrespondenzblatt 32*, 2002, 311–325.

Verpoorte, A. (2004). Eastern Central Europe during the Pleniglacial. *Antiquity 300*, 2004, 257–267. https://doi.org/10.1017/S0003598X0011292X

Verpoorte, A., Cosgrove, R., Wood, R., Petchey, F., Lenoble, A., Chadelle, J.-P., Smith, C., Kamermans, H. & Roebroeks, W. (2019). Improving the chronological framework for Laugeri-Haute Ouest (Dordogne, France). *Journal of Archaeological Science 23*, 2019, 574–582. https://doi.org/10.1016/j.jasrep.2018.11.017

Vignard, E. & Vacher, G. (1965). Quinze années de fouilles dans les Gros Monts des Beauregards de Nemours (Seine-et-Marne). *Bulletin de la Société Préhistorique Française, Études et Travaux 62*, 1965, 84–97.

Vogel, J. C. & Waterbolk, H. T. (1967). Groningen radiocarbon dates VII. *Radiocarbon 9*, 1967, 107–155.

Vogelsang, R., John, R. & Ossendorf, G. (in prep.). A question of style? Chronological trends in facially retouched points from MIS 3 assemblages from Mochena Borago Rockshelter, Ethiopia.

Vukosavljević, N. & Karavanić, I. (2017). Epigravettian shouldered

points in the eastern Adriatic and its hinterland: reconsidering their chronological position. *Acta Archaeologica Carparthica 52*, 2017, 5–21.

Walker, R., Eriksson, A., Ruiz, C., Newton, T. H. & Casalegno, F. (2021). Stabilization of cultural innovations depends on population density: Testing an epidemiological model of cultural evolution against a global dataset of rock art sites and climate-based estimates of ancient population densities. *Plos One 16(3)*, 2021, 0247973. https://doi.org/10.1371/journal.pone.0247973

Weber M.-J. (2009). Fabrication and use of Hamburgian shouldered points: new data from Poggenwisch and Teltwisch 1 (Ahrensbourg Valley, Schleswig-Holstein, Germany). *P@lethnologie 1*, 2009, 98–132. https://doi.org/10.4000/palethnologie.9361

Weber, M.-J. (2012). *From technology to tradition – Re-evaluating the Hamburgian-Magdalenian relationship*. Untersuchungen und Materialien zur Steinzeit in Schleswig–Holstein und im Ostseeraum, vol. 5. (Neumünster 2012).

Weißmüller, W. (1995). *Sesselfelsgrotte II. Die Silexartefakte der Unteren Schichten der Sesselfelsgrotte. Ein Beitrag zum Problem des Moustérien.* (Forschungsprojekt „Das Paläolithikum und Mesolithikum des Unteren Altmühltals 11" Teil II). Quartär-Bibliothek 6 (Saarbrücken 1995).

Weiss, M. (2020). The Lichtenberg Keilmesser - it's all about the angle. *PLoS ONE 15(10)*, 2020, e0239718. https://doi.org/10.1371/journal.pone.0239718

Weiss, M., Lauer, T., Wimmer, R. & Pop, C. (2018). The variability of the Keilmesser-Concept: A case study from central Germany. *Journal of Paleolithic Archaeology 1(3)*, 2018, 202–246. https://doi.org/10.1007/s41982-018-0013-y

Weninger, B. (2022). CalPal Edition 2022.7 [software]. *Zenodo*. https://doi.org/10.5281/zenodo.7215742

White, L. A. (1949). *The Science of Culture: A Study of Man and Civilization* (New York 1945).

White, L. A. (1959). *The Evolution of Culture* (New York 1959).

Whitehead, H., Laland, K. N., Rendell, L., Thorogood, R. & Whiten, A. (2019). The reach of gene–culture coevolution in animals. *Nature Communications, 10*, 2019, 2405. https://doi.org/10.1038/s41467-019-10293-y

Whiten, A. (2017). A second inheritance system: the extension of biology through culture. *Royal Society Interface Focus 7(5)*, 217.

Whiten, A., Hinde, R. A., Laland, K. N. & Stringer, C. B. (2011). Culture evolves. *Philosophical Transactions of the Royal Society B 366(1567)*, 2011, 938–948. https://doi.org/10.1098/rstb.2010.0372

Wickens, T. (1995). *The Geometry of Multivariate Statistics* (Hillsdale 1995).

Willey, G. R. (1953). Archaeological Theories and Interpretation: New World. In: Kroeber, A. L. (ed.), *Anthropology Today* (Chicago 1953), 361–385.

Wilczyński, J., Wojtal, P. & Sobczyk, K. (2012). Spatial organization of the Gravettian mammoth hunters' site at Kraków Spadzista (southern Poland). *Journal of Archaeological Science 39*, 2012, 3627–3642.

Wilczyński, J., Goslar, T., Wojtal, P., Oliva, M., Göhlich, U. B., Antl-Weiser, W., Šída, P., Verpoorte, A. & Lengyel, G. (2020). New radiocarbon dates for the late Gravettian in eastern central Europe. *Radiocarbon 62(1)*, 2020, 243–259. https://doi.org/10.1017/RDC.2019.111

Wojtal, P. & Sobczyk, K. (2005). Man and woolly mammoth at the Kraków Spadzista Street (B) taphonomy of the site. *Journal of Archaeological Science 32*, 2005, 193–206. https://doi.org/10.1016/j.jas.2004.08.005

Wojtal, P., Haynes, G., Klimowicz, J., Sobczyk, K., Tarasiuk, J., Wroński, S., Wilczyński, J. (2019). The earliest direct evidence of mammoth hunting in Central Europe – the Kraków Spadzista site (Poland). *Quaternary Science Review 213*, 2019, 162–166. https://doi.org/10.1016/j.quascirev.2019.04.004

Zaverniaev, F. M. (1991). Kremnëvyi inventar' Khotylëvskoi verkhnepaleoliticheskoi stoianki. *Sovetskaia Arkheologiia 4*, 1991, 164–181. (in Russian)

Zheltova, M. N. (2008). Kostënkovskie stoianki pervoi nadpoimennoi terrasy: varianty adaptatsii k okruzhaiushchei srede verkhnego Pleistotsena. In: Khlopachëv, G. A. (ed.), *Problemy biologicheskoi I kul'turnoi adaptatsii chelovecheskikh populiatsii. Tom 1: Arkheologiia: Adaptatsionnye strategii drevnego naseleniia Severnoi Evrazii: syr'ë i priëmy obrabotki* (Saint Petersburg 2008), 48–52.

Zheltova, M. N. & Zaretskaya, N. E. (2018). Novyye dannyye po khronostratigrafii Kostenok 1, sloi I. *Zapiski IIMK RAN 17*, 2018, 37–44. In Russian.

Zilhão, J. O. (1997). *Paleolítico Superior da Estremadura portuguesa* (Lisbon 1997).

Zilhão, J. O., Maurício, J. & Souto, P. (1991). A Arqueologia da Gruta do Almonada (Torres Novas). Resultados das Escavaçóes de 1988–89. In: Associação dos Arqueólogos Portugueses (ed.), *Actas das IV Jornadas Arqueológicas* (Lisboa 1991).

Zilhão, J. O., Angelucci, D. E., Arnold, L. J., d'Errico, F., Dayet, L., Demuro, M., Deschamps, M., Fewlass, H., Gomes, L., Linscott, B., Matias, E., Pike, A. W. G., Steier, P., Talamo, S. & Wild, E. M. (2021) Revisiting the Middle and Upper Palaeolithic archaeology of Gruta do Caldeirão (Tomar, Portugal). *PLoS ONE 16(10)*, 2021, e0259089. https://doi.org/10.1371/journal.pone.0259089

Zimmermann, W. (1937). Arbeitsweise der botanischen Phylogenetik und anderer Gruppierungswissenschaften. Abt. IX, Teil 3. In: Abderhalden, E. (ed.), *Handbuch der biologischen Arbeitsmethoden* (Berlin 1937).

Zimmermann, A. (1998). Neolithische Steinartefakte – ihre Merkmale und Aussagemöglichkeiten. In: Preuß, J. (ed.), *Das Neolithikum in Mitteleuropa 1/1. Teil A.* (Weissbach 1998), 137–158.

Zuberbühler Koch, K. (2002). Die magdalénienzeitliche Höhlenstation Winznau/Käsloch im Kanton Solothurn. *Archäologie und Denkmalpflege im Kanton Solothurn 7*, 2002, 7–49.

Züchner, A. (1969). Die spätjungpaläolithische Freilandstation Winznau-Köpfli. *Jahrbuch für Solothurnische Geschichte 42*, 1969, 138–201.

# PLATES

Stoneartefacts sorted alphabetically, scale = 1:1, reference object = 1x1 cm
completed areas of incomplete artefacts are indicated by black filling

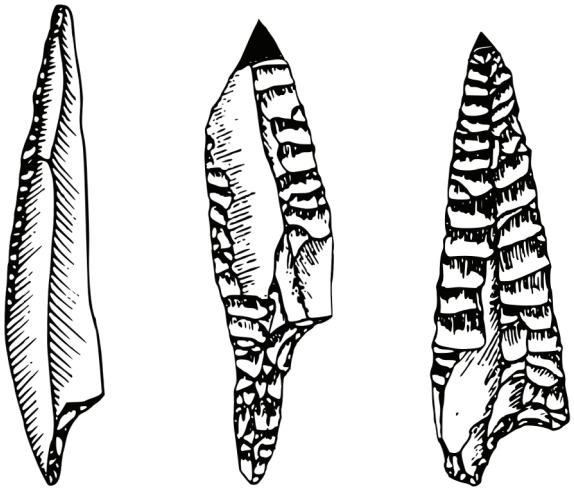


Plate 1: Abauntz
modified after Utrilla & Mazo 1994

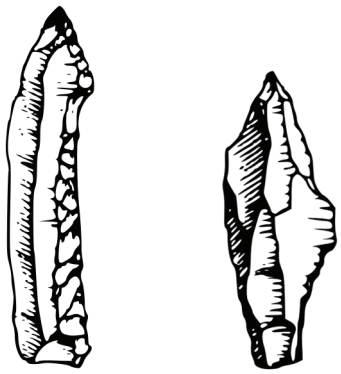


Plate 2: Abri de Fontalès
modified after Darasse & Guffroy 1960



Plate 3: Abri du Bois des Brousses, layer 3
modified after Bazile 2011

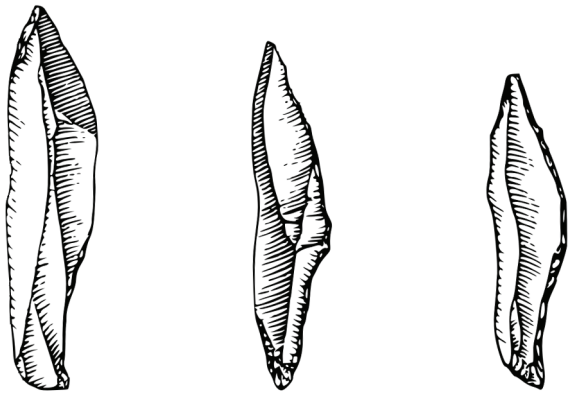


Plate 4: Abri du Rouet, layer 9b
modified after Brochier & Livache 2003

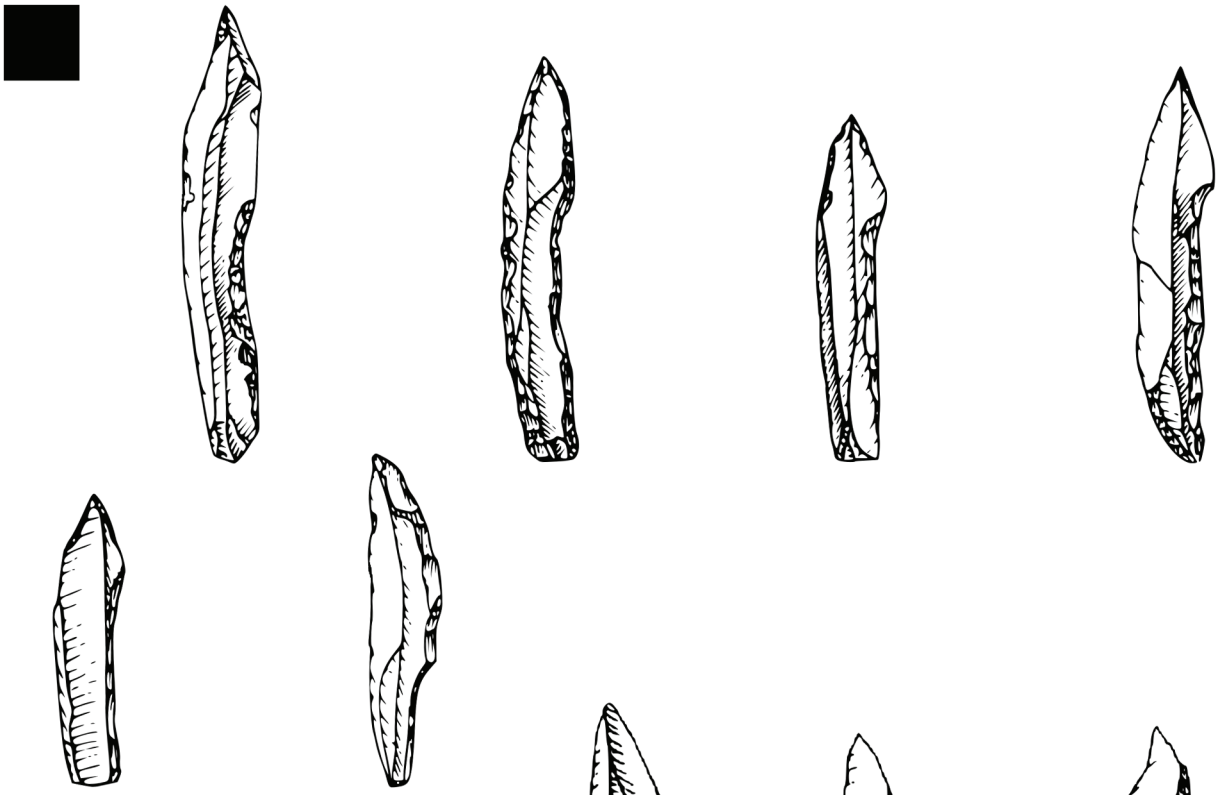


Plate 5: Abri Faustin, layer 1
modified after Lenoir & Terraza 1971

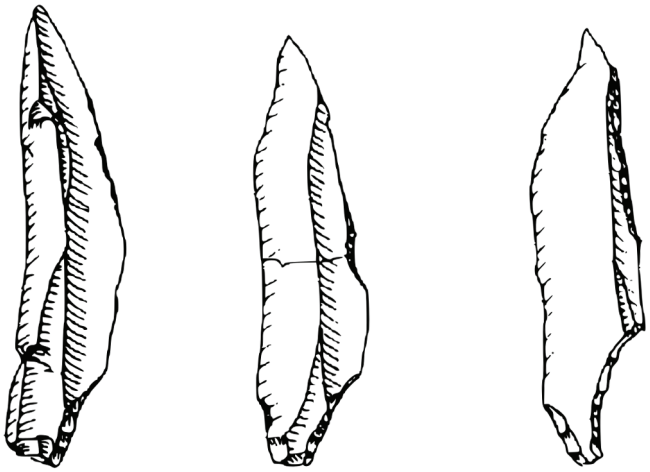


Plate 6: Abri Gandil, layer 20
modified after Ladier 2000

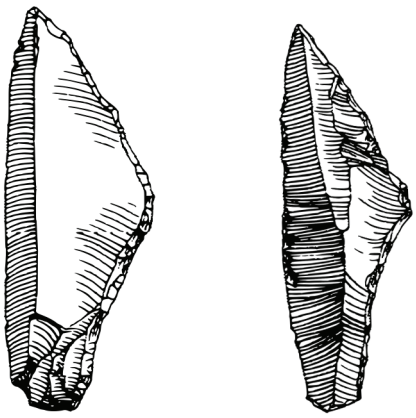


Plate 7: Abri Schweizersbild
modified after Höneisen & Peyer 1994



Plate 8: Ahrenshöft LA 73
modified after Clausen 1998

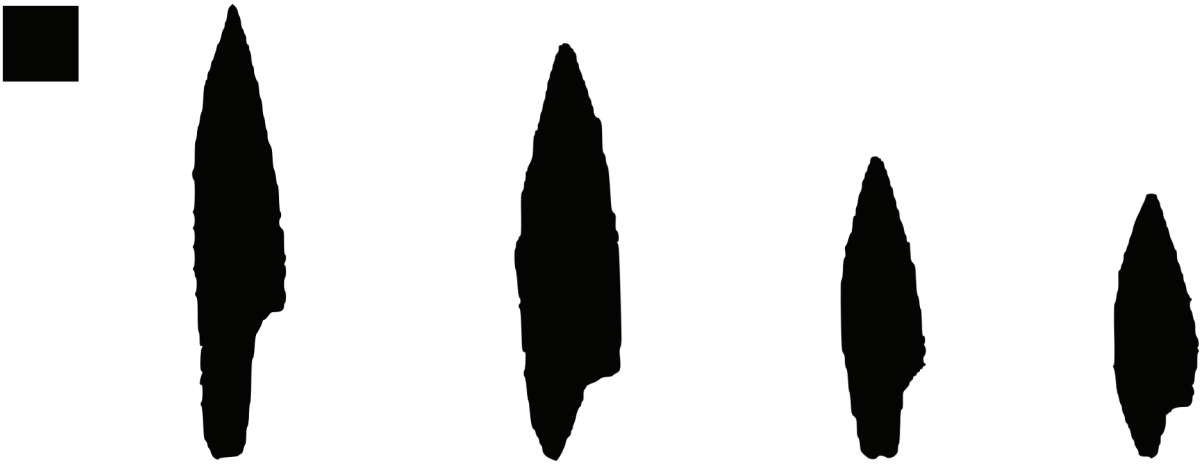


Plate 9: Aitzbarte IV
modified after images courtesy of I. Schmidt and G. Koert

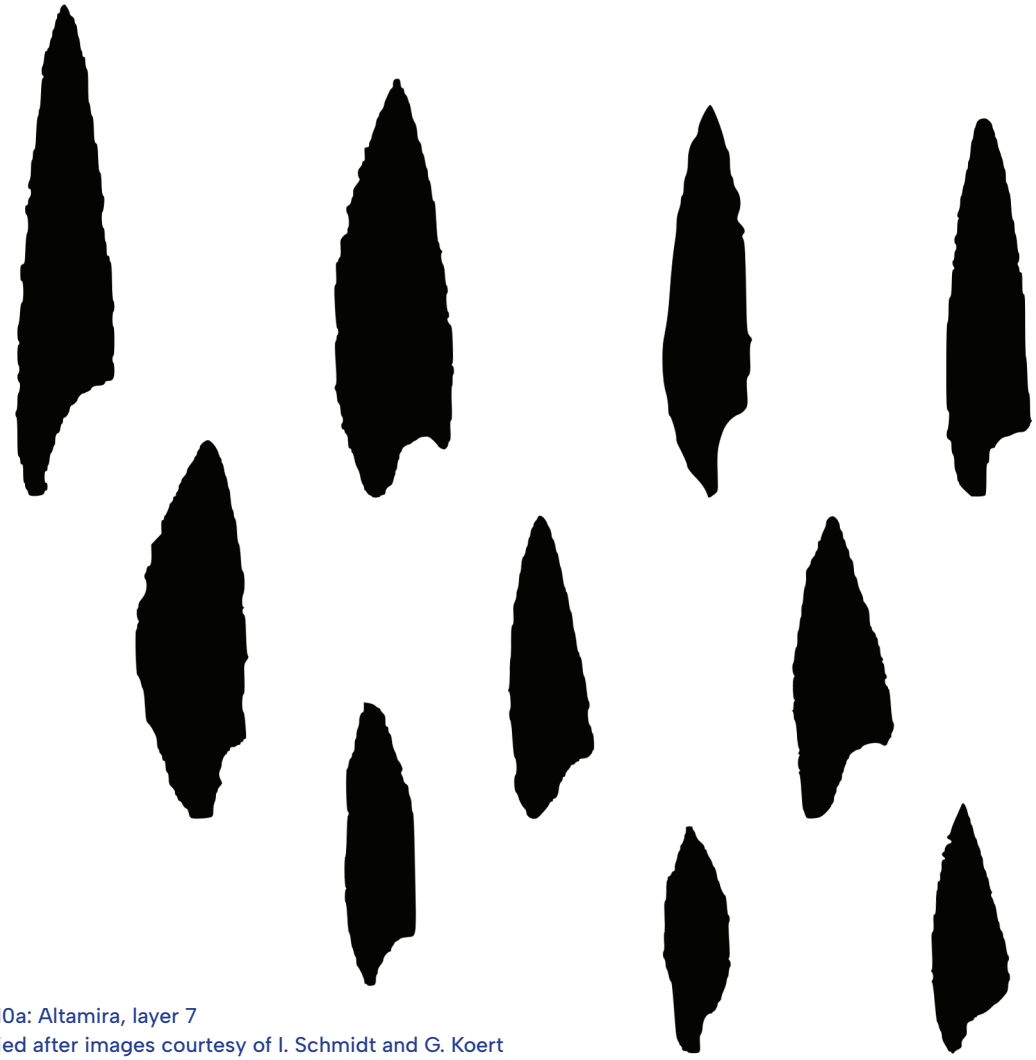


Plate 10a: Altamira, layer 7
modified after images courtesy of I. Schmidt and G. Koert

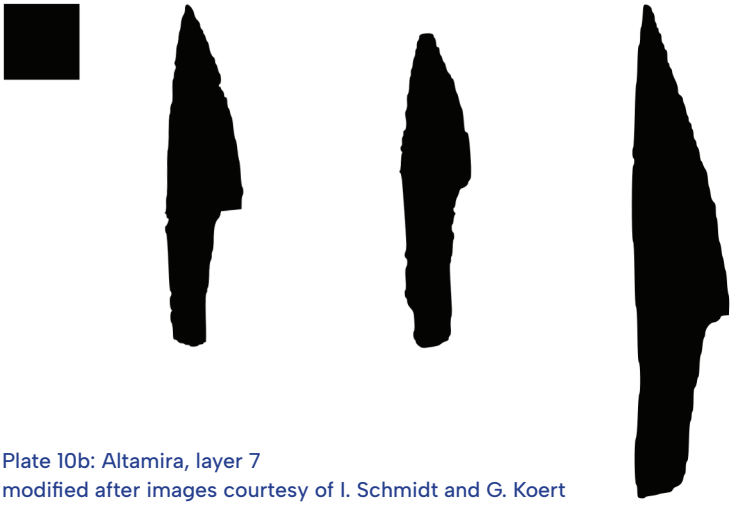


Plate 10b: Altamira, layer 7
modified after images courtesy of I. Schmidt and G. Koert

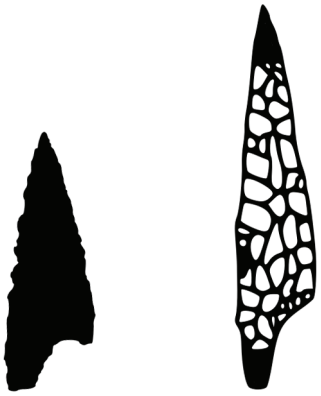


Plate 11: Amalda
modified after images courtesy of I. Schmidt and G. Koert

Plate 12: Atxuri
modified after Straus 1983

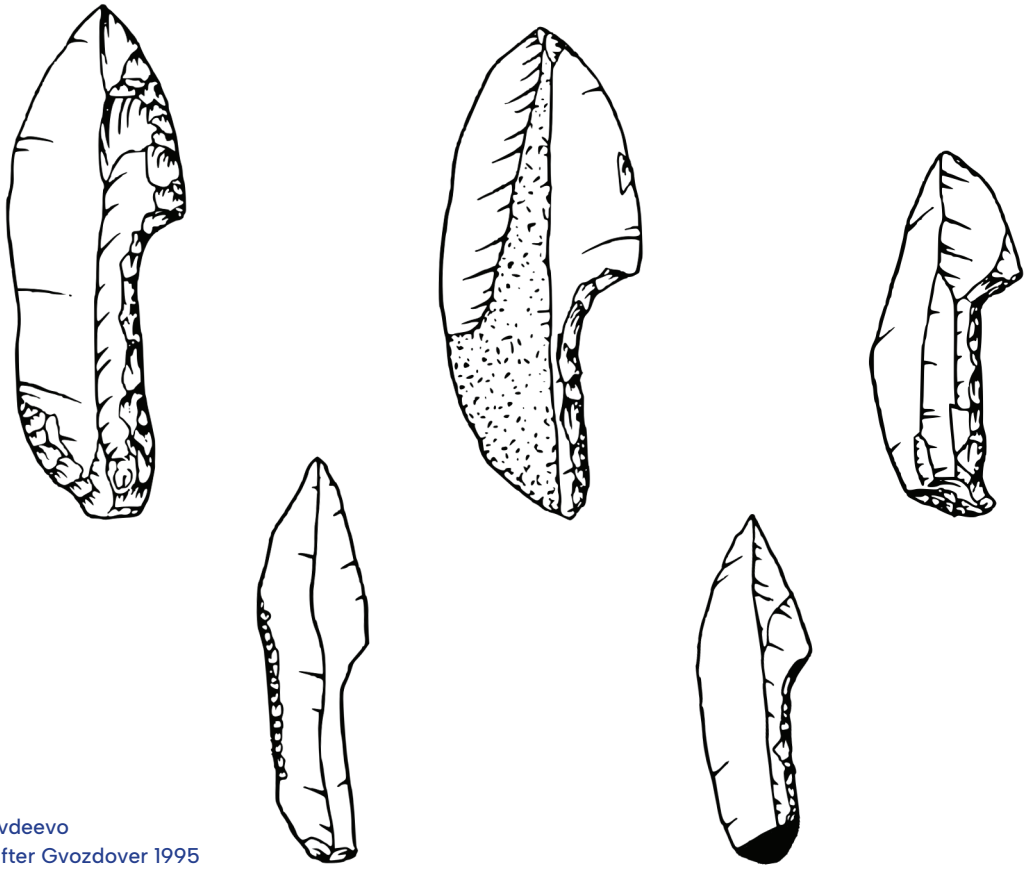


Plate 13: Avdeevo
modified after Gvozdover 1995

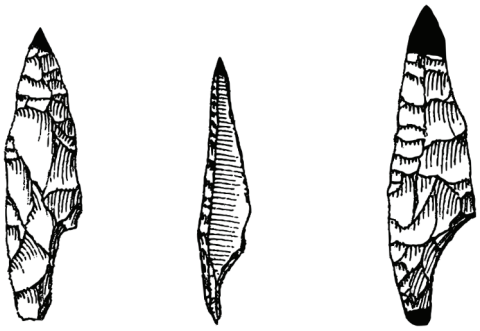


Plate 14: Baío
modified after Zilhão 1997



Plate 15: Banka–Horné farské role
modified after Alexandrowicz et al. 2000



Plate 16: Baume de Colle Rousse
modified after Combier 2003

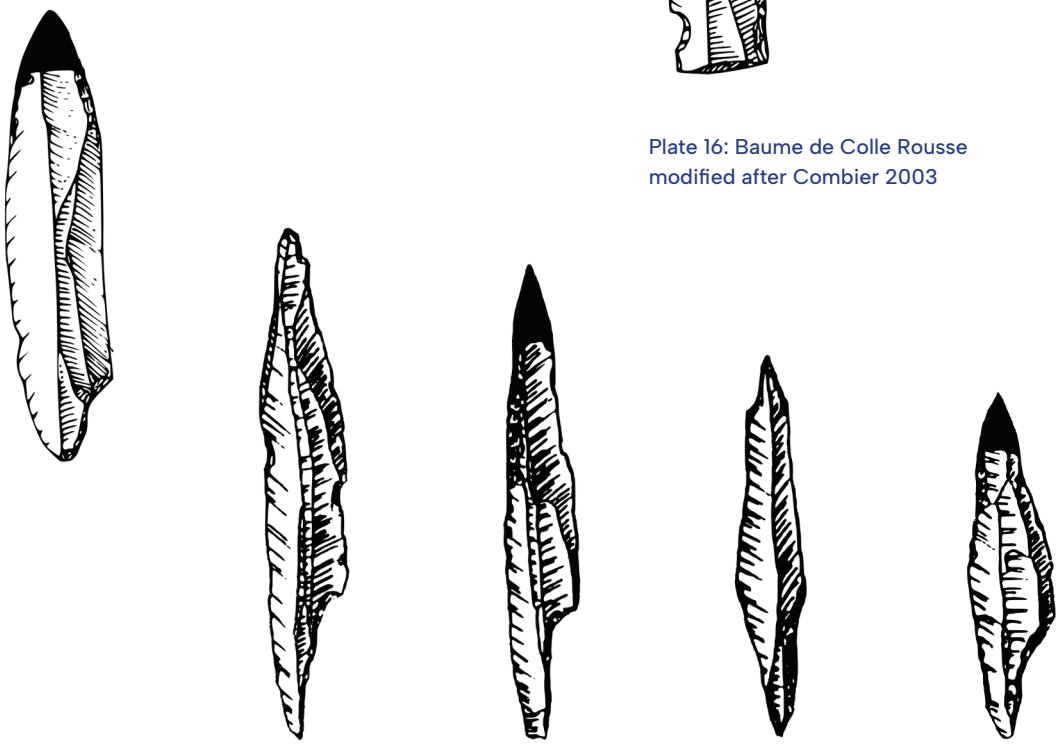


Plate 17: Baume d´Oullins, layer D
modified after Bazile 1990 and Boccacio 2005

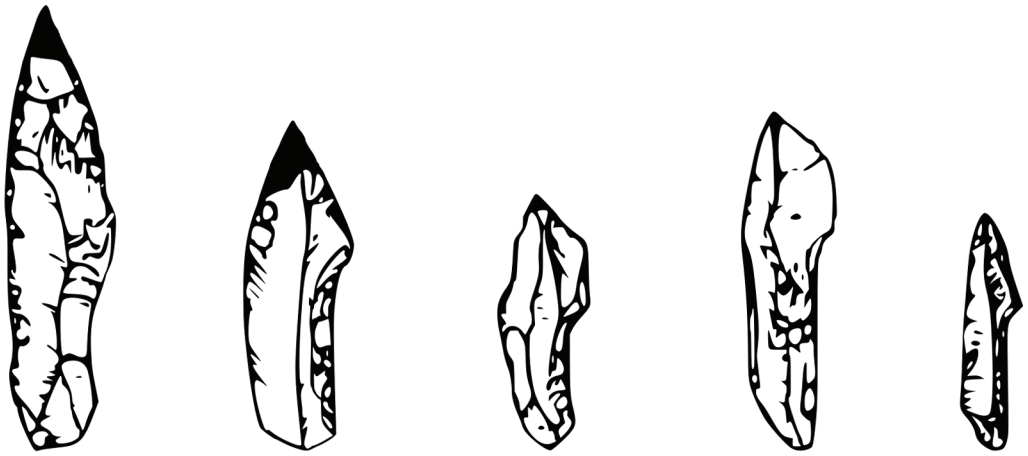


Plate 18: Berdyzh
modified after Kaletchitz 1984

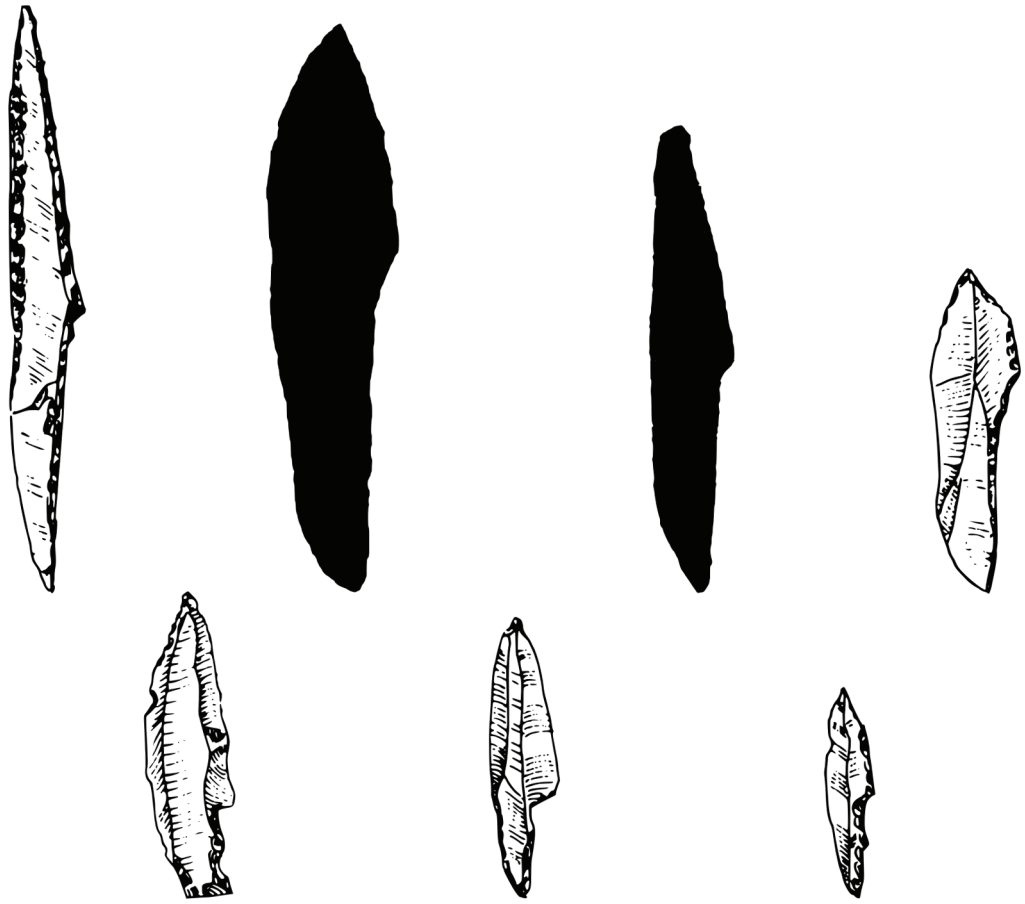


Plate 19: Bistricioara–Lutărie III AH 2.5
modified after Niţă et al. 2021 and images kindly prov. by Anghelinu & Niţă



Plate 20: Blazi Cave, Trench 5, layer 4
modified after Hauck et al. 2017

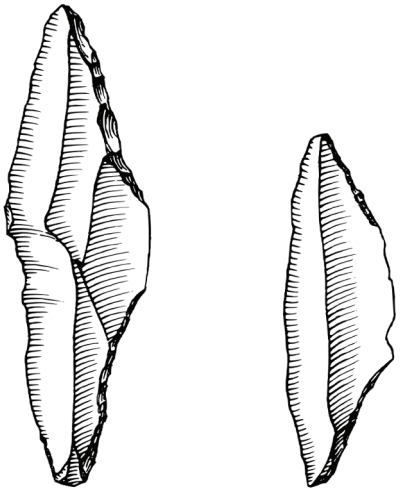


Plate 21: Bois Ragot, layer 5
modified after Chollet & Dujardin 2005

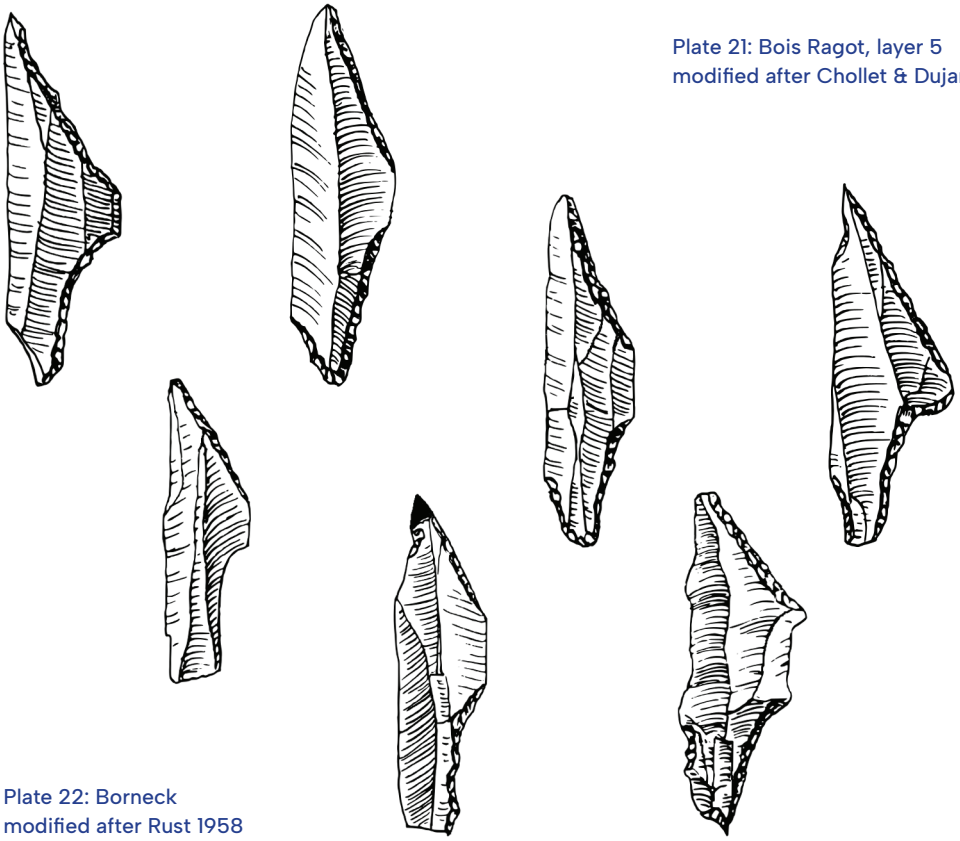


Plate 22: Borneck
modified after Rust 1958



Plate 23: Borshevo 1
modified after Nuzhnyi 2015



Plate 24: Brassempouy
modified after Smith 1966

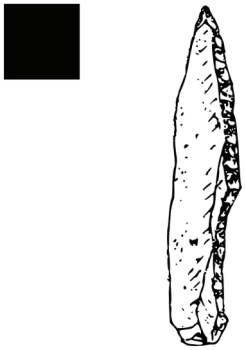


Plate 25: Buda, layer 1
modified after Bitiri-Ciortescu et al. 1989

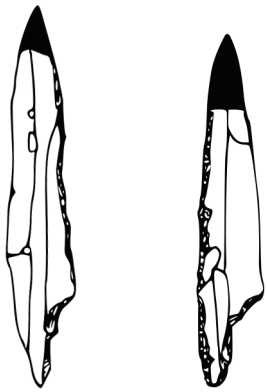


Plate 26: Cadenet
modified after Boccaccio 2005

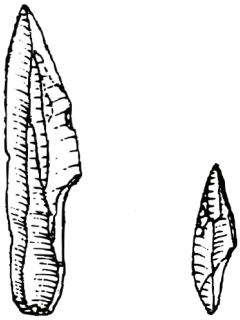


Plate 27: Cenciano Diruto, layer IV–I
modified after Pennacchioni & Tozzi 1984

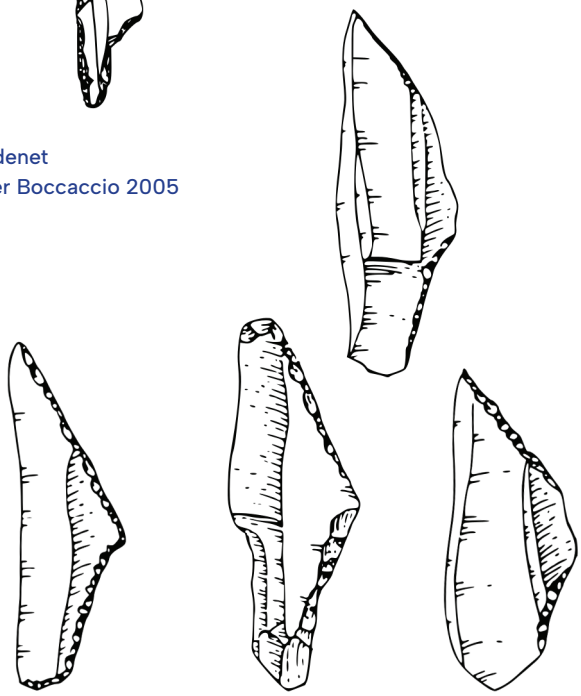


Plate 28: Cepoy/La Pierre aux Fées
modified after Allain 1974

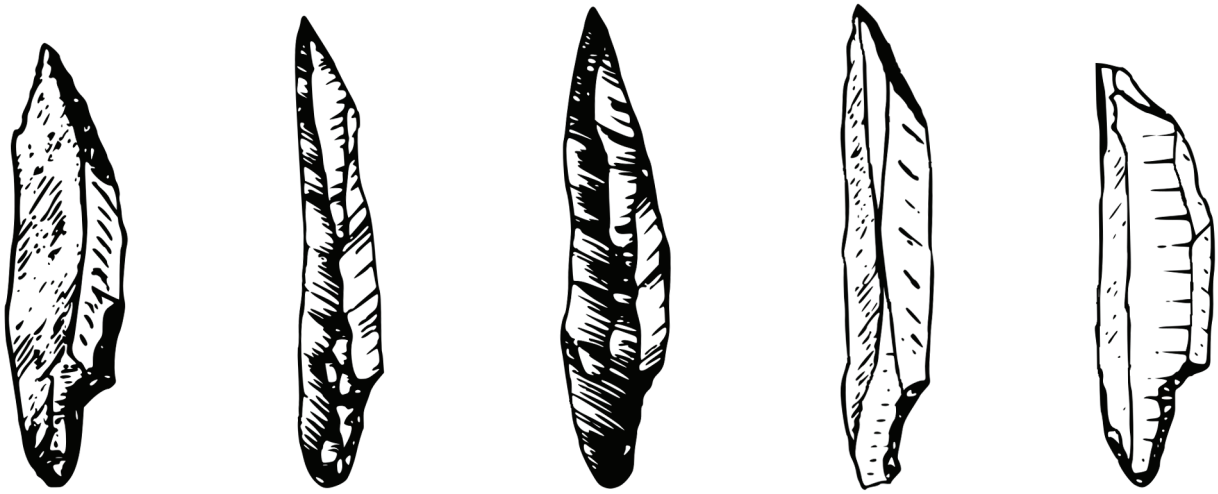


Plate 29: Chinchon 1, layer C
modified after Paccard 1964 and Paccard & Dumas 1977



Plate 30: Colombier
modified after Combier 2003

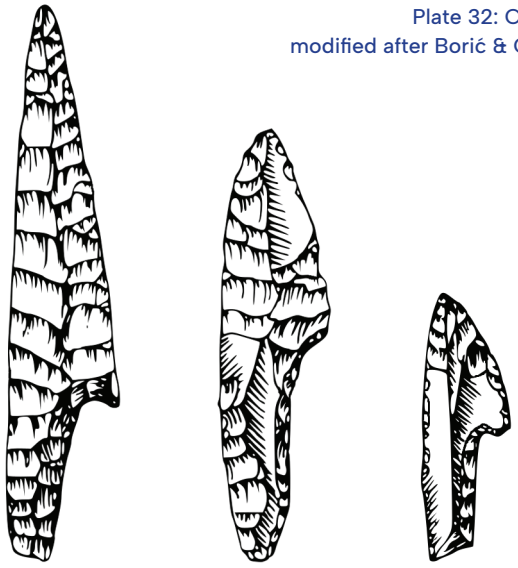


Plate 31: Combe-Saunière, layer IV
modified after Geneste & Plisson 1986



Plate 32: Crvena Stijena
modified after Borić & Cristiani 2016

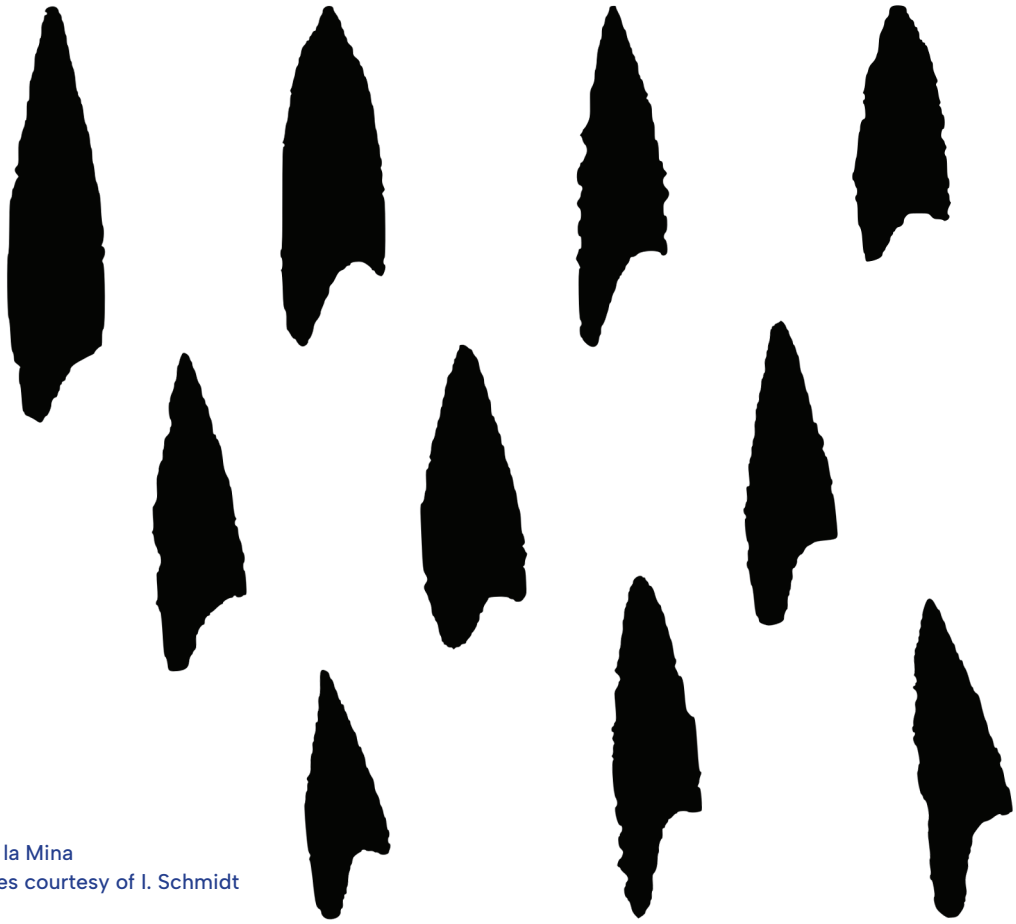


Plate 33a: Cueto de la Mina
modified after images courtesy of I. Schmidt
and G. Koert



Plate 33b: Cueto de la Mina
modified after images courtesy of I. Schmidt and G. Koert

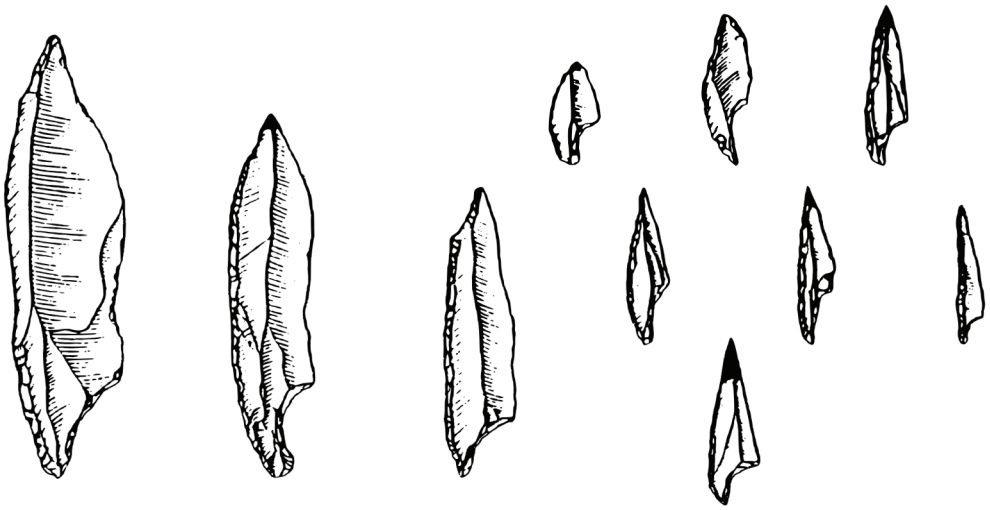


Plate 34: Cueva de Ambrosio, layer II
modified after Ripoll Lopez & Cacho Ouesada 1990

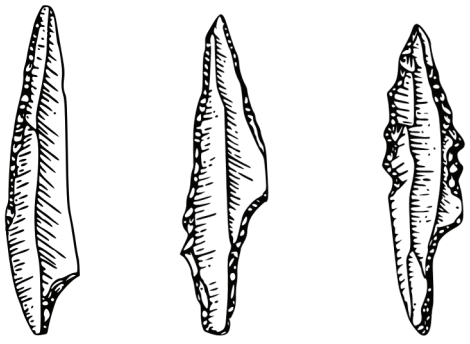


Plate 35: Cueva de Chaves
modified after Utrilla & Mazo 1994



Plate 36: Cueva de la Meaza
Image courtesy of I. Schmidt and G. Koert



Plate 37: Cueva de la Riera, layer 4
modified after Straus & Clark 1986

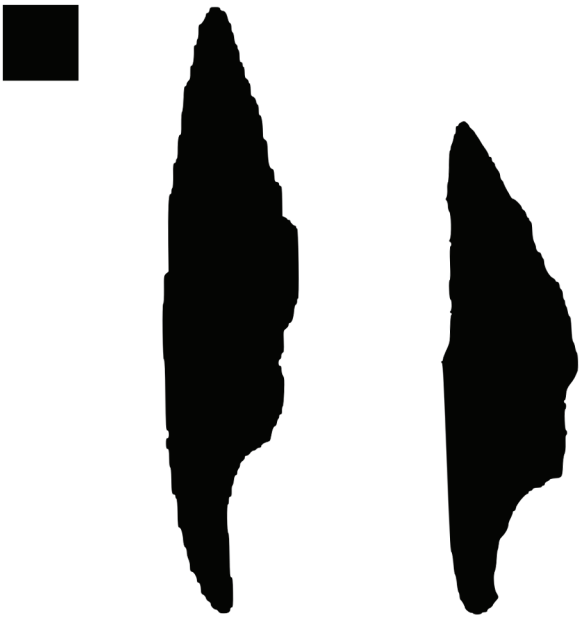


Plate 38: Cueva del Boquete Zafarraya
modified after images courtesy of I. Schmidt and G. Koert



Plate 39: Cueva de les Mallaetes, layer III
modified after Fortea Pérez & Jordá Cerda 1976



Plate 40: Cueva del Moro Chufin
modified after images courtesy of I. Schmidt and G. Koert

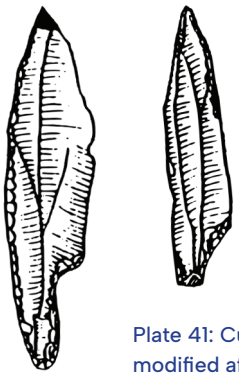
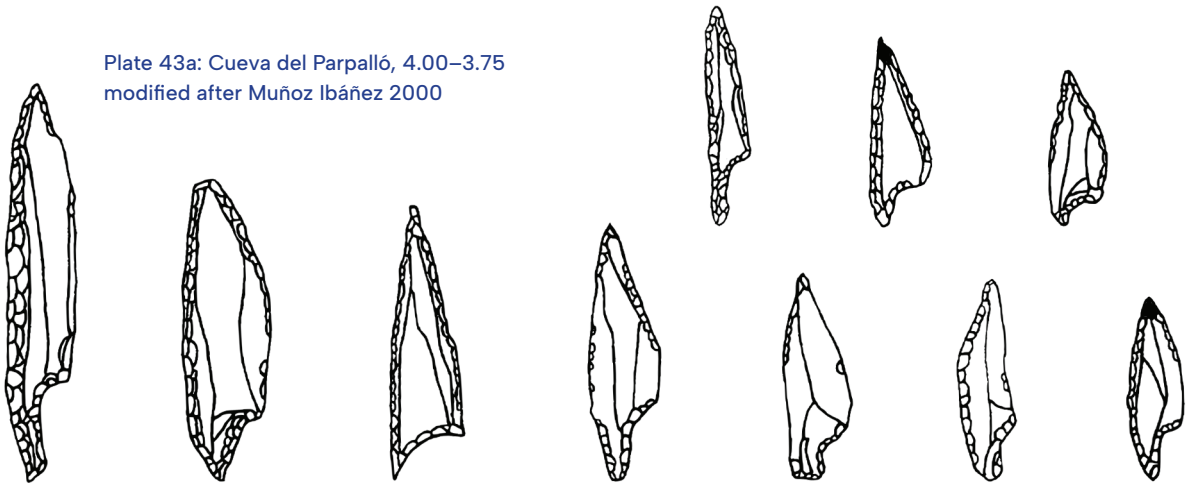


Plate 41: Cueva de los Morceguillos
modified after Ripoll Lopez & Cacho Ouesada 1990



Plate 42: Cueva del Pantano de Cubillas
modified after Ripoll Lopez & Cacho Ouesada 1990

Plate 43a: Cueva del Parpalló, 4.00–3.75
modified after Muñoz Ibáñez 2000



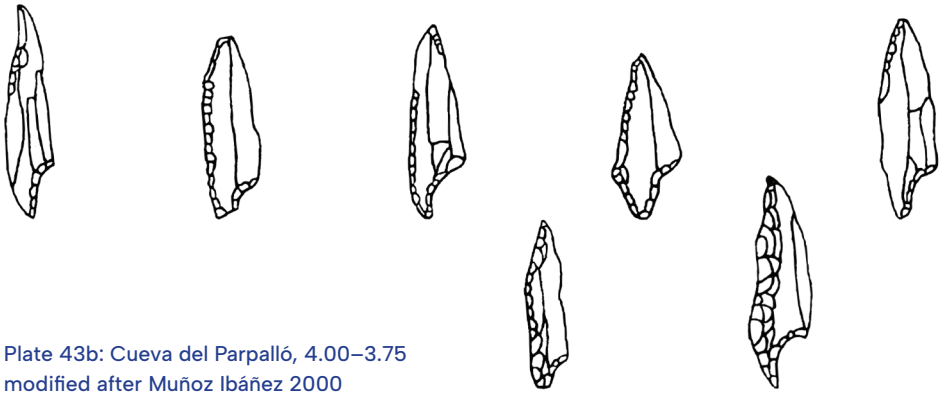


Plate 43b: Cueva del Parpalló, 4.00–3.75
modified after Muñoz Ibáñez 2000

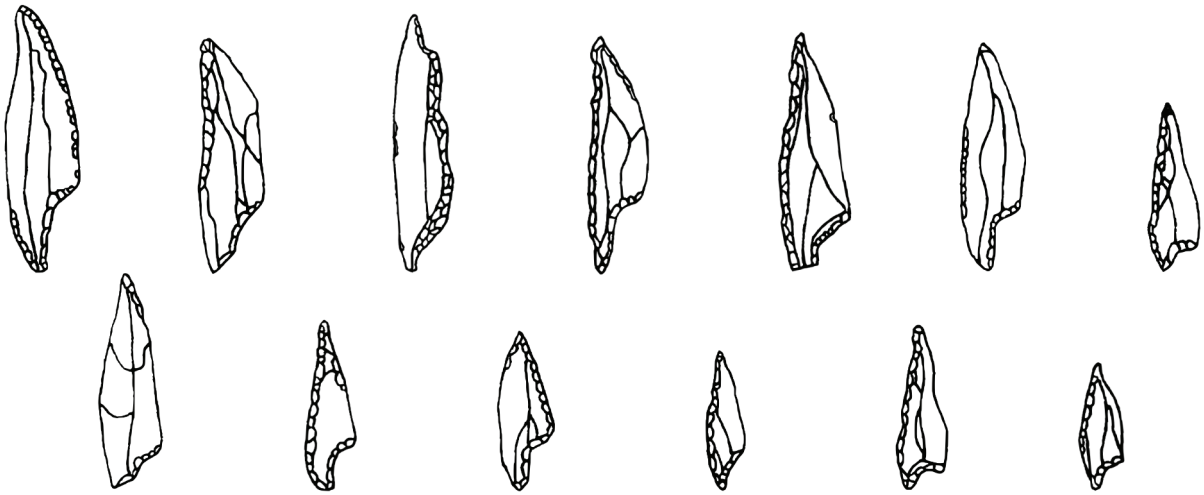


Plate 44: Cueva del Parpalló, 4.25–4.00
modified after Muñoz Ibáñez 2000

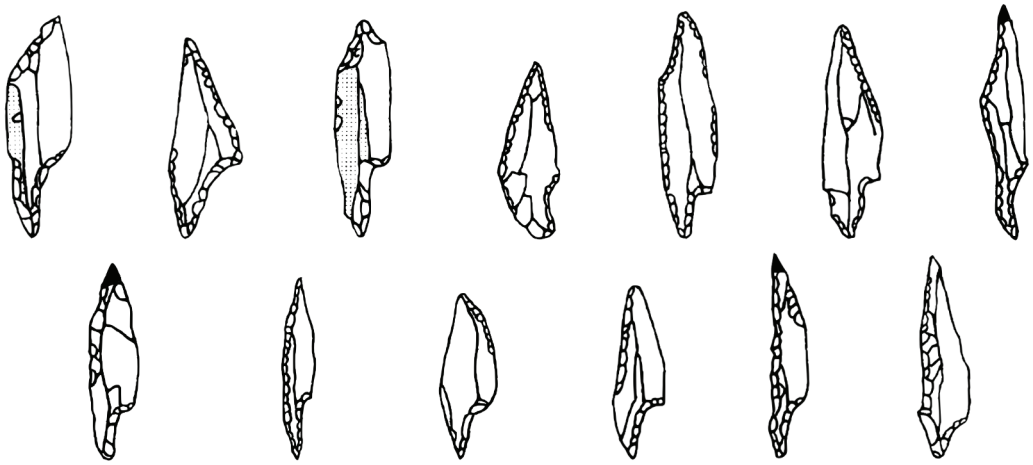


Plate 45a: Cueva del Parpalló, 4.50–4.25
modified after Muñoz Ibáñez 2000

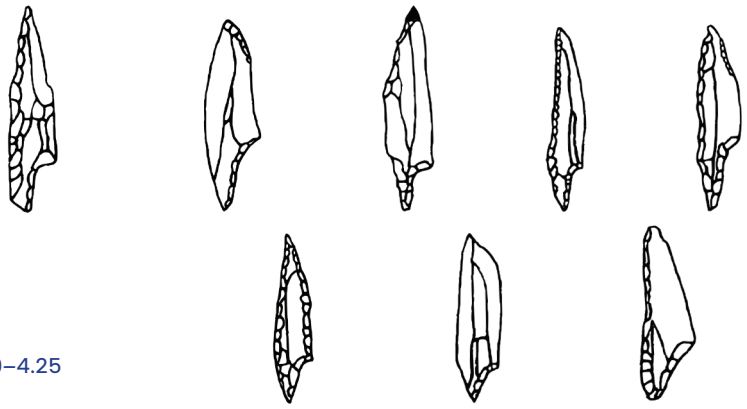


Plate 45b: Cueva del Parpalló, 4.50–4.25
modified after Muñoz Ibáñez 2000



Plate 46: Cueva del Reclau Viver
modified after images courtesy of I. Schmidt and G. Koert



Plate 47: Cueva Morín, layer 5a
modified after images courtesy of I. Schmidt and G. Koert



Plate 48: Davant Pau
modified after images courtesy of I. Schmidt and G. Koert

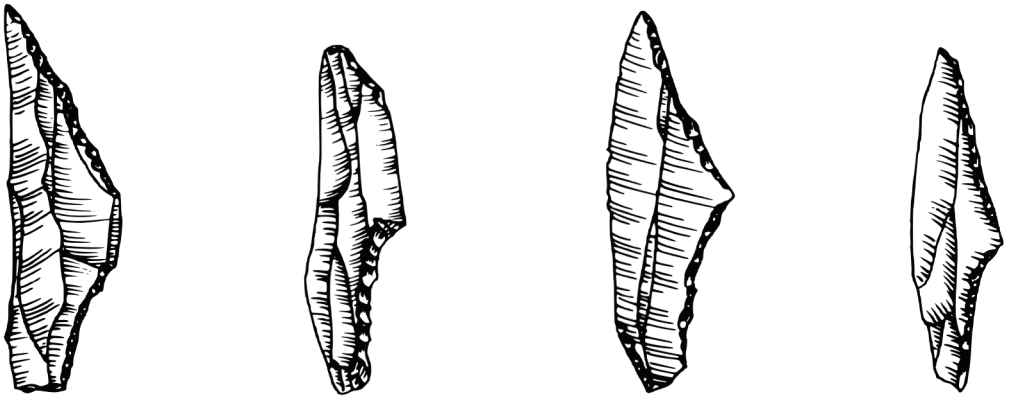


Plate 49a: Deimern 42
modified after Tromnau 1975a

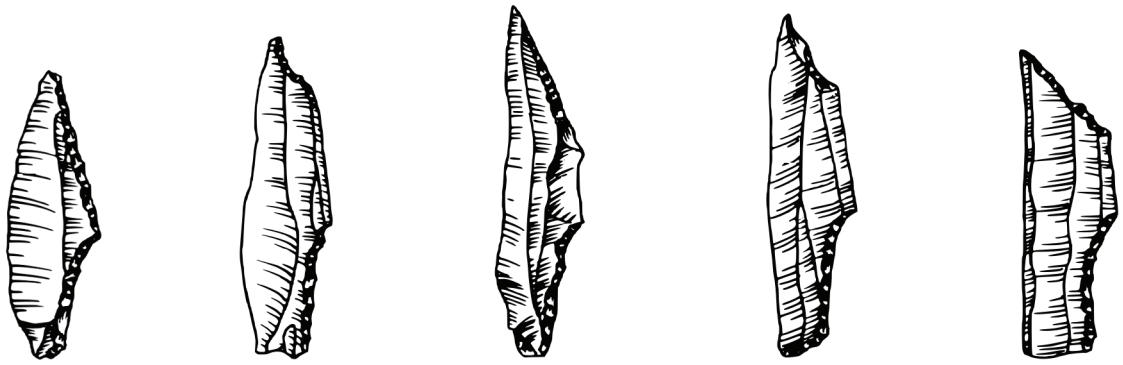


Plate 49b: Deimern 42 – modified after Tromnau 1975a



Plate 50: Deux-Avens, layer C
modified after Combier 2003

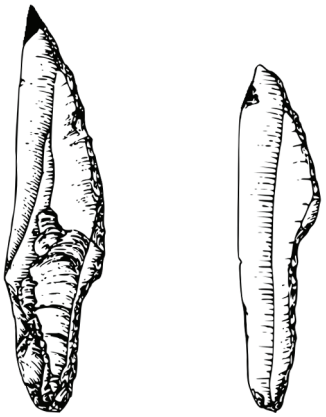


Plate 51: Dorotchivtsy III, layer 6
modified after Kulakovska et al. 2014

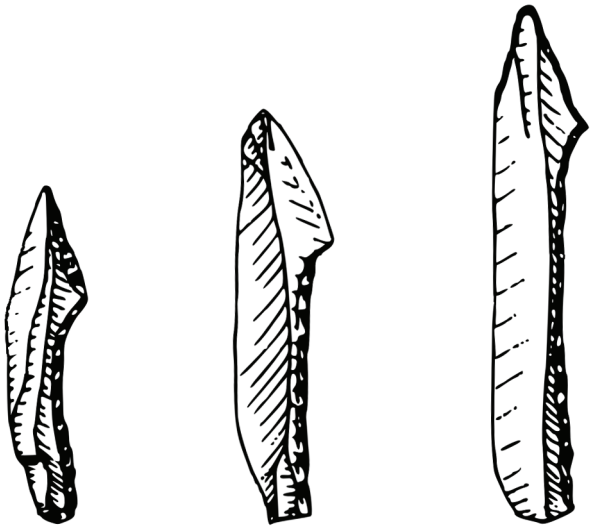


Plate 52: Duruthy, layer 3
modified after Arambourou et al. 1978



Plate 53: El Mirón
modified after Straus & Gonzáles Morales 2009

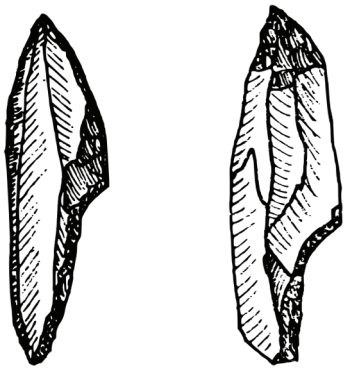
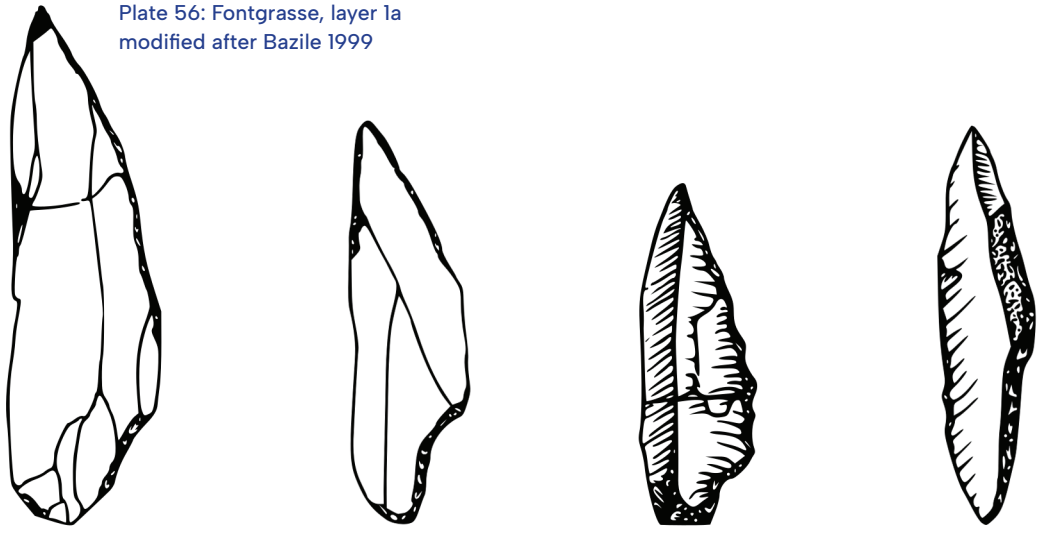


Plate 54: El Pendo
modified after Corchon 1971



Plate 55: Fondo Focone Trench B
modified after Cancellieri 2018

Plate 56: Fontgrasse, layer 1a
modified after Bazile 1999



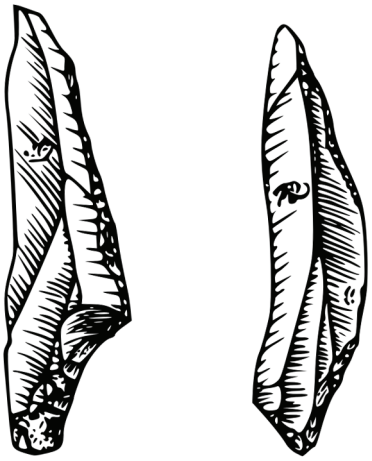


Plate 57: Fontgrasse, layer 3
modified after Bazile 1999

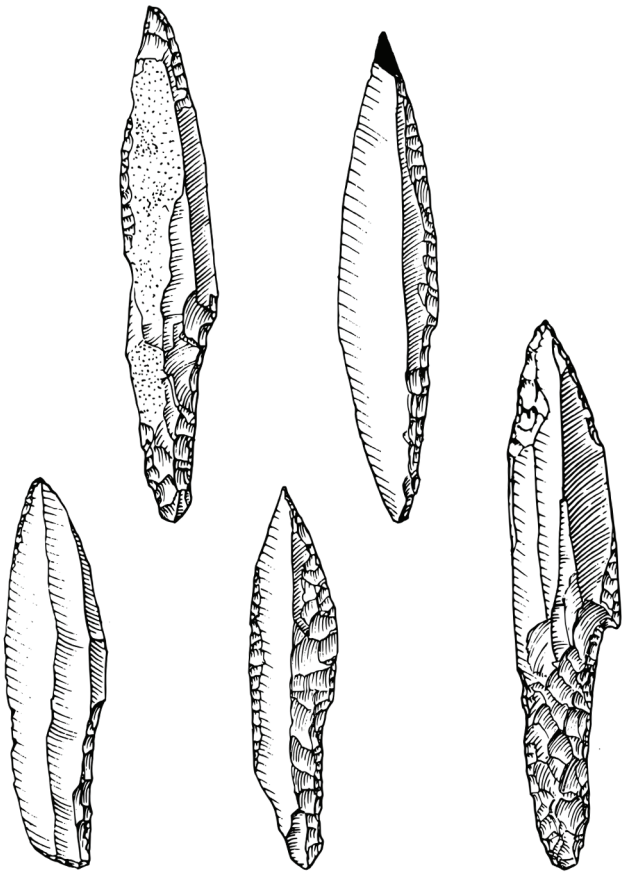


Plate 58: Fourneau du Diable, Solutreén superior I
modified after Smith 1966

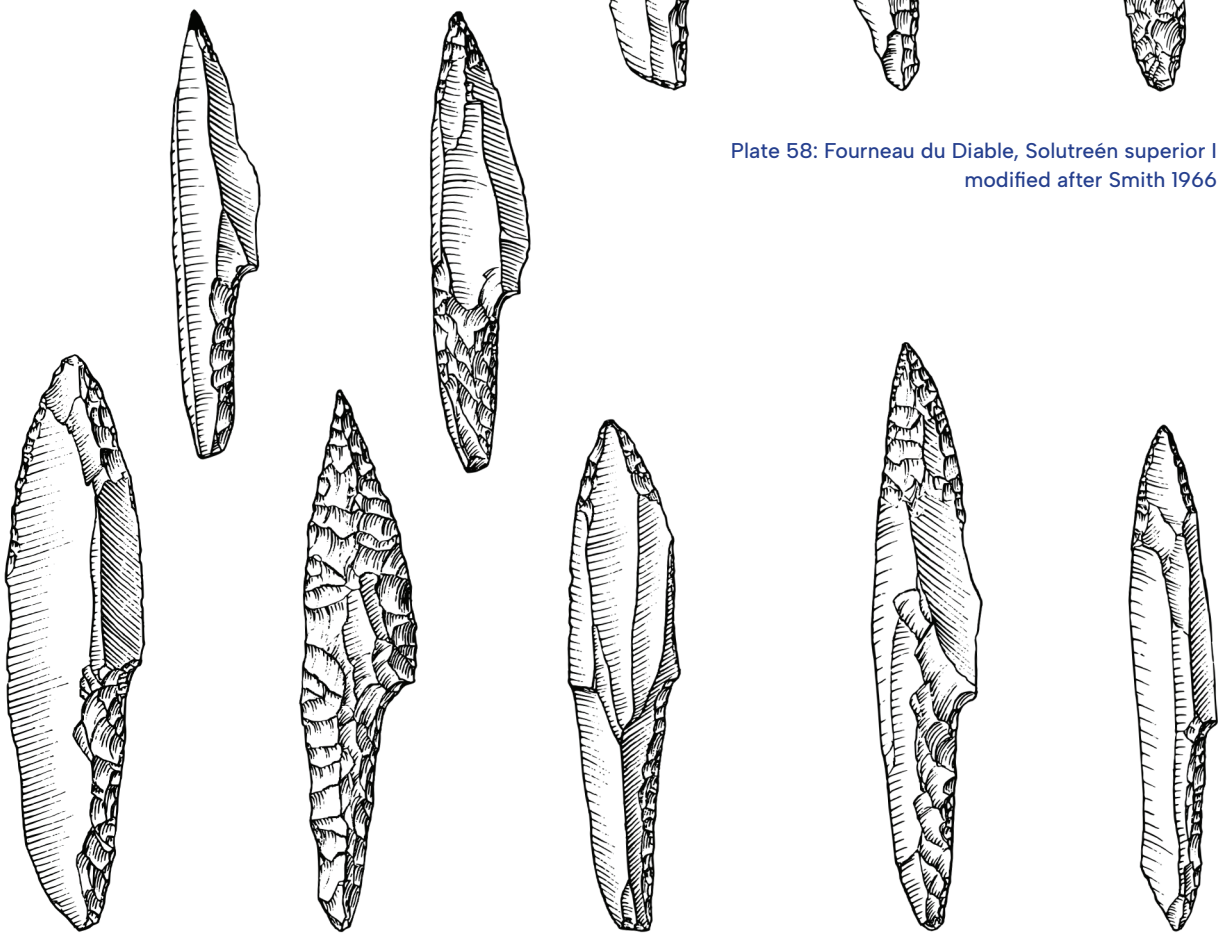


Plate 59a: Fourneau du Diable, Solutreén superior II – modified after Smith 1966

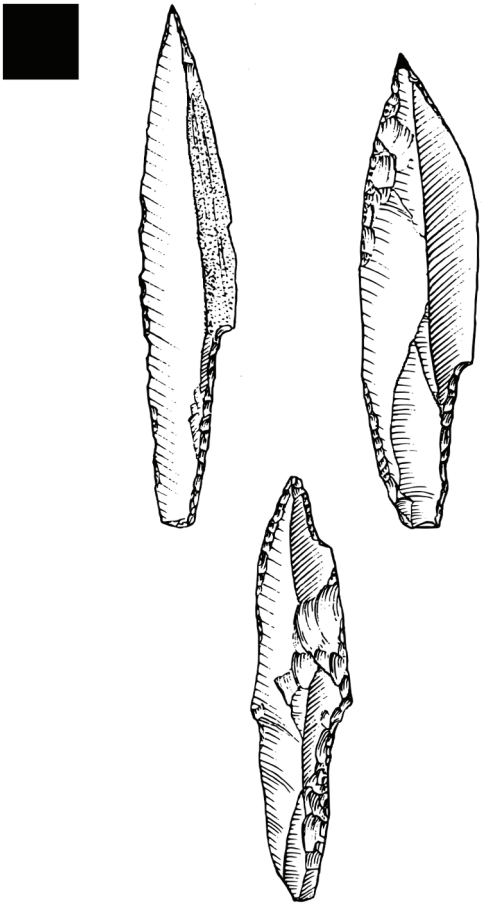


Plate 59b: Fourneau du Diable, Solutreén superior II
modified after Smith 1966

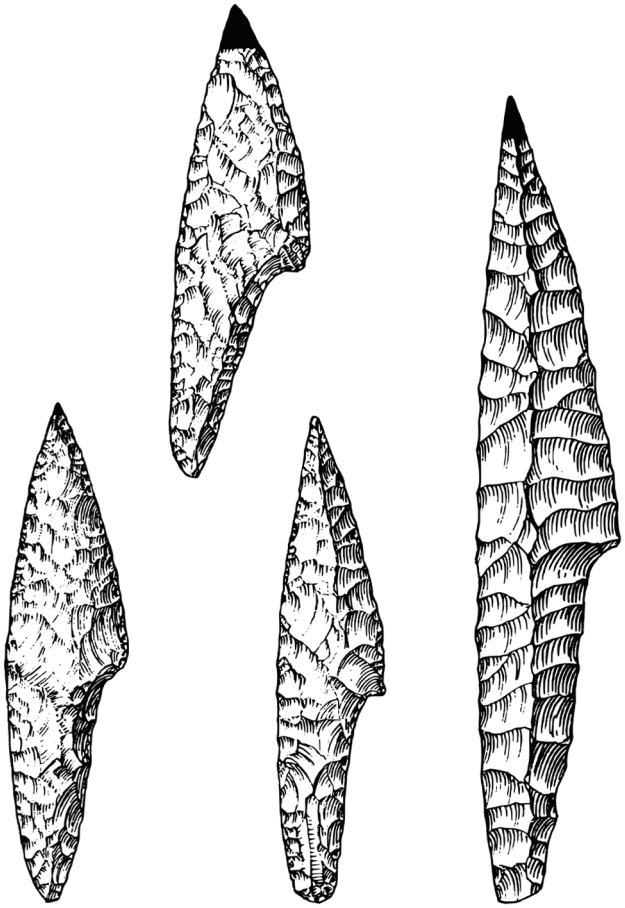


Plate 60a: Fourneau du Diable, Solutreén superior III
modified after Smith 1966

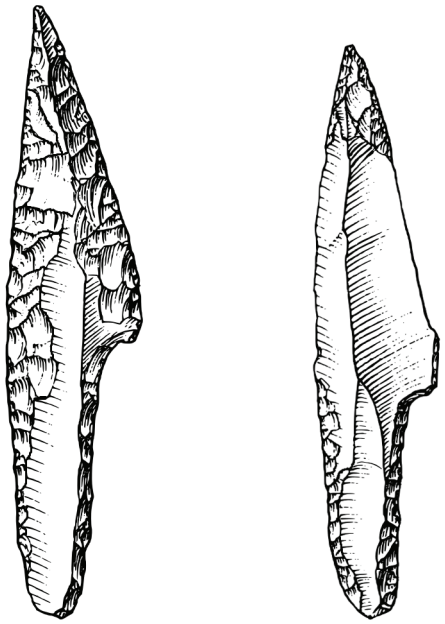


Plate 60b: Fourneau du Diable, Solutreén superior III
modified after Smith 1966

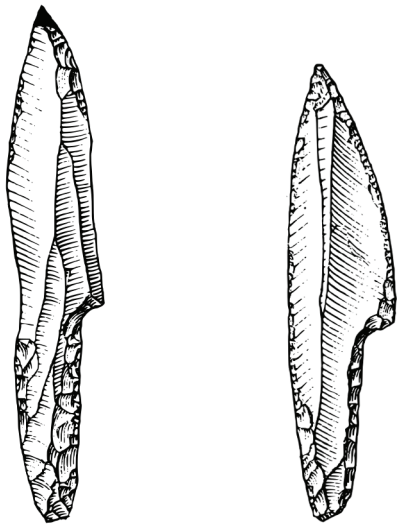




Plate 60c: Fourneau du Diable, Solutreén superior III
modified after Smith 1966

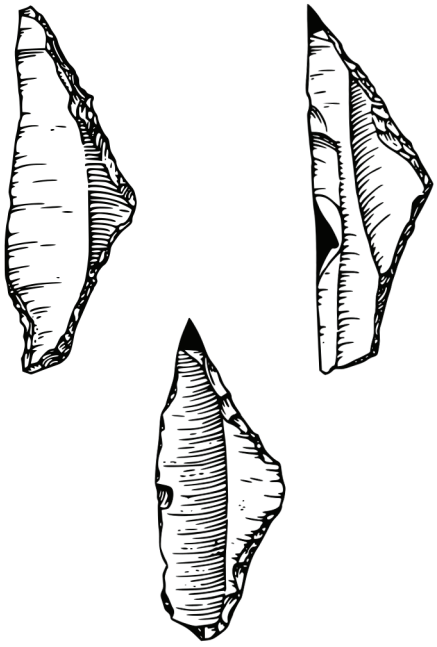


Plate 62: Fußgönheim II
modified after Stodiek 1987

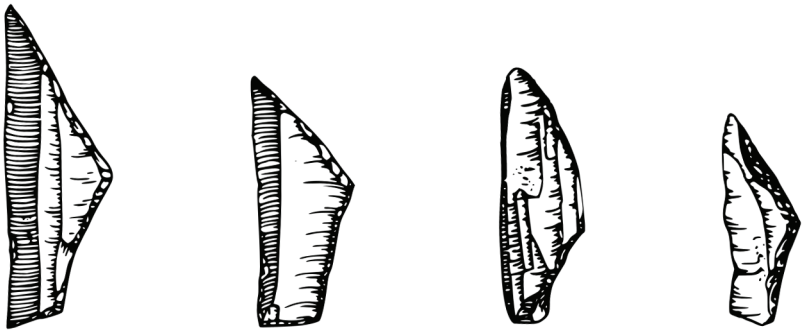


Plate 61: Fußgönheim I
modified after Stodiek 1987

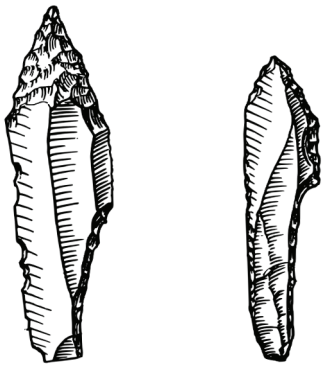


Plate 64: Gavechou
modified after Smith 1966

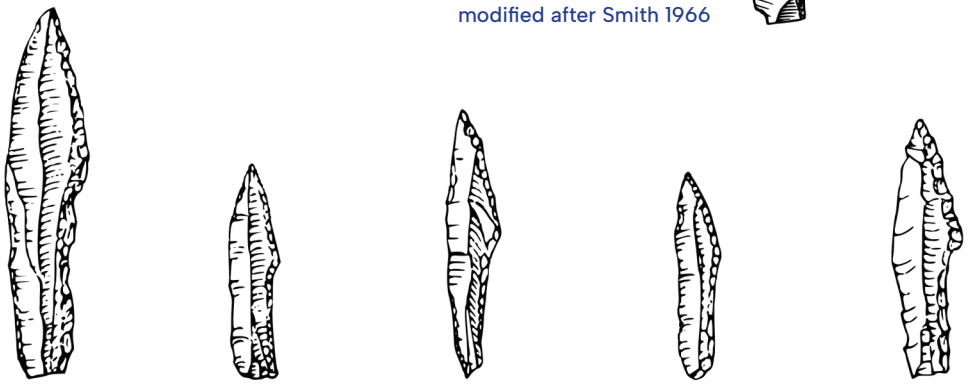


Plate 63: Gagarino
modified after Tarasov 1979

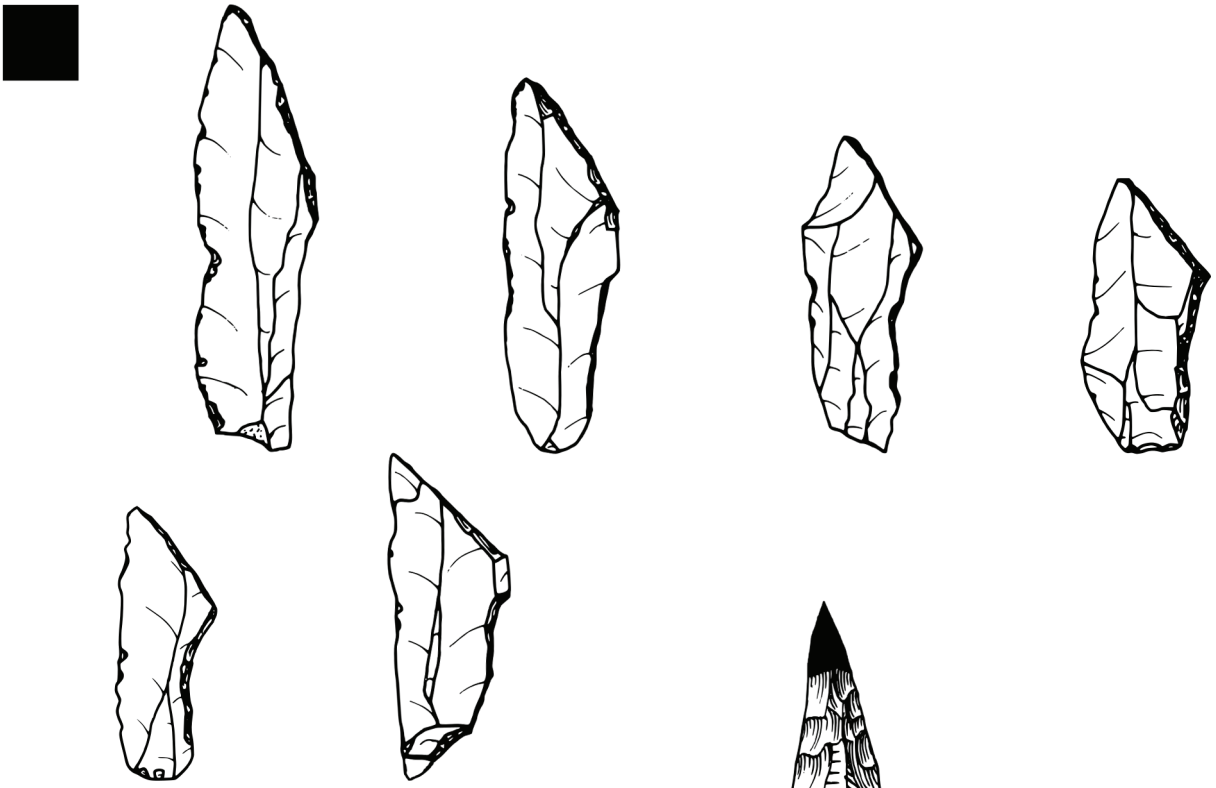


Plate 65: Gough's Cave, layer B
modified after Campbell 1977



Plate 66: Grand Abri de Mazerat
modified after Smith 1966

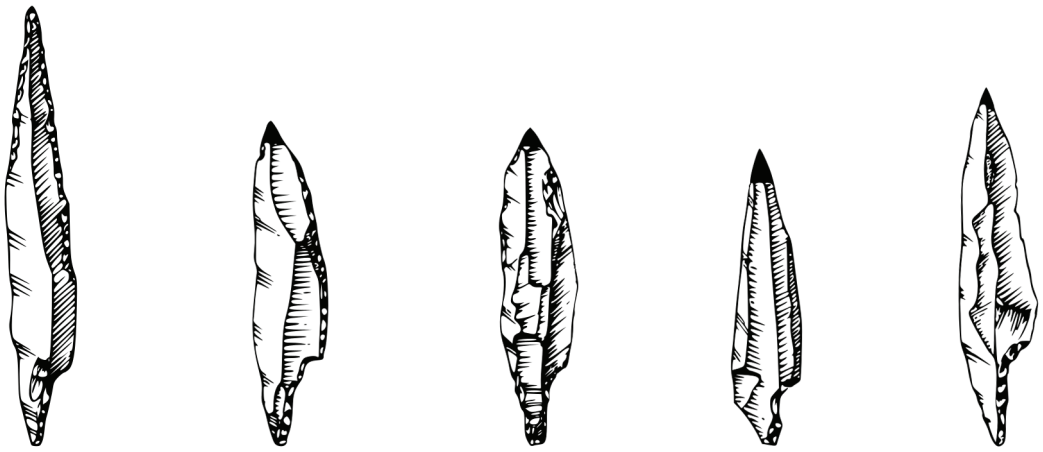


Plate 67: Grotta de la Salpêtriére, layer 6
modified after Onoratini 1982 and Boccaccio 2005



Plate 68: Grotta del Fanciulli, layer D–C
modified after Palma di Cesnola 1979



Plate 69: Grotta della Cala, layer P–M
modified after Martini 1978

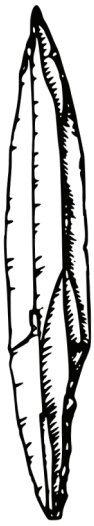


Plate 71: Grotta di Paina, layer 5
modified after Broglio et al. 1993

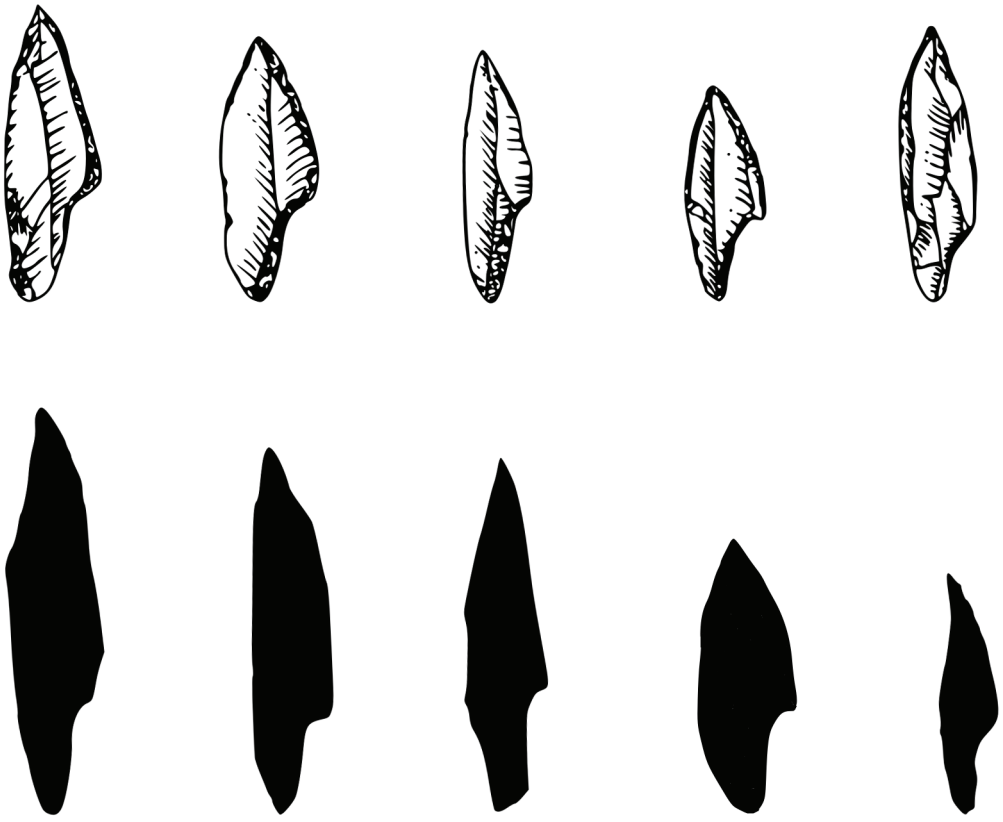


Plate 70: Grotta delle Settecannelle
modified after Ucelli Gnesutta & Cristiani 2002

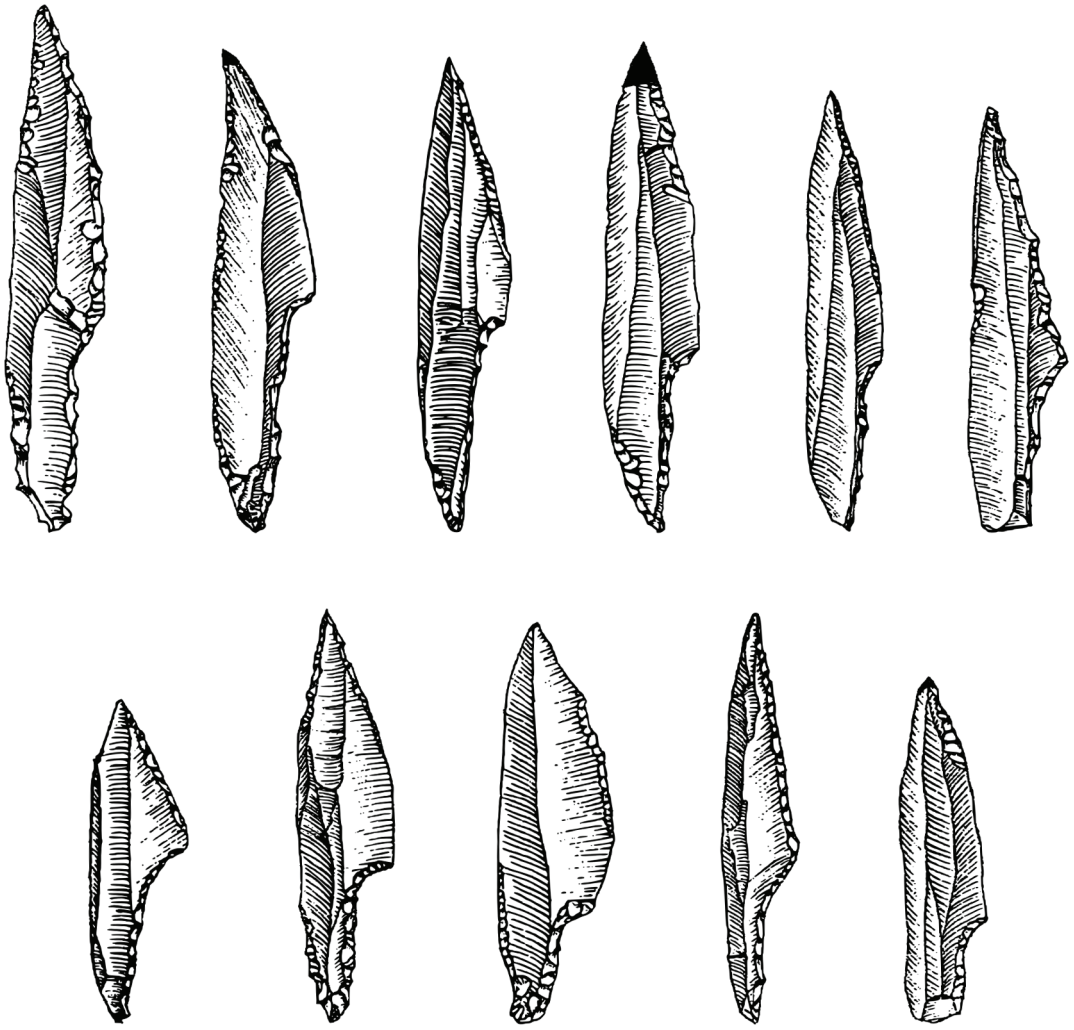


Plate 72a: Grotta Paglicci, layer 18a–10
modified after Mezzena & Palma di Cesnola 1967

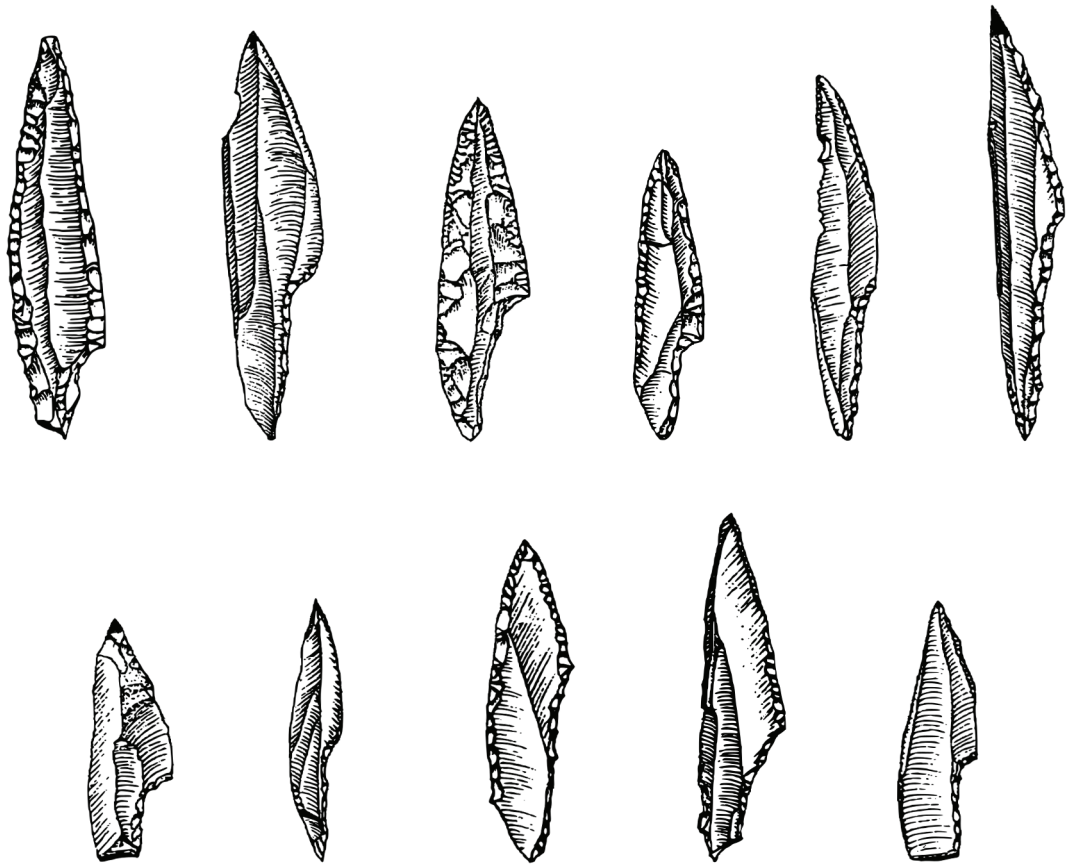


Plate 72b: Grotta Paglicci, layer 18a–10
modified after Mezzena & Palma di Cesnola 1976



Plate 73: Grotta Paglicci, layer 20
modified after Palma di Cesnola 1976



Plate 74: Grotta Paglicci, layer 23–22
modified after Palma di Cesnola 2006



Plate 75: Grotta Romanelli, layer E–B
modified after Palma di Cesnola 1985



Plate 76: Grotta Trene
modified after Broglio et al. 2009



Plate 77: Grotte de Cleves, Rinxent
modified after Fagnart 1984

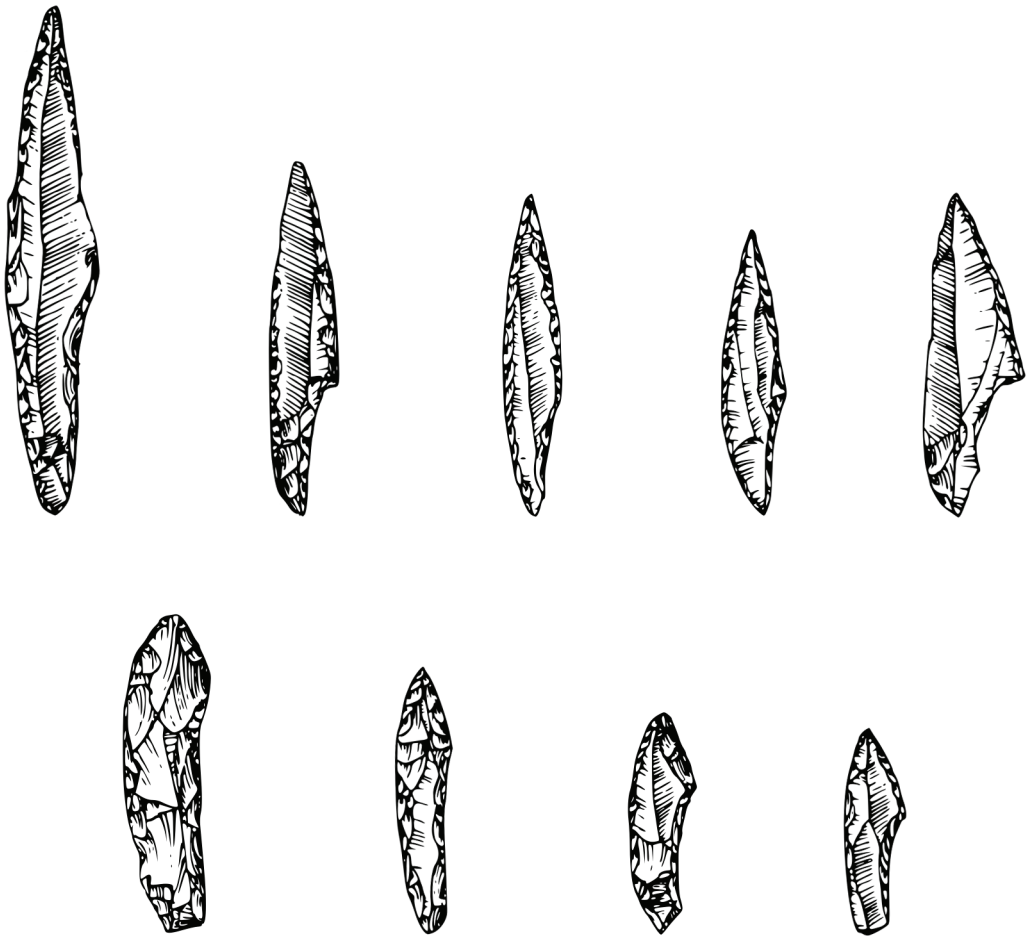


Plate 78: Grotte de la Bouviere
modified after Onoratini 1978

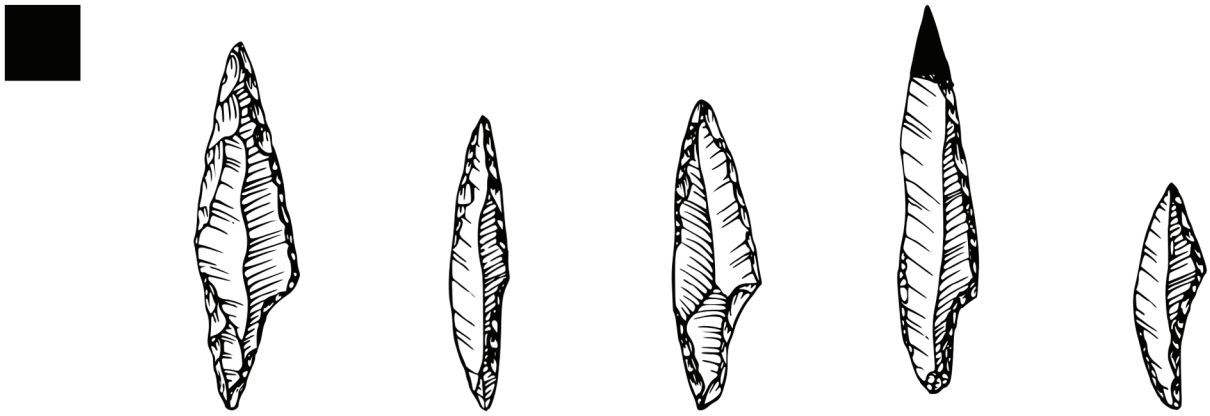


Plate 79: Grotte des Enfants à Grimaldi
modified after Onoratini 1978



Plate 80: Grotte des Eyzies
modified after Smith 1966



Plate 81: Grub-Kranawetberg, AH4
Images kindly provided by Antl-Weiser (unpubl.)

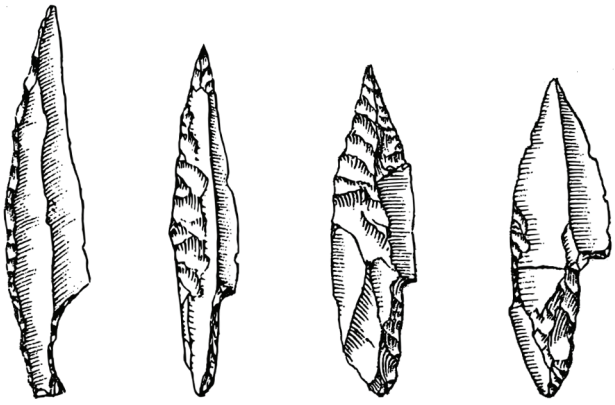


Plate 82: Gruta de Salemas
modified after Zilhão 1997

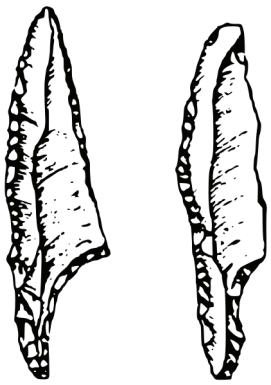


Plate 83: Gruta do Almonda
modified after Zilhão et al. 1991

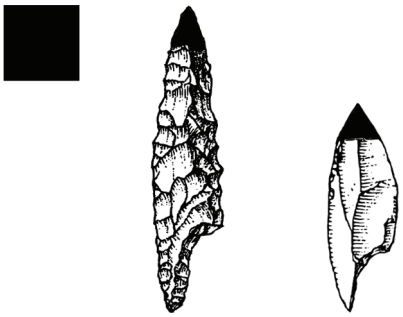


Plate 84: Gruta do Caldeirão, layer ABC–D/Eb
Zilhão 1997



Plate 85: Gruta do Ourão
modified after Zilhão 1997

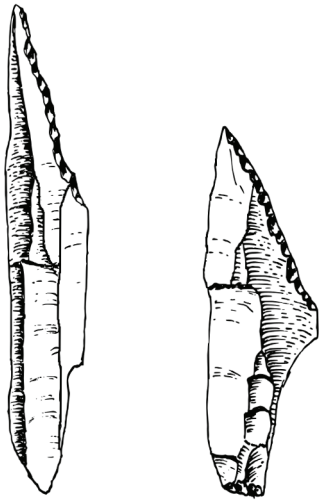


Plate 86: Hasewisch
modified after Rust 1958

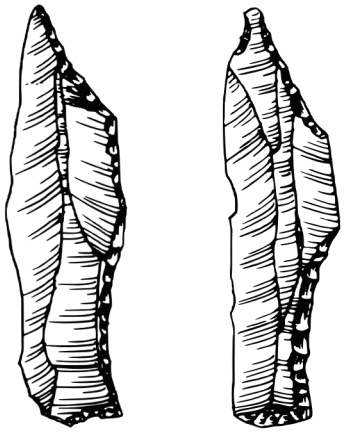
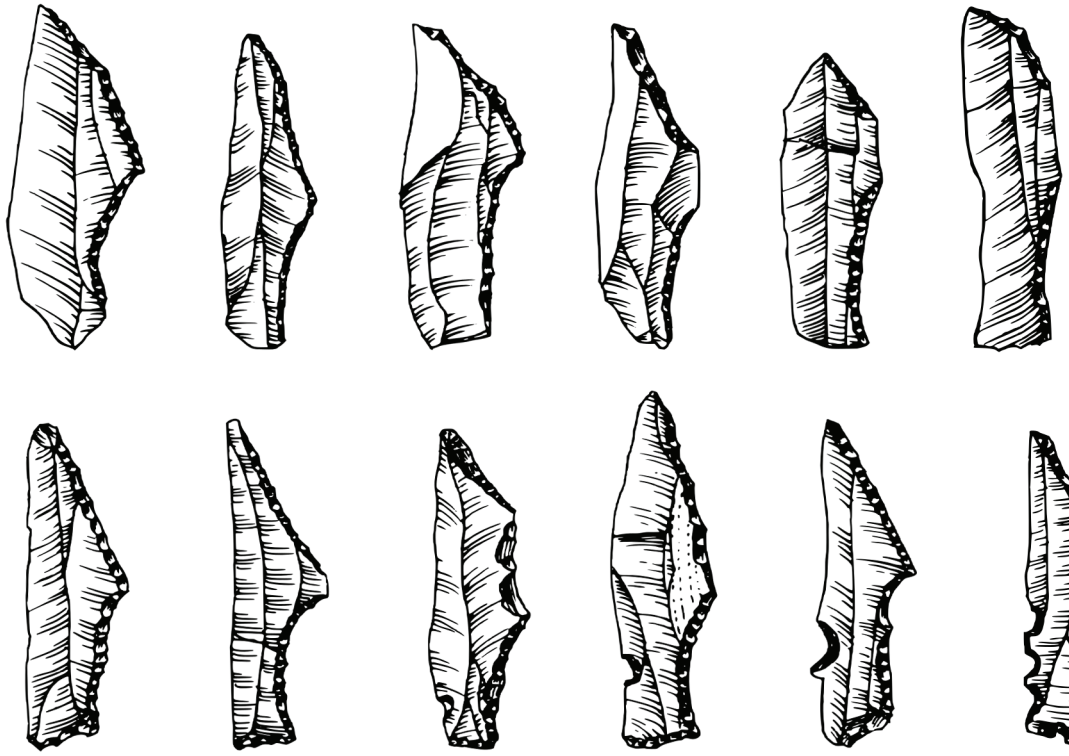


Plate 87: Heber 118
modified after Tromnau 1975a



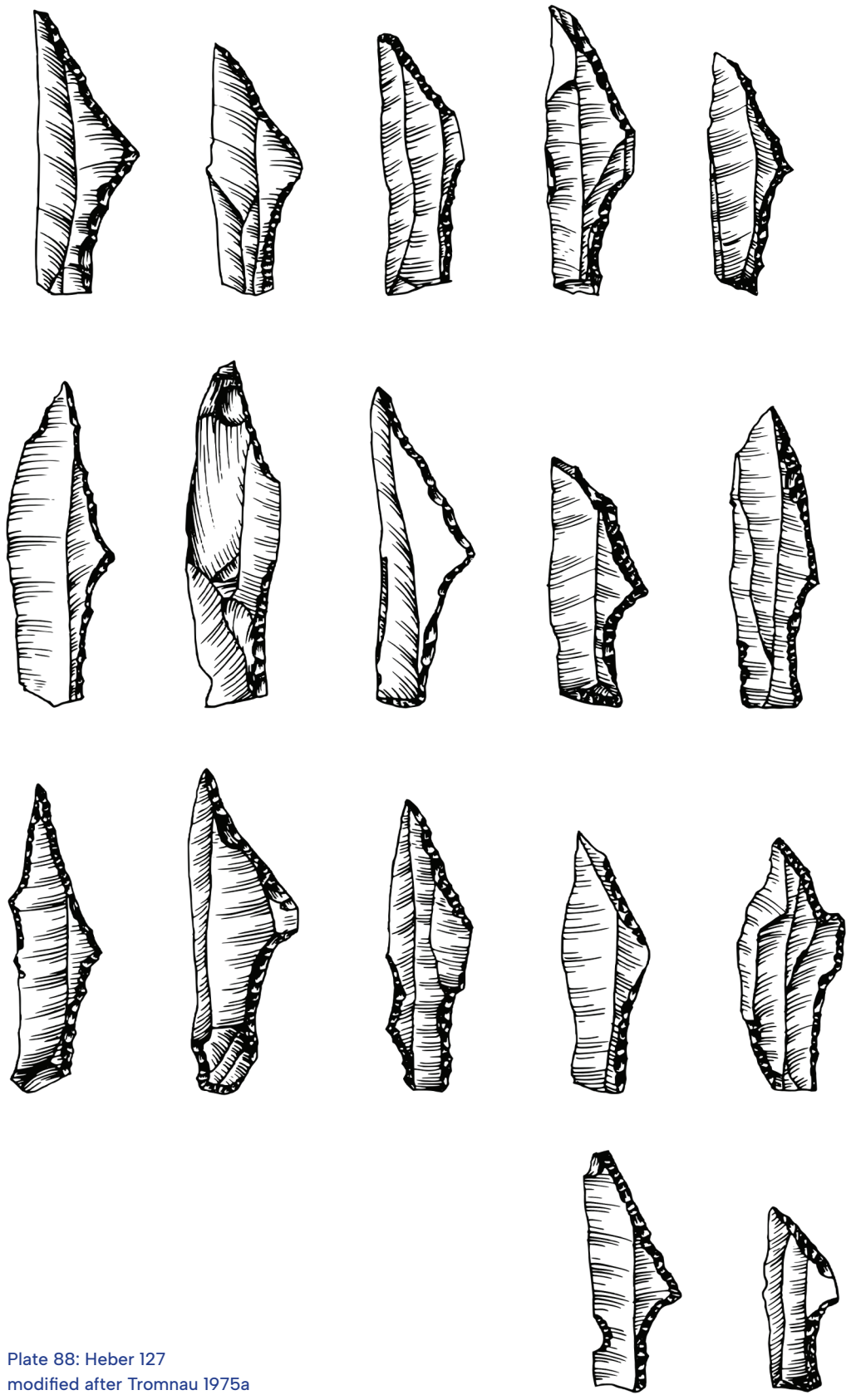


Plate 88: Heber 127
modified after Tromnau 1975a

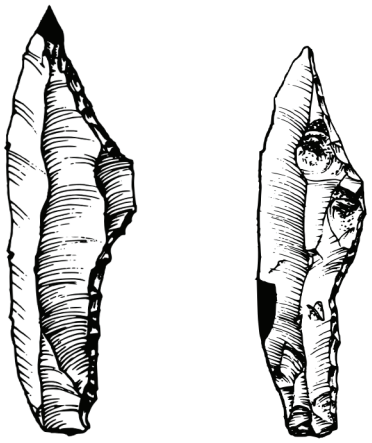


Plate 89: Hengistbury Head
modified after Barton 1992



Plate 90: Hubina
modified after Hromada & Žemla 2000



Plate 91: Jama v Lozi, layer 5
modified after Brodar 1986

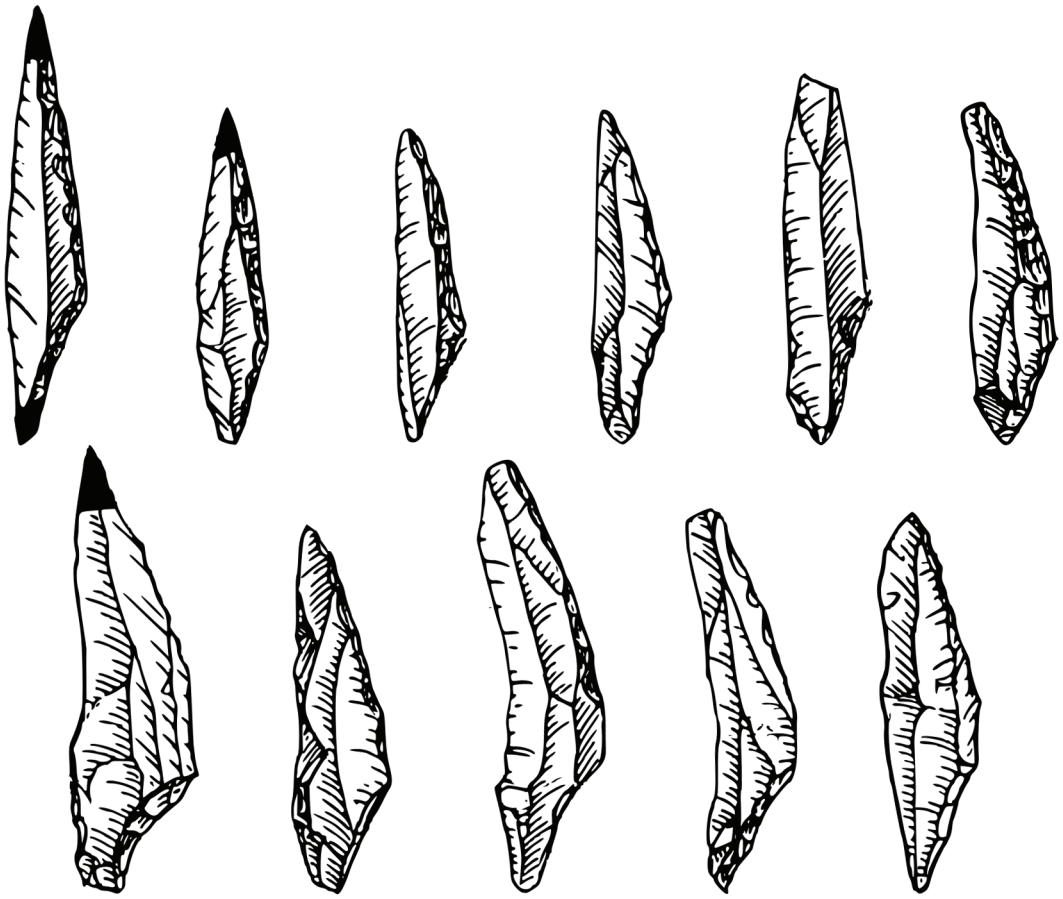


Plate 92: Jaurias
modified after Lenoir 2003

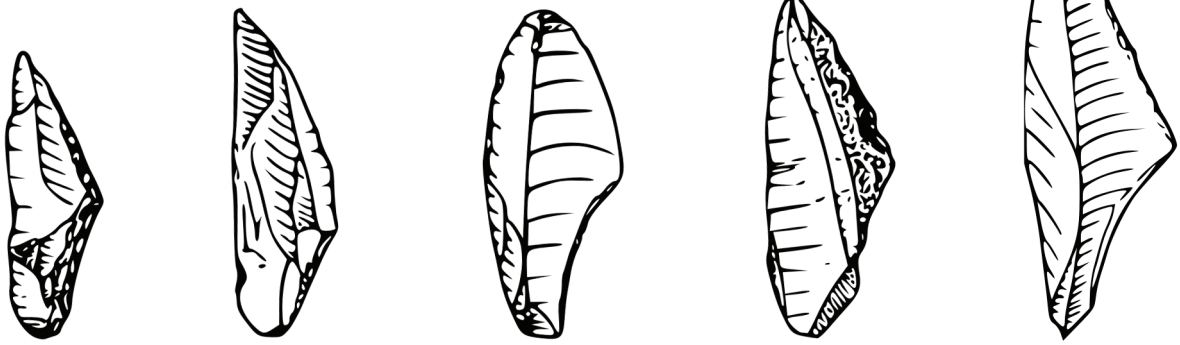


Plate 93: Käsloch
modified after Zuberbühler Koch 2002



Plate 94: Kamegg
modified after Neugebauer-Maresch 1999



Plate 95: Kammern-Grubgraben
(Krahuletzmuseum Eggenburg, Austria) images kindly prov. by V. Kaudela



Plate 96: Kastelhöhle-Nord
modified after Nielsen 2009

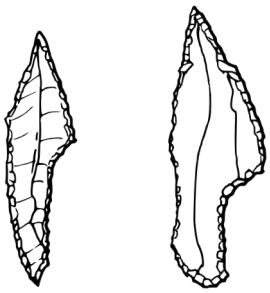


Plate 97: Kastrisa, layer 7/Straum 3
modified after Adam 2007



Plate 98: Kastrisa, Stratum 5
modified after Adam 2007

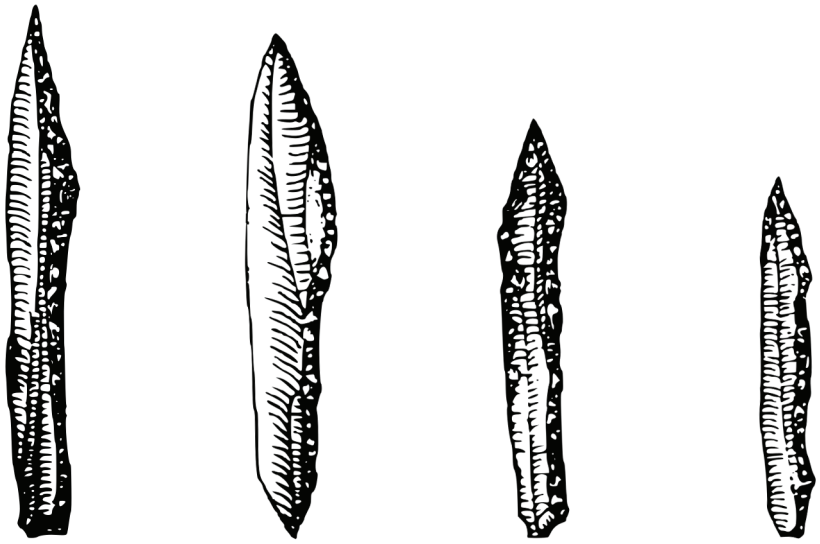


Plate 99: Khotylëvo 2
modified after Zaverniaev 1991



Plate 100: Kniegrotte, layer VIII
modified after Feustel 1974

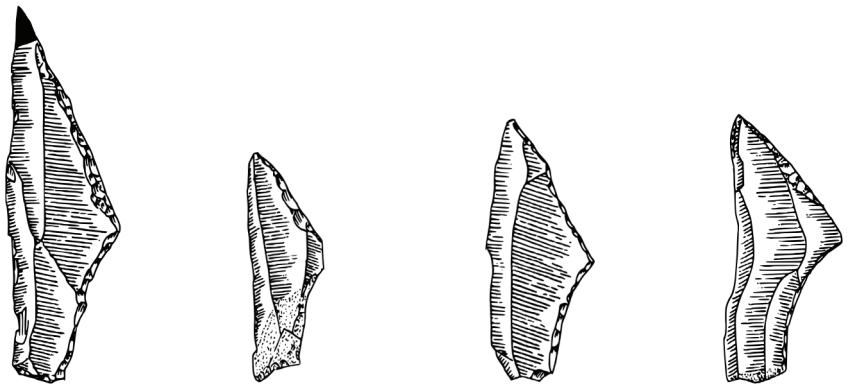


Plate 101: Köpfli
modified after Zürcher 1969

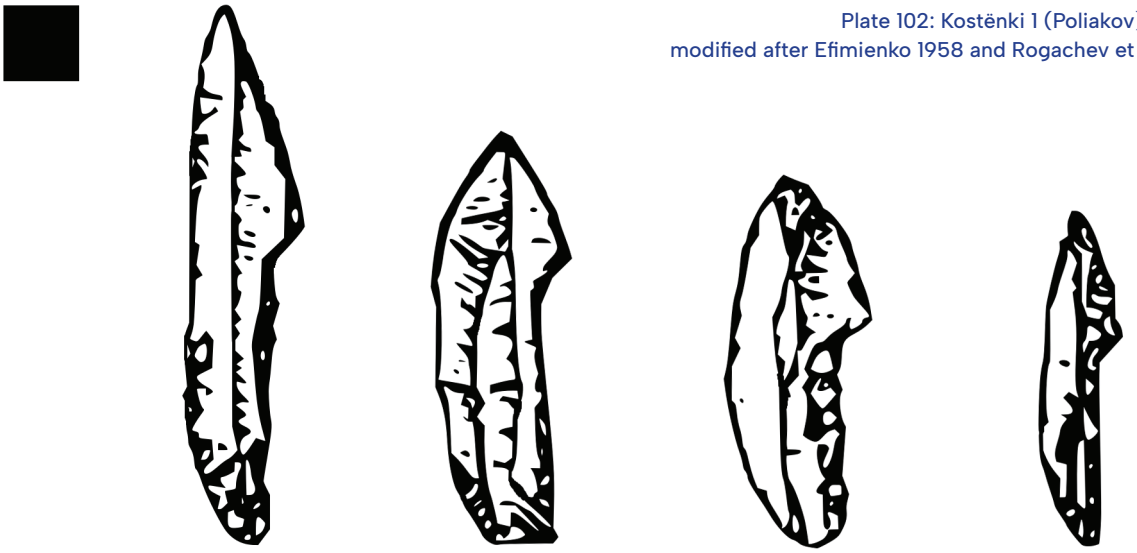


Plate 102: Kostënki 1 (Poliakov), layer I
modified after Efimienko 1958 and Rogachev et al. 1982

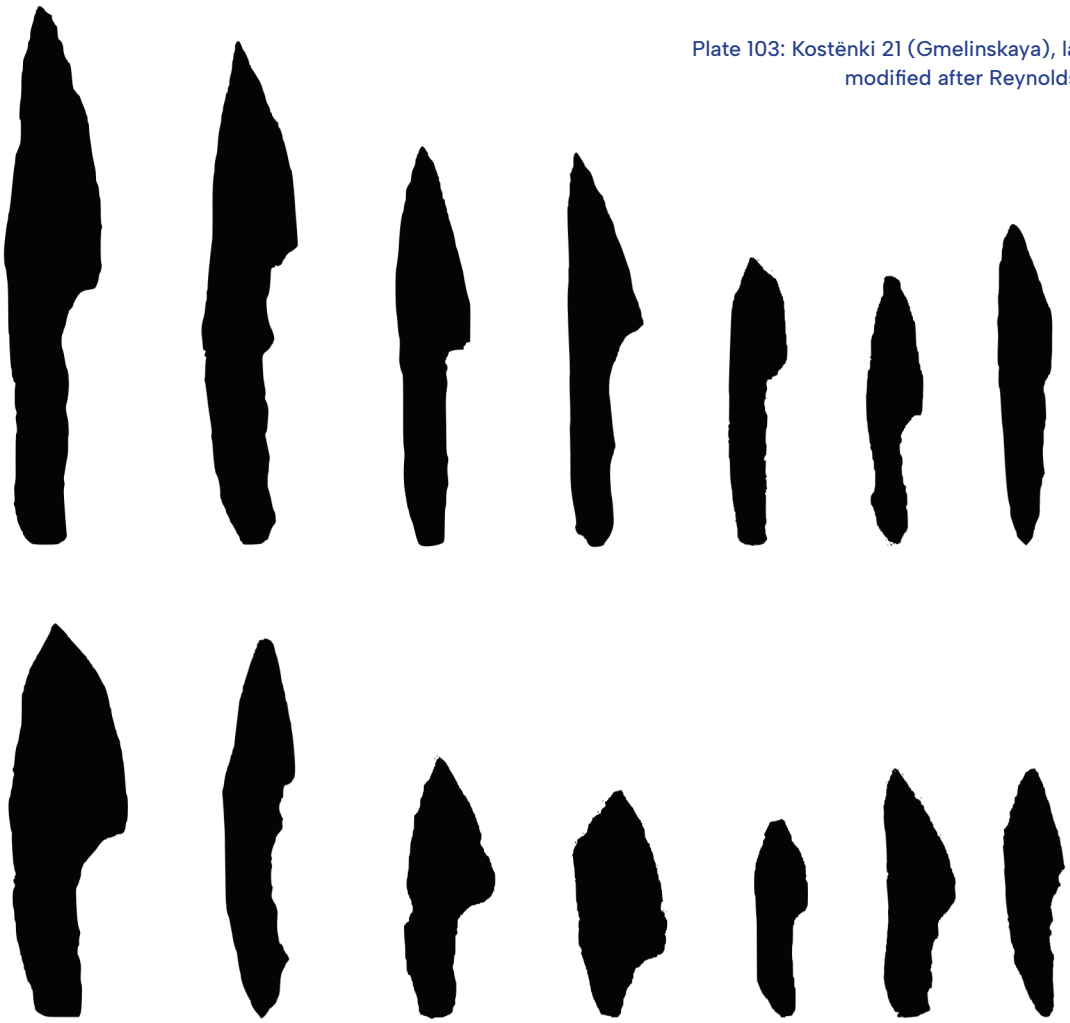


Plate 103: Kostënki 21 (Gmelinskaya), layer III
modified after Reynolds 2014

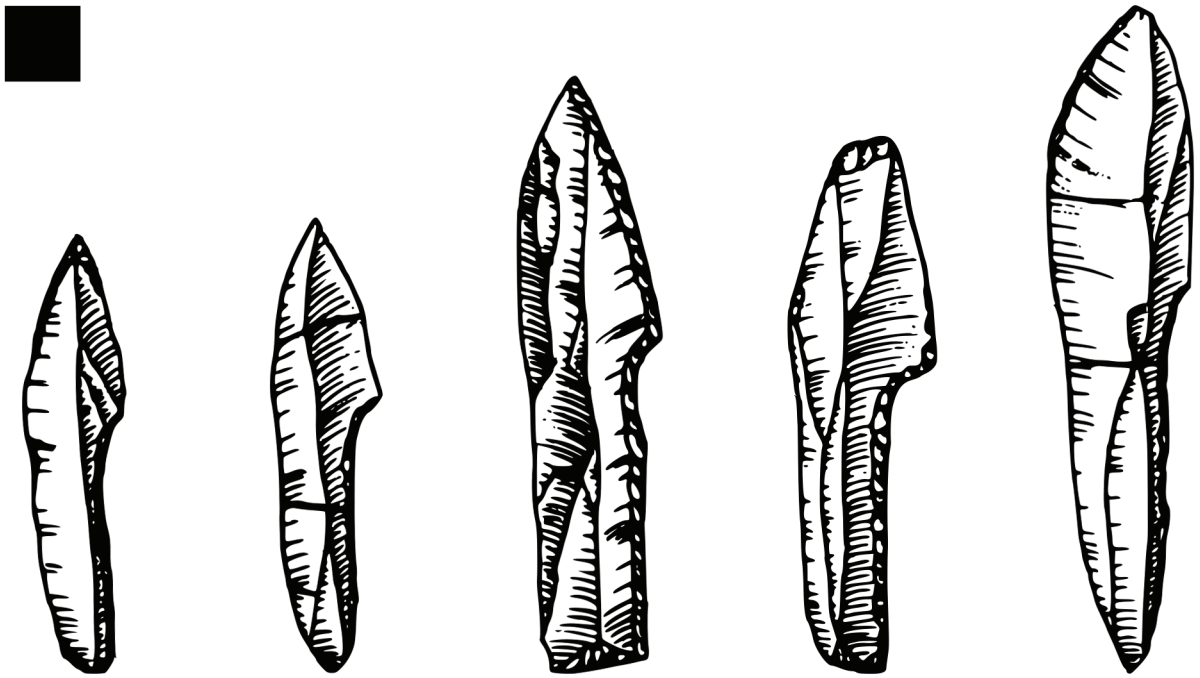


Plate 104: Kraków Spadzista B, layer 6
modified after Chmielewsky et al. 1975



Plate 105: La Balutie
modified after Smith 1966



Plate 106: Lacam
modified after Smith 1966

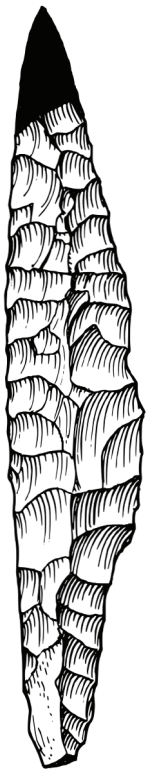


Plate 107: Lachaud
modified after Smith 1966

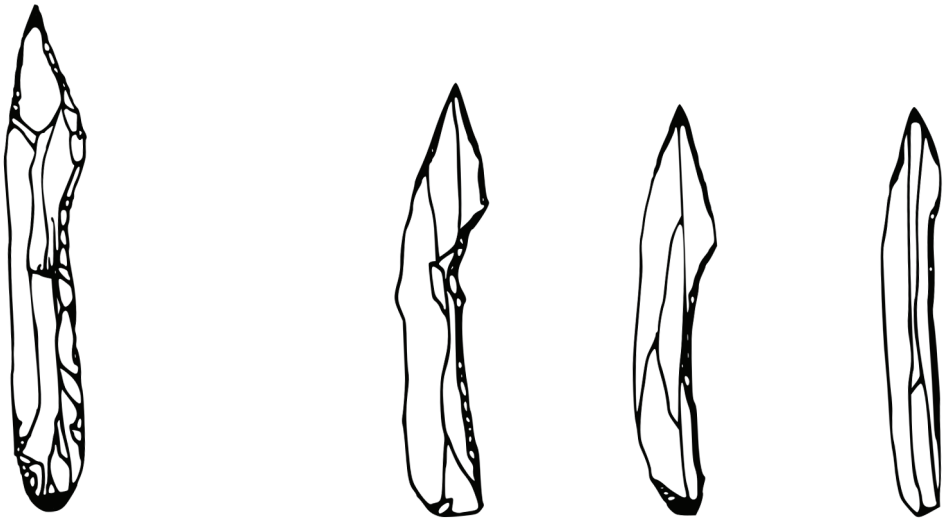


Plate 108: La Madeleine, layer B – Magdalenién V
modified after Taylor 2012

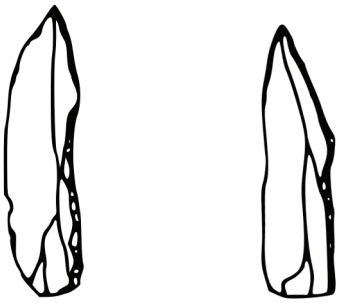


Plate 109: La Madeleine, layer C – Magdalenién VI
modified after Taylor 2012

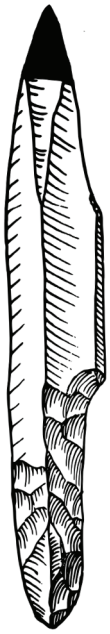


Plate 110: La Mouthe
modified after Smith 1966



Plate 111: La Pasiega
modified after Corchon 1971

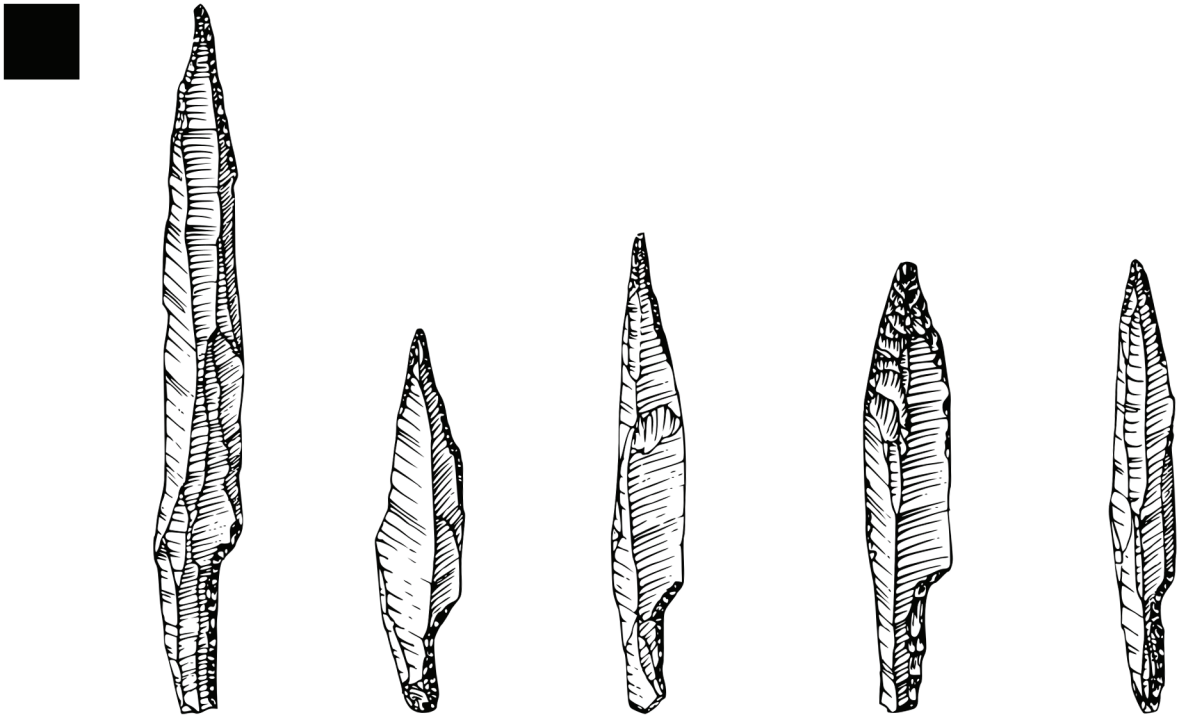


Plate 112: La Rouviére
modified after Gallet 1973

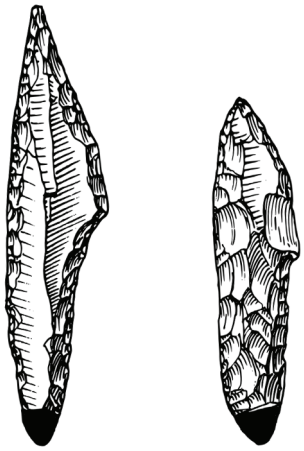


Plate 113: Laugerie-Haute Ouest,
Niveau de pointe à cran
Smith 1966

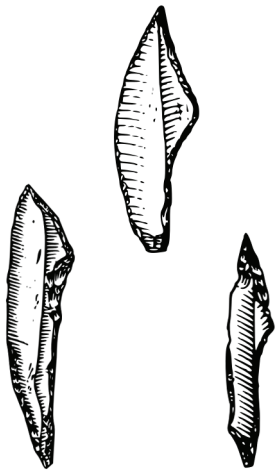


Plate 114: Le Cozoul de Vers, 21–16
modified after Ducasse et al. 2021

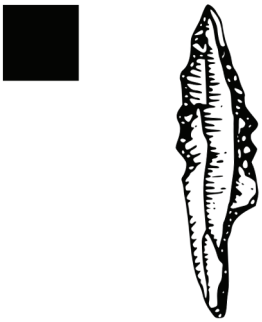


Plate 115: Legintxiqui
modified after Nuin 1988/1989

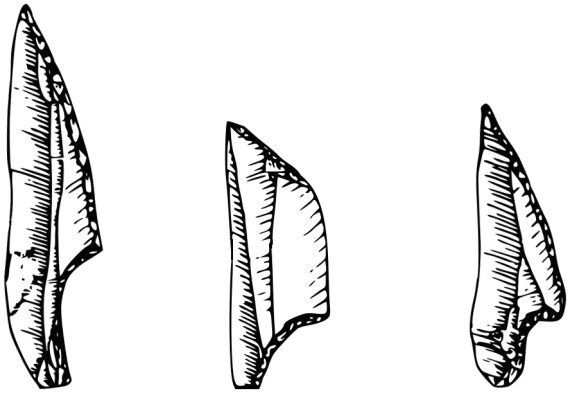


Plate 116: Le Martinet, layer IV
modified after Le Tensorer 1981

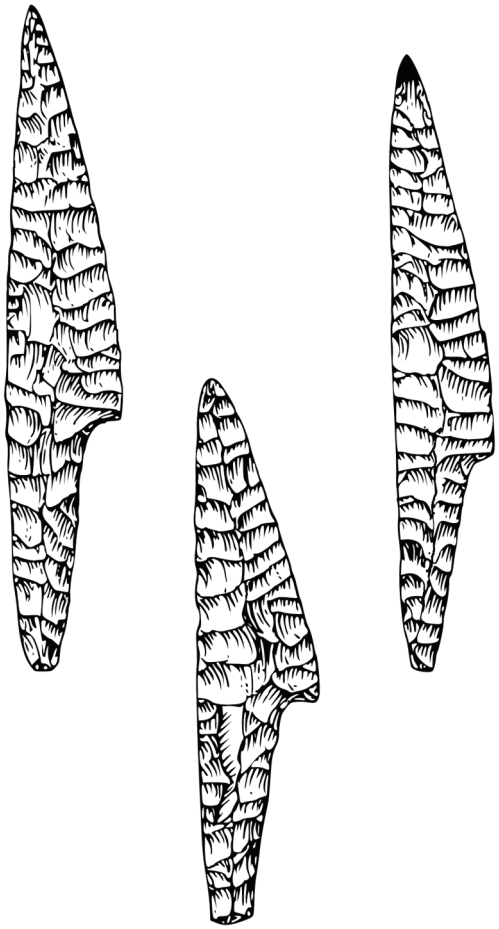


Plate 117a: Le Placard
modified after Smith 1966

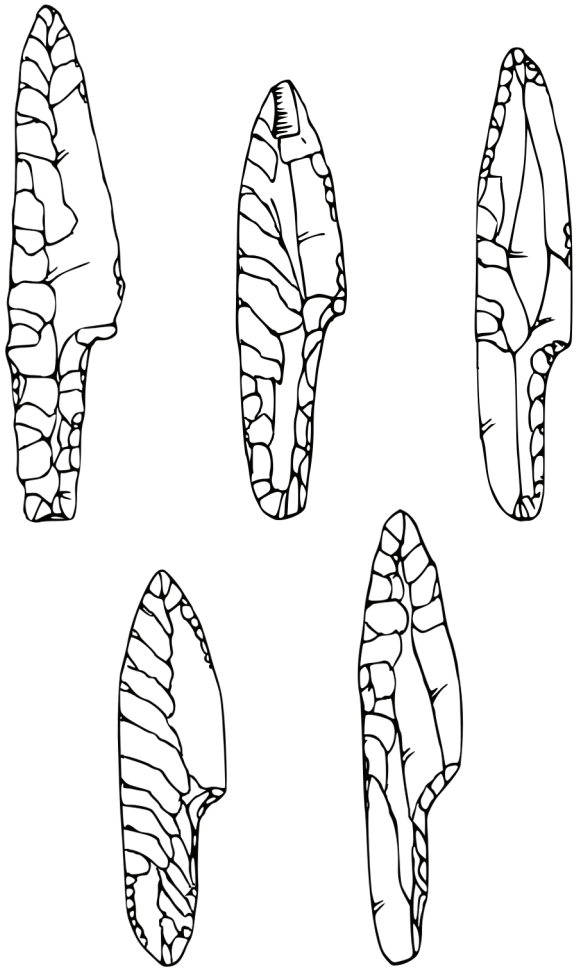


Plate 117b: Le Placard
modified after Geneste & Plisson 1989

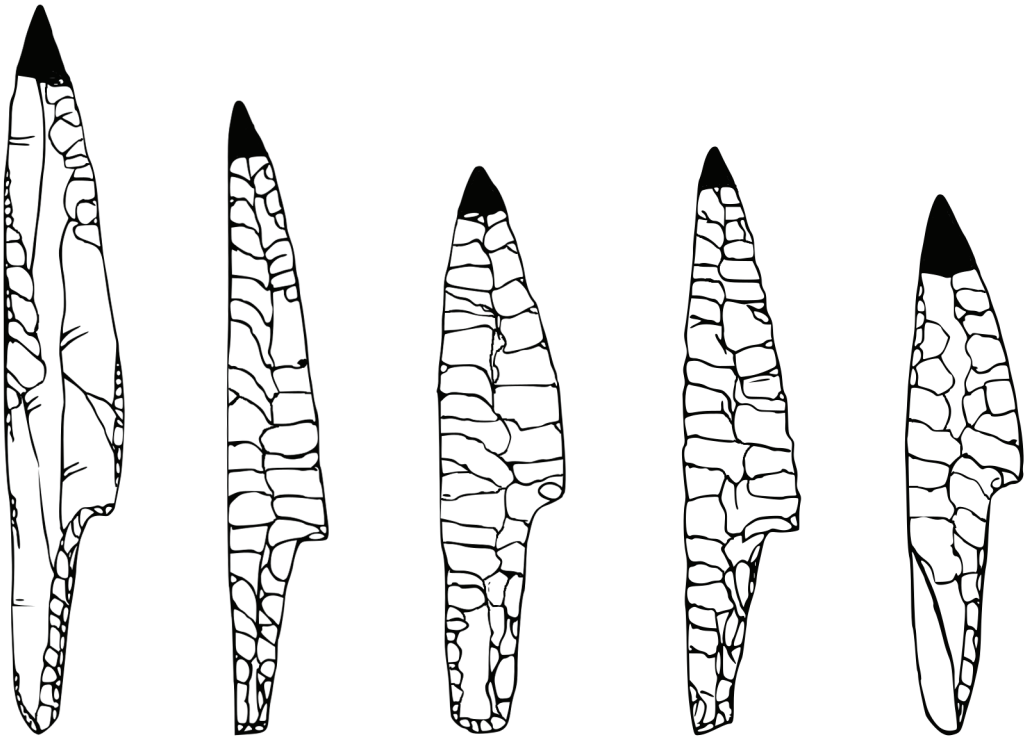


Plate 117c: Le Placard
modified after Geneste & Plisson 1989

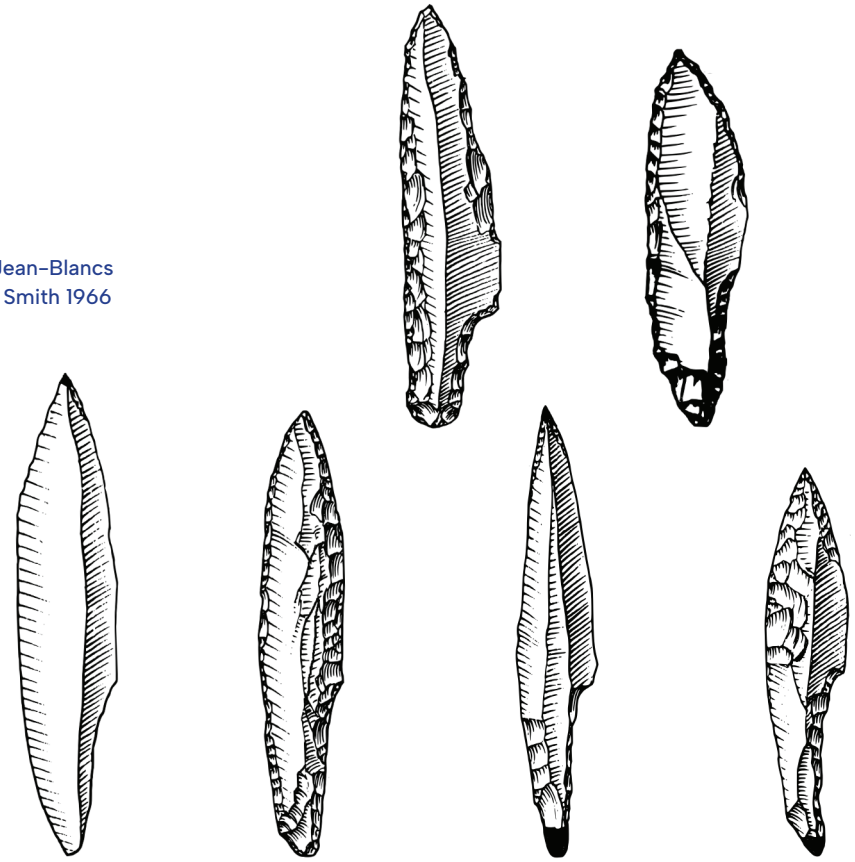


Plate 118: Les Jean-Blancs
modified after Smith 1966



Plate 119: Les Vachons
modified after Smith 1966

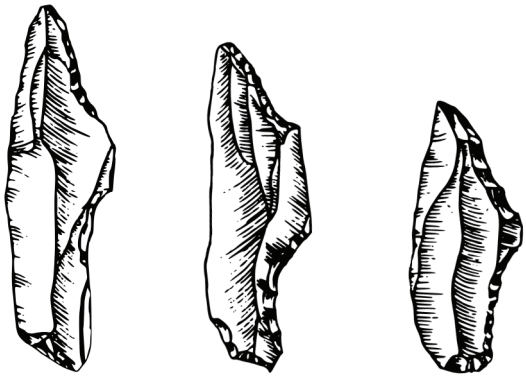


Plate 120: Liny 1
modified after Kobusiewicz 1975

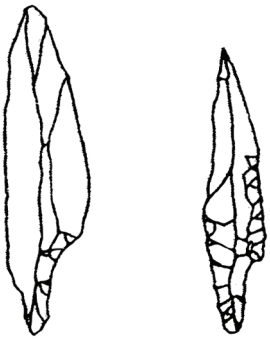


Plate 121: Madonna dell'Ospedale
modified after Silvestrini et al. 2008

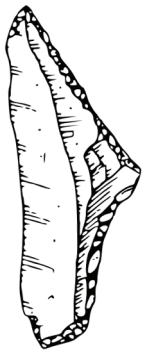


Plate 122: Marolles – Tureau des Gardes
modified after Burdukiewicz & Schmider 2000

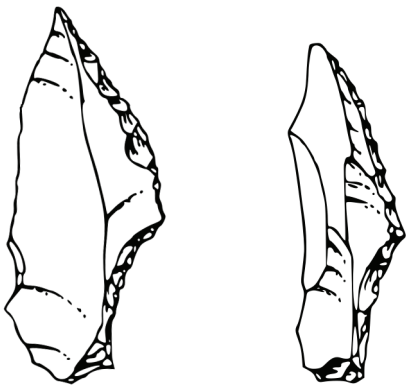


Plate 123: Marsagny
modified after Schmider 1992

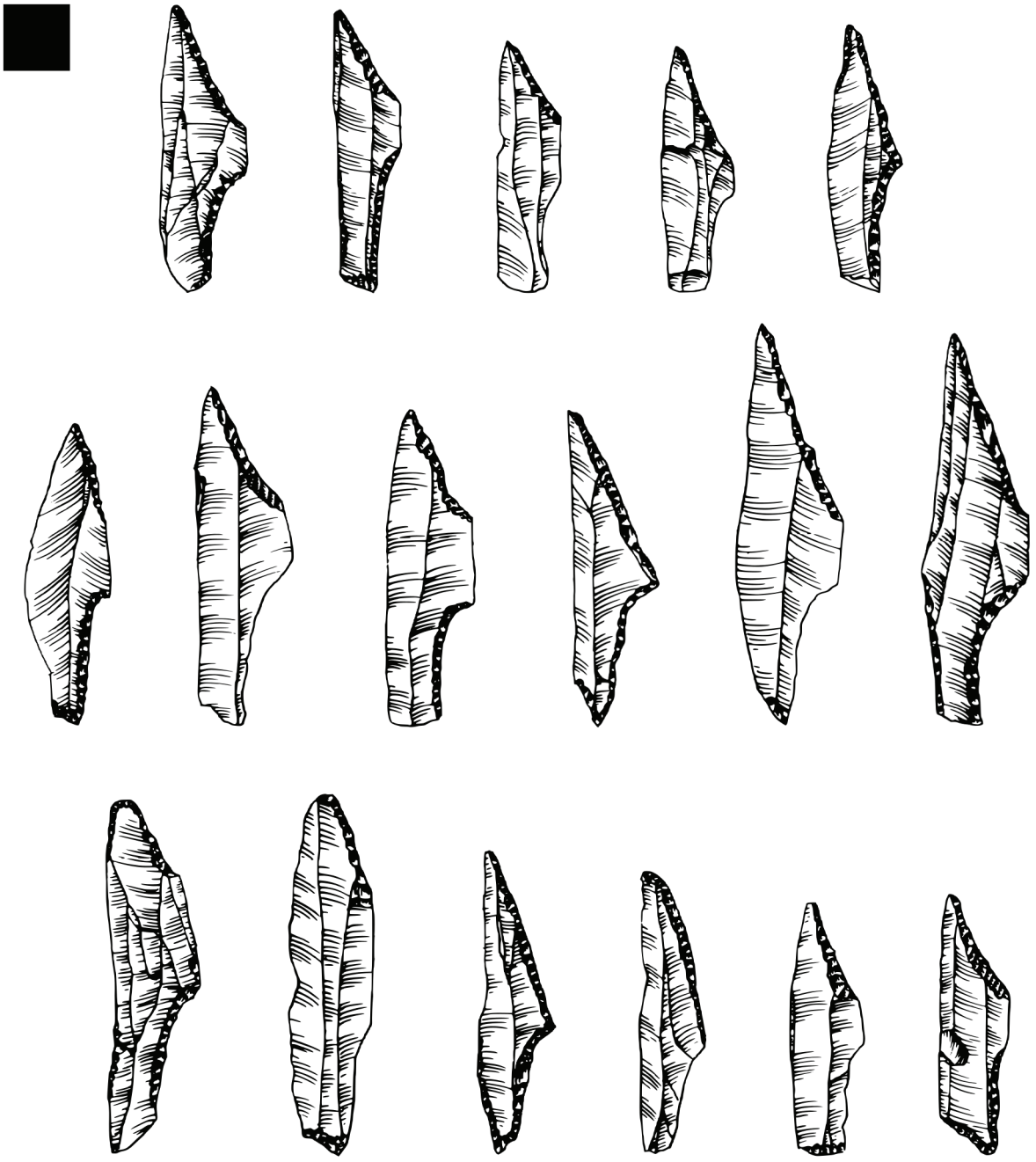


Plate 124: Meiendorf 2
modified after Rust 1937



Plate 125: Milovice I, section G
modified after Oliva 1999, 2009

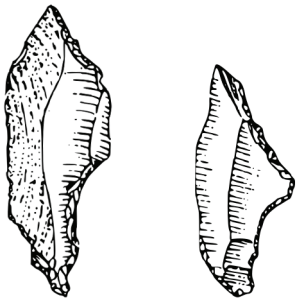


Plate 126: Mirkowice 33
modified after Chłodnicki & Kabaciński 1997

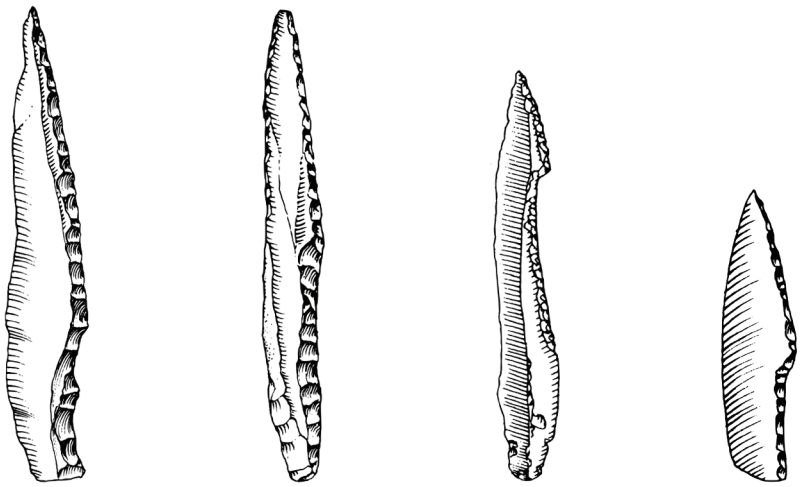


Plate 127: Mitoc-Malu Galben, layer 4a
modified after Otte et al. 2007

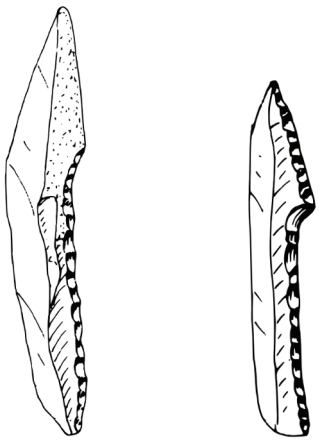


Plate 128: Molodova V, layer 7
modified after Chernysh 1961



Plate 129: Moravany nad Váhom-Lopata II
modified after Hromada 2000

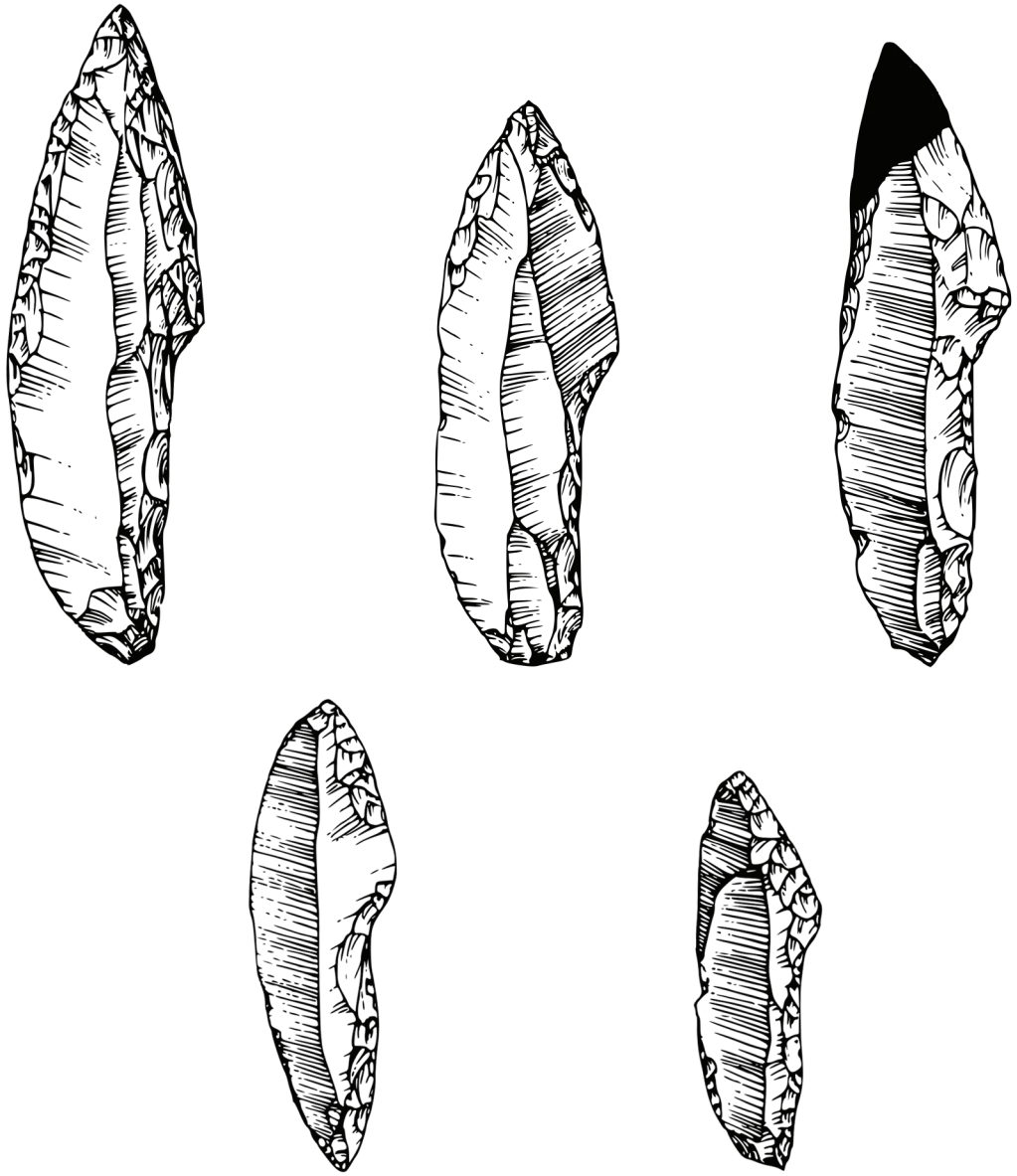


Plate 130a: Moravany nad Váhom–Noviny
modified after Bárta 1965

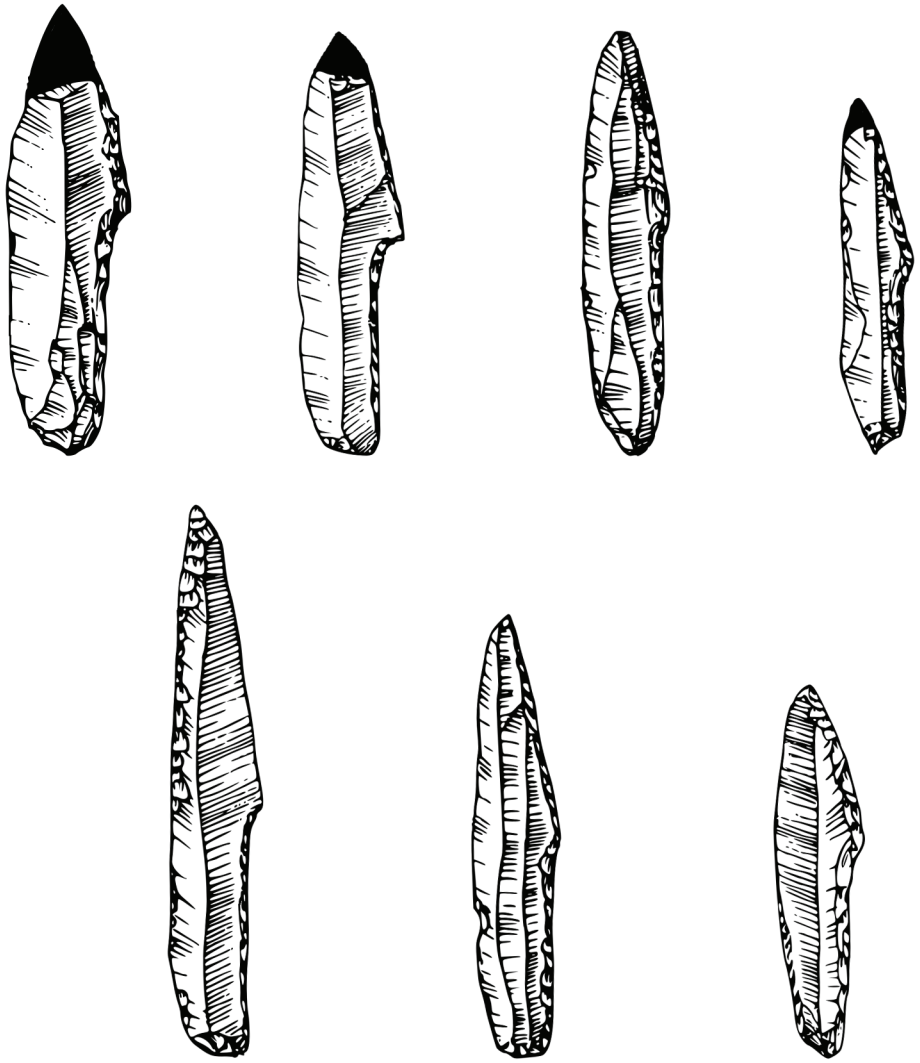


Plate 130b: Moravany nad Váhom–Noviny
modified after Bárta 1965

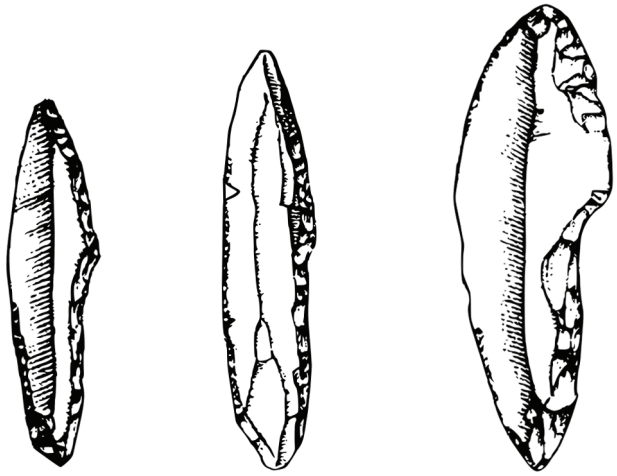


Plate 131: Moravany nad Váhom–Podkovica
modified after Bárta 1965

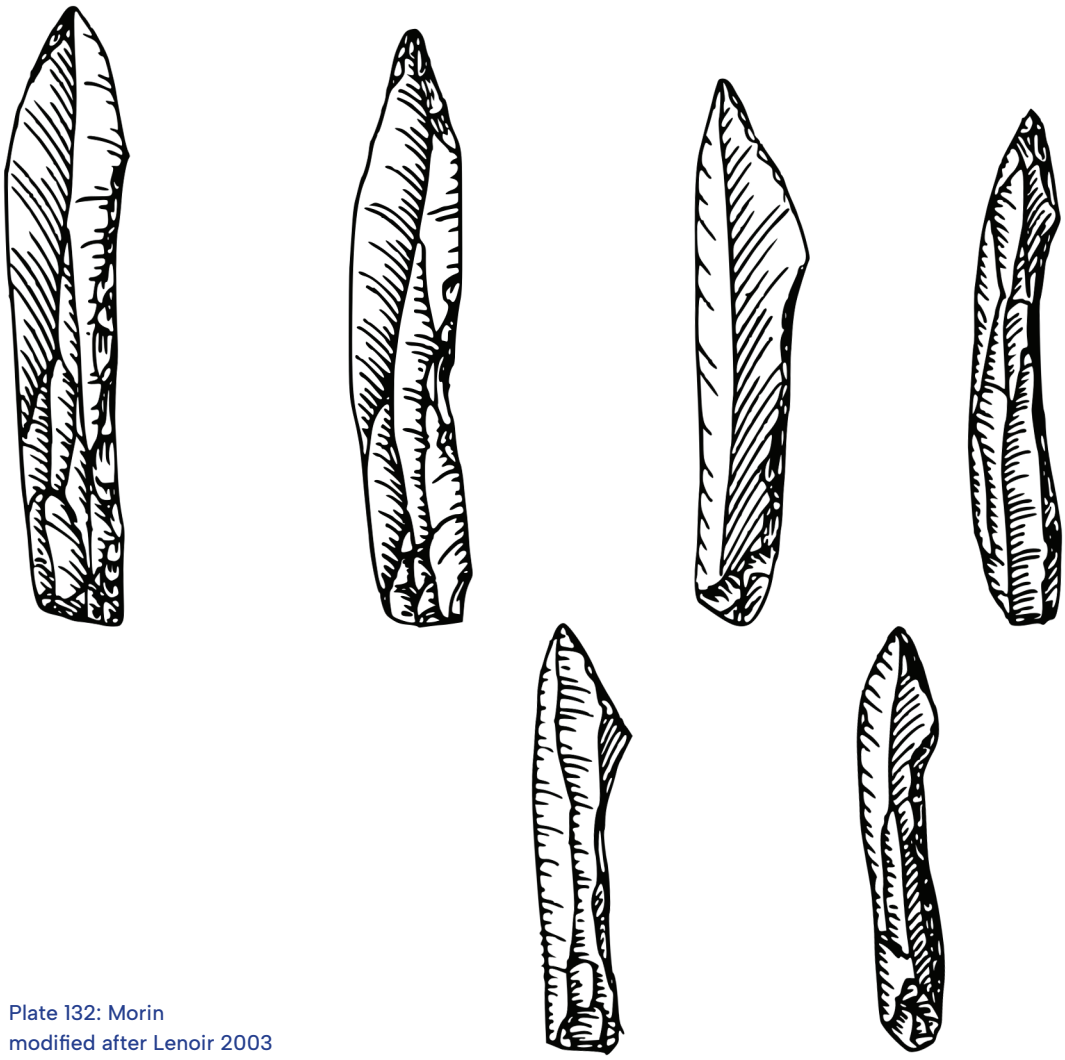


Plate 132: Morin
modified after Lenoir 2003

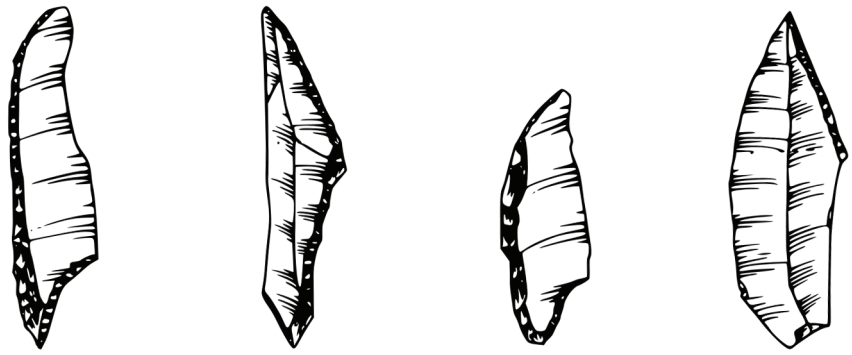


Plate 133: Mother Grundy´s Parlour, layers C/B and LB–SB
modified after Campbell 1977

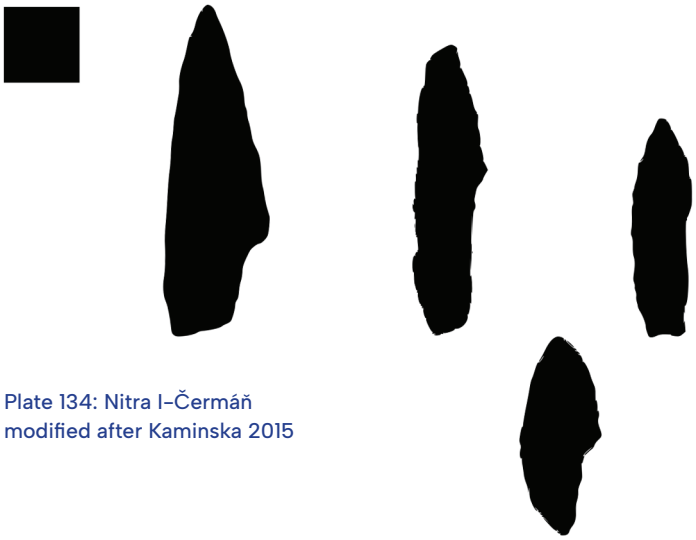


Plate 134: Nitra I–Čermáň
modified after Kaminska 2015



Plate 135: Noailles
modified after Smith 1966

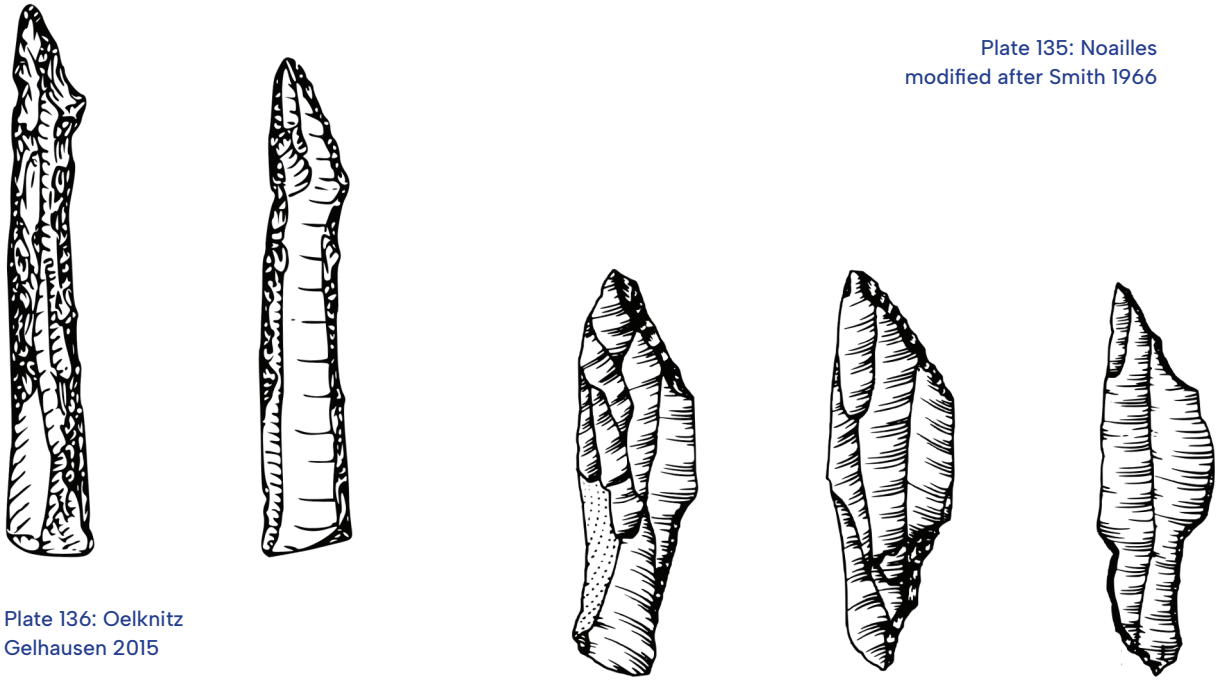


Plate 136: Oelknitz
Gelhausen 2015

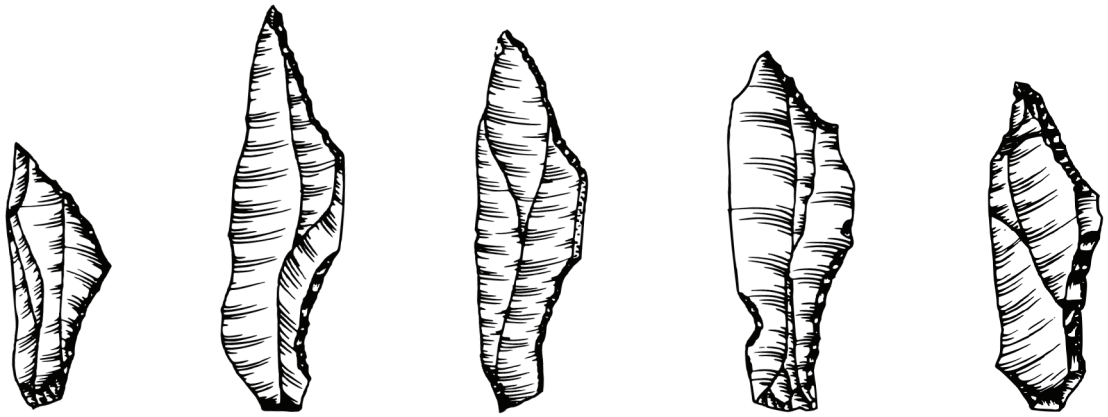


Plate 137: Olbrachcice 8
modified after Burdukiewicz 1981, 1986

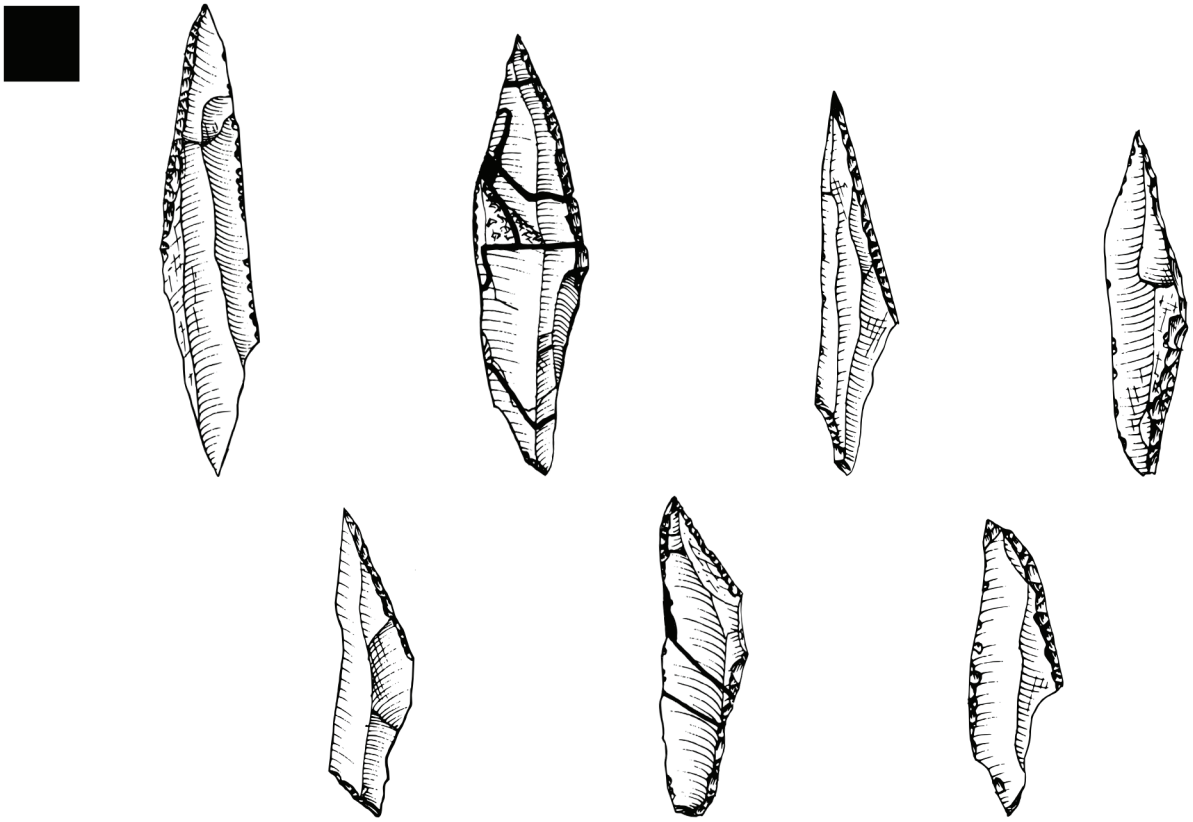


Plate 138: Oldeholtwolde
modified after Johansen & Stapert 2004

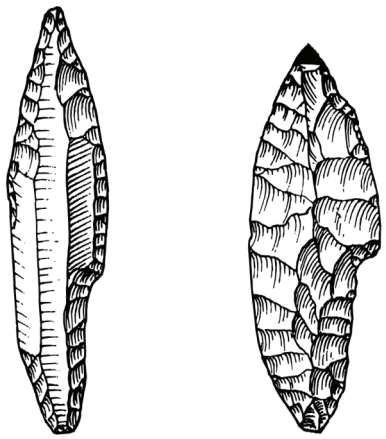


Plate 139: Oreille-d´Enfer
modified after Smith 1966

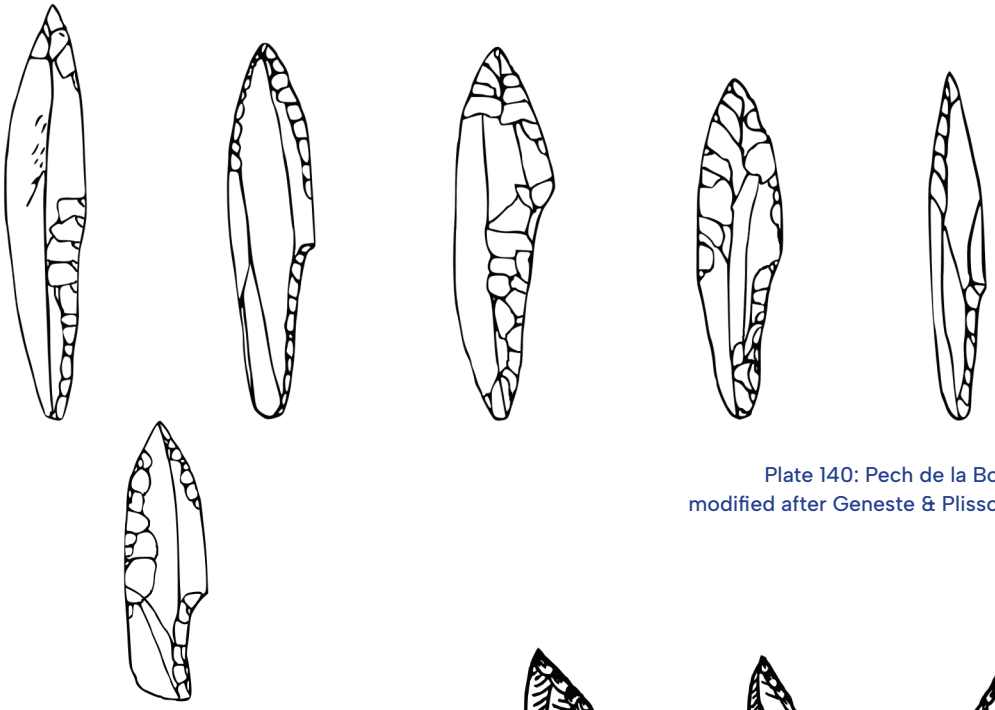


Plate 140: Pech de la Boissière
modified after Geneste & Plisson 1989

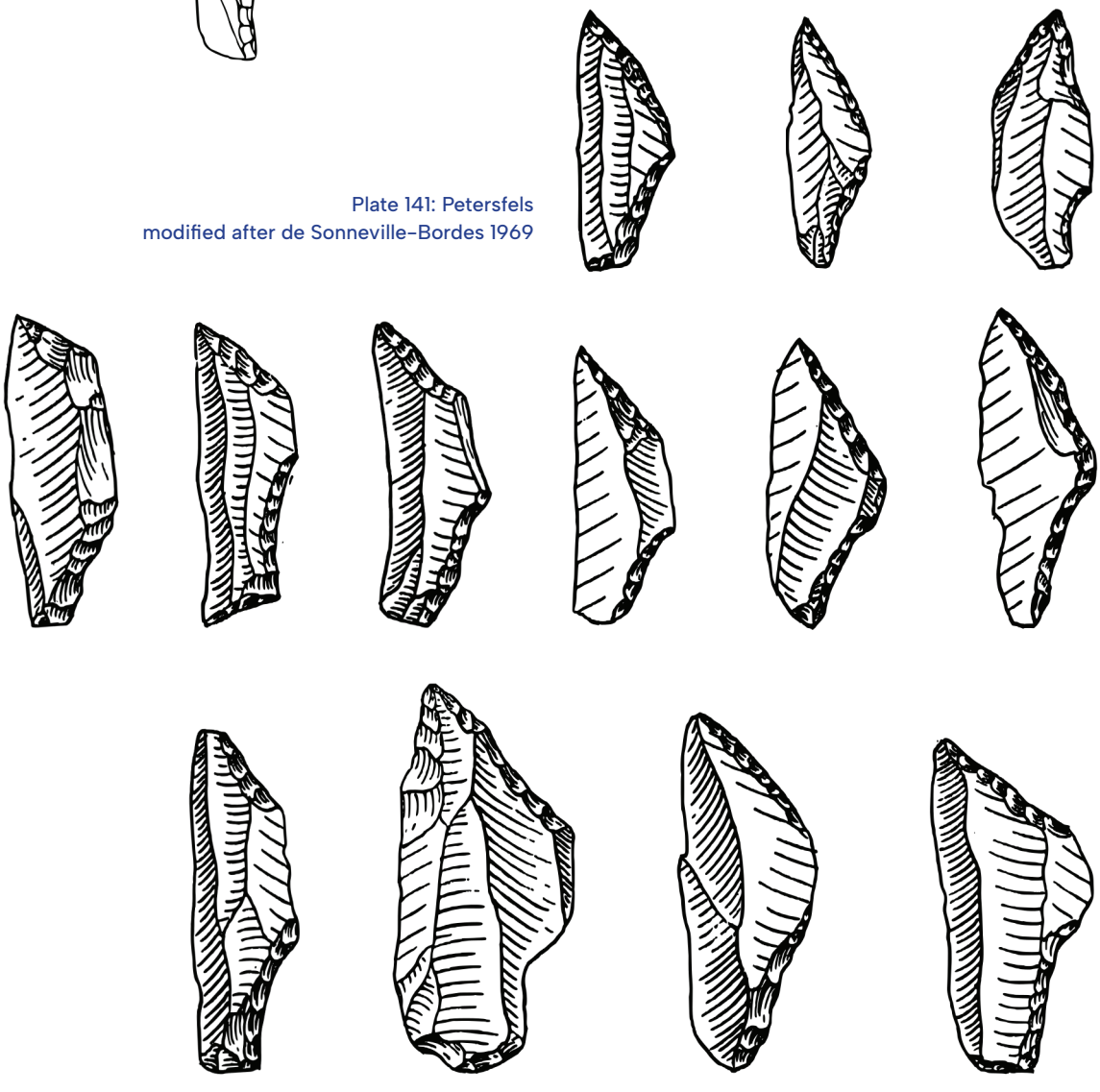


Plate 141: Petersfels
modified after de Sonneville-Bordes 1969

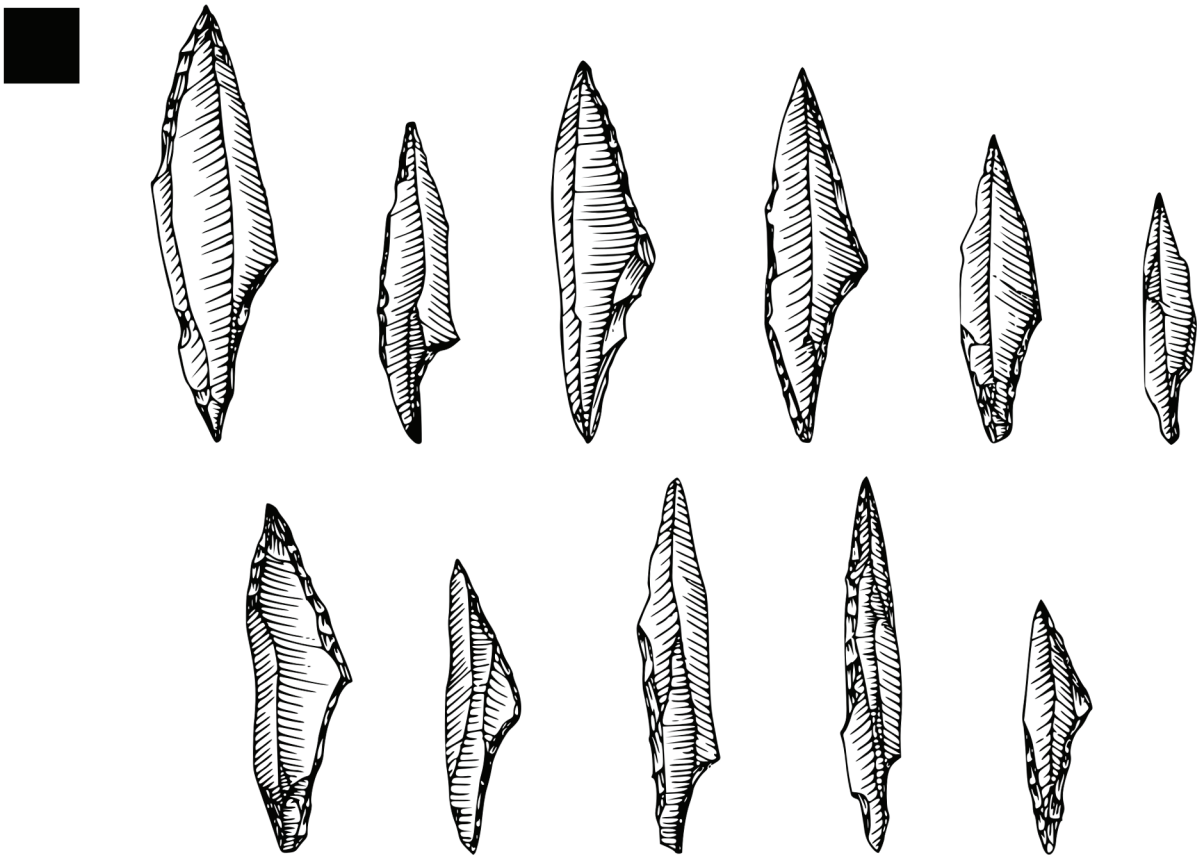


Plate 142: Petite Grotte de Bize
modified after Sacchi 1986

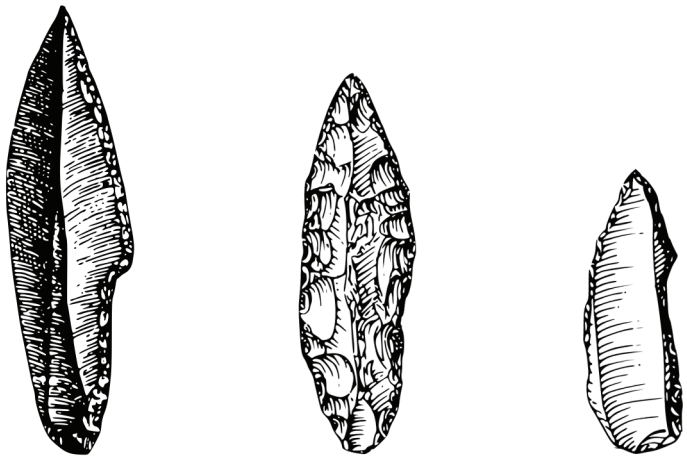


Plate 143: Petřkovice, layer 1a
modified after Novák 2008

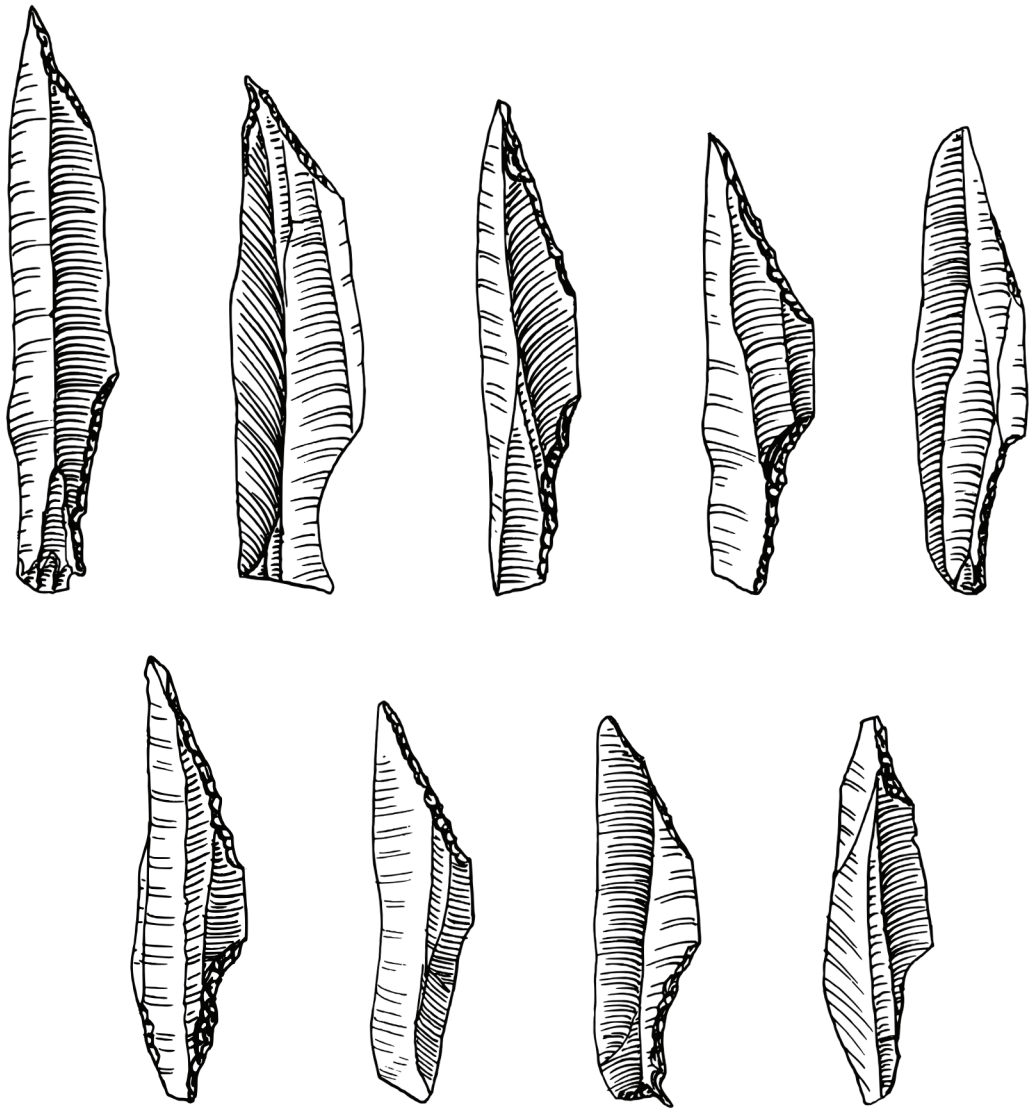


Plate 144a: Poggenwisch D
modified after Rust 1958

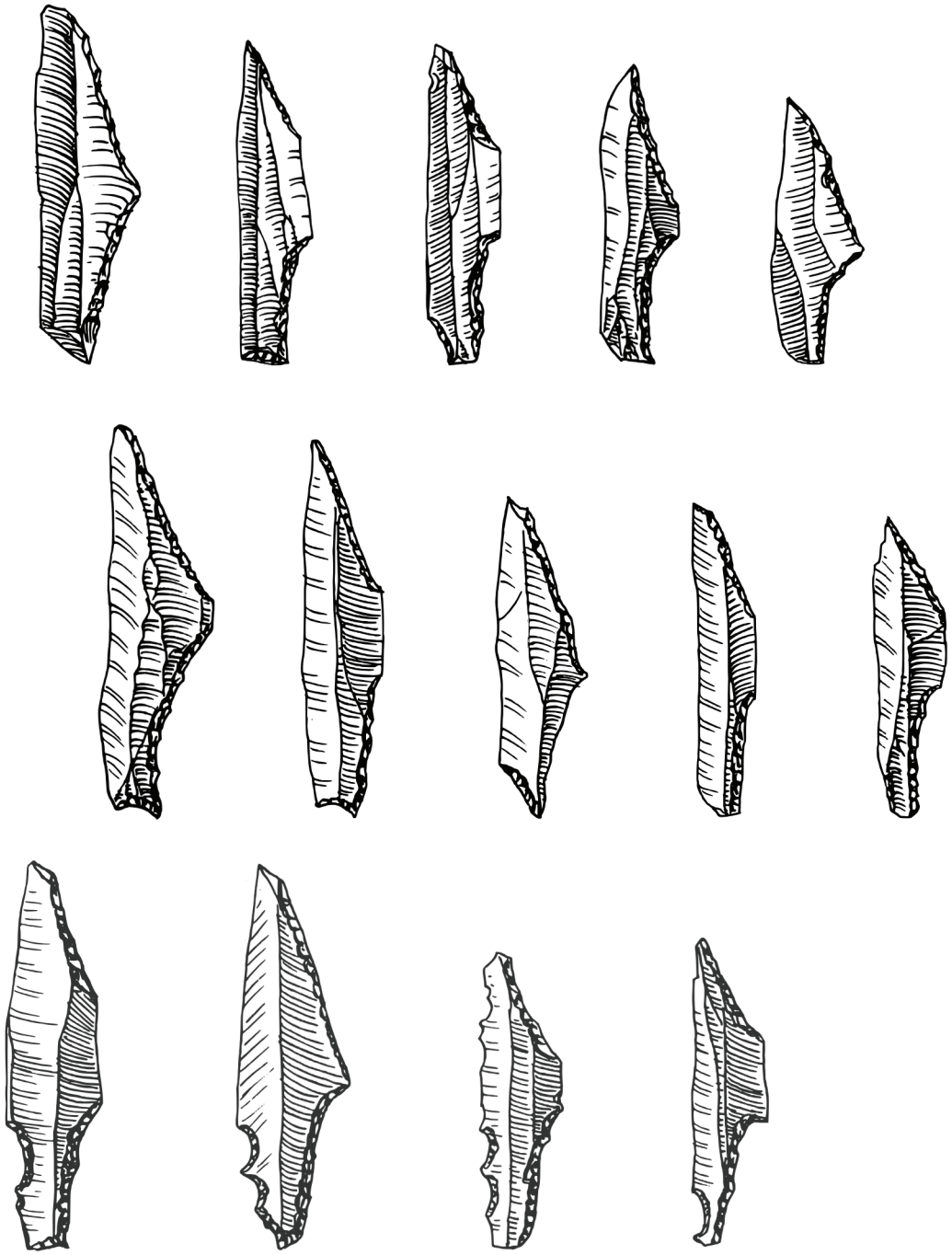


Plate 144b: Poggenwisch D
modified after Rust 1958

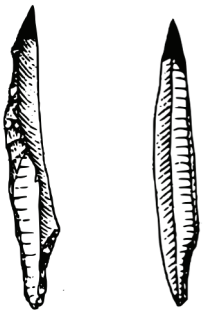


Plate 145: Ponte di Pietra
modified after Broglio & Lollini 1982



Plate 146: Pré-Aubert
modified after Smith 1966



Plate 147: Pushkari I
modified after Nuzhnyi 2015

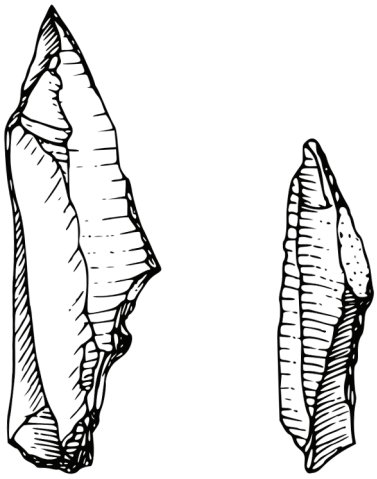


Plate 148: Ranchot, Abri des Cabônes
modified after David 1996

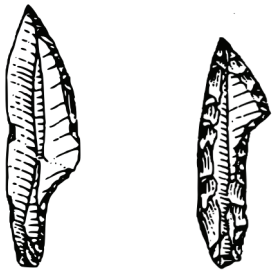


Plate 149: Riparo di Biedano, layer VI–II
modified after Pennacchioni & Tozzi 1986



Plate 150: Riparo Mochi, layer D
modified after Blanc 1953

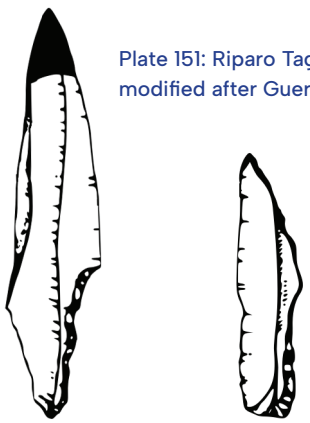


Plate 151: Riparo Tagliente, layer 15
modified after Guerreschi & Leonardi 1984



Plate 152: Roc de Sers
modified after Smith 1966

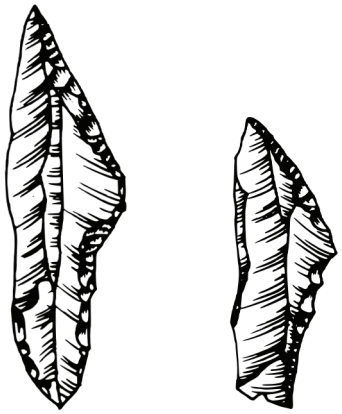


Plate 153: Rogow Opolski 9
modified after Rothert 1936



Plate 154: Saint-Front-de-Corgnac
modified after Smith 1966

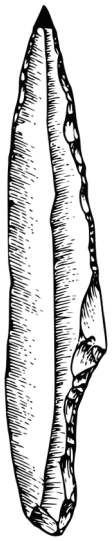


Plate 156: Sandalja II, layer c/d
modified after Malez 1987

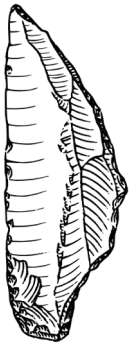


Plate 157: Schussenquelle, layer F
modified after Schuler 1994



Plate 155: Šalitrena Pecina, layer 4
modified after Mihailovic & Mihailovic 2007

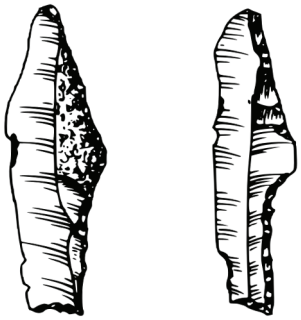
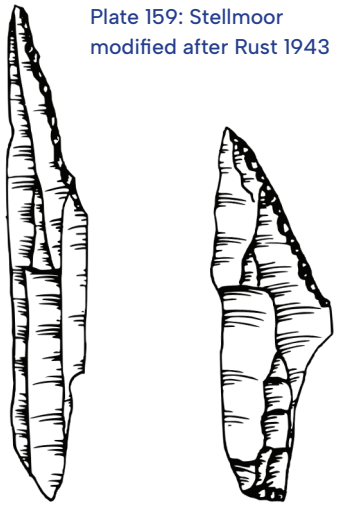


Plate 158: Siedlnica, layer 17a
modified after Burdukiewicz 1987

Plate 159: Stellmoor
modified after Rust 1943



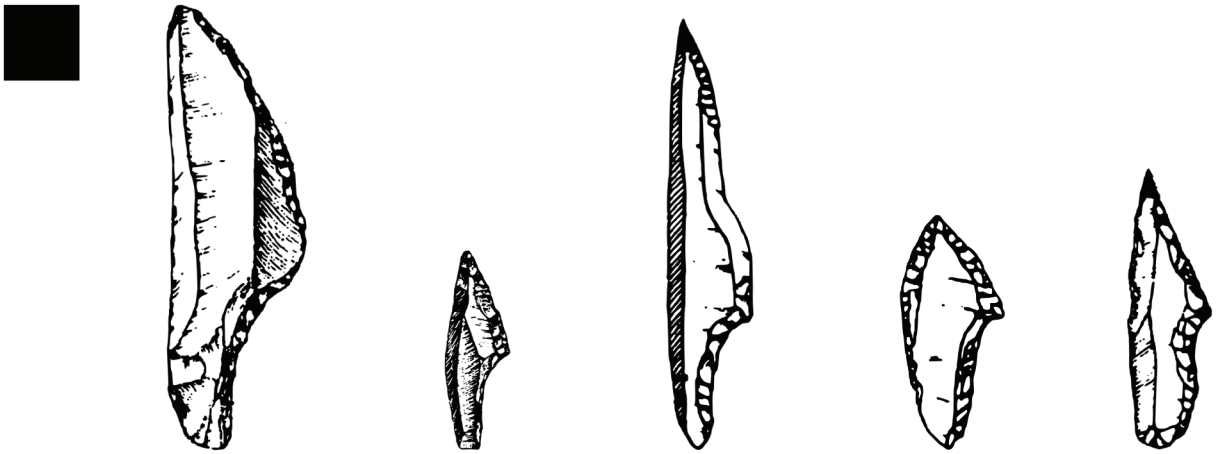


Plate 160: Taurisano, layer 23–6
modified after Bietti 1979

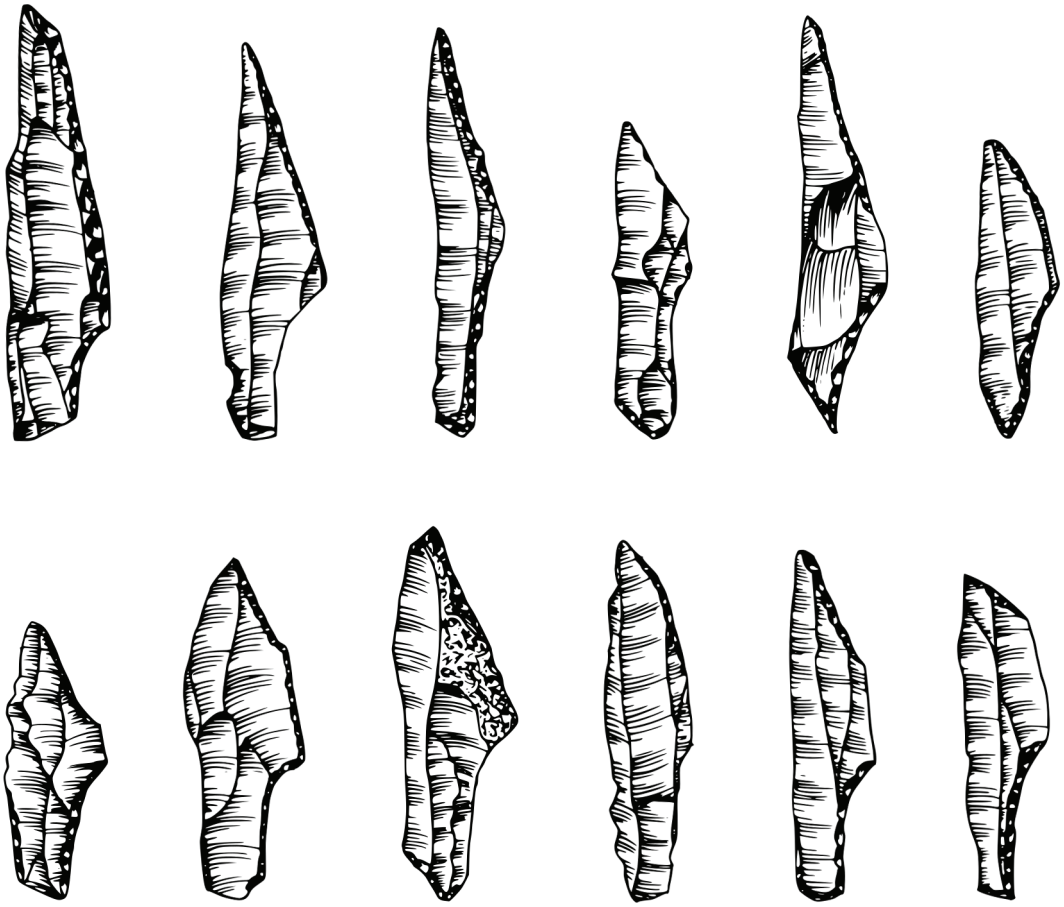


Plate 161: Teltwisch
modified after Tromnau 1975b

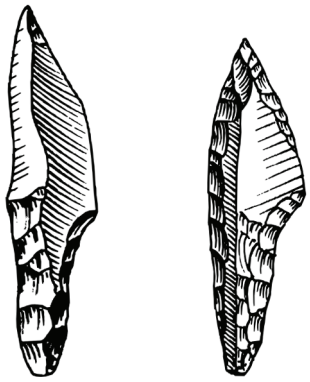


Plate 162: Tourtoirac
modified after Smith 1966

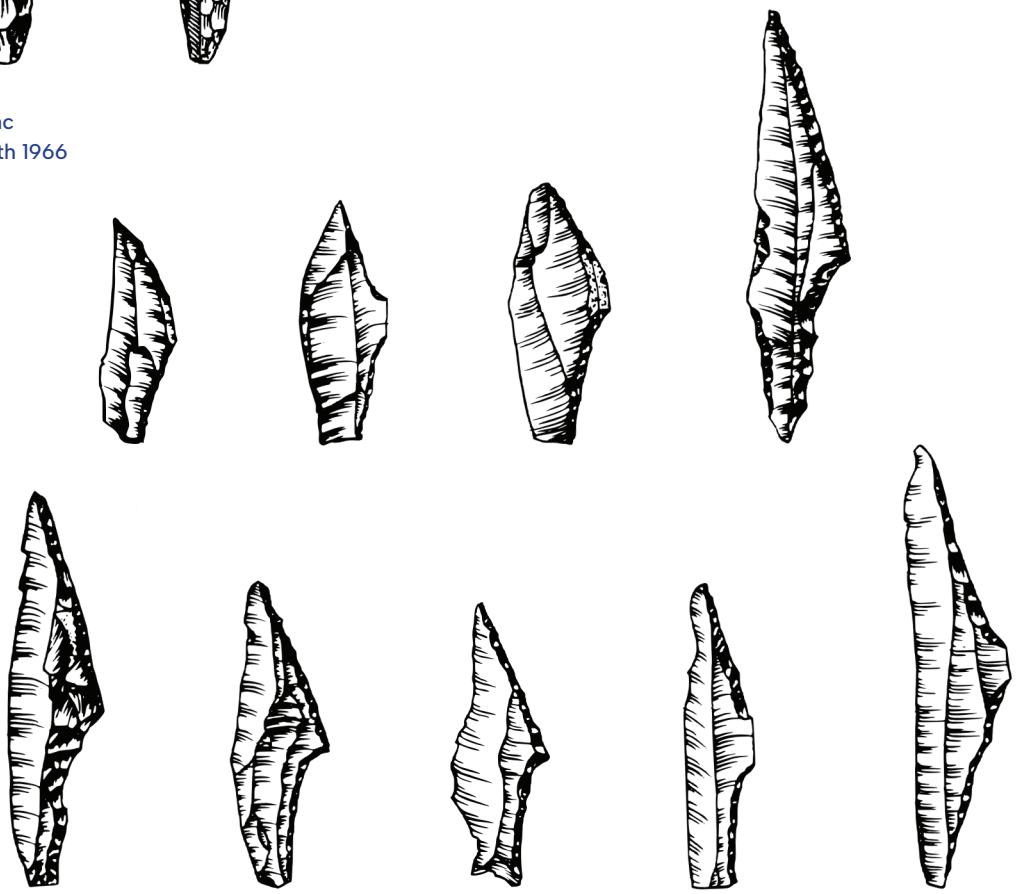


Plate 163: Ureterp 1
modified after Bohmers 1947



Plate 164: Vale Boi
modified after images courtesy of I. Schmidt and G. Koert



Plate 165: Vrbička Cave
modified after Boric & Christiani 2016

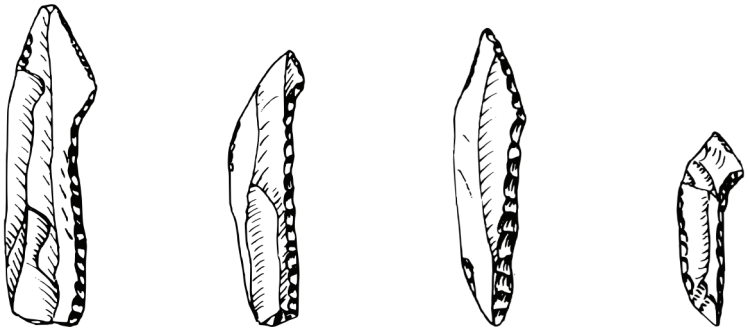


Plate 166: Willendorf II
modified after Felgenhauer 1957

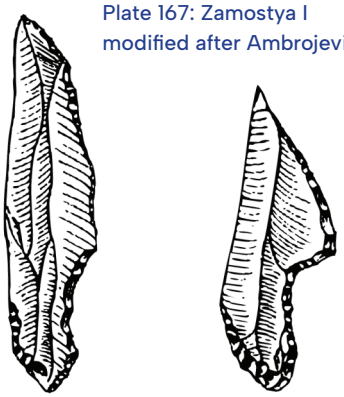


Plate 167: Zamostya I
modified after Ambrojevici & Popovici 1938

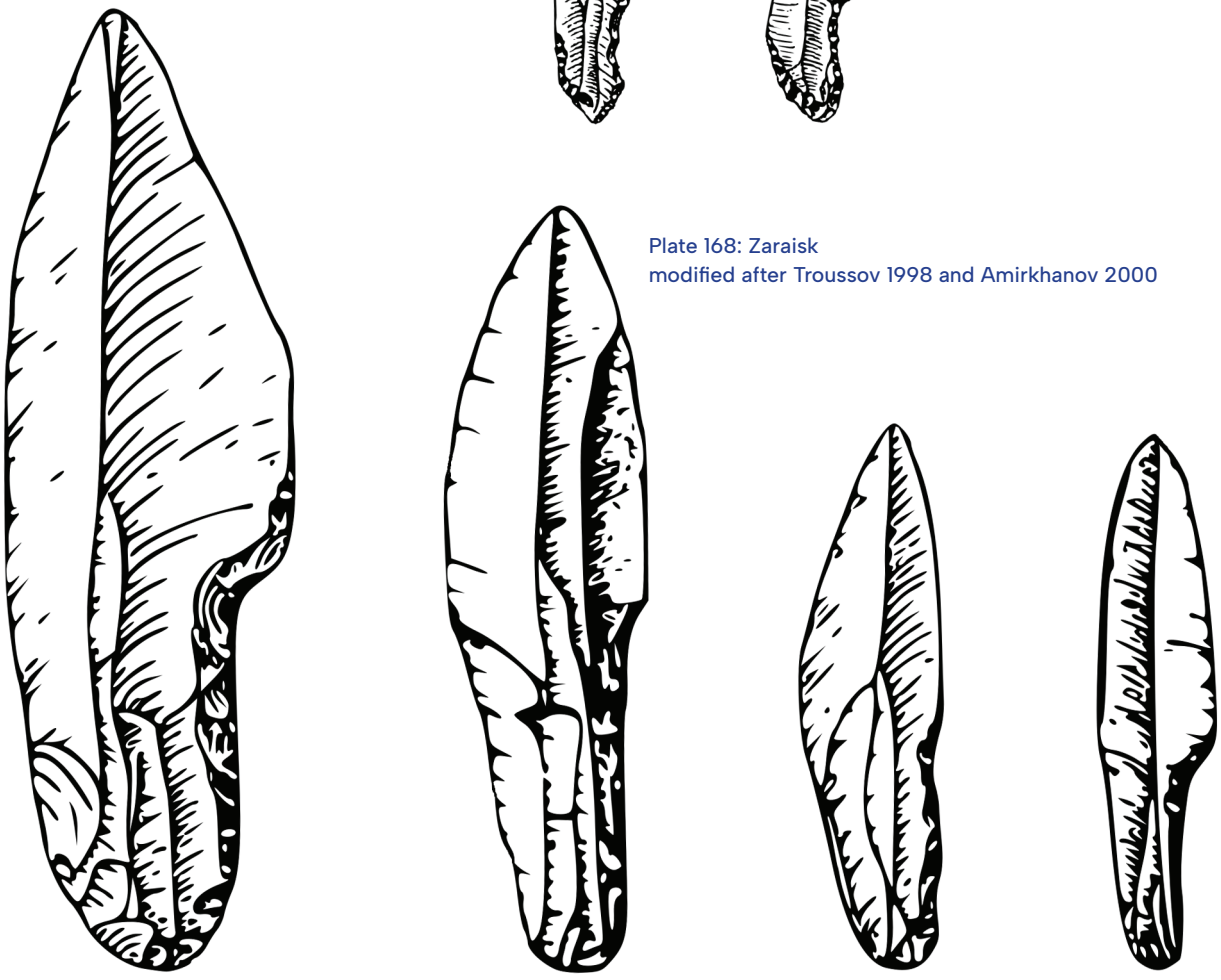


Plate 168: Zaraisk
modified after Troussov 1998 and Amirkhanov 2000

# APPENDIX TABLES

Appendix Table 1: RDA results with the calibrated ages ('ka calBP') as canonical variable on the 5000 year periodisation, category A assemblages only (dark red: p-value <= 0.05).

| mil. BP | 30th–26th | 26th–22th | 22th–18th | 18th–14th |
|---|---|---|---|---|
| SPs | 73 | 107 | 74 | 143 |
| assemblages | 16 | 20 | 11 | 24 |
| p | 0.08 | 0.003 | 0.029 | 0.134 |
| $R^2$ | 0.0268 | 0.0379 | 0.0347 | 0.0117 |

Appendix Table 2: RDA results with 'millennium BP' as canonical variable on the 5000 year periodisation (dark red: p-value <= 0.05).

| mil. BP | 30th–26th | 26th–22th | 22th–18th | 18th–14th |
|---|---|---|---|---|
| SPs | 79 | 112 | 78 | 154 |
| assemblages | 22 | 25 | 15 | 35 |
| p | 0.066 | 0.001 | 0.075 | 0.225 |
| $R^2$ | 0.0256 | 0.0418 | 0.0265 | 0.0091 |

Appendix Table 3: RDA results with the calibrated ages ('ka calBP') as canonical variable on the 4000 year periodisation, category A assemblages only (dark red: p-value <= 0.05).

| mil. BP | 30th–26th | 26th–23rd | 23rd–20th | 20th–17th | 17th–14th |
|---|---|---|---|---|---|
| SPs | 73 | 82 | 87 | 35 | 140 |
| assemblages | 16 | 16 | 12 | 6 | 23 |
| p | 0.08 | 0.004 | 0.009 | 0.037 | 0.153 |
| $R^2$ | 0.0268 | 0.0445 | 0.385 | 0.707 | 0.0114 |

Appendix Table 4: RDA results with 'millennium BP' as canonical variable on the 4000 year periodisation (dark red: p-value <= 0.05).

| mil. BP | 30th–26th | 26th–23rd | 23rd–20th | 20th–17th | 17th–14th |
|---|---|---|---|---|---|
| SPs | 79 | 87 | 90 | 39 | 150 |
| assemblages | 22 | 21 | 15 | 10 | 33 |
| p | 0.066 | 0.003 | 0.013 | 0.025 | 0.281 |
| $R^2$ | 0.0256 | 0.0553 | 0.0353 | 0.688 | 0.0083 |

Appendix Table 5: RDA results with the calibrated ages ('ka calBP') as canonical variable on the 3000 year periodisation, category A assemblages only (dark red: p-value <= 0.05).

| mil. BP | 30th–28th | 28th–26th | 26th–24th | 24th–22nd | 22nd–20th | 20th–18th | 18th–16th | 16th–14th |
|---|---|---|---|---|---|---|---|---|
| SPs | 75 | 59 | 66 | 76 | 71 | 22 | 55 | 55 |
| assemblages | 18 | 12 | 14 | 15 | 10 | 4 | 10 | 27 |
| p | 0.605 | 0.085 | 0.027 | 0.018 | 0.005 | 0.309 | 0.001 | 0.002 |
| $R^2$ | 0.0201 | 0.0334 | 0.0431 | 0.0405 | 0.0502 | 0.0573 | 0.1413 | 0.0431 |

Appendix Table 6: RDA results with 'millennium BP' as canonical variable on the 3000 year periodisation (dark red: p-value <= 0.05).

| mil. BP | 30th–28th | 28th–26th | 26th–24th | 24th–22nd | 22nd–20th | 20th–18th | 18th–16th | 16th–14th |
|---|---|---|---|---|---|---|---|---|
| SPs | 79 | 63 | 70 | 79 | 73 | 26 | 59 | 59 |
| assemblages | 22 | 16 | 18 | 18 | 12 | 8 | 14 | 31 |
| p | 0.098 | 0.126 | 0.003 | 0.001 | 0.036 | 0.87 | 0.001 | 0.001 |
| $R^2$ | 0.0463 | 0.0273 | 0.0623 | 0.0538 | 0.0348 | 0.0145 | 0.118 | 0.0359 |

Appendix Table 7: RDA results with the calibrated ages ('ka calBP') as canonical variable on the 2000 year periodisation, category A assemblages only (dark red: p-value <= 0.05).

| mil. BP | 30th–29th | 29th–28th | 28th–27th | 27th–26th | 26th–25th | 25th–24th | 24th–23rd | 23rd–22nd |
|---|---|---|---|---|---|---|---|---|
| SPs | 15 | 28 | 46 | 35 | 31 | 54 | 51 | 41 |
| assemblages | 5 | 6 | 9 | 7 | 5 | 12 | 11 | 6 |
| p | 0.115 | 0.179 | 0.05 | 0.003 | 0.002 | 0.004 | 0.437 | 0.234 |
| $R^2$ | 0.1377 | 0.0595 | 0.0461 | 0.1067 | 0.1467 | 0.085 | 0.0255 | 0.0322 |

| mil. BP | 22nd–21st | 21st–20th | 20th–19th | 19th–18th | 18th–17th | 17th–16th | 16th–15th | 15th–14th |
|---|---|---|---|---|---|---|---|---|
| SPs | 52 | 46 | 19 | 3 | 16 | 52 | 113 | 88 |
| assemblages | 7 | 5 | 3 | 1 | 3 | 9 | 19 | 14 |
| p | 0.008 | 0.006 | 0.079 | / | 0.082 | 0.001 | 0.001 | 0.222 |
| $R^2$ | 0.613 | 0.0758 | 0.0968 | / | 0.1307 | 0.1489 | 0.0502 | 0.0156 |

Appendix Table 8: RDA results with 'millennium BP' as canonical variable on the 2000 year periodisation (dark red: p-value <= 0.05).

| mil. BP | 30th–29th | 29th–28th | 28th–27th | 27th–26th | 26th–25th | 25th–24th | 24th–23rd | 23rd–22nd |
|---|---|---|---|---|---|---|---|---|
| SPs | 16 | 31 | 50 | 37 | 33 | 57 | 54 | 42 |
| assemblages | 6 | 9 | 13 | 9 | 7 | 15 | 14 | 7 |
| p | 0.04 | 0.086 | 0.277 | 0.107 | 0.005 | 0.002 | 0.418 | 0.233 |
| $R^2$ | 0.1552 | 0.0628 | 0.0247 | 0.0515 | 0.1057 | 0.0991 | 0.0197 | 0.032 |

| mil. BP | 22nd–21st | 21st–20th | 20th–19th | 19th–18th | 18th–17th | 17th–16th | 16th–15th | 15th–14th |
|---|---|---|---|---|---|---|---|---|
| SPs | 52 | 48 | 22 | 5 | 17 | 55 | 122 | 95 |
| assemblages | 7 | 7 | 6 | 3 | 4 | 12 | 28 | 21 |
| p | 0.007 | 0.006 | 0.079 | / | / | 0.001 | 0.001 | 0.72 |
| $R^2$ | 0.065 | 0.0705 | 0.0968 | / | / | 0.1207 | 0.0407 | 0.0063 |

Appendix Table 9: RDA results with the calibrated ages ('ka calBP') as canonical variable on the 1000 year periodisation, category A assemblages only (dark red: p-value <= 0.05).

| mil. BP | 30th | 29th | 28th | 27th | 26th | 25th | 24th | 23rd |
|---|---|---|---|---|---|---|---|---|
| SPs | 10 | 4 | 24 | 22 | 13 | 18 | 35 | 16 |
| assemblages | 3 | 1 | 5 | 4 | 3 | 2 | 9 | 2 |
| p | 0.205 | / | 0.005 | 0.005 | 0.002 | 0.002 | 0.07 | / |
| $R^2$ | 0.1603 | / | 0.1638 | 0.1466 | 0.3568 | 0.4074 | 0.0597 | / |

| mil. BP | 22nd | 21st | 20th | 19th | 18th | 17th | 16th | 15th | 14th |
|---|---|---|---|---|---|---|---|---|---|
| SPs | 25 | 27 | 19 | / | 3 | 13 | 39 | 74 | 14 |
| assemblages | 4 | 3 | 3 | / | 1 | 2 | 7 | 12 | 2 |
| p | 0.001 | 0.764 | 0.015 | / | / | 0.139 | 0.001 | 0.104 | 0.017 |
| $R^2$ | 0.22 | 0.0211 | 0.1728 | / | / | 0.146 | 0.2533 | 0.0249 | 0.2054 |

Appendix Table 10: Time-weight (0.01) matrix for Clustering Analysis (1000 years = 0.01).

| | GRA 30 | GRA 29 | GRA 28 | GRA 27 | GRA 26 | US 25 | US 24 | SAL 24 | EPI 24 | US 23 | LBA 23 | US 22 | TAR 22 | EPI 21 | LMA 21 | EPI 20 | LMA 20 | MMA 18 | MMA 17 | UMA-A 16 | UMA-B 16 | HAM 16 | UMA-A 15 | UMA-B 15 | HAM 15 | CRE 15 | HAM 14 | HAV 14 |
|---|---|---|---|---|---|---|---|---|---|---|---|---|---|---|---|---|---|---|---|---|---|---|---|---|---|---|---|---|
| **GRA 30** | | 0,01 | 0,02 | 0,03 | 0,04 | 0,05 | 0,06 | 0,06 | 0,06 | 0,07 | 0,07 | 0,08 | 0,08 | 0,09 | 0,09 | 0,10 | 0,10 | 0,12 | 0,13 | 0,14 | 0,14 | 0,14 | 0,15 | 0,15 | 0,15 | 0,15 | 0,16 | 0,16 |
| **GRA 29** | 0,01 | | 0,01 | 0,02 | 0,03 | 0,04 | 0,05 | 0,05 | 0,05 | 0,06 | 0,06 | 0,07 | 0,07 | 0,08 | 0,08 | 0,09 | 0,09 | 0,11 | 0,12 | 0,13 | 0,13 | 0,13 | 0,14 | 0,14 | 0,14 | 0,14 | 0,15 | 0,15 |
| **GRA 28** | 0,02 | 0,01 | | 0,01 | 0,02 | 0,03 | 0,04 | 0,04 | 0,04 | 0,05 | 0,05 | 0,06 | 0,06 | 0,07 | 0,07 | 0,08 | 0,08 | 0,10 | 0,11 | 0,12 | 0,12 | 0,12 | 0,13 | 0,13 | 0,13 | 0,13 | 0,14 | 0,14 |
| **GRA 27** | 0,03 | 0,02 | 0,01 | | 0,01 | 0,02 | 0,03 | 0,03 | 0,03 | 0,04 | 0,04 | 0,05 | 0,05 | 0,06 | 0,06 | 0,07 | 0,07 | 0,09 | 0,10 | 0,11 | 0,11 | 0,11 | 0,12 | 0,12 | 0,12 | 0,12 | 0,13 | 0,13 |
| **GRA 26** | 0,04 | 0,03 | 0,02 | 0,01 | | 0,01 | 0,02 | 0,02 | 0,02 | 0,03 | 0,03 | 0,04 | 0,04 | 0,05 | 0,05 | 0,06 | 0,06 | 0,08 | 0,09 | 0,10 | 0,10 | 0,10 | 0,11 | 0,11 | 0,11 | 0,11 | 0,12 | 0,12 |
| **US 25** | 0,05 | 0,04 | 0,03 | 0,02 | 0,01 | | 0,01 | 0,01 | 0,01 | 0,02 | 0,02 | 0,03 | 0,03 | 0,04 | 0,04 | 0,05 | 0,05 | 0,07 | 0,08 | 0,09 | 0,09 | 0,09 | 0,10 | 0,10 | 0,10 | 0,10 | 0,11 | 0,11 |
| **US 24** | 0,06 | 0,05 | 0,04 | 0,03 | 0,02 | 0,01 | | 0,00 | 0,00 | 0,01 | 0,01 | 0,02 | 0,02 | 0,03 | 0,03 | 0,04 | 0,04 | 0,06 | 0,07 | 0,08 | 0,08 | 0,08 | 0,09 | 0,09 | 0,09 | 0,09 | 0,10 | 0,10 |
| **SAL 24** | 0,06 | 0,05 | 0,04 | 0,03 | 0,02 | 0,01 | 0,00 | | 0,00 | 0,01 | 0,01 | 0,02 | 0,02 | 0,03 | 0,03 | 0,04 | 0,04 | 0,06 | 0,07 | 0,08 | 0,08 | 0,08 | 0,09 | 0,09 | 0,09 | 0,09 | 0,10 | 0,10 |
| **EPI 24** | 0,06 | 0,05 | 0,04 | 0,03 | 0,02 | 0,01 | 0,00 | 0,00 | | 0,01 | 0,01 | 0,02 | 0,02 | 0,03 | 0,03 | 0,04 | 0,04 | 0,06 | 0,07 | 0,08 | 0,08 | 0,08 | 0,09 | 0,09 | 0,09 | 0,09 | 0,10 | 0,10 |
| **US 23** | 0,07 | 0,06 | 0,05 | 0,04 | 0,03 | 0,02 | 0,01 | 0,01 | 0,01 | | 0,00 | 0,01 | 0,01 | 0,02 | 0,02 | 0,03 | 0,03 | 0,05 | 0,06 | 0,07 | 0,07 | 0,07 | 0,08 | 0,08 | 0,08 | 0,08 | 0,09 | 0,09 |
| **LBA 23** | 0,07 | 0,06 | 0,05 | 0,04 | 0,03 | 0,02 | 0,01 | 0,01 | 0,01 | 0,00 | | 0,01 | 0,01 | 0,02 | 0,02 | 0,03 | 0,03 | 0,05 | 0,06 | 0,07 | 0,07 | 0,07 | 0,08 | 0,08 | 0,08 | 0,08 | 0,09 | 0,09 |
| **US 22** | 0,08 | 0,07 | 0,06 | 0,05 | 0,04 | 0,03 | 0,02 | 0,02 | 0,02 | 0,01 | 0,01 | | 0,00 | 0,01 | 0,01 | 0,02 | 0,02 | 0,04 | 0,05 | 0,06 | 0,06 | 0,06 | 0,07 | 0,07 | 0,07 | 0,07 | 0,08 | 0,08 |
| **TAR 22** | 0,08 | 0,07 | 0,06 | 0,05 | 0,04 | 0,03 | 0,02 | 0,02 | 0,02 | 0,01 | 0,01 | 0,00 | | 0,01 | 0,01 | 0,02 | 0,02 | 0,04 | 0,05 | 0,06 | 0,06 | 0,06 | 0,07 | 0,07 | 0,07 | 0,07 | 0,08 | 0,08 |
| **EPI 21** | 0,09 | 0,08 | 0,07 | 0,06 | 0,05 | 0,04 | 0,03 | 0,03 | 0,03 | 0,02 | 0,02 | 0,01 | 0,01 | | 0,00 | 0,01 | 0,01 | 0,03 | 0,04 | 0,05 | 0,05 | 0,05 | 0,06 | 0,06 | 0,06 | 0,06 | 0,07 | 0,07 |
| **LMA 21** | 0,09 | 0,08 | 0,07 | 0,06 | 0,05 | 0,04 | 0,03 | 0,03 | 0,03 | 0,02 | 0,02 | 0,01 | 0,01 | 0,00 | | 0,01 | 0,01 | 0,03 | 0,04 | 0,05 | 0,05 | 0,05 | 0,06 | 0,06 | 0,06 | 0,06 | 0,07 | 0,07 |
| **EPI 20** | 0,10 | 0,09 | 0,08 | 0,07 | 0,06 | 0,05 | 0,04 | 0,04 | 0,04 | 0,03 | 0,03 | 0,02 | 0,02 | 0,01 | 0,01 | | 0,00 | 0,02 | 0,03 | 0,04 | 0,04 | 0,04 | 0,05 | 0,05 | 0,05 | 0,05 | 0,06 | 0,06 |
| **LMA 20** | 0,10 | 0,09 | 0,08 | 0,07 | 0,06 | 0,05 | 0,04 | 0,04 | 0,04 | 0,03 | 0,03 | 0,02 | 0,02 | 0,01 | 0,01 | 0,00 | | 0,02 | 0,03 | 0,04 | 0,04 | 0,04 | 0,05 | 0,05 | 0,05 | 0,05 | 0,06 | 0,06 |
| **MMA 18** | 0,12 | 0,11 | 0,10 | 0,09 | 0,08 | 0,07 | 0,06 | 0,06 | 0,06 | 0,05 | 0,05 | 0,04 | 0,04 | 0,03 | 0,03 | 0,02 | 0,02 | | 0,01 | 0,02 | 0,02 | 0,02 | 0,03 | 0,03 | 0,03 | 0,03 | 0,04 | 0,04 |
| **MMA 17** | 0,13 | 0,12 | 0,11 | 0,10 | 0,09 | 0,08 | 0,07 | 0,07 | 0,07 | 0,06 | 0,06 | 0,05 | 0,05 | 0,04 | 0,04 | 0,03 | 0,03 | 0,01 | | 0,01 | 0,01 | 0,01 | 0,02 | 0,02 | 0,02 | 0,02 | 0,03 | 0,03 |
| **UMA-A 16** | 0,14 | 0,13 | 0,12 | 0,11 | 0,10 | 0,09 | 0,08 | 0,08 | 0,08 | 0,07 | 0,07 | 0,06 | 0,06 | 0,05 | 0,05 | 0,04 | 0,04 | 0,02 | 0,01 | | 0,00 | 0,00 | 0,01 | 0,01 | 0,01 | 0,01 | 0,02 | 0,02 |
| **UMA-B 16** | 0,14 | 0,13 | 0,12 | 0,11 | 0,10 | 0,09 | 0,08 | 0,08 | 0,08 | 0,07 | 0,07 | 0,06 | 0,06 | 0,05 | 0,05 | 0,04 | 0,04 | 0,02 | 0,01 | 0,00 | | 0,00 | 0,01 | 0,01 | 0,01 | 0,01 | 0,02 | 0,02 |
| **HAM 16** | 0,14 | 0,13 | 0,12 | 0,11 | 0,10 | 0,09 | 0,08 | 0,08 | 0,08 | 0,07 | 0,07 | 0,06 | 0,06 | 0,05 | 0,05 | 0,04 | 0,04 | 0,02 | 0,01 | 0,00 | 0,00 | | 0,01 | 0,01 | 0,01 | 0,01 | 0,02 | 0,02 |
| **UMA-A 15** | 0,15 | 0,14 | 0,13 | 0,12 | 0,11 | 0,10 | 0,09 | 0,09 | 0,09 | 0,08 | 0,08 | 0,07 | 0,07 | 0,06 | 0,06 | 0,05 | 0,05 | 0,03 | 0,02 | 0,01 | 0,01 | 0,01 | | 0,00 | 0,00 | 0,00 | 0,01 | 0,01 |
| **UMA-B 15** | 0,15 | 0,14 | 0,13 | 0,12 | 0,11 | 0,10 | 0,09 | 0,09 | 0,09 | 0,08 | 0,08 | 0,07 | 0,07 | 0,06 | 0,06 | 0,05 | 0,05 | 0,03 | 0,02 | 0,01 | 0,01 | 0,01 | 0,00 | | 0,00 | 0,00 | 0,01 | 0,01 |
| **HAM 15** | 0,15 | 0,14 | 0,13 | 0,12 | 0,11 | 0,10 | 0,09 | 0,09 | 0,09 | 0,08 | 0,08 | 0,07 | 0,07 | 0,06 | 0,06 | 0,05 | 0,05 | 0,03 | 0,02 | 0,01 | 0,01 | 0,01 | 0,00 | 0,00 | | 0,00 | 0,01 | 0,01 |
| **CRE 15** | 0,15 | 0,14 | 0,13 | 0,12 | 0,11 | 0,10 | 0,09 | 0,09 | 0,09 | 0,08 | 0,08 | 0,07 | 0,07 | 0,06 | 0,06 | 0,05 | 0,05 | 0,03 | 0,02 | 0,01 | 0,01 | 0,01 | 0,00 | 0,00 | 0,00 | | 0,01 | 0,01 |
| **HAM 14** | 0,16 | 0,15 | 0,14 | 0,13 | 0,12 | 0,11 | 0,10 | 0,10 | 0,10 | 0,09 | 0,09 | 0,08 | 0,08 | 0,07 | 0,07 | 0,06 | 0,06 | 0,04 | 0,03 | 0,02 | 0,02 | 0,02 | 0,01 | 0,01 | 0,01 | 0,01 | | 0,00 |
| **HAV 14** | 0,16 | 0,15 | 0,14 | 0,13 | 0,12 | 0,11 | 0,10 | 0,10 | 0,10 | 0,09 | 0,09 | 0,08 | 0,08 | 0,07 | 0,07 | 0,06 | 0,06 | 0,04 | 0,03 | 0,02 | 0,02 | 0,02 | 0,01 | 0,01 | 0,01 | 0,01 | 0,00 | |

Appendix Table 11: Geographical distance weight matrix for Clustering Analysis (1000 km = 0.05).

| | GRA 30 | GRA 29 | GRA 28 | GRA 27 | GRA 26 | US 25 | US 24 | SAL 24 | EPI 24 | US 23 | LBA 23 | US 22 | TAR 22 | EPI 21 | LMA 21 | EPI 20 | LMA 20 | MMA 18 | MMA 17 | UMA-A 16 | UMA-B 16 | HAM 16 | UMA-A 15 | UMA-B 15 | HAM 15 | CRE 15 | HAM 14 | HAV 14 |
|---|---|---|---|---|---|---|---|---|---|---|---|---|---|---|---|---|---|---|---|---|---|---|---|---|---|---|---|---|
| **GRA 30** | | 0,02 | 0,04 | 0,02 | 0,10 | 0,15 | 0,13 | 0,08 | 0,04 | 0,13 | 0,10 | 0,13 | 0,08 | 0,04 | 0,09 | 0,05 | 0,08 | 0,06 | 0,11 | 0,11 | 0,07 | 0,02 | 0,08 | 0,07 | 0,05 | 0,12 | 0,06 | 0,08 |
| **GRA 29** | 0,02 | | 0,05 | 0,03 | 0,12 | 0,14 | 0,12 | 0,07 | 0,02 | 0,12 | 0,09 | 0,12 | 0,07 | 0,02 | 0,08 | 0,04 | 0,07 | 0,05 | 0,10 | 0,10 | 0,07 | 0,03 | 0,07 | 0,06 | 0,05 | 0,11 | 0,06 | 0,07 |
| **GRA 28** | 0,04 | 0,05 | | 0,02 | 0,06 | 0,19 | 0,17 | 0,12 | 0,07 | 0,17 | 0,14 | 0,17 | 0,12 | 0,07 | 0,13 | 0,09 | 0,12 | 0,10 | 0,15 | 0,15 | 0,11 | 0,05 | 0,12 | 0,11 | 0,08 | 0,16 | 0,09 | 0,11 |
| **GRA 27** | 0,02 | 0,03 | 0,02 | | 0,08 | 0,17 | 0,15 | 0,10 | 0,05 | 0,15 | 0,12 | 0,15 | 0,10 | 0,05 | 0,11 | 0,07 | 0,10 | 0,08 | 0,13 | 0,13 | 0,09 | 0,04 | 0,10 | 0,09 | 0,07 | 0,14 | 0,07 | 0,09 |
| **GRA 26** | 0,10 | 0,12 | 0,06 | 0,08 | | 0,25 | 0,24 | 0,19 | 0,13 | 0,23 | 0,20 | 0,23 | 0,18 | 0,13 | 0,19 | 0,15 | 0,19 | 0,16 | 0,21 | 0,21 | 0,18 | 0,12 | 0,19 | 0,17 | 0,14 | 0,22 | 0,15 | 0,17 |
| **US 25** | 0,15 | 0,14 | 0,19 | 0,17 | 0,25 | | 0,01 | 0,06 | 0,12 | 0,02 | 0,05 | 0,02 | 0,07 | 0,12 | 0,06 | 0,10 | 0,06 | 0,09 | 0,04 | 0,04 | 0,08 | 0,14 | 0,07 | 0,08 | 0,12 | 0,07 | 0,12 | 0,10 |
| **US 24** | 0,13 | 0,12 | 0,17 | 0,15 | 0,24 | 0,01 | | 0,05 | 0,11 | 0,01 | 0,04 | 0,02 | 0,05 | 0,11 | 0,04 | 0,09 | 0,05 | 0,08 | 0,03 | 0,03 | 0,06 | 0,13 | 0,06 | 0,07 | 0,11 | 0,07 | 0,11 | 0,09 |
| **SAL 24** | 0,08 | 0,07 | 0,12 | 0,10 | 0,19 | 0,06 | 0,05 | | 0,06 | 0,05 | 0,02 | 0,05 | 0,00 | 0,06 | 0,01 | 0,04 | 0,00 | 0,03 | 0,03 | 0,02 | 0,02 | 0,08 | 0,02 | 0,02 | 0,07 | 0,06 | 0,06 | 0,05 |
| **EPI 24** | 0,04 | 0,02 | 0,07 | 0,05 | 0,13 | 0,12 | 0,11 | 0,06 | | 0,11 | 0,08 | 0,11 | 0,06 | 0,01 | 0,07 | 0,02 | 0,06 | 0,04 | 0,09 | 0,08 | 0,06 | 0,05 | 0,06 | 0,06 | 0,06 | 0,11 | 0,06 | 0,07 |
| **US 23** | 0,13 | 0,12 | 0,17 | 0,15 | 0,23 | 0,02 | 0,01 | 0,05 | 0,11 | | 0,03 | 0,00 | 0,05 | 0,11 | 0,04 | 0,08 | 0,05 | 0,07 | 0,02 | 0,02 | 0,06 | 0,12 | 0,05 | 0,06 | 0,10 | 0,05 | 0,10 | 0,08 |
| **LBA 23** | 0,10 | 0,09 | 0,14 | 0,12 | 0,20 | 0,05 | 0,04 | 0,02 | 0,08 | 0,03 | | 0,03 | 0,02 | 0,08 | 0,01 | 0,06 | 0,02 | 0,04 | 0,01 | 0,01 | 0,03 | 0,09 | 0,02 | 0,03 | 0,08 | 0,05 | 0,07 | 0,05 |
| **US 22** | 0,13 | 0,12 | 0,17 | 0,15 | 0,23 | 0,02 | 0,02 | 0,05 | 0,11 | 0,00 | 0,03 | | 0,05 | 0,11 | 0,04 | 0,08 | 0,05 | 0,07 | 0,02 | 0,02 | 0,06 | 0,12 | 0,05 | 0,06 | 0,10 | 0,05 | 0,10 | 0,08 |
| **TAR 22** | 0,08 | 0,07 | 0,12 | 0,10 | 0,18 | 0,07 | 0,05 | 0,00 | 0,06 | 0,05 | 0,02 | 0,05 | | 0,06 | 0,01 | 0,04 | 0,00 | 0,02 | 0,03 | 0,03 | 0,02 | 0,08 | 0,02 | 0,02 | 0,06 | 0,06 | 0,06 | 0,05 |
| **EPI 21** | 0,04 | 0,02 | 0,07 | 0,05 | 0,13 | 0,12 | 0,11 | 0,06 | 0,01 | 0,11 | 0,08 | 0,11 | 0,06 | | 0,07 | 0,02 | 0,06 | 0,05 | 0,09 | 0,09 | 0,06 | 0,05 | 0,07 | 0,06 | 0,07 | 0,11 | 0,07 | 0,08 |
| **LMA 21** | 0,09 | 0,08 | 0,13 | 0,11 | 0,19 | 0,06 | 0,04 | 0,01 | 0,07 | 0,04 | 0,01 | 0,04 | 0,01 | 0,07 | | 0,05 | 0,01 | 0,03 | 0,02 | 0,02 | 0,02 | 0,09 | 0,02 | 0,03 | 0,07 | 0,05 | 0,07 | 0,05 |
| **EPI 20** | 0,05 | 0,04 | 0,09 | 0,07 | 0,15 | 0,10 | 0,09 | 0,04 | 0,02 | 0,08 | 0,06 | 0,08 | 0,04 | 0,02 | 0,05 | | 0,04 | 0,03 | 0,07 | 0,06 | 0,04 | 0,06 | 0,05 | 0,04 | 0,06 | 0,09 | 0,06 | 0,07 |
| **LMA 20** | 0,08 | 0,07 | 0,12 | 0,10 | 0,19 | 0,06 | 0,05 | 0,00 | 0,06 | 0,05 | 0,02 | 0,05 | 0,00 | 0,06 | 0,01 | 0,04 | | 0,03 | 0,03 | 0,02 | 0,02 | 0,08 | 0,02 | 0,02 | 0,07 | 0,06 | 0,06 | 0,05 |
| **MMA 18** | 0,06 | 0,05 | 0,10 | 0,08 | 0,16 | 0,09 | 0,08 | 0,03 | 0,04 | 0,07 | 0,04 | 0,07 | 0,02 | 0,05 | 0,03 | 0,03 | 0,03 | | 0,05 | 0,05 | 0,02 | 0,05 | 0,02 | 0,01 | 0,04 | 0,07 | 0,04 | 0,04 |
| **MMA 17** | 0,11 | 0,10 | 0,15 | 0,13 | 0,21 | 0,04 | 0,03 | 0,03 | 0,09 | 0,02 | 0,01 | 0,02 | 0,03 | 0,09 | 0,02 | 0,07 | 0,03 | 0,05 | | 0,00 | 0,03 | 0,10 | 0,03 | 0,04 | 0,08 | 0,04 | 0,08 | 0,06 |
| **UMA-A 16** | 0,11 | 0,10 | 0,15 | 0,13 | 0,21 | 0,04 | 0,03 | 0,02 | 0,08 | 0,02 | 0,01 | 0,02 | 0,03 | 0,09 | 0,02 | 0,06 | 0,02 | 0,05 | 0,00 | | 0,03 | 0,10 | 0,03 | 0,04 | 0,08 | 0,05 | 0,08 | 0,06 |
| **UMA-B 16** | 0,07 | 0,07 | 0,11 | 0,09 | 0,18 | 0,08 | 0,06 | 0,02 | 0,06 | 0,06 | 0,03 | 0,06 | 0,02 | 0,06 | 0,02 | 0,04 | 0,02 | 0,02 | 0,03 | 0,03 | | 0,07 | 0,01 | 0,00 | 0,05 | 0,05 | 0,04 | 0,03 |
| **HAM 16** | 0,02 | 0,03 | 0,05 | 0,04 | 0,12 | 0,14 | 0,13 | 0,08 | 0,05 | 0,12 | 0,09 | 0,12 | 0,08 | 0,05 | 0,09 | 0,06 | 0,08 | 0,05 | 0,10 | 0,10 | 0,07 | | 0,07 | 0,06 | 0,03 | 0,10 | 0,04 | 0,06 |
| **UMA-A 15** | 0,08 | 0,07 | 0,12 | 0,10 | 0,19 | 0,07 | 0,06 | 0,02 | 0,06 | 0,05 | 0,02 | 0,05 | 0,02 | 0,07 | 0,02 | 0,05 | 0,02 | 0,02 | 0,03 | 0,03 | 0,01 | 0,07 | | 0,01 | 0,06 | 0,05 | 0,05 | 0,03 |
| **UMA-B 15** | 0,07 | 0,06 | 0,11 | 0,09 | 0,17 | 0,08 | 0,07 | 0,02 | 0,06 | 0,06 | 0,03 | 0,06 | 0,02 | 0,06 | 0,03 | 0,04 | 0,02 | 0,01 | 0,04 | 0,04 | 0,00 | 0,06 | 0,01 | | 0,05 | 0,05 | 0,04 | 0,03 |
| **HAM 15** | 0,05 | 0,05 | 0,08 | 0,07 | 0,14 | 0,12 | 0,11 | 0,07 | 0,06 | 0,10 | 0,08 | 0,10 | 0,06 | 0,07 | 0,07 | 0,06 | 0,07 | 0,04 | 0,08 | 0,08 | 0,05 | 0,03 | 0,06 | 0,05 | | 0,08 | 0,01 | 0,03 |
| **CRE 15** | 0,12 | 0,11 | 0,16 | 0,14 | 0,22 | 0,07 | 0,07 | 0,06 | 0,11 | 0,05 | 0,05 | 0,05 | 0,06 | 0,11 | 0,05 | 0,09 | 0,06 | 0,07 | 0,04 | 0,05 | 0,05 | 0,10 | 0,05 | 0,05 | 0,08 | | 0,07 | 0,04 |
| **HAM 14** | 0,06 | 0,06 | 0,09 | 0,07 | 0,15 | 0,12 | 0,11 | 0,06 | 0,06 | 0,10 | 0,07 | 0,10 | 0,06 | 0,07 | 0,07 | 0,06 | 0,06 | 0,04 | 0,08 | 0,08 | 0,04 | 0,04 | 0,05 | 0,04 | 0,01 | 0,07 | | 0,02 |
| **HAV 14** | 0,08 | 0,07 | 0,11 | 0,09 | 0,17 | 0,10 | 0,09 | 0,05 | 0,07 | 0,08 | 0,05 | 0,08 | 0,05 | 0,08 | 0,05 | 0,07 | 0,05 | 0,04 | 0,06 | 0,06 | 0,03 | 0,06 | 0,03 | 0,03 | 0,03 | 0,04 | 0,02 | |

Appendix Table 12: Distance-Matrix for HCA based on the time-weighted (0.01) average change rates between averages of samples (colour scale: dark – light = pronounced morphometric differences – moderate differences – notable morphometric similarities (1.15 – 0.32 – 0.00). Abbreviations: GRA = Late Gravettian; US = Upper Solutrean; SAL = Salpetrian; LBA = Late Badegoulian; EPI = Epigravettian; TAR = Tardigravettian; LMA = Lower Magdalenian; MMA = Middle Magdalenian; UMA = Upper Magdalenian; HAM = Hamburgian; CRE = Creswellian; HAV = Havelte).

| | GRA 30 | GRA 29 | GRA 28 | GRA 27 | GRA 26 | US 25 | US 24 | SAL 24 | EPI 24 | US 23 | LBA 23 | US 22 | TAR 22 | EPI 21 | LMA 21 | EPI 20 | LMA 20 | MMA 18 | MMA 17 | UMA-A 16 | UMA-B 16 | HAM 16 | UMA-A 15 | UMA-B 15 | HAM 15 | CRE 15 | HAM 14 | HAV 14 |
|---|---|---|---|---|---|---|---|---|---|---|---|---|---|---|---|---|---|---|---|---|---|---|---|---|---|---|---|---|
| GRA 30 | | 0,31 | 0,25 | 0,18 | 0,28 | 0,55 | 0,51 | 0,62 | 0,45 | 0,46 | 0,24 | 0,45 | 0,94 | 0,44 | 0,76 | 0,38 | 0,72 | 0,61 | 0,63 | 0,42 | 0,56 | 0,53 | 0,39 | 0,59 | 0,54 | 0,44 | 0,49 | 0,47 |
| GRA 29 | 0,31 | | 0,22 | 0,17 | 0,31 | 0,34 | 0,37 | 0,37 | 0,27 | 0,23 | 0,36 | 0,31 | 0,54 | 0,20 | 0,44 | 0,32 | 0,45 | 0,43 | 0,36 | 0,42 | 0,47 | 0,42 | 0,34 | 0,47 | 0,31 | 0,40 | 0,38 | 0,25 |
| GRA 28 | 0,25 | 0,22 | | 0,12 | 0,12 | 0,57 | 0,55 | 0,63 | 0,48 | 0,41 | 0,31 | 0,44 | 0,66 | 0,35 | 0,50 | 0,41 | 0,45 | 0,58 | 0,52 | 0,27 | 0,42 | 0,34 | 0,32 | 0,42 | 0,40 | 0,34 | 0,40 | 0,41 |
| GRA 27 | 0,18 | 0,17 | 0,12 | | 0,15 | 0,43 | 0,44 | 0,52 | 0,39 | 0,28 | 0,24 | 0,33 | 0,69 | 0,26 | 0,53 | 0,30 | 0,49 | 0,48 | 0,43 | 0,37 | 0,40 | 0,34 | 0,37 | 0,40 | 0,35 | 0,28 | 0,32 | 0,29 |
| GRA 26 | 0,28 | 0,31 | 0,12 | 0,15 | | 0,54 | 0,53 | 0,65 | 0,50 | 0,40 | 0,29 | 0,39 | 0,71 | 0,38 | 0,52 | 0,37 | 0,44 | 0,54 | 0,54 | 0,35 | 0,33 | 0,29 | 0,40 | 0,35 | 0,38 | 0,26 | 0,33 | 0,41 |
| US 25 | 0,55 | 0,34 | 0,57 | 0,43 | 0,54 | | 0,14 | 0,12 | 0,22 | 0,13 | 0,33 | 0,15 | 0,37 | 0,20 | 0,35 | 0,21 | 0,41 | 0,19 | 0,25 | 0,58 | 0,47 | 0,46 | 0,50 | 0,47 | 0,31 | 0,39 | 0,39 | 0,26 |
| US 24 | 0,51 | 0,37 | 0,55 | 0,44 | 0,53 | 0,14 | | 0,16 | 0,15 | 0,23 | 0,21 | 0,24 | 0,56 | 0,32 | 0,49 | 0,25 | 0,56 | 0,27 | 0,36 | 0,67 | 0,58 | 0,59 | 0,54 | 0,59 | 0,42 | 0,50 | 0,50 | 0,36 |
| SAL 24 | 0,62 | 0,37 | 0,63 | 0,52 | 0,65 | 0,12 | 0,16 | | 0,16 | 0,15 | 0,32 | 0,23 | 0,36 | 0,22 | 0,40 | 0,27 | 0,48 | 0,28 | 0,29 | 0,55 | 0,54 | 0,52 | 0,43 | 0,53 | 0,36 | 0,46 | 0,44 | 0,27 |
| EPI 24 | 0,45 | 0,27 | 0,48 | 0,39 | 0,50 | 0,22 | 0,15 | 0,16 | | 0,20 | 0,29 | 0,26 | 0,54 | 0,28 | 0,49 | 0,30 | 0,54 | 0,32 | 0,34 | 0,56 | 0,59 | 0,59 | 0,42 | 0,59 | 0,42 | 0,52 | 0,50 | 0,32 |
| US 23 | 0,46 | 0,23 | 0,41 | 0,28 | 0,40 | 0,13 | 0,23 | 0,15 | 0,20 | | 0,56 | 0,11 | 0,35 | 0,10 | 0,27 | 0,20 | 0,29 | 0,20 | 0,17 | 0,47 | 0,40 | 0,37 | 0,42 | 0,38 | 0,22 | 0,33 | 0,31 | 0,15 |
| LBA 23 | 0,24 | 0,36 | 0,31 | 0,24 | 0,29 | 0,33 | 0,21 | 0,32 | 0,29 | 0,56 | | 0,53 | 1,18 | 0,56 | 0,96 | 0,42 | 0,92 | 0,70 | 0,77 | 0,64 | 0,72 | 0,68 | 0,54 | 0,75 | 0,66 | 0,57 | 0,60 | 0,56 |
| US 22 | 0,45 | 0,31 | 0,44 | 0,33 | 0,39 | 0,15 | 0,24 | 0,23 | 0,26 | 0,11 | 0,53 | | 0,26 | 0,15 | 0,29 | 0,11 | 0,28 | 0,12 | 0,20 | 0,56 | 0,32 | 0,32 | 0,50 | 0,33 | 0,20 | 0,27 | 0,27 | 0,23 |
| TAR 22 | 0,94 | 0,54 | 0,66 | 0,69 | 0,71 | 0,37 | 0,56 | 0,36 | 0,54 | 0,35 | 1,18 | 0,26 | | 0,24 | 0,09 | 0,35 | 0,22 | 0,26 | 0,20 | 0,52 | 0,36 | 0,32 | 0,53 | 0,34 | 0,27 | 0,39 | 0,33 | 0,37 |
| EPI 21 | 0,44 | 0,20 | 0,35 | 0,26 | 0,38 | 0,20 | 0,32 | 0,22 | 0,28 | 0,10 | 0,56 | 0,15 | 0,24 | | 0,21 | 0,16 | 0,26 | 0,23 | 0,16 | 0,43 | 0,34 | 0,31 | 0,37 | 0,33 | 0,15 | 0,28 | 0,27 | 0,13 |
| LMA 21 | 0,76 | 0,44 | 0,50 | 0,53 | 0,52 | 0,35 | 0,49 | 0,40 | 0,49 | 0,27 | 0,96 | 0,29 | 0,09 | 0,21 | | 0,29 | 0,14 | 0,19 | 0,16 | 0,49 | 0,30 | 0,26 | 0,50 | 0,28 | 0,22 | 0,33 | 0,29 | 0,32 |
| EPI 20 | 0,38 | 0,32 | 0,41 | 0,30 | 0,37 | 0,21 | 0,25 | 0,27 | 0,30 | 0,20 | 0,42 | 0,11 | 0,35 | 0,16 | 0,29 | | 0,20 | 0,18 | 0,29 | 0,55 | 0,31 | 0,31 | 0,51 | 0,31 | 0,22 | 0,24 | 0,29 | 0,23 |
| LMA 20 | 0,72 | 0,45 | 0,45 | 0,49 | 0,44 | 0,41 | 0,56 | 0,48 | 0,54 | 0,29 | 0,92 | 0,28 | 0,22 | 0,26 | 0,14 | 0,20 | | 0,23 | 0,24 | 0,45 | 0,25 | 0,20 | 0,47 | 0,23 | 0,22 | 0,25 | 0,29 | 0,30 |
| MMA 18 | 0,61 | 0,43 | 0,58 | 0,48 | 0,54 | 0,19 | 0,27 | 0,28 | 0,32 | 0,20 | 0,70 | 0,12 | 0,26 | 0,23 | 0,19 | 0,18 | 0,23 | | 0,14 | 0,60 | 0,28 | 0,28 | 0,54 | 0,29 | 0,19 | 0,26 | 0,23 | 0,26 |
| MMA 17 | 0,63 | 0,36 | 0,52 | 0,43 | 0,54 | 0,25 | 0,36 | 0,29 | 0,34 | 0,17 | 0,77 | 0,20 | 0,20 | 0,16 | 0,16 | 0,29 | 0,24 | 0,14 | | 0,51 | 0,28 | 0,27 | 0,45 | 0,26 | 0,13 | 0,28 | 0,20 | 0,19 |
| UMA-A 16 | 0,42 | 0,42 | 0,27 | 0,37 | 0,35 | 0,58 | 0,67 | 0,55 | 0,56 | 0,47 | 0,64 | 0,56 | 0,52 | 0,43 | 0,49 | 0,55 | 0,45 | 0,60 | 0,51 | | 0,57 | 0,44 | 0,12 | 0,52 | 0,51 | 0,41 | 0,44 | 0,49 |
| UMA-B 16 | 0,56 | 0,47 | 0,42 | 0,40 | 0,33 | 0,47 | 0,58 | 0,54 | 0,59 | 0,40 | 0,72 | 0,32 | 0,36 | 0,34 | 0,30 | 0,31 | 0,25 | 0,28 | 0,28 | 0,57 | | 0,10 | 0,58 | 0,05 | 0,22 | 0,14 | 0,20 | 0,34 |
| HAM 16 | 0,53 | 0,42 | 0,34 | 0,34 | 0,29 | 0,46 | 0,59 | 0,52 | 0,59 | 0,37 | 0,68 | 0,32 | 0,32 | 0,31 | 0,26 | 0,31 | 0,20 | 0,28 | 0,27 | 0,44 | 0,10 | | 0,47 | 0,10 | 0,18 | 0,10 | 0,16 | 0,29 |
| UMA-A 15 | 0,39 | 0,34 | 0,32 | 0,37 | 0,40 | 0,50 | 0,54 | 0,43 | 0,42 | 0,42 | 0,54 | 0,50 | 0,53 | 0,37 | 0,50 | 0,51 | 0,47 | 0,54 | 0,45 | 0,12 | 0,58 | 0,47 | | 0,55 | 0,37 | 0,42 | 0,41 | 0,46 |
| UMA-B 15 | 0,59 | 0,47 | 0,42 | 0,40 | 0,35 | 0,47 | 0,59 | 0,53 | 0,59 | 0,38 | 0,75 | 0,33 | 0,34 | 0,33 | 0,28 | 0,31 | 0,23 | 0,29 | 0,26 | 0,52 | 0,05 | 0,10 | 0,55 | | 0,18 | 0,13 | 0,17 | 0,29 |
| HAM 15 | 0,54 | 0,31 | 0,40 | 0,35 | 0,38 | 0,31 | 0,42 | 0,36 | 0,42 | 0,22 | 0,66 | 0,20 | 0,27 | 0,15 | 0,22 | 0,22 | 0,22 | 0,19 | 0,13 | 0,51 | 0,22 | 0,18 | 0,37 | 0,18 | | 0,17 | 0,15 | 0,12 |
| CRE 15 | 0,44 | 0,40 | 0,34 | 0,28 | 0,26 | 0,39 | 0,50 | 0,46 | 0,52 | 0,33 | 0,57 | 0,27 | 0,39 | 0,28 | 0,33 | 0,24 | 0,25 | 0,26 | 0,28 | 0,41 | 0,14 | 0,10 | 0,42 | 0,13 | 0,17 | | 0,13 | 0,25 |
| HAM 14 | 0,49 | 0,38 | 0,40 | 0,32 | 0,33 | 0,39 | 0,50 | 0,44 | 0,50 | 0,31 | 0,60 | 0,27 | 0,33 | 0,27 | 0,29 | 0,29 | 0,29 | 0,23 | 0,20 | 0,44 | 0,20 | 0,16 | 0,41 | 0,17 | 0,15 | 0,13 | | 0,20 |
| HAV 14 | 0,47 | 0,25 | 0,41 | 0,29 | 0,41 | 0,26 | 0,36 | 0,27 | 0,32 | 0,15 | 0,56 | 0,23 | 0,37 | 0,13 | 0,32 | 0,23 | 0,30 | 0,26 | 0,19 | 0,49 | 0,34 | 0,29 | 0,46 | 0,29 | 0,12 | 0,25 | 0,20 | |

Appendix Table 13: Distance-Matrix for HCA based on the time-weighted (0.02) average change rates between averages of samples (colour scale: dark – light = pronounced morphometric differences – moderate differences – notable morphometric similarities (1.15 – 0.32 – 0.00). Abbreviations: GRA = Late Gravettian; US = Upper Solutrean; SAL = Salpetrian; LBA = Late Badegoulian; EPI = Epigravettian; TAR = Tardigravettian; LMA = Lower Magdalenian; MMA = Middle Magdalenian; UMA = Upper Magdalenian; HAM = Hamburgian; CRE = Creswellian; HAV = Havelte).

| | GRA 30 | GRA 29 | GRA 28 | GRA 27 | GRA 26 | US 25 | US 24 | SAL 24 | EPI 24 | US 23 | LBA 23 | US 22 | TAR 22 | EPI 21 | LMA 21 | EPI 20 | LMA 20 | MMA 18 | MMA 17 | UMA-A 16 | UMA-B 16 | HAM 16 | UMA-A 15 | UMA-B 15 | HAM 15 | CRE 15 | HAM 14 | HAV 14 |
|---|---|---|---|---|---|---|---|---|---|---|---|---|---|---|---|---|---|---|---|---|---|---|---|---|---|---|---|---|
| GRA 30 | | 0,32 | 0,27 | 0,21 | 0,32 | 0,60 | 0,57 | 0,68 | 0,51 | 0,53 | 0,31 | 0,53 | 1,02 | 0,53 | 0,85 | 0,48 | 0,82 | 0,73 | 0,76 | 0,56 | 0,70 | 0,67 | 0,54 | 0,74 | 0,69 | 0,59 | 0,65 | 0,63 |
| GRA 29 | 0,32 | | 0,23 | 0,19 | 0,34 | 0,38 | 0,42 | 0,42 | 0,32 | 0,29 | 0,42 | 0,38 | 0,61 | 0,28 | 0,52 | 0,41 | 0,54 | 0,54 | 0,48 | 0,55 | 0,60 | 0,55 | 0,48 | 0,61 | 0,45 | 0,54 | 0,53 | 0,40 |
| GRA 28 | 0,27 | 0,23 | | 0,13 | 0,14 | 0,60 | 0,59 | 0,67 | 0,52 | 0,46 | 0,36 | 0,50 | 0,72 | 0,42 | 0,57 | 0,49 | 0,53 | 0,68 | 0,63 | 0,39 | 0,54 | 0,46 | 0,45 | 0,55 | 0,53 | 0,47 | 0,54 | 0,55 |
| GRA 27 | 0,21 | 0,19 | 0,13 | | 0,16 | 0,45 | 0,47 | 0,55 | 0,42 | 0,32 | 0,28 | 0,38 | 0,74 | 0,32 | 0,59 | 0,37 | 0,56 | 0,57 | 0,53 | 0,48 | 0,51 | 0,45 | 0,49 | 0,52 | 0,47 | 0,40 | 0,45 | 0,42 |
| GRA 26 | 0,32 | 0,34 | 0,14 | 0,16 | | 0,55 | 0,55 | 0,67 | 0,52 | 0,43 | 0,32 | 0,43 | 0,75 | 0,43 | 0,57 | 0,43 | 0,50 | 0,62 | 0,63 | 0,45 | 0,43 | 0,39 | 0,51 | 0,46 | 0,49 | 0,37 | 0,45 | 0,53 |
| US 25 | 0,60 | 0,38 | 0,60 | 0,45 | 0,55 | | 0,15 | 0,13 | 0,23 | 0,15 | 0,35 | 0,18 | 0,40 | 0,24 | 0,39 | 0,26 | 0,46 | 0,26 | 0,33 | 0,67 | 0,56 | 0,55 | 0,60 | 0,57 | 0,41 | 0,49 | 0,50 | 0,37 |
| US 24 | 0,57 | 0,42 | 0,59 | 0,47 | 0,55 | 0,15 | | 0,16 | 0,15 | 0,24 | 0,22 | 0,26 | 0,58 | 0,35 | 0,52 | 0,29 | 0,60 | 0,33 | 0,43 | 0,75 | 0,66 | 0,67 | 0,63 | 0,68 | 0,51 | 0,59 | 0,60 | 0,46 |
| SAL 24 | 0,68 | 0,42 | 0,67 | 0,55 | 0,67 | 0,13 | 0,16 | | 0,16 | 0,16 | 0,33 | 0,25 | 0,38 | 0,25 | 0,43 | 0,31 | 0,52 | 0,34 | 0,36 | 0,63 | 0,62 | 0,60 | 0,52 | 0,62 | 0,45 | 0,55 | 0,54 | 0,37 |
| EPI 24 | 0,51 | 0,32 | 0,52 | 0,42 | 0,52 | 0,23 | 0,15 | 0,16 | | 0,21 | 0,30 | 0,28 | 0,56 | 0,31 | 0,52 | 0,34 | 0,58 | 0,38 | 0,41 | 0,64 | 0,67 | 0,67 | 0,51 | 0,68 | 0,51 | 0,61 | 0,60 | 0,42 |
| US 23 | 0,53 | 0,29 | 0,46 | 0,32 | 0,43 | 0,15 | 0,24 | 0,16 | 0,21 | | 0,56 | 0,12 | 0,36 | 0,12 | 0,29 | 0,23 | 0,32 | 0,25 | 0,23 | 0,54 | 0,47 | 0,44 | 0,50 | 0,46 | 0,30 | 0,41 | 0,40 | 0,24 |
| LBA 23 | 0,31 | 0,42 | 0,36 | 0,28 | 0,32 | 0,35 | 0,22 | 0,33 | 0,30 | 0,56 | | 0,54 | 1,19 | 0,58 | 0,98 | 0,45 | 0,95 | 0,75 | 0,83 | 0,71 | 0,79 | 0,75 | 0,62 | 0,83 | 0,74 | 0,65 | 0,69 | 0,65 |
| US 22 | 0,53 | 0,38 | 0,50 | 0,38 | 0,43 | 0,18 | 0,26 | 0,25 | 0,28 | 0,12 | 0,54 | | 0,26 | 0,16 | 0,30 | 0,13 | 0,30 | 0,16 | 0,25 | 0,62 | 0,38 | 0,38 | 0,57 | 0,40 | 0,27 | 0,34 | 0,35 | 0,31 |
| TAR 22 | 1,02 | 0,61 | 0,72 | 0,74 | 0,75 | 0,40 | 0,58 | 0,38 | 0,56 | 0,36 | 1,19 | 0,26 | | 0,25 | 0,10 | 0,37 | 0,24 | 0,30 | 0,25 | 0,58 | 0,42 | 0,38 | 0,60 | 0,41 | 0,34 | 0,46 | 0,41 | 0,45 |
| EPI 21 | 0,53 | 0,28 | 0,42 | 0,32 | 0,43 | 0,24 | 0,35 | 0,25 | 0,31 | 0,12 | 0,58 | 0,16 | 0,25 | | 0,21 | 0,17 | 0,27 | 0,26 | 0,20 | 0,48 | 0,39 | 0,36 | 0,43 | 0,39 | 0,21 | 0,34 | 0,34 | 0,20 |
| LMA 21 | 0,85 | 0,52 | 0,57 | 0,59 | 0,57 | 0,39 | 0,52 | 0,43 | 0,52 | 0,29 | 0,98 | 0,30 | 0,10 | 0,21 | | 0,30 | 0,15 | 0,22 | 0,20 | 0,54 | 0,35 | 0,31 | 0,56 | 0,34 | 0,28 | 0,39 | 0,36 | 0,39 |
| EPI 20 | 0,48 | 0,41 | 0,49 | 0,37 | 0,43 | 0,26 | 0,29 | 0,31 | 0,34 | 0,23 | 0,45 | 0,13 | 0,37 | 0,17 | 0,30 | | 0,20 | 0,20 | 0,32 | 0,59 | 0,35 | 0,35 | 0,56 | 0,36 | 0,27 | 0,29 | 0,35 | 0,29 |
| LMA 20 | 0,82 | 0,54 | 0,53 | 0,56 | 0,50 | 0,46 | 0,60 | 0,52 | 0,58 | 0,32 | 0,95 | 0,30 | 0,24 | 0,27 | 0,15 | 0,20 | | 0,25 | 0,27 | 0,49 | 0,29 | 0,24 | 0,52 | 0,28 | 0,27 | 0,30 | 0,35 | 0,36 |
| MMA 18 | 0,73 | 0,54 | 0,68 | 0,57 | 0,62 | 0,26 | 0,33 | 0,34 | 0,38 | 0,25 | 0,75 | 0,16 | 0,30 | 0,26 | 0,22 | 0,20 | 0,25 | | 0,15 | 0,62 | 0,30 | 0,30 | 0,57 | 0,32 | 0,22 | 0,29 | 0,27 | 0,30 |
| MMA 17 | 0,76 | 0,48 | 0,63 | 0,53 | 0,63 | 0,33 | 0,43 | 0,36 | 0,41 | 0,23 | 0,83 | 0,25 | 0,25 | 0,20 | 0,20 | 0,32 | 0,27 | 0,15 | | 0,52 | 0,29 | 0,28 | 0,47 | 0,28 | 0,15 | 0,30 | 0,23 | 0,22 |
| UMA-A 16 | 0,56 | 0,55 | 0,39 | 0,48 | 0,45 | 0,67 | 0,75 | 0,63 | 0,64 | 0,54 | 0,71 | 0,62 | 0,58 | 0,48 | 0,54 | 0,59 | 0,49 | 0,62 | 0,52 | | 0,57 | 0,44 | 0,13 | 0,53 | 0,52 | 0,42 | 0,46 | 0,51 |
| UMA-B 16 | 0,70 | 0,60 | 0,54 | 0,51 | 0,43 | 0,56 | 0,66 | 0,62 | 0,67 | 0,47 | 0,79 | 0,38 | 0,42 | 0,39 | 0,35 | 0,35 | 0,29 | 0,30 | 0,29 | 0,57 | | 0,10 | 0,59 | 0,06 | 0,23 | 0,15 | 0,22 | 0,36 |
| HAM 16 | 0,67 | 0,55 | 0,46 | 0,45 | 0,39 | 0,55 | 0,67 | 0,60 | 0,67 | 0,44 | 0,75 | 0,38 | 0,38 | 0,36 | 0,31 | 0,35 | 0,24 | 0,30 | 0,28 | 0,44 | 0,10 | | 0,48 | 0,11 | 0,19 | 0,11 | 0,18 | 0,31 |
| UMA-A 15 | 0,54 | 0,48 | 0,45 | 0,49 | 0,51 | 0,60 | 0,63 | 0,52 | 0,51 | 0,50 | 0,62 | 0,57 | 0,60 | 0,43 | 0,56 | 0,56 | 0,52 | 0,57 | 0,47 | 0,13 | 0,59 | 0,48 | | 0,55 | 0,37 | 0,42 | 0,42 | 0,47 |
| UMA-B 15 | 0,74 | 0,61 | 0,55 | 0,52 | 0,46 | 0,57 | 0,68 | 0,62 | 0,68 | 0,46 | 0,83 | 0,40 | 0,41 | 0,39 | 0,34 | 0,36 | 0,28 | 0,32 | 0,28 | 0,53 | 0,06 | 0,11 | 0,55 | | 0,18 | 0,13 | 0,18 | 0,30 |
| HAM 15 | 0,69 | 0,45 | 0,53 | 0,47 | 0,49 | 0,41 | 0,51 | 0,45 | 0,51 | 0,30 | 0,74 | 0,27 | 0,34 | 0,21 | 0,28 | 0,27 | 0,27 | 0,22 | 0,15 | 0,52 | 0,23 | 0,19 | 0,37 | 0,18 | | 0,17 | 0,16 | 0,13 |
| CRE 15 | 0,59 | 0,54 | 0,47 | 0,40 | 0,37 | 0,49 | 0,59 | 0,55 | 0,61 | 0,41 | 0,65 | 0,34 | 0,46 | 0,34 | 0,39 | 0,29 | 0,30 | 0,29 | 0,30 | 0,42 | 0,15 | 0,11 | 0,42 | 0,13 | 0,17 | | 0,14 | 0,26 |
| HAM 14 | 0,65 | 0,53 | 0,54 | 0,45 | 0,45 | 0,50 | 0,60 | 0,54 | 0,60 | 0,40 | 0,69 | 0,35 | 0,41 | 0,34 | 0,36 | 0,35 | 0,35 | 0,27 | 0,23 | 0,46 | 0,22 | 0,18 | 0,42 | 0,18 | 0,16 | 0,14 | | 0,20 |
| HAV 14 | 0,63 | 0,40 | 0,55 | 0,42 | 0,53 | 0,37 | 0,46 | 0,37 | 0,42 | 0,24 | 0,65 | 0,31 | 0,45 | 0,20 | 0,39 | 0,29 | 0,36 | 0,30 | 0,22 | 0,51 | 0,36 | 0,31 | 0,47 | 0,30 | 0,13 | 0,26 | 0,20 | |

Appendix Table 14: Distance-Matrix for HCA based on the time- (0.01) and geographical distance-weighted average change rates between averages of samples (colour scale: dark – light = pronounced morphometric differences – moderate differences – notable morphometric similarities (1.15 – 0.32 – 0.00). Abbreviations: GRA = Late Gravettian; US = Upper Solutrean; SAL = Salpetrian; LBA = Late Badegoulian; EPI = Epigravettian; TAR = Tardigravettian; LMA = Lower Magdalenian; MMA = Middle Magdalenian; UMA = Upper Magdalenian; HAM = Hamburgian; CRE = Creswellian; HAV = Havelte).

| | GRA 30 | GRA 29 | GRA 28 | GRA 27 | GRA 26 | US 25 | US 24 | SAL 24 | EPI 24 | US 23 | LBA 23 | US 22 | TAR 22 | EPI 21 | LMA 21 | EPI 20 | LMA 20 | MMA 18 | MMA 17 | UMA-A 16 | UMA-B 16 | HAM 16 | UMA-A 15 | UMA-B 15 | HAM 15 | CRE 15 | HAM 14 | HAV 14 |
|---|---|---|---|---|---|---|---|---|---|---|---|---|---|---|---|---|---|---|---|---|---|---|---|---|---|---|---|---|
| GRA 30 | | 0,33 | 0,29 | 0,20 | 0,38 | 0,70 | 0,64 | 0,70 | 0,49 | 0,59 | 0,34 | 0,58 | 1,02 | 0,48 | 0,85 | 0,43 | 0,80 | 0,67 | 0,74 | 0,53 | 0,63 | 0,55 | 0,47 | 0,66 | 0,59 | 0,56 | 0,55 | 0,55 |
| GRA 29 | 0,33 | | 0,27 | 0,20 | 0,43 | 0,48 | 0,49 | 0,44 | 0,29 | 0,35 | 0,45 | 0,43 | 0,61 | 0,22 | 0,52 | 0,36 | 0,52 | 0,48 | 0,46 | 0,52 | 0,54 | 0,45 | 0,41 | 0,53 | 0,36 | 0,51 | 0,44 | 0,32 |
| GRA 28 | 0,29 | 0,27 | | 0,14 | 0,18 | 0,76 | 0,72 | 0,75 | 0,55 | 0,58 | 0,45 | 0,61 | 0,78 | 0,42 | 0,63 | 0,50 | 0,57 | 0,68 | 0,67 | 0,42 | 0,53 | 0,39 | 0,44 | 0,53 | 0,48 | 0,50 | 0,49 | 0,52 |
| GRA 27 | 0,20 | 0,20 | 0,14 | | 0,23 | 0,60 | 0,59 | 0,62 | 0,44 | 0,43 | 0,36 | 0,48 | 0,79 | 0,31 | 0,64 | 0,37 | 0,59 | 0,56 | 0,56 | 0,50 | 0,49 | 0,38 | 0,47 | 0,49 | 0,42 | 0,42 | 0,39 | 0,38 |
| GRA 26 | 0,38 | 0,43 | 0,18 | 0,23 | | 0,79 | 0,77 | 0,84 | 0,63 | 0,63 | 0,49 | 0,62 | 0,89 | 0,51 | 0,71 | 0,52 | 0,63 | 0,70 | 0,75 | 0,56 | 0,51 | 0,41 | 0,59 | 0,52 | 0,52 | 0,48 | 0,48 | 0,58 |
| US 25 | 0,70 | 0,48 | 0,76 | 0,60 | 0,79 | | 0,15 | 0,18 | 0,34 | 0,15 | 0,38 | 0,17 | 0,44 | 0,32 | 0,41 | 0,31 | 0,47 | 0,28 | 0,29 | 0,62 | 0,55 | 0,60 | 0,57 | 0,55 | 0,43 | 0,46 | 0,51 | 0,36 |
| US 24 | 0,64 | 0,49 | 0,72 | 0,59 | 0,77 | 0,15 | | 0,21 | 0,26 | 0,24 | 0,25 | 0,26 | 0,61 | 0,43 | 0,53 | 0,34 | 0,61 | 0,35 | 0,39 | 0,70 | 0,64 | 0,72 | 0,60 | 0,66 | 0,53 | 0,57 | 0,61 | 0,45 |
| SAL 24 | 0,70 | 0,44 | 0,75 | 0,62 | 0,84 | 0,18 | 0,21 | | 0,22 | 0,20 | 0,34 | 0,28 | 0,36 | 0,28 | 0,41 | 0,31 | 0,48 | 0,31 | 0,32 | 0,57 | 0,56 | 0,60 | 0,45 | 0,55 | 0,43 | 0,52 | 0,50 | 0,32 |
| EPI 24 | 0,49 | 0,29 | 0,55 | 0,44 | 0,63 | 0,34 | 0,26 | 0,22 | | 0,31 | 0,37 | 0,37 | 0,60 | 0,29 | 0,56 | 0,32 | 0,60 | 0,36 | 0,43 | 0,64 | 0,65 | 0,64 | 0,48 | 0,65 | 0,48 | 0,63 | 0,56 | 0,39 |
| US 23 | 0,59 | 0,35 | 0,58 | 0,43 | 0,63 | 0,15 | 0,24 | 0,20 | 0,31 | | 0,59 | 0,11 | 0,40 | 0,21 | 0,31 | 0,28 | 0,34 | 0,27 | 0,19 | 0,49 | 0,46 | 0,49 | 0,47 | 0,44 | 0,32 | 0,38 | 0,41 | 0,23 |
| LBA 23 | 0,34 | 0,45 | 0,45 | 0,36 | 0,49 | 0,38 | 0,25 | 0,34 | 0,37 | 0,59 | | 0,56 | 1,20 | 0,64 | 0,97 | 0,48 | 0,94 | 0,74 | 0,78 | 0,65 | 0,75 | 0,77 | 0,56 | 0,78 | 0,74 | 0,62 | 0,67 | 0,61 |
| US 22 | 0,58 | 0,43 | 0,61 | 0,48 | 0,62 | 0,17 | 0,26 | 0,28 | 0,37 | 0,11 | 0,56 | | 0,31 | 0,26 | 0,33 | 0,19 | 0,33 | 0,19 | 0,22 | 0,58 | 0,38 | 0,44 | 0,55 | 0,39 | 0,30 | 0,32 | 0,37 | 0,31 |
| TAR 22 | 1,02 | 0,61 | 0,78 | 0,79 | 0,89 | 0,44 | 0,61 | 0,36 | 0,60 | 0,40 | 1,20 | 0,31 | | 0,30 | 0,10 | 0,39 | 0,22 | 0,28 | 0,23 | 0,55 | 0,38 | 0,40 | 0,55 | 0,36 | 0,33 | 0,45 | 0,39 | 0,42 |
| EPI 21 | 0,48 | 0,22 | 0,42 | 0,31 | 0,51 | 0,32 | 0,43 | 0,28 | 0,29 | 0,21 | 0,64 | 0,26 | 0,30 | | 0,28 | 0,18 | 0,32 | 0,28 | 0,25 | 0,52 | 0,40 | 0,36 | 0,44 | 0,39 | 0,22 | 0,39 | 0,34 | 0,21 |
| LMA 21 | 0,85 | 0,52 | 0,63 | 0,64 | 0,71 | 0,41 | 0,53 | 0,41 | 0,56 | 0,31 | 0,97 | 0,33 | 0,10 | 0,28 | | 0,34 | 0,15 | 0,22 | 0,18 | 0,51 | 0,32 | 0,35 | 0,52 | 0,31 | 0,29 | 0,38 | 0,36 | 0,37 |
| EPI 20 | 0,43 | 0,36 | 0,50 | 0,37 | 0,52 | 0,31 | 0,34 | 0,31 | 0,32 | 0,28 | 0,48 | 0,19 | 0,39 | 0,18 | 0,34 | | 0,24 | 0,21 | 0,36 | 0,61 | 0,35 | 0,37 | 0,56 | 0,35 | 0,28 | 0,33 | 0,35 | 0,30 |
| LMA 20 | 0,80 | 0,52 | 0,57 | 0,59 | 0,63 | 0,47 | 0,61 | 0,48 | 0,60 | 0,34 | 0,94 | 0,33 | 0,22 | 0,32 | 0,15 | 0,24 | | 0,26 | 0,27 | 0,47 | 0,27 | 0,28 | 0,49 | 0,25 | 0,29 | 0,31 | 0,35 | 0,35 |
| MMA 18 | 0,67 | 0,48 | 0,68 | 0,56 | 0,70 | 0,28 | 0,35 | 0,31 | 0,36 | 0,27 | 0,74 | 0,19 | 0,28 | 0,28 | 0,22 | 0,21 | 0,26 | | 0,19 | 0,65 | 0,30 | 0,33 | 0,56 | 0,30 | 0,23 | 0,33 | 0,27 | 0,30 |
| MMA 17 | 0,74 | 0,46 | 0,67 | 0,56 | 0,75 | 0,29 | 0,39 | 0,32 | 0,43 | 0,19 | 0,78 | 0,22 | 0,23 | 0,25 | 0,18 | 0,36 | 0,27 | 0,19 | | 0,51 | 0,31 | 0,37 | 0,48 | 0,30 | 0,21 | 0,32 | 0,28 | 0,25 |
| UMA-A 16 | 0,53 | 0,52 | 0,42 | 0,50 | 0,56 | 0,62 | 0,70 | 0,57 | 0,64 | 0,49 | 0,65 | 0,58 | 0,55 | 0,52 | 0,51 | 0,61 | 0,47 | 0,65 | 0,51 | | 0,60 | 0,54 | 0,15 | 0,56 | 0,59 | 0,46 | 0,52 | 0,55 |
| UMA-B 16 | 0,63 | 0,54 | 0,53 | 0,49 | 0,51 | 0,55 | 0,64 | 0,56 | 0,65 | 0,46 | 0,75 | 0,38 | 0,38 | 0,40 | 0,32 | 0,35 | 0,27 | 0,30 | 0,31 | 0,60 | | 0,17 | 0,59 | 0,05 | 0,27 | 0,19 | 0,24 | 0,37 |
| HAM 16 | 0,55 | 0,45 | 0,39 | 0,38 | 0,41 | 0,60 | 0,72 | 0,60 | 0,64 | 0,49 | 0,77 | 0,44 | 0,40 | 0,36 | 0,35 | 0,37 | 0,28 | 0,33 | 0,37 | 0,54 | 0,17 | | 0,54 | 0,16 | 0,21 | 0,20 | 0,20 | 0,35 |
| UMA-A 15 | 0,47 | 0,41 | 0,44 | 0,47 | 0,59 | 0,57 | 0,60 | 0,45 | 0,48 | 0,47 | 0,56 | 0,55 | 0,55 | 0,44 | 0,52 | 0,56 | 0,49 | 0,56 | 0,48 | 0,15 | 0,59 | 0,54 | | 0,56 | 0,43 | 0,47 | 0,46 | 0,49 |
| UMA-B 15 | 0,66 | 0,53 | 0,53 | 0,49 | 0,52 | 0,55 | 0,66 | 0,55 | 0,65 | 0,44 | 0,78 | 0,39 | 0,36 | 0,39 | 0,31 | 0,35 | 0,25 | 0,30 | 0,30 | 0,56 | 0,05 | 0,16 | 0,56 | | 0,23 | 0,18 | 0,21 | 0,32 |
| HAM 15 | 0,59 | 0,36 | 0,48 | 0,42 | 0,52 | 0,43 | 0,53 | 0,43 | 0,48 | 0,32 | 0,74 | 0,30 | 0,33 | 0,22 | 0,29 | 0,28 | 0,29 | 0,23 | 0,21 | 0,59 | 0,27 | 0,21 | 0,43 | 0,23 | | 0,25 | 0,16 | 0,15 |
| CRE 15 | 0,56 | 0,51 | 0,50 | 0,42 | 0,48 | 0,46 | 0,57 | 0,52 | 0,63 | 0,38 | 0,62 | 0,32 | 0,45 | 0,39 | 0,38 | 0,33 | 0,31 | 0,33 | 0,32 | 0,46 | 0,19 | 0,20 | 0,47 | 0,18 | 0,25 | | 0,20 | 0,29 |
| HAM 14 | 0,55 | 0,44 | 0,49 | 0,39 | 0,48 | 0,51 | 0,61 | 0,50 | 0,56 | 0,41 | 0,67 | 0,37 | 0,39 | 0,34 | 0,36 | 0,35 | 0,35 | 0,27 | 0,28 | 0,52 | 0,24 | 0,20 | 0,46 | 0,21 | 0,16 | 0,20 | | 0,22 |
| HAV 14 | 0,55 | 0,32 | 0,52 | 0,38 | 0,58 | 0,36 | 0,45 | 0,32 | 0,39 | 0,23 | 0,61 | 0,31 | 0,42 | 0,21 | 0,37 | 0,30 | 0,35 | 0,30 | 0,25 | 0,55 | 0,37 | 0,35 | 0,49 | 0,32 | 0,15 | 0,29 | 0,22 | |

Appendix Table 15: Radiocarbon dates for the construction of the chronological framework. Abbreviations are explained on page ...

| site | layer/level/ conc./... | lab.-nr. | m. | material | BP | std. | % | calBP | std. | * | c. | P% | WA | std. | calBP | std. | reference |
|---|---|---|---|---|---|---|---|---|---|---|---|---|---|---|---|---|---|
| Oldeholtwolde | | GrN-12280 | CON | charcoal (*Salix* sp.) | 11080 | 280 | 2.5 | 13010 | 240 | | A, 1 | | | | | | Lanting & van der Pflicht 1996 |
| | | OxA-2560 | AMS | charcoal (*Pinus* sp.) | 11300 | 110 | 1.0 | 13206 | 92 | | 1 | | | | | | Hedges et al. 1992 |
| | | GrN-11264 | CON | charcoal | 11340 | 100 | 0.9 | 13233 | 87 | | 1 | | | | | | Johansen & Stapert 2003 |
| | hearth | OxA-2559 | AMS | charcoal (*Salix* sp.) | 11470 | 110 | 1.0 | 13339 | 107 | * | | | | | | | Hedges et al. 1992 |
| | hearth | GrN-10274 | CON | charcoal (*Salix* sp.) | 11540 | 270 | 2.3 | 13446 | 265 | * | A | | | | | | Lanting & van der Pflicht 1996 |
| | hearth | GrN-13083 | CON | charcoal (*Salix* sp.) | 11600 | 250 | 2.2 | 13495 | 248 | | A, 1 | | | | | | Lanting & van der Pflicht 1996 |
| | hearth | OxA-2561 | AMS | charcoal (*Salix* sp.) | 11680 | 120 | 1.0 | 13557 | 136 | * | | | | | | | Hedges et al. 1992 |
| | hearth | OxA-2558 | AMS | charcoal (*Salix* sp.) | 11810 | 110 | 0.9 | 13666 | 117 | * | | | | | | | Hedges et al. 1992 |
| | | | | | | | | | | | | 17.1 | 11646 | 63 | **13506** | **68** | |
| Crvena Stijena | VII | OxA-23313 | AMS | bone (*C. elaphus*) | 11755 | 55 | 0.5 | 13623 | 93 | * | | | | | | | Mercier et al. 2018 |
| | X | OxA-23343 | AMS | bone (*C. elaphus*) | 11790 | 50 | 0.4 | 13652 | 80 | * | | | | | | | Mercier et al. 2018 |
| | | | | | | | | | | | | 63.8 | 11774 | 37 | **13635** | **88** | |
| Borneck | | KIA-33950 | AMS | Tibia (*A.alces*) | 11770 | 55 | 0.5 | 13632 | 91 | * | | | | | | | Taute 1968 |
| | | KIA-33949 | AMS | Humerus (*R. tarandus*) | 11940 | 50 | 0.4 | 13853 | 111 | * | | | | | | | Taute 1968 |
| | | | | | | | | | | | | 2.2 | 11863 | 37 | **13700** | **66** | |
| Marsangy | | OxA-740 | AMS | bone | 12120 | 200 | 1.7 | **14181** | **358** | | | | | | | | Valentin & Pigeot 2000 |
| Ahrenshöft LA 73 | N, hearth A&D | KIA-3833 | AMS | charcoal (*Salix/Populus*) | 12130 | 60 | 0.5 | **13985** | **102** | | | | | | | | Clausen 1998 |
| Mother Grundy´s Parlour | C/B, LB-SB | OxA-5858 | AMS | charcoal | 11790 | 90 | 0.8 | 13645 | 102 | | B | | | | | | Hedges et al. 1996 |
| | | OxA-8738 | AMS | tooth (*E. ferus*) | 11970 | 75 | 0.6 | 13874 | 108 | | B | | | | | | Hedges et al. 1996 |
| | | OxA-5698 | AMS | tooth (*E. ferus*), cutm. | 12280 | 110 | 0.9 | 14418 | 297 | * | | | | | | | Hedges et al. 1996 |
| | | OxA-733 | AMS | bone fragment | 12060 | 160 | 1.3 | 13990 | 211 | * | | | | | | | Hedges et al. 1996 |
| | | OxA-8739 | AMS | tooth (*E. ferus*) | 12170 | 80 | 0.7 | 14059 | 139 | * | | | | | | | Hedges et al. 1996 |
| | | OxA-0734 | AMS | bone fragment | 12190 | 140 | 1.1 | 14227 | 298 | * | | | | | | | Hedges et al. 1996 |
| | | OxA-3398 | AMS | premolar tooth | 12280 | 110 | 0.9 | 14418 | 297 | * | | | | | | | Hedges et al. 1996 |
| | | OxA-3400 | AMS | molar tooth | 12340 | 110 | 0.9 | 14481 | 285 | * | | | | | | | Hedges et al. 1996 |
| | | OxA-4102 | AMS | molar tooth | 12540 | 140 | 1.1 | 14742 | 315 | | B | | | | | | Hedges et al. 1996 |
| | | | | | | | | | | | 67.1 | 12229 | 45 | **14151** | **67** | | |

Appendix Table 15: continued 1,

| site | layer/level/ conc./... | lab.-nr. | m. | material | BP | std. | % | calBP | std. | * | c. | P% | WA | std. | calBP | std. | reference |
|---|---|---|---|---|---|---|---|---|---|---|---|---|---|---|---|---|---|
| **Mirkowice 33** | | UtC-8617 | AMS | leaf (*S. plaris*) | 10210 | 120 | 1.2 | 11939 | 305 | | 5 | | | | | | Kabaciński & Schild 2005 |
| | | UtC-8598 | AMS | seed (*H. rhamnoides*) | 10930 | 80 | 0.7 | 12880 | 97 | | 5 | | | | | | Kabaciński & Schild 2005 |
| | | UtC-8619 | AMS | seed (*H. rhamnoides*) | 11010 | 100 | 0.9 | 12934 | 108 | | 5 | | | | | | Kabaciński & Schild 2005 |
| | | UtC-8618 | AMS | charcoal | 11820 | 200 | 1.7 | 13724 | 225 | | A, 5 | | | | | | Kabaciński & Schild 2005 |
| | | Gd-10892 | CON | wood branch | 11850 | 180 | 1.5 | 13746 | 208 | | A, 5 | | | | | | Kabaciński & Schild 2005 |
| | | Gd-12124 | CON | wood branch | 11950 | 110 | 0.9 | 13828 | 153 | | 5 | | | | | | Kabaciński & Schild 2005 |
| | | Gd-7851 | CON | wood fragment | 12160 | 80 | 0.7 | 14040 | 135 | * | 5 | | | | | | Kabaciński & Schild 2005 |
| | | UtC-8493 | AMS | charcoal | 12260 | 70 | 0.6 | 14263 | 155 | * | 5 | | | | | | Kabaciński & Schild 2005 |
| | | GrA-17715 | AMS | burned bone | 12290 | 70 | 0.6 | 14342 | 202 | * | | | | | | | Lanting et al. 2002 |
| | | Gd-10885 | CON | wood branch | 12400 | 230 | 1.9 | 14573 | 400 | * | A, 5 | | | | | | Kabaciński & Schild 2005 |
| | | Gd-10544 | CON | wood fragment | 12870 | 190 | 1.5 | 15363 | 280 | | A, 5 | | | | | | Kabaciński & Schild 2005 |
| | | Gd-10872 | CON | wood branch | 13110 | 200 | 1.5 | 15716 | 295 | | A, 5 | | | | | | Kabaciński & Schild 2005 |
| | | Gd-10876 | CON | wood branch | 16550 | 320 | 1.9 | 19986 | 384 | | A, 5 | | | | | | Kabaciński & Schild 2005 |
| | | | | | | | | | | | | 57.0 | 12248 | 41 | **14171** | **72** | |
| **Marolles/Tureau des Gardes** | | Ly-6989 | CON | bone (*R. tarandus*) | 11560 | 100 | 0.9 | 13423 | 95 | | B | | | | | | Bridault et al. 1997 |
| | | AA-44215 | AMS | bone (*E. ferus*) | 12160 | 120 | 1.0 | 14107 | 212 | * | | | | | | | Bignon 2008 |
| | | AA-44214 | AMS | bone (*E. ferus*) | 12170 | 130 | 1.1 | 14159 | 255 | * | | | | | | | Bignon 2008 |
| | | Ly-6988 | CON | bone | 12290 | 90 | 0.7 | 14416 | 277 | * | | | | | | | Bridault et al. 1997 |
| | | AA-44216 | AMS | bone | 12520 | 130 | 1.0 | 14715 | 302 | * | | | | | | | Bignon 2008 |
| | | | | | | | | | | | | 16.2 | 12282 | 57 | **14276** | **146** | |
| **Baume de Colle Rousse** | **2** | Gif-8657 | CON | ? | 12330 | 150 | 1.2 | **14478** | **318** | | | | | | | | Onoratini & Renault-Miskovsky 1999 |
| **Deux-Avens** | **C** | Ly-321 | CON | charcoal | 12320 | 600 | 4.9 | 14602 | 834 | * | A | | | | | | Onoratini & Renault-Miskovsky 1999 |
| | | Ly-322 | CON | bone | 12350 | 200 | 1.6 | 14510 | 367 | * | | | | | | | Onoratini & Renault-Miskovsky 1999 |
| | | | | | | | | | | | | 96.2 | 12347 | 190 | **14504** | **356** | |
| **Kastelhöhle-Nord** | **upper** | ETH-45026 | AMS | bone (*R. tarandus*) | 12215 | 45 | 0.4 | 14133 | 60 | | B | | | | | | Leesch & Müller 2012 |
| | | OxA-V-2793-54C | AMS | bone (*R. tarandus*) | 12270 | 60 | 0.5 | 14253 | 135 | * | | | | | | | Raede et al. 2020 |
| | | OxA-V-2793-55C | AMS | bone (*R. tarandus*) | 12380 | 50 | 0.4 | 14526 | 231 | * | | | | | | | Raede et al. 2020 |

Appendix Table 15: continued 2,

| site | layer/level/ conc./... | lab.-nr. | m. | material | BP | std. | % | calBP | std. | * | c. | P% | WA | std. | calBP | std. | reference |
|---|---|---|---|---|---|---|---|---|---|---|---|---|---|---|---|---|---|
| | | ETH-45025 | AMS | bone (*R. tarandus*) | 12395 | 45 | 0.4 | 14547 | 216 | * | | | | | | | Leesch & Müller 2012 |
| | | OxA-V-2748-25C | AMS | bone (*Equus* sp.) | 12560 | 50 | 0.4 | 14846 | 185 | | B | | | | | | Raede et al. 2020 |
| | | OxA-V-2754-48C | AMS | bone (*Equus* sp.) | 12880 | 50 | 0.4 | 15403 | 95 | | B | | | | | | Raede et al. 2020 |
| | | ETH-45024 | AMS | bone (Bos/Bison) | 13435 | 50 | 0.4 | 16181 | 88 | | B | | | | | | Leesch & Müller 2012 |
| | | OxA-V-2794-25C | AMS | bone (Bos/Bison) | 13550 | 60 | 0.4 | 16358 | 100 | | B | | | | | | Raede et al. 2020 |
| | | | | | | | | | | | | 22.1 | 12360 | 29 | **14506** | **241** | |
| **Abri Faustin** | 1 | OxA-26661 | AMS | bone (*C. elaphus*) | 12325 | 50 | 0.4 | 14444 | 256 | * | | | | | | | Barshay-Szmidt et al. 2016 |
| | | Lyon-10177 | AMS | bone (*E. ferus*) | 12370 | 60 | 0.5 | 14509 | 245 | * | | | | | | | Barshay-Szmidt et al. 2016 |
| | | Ly-2700 | CON | bone | 12370 | 220 | 1.8 | 14536 | 388 | * | | | | | | | Barshay-Szmidt et al. 2016 |
| | | OxA-26660 | AMS | bone (Bos/Bison) | 12415 | 50 | 0.4 | 14573 | 211 | * | | | | | | | Barshay-Szmidt et al. 2016 |
| | | Poz-52974 | AMS | bone (*R. tarandus*) | 12420 | 70 | 0.6 | 14578 | 230 | * | | | | | | | Barshay-Szmidt et al. 2016 |
| | | OxA-28079 | AMS | bone (*H. sapiens*) | 12700 | 55 | 0.4 | 15141 | 83 | | | | | | | | Barshay-Szmidt et al. 2016 |
| | | | | | | | | | | | | 72.7 | 12378 | 28 | **14533** | **221** | |
| **Meiendorf D** | | H-38-121C | CON | antler (*R. tarandus*) | 6150 | 500 | 8.1 | 6957 | 510 | | A, 1 | | | | | | Münnich 1957; Fischer & Tauber 1986 |
| | | Y-158.1 | CON | antler (*R. tarandus*) | 7060 | 400 | 5.7 | 7918 | 375 | | A, 1 | | | | | | Barendsen et al. 1957; Lanting & van der Plicht 1996 |
| | | Y-158 | CON | antler (*R. tarandus*) | 9540 | 130 | 1.4 | 10870 | 205 | | 1 | | | | | | Barendsen et al. 1957; Lanting & van der Plicht 1996 |
| | | Y-158.2 | CON | antler (*R. tarandus*) | 10760 | 250 | 2.3 | 12591 | 348 | | A, 1 | | | | | | Barendsen et al. 1957; Lanting & van der Plicht 1996 |
| | | W-264 | CON | antler (*R. tarandus*) | 11790 | 200 | 1.7 | 13693 | 223 | | A, 1 | | | | | | Rubin & Suess 1956; Rust 1958 |
| | | W-281 | CON | antler (b.s., *R. tarandus*) | 11870 | 200 | 1.7 | 13767 | 225 | | A, 1 | | | | | | Rubin & Suess 1956; Rust 1958 |
| | | H-38-121A | CON | antler (*R. tarandus*) | 12300 | 300 | 2.4 | 14463 | 485 | | A | | | | | | Münnich 1957; Rust 1958 |
| | | H-38-121B | CON | antler (*R. tarandus*) | 12300 | 200 | 1.6 | 14451 | 370 | | A, 1 | | | | | | Münnich 1957; Rust 1958 |
| | | K-4329 | CON | antler (*R. tarandus*) | 12360 | 110 | 0.9 | 14502 | 281 | * | | | | | | | Fischer & Tauber 1986 |
| | | KN-2220 | CON | bone (b.s.) | 12470 | 250 | 2.0 | 14662 | 431 | * | A | | | | | | Grimm & Weber 2008 |
| | | W-172 | CON | calcareous gyttja | 15750 | 800 | 5.1 | 19125 | 923 | | A, 1 | | | | | | Rubin & Suess 1956; Rust 1958 |
| | | | | | | | | | | | | 68.7 | 12378 | 101 | **14521** | **270** | |
| **Poggenwisch D** | | W-271 | CON | antler (b.s., *R. tarandus*) | 11750 | 200 | 1.7 | 13641 | 214 | | A, 1 | | | | | | Rubin & Suess 1956; Rust 1958 |
| | | KIA-32925 | AMS | antler (*R. tarandus*) | 12265 | 55 | 0.4 | 14218 | 105 | | B | | | | | | Grimm & Weber 2008 |
| | | OxA-V-2793-55C | AMS | bone (*R. tarandus*) | 12380 | 50 | 0.4 | 14526 | 231 | * | | | | | | | Raede et al. 2020 |

Appendix Table 15: continued 3,

| site | layer/level/ conc./... | lab.-nr. | m. | material | BP | std. | % | calBP | std. | * | c. | P% | WA | std. | calBP | std. | reference |
|---|---|---|---|---|---|---|---|---|---|---|---|---|---|---|---|---|---|
| | | KIA-32926 | AMS | antler (*R. tarandus*) | 12365 | 60 | 0.5 | 14503 | 249 | * | | | | | | | Grimm & Weber 2008 |
| | | K-4331 | CON | bone (*R. tarandus*) | 12440 | 115 | 0.9 | 14605 | 278 | * | | | | | | | Fischer & Tauber 1986 |
| | | K-4577 | CON | bone (*R. tarandus*) | 12440 | 115 | 0.9 | 14605 | 278 | * | | | | | | | Fischer & Tauber 1986 |
| | | GrN-11254 | CON | (H-136/116) | 12460 | 60 | 0.5 | 14645 | 216 | * | | | | | | | Lanting & van der Pflicht 1996 |
| | | KN-2754 | CON | bone (b.s.) | 12470 | 95 | 0.8 | 14648 | 257 | * | | | | | | | Grimm & Weber 2008 |
| | | K-4332 | CON | bone (*R. tarandus*) | 12570 | 115 | 0.9 | 14803 | 280 | * | | | | | | | Fischer & Tauber 1986 |
| | | H-32-118C | CON | calcareous gyttja | 12850 | 500 | 3.9 | 15223 | 802 | | A, 1 | | | | | | Münnich 1957; Rust 1958 |
| | | H-136-116 | CON | wood twigs | 12980 | 370 | 2.9 | 15440 | 606 | | A, 1 | | | | | | Münnich 1957; Rust 1958 |
| | | H-31-67 | CON | organic fraction bone | 13050 | 200 | 1.5 | 15634 | 291 | | D | | | | | | Münnich 1957; Rust 1958 |
| | | W-93 | CON | calcareous gyttja | 15150 | 150 | 1.0 | 18473 | 163 | | D | | | | | | Münnich 1957; Rust 1958 |
| | | H-32-60 | CON | calcareous gyttja | 15700 | 350 | 2.2 | 19038 | 376 | | A, 1 | | | | | | Münnich 1957; Rust 1958 |
| | | H-32-118A | CON | calcareous gyttja | 17100 | 560 | 3.3 | 20718 | 733 | | A, 1 | | | | | | Münnich 1957; Rust 1958 |
| | | | | | | | | | | | | 44.1 | 12409 | 29 | **14566** | **197** | |
| **Oelknitz** | | Bln-1908 | CON | charcoal | 10940 | 85 | 0.8 | 12891 | 103 | | B | | | | | | Musil 1985 |
| | | Bln-1724 | CON | charcoal | 11160 | 85 | 0.8 | 13048 | 97 | | B | | | | | | Musil 1985 |
| | | H-830/840 | CON | soil/charcoal | 11750 | 260 | 2.2 | 13668 | 287 | | B | | | | | | Musil 1985 |
| | | OxA-5715 | AMS | bone (*E. ferus*) | 11810 | 110 | 0.9 | 13666 | 117 | | B | | | | | | Brasser 2013 |
| | | OxA-5711 | AMS | bone (*E. ferus*), cutm. | 12050 | 110 | 0.9 | 13931 | 120 | | B | | | | | | Brasser 2013 |
| | | OxA-5710 | AMS | bone (*E. ferus*) | 12080 | 110 | 0.9 | 13961 | 129 | | B | | | | | | Brasser 2013 |
| | | OxA-5712 | AMS | bone (*R. tarandus*) | 12270 | 110 | 0.9 | 14402 | 294 | * | | | | | | | Brasser 2013 |
| | | OxA-5709 | AMS | bone (*E. ferus*), cutm. | 12270 | 120 | 1 | 14409 | 306 | * | | | | | | | Brasser 2013 |
| | | Bln-1726 | CON | bone | 12350 | 85 | 0.7 | 14486 | 268 | * | | | | | | | Musil 1985 |
| | | OxA-8074 | AMS | bone (*A. anser*) | 12390 | 70 | 0.6 | 14535 | 240 | * | | | | | | | Brasser 2013 |
| | | Bln-1565 | CON | bone | 12545 | 80 | 0.6 | 14788 | 231 | * | | | | | | | Musil 1985 |
| | | OxA-5714 | AMS | bone (*R. tarandus*), cutm. | 12620 | 120 | 1 | 14887 | 281 | * | | | | | | | Brasser 2013 |
| | | OxA-8076 | AMS | bone (*E. ferus*) | 12630 | 75 | 0.6 | 15016 | 133 | | B | | | | | | Brasser 2013 |
| | | OxA-8075 | AMS | bone (*E. ferus*) | 12660 | 80 | 0.6 | 15073 | 123 | | B | | | | | | Brasser 2013 |
| | | OxA-5717 | AMS | bone (*R. tarandus*) | 12670 | 110 | 0.9 | 15041 | 197 | | B | | | | | | Brasser 2013 |

Appendix Table 15: continued 4,

| site | layer/level/ conc./... | lab.-nr. | m. | material | BP | std. | % | calBP | std. | * | c. | P% | WA | std. | calBP | std. | reference |
|---|---|---|---|---|---|---|---|---|---|---|---|---|---|---|---|---|---|
| | | OxA-5713 | AMS | bone (*E. ferus*), cutm. | 12740 | 120 | 0.9 | 15193 | 189 | | B | | | | | | Brasser 2013 |
| | | OxA-5716 | AMS | bone (*E. ferus*) | 12790 | 110 | 0.9 | 15284 | 169 | | B | | | | | | Brasser 2013 |
| | | OxA-10240 | AMS | Ivory (*M. primigenius*) | 14100 | 100 | 0.7 | 17171 | 123 | | B | | | | | | Brasser 2013 |
| | | | | | | | | | | | | 9.2 | 12413 | 37 | **14571** | **201** | |
| **Käsloch** | | ETH-39771 | AMS | tooth (*Equus* sp.) | 12450 | 45 | 0.4 | 14632 | 199 | * | | | | | | | Leesch & Müller 2012 |
| | | ETH-39769 | AMS | tooth (*Equus* sp.) | 12505 | 45 | 0.4 | 14744 | 182 | * | | | | | | | Leesch & Müller 2012 |
| | | ETH-39770 | AMS | tooth (*Equus* sp.) | 13760 | 45 | 0.3 | 16694 | 108 | | | | | | | | Leesch & Müller 2012 |
| | | | | | | | | | | | | 38.7 | 12478 | 32 | **14705** | **171** | |
| **Abri du Rouet** | **9b** | GifA-93082 | AMS | charcoal | 12520 | 130 | 1.0 | **14715** | **302** | | | | | | | | Brochier & Livache 2003b |
| **Gough's Cave** | | OxA-2795 | AMS | bone (*H. sapiens*) | 11820 | 120 | 1.0 | 13683 | 132 | | | | | | | | Jacobi 2004 |
| | | OxA-2797 | AMS | Bâton p. antler (*R. tarandus*) | 11870 | 110 | 0.9 | 13756 | 148 | | | | | | | | Jacobi 2004 |
| | | OxA-1890 | AMS | ivory (*M. primigenius*) | 12170 | 130 | 1.1 | 14159 | 255 | | | | | | | | Jacobi 2004 |
| | | OxA-18067 | AMS | bone (*C. elaphus*) | 12245 | 55 | 0.4 | 14187 | 91 | | | | | | | | Jacobi & Higham 2009 |
| | | OxA-1071 | AMS | bone (*C. elaphus*) | 12300 | 180 | 1.5 | 14448 | 350 | * | | | | | | | Jacobi 2004 |
| | | OxA-2237 | AMS | bone (*H. sapiens*) | 12300 | 100 | 0.8 | 14438 | 289 | * | | | | | | | Jacobi 2004 |
| | | OxA-589 | AMS | bone (*E. ferus*) | 12340 | 150 | 1.2 | 14488 | 316 | * | | | | | | | Jacobi 2004 |
| | | OxA-465 | AMS | bone (*E. ferus*) | 12360 | 170 | 1.4 | 14515 | 335 | * | | | | | | | Jacobi 2004 |
| | | OxA-590 | AMS | bone (*E. ferus*) | 12370 | 150 | 1.2 | 14522 | 314 | * | | | | | | | Jacobi 2004 |
| | | OxA-2796 | AMS | bone (*H. sapiens*) | 12380 | 110 | 0.9 | 14525 | 277 | * | | | | | | | Jacobi 2004 |
| | | OxA-3452 | AMS | bone (*E. ferus*) | 12400 | 100 | 0.8 | 14548 | 264 | * | | | | | | | Jacobi 2004 |
| | | OxA-17832 | AMS | bone (*E. ferus*) | 12415 | 50 | 0.4 | 14573 | 211 | * | | | | | | | Jacobi & Higham 2009 |
| | | OxA-13585 | AMS | bone (*C. familiaris*) | 12440 | 55 | 0.4 | 14611 | 213 | * | | | | | | | Jacobi & Higham 2009 |
| | | OxA-18066 | AMS | bone (*L. lynx*) | 12440 | 55 | 0.4 | 14611 | 213 | * | | | | | | | Jacobi & Higham 2009 |
| | | OxA-464 | AMS | bone (*E. ferus*) | 12470 | 160 | 1.3 | 14647 | 328 | * | | | | | | | Jacobi 2004 |
| | | OxA-17846 | AMS | ivory (*M. primigenius*) | 12470 | 55 | 0.4 | 14667 | 207 | * | | | | | | | Jacobi & Higham 2009 |
| | | OxA-17848 | AMS | bone (*H. sapiens*) | 12485 | 50 | 0.4 | 14701 | 195 | * | | | | | | | Jacobi & Higham 2009 |
| | | OxA-18065 | AMS | bone (*E. ferus*) | 12490 | 55 | 0.4 | 14706 | 201 | * | | | | | | | Jacobi & Higham 2009 |

Appendix Table 15: continued 5,

| site | layer/level/ conc./... | lab.-nr. | m. | material | BP | std. | % | calBP | std. | * | c. | P% | WA | std. | calBP | std. | reference |
|---|---|---|---|---|---|---|---|---|---|---|---|---|---|---|---|---|---|
| | | OxA-3412 | AMS | bone (*C. elaphus*) | 12490 | 120 | 1.0 | 14672 | 287 | * | | | | | | | Jacobi 2004 |
| | | OxA-12104 | AMS | bone (*E. ferus*) | 12498 | 50 | 0.4 | 14727 | 191 | * | | | | | | | Jacobi & Higham 2009 |
| | | OxA-17845 | AMS | bone (*C. elaphus*) | 12500 | 50 | 0.4 | 14730 | 190 | * | | | | | | | Jacobi & Higham 2009 |
| | | OxA-16378 | AMS | bone (*C. elaphus*) | 12515 | 50 | 0.4 | 14758 | 188 | * | | | | | | | Jacobi & Higham 2009 |
| | | OxA-18068 | AMS | bone (*E. ferus*) | 12520 | 55 | 0.4 | 14763 | 195 | * | | | | | | | Jacobi & Higham 2009 |
| | | OxA-18064 | AMS | Bâton p. antler (*R. tarandus*) | 12535 | 55 | 0.4 | 14792 | 194 | * | | | | | | | Jacobi & Higham 2009 |
| | | OxA-4107 | AMS | bone (*L. timidus*) | 12550 | 130 | 1.0 | 14762 | 303 | * | | | | | | | Jacobi 2004 |
| | | OxA-17847 | AMS | bone (*H. sapiens*) | 12565 | 50 | 0.4 | 14856 | 184 | * | | | | | | | Jacobi & Higham 2009 |
| | | OxA-17833 | AMS | bone (*E. ferus*) | 12570 | 45 | 0.4 | 14873 | 172 | * | | | | | | | Jacobi & Higham 2009 |
| | | OxA-3414 | AMS | bone | 12570 | 120 | 1.0 | 14800 | 288 | * | | | | | | | Jacobi 2004 |
| | | OxA-16292 | AMS | bone (*E. ferus*) | 12585 | 55 | 0.4 | 14902 | 172 | * | | | | | | | Jacobi & Higham 2009 |
| | | OxA-17849 | AMS | bone (*H. sapiens*) | 12590 | 50 | 0.4 | 14972 | 107 | * | | | | | | | Jacobi & Higham 2009 |
| | | OxA-18035 | AMS | bone | 12600 | 80 | 0.6 | 14889 | 220 | * | | | | | | | Jacobi & Higham 2009 |
| | | OxA-3411 | AMS | bone (*L. lynx*) | 12650 | 120 | 0.9 | 14942 | 274 | * | | | | | | | Jacobi 2004 |
| | | OxA-4106 | AMS | bone (*E. ferus*) | 12670 | 120 | 0.9 | 14992 | 258 | * | | | | | | | Jacobi 2004 |
| | | OxA-466 | AMS | bone (*C. elaphus*) | 12800 | 470 | 3.7 | 15148 | 757 | * | A | | | | | | Jacobi 2004 |
| | | OxA-3413 | AMS | bone (*E. ferus*) | 12940 | 140 | 1.1 | 15479 | 196 | | | | | | | | Jacobi 2004 |
| | | | | | | | | | | | | 32.4 | 12506 | 12 | **14772** | **147** | |
| **Stellmoor** | | K-4328 | CON | bone (*R. tarandus*) | 12180 | 130 | 1.1 | 14183 | 266 | | 1 | | | | | | Fischer & Tauber 1986 |
| | | K-4261 | CON | antler (*R. tarandus*) | 12190 | 125 | 1.0 | 14198 | 263 | | 1 | | | | | | Fischer & Tauber 1986 |
| | | W-261 | CON | antler (*R. tarandus*) | 12450 | 200 | 1.6 | 14627 | 371 | | A, 1 | | | | | | Rubin & Suess 1956; Rust 1958 |
| | | KN-2224 | CON | bone/antler (b.s.) | 12530 | 160 | 1.3 | 14726 | 338 | * | | | | | | | Grimm & Weber 2008 |
| | | KN-2223 | CON | bone (b.s.) | 12590 | 80 | 0.6 | 14870 | 223 | * | | | | | | | Grimm & Weber 2008 |
| | | | | | | | | | | | | 73.7 | 12578 | 72 | **14857** | **214** | |
| **Ranchot, Abri des Cabônes** | **lower, D-F** | Ly-2296 | CON | bone | 12620 | 250 | 2 | **14862** | **462** | | A | | | | | | David 1996 |
| **La Madeleine** | **B - Magd. VI** | Ly-919 | CON | bone (*H. sapiens*) | 12640 | 260 | 2.1 | **14894** | **480** | | A | | | | | | Evin et al. 1976 |

Appendix Table 15: continued 6,

| site | layer/level/ conc./... | lab.-nr. | m. | material | BP | std. | % | calBP | std. | * | c. | P% | WA | std. | calBP | std. | reference |
|---|---|---|---|---|---|---|---|---|---|---|---|---|---|---|---|---|---|
| **Olbrachcice 8** | | Lod-111 | CON | charcoal | 12685 | 235 | 1.9 | **14964** | **454** | | A | | | | | | Burdukiewicz 1981 |
| **Petersfels** | | H-5210-4866 | CON | ? | 12160 | 95 | 0.8 | 14061 | 161 | | | | | | | | Hahn 1996 |
| | | H-7139-7300 | CON | bone (*Equus* sp.) | 12180 | 100 | 0.8 | 14109 | 182 | | | | | | | | Hahn 1996 |
| | | H-7215-7349 | CON | ? | 12270 | 95 | 0.8 | 14367 | 253 | | | | | | | | Hahn 1996 |
| | | H-7136-6890 | CON | bone (*R. tarandus*) | 12320 | 90 | 0.7 | 14456 | 280 | | | | | | | | Hahn 1996 |
| | | ETH-11518 | AMS | bone (*H. sapiens*) | 12440 | 100 | 0.8 | 14605 | 262 | * | | | | | | | Hahn 1996 |
| | | H-7137-7067 | CON | bone/teeth (*Equus* sp.) | 12470 | 100 | 0.8 | 14647 | 263 | * | | | | | | | Hahn 1996 |
| | | H-7134-6876 | CON | bone (*Lepus* sp.) | 12500 | 120 | 1 | 14687 | 288 | * | | | | | | | Hahn 1996 |
| | | H-7140-7058 | CON | bone (*R. tarandus*) | 12530 | 90 | 0.7 | 14752 | 248 | * | | | | | | | Hahn 1996 |
| | | H-7133-6877 | CON | bone (*R. tarandus*) | 12580 | 130 | 1 | 14810 | 300 | * | | | | | | | Hahn 1996 |
| | | H-4277-3531 | CON | ? | 12650 | 100 | 0.8 | 15007 | 192 | * | | | | | | | Hahn 1996 |
| | | H-7214-7350 | CON | ? | 12660 | 100 | 0.8 | 15037 | 177 | * | | | | | | | Hahn 1996 |
| | | H-7135-6879 | CON | bone (*R. tarandus*) | 12670 | 100 | 0.8 | 15061 | 167 | * | | | | | | | Hahn 1996 |
| | | H-7217-7364 | CON | ? | 12670 | 90 | 0.7 | 15079 | 140 | * | | | | | | | Hahn 1996 |
| | | H-7141-6985 | CON | ? | 12680 | 110 | 0.9 | 15067 | 187 | * | | | | | | | Hahn 1996 |
| | | H-7138-7057 | CON | bone (*R. tarandus*) | 12685 | 75 | 0.6 | 15116 | 108 | * | | | | | | | Hahn 1996 |
| | | | | | | | | | | | | 52.4 | 12602 | 30 | **15022** | **61** | |
| **Bois Ragot** | **5** | OxA-12079 | AMS | harpoon fragment | 12560 | 50 | 0.4 | 14846 | 185 | * | | | | | | | Dujardin & Oberlin 2005 |
| | | OxA-12080 | AMS | bone (*R. tarandus*) | 12615 | 70 | 0.6 | 14990 | 135 | * | | | | | | | Dujardin & Oberlin 2005 |
| | | OxA-12081 | AMS | bone (*C. elaphus*) | 12685 | 70 | 0.6 | 15118 | 101 | * | | | | | | | Dujardin & Oberlin 2005 |
| | | | | | | | | | | | | 34.4 | 12605 | 35 | **15023** | **65** | |
| **Morin** | **AIII** | OxA-28122 | AMS | premolar (*H. sapiens*) | 12275 | 60 | 0.5 | 14267 | 144 | | 4 | | | | | | Barshay-Szmidt et al. 2016 |
| | **AIV** | OxA-19829 | AMS | bone (*B. scandiacus*) | 12380 | 55 | 0.4 | 14524 | 234 | | | | | | | | Szmidt et al. 2009 |
| | **B1** | OxA-26670 | AMS | antler (cervid) | 12470 | 60 | 0.5 | 14663 | 214 | | 4 | | | | | | Barshay-Szmidt et al. 2016 |
| | **AIV** | OxA-27393 | AMS | antler (*C. elaphus*) | 12500 | 55 | 0.4 | 14725 | 198 | | | | | | | | Barshay-Szmidt et al. 2016 |
| | **AIV** | OxA-19827 | AMS | bone (cervid) | 12630 | 60 | 0.5 | 15042 | 95 | * | | | | | | | Szmidt et al. 2009 |
| | **AIV** | OxA-19828 | AMS | bone (cervid) | 12690 | 60 | 0.5 | 15127 | 89 | * | | | | | | | Szmidt et al. 2009 |

Appendix Table 15: continued 7,

| site | layer/level/ conc./... | lab.-nr. | m. | material | BP | std. | % | calBP | std. | * | c. | P% | WA | std. | calBP | std. | reference |
|---|---|---|---|---|---|---|---|---|---|---|---|---|---|---|---|---|---|
| | **AIII** | OxA-26667 | AMS | antler (cervid) | 12705 | 55 | 0.4 | **15147** | **82** | * | | | | | | | Barshay-Szmidt et al. 2016 |
| | **AIV** | OxA-26669 | AMS | antler (cervid) | 12785 | 60 | 0.5 | 15260 | 93 | * | 4 | | | | | | Barshay-Szmidt et al. 2016 |
| | **B1** | OxA-26666 | AMS | antler (cervid) | 12870 | 60 | 0.5 | 15392 | 105 | | 4 | | | | | | Barshay-Szmidt et al. 2016 |
| | **B1** | OxA-26668 | AMS | antler (cervid) | 12920 | 60 | 0.5 | 15450 | 105 | | | | | | | | Barshay-Szmidt et al. 2016 |
| | **B1** | OxA-19826 | AMS | bone (B. scandiacus) | 12945 | 50 | 0.4 | 15477 | 99 | | | | | | | | Szmidt et al. 2009 |
| | **B1** | OxA-19699 | AMS | bone (R. tarandus) | 13065 | 60 | 0.5 | 15661 | 89 | | | | | | | | Szmidt et al. 2009 |
| | | | | | | | | | | | | 33.4 | 12703 | 29 | **15152** | **57** | |
| **Duruthy** | **3** | OxA-28073 | AMS | antler (R. tarandus) | 12810 | 53 | 0.4 | 15300 | 94 | | | | | | | | Barshay-Szmidt et al. 2016 |
| | | Poz-15983 | AMS | bone (R. tarandus) | 12930 | 60 | 0.5 | 15461 | 106 | * | | | | | | | Langlais et al. 2012 |
| | | OxA-29996 | AMS | bone (R. tarandus) | 13130 | 55 | 0.4 | 15753 | 85 | * | | | | | | | Barshay-Szmidt et al. 2016 |
| | | | | | | | | | | | | 13.4 | 12863 | 40 | **15380** | **86** | |
| **La Madeleine** | **C - Magd. V** | Ly-920 | CON | bone | 12750 | 240 | 1.9 | 15067 | 458 | * | A | | | | | | Evin et al. 1976 |
| | | Ly-921 | CON | bone (H. sapiens) | 13070 | 190 | 1.5 | 15660 | 280 | * | | | | | | | Evin et al. 1976 |
| | | | | | | | | | | | | 29.6 | 12947 | 149 | **15489** | **209** | |
| **Rinxent, La Grotta de Cleves** | | OxA-1343 | AMS | antler | 13030 | 120 | 0.9 | **15592** | **183** | | | | | | | | Fagnart 1988 |
| **Colombier** | **17** | UtC-1737 | AMS | ? | 13280 | 110 | 0.8 | 15969 | 165 | * | | | | | | | Onoratini & Renault-Miskovsky 1999 |
| | | OxA-27208 | AMS | ? | 12995 | 60 | 0.5 | 15544 | 110 | * | | | | | | | Onoratini & Renault-Miskovsky 1999 |
| | | Ly-5292 | CON | ? | 14480 | 360 | 2.5 | 17625 | 458 | | A, C | | | | | | Onoratini & Renault-Miskovsky 1999 |
| | | | | | | | | | | | | 2.3 | 13060 | 53 | **15656** | **80** | |
| **Abri de Fontalès** | **I-III** | Poz-138702 | AMS | bone (R. tarandus) | 12900 | 70 | 0.5 | 15428 | 114 | * | | | | | | | Pétillon et al. 2024 |
| | | Poz-138701 | AMS | antler (R. tarandus) | 12970 | 70 | 0.5 | 15508 | 120 | * | | | | | | | Pétillon et al. 2024 |
| | | GifA-96327 | AMS | barbed point | 13140 | 120 | 0.9 | 15770 | 176 | * | | | | | | | Tisnerat-Laborde et al. 1997 |
| | | | | | | | | | | | | 22.4 | 12965 | 46 | **15503** | **96** | |
| **Kniegrotte** | **VIII** | OxA-4853 | AMS | bone (S. tatarica) | 13090 | 130 | 1 | 15687 | 199 | * | | | | | | | Street & Höck 1998 |
| | | OxA-4845 | AMS | bone (R. tarandus) | 13120 | 130 | 1 | 15736 | 194 | * | | | | | | | Street & Höck 1998 |
| | | OxA-4849 | AMS | bone (S. tatarica) | 13130 | 120 | 0.9 | 15754 | 177 | * | | | | | | | Street & Höck 1998 |
| | | OxA-4848 | AMS | bone (E. sp.) | 13150 | 130 | 1 | 15783 | 189 | * | | | | | | | Street & Höck 1998 |

Appendix Table 15: continued 8,

| site | layer/level/ conc./... | lab.-nr. | m. | material | BP | std. | % | calBP | std. | * | c. | P% | WA | std. | calBP | std. | reference |
|---|---|---|---|---|---|---|---|---|---|---|---|---|---|---|---|---|---|
| | | OxA-4850 | AMS | bone (*V. lagopus*) | 13160 | 140 | 1.1 | **15797** | **203** | * | | | | | | | Street & Höck 1998 |
| | | OxA-4846 | AMS | bone (*E.* sp.) | 13190 | 130 | 1 | 15843 | 187 | * | | | | | | | Street & Höck 1998 |
| | | OxA-4832 | AMS | bone (*R. tarandus*), cutm. | 13310 | 110 | 0.8 | 16007 | 166 | * | | | | | | | Street & Höck 1998 |
| | | OxA-4852 | AMS | bone (*E.* sp.) | 13520 | 130 | 1 | 16313 | 201 | * | | | | | | | Street & Höck 1998 |
| | | Bln-1564 | CON | ? | 13585 | 165 | 1.2 | 16427 | 261 | * | | | | | | | Street & Höck 1998 |
| | | OxA-4851 | AMS | bone (*M. primigenius*) | 14470 | 140 | 1 | 17673 | 215 | | B | | | | | | Street & Höck 1998 |
| | | | | | | | | | | | | 9.9 | 13238 | 43 | **15898** | **78** | |
| **Riparo Tagliente** | **15-16** | R-605 | CON | charcoal | 13330 | 160 | 1.2 | 16036 | 228 | * | | | | | | | Djindjan et al. 1999 |
| | | R-605a | CON | charcoal | 13430 | 180 | 1.3 | 16186 | 270 | * | | | | | | | Djindjan et al. 1999 |
| | | | | | | | | | | | | 67.8 | 13374 | 120 | **16091** | **178** | |
| **Jaurias** | **5** | Ly-3730 | CON | ? | 13580 | 140 | 1.0 | 16414 | 220 | * | | | | | | | Lenoir 2000 |
| | | Gd-2698 | CON | ? | 13500 | 200 | 1.5 | 16297 | 304 | * | | | | | | | Lenoir 2000 |
| | | Gd-2697 | CON | ? | 14660 | 200 | 1.4 | 17851 | 280 | | | | | | | | Lenoir 2000 |
| | | | | | | | | | | | | 74.3 | 13554 | 115 | **16365** | **178** | |
| **Kamegg** | | GrN-22883 | CON | ? | 13840 | 120 | 0.9 | 16779 | 182 | * | | | | | | | Verpoorte 2004 |
| | | GrN-23182 | CON | ? | 14130 | 110 | 0.8 | 17194 | 126 | * | | | | | | | Verpoorte 2004 |
| | | | | | | | | | | | | 7.5 | 13998 | 81 | **17026** | **126** | |
| **Le Martinet** | **IV** | Ly-1605 | CON | bone | 13600 | 1100 | 8.1 | 16228 | 1528 | * | A | | | | | | Le Tensorer 1981 |
| | | Ly-5069 | CON | bone | 14098 | 239 | 1.7 | 17135 | 353 | * | A | | | | | | Djindjan 2000 |
| | | | | | | | | | | | | 65.8 | 14076 | 234 | **17091** | **337** | |
| **Borshchëvo 1** | | ICFN-903 | CON | shell | 9900 | 70 | 0.7 | 11383 | 128 | | | | | | | | Lisitsyn & Dudin 2019 |
| | | GIN-11197 | CON | ? | 15140 | 100 | 0.7 | 18461 | 144 | * | | | | | | | Lisitsyn & Dudin 2019 |
| | | GIN-11198 | CON | ? | 15200 | 100 | 0.7 | 18487 | 148 | * | | | | | | | Lisitsyn & Dudin 2019 |
| | | GIN-11199 | CON | ? | 15200 | 200 | 1.3 | 18506 | 193 | * | | | | | | | Lisitsyn & Dudin 2019 |
| | | GIN-8085 | CON | bone (*M. primigenius*) | 15600 | 70 | 0.4 | 18884 | 60 | | | | | | | | Lisitsyn & Dudin 2019 |
| | | LE-3727 | CON | bone (*M. primigenius*) | 17200 | 150 | 0.9 | 20747 | 167 | | | | | | | | Lisitsyn & Dudin 2019 |
| | | | | | | | | | | | | 90.5 | 15173 | 67 | **18470** | **137** | |
| **Grotta delle Settecannelle** | | Ozc-165 | CON | ? | 15700 | 180 | 1.1 | **19029** | **186** | | | | | | | | Ucelli Gnesutta & Cristiani 2002 |

Appendix Table 15: continued 9,

| site | layer/level/ conc./... | lab.-nr. | m. | material | BP | std. | % | calBP | std. | * | c. | P% | WA | std. | calBP | std. | reference |
|---|---|---|---|---|---|---|---|---|---|---|---|---|---|---|---|---|---|
| Taurisano | 12-10 | R-1063 | CON | bone | 15600 | 120 | 0.8 | **18903** | **108** | * | | | | | | | Milliken 1998 |
| | 22-18 | R-1064 | CON | bone | 16000 | 150 | 0.9 | 19300 | 176 | * | | | | | | | Milliken 1998 |
| | 9-6 | R-1062 | CON | bone | 16050 | 160 | 1 | 19351 | 187 | * | | | | | | | Milliken 1998 |
| | | | | | | | | | | | | 3.3 | 15831 | 81 | **19109** | **116** | |
| Amalda | | I-11435 | CON | ? | 16090 | 240 | 1.5 | 19443 | 303 | * | | | | | | | Soto-Barreiro 2003 |
| | | I-11428 | CON | ? | 16200 | 380 | 2.3 | 19598 | 454 | * | A | | | | | | Soto-Barreiro 2003 |
| | | I-11355 | CON | ? | 17580 | 440 | 2.5 | 21310 | 568 | | A | | | | | | Soto-Barreiro 2003 |
| | | | | | | | | | | | | 80.7 | 16121 | 203 | **19468** | **270** | |
| Fontgrasse | 1a | Erl-8925 | AMS | charcoal (*Pinus* sp.) | 16338 | 143 | 0.9 | 19738 | 172 | * | | | | | | | Bazile 2006 |
| | | Erl-8928 | AMS | bone | 16338 | 153 | 0.9 | 19741 | 185 | * | | | | | | | Bazile 2006 |
| | | | | | | | | | | | | 100 | 16338 | 104 | **19726** | **131** | |
| Abri du Bois des Brousses | 3 | OxA-22941 | CON | ? | 16440 | 80 | 0.5 | **19813** | **147** | | | | | | | | Bazile 2011 |
| Fontgrasse | 3 | Erl-8926 | AMS | ? | 16518 | 133 | 0.8 | 19927 | 210 | * | | | | | | | Bazile 2006 |
| | | Erl-8927 | AMS | ? | 17100 | 144 | 0.8 | 20658 | 157 | * | | | | | | | Bazile 2006 |
| | | | | | | | | | | | | 0.3 | 16786 | 98 | **20287** | **128** | |
| Grotta Paglicci | 13a | GrN-14318 | CON | charcoal | 15480 | 150 | 1.0 | 18726 | 178 | | B | | | | | | Boschin et al. 2018 |
| | 14 b (a) | UtC- | AMS | ? | 15600 | 200 | 1.3 | 18914 | 201 | | B | | | | | | Boschin et al. 2018 |
| | 12c | GrN-14317 | CON | charcoal | 15730 | 330 | 2.1 | 19072 | 349 | | A | | | | | | Boschin et al. 2018 |
| | 15a | GrN-14323 | CON | charcoal | 15750 | 160 | 1.0 | 19073 | 177 | | B | | | | | | Boschin et al. 2018 |
| | 14b (b) | GrN-14322 | CON | charcoal | 15930 | 200 | 1.3 | 19240 | 223 | | B | | | | | | Boschin et al. 2018 |
| | 12a | GrN-14316 | CON | charcoal | 15950 | 350 | 2.2 | 19329 | 395 | | A | | | | | | Boschin et al. 2018 |
| | 13c | GrN-14320 | CON | charcoal | 15990 | 160 | 1.0 | 19290 | 186 | | B | | | | | | Boschin et al. 2018 |
| | 13d | GrN-14321 | CON | charcoal | 16030 | 190 | 1.2 | 19336 | 218 | | B | | | | | | Boschin et al. 2018 |
| | 15b | GrN-14324 | CON | charcoal | 16260 | 160 | 1.0 | 19641 | 204 | | B | | | | | | Boschin et al. 2018 |
| | 13b | GrN-14319 | CON | charcoal | 16310 | 350 | 2.1 | 19708 | 431 | | A | | | | | | Boschin et al. 2018 |
| | 16 b3 (a) | GrN-14326 | CON | charcoal | 16450 | 190 | 1.2 | 19875 | 247 | * | | | | | | | Boschin et al. 2018 |
| | 16 b7 | GrN-14872 | CON | ? | 16480 | 150 | 0.9 | 19891 | 218 | * | | | | | | | Boschin et al. 2018 |

Appendix Table 15: continued 10,

| site | layer/level/ conc./... | lab.-nr. | m. | material | BP | std. | % | calBP | std. | * | c. | P% | WA | std. | calBP | std. | reference |
|---|---|---|---|---|---|---|---|---|---|---|---|---|---|---|---|---|---|
| | **16 a3-1** | GrN-14325 | CON | charcoal | 16690 | 150 | 0.9 | 20159 | 196 | * | | | | | | | Boschin et al. 2018 |
| | **16 b5** | GrN-14871 | CON | ? | 16750 | 150 | 0.9 | 20225 | 191 | * | | | | | | | Boschin et al. 2018 |
| | **16 c2** | GrN-14873 | CON | ? | 16850 | 150 | 0.9 | 20346 | 181 | * | | | | | | | Boschin et al. 2018 |
| | **17 b** | GrN-14874 | CON | ? | 16890 | 160 | 0.9 | 20407 | 203 | * | | | | | | | Boschin et al. 2018 |
| | **17 e (b)** | GrN-14876 | CON | ? | 16940 | 160 | 0.9 | 20481 | 208 | * | | | | | | | Boschin et al. 2018 |
| | **16 b3 (b)** | GrN-14870 | CON | charcoal | 16970 | 130 | 0.8 | 20526 | 174 | * | | | | | | | Boschin et al. 2018 |
| | **17 d1** | GrN-14875 | CON | ? | 17050 | 160 | 0.9 | 20604 | 184 | * | | | | | | | Boschin et al. 2018 |
| | **15** | UtC-? | AMS | charcoal | 17100 | 300 | 1.8 | 20671 | 374 | | A | | | | | | Boschin et al. 2018 |
| | **16** | UtC-? | AMS | charcoal | 17200 | 300 | 1.7 | 20829 | 393 | | A | | | | | | Boschin et al. 2018 |
| | **17 e (a)** | UtC-? | AMS | ? | 19600 | 300 | 1.5 | 23556 | 340 | | C | | | | | | Boschin et al. 2018 |
| | | | | | | | | | | | | 8.3 | 16800 | 51 | **20323** | **82** | |
| **Abri Gandil** | | GifA-96416 | AMS | bone | 16980 | 170 | 1.0 | **20525** | **212** | | | | | | | | Djindjan 2000 |
| **Altamira** | **7 inf.** | GrA-30324 | AMS | bone | 18750 | 100 | 0.5 | 22690 | 152 | * | | | | | | | de las Heras et al. 2013 |
| | **7 med.** | GrA-30325 | AMS | bone | 19060 | 90 | 0.5 | 22996 | 67 | * | | | | | | | de las Heras et al. 2013 |
| | **7 sub.** | GrA-32761 | AMS | bone | 19630 | 80 | 0.4 | 23601 | 162 | | B | | | | | | de las Heras et al. 2013 |
| | | | | | | | | | | | | 2.1 | 18921 | 67 | **22817** | **127** | |
| **Cueva del Moro Chufin** | **(E) III** | CSIC-258 | CON | charcoal | 17420 | 200 | 1.1 | **21081** | **275** | | | | | | | | Cabrera & Bernaldo de Quirós 1977 |
| **Cueto de la Mina** | **E** | Ua-3588 | CON | bone | 17545 | 205 | 1.2 | **21286** | **320** | | | | | | | | Soto-Barreiro 2003 |
| | **E** | OxA-10122 | AMS | bone (*M. primigenius*) | 19700 | 500 | 2.5 | 23750 | 590 | | A | | | | | | Stuart et al. 2002 |
| **Chinchon 1** | **C** | Ly-5078 | AMS | egg shell | 17750 | 80 | 0.5 | **21570** | **164** | | | | | | | | Brochier 2016 |
| **Aitzbarte IV El Mirón** | | GrN-5993 | CON | bone | 17950 | 100 | 0.6 | 21782 | 206 | | | | | | | | Soto-Barreiro 2003 |
| | | GX-32655 | CON | bone collagen | 18390 | 300 | 1.6 | 22305 | 352 | * | A | | | | | | Straus & Gonzáles Morales 2007 |
| | | GX-24471 | CON | bone | 18950 | 350 | 1.8 | 22930 | 400 | * | A | | | | | | Straus et al. 2002 |
| | | GX-24470 | CON | bone | 18980 | 360 | 1.9 | 22967 | 419 | * | A | | | | | | Straus et al. 2002 |
| | | | | | | | | | | | | 33.9 | 18728 | 192 | **22669** | **195** | |

Appendix Table 15: continued 11,

| site | layer/level/ conc./... | lab.-nr. | m. | material | BP | std. | % | calBP | std. | * | c. | P% | WA | std. | calBP | std. | reference |
|---|---|---|---|---|---|---|---|---|---|---|---|---|---|---|---|---|---|
| **Cuzoul de Vers** | **21** | Lyon-9076 | AMS | antler | 18590 | 110 | 0.6 | 22566 | 158 | * | | | | | | | Ducasse et al. 2014 |
| | **19** | Lyon-9075 | AMS | antler | 18860 | 110 | 0.6 | 22753 | 151 | * | | | | | | | Ducasse et al. 2014 |
| | **18** | OxA-11118 | AMS | bone | 19020 | 110 | 0.6 | 22902 | 134 | * | | | | | | | Oberlin & Valladas 2012 |
| | | | | | | | | | | | | 30.4 | 18940 | 78 | **22827** | **131** | |
| **Kammern-Grubgraben** | **AL2b** | Lv-1821 | CON | bone (*E. ferus/R. tarandus*) | 17350 | 190 | 1.1 | | | | 3 | | | | | | Gilot 1997 |
| | **AL3** | Lv-1810 | CON | bone (*E. ferus/R. tarandus*) | 18030 | 270 | 1.5 | | | | 3 | | | | | | Gilot 1997 |
| | **AL2** | Lv-1823 | CON | bone (*E. ferus/R. tarandus*) | 18070 | 270 | 1.5 | | | | 3 | | | | | | Gilot 1997 |
| | **AL3** | Poz-105378 | AMS | ? | 18320 | 120 | 0.7 | | | | | | | | | | Lengyel et al. 2021 |
| | **AL2b** | Lv-1822 | CON | bone (*E. ferus/R. tarandus*) | 18620 | 220 | 1.2 | | | | 3 | | | | | | Gilot 1997 |
| | **AL2** | Poz-105373 | AMS | bone | 18810 | 140 | 0.7 | | | * | | | | | | | Lengyel et al. 2021 |
| | **AL2** | MAMS-40115 | AMS | bone | 18860 | 60 | 0.3 | | | * | | | | | | | Händel et al. 2021 |
| | **AL2** | GrN-21529 | CON | bone | 18890 | 180 | 1 | | | * | | | | | | | Haesaerts et al. 2016 |
| | **AL2** | Poz-105374 | AMS | bone | 18910 | 140 | 0.7 | | | * | | | | | | | Lengyel et al. 2021 |
| | **AL3** | GrN-21530 | CON | bone | 18920 | 90 | 0.5 | | | * | | | | | | | Haesaerts et al. 2016 |
| | **AL3** | Poz-105376 | AMS | bone | 18930 | 140 | 0.7 | | | * | | | | | | | Lengyel et al. 2021 |
| | **AL3** | MAMS-22871 | AMS | tooth (*R. tarandus*) | 19070 | 70 | 0.4 | | | * | | | | | | | Haesaerts et al. 2016 |
| | **AL3** | MAMS-25870 | AMS | tooth (*R. tarandus*) | 19170 | 60 | 0.3 | | | * | | | | | | | Haesaerts et al. 2016 |
| | **AL2** | MAMS-40116 | AMS | bone | 19230 | 60 | 0.3 | | | * | | | | | | | Händel et al. 2021 |
| | **AL2** | MAMS-30165 | AMS | bone | 19250 | 70 | 0.4 | | | | | | | | | | Händel et al. 2021 |
| | **AL3** | Poz-105375 | AMS | bone | 19290 | 140 | 0.7 | | | | | | | | | | Lengyel et al. 2021 |
| | **AL2** | MAMS-25868 | AMS | tooth (*R. tarandus*) | 19320 | 60 | 0.3 | | | | | | | | | | Haesaerts et al. 2016 |
| | **AL2** | MAMS-25869 | AMS | tooth (*R. tarandus*) | 19330 | 70 | 0.4 | | | | | | | | | | Haesaerts et al. 2016 |
| | | | | | | | | | | | | 2.1 | 19102 | 31 | **23007** | **34** | |
| **La Salpêtriére** | **6** | Ly-937 | CON | bone | 10680 | 300 | 2.8 | 12450 | 416 | | A, C | | | | | | Brochier 2016 |
| | **6** | MC-2083 | CON | charcoal | 18800 | 300 | 1.6 | 22731 | 284 | * | | | | | | | Onoratini & Renault-Miskovsky 1999 |
| | | Ly-939 | CON | bone | 18880 | 300 | 1.6 | 22823 | 315 | * | | | | | | | Brochier 2016 |
| | | MC-2168 | CON | charcoal | 19530 | 270 | 1.4 | 23479 | 296 | * | | | | | | | Onoratini & Renault-Miskovsky 1999 |
| | | | | | | | | | | | | 13.0 | 19103 | 167 | **23076** | **214** | |

Appendix Table 15: continued 12,

| site | layer/level/ conc./... | lab.-nr. | m. | material | BP | std. | % | calBP | std. | * | c. | P% | WA | std. | calBP | std. | reference |
|---|---|---|---|---|---|---|---|---|---|---|---|---|---|---|---|---|---|
| Cueva de Ambrosio | II | Gif-7276 | CON | charcoal | 16500 | 280 | 1.7 | 19933 | 340 | | A | | | | | | Ripoll López 1988 |
| | | GifA-A-II.4 | AMS | charcoal | 19110 | 90 | 0.5 | 23049 | 81 | * | | | | | | | Jordá Cerdá et al. 2012 |
| | | GifA-A-II.2 | AMS | charcoal | 19170 | 190 | 1 | 23244 | 290 | * | | | | | | | Jordá Cerdá et al. 2012 |
| | | Gif-9883 | CON | charcoal | 19250 | 70 | 0.4 | 23182 | 124 | * | | | | | | | Jordá Cerdá et al. 2012 |
| | | GifA-A-II.6 | AMS | charcoal | 19300 | 190 | 1 | 23350 | 278 | * | | | | | | | Jordá Cerdá et al. 2012 |
| | | GifA-95577 | AMS | charcoal | 19950 | 210 | 1.1 | 24018 | 209 | | B | | | | | | Jordá Cerdá et al. 2012 |
| | | GifA-95576? | AMS | charcoal | 20150 | 200 | 1 | 24238 | 272 | | B | | | | | | Jordá Cerdá et al. 2012 |
| | | | | | | | | | | | | 62.5 | 19180 | 44 | **23074** | **62** | |
| Combe-Saunière | IVb | OxA-755 | AMS | bone | 14890 | 200 | 1.3 | 18215 | 294 | | C | | | | | | Geneste & Plisson 1986 |
| | IVb | OxA-756 | AMS | bone | 15120 | 200 | 1.3 | 18455 | 192 | | C | | | | | | Geneste & Plisson 1986 |
| | IVb | OxA-751 | AMS | bone | 15190 | 200 | 1.3 | 18500 | 193 | | C | | | | | | Geneste & Plisson 1986 |
| | IVb | OxA-754 | AMS | bone | 15200 | 200 | 1.3 | 18506 | 193 | | C | | | | | | Geneste & Plisson 1986 |
| | IVa | OXA-488 | AMS | Bone | 17700 | 290 | 1.6 | 21459 | 409 | | A, C | | | | | | Geneste & Plisson 1986 |
| | IVb | OxA-757 | AMS | bone | 18860 | 320 | 1.7 | 22812 | 332 | * | A | | | | | | Geneste & Plisson 1986 |
| | IV | OxA-489 | AMS | bone | 19450 | 330 | 1.7 | 23421 | 341 | * | A | | | | | | Geneste & Plisson 1986 |
| | IVb | OxA-752 | AMS | bone | 19490 | 350 | 1.8 | 23458 | 363 | * | A | | | | | | Geneste & Plisson 1986 |
| | IVb | OxA-753 | AMS | bone | 19630 | 320 | 1.6 | 23600 | 374 | * | A | | | | | | Geneste & Plisson 1986 |
| | | | | | | | | | | | | 33.9 | 19350 | 165 | **23380** | **262** | |
| Ponte di Pietra | II-US66 | CRG-1019 | CON | charcoal | 18515 | 618 | 3.3 | 22323 | 743 | * | A | | | | | | Broglio 1997 |
| | II-US66 | CRG-1018 | CON | charcoal | 19940 | 471 | 2.4 | 24022 | 599 | * | A | | | | | | Broglio 1997 |
| | | | | | | | | | | | | 6.7 | 19416 | 375 | **23394** | **381** | |
| Laugerie-Haute Ouest | 4 | Wk-39841 | AMS | bone (*R. tarandus*) | 19388 | 103 | 0.5 | 23414 | 235 | * | | | | | | | Verpoorte et al. 2019 |
| | H‴ – 1-7 | Lyon-1173 | CON | burned bone | 19524 | 155 | 0.8 | 23485 | 220 | * | | | | | | | Roque et al. 2001 |
| | H‴ – 1-7 | GifA-100634 | CON | bone | 19550 | 340 | 1.7 | 23517 | 368 | * | | | | | | | Roque et al. 2001 |
| | H‴ – 1-7 | GifA-100630 | CON | burned bone | 19600 | 200 | 1 | 23533 | 246 | * | | | | | | | Roque et al. 2001 |
| | H‴ – 5 | GrN-4442 | CON | burned bone | 19650 | 140 | 0.7 | 23595 | 193 | * | | | | | | | Vogel & Waterbolk 1967 |
| | 4 | Wk-35666 | AMS | bone (*R. tarandus*) | 19676 | 112 | 0.6 | 23620 | 178 | * | | | | | | | Verpoorte et al. 2019 |
| | H‴ – 2 | GrN-4605 | CON | burned bone | 19870 | 190 | 1 | 23913 | 214 | * | | | | | | | Vogel & Waterbolk 1967 |

Appendix Table 15: continued 13,

| site | layer/level/ conc./... | lab.-nr. | m. | material | BP | std. | % | calBP | std. | * | c. | P% | WA | std. | calBP | std. | reference |
|---|---|---|---|---|---|---|---|---|---|---|---|---|---|---|---|---|---|
| | H˝ – 5 | GrN-4495 | CON | burned bone | 19900 | 200 | 1 | 23961 | 202 | * | | | | | | | Vogel & Waterbolk 1967 |
| | H˝ – 2 | GrN-4441 | CON | burned bone | 20000 | 240 | 1.2 | 24101 | 271 | * | | | | | | | Vogel & Waterbolk 1967 |
| | | | | | | | | | | | | 15.1 | 19619 | 52 | **23601** | **154** | |
| **Kastritsa** | **3** | Beta-143302 | CON | ? | 19660 | 160 | 0.8 | **23599** | **209** | | | | | | | | Djindjian et al. 1999 |
| **Grotta di Paina** | **5** | UtC-2698 | AMS | bone | 10760 | 100 | 0.9 | 12733 | 78 | | C | | | | | | Broglio & Improta 1995 |
| | **6** | UtC-2043 | AMS | bone | 19430 | 150 | 0.8 | 23426 | 237 | * | | | | | | | Broglio & Improta 1995 |
| | **5** | ETH-79366 | AMS | bone | 19686 | 54 | 0.3 | 23635 | 161 | * | | | | | | | Broglio & Improta 1995 |
| | **6** | UtC-2696 | AMS | bone | 20120 | 220 | 1.1 | 24220 | 284 | * | | | | | | | Broglio & Improta 1995 |
| | | | | | | | | | | | | 3.4 | 19680 | 50 | **23632** | **160** | |
| **Cueva de Chaves** | | GrN-12681 | CON | charcoal | 19700 | 310 | 1.6 | **23676** | **382** | | A | | | | | | Utrilla 1995 |
| **Gruta de Salemas** | | ICEN-367 | CON | bone | 17770 | 420 | 2.4 | 21515 | 526 | | | | | | | | Zilhão 1997 |
| | | ICEN-385 | CON | bone | 19220 | 300 | 1.6 | 23241 | 375 | * | | | | | | | Zilhão 1997 |
| | | ICEN-376 | CON | bone | 20250 | 320 | 1.6 | 24403 | 412 | * | | | | | | | Zilhão 1997 |
| | | | | | | | | | | | | 1.9 | 19702 | 219 | **23657** | **285** | |
| **Cueva de la Riera** | **4** | OxA-X-2491-15 | AMS | bone (*C. pyrenaica*) | 19710 | 120 | 0.6 | 23646 | 189 | * | | | | | | | Monge Soares et al. 2016 |
| | | OxA-27116 | AMS | P. vulgata | 19990 | 90 | 0.5 | 24008 | 118 | * | | | | | | | Monge Soares et al. 2016 |
| | | GaK-6984 | CON | | 20970 | 620 | 3.0 | 25101 | 688 | | A, D | | | | | | Straus 1983 |
| | | | | | | | | | | | | 6.2 | 19889 | 72 | **23929** | **98** | |
| **Cueva Morín** | | Si-953 | CON | | 20124 | 340 | 1.7 | **24273** | **413** | | | | | | | | Gonzáles Echegaray & Freeman 1978 |
| **Le Placard** | **GLD, layer 8** | Gif-8802 | CON | bone | 18470 | 300 | 1.6 | 22413 | 338 | * | 2 | | | | | | Dujardin & Pinçon 2000 |
| | **GLD, e. panel** | GifTAN 91.84 | AMS | burned bone | 19970 | 250 | 1.3 | 24062 | 276 | * | | | | | | | Clottes et al. 1991 |
| | **GLD, layer 17** | GifA-92084 | AMS | bone | 20210 | 260 | 1.3 | 24336 | 344 | * | | | | | | | Clottes 1994; Clottes et al.1994 |
| | **GLD, layer 14** | GifA-92083 | AMS | bone | 20310 | 220 | 1.1 | 24445 | 314 | * | | | | | | | Clottes 1994; Clottes et al.1994 |
| | | | | | | | | | | | | 58.7 | 20176 | 139 | **24235** | **223** | |

Appendix Table 15: continued 14,

| site | layer/level/ conc./... | lab.-nr. | m. | material | BP | std. | % | calBP | std. | * | c. | P% | WA | std. | calBP | std. | reference |
|---|---|---|---|---|---|---|---|---|---|---|---|---|---|---|---|---|---|
| Pushkari 1 | | QC-899 | CON | burned bone | 16775 | 605 | 3.6 | 20312 | 747 | | A | | | | | | Belyaeva 2002; Gribchenko et al. 2011; 1 |
| | | AA-1389 | CON | burned bone | 19010 | 220 | 1.2 | 22927 | 282 | | B | | | | | | Belyaeva 2002; Gribchenko et al. 2011; 1 |
| | | Ki-11901 | CON | horse bone | 19500 | 240 | 1.2 | 23455 | 274 | | B | | | | | | Belyaeva 2002; Gribchenko et al. 2011; 1 |
| | | GIN-11310 | CON | burned bone | 20160 | 180 | 0.9 | 24236 | 256 | * | | | | | | | Belyaeva 2002; Gribchenko et al. 2011; 1 |
| | | GIN-10195 | CON | burned bone | 20350 | 180 | 0.9 | 24494 | 265 | * | | | | | | | Belyaeva 2002; Gribchenko et al. 2011; 1 |
| | | GIN-11311 | CON | bone (*M. primigenius*) | 20500 | 500 | 2.4 | 24670 | 592 | | A | | | | | | Belyaeva 2002; Gribchenko et al. 2011; 1 |
| | | GIN11311b | CON | bone (*M. primigenius*) | 20500 | 500 | 2.4 | 24670 | 592 | | A | | | | | | Belyaeva 2002; Gribchenko et al. 2011; 1 |
| | | GIN-8529 | CON | tooth (*M. primigenius*) | 20600 | 1200 | 5.8 | 24673 | 1294 | | A | | | | | | Belyaeva 2002; Gribchenko et al. 2011; 1 |
| | | GIN-8529a | CON | tooth (*M. primigenius*) | 20700 | 500 | 2.4 | 24880 | 597 | | A | | | | | | Belyaeva 2002; Gribchenko et al. 2011; 1 |
| | | GIN-11309 | CON | burned bone | 20840 | 190 | 0.9 | 25124 | 289 | | B | | | | | | Belyaeva 2002; Gribchenko et al. 2011; 1 |
| | | GIN-11311a | CON | tooth (*M. primigenius*) | 20900 | 600 | 2.9 | 25038 | 671 | | A | | | | | | Belyaeva 2002; Gribchenko et al. 2011; 1 |
| | | GIN-3381 | CON | burned bone | 21100 | 400 | 1.9 | 25297 | 445 | | A | | | | | | Belyaeva 2002; Gribchenko et al. 2011; 1 |
| | | GIN-3382 | CON | burned bone | 21100 | 400 | 1.9 | 25297 | 445 | | A | | | | | | Belyaeva 2002; Gribchenko et al. 2011; 1 |
| | | GIN-11307 | CON | burned bone | 22350 | 150 | 0.7 | 26685 | 223 | | B | | | | | | Belyaeva 2002; Gribchenko et al. 2011; 1 |
| | | | | | | | | | | | | 45.5 | 20255 | 127 | **24343** | **194** | |
| Vale Boi | **B6** | Wk-24765 | AMS | shell | 18859 | 90 | 0.5 | 22759 | 143 | | | | | | | | Cascalheira et al. 2012 |
| | **C1** | Wk-24765 | AMS | charcoal | 19533 | 92 | 0.5 | 23531 | 173 | | | | | | | | Cascalheira et al. 2012 |
| | **B1** | Wk-17840 | AMS | bone | 20339 | 161 | 0.8 | 24473 | 238 | * | | | | | | | Cascalheira et al. 2012 |
| | **C** | Wk-26802 | AMS | charcoal | 20570 | 158 | 0.8 | 24745 | 246 | * | | | | | | | Cascalheira et al. 2012 |
| | **C4** | Wk-26800 | AMS | charcoal | 20620 | 160 | 0.8 | 24815 | 235 | * | | | | | | | Cascalheira et al. 2012 |
| | | | | | | | | | | | | 41.8 | 20511 | 92 | **24689** | **188** | |
| Avdeevo | | IGAN-151 | CON | tooth (*M. primigenius*) | 11950 | 310 | 2.6 | 14017 | 457 | | A | | | | | | Abramova et al. 2001 |
| | | IGAN-78 | CON | tooth (*M. primigenius*) | 13900 | 200 | 1.4 | 16844 | 287 | | C | | | | | | Abramova et al. 2001 |
| | | QC-886 | CON | bone (*M. primigenius*) | 16565 | 270 | 1.6 | 19997 | 336 | | A | | | | | | Abramova et al. 2001 |
| | | QC-621 | CON | bone (*M. primigenius*) | 16960 | 420 | 2.5 | 20498 | 535 | | A | | | | | | Abramova et al. 2001 |
| | | GIN-1571b | CON | burned bone | 17200 | 1800 | 10.5 | 20763 | 2094 | | A | | | | | | Abramova et al. 2001 |
| | | QC-887 | CON | bone | 18500 | 2100 | 11.4 | 22232 | 2426 | | A | | | | | | Abramova et al. 2001 |
| | | GIN-7727 | CON | tooth (*M. primigenius*) | 19500 | 500 | 2.6 | 23522 | 546 | | A | | | | | | Abramova et al. 2001 |

Appendix Table 15: continued 15,

| site | layer/level/ conc./... | lab.-nr. | m. | material | BP | std. | % | calBP | std. | * | c. | P% | WA | std. | calBP | std. | reference |
|---|---|---|---|---|---|---|---|---|---|---|---|---|---|---|---|---|---|
| | | GIN-1570a | CON | charcoal | 19800 | 1200 | 6.1 | 23848 | 1344 | | A | | | | | | Abramova et al. 2001 |
| | | GIN-1746 | CON | burned bone | 20100 | 500 | 2.5 | 24213 | 636 | | A | | | | | | Abramova et al. 2001 |
| | | GIN-6592 | CON | burned bone, hearth | 20100 | 300 | 1.5 | 24234 | 362 | | B | | | | | | Abramova et al. 2001 |
| | | GIN-6593 | CON | burned bone | 20100 | 200 | 1 | 24189 | 260 | | B | | | | | | Abramova et al. 2001 |
| | | GIN-6594 | CON | burned bone | 20100 | 400 | 2 | 24249 | 486 | | A | | | | | | Abramova et al. 2001 |
| | | GIN-1747 | CON | burned bone | 20800 | 200 | 1 | 25050 | 292 | * | | | | | | | Abramova et al. 2001 |
| | | GIN-1748 | CON | burned bone | 21000 | 200 | 1 | 25330 | 249 | * | | | | | | | Abramova et al. 2001 |
| | | GIN-2535 | CON | burned bone | 21000 | 800 | 3.8 | 25129 | 869 | * | A | | | | | | Abramova et al. 2001 |
| | | GIN-1569 | CON | burned bone | 21200 | 200 | 0.9 | 25507 | 216 | * | | | | | | | Abramova et al. 2001 |
| | | GIN-4693 | CON | burned bone, hearth | 21600 | 400 | 1.9 | 25870 | 431 | * | A | | | | | | Abramova et al. 2001 |
| | | GIN-1970 | CON | burned bone | 22200 | 700 | 3.2 | 26474 | 656 | * | A | | | | | | Abramova et al. 2001 |
| | | GIN-1969 | CON | burned bone | 22400 | 500 | 2.2 | 26654 | 486 | | A | | | | | | Abramova et al. 2001 |
| | | GIN-1571g | CON | burned bone | 22700 | 700 | 3.1 | 26915 | 669 | | A | | | | | | Abramova et al. 2001 |
| | | GIN-7729 | CON | tooth (*M. primigenius*) | 23400 | 700 | 3 | 27670 | 725 | | A | | | | | | Abramova et al. 2001 |
| | | | | | | | | | | | | 24.1 | 21073 | 109 | **25427** | **156** | |
| **Abauntz** | **f** | GrN-21011 | CON | bone | 21600 | 210 | 1 | **25912** | **192** | | | | | | | | Vermeersch 2023 |
| **Gagarino** | | GIN-7991 | CON | tusk (*M. primigenius*) | 17900 | 120 | 0.7 | 21728 | 216 | | C | | | | | | Sinitsyn et al. 1997 |
| | | LE-1432a | CON | tooth (*M. primigenius*) | 17930 | 100 | 0.6 | 21759 | 208 | | C | | | | | | Arslanov & Svezhentsev 1993 |
| | | GIN-7990 | CON | tusk (*M. primigenius*) | 19160 | 130 | 0.7 | 23150 | 160 | | | | | | | | Sinitsyn et al. 1997 |
| | | LE-1432b | CON | tooth (*M. primigenius*) | 20150 | 300 | 1.5 | 24288 | 372 | | | | | | | | Arslanov & Svezhentsev 1993 |
| | | LE-1432c | CON | tooth (*M. primigenius*) | 20820 | 300 | 1.4 | 25060 | 412 | * | | | | | | | Arslanov & Svezhentsev 1993 |
| | | GIN-7989 | CON | tusk (*M. primigenius*) | 21600 | 140 | 0.6 | 25881 | 91 | * | | | | | | | Sinitsyn et al. 1997 |
| | | GIN-1872 | CON | burned bone | 21800 | 300 | 1.4 | 26111 | 269 | * | | | | | | | Svezhentsev & Popov 1993 |
| | | IGAN-83 | CON | tooth (*M. primigenius*) | 30000 | 1900 | 6.3 | 34349 | 2087 | | A | | | | | | Sinitsyn et al. 1997 |
| | | | | | | | | | | | | 54.6 | 21636 | 127 | **25906** | **83** | |
| **Grotta Paglicci** | **20** | F-47 | CON | charcoal | 21260 | 340 | 1.6 | 25503 | 332 | * | | | | | | | Azzi et al. 1974 |
| | | F-49 | CON | burned bones | 22110 | 330 | 1.5 | 26457 | 388 | * | | | | | | | Azzi et al. 1974 |

Appendix Table 15: continued 16,

| site | layer/level/ conc./... | lab.-nr. | m. | material | BP | std. | % | calBP | std. | * | c. | P% | WA | std. | calBP | std. | reference |
|---|---|---|---|---|---|---|---|---|---|---|---|---|---|---|---|---|---|
| | | F-48 | CON | charcoal | 22220 | 360 | 1.6 | 26532 | 404 | * | | | | | | | Azzi et al. 1974 |
| | | F-50 | CON | charcoal | 22630 | 390 | 1.7 | 26851 | 387 | | A | | | | | | Azzi et al. 1974 |
| | | | | | | | | | | | | 9.6 | 21855 | 198 | **26136** | **180** | |
| **Petřkovice** | **1a** | GrN-19540 | CONv | exc.1953 (Klíma) | 20790 | 270 | 1.3 | 25032 | 381 | | B | | | | | | Svoboda 2008 |
| | | GrA-35446 | AMS | burned bone | 21790 | 110 | 0.5 | 26089 | 148 | | B | | | | | | Svoboda 2008 |
| | | GrA-35447 | AMS | burned bone | 21970 | 110 | 0.5 | 26185 | 135 | * | | | | | | | Svoboda 2008 |
| | | GrA-35449 | AMS | burned bone | 22260 | 110 | 0.5 | 26617 | 215 | * | | | | | | | Svoboda 2008 |
| | | GrA-891 | AMS | charcoal | 23370 | 160 | 0.7 | 27556 | 147 | | B | | | | | | Svoboda 2008 |
| | | | | | | | | | | | | 6.2 | 22115 | 78 | **26259** | **143** | |
| **Banka-Horne farske role** | | GrA-19909 | AMS | bone (*R. tarandus*), cutm. | 22010 | 210 | 1 | 26285 | 241 | * | | | | | | | Verpoorte 2002 |
| | | GrA-19910 | AMS | bone (*R. tarandus*), cutm. | 22320 | 220 | 1 | 26643 | 284 | * | | | | | | | Verpoorte 2002 |
| | | | | | | | | | | | | 30.8 | 22158 | 152 | **26452** | **309** | |
| **Dorotchivtsy III** | **6** | GrA-44217 | AMS | charcoal | 22300 | 100 | 0.4 | **26649** | **202** | | | | | | | | Kulakovska et al. 2014 |
| **Moravany nad Váhom-Podkovica** | | GrN-26749 | CON | bone | 22680 | 400 | 1.8 | 26890 | 402 | * | A | | | | | | Verpoorte 2002 |
| | | GrN-26750 | CON | bone | 22200 | 220 | 1 | 26507 | 336 | * | | | | | | | Verpoorte 2002 |
| | | | | | | | | | | | | 29.3 | 22311 | 193 | **26644** | **262** | |
| **Kostënki 21 (Gmelinskaya)** | **III** | LE-1043 | CON | charcoal | 16960 | 300 | 1.8 | 20469 | 364 | | A, C | | | | | | Praslov & Ivanova 1982 |
| | | LE-1437d | CON | bone | 19050 | 130 | 0.7 | 22955 | 158 | | C | | | | | | Arslanov & Svezhentsev 1993 |
| | | LE-1437a | CON | bone | 19100 | 150 | 0.8 | 23070 | 176 | | C | | | | | | Arslanov & Svezhentsev 1993 |
| | | LE-1437b | CON | bone | 20250 | 100 | 0.5 | 24341 | 163 | | B, D | | | | | | Arslanov & Svezhentsev 1993 |
| | | OxA-26759 | AMS | bone (large mammal) | 21100 | 130 | 0.6 | 25445 | 168 | | B | | | | | | Dinnis et al. 2021 |
| | | GrN-10513 | CON | charcoal | 21260 | 340 | 1.6 | 25503 | 332 | | A | | | | | | Praslov & Ivanova 1982 |
| | | OxA-27217 | AMS | bone (burned?) | 21570 | 130 | 0.6 | 25860 | 84 | | B | | | | | | Dinnis et al. 2021 |
| | | GrA-14669 | AMS | charcoal | 22230 | 100 | 0.4 | 26589 | 221 | * | | | | | | | Zheltova 2008 |
| | | GrN-7363 | CON | charcoal | 22270 | 150 | 0.7 | 26616 | 240 | * | | | | | | | Praslov & Ivanova 1982 |
| | | OxA-26760 | AMS | retoucher, bone | 22570 | 150 | 0.7 | 26830 | 263 | * | | | | | | | Dinnis et al. 2021 |
| | | GrN-24968 | CON | charcoal | 22860 | 320 | 1.4 | 27056 | 387 | * | | | | | | | Zheltova 2008 |

Appendix Table 15: continued 17,

| site | layer/level/ conc./... | lab.-nr. | m. | material | BP | std. | % | calBP | std. | * | c. | P% | WA | std. | calBP | std. | reference |
|---|---|---|---|---|---|---|---|---|---|---|---|---|---|---|---|---|---|
| | | LE-1437c | CON | bone | 22900 | 150 | 0.7 | 27213 | 114 | | B | | | | | | Arslanov & Svezhentsev 1993 |
| | | | | | | | | | | | | 9.3 | 22346 | 71 | **26673** | **185** | |
| **Moravany nad Váhom-Lopata II** | | Gd-9246 | CON | bone | 21400 | 610 | 2.9 | 25610 | 680 | | A | | | | | | Kozłowski Ed. 1998 |
| | | GrA-20460 | AMS | bone (*R. tarandus*), cutm.? | 22030 | 190 | 0.9 | 26273 | 215 | * | | | | | | | Verpoorte 2004 |
| | | GrA-19999 | AMS | bone (*R. tarandus*), cutm.? | 23310 | 320 | 1.4 | 27533 | 230 | * | | | | | | | Verpoorte 2002 |
| | | Gd-10555 | CON | bone | 24100 | 800 | 3.3 | 28373 | 777 | | A | | | | | | Kozłowski Ed. 1998 |
| | | | | | | | | | | | | 0.1 | 22364 | 163 | **26695** | **231** | |
| **Nitra I-Cerman** | | GrN-2449 | CON | charcoal | 23000 | 330 | 1.4 | **27249** | **331** | | | | | | | | Bárta 1966 |
| | | GrN-2456 | CON | charcoal | 24020 | 640 | 2.7 | 28288 | 620 | | A | | | | | | Bárta 1966 |
| **Khotylevo 2** | | OxA-27225 | AMS | bone (large mammal) | 19600 | 450 | 2.3 | 23615 | 507 | | A | | | | | | Garilov et al. 2015 |
| | | GIN-15036 | CON | soil/humus | 20190 | 80 | 0.4 | 24239 | 153 | | B | | | | | | Djindjian et al. 1999 |
| | | LU-359 | CON | tooth (*M. primigenius*) | 20550 | 210 | 1 | 24710 | 305 | | B | | | | | | Djindjian et al. 1999 |
| | | GIN-8495 | CON | tooth (*M. primigenius*) | 20570 | 110 | 0.5 | 24773 | 182 | | B | | | | | | Djindjian et al. 1999 |
| | | GIN-8886 | CON | bone | 20720 | 170 | 0.8 | 24931 | 235 | | B | | | | | | Djindjian et al. 1999 |
| | | GIN-8406 | CON | tooth (*M. primigenius*) | 20830 | 100 | 0.5 | 25104 | 121 | | B | | | | | | Djindjian et al. 1999 |
| | | OxA-27000 | AMS | bone (large mammal) | 21170 | 260 | 1.2 | 25462 | 265 | | B | | | | | | Garilov et al. 2015 |
| | | GIN-15037 | CON | bone/charcoal | 21670 | 80 | 0.4 | 25920 | 54 | | B | | | | | | Djindjian et al. 1999 |
| | | GrN-21899 | CON | bone | 21720 | 170 | 0.8 | 26043 | 179 | | B | | | | | | Djindjian et al. 1999 |
| | | GrN-22216 | CON | bone | 21850 | 170 | 0.8 | 26131 | 166 | | B | | | | | | Djindjian et al. 1999 |
| | | GIN-8497 | CON | tooth (*M. primigenius*) | 22660 | 120 | 0.5 | 26911 | 244 | | B | | | | | | Djindjian et al. 1999 |
| | | IGAN-73 | CON | tooth (*M. primigenius*) | 22700 | 200 | 0.9 | 26902 | 287 | | B | | | | | | Djindjian et al. 1999 |
| | | OxA-X-2500-11 | AMS | bone (*R. tarandus*) | 22700 | 450 | 2 | 26911 | 445 | | A | | | | | | Garilov et al. 2015 |
| | | GIN-12855 | CON | bone/charcoal | 22720 | 150 | 0.7 | 26962 | 230 | | B | | | | | | Djindjian et al. 1999 |
| | | GIN-12856 | CON | 'Ash pan' - bone/charcoal | 22900 | 150 | 0.7 | 27213 | 114 | * | | | | | | | Djindjian et al. 1999 |
| | | GIN-13075 | CON | 'Ash pan' - bone/charcoal | 23020 | 210 | 0.9 | 27362 | 189 | * | | | | | | | Djindjian et al. 1999 |
| | | GIN-12857 | CON | 'Ash pan' - bone/charcoal | 23050 | 150 | 0.7 | 27388 | 146 | * | | | | | | | Djindjian et al. 1999 |
| | | GIN-12858 | CON | 'Ash pan' - bone/charcoal | 23160 | 160 | 0.7 | 27455 | 151 | * | | | | | | | Djindjian et al. 1999 |

Appendix Table 15: continued 18,

| site | layer/level/ conc./... | lab.-nr. | m. | material | BP | std. | % | calBP | std. | * | c. | P% | WA | std. | calBP | std. | reference |
|---|---|---|---|---|---|---|---|---|---|---|---|---|---|---|---|---|---|
| | | GIN-12859 | CON | tooth (*M. primigenius*) | 23240 | 160 | 0.7 | 27496 | 148 | * | | | | | | | Djindjian et al. 1999 |
| | | OxA-27002 | AMS | bone (*M. primigenius*) | 23300 | 300 | 1.3 | 27525 | 215 | * | | | | | | | Garilov et al. 2015 |
| | | Gin-12861 | CON | tooth (*M. primigenius*) | 23470 | 170 | 0.7 | 27603 | 154 | * | | | | | | | Djindjian et al. 1999 |
| | | OxA-27001 | AMS | bone (*M. primigenius*) | 23660 | 270 | 1.1 | 27882 | 316 | * | | | | | | | Garilov et al. 2015 |
| | | GIN-8497a | CON | tooth (*M. primigenius*) | 23870 | 160 | 0.7 | 28069 | 213 | | B | | | | | | Djindjian et al. 1999 |
| | | GIN-8496 | CON | tooth (*M. primigenius*) | 24220 | 110 | 0.5 | 28390 | 205 | | B | | | | | | Djindjian et al. 1999 |
| | | OxA-27224 | AMS | bone (bird) | 24960 | 400 | 1.6 | 29259 | 454 | | A | | | | | | Garilov et al. 2015 |
| | | OxA-27223 | AMS | bone (*C. canis*) | 29090 | 350 | 1.2 | **33506** | **471** | | C | | | | | | Garilov et al. 2015 |
| | | | | | | | | | | | | 30.1 | 23229 | 70 | **27483** | **115** | |
| **Bistricioara-Lutărie III** | **AH 2.5** | RoAMS-1070.101 | AMS | ? | 23332 | 185 | 0.8 | 27538 | 156 | * | | | | | | | Anghelinu et al. 2021 |
| | | RoAMS-1413.101 | AMS | ? | 23284 | 139 | 0.6 | 27518 | 140 | * | | | | | | | Anghelinu et al. 2021 |
| | | RoAMS-1417.101 | AMS | ? | 23699 | 137 | 0.6 | 27868 | 124 | * | | | | | | | Anghelinu et al. 2021 |
| | | DeA-7462 | CON | charcoal | 23342 | 133 | 0.6 | 27546 | 137 | * | | | | | | | Anghelinu et al. 2021 |
| | | | | | | | | | | | | 12.9 | 23424 | 72 | **27601** | **119** | |
| **Buda** | **I** | GrN-23072 | CON | bone | 23810 | 190 | 0.8 | 28039 | 228 | * | | | | | | | Păunescu 1998 |
| | | OxA-29525 | AMS | bone | 23300 | 160 | 0.7 | 27525 | 147 | * | | | | | | | Tuffreau et al. 2018 |
| | | OxA-29526 | AMS | bone | 23440 | 160 | 0.7 | 27589 | 149 | * | | | | | | | Tuffreau et al. 2018 |
| | | | | | | | | | | | | 11.4 | 23485 | 97 | **27633** | **119** | |
| **Kostënki 1 (Poliakov)** | **I** | LE-3280 | CON | burned bone | 18230 | 620 | 3.4 | 21993 | 757 | | A | | | | | | Damblon et al. 1996 |
| | | LE-4351 | CON | tooth (*M. primigenius*) | 18400 | 3300 | 17.9 | 21796 | 3805 | | A | | | | | | Sinitsyn et al. 1997 |
| | | LE-2950 | CON | tooth (*M. primigenius*) | 19010 | 120 | 0.6 | 22879 | 154 | | | | | | | | Damblon et al. 1996 |
| | | LE-3292 | CON | burned bone | 19540 | 580 | 3 | 23585 | 647 | | A | | | | | | Damblon et al. 1996 |
| | | LE-3281 | CON | burned bone | 19620 | 460 | 2.3 | 23639 | 521 | | A | | | | | | Damblon et al. 1996 |
| | | LE-2949 | CON | bone (*M. primigenius*) | 19860 | 200 | 1 | 23846 | 281 | | | | | | | | Damblon et al. 1996 |
| | | LE-3277 | CON | burned bone | 20100 | 680 | 3.4 | 24216 | 807 | | A | | | | | | Damblon et al. 1996 |
| | | AA-4800 | CON | burned bone | 20315 | 200 | 1 | 24448 | 290 | | | | | | | | Damblon et al. 1996 |
| | | GIN-4851 | CON | burned bone | 20800 | 300 | 1.4 | 25036 | 413 | | | | | | | | Damblon et al. 1996 |
| | | GIN-4892 | CON | burned bone | 20850 | 160 | 0.8 | 25149 | 239 | | | | | | | | Zheltova & Zaretskaya 2018 |

Appendix Table 15: continued 19,

| site | layer/level/ conc./... | lab.-nr. | m. | material | BP | std. | % | calBP | std. | * | c. | P% | WA | std. | calBP | std. | reference |
|---|---|---|---|---|---|---|---|---|---|---|---|---|---|---|---|---|---|
| | | AA-4799 | CON | burned bone | 20855 | 260 | 1.2 | 25117 | 369 | | | | | | | | Damblon et al. 1996 |
| | | GrN-17120 | CON | burned bone | 20950 | 100 | 0.5 | 25317 | 176 | | | | | | | | Sinitsyn et al. 1997 |
| | | GIN-4231 | CON | burned bone | 21150 | 200 | 0.9 | 25471 | 217 | | | | | | | | Sinitsyn et al. 1997 |
| | | GrN-17119 | CON | burned bone | 21180 | 100 | 0.5 | 25504 | 159 | | | | | | | | Sinitsyn et al. 1997 |
| | | GIN-4896 | CON | burned bone | 21200 | 100 | 0.5 | 25520 | 162 | | | | | | | | Zheltova & Zaretskaya 2018 |
| | | GIN-4904 | CON | burned bone | 21210 | 150 | 0.7 | 25523 | 188 | | | | | | | | Zheltova & Zaretskaya 2018 |
| | | GIN-2534 | CON | burned bone | 21300 | 400 | 1.9 | 25520 | 399 | | A | | | | | | Damblon et al. 1996 |
| | | GIN-4900 | CON | burned bone | 21600 | 90 | 0.4 | 25883 | 61 | | | | | | | | Zheltova & Zaretskaya 2018 |
| | | LE-3279 | CON | tooth (*M. primigenius*) | 21680 | 700 | 3.2 | 25952 | 779 | | A | | | | | | Damblon et al. 1996 |
| | | LE-2801 | CON | not stated | 21800 | 200 | 0.9 | 26102 | 188 | | | | | | | | Damblon et al. 1996 |
| | | GIN-4901 | CON | burned bone | 21880 | 200 | 0.9 | 26152 | 180 | | | | | | | | Zheltova & Zaretskaya 2018 |
| | | GIN-8041 | CON | tooth (*M. primigenius*) | 21950 | 250 | 1.1 | 26256 | 259 | | | | | | | | Sinitsyn et al. 1997 |
| | | LE-3282 | CON | tooth (*M. primigenius*) | 22020 | 310 | 1.4 | 26391 | 372 | | | | | | | | Damblon et al. 1996 |
| | | LE-3290 | CON | bone | 22060 | 500 | 2.3 | 26412 | 499 | | A | | | | | | Damblon et al. 1996 |
| | | GIN-3634 | CON | burned bone | 22200 | 300 | 1.4 | 26515 | 374 | | | | | | | | Sinitsyn et al. 1997 |
| | | GIN-4903 | CON | burned bone | 22200 | 500 | 2.3 | 26517 | 488 | | A | | | | | | Sinitsyn et al. 1997 |
| | | GIN-1870 | CON | burned bone | 22300 | 230 | 1 | 26615 | 304 | | | | | | | | Damblon et al. 1996 |
| | | GIN-2533 | CON | burned bone | 22300 | 200 | 0.9 | 26629 | 273 | | | | | | | | Damblon et al. 1996 |
| | | GrN-17118 | CON | charcoal | 22330 | 150 | 0.7 | 26670 | 225 | | | | | | | | Sinitsyn et al. 1997 |
| | | GIN-3633 | CON | burned bone | 22600 | 300 | 1.3 | 26833 | 325 | | | | | | | | Sinitsyn et al. 1997 |
| | | GIN-6249 | CON | tooth (*M. primigenius*) | 22600 | 300 | 1.3 | 26833 | 325 | | | | | | | | Sinitsyn et al. 1997 |
| | | LE-2969 | CON | tooth (*M. primigenius*) | 22700 | 250 | 1.1 | 26898 | 310 | | | | | | | | Damblon et al. 1996 |
| | | LE-2800 | CON | tooth (*M. primigenius*) | 22760 | 250 | 1.1 | 26944 | 316 | | | | | | | | Damblon et al. 1996 |
| | | GIN-2530 | CON | burned bone | 22800 | 200 | 0.9 | 27025 | 243 | | | | | | | | Damblon et al. 1996 |
| | | GIN-3632 | CON | burned bone | 22800 | 300 | 1.3 | 26986 | 359 | | | | | | | | Sinitsyn et al. 1997 |
| | | GIN-2528 | CON | burned bone | 23000 | 500 | 2.2 | 27158 | 514 | | A | | | | | | Damblon et al. 1996 |
| | | LE-3276 | CON | tooth (*M. primigenius*) | 23010 | 300 | 1.3 | 27289 | 287 | | | | | | | | Damblon et al. 1996 |
| | | LE-3287 | CON | tooth (*M. primigenius*) | 23260 | 420 | 1.8 | 27495 | 347 | | A | | | | | | Damblon et al. 1996 |

Appendix Table 15: continued 20,

| site | layer/level/ conc./... | lab.-nr. | m. | material | BP | std. | % | calBP | std. | * | c. | P% | WA | std. | calBP | std. | reference |
|---|---|---|---|---|---|---|---|---|---|---|---|---|---|---|---|---|---|
| | | LE-3289 | CON | tooth (*M. primigenius*) | 23260 | 680 | 2.9 | 27495 | 727 | | A | | | | | | Svezhentsev & Popov 1993 |
| | | OxA-26765 | AMS | awl (*E. ferus*) | 23260 | 160 | 0.7 | 27506 | 148 | * | | | | | | | Sinitsyn et al. 1997 |
| | | LE-3286 | CON | burned bone | 23490 | 420 | 1.8 | 27778 | 415 | | A | | | | | | Damblon et al. 1996 |
| | | GIN-2527 | CON | burned bone | 23500 | 200 | 0.9 | 27625 | 173 | | | | | | | | Damblon et al. 1996 |
| | | OxA-26766 | AMS | (*Vulpes/Leporidae*), cutm. | 23510 | 160 | 0.7 | 27627 | 151 | * | | | | | | | Sinitsyn et al. 1997 |
| | | OxA-26764 | AMS | bone | 23530 | 170 | 0.7 | 27641 | 157 | * | | | | | | | Sinitsyn et al. 1997 |
| | | GrA-5244 | AMS | charcoal (*Picea* sp.) | 23600 | 440 | 1.9 | 27887 | 455 | * | A | | | | | | Sinitsyn et al. 1997 |
| | | LE-3283 | CON | tusk (*M. primigenius*) | 23640 | 320 | 1.4 | 27880 | 363 | | | | | | | | Damblon et al. 1996 |
| | | LE-2951 | CON | tooth (*M. primigenius*) | 23770 | 200 | 0.8 | 28005 | 231 | | | | | | | | Sinitsyn et al. 1997 |
| | | GrA-5143 | AMS | charcoal | 24030 | 440 | 1.8 | 28266 | 431 | * | A | | | | | | Sinitsyn et al. 1997 |
| | | GrA-5243 | AMS | charcoal (*Picea* sp.) | 24030 | 440 | 1.8 | 28266 | 431 | * | A | | | | | | Sinitsyn et al. 1997 |
| | | GIN-2529 | CON | burned bone | 24100 | 500 | 2.1 | 28337 | 489 | | A | | | | | | Zheltova & Zaretskaya 2018 |
| | | LE-4352 | CON | tooth (*M. primigenius*) | 24570 | 3950 | 16.1 | 28691 | 4221 | | A | | | | | | Sinitsyn et al. 1997 |
| | | | | | | | | | | | | 39.1 | 23485 | 88 | **27640** | **112** | |
| **Krakow Spadzista B** | **6** | Poz-58706 | AMS | bone (*M. primigenius*) | 11690 | 130 | 1.1 | 13566 | 143 | | C | | | | | | Damblon et al. 1996 |
| | | Poz-86236 | AMS | carbonized bone | 17670 | 100 | 0.6 | 21409 | 240 | | C | | | | | | Wilczyński et al. 2020 |
| | | Poz-77076 | AMS | burned bone (*M. primigenius*) | 17870 | 90 | 0.5 | 21699 | 189 | | C | | | | | | Wilczyński et al. 2020 |
| | | Poz-87042 | AMS | bone (*M. primigenius*) (2016) | 18740 | 100 | 0.5 | 22684 | 153 | | C | | | | | | Wilczyński et al. 2020 |
| | | Poz-31039 | AMS | bone (*M. primigenius*) | 19450 | 120 | 0.6 | 23449 | 219 | | C | | | | | | Wilczyński et al. 2012 |
| | | Poz-100023 | AMS | carbonized bone | 19720 | 200 | 1 | 23678 | 271 | | C | | | | | | Wilczyński et al. 2020 |
| | | Ly-631 | CON | bone (*M. primigenius*) | 20600 | 1050 | 5.1 | 24682 | 1142 | | A | | | | | | Kozlowski et al. 1974 |
| | | Poz-48407 | AMS | bone (*M. primigenius*) | 21620 | 140 | 0.6 | 25897 | 93 | | C | | | | | | Sobczyk 1995 |
| | | Poz-67404 | AMS | bone coll. (*M. primigenius*) | 21700 | 120 | 0.6 | 25987 | 118 | | C | | | | | | Wilczyński et al. 2020 |
| | | Poz-86231 | AMS | bone (*M. primigenius*) | 21710 | 110 | 0.5 | 25988 | 109 | | C | | | | | | Wilczyński et al. 2020 |
| | | Poz-58707 | AMS | burned bone (*M. primigenius*) | 22030 | 110 | 0.5 | 26212 | 139 | | B | | | | | | Damblon et al. 1996 |
| | | Poz-87043 | AMS | bone (*M. primigenius*) (2016) | 22460 | 140 | 0.6 | 26758 | 231 | | B | | | | | | Wilczyński et al. 2020 |
| | | Poz-242 | AMS | bone (*M. primigenius*) | 23020 | 180 | 0.8 | 27368 | 164 | | B | | | | | | Wojtal & Sobczyk 2005 |
| | | GrN-6636 | CON | carbonized bone | 23040 | 170 | 0.7 | 27384 | 158 | | B | | | | | | Kozłowski et al. 1974 |

Appendix Table 15: continued 21,

| site | layer/level/ conc./... | lab.-nr. | m. | material | BP | std. | % | calBP | std. | * | c. | P% | WA | std. | calBP | std. | reference |
|---|---|---|---|---|---|---|---|---|---|---|---|---|---|---|---|---|---|
| | | Poz-86233 | AMS | bone (*M. primigenius*) | 23370 | 130 | 0.6 | 27560 | 137 | | B | | | | | | Wilczyński et al. 2020 |
| | | Poz-86230 | AMS | bone (*M. primigenius*) (2016) | 23440 | 140 | 0.6 | 27591 | 142 | * | | | | | | | Wilczyński et al. 2020 |
| | | Poz-86232 | AMS | bone (*M. primigenius*) | 23570 | 140 | 0.6 | 27685 | 126 | * | | | | | | | Wilczyński et al. 2020 |
| | | Poz-58704 | AMS | burned bone (*M. primigenius*) | 23590 | 120 | 0.5 | 27724 | 91 | * | | | | | | | Damblon et al. 1996 |
| | | Poz-86229 | AMS | bone (*M. primigenius*) (2016) | 23710 | 140 | 0.6 | 27884 | 132 | * | | | | | | | Wilczyński et al. 2020 |
| | | LuS-7417 | AMS | bone (*M. primigenius*) | 23750 | 150 | 0.6 | 27948 | 169 | * | | | | | | | Arppe & Karhu 2010 |
| | | Poz-1248 | AMS | bone (*M. primigenius*) | 23750 | 140 | 0.6 | 27936 | 154 | * | | | | | | | Wojtal & Sobczyk 2005 |
| | | Poz-1251 | AMS | bone (*M. primigenius*) | 23770 | 160 | 0.7 | 27979 | 188 | * | | | | | | | Wojtal & Sobczyk 2005 |
| | | Poz-86237 | AMS | bone (*M. primigenius*) | 23850 | 200 | 0.8 | 28080 | 244 | * | | | | | | | Wilczyński et al. 2020 |
| | | Poz-77075 | AMS | carbonized bone | 23970 | 160 | 0.7 | 28155 | 238 | * | | | | | | | Wilczyński et al. 2020 |
| | | Poz-225 | AMS | bone (*M. primigenius*) | 23980 | 280 | 1.2 | 28204 | 313 | * | | | | | | | Wilczyński et al. 2012 |
| | | Poz-268 | AMS | bone (*M. primigenius*) | 24000 | 300 | 1.3 | 28221 | 327 | * | | | | | | | Wojtal & Sobczyk 2005 |
| | | Poz-101183 | AMS | bone (*M. primigenius*) (2016) | 24200 | 250 | 1 | 28353 | 312 | * | | | | | | | Wilczyński et al. 2020 |
| | | Poz-28735 | AMS | bone (*M. primigenius*) | 24240 | 160 | 0.7 | 28388 | 249 | | B | | | | | | Wojtal & Sobczyk 2005 |
| | | Poz-61263 | AMS | burned bone (*M. primigenius*) | 24480 | 180 | 0.7 | 28712 | 236 | | B | | | | | | Damblon et al. 1996 |
| | | Poz-59976 | AMS | bone (*M. primigenius*) | 24800 | 160 | 0.6 | 29002 | 151 | | B | | | | | | Damblon et al. 1996 |
| | | Poz-101206 | AMS | bone (*M. primigenius*) (2017) | 25120 | 320 | 1.3 | 29424 | 358 | | B | | | | | | Wilczyński et al. 2020 |
| | | Poz-67406 | AMS | carbonized bone | 25830 | 190 | 0.7 | 30135 | 160 | | C | | | | | | Wilczyński et al. 2020 |
| | | | | | | | | | | | | 19.2 | 23721 | 47 | **27820** | **41** | |
| **Mitoc-Malu Galben** | **4a** | GrA-14671 | AMS | charcoal (*Picea* sp.) | 23290 | 100 | 0.4 | 27522 | 125 | | B | | | | | | Haesaerts et al. 2010 |
| | | GrN-20438 | AMS | charcoal (*Picea* sp.) | 23390 | 280 | 1.2 | 27578 | 208 | * | | | | | | | Haesaerts et al. 2010 |
| | | GrA-1353 | AMS | charcoal (*Picea* sp.) | 23850 | 100 | 0.4 | 27994 | 151 | * | | | | | | | Noiret 2007 |
| | | | | | | | | | | | | 12.2 | 23798 | 94 | **27928** | **114** | |
| **Riparo Mochi** | **D** | OxA-19800 | AMS | shell (*C. neritea*) | 24600 | 100 | 0.7 | 28883 | 130 | | | | | | | | Douka et al. 2011 |
| **Willendorf II** | **9/B1** | Poz-100126 | AMS | bone (*R. tarandus*) | 10080 | 70 | 0.7 | 11605 | 164 | | C | | | | | | Wilczyński et al. 2020 |
| | | Poz-99666 | AMS | bone (*R. tarandus*) | 12910 | 100 | 0.8 | 15440 | 146 | | C | | | | | | Wilczyński et al. 2020 |
| | | Poz-99661 | AMS | bone (*Vulpes/Alopex*) | 13270 | 100 | 0.8 | 15955 | 152 | | C | | | | | | Wilczyński et al. 2020 |

Appendix Table 15: continued 22,

| site | layer/level/ conc./... | lab.-nr. | m. | material | BP | std. | % | calBP | std. | * | c. | P% | WA | std. | calBP | std. | reference |
|---|---|---|---|---|---|---|---|---|---|---|---|---|---|---|---|---|---|
| | | Poz-99668 | AMS | tooth (*E. ferus*) | 13350 | 100 | 0.7 | 16059 | 154 | | C | | | | | | Wilczyński et al. 2020 |
| | | Poz-99662 | AMS | bone (*Vulpes/Alopex*) | 15690 | 130 | 0.8 | 18990 | 126 | | C | | | | | | Wilczyński et al. 2020 |
| | | Poz-99664 | AMS | bone (*M. primigenius*) | 17130 | 140 | 0.8 | 20683 | 151 | | C | | | | | | Wilczyński et al. 2020 |
| | | Poz-99952 | AMS | bone( *R. tarandus*) | 18400 | 100 | 0.5 | 22314 | 90 | | C | | | | | | Wilczyński et al. 2020 |
| | | Poz-99665 | AMS | bone (*M. primigenius*) | 19370 | 180 | 0.9 | 23387 | 261 | | B | | | | | | Wilczyński et al. 2020 |
| | | Poz-99994 | AMS | bone (*M. primigenius*) | 21400 | 140 | 0.7 | 25713 | 137 | | B | | | | | | Wilczyński et al. 2020 |
| | | GrN-21898 | CON | bone | 23860 | 270 | 1.1 | 28115 | 303 | | B | | | | | | Haesaerts et al. 1996 |
| | | GrN-22208 | CON | bone | 24370 | 290 | 1.2 | 28522 | 368 | * | | | | | | | Haesaerts et al. 1996 |
| | | GrA-5006 | AMS | bone | 24910 | 150 | 0.6 | 29116 | 178 | * | | | | | | | Haesaerts et al. 1996 |
| | | GrA-5006 | AMS | long bone | 24910 | 150 | 0.6 | 29116 | 178 | * | | | | | | | Haesaerts et al. 1996 |
| | | | | | | | | | | | | 21.7 | 24846 | 100 | **29037** | **120** | |
| **Grub-Kranawetberg** | **AH 4** | GrA-9063 | AMS | charcoal | 24620 | 230 | 0.9 | 28849 | 231 | | B | | | | | | Antl-Weiser et al. 2010 |
| | | GrA-9065 | AMS | charcoal | 24930 | 240 | 1 | 29242 | 330 | * | | | | | | | Antl-Weiser et al. 2010 |
| | | GrA-9066 | AMS | charcoal | 24830 | 230 | 0.9 | 29092 | 260 | * | | | | | | | Antl-Weiser et al. 2010 |
| | | VERA-364 | AMS | charcoal | 25300 | 90 | 0.4 | 29565 | 222 | * | | | | | | | Antl-Weiser et al. 2010 |
| | | | | | | | | | | | | 7.9 | 25204 | 79 | **29495** | **202** | |
| **Molodova 5** | **7** | GrA-9443 | AMS | bone (*E. ferus*) | 21070 | 150 | 0.7 | 25420 | 184 | | | | | | | | Noiret 2007 |
| | | GrA-9455 | AMS | charcoal (*Pinus* sp.) | 23000 | 170 | 0.7 | 27348 | 155 | | | | | | | | Noiret 2007 |
| | | Mo-11 | CON | charcoal (*Pinus* sp.) | 23000 | 800 | 3.5 | 27238 | 802 | | A | | | | | | Noiret 2007 |
| | | GrA-22909 | AMS | charcoal (*Pinus* sp.) | 23650 | 140 | 0.6 | 27802 | 116 | | | | | | | | Haesaerts et al. 2010 |
| | | GIN-10 | CON | soil | 23700 | 320 | 1.4 | 27949 | 364 | | | | | | | | Noiret 2007 |
| | | GrA-9564 | AMS | charcoal (*Pinus* sp.) | 25130 | 220 | 0.9 | 29467 | 279 | * | | | | | | | Noiret 2007 |
| | | GrA-9457 | AMS | charcoal (*Pinus* sp.) | 25170 | 210 | 0.8 | 29498 | 267 | * | | | | | | | Noiret 2007 |
| | | GrA-9456 | AMS | charcoal (*Pinus* sp.) | 25280 | 210 | 0.8 | 29564 | 264 | * | | | | | | | Noiret 2007 |
| | | GrA-9458 | AMS | charcoal (*Pinus* sp.) | 25280 | 210 | 0.8 | 29564 | 264 | * | | | | | | | Haesaerts et al. 2010 |
| | | | | | | | | | | | | 94.3 | 25217 | 106 | **29515** | **216** | |
| **Milovice I** | **section G** | ISGS-1691 | CON | charcoal | 21200 | 1100 | 5.2 | 25337 | 1199 | | A | | | | | | Oliva 2009 |
| | | ISGS-1690 | CON | charcoal | 22900 | 490 | 2.1 | 27078 | 507 | | A | | | | | | Oliva 2009 |

Appendix Table 15: continued 23.

| site | layer/level/ conc./... | lab.-nr. | m. | material | BP | std. | % | calBP | std. | * | c. | P% | WA | std. | calBP | std. | reference |
|---|---|---|---|---|---|---|---|---|---|---|---|---|---|---|---|---|---|
| | | ISGS-1903 | CON | bone | 24130 | 460 | 1.9 | 28350 | 459 | | A | | | | | | Oliva 2009 |
| | | Poz-99607 | AMS | tooth (*M. primigenius*) | 24900 | 200 | 0.8 | 29177 | 274 | | | | | | | | Wilczyński et al. 2020 |
| | | GrN-14824 | CON | charcoal | 25220 | 280 | 1.1 | 29520 | 302 | * | | | | | | | Oliva 2009 |
| | | GrN-22105 | CON | charcoal | 25570 | 170 | 0.7 | 29752 | 250 | * | | | | | | | Oliva 2009 |
| | | Poz-99606 | AMS | tooth (*M. primigenius*) | 25770 | 210 | 0.8 | 30039 | 208 | * | | | | | | | Wilczyński et al. 2020 |
| | | Poz-996610 | AMS | tooth (*M. primigenius*) | 25880 | 220 | 0.9 | 30210 | 213 | * | | | | | | | Wilczyński et al. 2020 |
| | | Poz-99608 | AMS | tooth (*M. primigenius*) | 26010 | 230 | 0.9 | 30369 | 276 | * | | | | | | | Wilczyński et al. 2020 |
| | | | | | | | | | | | | 19.1 | 25705 | 96 | **30015** | **67** | |

Abbreviations:

m. = method: AMS = Accelerator Mass Spectrometry, CON = conventional

material: b.s. = bulked sample

BP = before present

std. = standard deviation

% = percentage of std. from BP

calBP = calibrated date BP (using IntCal20)

* = used for weighted average (WA)

c. = comment: A = Std., B = z-test, C = too young/too old/outlier, D = conflict with AMS date, 1 = problematic/rejected (Grimm & Weber 2008), 2 = problematic/rejected (Delage 2018), 3 = problematic/rejected (Haesearts et al. 2016), 4 = problematic/rejected (Barshay-Szmidt et al. 2016), 5 = stratigraphic association only

P% = probability of WA

WA = weighted average

1 = Demay et al. 2015

Appendix Table 16: Radiocarbon dates for assemblages excluded from the chronological analysis due to varying quality concerns affecting either individual measurements or the reliability of the entire archaeological context (see r.). (The Abbreviations are explained on previous page.)

| site | layer/level/ conc./... | lab.-nr. | m. | material | BP | std. | % | calBP | std. | * | c. | P% | WA | std. | calBP | std. | reference |
|---|---|---|---|---|---|---|---|---|---|---|---|---|---|---|---|---|---|
| **Abris Schweizersbild** | | OxA-5744 | AMS | bone (*R. tarandus*), cutm. | 11780 | 90 | 0.8 | 13639 | 103 | | | | | | | | Leesch & Müller 2012 |
| | | ETH-44391 | AMS | tooth (*E. ferus*) | 12240 | 50 | 0.4 | 14172 | 80 | | | | | | | | Leesch & Müller 2012 |
| | | ETH-44390 | AMS | tooth (*E. ferus*) | 12240 | 60 | 0.5 | 14188 | 97 | | | | | | | | Leesch & Müller 2012 |
| | | ETH-44392 | AMS | tooth (*E. ferus*) | 12690 | 50 | 0.4 | 15129 | 79 | | | | | | | | Leesch & Müller 2012 |
| | | OxA-5745 | AMS | bone, worked | 13940 | 100 | 0.7 | 16904 | 151 | | | | | | | | Leesch & Müller 2012 |
| | | ETH-5204 | AMS | antler (*R. tarandus*) | 14500 | 115 | 0.8 | 17698 | 196 | | | | | | | | Leesch & Müller 2012 |
| **Baume d´Oullins** | D | Ly-1985 | CON | | 20060 | 450 | 2.2 | 24163 | 585 | * | A | | | | | | Bazile 1990 |
| | | Ly-1984 | CON | bone | 20100 | 500 | 2.5 | 24213 | 636 | * | A | | | | | | Bazile 1990 |
| | | MC-2358 | CON | | 20920 | 300 | 1.4 | 25167 | 391 | * | | | | | | | Bazile 1990 |
| | | | | | | | | | | | | 17.2 | 20545 | 223 | **24705** | | |
| **Berdyzh** | | OxA-716 | AMS | bone (*M.primigenius*) | 15100 | 250 | 1.7 | 18416 | 246 | | A, C | | | | | | Kaletchitz 1984 |
| | | GIN-2695 | CON | bone | 22500 | 200 | 0.9 | 26786 | 266 | | | | | | | | Demay et al. 2021 |
| | | LU-104 | CON | bone (*M. primigenius*) | 23430 | 180 | 0.8 | 27583 | 157 | | | | | | | | Sinitsyn 2007 |
| **Cueva del Boquete Zafarraya** | | OxA-7114 | AMS | charcoal | 18920 | 420 | 2.2 | 22914 | 465 | | A | | | | | | Santamaría Álvarez & de la Rasilla Vives 2013 |
| **Cueva de les Mallaetes** | | KN-1918 | CON | charcoal | 16300 | 1500 | 9.2 | 19728 | 1829 | | A | | | | | | Fortea Pérez & Jordá Cerda 1976 |
| **Cueva del Parpalló** | | BIRM-521 | CON | bone | 17896 | 340 | 1.9 | 21649 | 451 | | A | | | | | | Bofinger & Davidson 1977 |
| **Cueva del Reclau Viver** | | M-1019 | CON | bone | 13299 | 600 | 4.5 | 15913 | 915 | | A, C | | | | | | Straus 1990 |
| **Deimern 42** | | GrN-10269 | CON | charcoal | 6595 | 45 | 0.7 | 7494 | 49 | | C | | | | | | Lanting & van der Pflicht 1996 |
| **Grotta della Cala** | M | F-112 | CON | charcoal | 14740 | 850 | 5.8 | 17759 | 1050 | | A | | | | | | Bietti et al. 1983 |
| | N | F-113 | CON | charcoal | 16320 | 850 | 5.2 | 19822 | 982 | | A | | | | | | Bietti et al. 1983 |

Appendix Table 16: continued 1,

| site | layer/level/ conc./... | lab.-nr. | m. | material | BP | std. | % | calBP | std. | * | c. | P% | WA | std. | calBP | std. | reference |
|---|---|---|---|---|---|---|---|---|---|---|---|---|---|---|---|---|---|
| **Grotta Paglicci** | **23** | UtC-1415 | AMS | charcoal | 26300 | 400 | 1.5 | 30537 | 355 | * | | | | | | | Boschin et al. 2018 |
| | **22** | UtC-1412 | AMS | charcoal | 26800 | 300 | 1.1 | 30856 | 282 | * | | | | | | | Boschin et al. 2018 |
| | **23** | UtC-1414 | AMS | charcoal | 28100 | 400 | 1.4 | 32299 | 572 | | C | | | | | | Boschin et al. 2018 |
| | **22** | UtC-1413 | AMS | charcoal | 28300 | 400 | 1.4 | 32502 | 571 | | C | | | | | | Boschin et al. 2018 |
| | | | | | | | | | | | | 31.7 | 26620 | 240 | **30758** | **265** | |
| **Grotta Romanelli** | **C1** | LTL-17741A | AMS | bone | 9657 | 65 | 0.7 | 10998 | 150 | | | | | | | | Calgagnile et al. 2019 |
| | | LTL-17295A | AMS | bone | 9774 | 40 | 0.4 | 11206 | 28 | | | | | | | | Calgagnile et al. 2019 |
| | | GrN-2154 | CON | charcoal | 9790 | 80 | 0.8 | 11192 | 88 | | | | | | | | Sardella et al. 2018 |
| | | LTL-17299A | AMS | bone | 9822 | 45 | 0.5 | 11234 | 32 | | | | | | | | Calgagnile et al. 2019 |
| | | LTL-17300A | AMS | bone | 10100 | 80 | 0.8 | 11636 | 180 | * | | | | | | | Calgagnile et al. 2019 |
| | | LTL-17298A | AMS | bone | 10277 | 45 | 0.4 | 12082 | 168 | * | | | | | | | Calgagnile et al. 2019 |
| | | LTL-17740Z | AMS | bone | 10295 | 75 | 0.7 | 12147 | 220 | * | | | | | | | Calgagnile et al. 2019 |
| | | GrN-2153 | CON | charcoal | 10390 | 80 | 0.8 | 12256 | 192 | * | | | | | | | Sardella et al. 2018 |
| | | SacA-61166 LTL | AMS | tooth | 10880 | 50 | 0.5 | 12806 | 47 | | | | | | | | Calgagnile et al. 2019 |
| | | LTL-17292A | AMS | bone | 11328 | 60 | 0.5 | 13217 | 62 | | | | | | | | Calgagnile et al. 2019 |
| | | | | | | | | | | | | 7.5 | 10270 | 32 | **11998** | **93** | |
| **Grotta Trene** | | UtC-2691 | AMS | bone | 17640 | 140 | 0.8 | 21375 | 275 | | | | | | | | Broglio & Improta 1995 |
| | | UtC-2692 | AMS | bone | 18630 | 150 | 0.8 | 22612 | 187 | | | | | | | | Broglio & Improta 1995 |
| | | ETH-79368 | AMS | bone | 19948 | 55 | 0.3 | 23968 | 99 | | | | | | | | Terlato et al. 2019 |
| **Grotte des Enfants á Grimaldi** | **burial layer** | MC-402 | CON | shell (*Monodonta turbinata*) | 12200 | 400 | 3.3 | 14379 | 592 | | A | | | | | | Thommeret & Thommeret 1973 |
| | | | | | | | | | | | | | | | **14379** | **592** | |
| **Hengestbury Head** | | OxA-399 | AMS | charcoal | 4770 | 180 | 3.8 | 5456 | 228 | | C | | | | | | Gillespie et al. 1985 |
| | | OxA-411 | AMS | charcoal | 7690 | 110 | 1.4 | 8497 | 100 | | C | | | | | | Gillespie et al. 1985 |
| | | OxA-413 | AMS | charcoal | 7910 | 140 | 1.8 | 8771 | 186 | | C | | | | | | Gillespie et al. 1985 |
| | | OxA-413 | AMS | humic extraction of OxA-412 | 7910 | 140 | 1.8 | 8771 | 186 | | C | | | | | | Gillespie et al. 1985 |
| | | OxA-412 | AMS | charcoal | 8140 | 120 | 1.5 | 9062 | 203 | | C | | | | | | Gillespie et al. 1985 |
| | | OxA-398 | AMS | charcoal | 8590 | 120 | 1.4 | 9640 | 149 | | C | | | | | | Gillespie et al. 1985 |

Appendix Table 16: continued 2.

| site | layer/level/ conc./... | lab.-nr. | m. | material | BP | std. | % | calBP | std. | * | c. | P% | WA | std. | calBP | std. | reference |
|---|---|---|---|---|---|---|---|---|---|---|---|---|---|---|---|---|---|
| Kastrisa | 5 | B-132437 | AMS | charcoal | 20000 | 80 | 0.4 | 24012 | 114 | | | | | | | | Galanidou & Tzedakis 2001 |
| | | B-143307 | AMS | charcoal | 20590 | 70 | 0.3 | 24811 | 136 | | | | | | | | Galanidou & Tzedakis 2001 |
| | | B-131047 | AMS | charcoal | 21350 | 80 | 0.4 | 25719 | 80 | | | | | | | | Galanidou & Tzedakis 2001 |
| | | B-143305 | AMS | charcoal | 22230 | 210 | 0.9 | 26537 | 322 | | | | | | | | Galanidou & Tzedakis 2001 |
| Sandalja II | c/d | Z-193 | CON | charcoal | 20750 | 400 | 1.9 | 24944 | 516 | | A | | | | | | Srdoč et al. 1973 |
| Siedlnica | 17a | GrA-15832 | CON | bone | 8450 | 60 | 0.7 | 9459 | 55 | | C | | | | | | Lanting et al. 2002 |
| Vrbička Cave | | OxA-27861 | AMS | | 23120 | 160 | 0.7 | 27434 | 152 | | | | | | | | Borić et al. 2014; Christiani 2013; 2014 |
| Zaraisk | | GIN-6095 | CON | burned bone | 15600 | 300 | 1.9 | 18901 | 350 | | C | | | | | | Velichko & Zelikson 2005 |
| | | GIN-2487 | CON | burned bone | 16200 | 1000 | 6.2 | 19668 | 1181 | | C | | | | | | Velichko & Zelikson 2005 |
| | | GIN-3727 | CON | bone (M. primigenius) | 18300 | 200 | 1.1 | 22203 | 193 | | | | | | | | Velichko & Zelikson 2005 |
| | | GIN-8975 | CON | burned bone | 19000 | 200 | 1.1 | 22898 | 252 | | | | | | | | Velichko & Zelikson 2005 |
| | | GIN-8396 | CON | burned bone | 19100 | 200 | 1 | 23065 | 280 | | | | | | | | Velichko & Zelikson 2005 |
| | | GIN-8397 | CON | burned bone | 19100 | 260 | 1.4 | 23087 | 367 | | | | | | | | Velichko & Zelikson 2005 |
| | | GIN-8486 | CON | burned bone | 19200 | 300 | 1.6 | 23218 | 388 | | | | | | | | Velichko & Zelikson 2005 |
| | | GIN-8484 | CON | burned bone | 19900 | 260 | 1.3 | 23895 | 346 | | | | | | | | Velichko & Zelikson 2005 |
| | | GIN-8975 | CON | tooth (M. primigenius) | 21000 | 430 | 2 | 25181 | 498 | | | | | | | | Velichko & Zelikson 2005 |
| | | GIN-8488 | CON | burned bone | 21400 | 50 | 0.2 | 25767 | 58 | | | | | | | | Velichko & Zelikson 2005 |
| | | GIN-3998 | CON | tooth (M. primigenius) | 22300 | 300 | 1.3 | 26594 | 362 | | | | | | | | Velichko & Zelikson 2005 |

Appendix Table 17: Table of main metrical features for all artefacts. All measurements in mm, area in mm²
Abbreviations: l = length, w = width, MP = midpoint, CM = centre of mass

| ID | width | length | l-w-index | area | upper-lower ratio | left-right ratio | tip angle | MP-CM-x-offset | MP-CM-y-offset |
|---|---|---|---|---|---|---|---|---|---|
| Abauntz_01 | 12 | 63 | 5.2 | 517 | 4.2 | 1 | 31 | -0.3 | -2.1 |
| Abauntz_02 | 16 | 61 | 3.8 | 636 | 1.7 | 0.7 | 57 | -0.5 | 2 |
| Abauntz_03 | 18 | 59 | 3.3 | 693 | 5.1 | 0.5 | 37 | -1 | -3.2 |
| Abri-de-Fontales_01 | 10 | 47 | 4.7 | 414 | 0.3 | 1.6 | 71 | -0.5 | -1.4 |
| Abri-de-Fontales_02 | 14 | 39 | 2.8 | 373 | 1 | 0.8 | 61 | -0.8 | -0.6 |
| Abri-du-Bois-des-Brousses_layer-3_01 | 9 | 26 | 2.9 | 156 | 0.7 | 1 | 65 | -0.5 | 0.2 |
| Abri-du-Rouet_layer-9b_01 | 11 | 50 | 4.5 | 452 | 1.1 | 0.6 | 63 | -0.8 | 0.2 |
| Abri-du-Rouet_ layer-9b_02 | 10 | 45 | 4.5 | 315 | 1.4 | 0.4 | 43 | -1 | -0.2 |
| Abri-du-Rouet_ layer-9b_03 | 10 | 41 | 4.1 | 291 | 1.3 | 0.8 | 50 | -0.5 | 0 |
| Abri-Faustin_01 | 10 | 60 | 6 | 465 | 0.6 | 1.4 | 42 | 0.2 | -0.6 |
| Abri-Faustin_02 | 8 | 38 | 4.8 | 274 | 0.4 | 0.9 | 64 | 0 | -1 |
| Abri-Faustin_03 | 9 | 53 | 5.9 | 396 | 0.5 | 1.4 | 58 | 0 | -1.1 |
| Abri-Faustin_04 | 9 | 44 | 4.9 | 299 | 0.8 | 0.2 | 55 | -0.8 | 0.7 |
| Abri-Faustin_05 | 8 | 45 | 5.6 | 323 | 0.4 | 0.9 | 65 | 0 | -0.6 |
| Abri-Faustin_06 | 10 | 52 | 5.2 | 387 | 0.5 | 1.4 | 49 | -0.3 | -0.5 |
| Abri-Gandil_layer-20_01 | 13 | 61 | 4.7 | 617 | 1.1 | 0.3 | 46 | -0.3 | -1.9 |
| Abri-Gandil_layer-20_02 | 14 | 57 | 4.1 | 592 | 2.1 | 0.4 | 43 | -1 | -2.3 |
| Abri-Gandil_layer-20_03 | 14 | 57 | 4.1 | 565 | 2.2 | 0.9 | 50 | -0.4 | -0.3 |
| Abri-Schweizersbild_01 | 20 | 53 | 2.6 | 711 | 0.9 | 0.3 | 66 | -1.9 | -0.9 |
| Abri-Schweizersbild_02 | 17 | 50 | 2.9 | 558 | 1 | 0.3 | 61 | -1.9 | -0.5 |
| Ahrenshoeft-LA-73-Nord_01 | 9 | 34 | 3.8 | 232 | 1.5 | 0.6 | 39 | -0.4 | -1.9 |
| Aitzbitarte-IV_01 | 12 | 59 | 4.9 | 490 | 1.9 | 0.8 | 37 | -0.8 | -0.8 |
| Aitzbitarte-IV_02 | 13 | 55 | 4.2 | 523 | 4 | 0.8 | 45 | -0.2 | -1 |
| Aitzbitarte-IV_03 | 11 | 40 | 3.6 | 299 | 2.3 | 1.1 | 46 | -0.4 | -1 |
| Aitzbitarte-IV_04 | 11 | 35 | 3.2 | 262 | 4 | 0.8 | 51 | -0.6 | -0.7 |
| Altamira_01_01 | 12 | 65 | 5.4 | 528 | 3.3 | 0.4 | 31 | -1.3 | -1.4 |
| Altamira_01_02 | 14 | 50 | 3.6 | 509 | 3.5 | 1.6 | 52 | 0.4 | -0.7 |
| Altamira_01_03 | 9 | 37 | 4.1 | 261 | 4.3 | 0.5 | 47 | -0.3 | -0.4 |
| Altamira_01_04 | 15 | 55 | 3.7 | 592 | 4.5 | 0.7 | 42 | -0.1 | -2.1 |
| Altamira_01_05 | 10 | 40 | 4 | 289 | 2.8 | 0.4 | 40 | -0.9 | -1.4 |
| Altamira_01_06 | 8 | 30 | 3.8 | 182 | 4 | 0.9 | 54 | -0.3 | 0 |
| Altamira_01_07 | 11 | 51 | 4.6 | 395 | 3.6 | 1.2 | 36 | -0.1 | -0.8 |
| Altamira_01_08 | 13 | 40 | 3.1 | 324 | 2.6 | 0.4 | 45 | -1.3 | -0.8 |
| Altamira_01_09 | 10 | 33 | 3.3 | 212 | 3.1 | 0.5 | 40 | -0.8 | -1.2 |
| Altamira_01_10 | 11 | 50 | 4.5 | 387 | 4.5 | 0.8 | 36 | -0.5 | -1.6 |
| Altamira_02_01 | 12 | 64 | 5.3 | 521 | 1.5 | 0.2 | 28 | -1.6 | -1.9 |

Appendix Table 17: continued 1,

| ID | width | length | l-w-index | area | upper-lower ratio | left-right ratio | tip angle | MP-CM-x-offset | MP-CM-y-offset |
|---|---|---|---|---|---|---|---|---|---|
| Altamira_02_02 | 10 | 45 | 4.5 | 282 | 1.2 | 0.5 | 39 | -0.9 | -0.2 |
| Altamira_02_03 | 9 | 41 | 4.6 | 264 | 0.8 | 0.7 | 52 | -0.6 | 0.3 |
| Amalda_01 | 11 | 34 | 3.1 | 245 | 3.8 | 0.4 | 42 | -1 | -1.6 |
| Atxuri_01 | 10 | 50 | 5 | 344 | 2 | 0.5 | 30 | -0.7 | -2 |
| Avdeevo_01 | 23 | 67 | 2.9 | 1113 | 0.7 | 1.1 | 81 | -0.6 | -0.2 |
| Avdeevo_02 | 14 | 53 | 3.8 | 548 | 0.6 | 1.5 | 63 | -0.3 | -0.2 |
| Avdeevo_03 | 27 | 65 | 2.4 | 1166 | 0.9 | 1.3 | 91 | -0.8 | 1.9 |
| Avdeevo_04 | 15 | 46 | 3.1 | 482 | 0.7 | 1.1 | 63 | -0.5 | -0.8 |
| Avdeevo_05 | 17 | 48 | 2.8 | 611 | 0.5 | 0.8 | 90 | -0.7 | -0.5 |
| Baio_01 | 10 | 38 | 3.8 | 265 | 1.6 | 0.7 | 47 | -0.5 | -0.6 |
| Baio_02 | 6 | 35 | 5.8 | 141 | 1.3 | 0.5 | 31 | -0.3 | -0.5 |
| Baio_03 | 11 | 42 | 3.8 | 305 | 1.6 | 0.6 | 45 | -0.8 | -0.5 |
| Banka-Horne-farske-role_01 | 14 | 43 | 3.1 | 456 | 0.6 | 1.3 | 81 | -0.8 | 0.3 |
| Baume-de-Colle-Rousse_01 | 14 | 48 | 3.4 | 517 | 1.2 | 0.6 | 48 | -0.4 | -3 |
| Baume-dOullins_layer-D&C_01 | 13 | 59 | 4.5 | 618 | 2.9 | 1.1 | 56 | -0.1 | -0.4 |
| Baume-dOullins_layer-D&C_02 | 11 | 66 | 6 | 510 | 2.3 | 0.5 | 48 | -0.5 | 0.7 |
| Baume-dOullins_layer-D&C_03 | 9 | 63 | 7 | 407 | 2.7 | 0.8 | 31 | -0.3 | -1 |
| Baume-dOullins_layer-D&C_04 | 9 | 50 | 5.6 | 302 | 1.5 | 1.4 | 41 | 0.3 | -0.3 |
| Baume-dOullins_layer-D&C_05 | 11 | 45 | 4.1 | 326 | 1.8 | 0.8 | 46 | -0.5 | -0.6 |
| Berdyzh_01 | 14 | 58 | 4.1 | 611 | 0.9 | 0.5 | 47 | -0.8 | -1.8 |
| Berdyzh_02 | 14 | 43 | 3.1 | 441 | 0.6 | 0.9 | 61 | -0.7 | -1.4 |
| Berdyzh_03 | 12 | 33 | 2.8 | 272 | 0.8 | 1 | 69 | -0.1 | 0.2 |
| Berdyzh_04 | 12 | 44 | 3.7 | 398 | 0.5 | 0.8 | 81 | -0.8 | 0.8 |
| Berdyzh_05 | 7 | 31 | 4.4 | 170 | 0.7 | 0.7 | 64 | -0.4 | -0.4 |
| Bistricioara-Lutarie-III_layer-AH2-5_01 | 9 | 77 | 8.6 | 468 | 1.1 | 0.6 | 26 | -0.8 | 0.4 |
| Bistricioara-Lutarie-III_layer-AH2-5_02 | 11 | 40 | 3.6 | 327 | 1 | 1.6 | 50 | 0.3 | -1.4 |
| Bistricioara-Lutarie-III_layer-AH2-5_03 | 17 | 75 | 4.4 | 881 | 0.6 | 1.5 | 64 | -0.8 | 1.9 |
| Bistricioara-Lutarie-III_layer-AH2-5_04 | 9 | 37 | 4.1 | 219 | 1.3 | 0.8 | 54 | -0.7 | 0.8 |
| Bistricioara-Lutarie-III_layer-AH2-5_05 | 11 | 60 | 5.5 | 475 | 0.9 | 1 | 48 | -1.1 | 0.2 |
| Bistricioara-Lutarie-III_layer-AH2-5_06 | 6 | 28 | 4.7 | 121 | 1 | 1 | 53 | -0.3 | 0.4 |
| Bistricioara-Lutarie-III_layer-AH2-5_07 | 12 | 43 | 3.6 | 335 | 0.5 | 1 | 70 | -0.8 | 1.1 |
| Blazi-Cave_layer-4-trench-5_01 | 9 | 31 | 3.4 | 213 | 0.6 | 0.6 | 67 | -0.4 | -0.3 |
| Blazi-Cave_layer-4-trench-5_02 | 6 | 26 | 4.3 | 132 | 2.4 | 0.6 | 52 | -0.5 | -0.5 |
| Bois-Ragot_01 | 19 | 63 | 3.3 | 759 | 0.9 | 0.7 | 59 | -0.6 | 0.3 |
| Bois-Ragot_02 | 14 | 46 | 3.3 | 468 | 1 | 0.5 | 62 | -0.9 | 0.4 |
| Borneck_01 | 15 | 49 | 3.3 | 418 | 1 | 0.2 | 34 | -1.6 | -1.4 |
| Borneck_02 | 11 | 40 | 3.6 | 302 | 0.8 | 0.2 | 47 | -1.1 | -0.8 |

Appendix Table 17: continued 2,

| ID | width | length | l-w-index | area | upper-lower ratio | left-right ratio | tip angle | MP-CM-x-offset | MP-CM-y-offset |
|---|---|---|---|---|---|---|---|---|---|
| Borneck_03 | 13 | 50 | 3.8 | 469 | 0.8 | 0.6 | 54 | -1 | -0.3 |
| Borneck_04 | 12 | 45 | 3.8 | 380 | 0.7 | 0.6 | 48 | -0.7 | -0.9 |
| Borneck_05 | 12 | 46 | 3.8 | 378 | 1.3 | 0.5 | 45 | -0.8 | -1.2 |
| Borneck_06 | 15 | 45 | 3 | 440 | 0.6 | 0.3 | 64 | -1.5 | 0.6 |
| Borneck_07 | 16 | 48 | 3 | 430 | 1.4 | 0.2 | 34 | -2 | -1.4 |
| Borshevo-1_01 | 11 | 37 | 3.4 | 278 | 0.8 | 0.8 | 66 | -0.5 | 0.3 |
| Brassempouy_01 | 13 | 51 | 3.9 | 416 | 1.3 | 0.3 | 47 | -1.9 | 0.1 |
| Buda_layer-1_01 | 9 | 45 | 5 | 314 | 1.1 | 0.6 | 46 | -0.6 | -1.5 |
| Cadenet_01 | 8 | 50 | 6.2 | 301 | 1.9 | 1 | 35 | -0.3 | -0.4 |
| Cadenet_02 | 9 | 45 | 5 | 281 | 2.7 | 0.7 | 33 | -0.6 | -1.1 |
| Cenciano-Diruto_01 | 10 | 41 | 4.1 | 297 | 1.2 | 0.4 | 50 | -1 | -0.9 |
| Cenciano-Diruto_02 | 5 | 20 | 4 | 74 | 1.1 | 0.9 | 48 | -0.3 | -0.2 |
| Cepoy-La-Pierre-aux-Fees_01 | 16 | 48 | 3 | 516 | 1.2 | 0.4 | 53 | -1.3 | -1.4 |
| Cepoy-La-Pierre-aux-Fees_02 | 14 | 46 | 3.3 | 406 | 1.4 | 0.1 | 46 | -1.9 | -1.8 |
| Cepoy-La-Pierre-aux-Fees_03 | 17 | 49 | 2.9 | 514 | 1 | 0.6 | 67 | -1.2 | 0.5 |
| Cepoy-La-Pierre-aux-Fees_04 | 17 | 42 | 2.5 | 487 | 1.5 | 0.4 | 53 | -0.9 | -2 |
| Chinchon-1_layer-C_01 | 15 | 58 | 3.9 | 652 | 3.1 | 0.6 | 51 | -0.7 | -0.7 |
| Chinchon-1_layer-C_02 | 12 | 63 | 5.2 | 612 | 3.2 | 0.3 | 46 | -0.4 | -0.7 |
| Chinchon-1_layer-C_03 | 11 | 62 | 5.6 | 506 | 3.1 | 0.4 | 34 | -0.3 | -2.5 |
| Chinchon-1_layer-C_04 | 15 | 56 | 3.7 | 643 | 2.7 | 0.3 | 51 | -0.7 | 0.1 |
| Chinchon-1_layer-C_05 | 14 | 63 | 4.5 | 626 | 2.9 | 0.7 | 37 | -0.5 | -1.9 |
| Columbier_01 | 9 | 47 | 5.2 | 318 | 1.1 | 0.6 | 38 | 0.1 | -1.4 |
| Combe-Sauniere_layer-IV_01 | 14 | 73 | 5.2 | 681 | 2.4 | 0.4 | 29 | -2.3 | -1.8 |
| Combe-Sauniere_layer-IV_02 | 14 | 57 | 4.1 | 547 | 0.7 | 0.7 | 63 | -1.3 | 1.2 |
| Combe-Sauniere_layer-IV_03 | 11 | 35 | 3.2 | 271 | 1 | 0.3 | 66 | -1.4 | 0.5 |
| Crvena-Stijena_01 | 14 | 39 | 2.8 | 382 | 1.3 | 0.6 | 63 | -1.3 | -0.7 |
| Cueto-de-la-Mina_01_01 | 12 | 53 | 4.4 | 484 | 4.3 | 0.7 | 35 | -0.2 | -2.2 |
| Cueto-de-la-Mina_01_02 | 11 | 42 | 3.8 | 311 | 2.8 | 0.3 | 37 | -1 | -1.4 |
| Cueto-de-la-Mina_01_03 | 11 | 33 | 3 | 205 | 2.1 | 0.4 | 35 | -1.1 | -1.2 |
| Cueto-de-la-Mina_01_04 | 13 | 45 | 3.5 | 421 | 2.9 | 0.4 | 55 | -0.9 | 0.1 |
| Cueto-de-la-Mina_01_05 | 13 | 40 | 3.1 | 362 | 4 | 0.5 | 45 | -0.7 | -1.6 |
| Cueto-de-la-Mina_01_06 | 11 | 45 | 4.1 | 326 | 2 | 0.5 | 47 | -1 | 0.6 |
| Cueto-de-la-Mina_01_07 | 11 | 45 | 4.1 | 322 | 2.2 | 0.4 | 41 | -1 | -0.3 |
| Cueto-de-la-Mina_01_08 | 12 | 40 | 3.3 | 294 | 2.1 | 0.5 | 41 | -1 | -0.9 |
| Cueto-de-la-Mina_01_09 | 11 | 42 | 3.8 | 296 | 2 | 0.3 | 43 | -1.4 | -0.4 |
| Cueto-de-la-Mina_01_10 | 12 | 34 | 2.8 | 285 | 3.4 | 0.4 | 57 | -0.8 | -0.3 |
| Cueto-de-la-Mina_02_01 | 16 | 50 | 3.1 | 532 | 2.3 | 0.4 | 51 | -1.4 | -0.7 |

Appendix Table 17: continued 3,

| ID | width | length | l-w-index | area | upper-lower ratio | left-right ratio | tip angle | MP-CM-x-offset | MP-CM-y-offset |
|---|---|---|---|---|---|---|---|---|---|
| Cueto-de-la-Mina_02_02 | 11 | 55 | 5 | 398 | 1.1 | 0.4 | 38 | -1.3 | -0.2 |
| Cueto-de-la-Mina_02_03 | 12 | 34 | 2.8 | 311 | 3.2 | 0.5 | 64 | -0.6 | 0.3 |
| Cueto-de-la-Mina_02_04 | 8 | 47 | 5.9 | 281 | 2.2 | 0.7 | 32 | -0.4 | -0.1 |
| Cueva-de-Ambrosio_layer-II_01 | 16 | 56 | 3.5 | 647 | 3.3 | 0.7 | 58 | -0.8 | -0.3 |
| Cueva-de-Ambrosio_layer-II_02 | 6 | 13 | 2.2 | 59 | 1.1 | 0.9 | 85 | -0.4 | 0.1 |
| Cueva-de-Ambrosio_layer-II_03 | 5 | 21 | 4.2 | 78 | 2.5 | 0.9 | 44 | -0.3 | -0.4 |
| Cueva-de-Ambrosio_layer-II_04 | 6 | 20 | 3.3 | 81 | 2.5 | 1.2 | 73 | -0.1 | 0.8 |
| Cueva-de-Ambrosio_layer-II_05 | 11 | 48 | 4.4 | 401 | 2.7 | 1 | 56 | -0.2 | 0.5 |
| Cueva-de-Ambrosio_layer-II_06 | 5 | 20 | 4 | 70 | 1.5 | 0.8 | 32 | -0.3 | -0.5 |
| Cueva-de-Ambrosio_layer-II_07 | 5 | 20 | 4 | 66 | 1.5 | 0.4 | 39 | -0.5 | -0.2 |
| Cueva-de-Ambrosio_layer-II_08 | 4 | 18 | 4.5 | 46 | 3.5 | 0.5 | 32 | -0.2 | -0.6 |
| Cueva-de-Ambrosio_layer-II_09 | 9 | 38 | 4.2 | 260 | 2.8 | 0.7 | 48 | -0.8 | -0.6 |
| Cueva-de-Ambrosio_layer-II_10 | 6 | 22 | 3.7 | 87 | 2.6 | 0.5 | 34 | -0.8 | -1.1 |
| Cueva-de-Chaves_01 | 9 | 43 | 4.8 | 278 | 3.5 | 0.8 | 34 | -0.3 | -1.4 |
| Cueva-de-Chaves_02 | 10 | 42 | 4.2 | 286 | 1.4 | 0.6 | 42 | -0.4 | -0.7 |
| Cueva-de-Chaves_03 | 10 | 41 | 4.1 | 269 | 1.5 | 0.9 | 53 | -0.4 | 0.8 |
| Cueva-de-la-Meaza_01 | 17 | 57 | 3.4 | 617 | 2.1 | 0.2 | 52 | -1.9 | 0.3 |
| Cueva-de-la-Riera_layer-4_01 | 12 | 47 | 3.9 | 352 | 1.5 | 0.5 | 38 | -1.1 | -0.4 |
| Cueva-de-les-Mallaetes_01 | 10 | 36 | 3.6 | 282 | 3 | 0.4 | 66 | -0.5 | 0.6 |
| Cueva-de-les-Mallaetes_02 | 6 | 30 | 5 | 125 | 1.4 | 0.3 | 39 | -0.2 | 0.7 |
| Cueva-de-les-Mallaetes_03 | 7 | 33 | 4.7 | 164 | 3 | 0.6 | 41 | -0.3 | 0 |
| Cueva-de-los-Morceguillos_01 | 11 | 48 | 4.4 | 384 | 2.3 | 0.7 | 56 | -0.5 | 0.7 |
| Cueva-de-los-Morceguillos_02 | 8 | 36 | 4.5 | 233 | 4.1 | 0.8 | 47 | -0.1 | -1.4 |
| Cueva-del-Boquete-de-Zafarraya_01 | 17 | 80 | 4.7 | 897 | 1.9 | 0.7 | 42 | -1.2 | 1.4 |
| Cueva-del-Boquete-de-Zafarraya_02 | 18 | 65 | 3.6 | 730 | 2.3 | 0.3 | 48 | -1.7 | 0 |
| Cueva-del-Moro-Chufin_01 | 10 | 29 | 2.9 | 183 | 1 | 0.9 | 59 | -0.4 | 0.3 |
| Cueva-del-Moro-Chufin_02 | 8 | 18 | 2.2 | 93 | 0.9 | 0.4 | 81 | -0.7 | 0.4 |
| Cueva-del-Pantano-de-Cubillas_01 | 14 | 60 | 4.3 | 546 | 3 | 0.5 | 37 | -1.3 | -1.4 |
| Cueva-del-Parpallo_layer-400-375_01 | 9 | 52 | 5.8 | 360 | 2.5 | 0.7 | 47 | -0.3 | 1 |
| Cueva-del-Parpallo_layer-400-375_02 | 7 | 24 | 3.4 | 123 | 2 | 0.7 | 59 | -0.3 | 0.2 |
| Cueva-del-Parpallo_layer-400-375_03 | 7 | 20 | 2.9 | 111 | 4 | 0.4 | 51 | -0.5 | -0.7 |
| Cueva-del-Parpallo_layer-400-375_04 | 12 | 39 | 3.2 | 350 | 2.9 | 0.6 | 70 | -0.5 | 0.4 |
| Cueva-del-Parpallo_layer-400-375_05 | 6 | 28 | 4.7 | 119 | 3 | 1 | 31 | -0.1 | -0.8 |
| Cueva-del-Parpallo_layer-400-375_06 | 8 | 22 | 2.8 | 122 | 1.9 | 0.9 | 53 | -0.3 | -0.7 |
| Cueva-del-Parpallo_layer-400-375_07 | 10 | 36 | 3.6 | 218 | 4.4 | 0.1 | 31 | -1.2 | -1.5 |
| Cueva-del-Parpallo_layer-400-375_08 | 7 | 24 | 3.4 | 136 | 5 | 0.5 | 64 | -0.3 | -0.2 |
| Cueva-del-Parpallo_layer-400-375_09 | 5 | 22 | 4.4 | 88 | 4 | 0.6 | 40 | -0.2 | -0.7 |

Appendix Table 17: continued 4,

| ID | width | length | l-w-index | area | upper-lower ratio | left-right ratio | tip angle | MP-CM-x-offset | MP-CM-y-offset |
|---|---|---|---|---|---|---|---|---|---|
| Cueva-del-Parpallo_layer-400-375_10 | 9 | 34 | 3.8 | 204 | 2.1 | 0.5 | 42 | -0.8 | -0.6 |
| Cueva-del-Parpallo_layer-400-375_11 | 7 | 25 | 3.6 | 125 | 2.1 | 0.6 | 49 | -0.8 | -0.3 |
| Cueva-del-Parpallo_layer-400-375_12 | 7 | 26 | 3.7 | 142 | 2.5 | 0.6 | 53 | -0.3 | 0.1 |
| Cueva-del-Parpallo_layer-400-375_13 | 8 | 27 | 3.4 | 165 | 1.8 | 0.6 | 43 | -0.7 | -1.3 |
| Cueva-del-Parpallo_layer-400-375_14 | 5 | 28 | 5.6 | 110 | 2.1 | 0.5 | 41 | -0.5 | 0.3 |
| Cueva-del-Parpallo_layer-400-375_15 | 8 | 28 | 3.5 | 149 | 3 | 0.7 | 45 | 0 | 0 |
| Cueva-del-Parpallo_layer-400-375_16 | 8 | 25 | 3.1 | 129 | 2.6 | 0.3 | 44 | -0.9 | -0.7 |
| Cueva-del-Parpallo_layer-400-375_17 | 7 | 26 | 3.7 | 134 | 2 | 1.3 | 41 | -0.3 | -0.8 |
| Cueva-del-Parpallo_layer-425-400_01 | 10 | 35 | 3.5 | 236 | 1.8 | 0.6 | 46 | -0.5 | -0.1 |
| Cueva-del-Parpallo_layer-425-400_02 | 8 | 28 | 3.5 | 157 | 3.6 | 0.4 | 39 | -0.5 | -1.4 |
| Cueva-del-Parpallo_layer-425-400_03 | 9 | 31 | 3.4 | 196 | 1.8 | 0.3 | 58 | -0.4 | 0.2 |
| Cueva-del-Parpallo_layer-425-400_04 | 7 | 22 | 3.1 | 98 | 4.5 | 0.6 | 37 | -0.3 | -1.3 |
| Cueva-del-Parpallo_layer-425-400_05 | 6 | 21 | 3.5 | 94 | 2.2 | 0.4 | 37 | -0.8 | -1.3 |
| Cueva-del-Parpallo_layer-425-400_06 | 7 | 34 | 4.9 | 189 | 4.2 | 0.5 | 49 | -0.6 | -0.5 |
| Cueva-del-Parpallo_layer-425-400_07 | 6 | 16 | 2.7 | 65 | 2.2 | 0.8 | 44 | -0.2 | -0.4 |
| Cueva-del-Parpallo_layer-425-400_08 | 7 | 21 | 3 | 97 | 1.3 | 0.6 | 54 | -0.6 | -0.2 |
| Cueva-del-Parpallo_layer-425-400_09 | 8 | 31 | 3.9 | 163 | 1.6 | 0.3 | 44 | -0.8 | 0.5 |
| Cueva-del-Parpallo_layer-425-400_10 | 5 | 18 | 3.6 | 64 | 1.7 | 0.7 | 44 | -0.3 | -0.5 |
| Cueva-del-Parpallo_layer-425-400_11 | 9 | 31 | 3.4 | 193 | 2.7 | 0.3 | 41 | -0.8 | -1.6 |
| Cueva-del-Parpallo_layer-425-400_12 | 7 | 21 | 3 | 93 | 4.2 | 0.4 | 36 | -0.3 | -1.4 |
| Cueva-del-Parpallo_layer-425-400_13 | 8 | 30 | 3.8 | 172 | 1.7 | 0.6 | 48 | -0.5 | -0.3 |
| Cueva-del-Parpallo_layer-450-425_01 | 9 | 29 | 3.2 | 171 | 1.3 | 1.5 | 60 | -0.1 | 1 |
| Cueva-del-Parpallo_layer-450-425_02 | 6 | 26 | 4.3 | 118 | 2.3 | 0.8 | 53 | -0.3 | 0 |
| Cueva-del-Parpallo_layer-450-425_03 | 9 | 26 | 2.9 | 141 | 1.6 | 0.3 | 45 | -0.9 | -0.3 |
| Cueva-del-Parpallo_layer-450-425_04 | 6 | 27 | 4.5 | 118 | 2.9 | 0.7 | 35 | -0.5 | -0.9 |
| Cueva-del-Parpallo_layer-450-425_05 | 5 | 22 | 4.4 | 78 | 2.8 | 0.7 | 34 | -0.1 | -0.5 |
| Cueva-del-Parpallo_layer-450-425_06 | 4 | 24 | 6 | 72 | 2 | 0.9 | 34 | -0.3 | 0.2 |
| Cueva-del-Parpallo_layer-450-425_07 | 7 | 28 | 4 | 155 | 1.6 | 1 | 70 | -0.1 | 1.1 |
| Cueva-del-Parpallo_layer-450-425_08 | 7 | 25 | 3.6 | 120 | 1.4 | 0.6 | 59 | -0.5 | 0.7 |
| Cueva-del-Parpallo_layer-450-425_09 | 7 | 22 | 3.1 | 105 | 1.8 | 0.6 | 65 | -0.3 | 0.6 |
| Cueva-del-Parpallo_layer-450-425_10 | 6 | 22 | 3.7 | 101 | 3.4 | 0.6 | 66 | -0.1 | 0.2 |
| Cueva-del-Parpallo_layer-450-425_11 | 8 | 23 | 2.9 | 123 | 1.7 | 1.8 | 48 | 0.3 | -1 |
| Cueva-del-Parpallo_layer-450-425_12 | 6 | 27 | 4.5 | 117 | 2.4 | 0.9 | 45 | -0.1 | -0.1 |
| Cueva-del-Parpallo_layer-450-425_13 | 7 | 23 | 3.3 | 100 | 2 | 0.8 | 51 | -0.3 | 0.3 |
| Cueva-del-Parpallo_layer-450-425_14 | 7 | 23 | 3.3 | 112 | 1.7 | 0.3 | 56 | -0.8 | -0.3 |
| Cueva-del-Parpallo_layer-450-425_15 | 7 | 30 | 4.3 | 163 | 2.7 | 0.9 | 53 | -0.3 | 0 |
| Cueva-del-Parpallo_layer-450-425_16 | 5 | 24 | 4.8 | 81 | 2.5 | 0.8 | 33 | 0 | -0.2 |

Appendix Table 17: continued 5,

| ID | width | length | l-w-index | area | upper-lower ratio | left-right ratio | tip angle | MP-CM-x-offset | MP-CM-y-offset |
|---|---|---|---|---|---|---|---|---|---|
| Cueva-del-Parpallo_layer-450-425_17 | 5 | 26 | 5.2 | 95 | 1.9 | 0.3 | 43 | -0.6 | -0.1 |
| Cueva-del-Parpallo_layer-450-425_18 | 8 | 28 | 3.5 | 153 | 2.5 | 0.7 | 46 | -0.5 | -0.5 |
| Cueva-del-Parpallo_layer-450-425_19 | 6 | 24 | 4 | 99 | 1.4 | 0.5 | 59 | -0.4 | 0.6 |
| Cueva-del-Parpallo_layer-450-425_20 | 6 | 25 | 4.2 | 119 | 3.5 | 0.5 | 40 | -0.4 | -1.2 |
| Cueva-del-Parpallo_layer-450-425_21 | 6 | 31 | 5.2 | 114 | 2.1 | 1.8 | 39 | 0.3 | 0.3 |
| Cueva-del-Reclau-Viver_01 | 9 | 27 | 3 | 168 | 1.3 | 0.8 | 66 | -0.5 | 0.3 |
| Cueva-del-Reclau-Viver_02 | 10 | 21 | 2.1 | 140 | 1.2 | 0.8 | 78 | -0.6 | -0.1 |
| Cueva-del-Reclau-Viver_03 | 10 | 21 | 2.1 | 124 | 0.9 | 0.5 | 86 | -0.8 | 0.8 |
| Cueva-Morin_01 | 12 | 50 | 4.2 | 436 | 3.5 | 0.7 | 41 | -0.3 | -2 |
| Davant-Pau_01 | 10 | 34 | 3.4 | 219 | 2.3 | 0.4 | 33 | -0.8 | -2 |
| Davant-Pau_02 | 9 | 27 | 3 | 157 | 1.2 | 0.9 | 51 | -0.4 | 0.1 |
| Deimern-42_01 | 14 | 51 | 3.6 | 504 | 1.8 | 0.1 | 38 | -1.2 | -2.5 |
| Deimern-42_02 | 12 | 45 | 3.8 | 337 | 1.3 | 0.8 | 46 | -0.8 | -0.2 |
| Deimern-42_03 | 12 | 38 | 3.2 | 307 | 1.3 | 0.7 | 52 | -0.9 | -0.8 |
| Deimern-42_04 | 12 | 46 | 3.8 | 394 | 1.1 | 0.4 | 71 | -0.8 | 0.8 |
| Deimern-42_05 | 11 | 45 | 4.1 | 360 | 1.3 | 0.3 | 43 | -0.9 | -0.6 |
| Deimern-42_06 | 12 | 40 | 3.3 | 380 | 1.2 | 0.2 | 47 | -0.8 | -1.8 |
| Deimern-42_07 | 17 | 50 | 2.9 | 508 | 0.9 | 0.5 | 55 | -1.8 | -0.8 |
| Deimern-42_08 | 12 | 42 | 3.5 | 359 | 1.2 | 0.4 | 57 | -0.5 | -1.4 |
| Deimern-42_09 | 11 | 46 | 4.2 | 343 | 1.6 | 0.3 | 37 | -0.5 | -1.6 |
| Deux-Avens_01 | 11 | 60 | 5.5 | 484 | 2.4 | 0.7 | 32 | -0.4 | -3.1 |
| Dorotchivtsy-III_layer-6_01 | 13 | 53 | 4.1 | 468 | 1.7 | 0.7 | 40 | -0.3 | -1.6 |
| Dorotchivtsy-III_layer-6_02 | 10 | 46 | 4.6 | 339 | 0.7 | 0.5 | 64 | -1.1 | 1.1 |
| Duruthy_layer-3_01 | 12 | 68 | 5.7 | 627 | 0.3 | 0.7 | 57 | -1.2 | -1.4 |
| Duruthy_layer-3_02 | 13 | 55 | 4.2 | 494 | 0.5 | 0.5 | 74 | -1.4 | 0.4 |
| Duruthy_layer-3_03 | 10 | 44 | 4.4 | 309 | 0.5 | 1.1 | 54 | -0.6 | -0.5 |
| El-Miron_01 | 12 | 48 | 4 | 387 | 2.4 | 1.1 | 40 | -0.2 | -0.8 |
| El-Pendo_01 | 13 | 46 | 3.5 | 414 | 0.7 | 0.5 | 70 | -1.2 | 1.1 |
| El-Pendo_02 | 15 | 47 | 3.1 | 497 | 1.3 | 0.7 | 64 | -0.6 | 0 |
| Fondo-Focone_layer-Trench-B_01 | 15 | 64 | 4.3 | 611 | 1.3 | 0.6 | 46 | -0.8 | 0.6 |
| Fondo-Focone_layer-Trench-B_02 | 19 | 41 | 2.2 | 505 | 1.3 | 0.8 | 75 | -0.9 | 0 |
| Fondo-Focone_layer-Trench-B_03 | 18 | 66 | 3.7 | 779 | 1.6 | 0.8 | 45 | -0.3 | -1.3 |
| Fondo-Focone_layer-Trench-B_04 | 14 | 43 | 3.1 | 417 | 1.3 | 0.5 | 65 | -1.4 | 0 |
| Fondo-Focone_layer-Trench-B_05 | 12 | 59 | 4.9 | 523 | 1 | 0.9 | 56 | -0.3 | 0.2 |
| Fontgrasse_layer-1a_01 | 20 | 68 | 3.4 | 997 | 2.6 | 0.6 | 48 | -0.8 | -3.4 |
| Fontgrasse_layer-1a_02 | 15 | 53 | 3.5 | 589 | 2.1 | 0.5 | 46 | -0.6 | -1.6 |
| Fontgrasse_layer-1a_03 | 15 | 45 | 3 | 500 | 1.4 | 0.5 | 54 | -1.1 | -2.4 |

Appendix Table 17: continued 6,

| ID | width | length | l–w–index | area | upper–lower ratio | left–right ratio | tip angle | MP–CM–x–offset | MP–CM–y–offset |
|---|---|---|---|---|---|---|---|---|---|
| Fontgrasse_layer–1a_04 | 12 | 52 | 4.3 | 466 | 0.9 | 0.8 | 54 | –0.8 | –0.3 |
| Fontgrasse_layer–3_01 | 16 | 59 | 3.7 | 641 | 2.2 | 0.2 | 47 | –1.4 | –1.6 |
| Fontgrasse_layer–3_02 | 13 | 57 | 4.4 | 565 | 2.9 | 0.6 | 42 | –0.2 | –1.5 |
| Forneau–du–Diable_layer–Sol–sup–I_01 | 14 | 72 | 5.1 | 735 | 1.1 | 0.8 | 49 | –1 | 1.3 |
| Forneau–du–Diable_layer–Sol–sup–I_02 | 11 | 50 | 4.5 | 413 | 0.7 | 1 | 49 | –0.4 | 0.1 |
| Forneau–du–Diable_layer–Sol–sup–I_03 | 12 | 68 | 5.7 | 601 | 0.9 | 0.9 | 45 | –0.6 | 0.3 |
| Forneau–du–Diable_layer–Sol–sup–I_04 | 13 | 52 | 4 | 518 | 0.9 | 1 | 60 | –0.5 | –0.6 |
| Forneau–du–Diable_layer–Sol–sup–I_05 | 13 | 65 | 5 | 586 | 1.3 | 1.1 | 37 | 0.1 | –0.7 |
| Forneau–du–Diable_layer–Sol–sup–III_01_01 | 19 | 106 | 5.6 | 1284 | 1.2 | 0.3 | 29 | –2.1 | –1.9 |
| Forneau–du–Diable_layer–Sol–sup–III_01_02 | 14 | 64 | 4.6 | 590 | 1.3 | 0.5 | 37 | –1.2 | –1.1 |
| Forneau–du–Diable_layer–Sol–sup–III_01_03 | 16 | 66 | 4.1 | 662 | 1 | 0.6 | 45 | –1.1 | –0.1 |
| Forneau–du–Diable_layer–Sol–sup–III_01_04 | 17 | 62 | 3.6 | 655 | 1 | 0.4 | 48 | –1.5 | 1 |
| Forneau–du–Diable_layer–Sol–sup–III_02_01 | 18 | 81 | 4.5 | 883 | 1.1 | 0.5 | 35 | –1.7 | –1.1 |
| Forneau–du–Diable_layer–Sol–sup–III_02_02 | 16 | 76 | 4.8 | 790 | 1.3 | 0.7 | 39 | –1.4 | –1.2 |
| Forneau–du–Diable_layer–Sol–sup–III_02_03 | 11 | 68 | 6.2 | 593 | 1.6 | 1 | 51 | –0.6 | 0.3 |
| Forneau–du–Diable_layer–Sol–sup–III_02_04 | 14 | 60 | 4.3 | 581 | 1.1 | 0.4 | 50 | –1 | 0.4 |
| Forneau–du–Diable_layer–Sol–sup–III_03_01 | 13 | 51 | 3.9 | 448 | 0.3 | 0.6 | 89 | –1.1 | 1.7 |
| Forneau–du–Diable_layer–Sol–sup–II_01_01 | 18 | 76 | 4.2 | 1027 | 0.6 | 1 | 67 | –0.3 | 0.8 |
| Forneau–du–Diable_layer–Sol–sup–II_01_02 | 10 | 67 | 6.7 | 544 | 1 | 0.8 | 44 | –0.4 | 0.3 |
| Forneau–du–Diable_layer–Sol–sup–II_01_03 | 15 | 68 | 4.5 | 675 | 1 | 0.5 | 46 | –1.2 | 0.8 |
| Forneau–du–Diable_layer–Sol–sup–II_01_04 | 11 | 59 | 5.4 | 465 | 0.7 | 0.4 | 42 | –1.4 | –0.3 |
| Forneau–du–Diable_layer–Sol–sup–II_01_05 | 14 | 67 | 4.8 | 709 | 1 | 1.1 | 58 | –0.4 | 1.5 |
| Forneau–du–Diable_layer–Sol–sup–II_01_06 | 13 | 60 | 4.6 | 540 | 1 | 0.5 | 47 | –1.2 | 0.3 |
| Forneau–du–Diable_layer–Sol–sup–II_01_07 | 14 | 77 | 5.5 | 750 | 0.8 | 0.7 | 44 | –0.8 | 0.4 |
| Forneau–du–Diable_layer–Sol–sup–II_02_01 | 13 | 69 | 5.3 | 601 | 1.2 | 0.7 | 35 | –0.7 | –0.9 |
| Forneau–du–Diable_layer–Sol–sup–II_02_02 | 16 | 62 | 3.9 | 717 | 0.9 | 0.6 | 50 | –0.5 | –0.6 |
| Forneau–du–Diable_layer–Sol–sup–II_02_03 | 13 | 56 | 4.3 | 502 | 1.1 | 0.7 | 49 | –0.6 | 0.3 |
| Fussgoenheim–I_01 | 14 | 42 | 3 | 367 | 1.2 | 0.1 | 41 | –2.1 | –1.7 |
| Fussgoenheim–I_02 | 12 | 33 | 2.8 | 299 | 0.8 | 0 | 54 | –1.5 | –1.5 |
| Fussgoenheim–I_03 | 11 | 33 | 3 | 280 | 1.7 | 0.3 | 65 | –1.1 | –0.3 |
| Fussgoenheim–I_04 | 9 | 28 | 3.1 | 182 | 1.2 | 0.4 | 53 | –0.7 | –1 |
| Fussgoenheim–II_01 | 16 | 48 | 3 | 499 | 1.1 | 0.2 | 53 | –1.8 | –0.9 |
| Fussgoenheim–II_02 | 17 | 42 | 2.5 | 449 | 1.2 | 0.5 | 44 | –1.5 | –1.9 |
| Gagarino_01 | 11 | 48 | 4.4 | 392 | 0.8 | 0.9 | 60 | –0.1 | –0.5 |
| Gagarino_02 | 6 | 28 | 4.7 | 145 | 0.9 | 0.8 | 48 | –0.3 | –1.2 |
| Gagarino_03 | 7 | 35 | 5 | 169 | 0.8 | 0.5 | 49 | –0.7 | 0.3 |
| Gagarino_04 | 6 | 27 | 4.5 | 124 | 0.6 | 0.6 | 58 | –0.3 | –0.3 |

Appendix Table 17: continued 7,

| ID | width | length | l-w-index | area | upper-lower ratio | left-right ratio | tip angle | MP-CM-x-offset | MP-CM-y-offset |
|---|---|---|---|---|---|---|---|---|---|
| Gagarino_05 | 9 | 34 | 3.8 | 211 | 0.9 | 0.6 | 56 | -0.3 | -0.6 |
| Gavechou_01 | 13 | 47 | 3.6 | 443 | 1.1 | 0.7 | 56 | -0.2 | -0.2 |
| Gavechou_02 | 10 | 40 | 4 | 279 | 0.5 | 0.7 | 75 | -0.8 | 1.3 |
| Goughs-Cave_layer-B_01 | 16 | 59 | 3.7 | 692 | 0.7 | 0.7 | 56 | -0.3 | -1.4 |
| Goughs-Cave_layer-B_02 | 12 | 36 | 3 | 331 | 0.7 | 0.3 | 69 | -1.1 | -0.8 |
| Goughs-Cave_layer-B_03 | 15 | 49 | 3.3 | 557 | 0.8 | 0.4 | 64 | -1 | -0.6 |
| Goughs-Cave_layer-B_04 | 16 | 43 | 2.7 | 457 | 0.6 | 0.1 | 59 | -1.5 | -0.3 |
| Goughs-Cave_layer-B_05 | 15 | 42 | 2.8 | 431 | 0.6 | 1 | 73 | -1.2 | -0.1 |
| Goughs-Cave_layer-B_06 | 15 | 36 | 2.4 | 424 | 0.6 | 0.4 | 86 | -0.8 | -1.2 |
| Grand-Abri-de-Mazerat_01 | 15 | 72 | 4.8 | 692 | 1.5 | 0.6 | 32 | -1 | -1.5 |
| Grotta-de-la-Salpetriere_layer-6_01 | 8 | 58 | 7.2 | 346 | 3.8 | 0.7 | 22 | -0.4 | -1.8 |
| Grotta-de-la-Salpetriere_layer-6_02 | 10 | 42 | 4.2 | 296 | 2.5 | 0.4 | 52 | -0.6 | 0.4 |
| Grotta-de-la-Salpetriere_layer-6_03 | 10 | 42 | 4.2 | 300 | 2.8 | 0.6 | 60 | -0.4 | 0.8 |
| Grotta-de-la-Salpetriere_layer-6_04 | 9 | 39 | 4.3 | 240 | 2.9 | 1.1 | 31 | 0.1 | -1.7 |
| Grotta-de-la-Salpetriere_layer-6_05 | 10 | 47 | 4.7 | 304 | 2.1 | 0.8 | 39 | -0.6 | -0.2 |
| Grotta-del-Fanciulli_layer-D-C_01 | 10 | 39 | 3.9 | 262 | 0.8 | 3.5 | 49 | 1 | -0.4 |
| Grotta-della-Cala_layer-P-M_01 | 6 | 23 | 3.8 | 103 | 1.6 | 0.7 | 53 | -0.4 | 0.3 |
| Grotta-delle-Settecannelle_01 | 13 | 39 | 3 | 327 | 1.4 | 0.5 | 55 | -1.2 | -0.5 |
| Grotta-delle-Settecannelle_02 | 12 | 53 | 4.4 | 435 | 1.5 | 0.7 | 41 | -0.4 | -0.2 |
| Grotta-delle-Settecannelle_03 | 13 | 35 | 2.7 | 300 | 1.2 | 0.7 | 67 | -0.8 | 0.3 |
| Grotta-delle-Settecannelle_04 | 10 | 48 | 4.8 | 368 | 2 | 0.5 | 43 | -0.7 | -0.3 |
| Grotta-delle-Settecannelle_05 | 9 | 33 | 3.7 | 209 | 1.2 | 0.5 | 54 | -0.8 | -0.1 |
| Grotta-delle-Settecannelle_06 | 10 | 46 | 4.6 | 321 | 1.8 | 0.8 | 36 | -0.4 | -1.2 |
| Grotta-delle-Settecannelle_07 | 10 | 28 | 2.8 | 190 | 1.2 | 0.7 | 66 | -0.6 | 0.6 |
| Grotta-delle-Settecannelle_08 | 13 | 36 | 2.8 | 316 | 1.5 | 0.8 | 61 | -0.5 | -0.3 |
| Grotta-delle-Settecannelle_09 | 10 | 36 | 3.6 | 262 | 2 | 0.8 | 53 | -0.4 | -0.3 |
| Grotta-delle-Settecannelle_10 | 7 | 31 | 4.4 | 150 | 1.3 | 0.5 | 36 | -0.5 | -0.7 |
| Grotta-di-Paina_01 | 11 | 68 | 6.2 | 548 | 2 | 1 | 38 | -0.1 | -0.3 |
| Grotta-Paglicci_layer-18a-10_01_01 | 12 | 69 | 5.8 | 612 | 1.4 | 0.7 | 32 | -0.3 | -0.8 |
| Grotta-Paglicci_layer-18a-10_01_02 | 13 | 42 | 3.2 | 322 | 0.8 | 0.5 | 60 | -1.8 | 1.3 |
| Grotta-Paglicci_layer-18a-10_01_03 | 13 | 64 | 4.9 | 546 | 1 | 0.4 | 34 | -0.7 | -0.5 |
| Grotta-Paglicci_layer-18a-10_01_04 | 13 | 54 | 4.2 | 446 | 1.6 | 0.6 | 38 | -0.9 | 0 |
| Grotta-Paglicci_layer-18a-10_01_05 | 12 | 62 | 5.2 | 476 | 1.1 | 0.6 | 37 | -1.1 | 0.8 |
| Grotta-Paglicci_layer-18a-10_01_06 | 15 | 53 | 3.5 | 547 | 2.3 | 0.4 | 56 | -1.5 | 0.3 |
| Grotta-Paglicci_layer-18a-10_01_07 | 13 | 65 | 5 | 557 | 1.5 | 1.1 | 40 | -0.4 | 0.1 |
| Grotta-Paglicci_layer-18a-10_01_08 | 10 | 54 | 5.4 | 327 | 1.3 | 0.7 | 32 | -1 | -0.2 |
| Grotta-Paglicci_layer-18a-10_01_09 | 10 | 58 | 5.8 | 416 | 1.2 | 0.9 | 34 | -0.4 | -1 |

Appendix Table 17: continued 8,

| ID | width | length | l-w-index | area | upper-lower ratio | left-right ratio | tip angle | MP-CM-x-offset | MP-CM-y-offset |
|---|---|---|---|---|---|---|---|---|---|
| Grotta-Paglicci_layer-18a-10_01_10 | 11 | 45 | 4.1 | 378 | 2.4 | 0.5 | 44 | -0.7 | -1.4 |
| Grotta-Paglicci_layer-18a-10_01_11 | 12 | 55 | 4.6 | 461 | 1.5 | 0.3 | 33 | -1.7 | -2.7 |
| Grotta-Paglicci_layer-18a-10_02_01 | 12 | 53 | 4.4 | 448 | 3.1 | 1.1 | 38 | -0.2 | -1.2 |
| Grotta-Paglicci_layer-18a-10_02_02 | 11 | 32 | 2.9 | 239 | 1.3 | 0.3 | 54 | -1.2 | -0.9 |
| Grotta-Paglicci_layer-18a-10_02_03 | 13 | 54 | 4.2 | 452 | 0.9 | 0.7 | 49 | -1.1 | 0.9 |
| Grotta-Paglicci_layer-18a-10_02_04 | 7 | 34 | 4.9 | 154 | 1 | 1.3 | 40 | -0.2 | 0.4 |
| Grotta-Paglicci_layer-18a-10_02_05 | 12 | 45 | 3.8 | 344 | 1.4 | 0.6 | 48 | -1.2 | 0.3 |
| Grotta-Paglicci_layer-18a-10_02_06 | 11 | 42 | 3.8 | 324 | 0.7 | 0.8 | 60 | -0.8 | -0.1 |
| Grotta-Paglicci_layer-18a-10_02_07 | 9 | 38 | 4.2 | 247 | 1.7 | 0.7 | 52 | -0.8 | 0 |
| Grotta-Paglicci_layer-18a-10_02_08 | 11 | 46 | 4.2 | 333 | 1.6 | 0.3 | 39 | -1.4 | -0.7 |
| Grotta-Paglicci_layer-18a-10_02_09 | 8 | 48 | 6 | 282 | 1.3 | 0.6 | 37 | -0.3 | 0 |
| Grotta-Paglicci_layer-18a-10_02_10 | 10 | 34 | 3.4 | 246 | 1.3 | 0.4 | 47 | -0.4 | -1.8 |
| Grotta-Paglicci_layer-18a-10_02_11 | 9 | 57 | 6.3 | 347 | 1 | 0.3 | 34 | -1.1 | 0.6 |
| Grotta-Paglicci_layer-20_01 | 12 | 51 | 4.2 | 424 | 1.3 | 0.7 | 44 | -0.5 | -0.1 |
| Grotta-Paglicci_layer-23&22_01 | 11 | 41 | 3.7 | 313 | 0.8 | 0.5 | 58 | -1.2 | 0.7 |
| Grotta-Romanelli_01 | 4 | 29 | 7.2 | 101 | 1.1 | 0.8 | 39 | -0.3 | -0.4 |
| Grotta-Trene_01 | 11 | 49 | 4.5 | 376 | 1.2 | 0.4 | 44 | -1 | -0.6 |
| Grotte-de-Cleves_01 | 14 | 62 | 4.4 | 615 | 1.1 | 0.1 | 43 | -1.4 | -0.4 |
| Grotte-de-La-Bouviere_01 | 12 | 66 | 5.5 | 533 | 1.1 | 0.9 | 35 | -0.4 | -1 |
| Grotte-de-La-Bouviere_02 | 11 | 42 | 3.8 | 376 | 0.4 | 1.4 | 93 | 0.2 | 0.3 |
| Grotte-de-La-Bouviere_03 | 9 | 47 | 5.2 | 290 | 1.4 | 0.8 | 38 | -0.5 | -0.1 |
| Grotte-de-La-Bouviere_04 | 7 | 35 | 5 | 193 | 0.5 | 1 | 63 | -0.3 | 0.2 |
| Grotte-de-La-Bouviere_05 | 8 | 42 | 5.2 | 231 | 1.3 | 1 | 38 | -0.3 | -0.3 |
| Grotte-de-La-Bouviere_06 | 8 | 29 | 3.6 | 176 | 0.5 | 1.1 | 76 | -0.4 | 0.5 |
| Grotte-de-La-Bouviere_07 | 8 | 36 | 4.5 | 214 | 1.4 | 1 | 37 | -0.3 | -0.8 |
| Grotte-de-La-Bouviere_08 | 8 | 27 | 3.4 | 157 | 0.8 | 0.7 | 66 | -0.8 | -0.2 |
| Grotte-de-La-Bouviere_09 | 13 | 42 | 3.2 | 332 | 1.3 | 0.5 | 50 | -1.4 | -0.1 |
| Grotte-des-Enfants-a-Grimaldi_01 | 13 | 48 | 3.7 | 395 | 1.4 | 0.7 | 43 | -0.8 | -0.3 |
| Grotte-des-Enfants-a-Grimaldi_02 | 8 | 38 | 4.8 | 212 | 1.2 | 1.4 | 42 | -0.1 | -0.3 |
| Grotte-des-Enfants-a-Grimaldi_03 | 12 | 41 | 3.4 | 315 | 1.4 | 0.5 | 52 | -0.9 | 0.1 |
| Grotte-des-Enfants-a-Grimaldi_04 | 10 | 51 | 5.1 | 362 | 2.4 | 0.7 | 32 | -0.5 | -2 |
| Grotte-des-Enfants-a-Grimaldi_05 | 9 | 29 | 3.2 | 175 | 0.7 | 1.1 | 65 | -0.5 | 0.5 |
| Grotte-des-Eyzies_01 | 13 | 65 | 5 | 614 | 1.7 | 1.2 | 43 | 0 | 0.1 |
| Grub-Kranawetberg_01 | 14 | 56 | 4 | 520 | 1.1 | 0.4 | 45 | -1.3 | -0.8 |
| Grub-Kranawetberg_02 | 8 | 38 | 4.8 | 204 | 1.8 | 0.4 | 43 | -1 | 0.6 |
| Grub-Kranawetberg_03 | 9 | 29 | 3.2 | 202 | 0.8 | 0.2 | 57 | -0.9 | -0.5 |
| Gruta-de-Salemas_01 | 11 | 52 | 4.7 | 353 | 2.2 | 0.7 | 28 | -0.7 | -1.4 |

Appendix Table 17: continued 9,

| ID | width | length | l-w-index | area | upper-lower ratio | left-right ratio | tip angle | MP-CM-x-offset | MP-CM-y-offset |
|---|---|---|---|---|---|---|---|---|---|
| Gruta-de-Salemas_02 | 9 | 46 | 5.1 | 265 | 2.3 | 0.9 | 29 | -0.2 | -0.8 |
| Gruta-de-Salemas_03 | 11 | 43 | 3.9 | 345 | 1.6 | 1.1 | 39 | -0.1 | -1.2 |
| Gruta-de-Salemas_04 | 13 | 42 | 3.2 | 359 | 1.1 | 0.8 | 53 | -0.8 | -0.1 |
| Gruta-do-Almonda_01 | 13 | 49 | 3.8 | 390 | 2 | 0.6 | 48 | -1.4 | 0.7 |
| Gruta-do-Almonda_02 | 11 | 47 | 4.3 | 367 | 3.6 | 1.5 | 63 | 0.3 | 1.3 |
| Gruta-do-Caldeirao_01 | 9 | 40 | 4.4 | 249 | 2.1 | 0.7 | 48 | -0.6 | -0.1 |
| Gruta-do-Caldeirao_02 | 9 | 27 | 3 | 169 | 2 | 0.6 | 66 | -0.6 | 0.7 |
| Gruta-do-Ourao_01 | 9 | 45 | 5 | 257 | 2.2 | 0.7 | 30 | -0.5 | -0.8 |
| Hasewisch_01 | 11 | 64 | 5.8 | 479 | 2.3 | 0.4 | 29 | -0.7 | -2.1 |
| Hasewisch_02 | 14 | 49 | 3.5 | 453 | 1.4 | 0.4 | 45 | -1.4 | -1.1 |
| Heber-118_01_01 | 17 | 46 | 2.7 | 510 | 1 | 0.5 | 60 | -0.9 | -0.5 |
| Heber-118_01_02 | 13 | 43 | 3.3 | 405 | 1.1 | 0.2 | 61 | -1.6 | -1.1 |
| Heber-118_01_03 | 12 | 41 | 3.4 | 344 | 1.1 | 0.6 | 58 | -1 | -1.1 |
| Heber-118_01_04 | 12 | 43 | 3.6 | 333 | 1.2 | 0.1 | 40 | -2.1 | -1.7 |
| Heber-118_01_05 | 16 | 43 | 2.7 | 470 | 0.7 | 0.2 | 59 | -1.4 | -0.7 |
| Heber-118_01_06 | 13 | 42 | 3.2 | 382 | 1.5 | 0.6 | 52 | -0.6 | -0.8 |
| Heber-118_01_07 | 14 | 43 | 3.1 | 390 | 1 | 0.7 | 48 | -0.5 | -1.1 |
| Heber-118_01_08 | 16 | 56 | 3.5 | 632 | 1 | 0.7 | 47 | -0.4 | -1.9 |
| Heber-118_01_09 | 13 | 39 | 3 | 399 | 0.8 | 0.9 | 81 | -0.9 | -0.5 |
| Heber-118_01_10 | 14 | 55 | 3.9 | 595 | 1 | 0.4 | 54 | -1.4 | -1.4 |
| Heber-118_01_11 | 12 | 45 | 3.8 | 448 | 0.6 | 0.2 | 82 | -0.6 | 0.2 |
| Heber-118_02_01 | 13 | 47 | 3.6 | 446 | 1.2 | 0.7 | 49 | -0.7 | -1.4 |
| Heber-118_02_02 | 12 | 43 | 3.6 | 354 | 1 | 0.2 | 51 | -0.8 | -1.8 |
| Heber-118_02_03 | 11 | 42 | 3.8 | 349 | 1 | 0.7 | 47 | 0 | -1.4 |
| Heber-127_01_01 | 16 | 45 | 2.8 | 437 | 1.1 | 0.1 | 40 | -2.1 | -2.3 |
| Heber-127_01_02 | 17 | 51 | 3 | 557 | 1.2 | 1 | 48 | -1.1 | -1.9 |
| Heber-127_01_03 | 15 | 40 | 2.7 | 376 | 1.1 | 0.4 | 51 | -1.4 | -1.5 |
| Heber-127_01_04 | 15 | 55 | 3.7 | 606 | 0.8 | 0.6 | 56 | -0.2 | -1.3 |
| Heber-127_01_05 | 13 | 41 | 3.2 | 407 | 0.9 | 0.1 | 56 | -1.1 | -1.3 |
| Heber-127_01_06 | 15 | 51 | 3.4 | 469 | 1.2 | 0.1 | 39 | -1.9 | -1.9 |
| Heber-127_01_07 | 14 | 46 | 3.3 | 440 | 1.3 | 0.1 | 51 | -0.7 | -0.8 |
| Heber-127_01_08 | 16 | 41 | 2.6 | 404 | 1.4 | 0.7 | 55 | -0.5 | -0.7 |
| Heber-127_01_09 | 13 | 39 | 3 | 323 | 1.1 | 0.5 | 59 | -1 | -0.4 |
| Heber-127_01_10 | 14 | 48 | 3.4 | 497 | 1.4 | 0.8 | 62 | -0.8 | -1.1 |
| Heber-127_02_01 | 13 | 49 | 3.8 | 408 | 1.2 | 0.3 | 32 | -1 | -2.8 |
| Heber-127_02_02 | 17 | 40 | 2.4 | 454 | 0.9 | 1.1 | 59 | -1 | -0.8 |
| Heber-127_02_03 | 17 | 52 | 3.1 | 535 | 1 | 0.3 | 45 | -2.1 | -1.3 |

Appendix Table 17: continued 10,

| ID | width | length | l-w-index | area | upper-lower ratio | left-right ratio | tip angle | MP-CM-x-offset | MP-CM-y-offset |
|---|---|---|---|---|---|---|---|---|---|
| Heber-127_02_04 | 14 | 38 | 2.7 | 345 | 1.7 | 0.6 | 59 | -1.5 | -0.8 |
| Heber-127_02_05 | 13 | 46 | 3.5 | 424 | 1.4 | 0.4 | 51 | -0.8 | -1.3 |
| Heber-127_02_06 | 12 | 29 | 2.4 | 238 | 1.1 | 0.6 | 68 | -0.7 | -0.6 |
| Heber-127_02_07 | 14 | 41 | 2.9 | 379 | 1 | 0.4 | 55 | -1.1 | -1.2 |
| Hengistbury-Head_01 | 16 | 56 | 3.5 | 625 | 0.9 | 0.7 | 47 | -1.5 | -1.4 |
| Hengistbury-Head_02 | 14 | 51 | 3.6 | 500 | 0.8 | 1 | 51 | -0.9 | -0.8 |
| Hubina_01 | 15 | 51 | 3.4 | 518 | 0.9 | 0.7 | 60 | -1.3 | 0 |
| Jama-v-Lozi_01 | 11 | 52 | 4.7 | 372 | 1 | 0.4 | 35 | -1.2 | -1 |
| Jaurias_01 | 17 | 59 | 3.5 | 626 | 3 | 0.5 | 35 | -0.8 | -3.1 |
| Jaurias_02 | 9 | 44 | 4.9 | 287 | 2.3 | 0.9 | 32 | -0.3 | -1.9 |
| Jaurias_03 | 13 | 48 | 3.7 | 416 | 2.4 | 0.6 | 39 | -0.3 | -2 |
| Jaurias_04 | 9 | 41 | 4.6 | 261 | 1.7 | 0.3 | 44 | -1.1 | -0.3 |
| Jaurias_05 | 13 | 57 | 4.4 | 547 | 2.1 | 0.2 | 50 | -0.7 | 0.2 |
| Jaurias_06 | 10 | 44 | 4.4 | 298 | 1.3 | 0.4 | 40 | -0.8 | -1 |
| Jaurias_07 | 11 | 50 | 4.5 | 411 | 2 | 0.1 | 47 | -0.9 | 0.3 |
| Jaurias_08 | 11 | 48 | 4.4 | 414 | 1.6 | 0.5 | 55 | -0.8 | 0.2 |
| Jaurias_09 | 13 | 50 | 3.8 | 440 | 1.6 | 0.6 | 61 | -0.8 | 0.6 |
| Jaurias_10 | 11 | 45 | 4.1 | 364 | 2.3 | 0.4 | 41 | -0.7 | -1.2 |
| Kaesloch_01 | 20 | 53 | 2.6 | 621 | 1.1 | 0.4 | 67 | -2.4 | 1.3 |
| Kaesloch_02 | 13 | 43 | 3.3 | 420 | 2.3 | 0.5 | 47 | -0.5 | -1.8 |
| Kaesloch_03 | 18 | 43 | 2.4 | 542 | 0.9 | 0.8 | 94 | -1 | 1.3 |
| Kaesloch_04 | 12 | 38 | 3.2 | 317 | 1.2 | 0.3 | 53 | -1.2 | -1.1 |
| Kaesloch_05 | 17 | 45 | 2.6 | 521 | 1.1 | 0.4 | 66 | -1.5 | -1 |
| Kamegg_01 | 11 | 40 | 3.6 | 320 | 1.8 | 1 | 43 | -0.7 | -1.9 |
| Kammern-Grubgraben_01 | 12 | 47 | 3.9 | 342 | 0.9 | 0.2 | 39 | -1.8 | -1.3 |
| Kammern-Grubgraben_02 | 11 | 30 | 2.7 | 249 | 1.2 | 1.2 | 73 | -0.6 | -0.2 |
| Kammern-Grubgraben_03 | 13 | 35 | 2.7 | 310 | 0.9 | 0.8 | 70 | -0.8 | 0.3 |
| Kammern-Grubgraben_04 | 10 | 36 | 3.6 | 259 | 1.3 | 0.9 | 50 | -0.4 | -0.2 |
| Kastelhoehle_layer-upper_01 | 11 | 34 | 3.1 | 249 | 1.3 | 0.4 | 49 | -1.3 | -0.9 |
| Kastritsa-3_01 | 9 | 33 | 3.7 | 183 | 0.7 | 0.8 | 44 | -0.8 | 0.5 |
| Kastritsa-3_02 | 12 | 37 | 3.1 | 294 | 1.1 | 0.5 | 48 | -1.1 | -0.5 |
| Kastritsa-5_01 | 14 | 53 | 3.8 | 515 | 1.2 | 1.5 | 68 | 0.3 | 1.7 |
| Khotylevo-2_01 | 9 | 70 | 7.8 | 482 | 0.5 | 0.6 | 28 | -0.4 | -2.4 |
| Khotylevo-2_02 | 12 | 66 | 5.5 | 569 | 0.7 | 0.7 | 48 | -0.8 | 0.9 |
| Khotylevo-2_03 | 8 | 55 | 6.9 | 368 | 0.4 | 1.3 | 46 | 0.1 | -0.7 |
| Khotylevo-2_04 | 6 | 47 | 7.8 | 267 | 0.4 | 0.8 | 43 | -0.4 | -1.1 |
| Kniegrotte_01 | 11 | 27 | 2.5 | 188 | 1.3 | 0.3 | 54 | -1.3 | -0.5 |

Appendix Table 17: continued 11,

| ID | width | length | l-w-index | area | upper-lower ratio | left-right ratio | tip angle | MP-CM-x-offset | MP-CM-y-offset |
|---|---|---|---|---|---|---|---|---|---|
| Koepfli_01 | 15 | 50 | 3.3 | 442 | 1.5 | 0.4 | 34 | -1.2 | -2.6 |
| Koepfli_02 | 9 | 30 | 3.3 | 205 | 1 | 0.1 | 65 | -1.1 | -0.1 |
| Koepfli_03 | 13 | 34 | 2.6 | 308 | 1.2 | 0.3 | 60 | -1.4 | -1.2 |
| Koepfli_04 | 14 | 35 | 2.5 | 318 | 1 | 0.1 | 62 | -1.6 | -0.8 |
| Kostenki-1_layer-1_01 | 15 | 71 | 4.7 | 732 | 0.7 | 0.6 | 49 | -1.1 | -0.3 |
| Kostenki-1_layer-1_02 | 18 | 54 | 3 | 709 | 0.4 | 0.9 | 81 | -0.7 | -0.8 |
| Kostenki-1_layer-1_03 | 18 | 49 | 2.7 | 645 | 0.7 | 0.8 | 85 | -0.6 | 0.2 |
| Kostenki-1_layer-1_04 | 10 | 44 | 4.4 | 312 | 0.6 | 0.8 | 64 | -0.7 | 0.1 |
| Kostenki-21_layer-3_01 | 12 | 71 | 5.9 | 574 | 0.9 | 0.6 | 41 | -0.8 | 0.5 |
| Kostenki-21_layer-3_02 | 15 | 52 | 3.5 | 528 | 0.9 | 0.7 | 70 | -1.3 | 0.9 |
| Kostenki-21_layer-3_03 | 11 | 66 | 6 | 509 | 0.7 | 0.5 | 38 | -0.7 | -0.2 |
| Kostenki-21_layer-3_04 | 9 | 49 | 5.4 | 312 | 0.6 | 1.6 | 54 | -0.1 | 0.4 |
| Kostenki-21_layer-3_05 | 9 | 52 | 5.8 | 332 | 0.7 | 0.8 | 44 | -1 | 0.3 |
| Kostenki-21_layer-3_06 | 11 | 34 | 3.1 | 248 | 0.9 | 0.4 | 65 | -1.1 | 0.2 |
| Kostenki-21_layer-3_07 | 10 | 51 | 5.1 | 309 | 0.8 | 0.3 | 43 | -1.9 | 0.2 |
| Kostenki-21_layer-3_08 | 11 | 30 | 2.7 | 246 | 1.4 | 0.8 | 75 | -0.4 | 0.3 |
| Kostenki-21_layer-3_09 | 7 | 38 | 5.4 | 198 | 0.5 | 0.7 | 72 | -0.7 | 1.1 |
| Kostenki-21_layer-3_10 | 7 | 26 | 3.7 | 133 | 0.5 | 1.1 | 76 | -0.3 | 0.5 |
| Kostenki-21_layer-3_11 | 7 | 35 | 5 | 172 | 0.8 | 0.8 | 52 | -0.3 | 0.8 |
| Kostenki-21_layer-3_12 | 9 | 32 | 3.6 | 210 | 0.8 | 0.2 | 57 | -0.9 | -0.6 |
| Kostenki-21_layer-3_13 | 7 | 41 | 5.9 | 220 | 0.4 | 0.8 | 62 | -0.4 | 0.8 |
| Kostenki-21_layer-3_14 | 8 | 32 | 4 | 175 | 0.7 | 1.3 | 60 | -0.6 | 0.8 |
| Krakow-Spadzista-B_01 | 19 | 87 | 4.6 | 1195 | 0.6 | 1.4 | 86 | 0.1 | 4.3 |
| Krakow-Spadzista-B_02 | 13 | 58 | 4.5 | 538 | 0.6 | 1.4 | 60 | -0.2 | 0 |
| Krakow-Spadzista-B_03 | 19 | 79 | 4.2 | 1109 | 0.7 | 0.6 | 58 | -0.6 | -1.8 |
| Krakow-Spadzista-B_04 | 14 | 60 | 4.3 | 577 | 0.6 | 0.8 | 60 | -1 | 0.6 |
| Krakow-Spadzista-B_05 | 19 | 71 | 3.7 | 926 | 0.6 | 1.5 | 77 | -0.9 | 1.9 |
| La-Balutie_01 | 17 | 115 | 6.8 | 1278 | 2.5 | 0.5 | 23 | -2.1 | -4.2 |
| La-Madeleine_layer-B-MV_01 | 10 | 67 | 6.7 | 533 | 0.4 | 0.8 | 39 | -0.6 | -1.9 |
| La-Madeleine_layer-C-MVI_01 | 10 | 57 | 5.7 | 458 | 0.4 | 1.2 | 47 | -0.1 | -2.3 |
| La-Madeleine_layer-C-MVI_02 | 9 | 38 | 4.2 | 315 | 0.6 | 2.1 | 54 | 0.1 | -1.3 |
| La-Madeleine_layer-C-MVI_03 | 10 | 54 | 5.4 | 386 | 0.5 | 1.2 | 43 | -0.5 | -1 |
| La-Madeleine_layer-C-MVI_04 | 9 | 36 | 4 | 282 | 0.7 | 0.9 | 45 | -0.2 | -2.3 |
| La-Madeleine_layer-C-MVI_05 | 7 | 54 | 7.7 | 334 | 0.4 | 1.8 | 47 | 0.2 | -0.7 |
| La-Mouthe_01 | 13 | 82 | 6.3 | 788 | 2.3 | 0.9 | 43 | -0.4 | -0.8 |
| La-Pasiega_01 | 16 | 58 | 3.6 | 637 | 2.4 | 0.5 | 58 | -1.1 | 0.6 |
| La-Rouviere_01 | 11 | 93 | 8.5 | 780 | 2.8 | 0.6 | 26 | -0.5 | -2.4 |

Appendix Table 17: continued 12,

| ID | width | length | l-w-index | area | upper-lower ratio | left-right ratio | tip angle | MP-CM-x-offset | MP-CM-y-offset |
|---|---|---|---|---|---|---|---|---|---|
| La-Rouviere_02 | 11 | 50 | 4.5 | 374 | 1.9 | 1.1 | 31 | 0.3 | -1.4 |
| La-Rouviere_03 | 9 | 63 | 7 | 421 | 2.5 | 0.8 | 24 | -0.3 | -1.9 |
| La-Rouviere_04 | 11 | 59 | 5.4 | 506 | 1.6 | 0.7 | 51 | -0.3 | 0.8 |
| La-Rouviere_05 | 8 | 60 | 7.5 | 372 | 2 | 1 | 33 | 0.1 | -0.3 |
| Lacam_01 | 12 | 47 | 3.9 | 385 | 0.4 | 0.6 | 83 | -1.1 | 1.1 |
| Lachaud_01 | 18 | 100 | 5.6 | 1232 | 1.1 | 0.4 | 35 | -1.4 | -1.6 |
| Laugerie-Haute-Ouest_01 | 13 | 58 | 4.5 | 480 | 0.9 | 0.5 | 38 | -1.3 | -0.1 |
| Laugerie-Haute-Ouest_02 | 11 | 46 | 4.2 | 380 | 0.8 | 0.7 | 64 | -0.9 | 0.3 |
| Le-Cuzoul-de-Vers_layer-21-16_01 | 8 | 37 | 4.6 | 211 | 0.4 | 0.6 | 74 | -0.7 | 1.7 |
| Le-Cuzoul-de-Vers_layer-21-16_02 | 11 | 32 | 2.9 | 221 | 0.8 | 1.2 | 49 | -0.6 | -0.3 |
| Le-Cuzoul-de-Vers_layer-21-16_03 | 6 | 31 | 5.2 | 120 | 0.7 | 0.7 | 42 | -0.6 | 0 |
| Le-Martinet_layer-IV_01 | 12 | 50 | 4.2 | 408 | 1.8 | 0.5 | 40 | -0.9 | -1 |
| Le-Martinet_layer-IV_02 | 13 | 35 | 2.7 | 339 | 2.3 | 0.2 | 60 | -0.8 | -0.2 |
| Le-Martinet_layer-IV_03 | 12 | 37 | 3.1 | 283 | 2.5 | 0.3 | 39 | -0.8 | -1.9 |
| Le-Placard_01_01 | 15 | 88 | 5.9 | 857 | 1.4 | 0.4 | 29 | -1.3 | -1 |
| Le-Placard_01_02 | 16 | 72 | 4.5 | 725 | 1.3 | 0.2 | 40 | -2.1 | -0.3 |
| Le-Placard_01_03 | 13 | 81 | 6.2 | 708 | 1.5 | 0.3 | 30 | -1.8 | -0.5 |
| Le-Placard_02_01 | 15 | 68 | 4.5 | 714 | 1.2 | 0.4 | 51 | -1.5 | -0.3 |
| Le-Placard_02_02 | 14 | 52 | 3.7 | 542 | 1.1 | 0.8 | 65 | -0.8 | 0.4 |
| Le-Placard_02_03 | 14 | 58 | 4.1 | 600 | 1 | 0.8 | 62 | -0.9 | 0.6 |
| Le-Placard_02_04 | 13 | 60 | 4.6 | 566 | 1.2 | 0.6 | 61 | -0.7 | 1.2 |
| Le-Placard_02_05 | 13 | 62 | 4.8 | 614 | 1.3 | 0.9 | 49 | -0.4 | 0.3 |
| Le-Placard_03_01 | 16 | 96 | 6 | 1036 | 2.1 | 0.5 | 37 | -1.5 | 0.4 |
| Le-Placard_03_02 | 13 | 83 | 6.4 | 722 | 2.1 | 0.2 | 28 | -2.2 | -0.5 |
| Le-Placard_03_03 | 16 | 75 | 4.7 | 857 | 1.3 | 0.6 | 45 | -1.5 | -0.4 |
| Le-Placard_03_04 | 15 | 77 | 5.1 | 756 | 1.6 | 0.2 | 35 | -1.7 | -0.3 |
| Le-Placard_03_05 | 15 | 71 | 4.7 | 720 | 1 | 0.5 | 46 | -1.4 | 0.3 |
| Legintxiqui_01 | 10 | 41 | 4.1 | 268 | 1.4 | 0.8 | 51 | -0.5 | 0.8 |
| Les-Jean-Blancs_01 | 13 | 63 | 4.8 | 607 | 1.3 | 0.9 | 47 | -0.3 | 0.3 |
| Les-Jean-Blancs_02 | 13 | 56 | 4.3 | 529 | 2.1 | 0.5 | 45 | -1.2 | -1.1 |
| Les-Jean-Blancs_03 | 11 | 59 | 5.4 | 506 | 1.4 | 1.2 | 52 | -0.1 | 0.4 |
| Les-Jean-Blancs_04 | 13 | 50 | 3.8 | 489 | 0.7 | 0.7 | 73 | -0.5 | 0.5 |
| Les-Jean-Blancs_05 | 10 | 59 | 5.9 | 395 | 1.4 | 0.9 | 33 | -0.3 | 0 |
| Les-Jean-Blancs_06 | 11 | 51 | 4.6 | 366 | 0.8 | 1.1 | 49 | -0.5 | 1.4 |
| Les-Vachons_01 | 17 | 68 | 4 | 812 | 1.4 | 1.3 | 63 | -0.2 | 1 |
| Liny-1_01 | 14 | 48 | 3.4 | 470 | 1.1 | 1.2 | 54 | -1.1 | -0.7 |
| Liny-1_02 | 13 | 43 | 3.3 | 417 | 1.5 | 0.8 | 56 | -0.3 | -0.2 |

Appendix Table 17: continued 13,

| ID | width | length | l-w-index | area | upper-lower ratio | left-right ratio | tip angle | MP-CM-x-offset | MP-CM-y-offset |
|---|---|---|---|---|---|---|---|---|---|
| Liny-1_03 | 14 | 36 | 2.6 | 358 | 0.9 | 0.5 | 66 | -1.1 | -1.3 |
| Madonna-dell-Ospedale_01 | 11 | 43 | 3.9 | 340 | 1.7 | 0.5 | 57 | -0.8 | 0.6 |
| Madonna-dell-Ospedale_02 | 8 | 36 | 4.5 | 200 | 2.3 | 1.1 | 33 | 0.2 | -1 |
| Marolles-Tureau-des-Gardes_01 | 16 | 45 | 2.8 | 457 | 1 | 0.2 | 59 | -2.3 | -1 |
| Marsangy_01 | 20 | 49 | 2.4 | 662 | 1.3 | 0.5 | 59 | -1 | -1.6 |
| Marsangy_02 | 13 | 45 | 3.5 | 431 | 1.4 | 0.5 | 53 | -0.6 | -1.4 |
| Meiendorf-2_01_01 | 13 | 43 | 3.3 | 353 | 1.3 | 0.4 | 42 | -1.3 | -1.1 |
| Meiendorf-2_01_02 | 14 | 51 | 3.6 | 449 | 1 | 0.4 | 44 | -1.4 | -0.3 |
| Meiendorf-2_01_03 | 10 | 42 | 4.2 | 285 | 0.8 | 0.4 | 48 | -0.7 | -0.2 |
| Meiendorf-2_01_04 | 13 | 47 | 3.6 | 445 | 1.1 | 0.4 | 50 | -1.2 | -1.1 |
| Meiendorf-2_01_05 | 9 | 38 | 4.2 | 276 | 1.3 | 0.5 | 49 | -0.5 | -1 |
| Meiendorf-2_01_06 | 12 | 47 | 3.9 | 336 | 1.3 | 0.2 | 35 | -1.4 | -0.4 |
| Meiendorf-2_01_07 | 11 | 37 | 3.4 | 266 | 1.3 | 0.4 | 41 | -1.2 | -1.6 |
| Meiendorf-2_01_08 | 16 | 60 | 3.8 | 548 | 1.7 | 0.5 | 32 | -1.2 | -1.4 |
| Meiendorf-2_01_09 | 11 | 40 | 3.6 | 277 | 1.2 | 1 | 39 | -0.8 | -0.9 |
| Meiendorf-2_01_10 | 16 | 59 | 3.7 | 546 | 1.5 | 0.7 | 32 | -0.9 | -1.9 |
| Meiendorf-2_02_01 | 13 | 53 | 4.1 | 486 | 1 | 0.1 | 61 | -1.6 | 1.2 |
| Meiendorf-2_02_02 | 13 | 45 | 3.5 | 372 | 1.1 | 1.5 | 54 | 0 | 0.1 |
| Meiendorf-2_02_03 | 13 | 53 | 4.1 | 539 | 1.4 | 1.1 | 71 | -0.3 | 0.3 |
| Meiendorf-2_02_04 | 11 | 45 | 4.1 | 296 | 1.4 | 0.3 | 34 | -1.3 | -1.1 |
| Meiendorf-2_02_05 | 10 | 42 | 4.2 | 297 | 1.4 | 0.3 | 50 | -1.4 | -0.3 |
| Meiendorf-2_02_06 | 11 | 38 | 3.5 | 298 | 1.2 | 0.5 | 44 | -1 | -1.6 |
| Meiendorf-2_02_07 | 10 | 39 | 3.9 | 296 | 1.1 | 0.6 | 45 | -0.3 | -1.3 |
| Milovice-I-section-G_01 | 9 | 42 | 4.7 | 266 | 1.3 | 0.9 | 38 | -0.6 | -0.9 |
| Mirkowice-33_01 | 14 | 38 | 2.7 | 347 | 1.8 | 1 | 71 | -0.8 | 1.2 |
| Mirkowice-33_02 | 13 | 30 | 2.3 | 236 | 1.1 | 0.5 | 57 | -1.4 | -0.6 |
| Mitoc-Malu-Galben_layer-4_01 | 11 | 62 | 5.6 | 469 | 2 | 0.7 | 27 | -0.3 | -3.8 |
| Mitoc-Malu-Galben_layer-4_02 | 8 | 62 | 7.8 | 384 | 1 | 0.9 | 34 | -0.5 | -1.4 |
| Mitoc-Malu-Galben_layer-4_03 | 8 | 54 | 6.8 | 319 | 0.3 | 0.8 | 34 | -0.3 | -2 |
| Mitoc-Malu-Galben_layer-4_04 | 10 | 38 | 3.8 | 276 | 1.4 | 1.1 | 48 | -0.3 | -1.5 |
| Molodova-5_layer-7_01 | 10 | 56 | 5.6 | 412 | 0.5 | 3 | 46 | 0.5 | -0.4 |
| Molodova-5_layer-7_02 | 8 | 46 | 5.8 | 300 | 0.6 | 0.7 | 56 | -0.8 | -0.6 |
| Molodova-5_layer-7_03 | 10 | 48 | 4.8 | 367 | 0.3 | 1.2 | 75 | -0.5 | 0.5 |
| Moravany-nad-Vahom-Lopata-II_01 | 14 | 58 | 4.1 | 628 | 0.4 | 1.3 | 87 | 0.1 | 1.3 |
| Moravany-nad-Vahom-Noviny_01_01 | 26 | 88 | 3.4 | 1549 | 0.9 | 1.4 | 54 | -0.3 | -1.1 |
| Moravany-nad-Vahom-Noviny_01_02 | 19 | 62 | 3.3 | 837 | 0.6 | 1.4 | 84 | -0.3 | 1.8 |
| Moravany-nad-Vahom-Noviny_01_03 | 24 | 75 | 3.1 | 1319 | 0.7 | 1 | 71 | -1 | -1.4 |

Appendix Table 17: continued 14,

| ID | width | length | l–w–index | area | upper–lower ratio | left–right ratio | tip angle | MP–CM–x–offset | MP–CM–y–offset |
|---|---|---|---|---|---|---|---|---|---|
| Moravany–nad–Vahom–Noviny_01_04 | 16 | 53 | 3.3 | 636 | 0.6 | 0.9 | 75 | –0.9 | 0.3 |
| Moravany–nad–Vahom–Noviny_01_05 | 22 | 83 | 3.8 | 1300 | 0.7 | 0.7 | 62 | –1.2 | –0.5 |
| Moravany–nad–Vahom–Noviny_02_01 | 16 | 59 | 3.7 | 695 | 0.8 | 0.9 | 58 | –0.9 | –1 |
| Moravany–nad–Vahom–Noviny_02_02 | 12 | 73 | 6.1 | 660 | 1.2 | 1.1 | 34 | –0.1 | –2.8 |
| Moravany–nad–Vahom–Noviny_02_03 | 14 | 56 | 4 | 562 | 1 | 0.9 | 62 | –0.8 | –0.5 |
| Moravany–nad–Vahom–Noviny_02_04 | 11 | 58 | 5.3 | 512 | 1 | 0.8 | 43 | –0.3 | –2.2 |
| Moravany–nad–Vahom–Noviny_02_05 | 11 | 56 | 5.1 | 506 | 0.7 | 1 | 57 | –0.2 | –0.6 |
| Moravany–nad–Vahom–Noviny_02_06 | 12 | 49 | 4.1 | 417 | 0.7 | 0.9 | 63 | –0.7 | 0.3 |
| Moravany–nad–Vahom–Noviny_02_07 | 9 | 44 | 4.9 | 332 | 0.7 | 0.7 | 75 | –0.6 | –0.7 |
| Moravany–nad–Vahom–Podkovica_01 | 20 | 61 | 3 | 865 | 0.6 | 1.3 | 89 | –0.1 | 2.1 |
| Moravany–nad–Vahom–Podkovica_02 | 12 | 55 | 4.6 | 533 | 0.8 | 0.9 | 60 | –0.3 | –0.6 |
| Moravany–nad–Vahom–Podkovica_03 | 12 | 48 | 4 | 409 | 0.8 | 1 | 61 | –0.5 | 0.3 |
| Morin_01 | 16 | 82 | 5.1 | 1042 | 0.3 | 1.5 | 73 | –0.9 | –0.4 |
| Morin_02 | 13 | 57 | 4.4 | 525 | 0.4 | 0.7 | 67 | –1.4 | –0.6 |
| Morin_03 | 15 | 79 | 5.3 | 963 | 0.7 | 1.6 | 47 | 0.3 | –2.8 |
| Morin_04 | 11 | 56 | 5.1 | 470 | 0.3 | 1.2 | 73 | 0 | –0.3 |
| Morin_05 | 15 | 71 | 4.7 | 797 | 0.5 | 0.4 | 53 | –1.4 | –0.7 |
| Morin_06 | 11 | 68 | 6.2 | 620 | 0.3 | 2 | 39 | 0.1 | –2.5 |
| Mother–Grundys–Parlour_layer–CB–LB–SB_01 | 11 | 45 | 4.1 | 353 | 2.3 | 0.6 | 45 | –0.9 | 0.3 |
| Mother–Grundys–Parlour_layer–CB–LB–SB_02 | 10 | 45 | 4.5 | 301 | 1 | 0.2 | 42 | –0.7 | –0.1 |
| Mother–Grundys–Parlour_layer–CB–LB–SB_03 | 12 | 33 | 2.8 | 277 | 1.6 | 1.2 | 55 | –0.3 | –0.5 |
| Mother–Grundys–Parlour_layer–CB–LB–SB_04 | 15 | 44 | 2.9 | 470 | 0.8 | 1 | 55 | –0.3 | –1.4 |
| Nitra–I–Cerman_01 | 13 | 43 | 3.3 | 412 | 1.9 | 0.4 | 47 | –1.4 | –1.9 |
| Nitra–I–Cerman_02 | 9 | 38 | 4.2 | 271 | 0.8 | 0.7 | 65 | –0.5 | –0.3 |
| Nitra–I–Cerman_03 | 7 | 28 | 4 | 180 | 0.6 | 0.8 | 70 | 0.1 | –0.7 |
| Nitra–I–Cerman_04 | 10 | 26 | 2.6 | 187 | 1 | 0.9 | 81 | –0.3 | 0.5 |
| Noailles_01 | 11 | 41 | 3.7 | 320 | 1 | 1 | 52 | –0.3 | 0.1 |
| Oelknitz_01 | 11 | 73 | 6.6 | 622 | 0.2 | 2.6 | 28 | –0.2 | –3.5 |
| Oelknitz_02 | 11 | 66 | 6 | 630 | 0.3 | 0.1 | 36 | –1.4 | –2.6 |
| Olbrachcice–8_01 | 15 | 53 | 3.5 | 627 | 0.9 | 0.7 | 64 | –0.3 | –0.4 |
| Olbrachcice–8_02 | 14 | 50 | 3.6 | 505 | 1.1 | 0.3 | 59 | –1.2 | –0.1 |
| Olbrachcice–8_03 | 13 | 35 | 2.7 | 298 | 0.9 | 0.2 | 56 | –1.7 | –0.4 |
| Olbrachcice–8_04 | 17 | 53 | 3.1 | 611 | 1 | 0.6 | 66 | –0.8 | 0.8 |
| Olbrachcice–8_05 | 16 | 47 | 2.9 | 554 | 1 | 0.6 | 70 | –1.4 | 0.2 |
| Olbrachcice–8_06 | 15 | 52 | 3.5 | 510 | 1.1 | 0.5 | 42 | –0.8 | –0.6 |
| Olbrachcice–8_07 | 15 | 43 | 2.9 | 453 | 0.8 | 0.6 | 55 | –0.8 | –1 |
| Olbrachcice–8_08 | 15 | 53 | 3.5 | 552 | 1.3 | 0.6 | 43 | –0.5 | –2.3 |

Appendix Table 17: continued 15,

| ID | width | length | l–w–index | area | upper–lower ratio | left–right ratio | tip angle | MP–CM–x–offset | MP–CM–y–offset |
|---|---|---|---|---|---|---|---|---|---|
| Oldeholtwolde_01 | 11 | 62 | 5.6 | 498 | 1.5 | 1.2 | 36 | 0.1 | −0.2 |
| Oldeholtwolde_02 | 10 | 41 | 4.1 | 276 | 1.9 | 0.7 | 33 | 0 | −1.8 |
| Oldeholtwolde_03 | 15 | 57 | 3.8 | 563 | 1.1 | 1.1 | 43 | −0.7 | −0.5 |
| Oldeholtwolde_04 | 11 | 42 | 3.8 | 340 | 1 | 0.4 | 53 | −0.8 | −0.6 |
| Oldeholtwolde_05 | 10 | 50 | 5 | 307 | 1.5 | 0.4 | 28 | −0.9 | −1.5 |
| Oldeholtwolde_06 | 12 | 39 | 3.2 | 299 | 1.3 | 0.5 | 54 | −0.7 | 0.6 |
| Oldeholtwolde_07 | 10 | 45 | 4.5 | 321 | 1 | 0.8 | 37 | −0.6 | −1.1 |
| Oreile-dEnfer_01 | 13 | 56 | 4.3 | 522 | 1.2 | 1.1 | 50 | −0.3 | −0.1 |
| Oreile-dEnfer_02 | 17 | 51 | 3 | 610 | 1.1 | 0.9 | 64 | −0.7 | 0 |
| Pech-de-la-Boissiere_01 | 11 | 55 | 5 | 430 | 0.9 | 1.7 | 48 | 0.2 | 0.4 |
| Pech-de-la-Boissiere_02 | 11 | 49 | 4.5 | 408 | 0.9 | 0.9 | 59 | −0.3 | 0.9 |
| Pech-de-la-Boissiere_03 | 7 | 46 | 6.6 | 249 | 1 | 0.9 | 33 | −0.4 | −0.8 |
| Pech-de-la-Boissiere_04 | 11 | 37 | 3.4 | 309 | 1.4 | 1.3 | 63 | −0.3 | −0.6 |
| Pech-de-la-Boissiere_05 | 13 | 49 | 3.8 | 435 | 0.6 | 0.7 | 69 | −0.9 | 1.2 |
| Pech-de-la-Boissiere_06 | 11 | 45 | 4.1 | 363 | 0.8 | 0.9 | 64 | −0.3 | 0.8 |
| Petersfels_01 | 13 | 36 | 2.8 | 337 | 1.2 | 0.2 | 61 | −1.4 | −0.9 |
| Petersfels_02 | 13 | 38 | 2.9 | 377 | 2 | 0.2 | 52 | −0.8 | −1.4 |
| Petersfels_03 | 24 | 53 | 2.2 | 930 | 1 | 0.5 | 70 | −1.3 | −1.8 |
| Petersfels_04 | 14 | 35 | 2.5 | 361 | 1.4 | 1.3 | 65 | −0.2 | −0.8 |
| Petersfels_05 | 14 | 42 | 3 | 433 | 1.5 | 0.3 | 57 | −0.3 | −1.1 |
| Petersfels_06 | 11 | 34 | 3.1 | 263 | 1.2 | 0.5 | 55 | −1 | −0.7 |
| Petersfels_07 | 19 | 49 | 2.6 | 653 | 0.8 | 0.4 | 76 | −1.6 | 0.1 |
| Petersfels_08 | 14 | 42 | 3 | 432 | 0.8 | 0.1 | 67 | −1.1 | 0.2 |
| Petersfels_09 | 16 | 40 | 2.5 | 419 | 1.1 | 0.5 | 66 | −1.4 | −0.4 |
| Petersfels_10 | 14 | 43 | 3.1 | 495 | 1.3 | 0.3 | 75 | −0.6 | 0.3 |
| Petersfels_11 | 21 | 47 | 2.2 | 668 | 1 | 0.4 | 71 | −1.4 | −0.6 |
| Petersfels_12 | 16 | 44 | 2.8 | 442 | 1 | 0.5 | 69 | −1.3 | 0.4 |
| Petersfels_13 | 15 | 47 | 3.1 | 527 | 1.6 | 0.3 | 62 | −1.3 | −0.3 |
| Petite-Grotte-de-Bize_01 | 15 | 57 | 3.8 | 550 | 1.1 | 0.9 | 50 | −0.5 | 0.8 |
| Petite-Grotte-de-Bize_02 | 12 | 46 | 3.8 | 379 | 1.1 | 0.3 | 48 | −1.5 | −0.2 |
| Petite-Grotte-de-Bize_03 | 10 | 42 | 4.2 | 265 | 2.1 | 0.9 | 35 | −0.5 | −0.1 |
| Petite-Grotte-de-Bize_04 | 10 | 39 | 3.9 | 224 | 1.1 | 0.4 | 40 | −1 | 0.1 |
| Petite-Grotte-de-Bize_05 | 13 | 50 | 3.8 | 399 | 1.1 | 0.4 | 48 | −1.4 | 0.5 |
| Petite-Grotte-de-Bize_06 | 9 | 49 | 5.4 | 324 | 2.5 | 1.3 | 39 | −0.3 | −0.4 |
| Petite-Grotte-de-Bize_07 | 13 | 49 | 3.8 | 377 | 1.2 | 0.6 | 42 | −1.3 | 0.2 |
| Petite-Grotte-de-Bize_08 | 8 | 49 | 6.1 | 265 | 2.1 | 1.3 | 28 | 0.1 | −0.8 |
| Petite-Grotte-de-Bize_09 | 10 | 40 | 4 | 272 | 1.5 | 0.7 | 36 | −0.6 | −0.8 |

Appendix Table 17: continued 16,

| ID | width | length | l–w–index | area | upper–lower ratio | left–right ratio | tip angle | MP–CM–x–offset | MP–CM–y–offset |
|---|---|---|---|---|---|---|---|---|---|
| Petite-Grotte-de-Bize_10 | 9 | 33 | 3.7 | 170 | 0.8 | 0.5 | 46 | −0.9 | 0.6 |
| Petite-Grotte-de-Bize_11 | 7 | 33 | 4.7 | 155 | 1.8 | 0.8 | 32 | −0.5 | −0.3 |
| Petrkovice-1a_01 | 16 | 57 | 3.6 | 669 | 1.3 | 1.4 | 52 | −0.7 | −0.8 |
| Petrkovice-1a_02 | 15 | 50 | 3.3 | 561 | 1 | 1 | 62 | −0.3 | −0.9 |
| Petrkovice-1a_03 | 12 | 37 | 3.1 | 361 | 0.5 | 1 | 55 | 0 | −1.8 |
| Poggenwisch-D_01_01 | 14 | 77 | 5.5 | 801 | 1.7 | 0.4 | 37 | −0.9 | −1.8 |
| Poggenwisch-D_01_02 | 15 | 59 | 3.9 | 555 | 1.9 | 0.7 | 33 | −0.4 | −2.4 |
| Poggenwisch-D_01_03 | 17 | 69 | 4.1 | 868 | 1.9 | 0.9 | 42 | 0.6 | −2 |
| Poggenwisch-D_01_04 | 13 | 53 | 4.1 | 482 | 1 | 0.4 | 43 | −0.6 | −1.8 |
| Poggenwisch-D_01_05 | 13 | 65 | 5 | 617 | 1.2 | 0.3 | 42 | −0.9 | −1.4 |
| Poggenwisch-D_01_06 | 14 | 52 | 3.7 | 506 | 1.3 | 0.8 | 49 | −0.3 | −0.9 |
| Poggenwisch-D_01_07 | 15 | 61 | 4.1 | 596 | 1.6 | 0.5 | 33 | −1 | −1.9 |
| Poggenwisch-D_01_08 | 14 | 51 | 3.6 | 474 | 1.4 | 0.7 | 45 | −0.8 | −0.3 |
| Poggenwisch-D_01_09 | 15 | 62 | 4.1 | 655 | 1.3 | 0.8 | 48 | −0.7 | −0.4 |
| Poggenwisch-D_02_01 | 14 | 52 | 3.7 | 504 | 1.3 | 0.5 | 52 | −0.8 | −0.3 |
| Poggenwisch-D_02_02 | 15 | 57 | 3.8 | 529 | 0.9 | 0.4 | 44 | −1.4 | −1 |
| Poggenwisch-D_02_03 | 10 | 46 | 4.6 | 350 | 1.6 | 0.4 | 33 | −0.5 | −1.6 |
| Poggenwisch-D_02_04 | 12 | 54 | 4.5 | 450 | 1.4 | 0.8 | 34 | −0.8 | −2.1 |
| Poggenwisch-D_02_05 | 11 | 46 | 4.2 | 364 | 1.2 | 0.4 | 45 | −0.7 | −0.8 |
| Poggenwisch-D_02_06 | 12 | 46 | 3.8 | 362 | 1.4 | 0.4 | 46 | −0.8 | 0.1 |
| Poggenwisch-D_02_07 | 10 | 43 | 4.3 | 320 | 1.4 | 1.2 | 46 | −0.7 | −0.8 |
| Poggenwisch-D_02_08 | 8 | 45 | 5.6 | 298 | 1.5 | 0.2 | 45 | −0.3 | −0.9 |
| Poggenwisch-D_02_09 | 13 | 38 | 2.9 | 303 | 1.4 | 0.4 | 47 | −1.4 | −1.3 |
| Poggenwisch-D_02_10 | 10 | 43 | 4.3 | 302 | 1.2 | 0.4 | 52 | −1 | 0.5 |
| Poggenwisch-D_03_01 | 14 | 56 | 4 | 538 | 1.6 | 0.5 | 43 | −0.8 | −0.8 |
| Poggenwisch-D_03_02 | 16 | 55 | 3.4 | 538 | 1.4 | 0.5 | 43 | −1.2 | −0.8 |
| Poggenwisch-D_03_03 | 12 | 42 | 3.5 | 344 | 0.9 | 0.3 | 55 | −1 | −0.6 |
| Poggenwisch-D_03_04 | 11 | 44 | 4 | 305 | 1 | 0.2 | 40 | −1.3 | 0.3 |
| Ponte-di-Pietra_01 | 6 | 40 | 6.7 | 162 | 2.8 | 0.8 | 26 | −0.3 | −1 |
| Ponte-di-Pietra_02 | 5 | 38 | 7.6 | 156 | 2.8 | 1.3 | 33 | −0.1 | −0.7 |
| Pre-Aubert_01 | 14 | 91 | 6.5 | 856 | 1.8 | 0.3 | 28 | −1.4 | −0.8 |
| Pushkari-I_01 | 10 | 37 | 3.7 | 273 | 0.6 | 0.9 | 64 | −0.1 | −0.9 |
| Ranchot-Abri-des-Cabones_01 | 19 | 62 | 3.3 | 793 | 1.3 | 0.5 | 50 | −1.8 | −1.9 |
| Ranchot-Abri-des-Cabones_02 | 12 | 44 | 3.7 | 386 | 0.9 | 0.5 | 56 | −0.7 | −0.8 |
| Riparo-di-Biedano_01 | 10 | 34 | 3.4 | 231 | 1.4 | 0.5 | 57 | −0.8 | 0.3 |
| Riparo-di-Biedano_02 | 9 | 30 | 3.3 | 186 | 0.5 | 0.4 | 70 | −1.1 | 0.1 |
| Riparo-Mochi_layer-D_01 | 17 | 46 | 2.7 | 510 | 0.9 | 0.7 | 64 | −1.4 | −0.8 |

Appendix Table 17: continued 17,

| ID | width | length | l–w–index | area | upper–lower ratio | left–right ratio | tip angle | MP–CM–x–offset | MP–CM–y–offset |
|---|---|---|---|---|---|---|---|---|---|
| Riparo–Taglient_01 | 11 | 54 | 4.9 | 427 | 1.7 | 0.8 | 41 | 0 | –0.4 |
| Riparo–Taglient_02 | 8 | 35 | 4.4 | 222 | 1 | 0.7 | 50 | –0.3 | –1.4 |
| Roc–de–Sers_01 | 13 | 53 | 4.1 | 508 | 2 | 0.7 | 41 | –0.7 | –1.9 |
| Rogow–Opolski–9_01 | 16 | 52 | 3.2 | 533 | 0.9 | 0.5 | 48 | –1.5 | –0.7 |
| Rogow–Opolski–9_02 | 13 | 38 | 2.9 | 349 | 1 | 0.5 | 66 | –0.8 | –0.3 |
| Saint–Front–de–Corgnac_01 | 11 | 44 | 4 | 326 | 1.2 | 0.7 | 49 | –0.6 | 0.3 |
| Salitrena–Pecina_01 | 13 | 52 | 4 | 494 | 1.8 | 0.5 | 47 | –0.8 | –0.6 |
| Sandalja–II_layer–c–d_01 | 13 | 70 | 5.4 | 631 | 1.8 | 0.8 | 34 | –0.8 | –1.9 |
| Schussenquelle_layer–F_01 | 16 | 44 | 2.8 | 485 | 1.4 | 0.4 | 56 | –1 | –1.4 |
| Siedlnica–17a_01 | 13 | 41 | 3.2 | 366 | 1.1 | 1.4 | 52 | –0.9 | –0.8 |
| Siedlnica–17a_02 | 11 | 40 | 3.6 | 303 | 1 | 1.1 | 67 | –0.8 | 0.5 |
| Stellmoor_01 | 10 | 65 | 6.5 | 488 | 2.4 | 0.5 | 33 | –0.6 | –1.9 |
| Stellmoor_02 | 15 | 50 | 3.3 | 481 | 1.4 | 0.5 | 46 | –1.2 | –1 |
| Taurisano_01 | 18 | 58 | 3.2 | 706 | 1.2 | 0.3 | 58 | –1.2 | 0.6 |
| Taurisano_02 | 8 | 26 | 3.2 | 132 | 1 | 0.4 | 52 | –0.9 | –0.1 |
| Taurisano_03 | 11 | 55 | 5 | 405 | 2 | 0.3 | 35 | –1.3 | –1.4 |
| Taurisano_04 | 13 | 31 | 2.4 | 262 | 0.7 | 0.7 | 82 | –1.1 | 0.8 |
| Taurisano_05 | 10 | 36 | 3.6 | 266 | 1.1 | 0.3 | 39 | –1 | –2 |
| Teltwisch–1_01 | 13 | 37 | 2.8 | 311 | 1.1 | 0.7 | 56 | –1 | –0.7 |
| Teltwisch–1_02 | 13 | 57 | 4.4 | 559 | 2.7 | 0.3 | 36 | –1.1 | –2.4 |
| Teltwisch–1_03 | 15 | 45 | 3 | 458 | 1.1 | 0.9 | 63 | –0.8 | –0.2 |
| Teltwisch–1_04 | 14 | 52 | 3.7 | 411 | 1.5 | 0.4 | 30 | –1.3 | –2.4 |
| Teltwisch–1_05 | 15 | 49 | 3.3 | 481 | 1.1 | 0.5 | 55 | –1.7 | 0.2 |
| Teltwisch–1_06 | 9 | 53 | 5.9 | 331 | 1 | 0.1 | 33 | –1.1 | –0.9 |
| Teltwisch–1_07 | 11 | 47 | 4.3 | 401 | 1 | 0.4 | 48 | –0.5 | –0.4 |
| Teltwisch–1_08 | 10 | 42 | 4.2 | 301 | 0.9 | 0.6 | 49 | –0.4 | –0.9 |
| Teltwisch–1_09 | 11 | 46 | 4.2 | 358 | 1.4 | 0.3 | 43 | –1.3 | –0.7 |
| Teltwisch–1_10 | 11 | 55 | 5 | 392 | 1.8 | 0.5 | 28 | –0.3 | –1.7 |
| Teltwisch–1_11 | 11 | 43 | 3.9 | 338 | 0.8 | 0.4 | 62 | –0.7 | 1.4 |
| Teltwisch–1_12 | 11 | 39 | 3.5 | 288 | 1 | 0.4 | 58 | –1 | 0.6 |
| Tourtoirac_01 | 12 | 48 | 4 | 388 | 1 | 0.6 | 46 | –0.7 | –0.3 |
| Tourtoirac_02 | 13 | 44 | 3.4 | 366 | 0.8 | 0.6 | 54 | –1.1 | 0.5 |
| Ureterp–1_01 | 12 | 52 | 4.3 | 407 | 1.2 | 0.3 | 39 | –1.4 | –1 |
| Ureterp–1_02 | 9 | 30 | 3.3 | 192 | 1.2 | 0.3 | 47 | –0.3 | –1 |
| Ureterp–1_03 | 13 | 40 | 3.1 | 305 | 1.3 | 0.6 | 50 | –0.9 | –0.8 |
| Ureterp–1_04 | 11 | 32 | 2.9 | 246 | 1 | 0.6 | 51 | –0.3 | –0.8 |
| Ureterp–1_05 | 13 | 37 | 2.8 | 265 | 1.3 | 1 | 37 | –0.4 | –1.5 |

Appendix Table 17: continued 18.

| ID | width | length | l–w–index | area | upper–lower ratio | left–right ratio | tip angle | MP–CM–x–offset | MP–CM–y–offset |
|---|---|---|---|---|---|---|---|---|---|
| Ureterp–I_06 | 13 | 34 | 2.6 | 307 | 0.8 | 0.9 | 72 | –0.8 | 0 |
| Ureterp–I_07 | 9 | 40 | 4.4 | 260 | 1.4 | 0.3 | 35 | –0.8 | –1.8 |
| Ureterp–I_08 | 13 | 57 | 4.4 | 437 | 1.4 | 0.4 | 33 | –0.8 | –0.6 |
| Ureterp–I_09 | 12 | 58 | 4.8 | 457 | 1.1 | 0.2 | 41 | –1.9 | –0.6 |
| Vale–Boi_01 | 8 | 31 | 3.9 | 186 | 1 | 0.9 | 40 | –0.1 | –0.9 |
| Vale–Boi_02 | 8 | 25 | 3.1 | 115 | 1 | 0.7 | 49 | –0.6 | 0.3 |
| Vale–Boi_03 | 9 | 25 | 2.8 | 130 | 2.5 | 0.2 | 38 | –1.2 | –1.2 |
| Vale–Boi_04 | 7 | 26 | 3.7 | 129 | 1.7 | 1.1 | 49 | –0.3 | 0.1 |
| Vale–Boi_05 | 4 | 23 | 5.8 | 80 | 1.6 | 0.3 | 41 | –0.5 | –0.2 |
| Vrbicka–Cave_01 | 15 | 40 | 2.7 | 445 | 1.4 | 0.5 | 79 | –1.3 | 0 |
| Willendorf–II_layer–9_01 | 11 | 42 | 3.8 | 399 | 0.4 | 0.9 | 82 | –0.3 | –1.3 |
| Willendorf–II_layer–9_02 | 8 | 36 | 4.5 | 257 | 0.2 | 3 | 60 | 0.3 | –0.8 |
| Willendorf–II_layer–9_03 | 9 | 39 | 4.3 | 265 | 0.5 | 1 | 59 | –0.5 | 0.2 |
| Willendorf–II_layer–9_04 | 8 | 25 | 3.1 | 142 | 0.3 | 1.2 | 91 | –0.7 | 0.8 |
| Zamostya–I_01 | 12 | 49 | 4.1 | 440 | 1.3 | 0.7 | 62 | –0.7 | –0.4 |
| Zamostya–I_02 | 14 | 40 | 2.9 | 340 | 1.3 | 0.5 | 42 | –0.8 | –1.4 |
| Zaraisk_01 | 38 | 127 | 3.3 | 3488 | 1.2 | 0.8 | 58 | –1.8 | –1.7 |
| Zaraisk_02 | 19 | 72 | 3.8 | 1025 | 1 | 2.6 | 57 | 1.3 | –1.2 |
| Zaraisk_03 | 16 | 71 | 4.4 | 811 | 1.1 | 1 | 58 | –0.5 | 1.3 |
| Zaraisk_04 | 27 | 101 | 3.7 | 1973 | 0.8 | 1.5 | 71 | 0.7 | 1.3 |

Appendix Table 18: Table of main metrical features for the scalene bladelets discussed in the text.
all measurements in mm, area in mm². Abbreviations: l = length, w = width, MP = midpoint, CM = centre of mass

| ID | width | length | l–w–index | area | upper–lower ratio | left–right ratio | tip angle | MP–CM–x–offset | MP–CM–y–offset |
|---|---|---|---|---|---|---|---|---|---|
| Scalene_bladelet_01 | 6 | 23 | 3.8 | 119 | 0.4 | 0.7 | 82 | –0.3 | 0.3 |
| Scalene_bladelet_02 | 8 | 29 | 3.6 | 180 | 0.4 | 0.2 | 83 | –0.6 | 0.1 |
| Scalene_bladelet_03 | 7 | 27 | 3.9 | 158 | 0.4 | 0.2 | 79 | –0.6 | 0.4 |
| Scalene_bladelet_04 | 6 | 21 | 3.5 | 112 | 0.4 | 0.3 | 90 | –0.3 | 0 |
| Scalene_bladelet_05 | 6 | 27 | 4.5 | 125 | 0.4 | 0.4 | 79 | –0.8 | 0.9 |
| Scalene_bladelet_06 | 6 | 21 | 3.5 | 89 | 0.6 | 0.3 | 64 | –0.6 | 0.3 |
| Scalene_bladelet_07 | 6 | 29 | 4.8 | 131 | 0.3 | 0.3 | 77 | –0.6 | 1 |
| Scalene_bladelet_08 | 5 | 22 | 4.4 | 97 | 0.4 | 0.8 | 84 | –0.3 | 0.3 |
| Scalene_bladelet_09 | 7 | 28 | 4 | 167 | 0.3 | 0.4 | 87 | –0.3 | 0.4 |
| Scalene_bladelet_10 | 6 | 26 | 4.3 | 119 | 0.3 | 0.2 | 93 | –0.5 | 1.3 |